



TESTING CERT # 2937.01

*Research Project Number TPF-5(193) Suppl. #15  
NDOR Sponsoring Agency Code RFPF-WISC-4*

# **DEVELOPMENT OF A RETROFIT, LOW-DEFLECTION, TEMPORARY CONCRETE BARRIER SYSTEM**

Submitted by

Robert W. Bielenberg, M.S.M.E., E.I.T.  
Research Associate Engineer

Tyson E. Quinn  
Former Undergraduate Research Assistant

Ronald K. Faller, Ph.D., P.E.  
Research Associate Professor  
MwRSF Director

Dean L. Sicking, Ph.D., P.E.  
Emeritus Professor

John D. Reid, Ph.D.  
Professor

## **MIDWEST ROADSIDE SAFETY FACILITY**

Nebraska Transportation Center  
University of Nebraska-Lincoln  
130 Whittier Research Center  
2200 Vine Street  
Lincoln, Nebraska 68583-0853  
(402) 472-0965

Submitted to

## **WISCONSIN DEPARTMENT OF TRANSPORTATION**

Bureau of Project Development  
4802 Sheboygan Avenue – Room 651  
P.O. Box 7916  
Madison, Wisconsin 53707-7916

MwRSF Research Report No. TRP-03-295-14

March 31, 2014

## TECHNICAL REPORT DOCUMENTATION PAGE

1. Report No. <b>TRP-03-295-14</b>	2.	3. Recipient's Accession No.	
4. Title and Subtitle <b>Development of a Retrofit, Low-Deflection, Temporary Concrete Barrier System</b>		5. Report Date <b>March 31, 2014</b>	
		6.	
7. Author(s) <b>Bielenberg, R.W., Quinn, T.E., Faller, R.K., Sicking, D.L., and Reid, J.D.</b>		8. Performing Organization Report No. <b>TRP-03-295-14</b>	
9. Performing Organization Name and Address <b>Midwest Roadside Safety Facility (MwRSF) Nebraska Transportation Center University of Nebraska-Lincoln 130 Whittier Research Center 2200 Vine Street Lincoln, Nebraska 68583-0853</b>		10. Project/Task/Work Unit No.	
		11. Contract © or Grant (G) No. <b>TPF-5(193) Suppl. #15</b>	
12. Sponsoring Organization Name and Address <b>Midwest States Regional Pooled Fund Program Nebraska Department of Roads 1500 Nebraska Highway 2 Lincoln, Nebraska 68502</b>		13. Type of Report and Period Covered <b>Final Report: 2009 – 2014</b>	
		14. Sponsoring Agency Code <b>RPPF-WISC-4</b>	
15. Supplementary Notes <b>Prepared in cooperation with U.S. Department of Transportation, Federal Highway Administration.</b>			
16. Abstract (Limit: 200 words) <p>The objective of this research effort was to develop a stiffening mechanism for use in reducing the deflection of temporary concrete barrier (TCB) installations without requiring anchorage of the barrier segments to the road surface. The joint- stiffening mechanism was developed for use with the Midwest Pooled Fund States' 12.5-ft (3.8-m) long, F-shape, temporary concrete barrier.</p> <p>The research effort included development and analysis of mechanisms for limiting deflections through engineering analysis and LS-DYNA computer simulation. Following analysis of the candidate designs, an initial prototype design was full-scale crash tested. Following the first full-scale crash test, the low-deflection TCB system was modified to further reduce deflections and full-scale crash tested a second time. The final version of the low-deflection TCB system was capable of reducing dynamic barrier deflections almost 50% over free-standing TCB installations while still safely redirecting errant vehicles.</p> <p>LS-DYNA simulations of a pickup truck striking the low-deflection TCB system at the 85<sup>th</sup> percentile impact severity were conducted to estimate the deflection of the barrier. The predicted deflection was then used to set placement criteria for non-critical installations.</p>			
17. Document Analysis/Descriptors <b>Highway Safety, Crash Test, Roadside Appurtenances, Compliance Test, MASH, Temporary Concrete Barrier, Deflection, Portable Concrete Barrier</b>		18. Availability Statement <b>No restrictions. Document available from: National Technical Information Services, Springfield, Virginia 22161</b>	
19. Security Class (this report) <b>Unclassified</b>	20. Security Class (this page) <b>Unclassified</b>	21. No. of Pages <b>366</b>	22. Price

## **DISCLAIMER STATEMENT**

This report was completed with funding from the Wisconsin Department of Transportation and the Federal Highway Administration, U.S. Department of Transportation. The contents of this report reflect the views and opinions of the authors who are responsible for the facts and the accuracy of the data presented herein. The contents do not necessarily reflect the official views or policies of the Wisconsin Department of Transportation nor the Federal Highway Administration, U.S. Department of Transportation. This report does not constitute a standard, specification, regulation, product endorsement, or an endorsement of manufacturers.

## **UNCERTAINTY OF MEASUREMENT STATEMENT**

The Midwest Roadside Safety Facility (MwRSF) has determined the uncertainty of measurements for several parameters involved in standard full-scale crash testing and non-standard testing of roadside safety features. Information regarding the uncertainty of measurements for critical parameters is available upon request by the sponsor and the Federal Highway Administration. Test nos. TCBF-1 through TCBF-6 were non-certified component tests conducted for research and development purposes only.

## **INDEPENDENT APPROVING AUTHORITY**

The Independent Approving Authority (IAA) for the data contained herein was Dr. Cody Stolle, Post-Doctoral Research Associate.

## **ACKNOWLEDGEMENTS**

The authors wish to acknowledge several sources that made a contribution to this project:

(1) the Wisconsin Department of Transportation and the Federal Highway Administration for sponsoring this project and (2) MwRSF personnel for constructing the barriers and conducting the crash tests.

Acknowledgement is also given to the following individuals who made a contribution to the completion of this research project.

### **Midwest Roadside Safety Facility**

J.C. Holloway, M.S.C.E., E.I.T., Test Site Manager  
K.A. Lechtenberg, M.S.M.E., E.I.T., Research Associate Engineer  
S.K. Rosenbaugh, M.S.C.E., E.I.T., Research Associate Engineer  
C.S. Stolle, Ph.D., E.I.T., Post-doctoral Research Associate  
J.D. Schmidt, Ph.D., P.E., Post-doctoral Research Associate  
A.T. Russell, B.S.B.A., Shop Manager  
K.L. Krenk, B.S.M.A., Maintenance Mechanic  
D.S. Charroin, Laboratory Mechanic  
S.M. Tighe, Laboratory Mechanic  
Undergraduate and Graduate Research Assistants

### **Wisconsin Department of Transportation**

Jerry Zogg, P.E., Chief Roadway Standards Engineer  
Erik Emerson, P.E., Standards Development Engineer

## TABLE OF CONTENTS

TECHNICAL REPORT DOCUMENTATION PAGE .....	i
DISCLAIMER STATEMENT .....	ii
UNCERTAINTY OF MEASUREMENT STATEMENT .....	ii
INDEPENDENT APPROVING AUTHORITY.....	ii
ACKNOWLEDGEMENTS .....	iii
TABLE OF CONTENTS.....	iv
LIST OF FIGURES .....	vii
LIST OF TABLES .....	xiii
1 INTRODUCTION .....	1
1.1 Background.....	1
1.2 Objective.....	2
1.3 Scope.....	3
2 LITERATURE REVIEW .....	4
2.1 MwRSF Free-Standing F-shape TCB.....	4
2.2 Reduced-Deflection TCB Designs.....	6
2.3 Comparison of Previous Reduced-Deflection Designs.....	10
3 DEVELOPMENT OF DESIGN CONCEPTS.....	13
3.1 Design Criteria.....	13
3.2 Design Concepts .....	13
4 SIMULATION OF REDUCED-DEFLECTION MECHANISMS .....	28
4.1 Methodology .....	28
4.2 Baseline Model .....	28
4.2.1 Baseline Model Description.....	28
4.2.2 Simulation of Baseline Model and Comparison with Test No. TB-2.....	31
4.3.1 Increased Barrier Mass .....	38
4.3.2 Increased Barrier-to-Ground Friction .....	41
4.3.3 Reduced Joint Tolerance.....	41
4.3.4 Composite Action .....	44
5 COMPONENT TESTING OF TCB FRICTION COEFFICIENTS .....	53
5.1 Purpose.....	53
5.2 Scope.....	53
5.3 Equipment and Instrumentation.....	60
5.3.1 Tensile-Load Cells.....	60
5.3.2 Digital Photography.....	61
5.4 Data Processing.....	61

6 FRICTION TESTING RESULTS AND DISCUSSION.....	63
6.1 Test Results.....	63
6.1.1 Test No. TCBF-1 .....	64
6.1.2 Test No. TCBF-2 .....	66
6.1.3 Test No. TCBF-3 .....	68
6.1.4 Test No. TCBF-4 .....	69
6.1.5 Test No. TCBF-5 .....	72
6.1.6 Test No. TCBF-6 .....	72
6.2 Test Results.....	72
7 CONCRETE MATERIAL MODELING .....	78
7.1 MAT_159_CSCM.....	78
7.2 Concrete Cylinder Models .....	81
7.2.1 Compression Cylinder Simulations .....	83
7.2.2 Tension Cylinder Simulations.....	93
7.2.1 Concrete Cylinder Simulation Discussion.....	98
7.3 Concrete Beam Models.....	98
7.4 Concrete Material Model Recommendations .....	109
8 TEST REQUIREMENTS AND EVALUATION CRITERIA .....	110
8.1 Test Requirements .....	110
8.2 Evaluation Criteria.....	111
9 TEST CONDITIONS.....	113
9.1 Test Facility .....	113
9.2 Vehicle Tow and Guidance System.....	113
9.3 Test Vehicles.....	113
9.4 Simulated Occupant .....	121
9.5 Data Acquisition Systems .....	121
9.5.1 Accelerometers .....	121
9.5.2 Rate Transducers.....	122
9.5.3 Speed Trap .....	123
9.5.4 Digital Photography.....	124
10 DESIGN DETAILS FOR TEST NO. RDTCB-1 .....	127
10.1 Design Considerations .....	127
10.2 Design Details.....	132
11 FULL-SCALE CRASH TEST NO. RDTCB-1 .....	152
11.1 Test No. RDTCB-1 .....	152
11.2 Weather Conditions .....	152
11.3 Test Description .....	152
11.4 Barrier Damage.....	154
11.5 Vehicle Damage.....	156
11.6 Occupant Risk.....	157
11.7 Discussion.....	158
12 ANALYSIS AND REFINEMENT OF LOW-DEFLECTION TCB DESIGN .....	171

12.1 Simulation and Validation of Test No. RDTCB-1.....	173
12.2 Simulation of Proposed Design Modifications .....	185
12.2.1 Increased Barrier-to-Ground Friction .....	186
12.2.2 Tube Thickness .....	186
12.2.3 Cap Thickness .....	187
12.2.4 Reduced Joint Gap Tolerance .....	187
12.2.5 Additional Tube Attachments .....	188
13 DESIGN DETAILS FOR TEST NO. RDTCB-2 .....	194
14 FULL-SCALE CRASH TEST NO. RDTCB-2 .....	217
14.1 Test No. RDTCB-2 .....	217
14.2 Weather Conditions .....	217
14.3 Test Description .....	217
14.4 Barrier Damage .....	219
14.5 Vehicle Damage .....	221
14.6 Occupant Risk .....	222
14.7 Discussion .....	223
15 EVALUATION OF DEFLECTION LIMITS .....	239
16 SUMMARY, CONCLUSIONS, AND RECOMMENDATIONS .....	245
16.1 Recommendations .....	249
17 REFERENCES .....	253
18 APPENDICES .....	257
Appendix A. Component Test Material Specifications .....	258
Appendix B. Material Specifications, Test No. RDTCB-1 .....	264
Appendix C. Material Specifications, Test No. RDTCB-2 .....	280
Appendix D. Vehicle Center of Gravity Determination .....	302
Appendix E. Vehicle Deformation Records .....	305
Appendix F. Accelerometer and Rate Transducer Data Plots, Test No. RDTCB-1 ....	318
Appendix G. Accelerometer and Rate Transducer Data Plots, Test No. RDTCB-2....	342

## LIST OF FIGURES

Figure 1. Ballast Base Plate A .....	15
Figure 2. Ballast Base Plate B.....	16
Figure 3. Ballast Concrete Cap .....	17
Figure 4. Composite Action – Beam.....	18
Figure 5. Composite Action – Tube.....	19
Figure 6. Composite Action – Cap .....	20
Figure 7. Composite Action – Cap with Continuous Tubes .....	21
Figure 8. Composite Action – Tie-Down Hole Plate.....	22
Figure 9. Composite Action – Tie-Down Hole Plate – V2.....	23
Figure 10. Friction – Adhesive .....	24
Figure 11. Friction – Base Covering.....	25
Figure 12. Joint Tolerance – Gap Shim .....	26
Figure 13. Joint Tolerance – Gap Shim – Tall.....	27
Figure 14. F-shape TCB Barrier Model .....	29
Figure 16. Baseline Model Impact Point .....	32
Figure 17. Overhead Sequential Views, Baseline Model and Test No. TB-2 .....	33
Figure 18. Overhead Sequential Views, Baseline Model and Test No. TB-2 .....	34
Figure 19. Downstream Sequential Views, Baseline Model and Test No. TB-2 .....	35
Figure 20. Downstream Sequential Views, Baseline Model and Test No. TB-2 .....	36
Figure 21. Low-Deflection TCB Parametric Study, Segment Mass = 8,366 lb (3,795 kg).....	39
Figure 22. Low-Deflection TCB Parametric Study, Segment Mass = 11,155 lb (5,060 kg).....	40
Figure 23. Low-Deflection TCB Parametric Study, Friction Coefficient = 0.6 .....	42
Figure 24. Low-Deflection TCB Parametric Study, Friction Coefficient = 0.8 .....	43
Figure 25. Low-Deflection TCB Parametric Study, Reduced Joint Gap Spacer .....	45
Figure 26. Low-Deflection TCB Parametric Study, Reduced Joint Gap.....	46
Figure 27. Low-Deflection TCB Parametric Study, Composite Action Models.....	48
Figure 28. Low-Deflection TCB Parametric Study, Composite Action – Plate.....	49
Figure 29. Low-Deflection TCB Parametric Study, Composite Action – Tube.....	50
Figure 30. Friction Pull Test Setup .....	54
Figure 31. Friction Pull Test Setup .....	55
Figure 32. Friction Pull Test Setup .....	56
Figure 33. Friction Pull Test Setup .....	57
Figure 34. Friction Pull Test Setup .....	58
Figure 35. Friction Pull Test Setup .....	59
Figure 36. Load Cell Arrangement, Test Nos. TCBF-1 through TCBF-6.....	61
Figure 37. Pull Test Setup, Test No. TCBF-1.....	64
Figure 38. Force vs. Time, Test No. TCBF-1 .....	65
Figure 39. Pull Test Setup, Test No. TCBF-2.....	66
Figure 40. Force vs. Time, Test No. TCBF-2.....	67
Figure 41. Pull Test Setup, Test No. TCBF-3.....	68
Figure 42. Force vs. Time, Test No. TCBF-4 .....	70
Figure 43. Rubber Wear Marks, Test No. TCBF-4 .....	71
Figure 44. Force vs. Time, Test No. TCBF-6.....	73
Figure 44. Force vs. Time, Test No. TCBF-6.....	75
Figure 46. Concrete Cylinder Compression Model Setup .....	83

Figure 47. Force and Internal Energy Vs. Time, Concrete Cylinder Compression – Run 1 .....	86
Figure 48. Deformation and Damage, Concrete Cylinder Compression – Run 1 .....	87
Figure 49. Force and Internal Energy Vs. Time, Concrete Cylinder Compression – Run 2 .....	89
Figure 50. Deformation and Damage, Concrete Cylinder Compression – Run 2 .....	90
Figure 51. Deformation and Damage, Concrete Cylinder Compression – Run 3 .....	91
Figure 52. Deformation and Damage, Concrete Cylinder Compression – Run 4 .....	92
Figure 53. Force and Internal Energy Vs. Time, Concrete Cylinder Compression – Run 4 .....	94
Figure 54. Concrete Cylinder Tension Model Setup .....	95
Figure 55. Force and Internal Energy Vs. Time, Concrete Cylinder Tension – Run 6 .....	96
Figure 56. Deformation and Damage, Concrete Cylinder Tension – Run 5.....	97
Figure 57. Reinforced Concrete Beam Test Setup.....	99
Figure 58. Reinforced Concrete Beam Simulation Model.....	101
Figure 59. Deformation and Damage, Simulation and Test No. ABC-3.....	106
Figure 60. Beam Deflection, Simulation and Test No. ABC-3 .....	107
Figure 61. Beam Moment, Simulation and Test No. ABC-3.....	107
Figure 62. Deformation and Damage, Simulation and Test No. ABC-2.....	108
Figure 63. Test Vehicle, Test No. RDTCB-1 .....	114
Figure 64. Vehicle Dimensions, Test No. RDTCB-1 .....	115
Figure 65. Test Vehicle, Test No. RDTCB-2 .....	117
Figure 66. Vehicle Dimensions, Test No. RDTCB-2 .....	118
Figure 67. Target Geometry, Test No. RDTCB-1 .....	119
Figure 68. Target Geometry, Test No. RDTCB-2 .....	120
Figure 69. Camera Locations, Speeds, and Lens Settings, Test No. RDTCB-1.....	125
Figure 70. Camera Locations, Speeds, and Lens Settings, Test No. RDTCB-2.....	126
Figure 71. Low-Deflection TCB Prototype, Version 3.....	129
Figure 72. Low-Deflection TCB Prototype, Version 5.....	130
Figure 73. Low-Deflection TCB Prototype, Version 6.....	131
Figure 74. Test Installation Layout, Test No. RDTCB-1 .....	134
Figure 75. Test Installation Layout, Test No. RDTCB-1 .....	135
Figure 76. Test Installation Layout, Test No. RDTCB-1 .....	136
Figure 77. Test Installation Layout, Test No. RDTCB-1 .....	137
Figure 78. Test Installation Layout, Test No. RDTCB-1 .....	138
Figure 79. Test Installation Layout, Test No. RDTCB-1 .....	139
Figure 80. Test Installation Layout, Test No. RDTCB-1 .....	140
Figure 81. Test Installation Layout, Test No. RDTCB-1 .....	141
Figure 82. Test Installation Layout, Test No. RDTCB-1 .....	142
Figure 83. Test Installation Layout, Test No. RDTCB-1 .....	143
Figure 84. Test Installation Layout, Test No. RDTCB-1 .....	144
Figure 85. Test Installation Layout, Test No. RDTCB-1 .....	145
Figure 86. Test Installation Layout, Test No. RDTCB-1 .....	146
Figure 87. Test Installation Layout, Test No. RDTCB-1 .....	147
Figure 88. Test Installation Layout, Test No. RDTCB-1 .....	148
Figure 89. Test Installation Layout, Test No. RDTCB-1 .....	149
Figure 90. Stiffened TCB Test Installation, Test No. RDTCB-1 .....	150
Figure 91. Barrier Segment Connection Designs, Test No. RDTCB-1 .....	151
Figure 92. Summary of Test Results and Sequential Photographs, Test No. RDTCB-1 .....	159
Figure 93. Additional Sequential Photographs, Test No. RDTCB-1.....	160

Figure 94. Additional Sequential Photographs, Test No. RDTCB-1 .....	161
Figure 95. Documentary Photographs, Test No. RDTCB-1 .....	162
Figure 96. Impact Location, Test No. RDTCB-1 .....	163
Figure 97. Vehicle Final Position and Trajectory Marks, Test No. RDTCB-1 .....	164
Figure 98. Overall System Damage, Test No. RDTCB-1.....	165
Figure 99. System Damage at Barrier Nos. 8 and 9, Test No. RDTCB-1 .....	166
Figure 100. Rail Splice at Barrier Nos. 8 and 9, Test No. RDTCB-1.....	167
Figure 101. Permanent Barrier Deflection, Test No. RDTCB-1 .....	168
Figure 102. Vehicle Damage, Test No. RDTCB-1 .....	169
Figure 103. Vehicle Damage, Test No. RDTCB-1 .....	170
Figure 104. Steel Tube Deformation and Deflection, Test No. RDTCB-1 .....	172
Figure 105. Steel Cap Deformation, Test No. RDTCB-1.....	174
Figure 106. RDTCB-1 Baseline Model .....	176
Figure 107. Overhead Sequential Views, Simulation Model and Test No. RDTCB-1 .....	177
Figure 108. Overhead Sequential Views, Simulation Model and Test No. RDTCB-1 .....	178
Figure 109. Downstream Sequential Views, Simulation Model and Test No. RDTCB-1 .....	179
Figure 110. Downstream Sequential Views, Simulation Model and Test No. RDTCB-1 .....	180
Figure 111. System Damage and Deformation, Simulation Model and Test No. RDTCB-1.....	182
Figure 112. RSVVP, X-Acceleration, Simulation Model and Test No. RDTCB-1 .....	182
Figure 113. RSVVP, Y-Acceleration, Simulation Model and Test No. RDTCB-1 .....	183
Figure 114. RSVVP, Yaw, Simulation Model and Test No. RDTCB-1 .....	183
Figure 115. RSVVP, Roll, Simulation Model and Test No. RDTCB-1 .....	184
Figure 116. RSVVP, Pitch, Simulation Model and Test No. RDTCB-1.....	184
Figure 117. RSVVP, Multi-Channel Comparison, Simulation Model and Test No. RDTCB-1	185
Figure 118. Additional Tube Attachments – Run 1 .....	190
Figure 119. Additional Tube Attachments – Run 3b.....	191
Figure 120. Test Installation Layout, Test No. RDTCB-2 .....	196
Figure 121. Design Details, Test No. RDTCB-2 .....	197
Figure 122. Design Details, Test No. RDTCB-2.....	198
Figure 123. Design Details, Test No. RDTCB-2.....	199
Figure 124. Design Details, Test No. RDTCB-2.....	200
Figure 125. Design Details, Test No. RDTCB-2.....	201
Figure 126. Design Details, Test No. RDTCB-2.....	202
Figure 127. Design Details, Test No. RDTCB-2.....	203
Figure 128. Design Details, Test No. RDTCB-2.....	204
Figure 129. Design Details, Test No. RDTCB-2.....	205
Figure 130. Design Details, Test No. RDTCB-2.....	206
Figure 131. Design Details, Test No. RDTCB-2.....	207
Figure 132. Design Details, Test No. RDTCB-2.....	208
Figure 133. Design Details, Test No. RDTCB-2.....	209
Figure 134. Design Details, Test No. RDTCB-2.....	210
Figure 135. Design Details, Test No. RDTCB-2.....	211
Figure 136. Design Details, Test No. RDTCB-2.....	212
Figure 137. Design Details, Test No. RDTCB-2.....	213
Figure 138. Design Details, Test No. RDTCB-2.....	214
Figure 139. Test Installation, Test No. RDTCB-2.....	215
Figure 140. Barrier Segment Connection Designs, Test No. RDTCB-2.....	216

Figure 141. Summary of Test Results and Sequential Photographs, Test No. RDTCB-2 .....	226
Figure 142. Additional Sequential Photographs, Test No. RDTCB-2.....	227
Figure 143. Additional Sequential Photographs, Test No. RDTCB-2.....	228
Figure 144. Documentary Photographs, Test No. RDTCB-2.....	229
Figure 145. Impact Location, Test No. RDTCB-2 .....	230
Figure 146. Vehicle Final Position and Trajectory Marks, Test No. RDTCB-2 .....	231
Figure 147. Overall System Damage, Test No. RDTCB-2.....	232
Figure 148. System Damage at Barrier Nos. 8 and 9, Test No. RDTCB-2 .....	233
Figure 149. Rail Splices at Barrier Nos. 8 and 9, Test No. RDTCB-2.....	234
Figure 150. Barrier Segment Damage Due to Reverse Bending, Test No. RDTCB-2.....	235
Figure 151. Permanent System Deflection, Test No. RDTCB-2.....	236
Figure 152. Vehicle Damage, Test No. RDTCB-2.....	237
Figure 153. Vehicle Damage, Test No. RDTCB-2.....	238
Figure 154. NCHRP 22-17 IS Distribution for Freeways.....	241
Figure 155. Simulation Model of System, Test No. RDTCB-2.....	243
Figure A-1. Summary of Material Certifications, Test Nos. TCBF-1 through TCBF-6 .....	259
Figure A-2. 50-Durometer Rubber Bearing Pad, Test Nos. TCBF-5 and TCBF-6.....	260
Figure A-3. 70-Durometer Rubber Bearing Pad, Test No. TCBF-4.....	260
Figure A-4. Polyurethane Adhesive Specifications, Test Nos. TCBF-4 through TCBF-6.....	261
Figure A-5. Polyurethane Adhesive Specifications, Test Nos. TCBF-4 through TCBF-6.....	262
Figure A-6. Polyurethane Adhesive Specifications, Test Nos. TCBF-4 through TCBF-6.....	263
Figure B-1. Concrete Barrier Mix Specifications .....	266
Figure B-2. Reinforcement Bar Specifications .....	267
Figure B-3. Loop Connection Bar Specifications.....	268
Figure B-4. Reinforcing Steel Bar Specifications.....	269
Figure B-5. Connector Pin Specifications .....	270
Figure B-6. Long Splice Main Tube Specifications .....	271
Figure B-7. Long Splice Insert Specifications.....	272
Figure B-8. 10 Gauge Mounting Bracket Plate Specifications.....	273
Figure B-9. 1-in. Flat Washer Specifications.....	274
Figure B-10. 1 in.-8 x 14 in. Bolt Specifications .....	275
Figure B-11. 1 in.-8 Hex Nut Specifications .....	276
Figure B-12. ¾ in. Flat Washer Specifications .....	277
Figure B-13. ¾ in.-10 x 6 ½ in. Bolt Specifications.....	278
Figure B-14. ¾ in.-10 Hex Nut Specifications .....	279
Figure C-1. Concrete Barrier Mix Specifications .....	282
Figure C-2. Reinforcement Bar Specifications.....	283
Figure C-3. Loop Connection Bar Specifications.....	284
Figure C-4. Reinforcing Steel Bar Specifications.....	285
Figure C-5. Connector Pin Specifications .....	286
Figure C-6. Long Splice Main Tube Specifications .....	287
Figure C-7. Long Splice Insert and Long L-Bracket Specifications .....	288
Figure C-8. 10 Gauge Mounting Bracket Plate Specifications.....	289
Figure C-9. 1-in. Flat Washer Specifications.....	290
Figure C-10. 1 in.-8 x 14 in. Bolt Specifications .....	291
Figure C-11. 1 in.-8 Hex Nut Specifications .....	292
Figure C-12. 1 in.-8 Hex Nut Specifications .....	293

Figure C-13. 3/4 in. Flat Washer Specifications ..... 294  
Figure C-14. 3/4 in.-10 x 6 1/2 in. Bolt Specifications ..... 295  
Figure C-15. 3/4 in.-10 Hex Nut Specifications ..... 296  
Figure C-16. 3/4 in.-10 Hex Nut Specifications ..... 297  
Figure C-17. 3/4 in.-10 Hex Nut Specifications ..... 298  
Figure C-18. 3/4 in.-10 x 13 in. Bolt Specifications ..... 299  
Figure C-19. 3/4 in.-10 x 13 in. Bolt Specifications ..... 300  
Figure C-20. 3/4 in.-10 x 13 in. Bolt Specifications ..... 301  
Figure D-1. Vehicle Mass Distribution, Test No. RDTCB-1 ..... 303  
Figure D-2. Vehicle Mass Distribution, Test No. RDTCB-2 ..... 304  
Figure E-1. Floor Pan Deformation Data – Set 1, Test No. RDTCB-1 ..... 306  
Figure E-2. Floor Pan Deformation Data – Set 2, Test No. RDTCB-1 ..... 307  
Figure E-3. Occupant Compartment Deformation Data – Set 1, Test No. RDTCB-1 ..... 308  
Figure E-4. Occupant Compartment Deformation Data – Set 2, Test No. RDTCB-1 ..... 309  
Figure E-5. Exterior Vehicle Crush (NASS) – Front, Test No. RDTCB-1 ..... 310  
Figure E-6. Exterior Vehicle Crush (NASS) – Side, Test No. RDTCB-1 ..... 311  
Figure E-7. Floor Pan Deformation Data – Set 1, Test No. RDTCB-2 ..... 312  
Figure E-8. Floor Pan Deformation Data – Set 2, Test No. RDTCB-2 ..... 313  
Figure E-9. Occupant Compartment Deformation Data – Set 1, Test No. RDTCB-2 ..... 314  
Figure E-10. Occupant Compartment Deformation Data – Set 2, Test No. RDTCB-2 ..... 315  
Figure E-11. Exterior Vehicle Crush (NASS) – Front, Test No. RDTCB-2 ..... 316  
Figure E-12. Exterior Vehicle Crush (NASS) – Side, Test No. RDTCB-2 ..... 317  
Figure F-1. 10-ms Average Longitudinal Deceleration (DTS), Test No. RDTCB-1 ..... 319  
Figure F-2. Longitudinal Change in Velocity (DTS), Test No. RDTCB-1 ..... 320  
Figure F-3. Longitudinal Change in Displacement (DTS), Test No. RDTCB-1 ..... 321  
Figure F-4. 10-ms Average Lateral Deceleration (DTS), Test No. RDTCB-1 ..... 322  
Figure F-5. Lateral Change in Velocity (DTS), Test No. RDTCB-1 ..... 323  
Figure F-6. Lateral Occupant Displacement (DTS), Test No. RDTCB-1 ..... 324  
Figure F-7. Vehicle Angular Displacements (DTS), Test No. RDTCB-1 ..... 325  
Figure F-8. Acceleration Severity Index (DTS), Test No. RDTCB-1 ..... 326  
Figure F-9. 10-ms Average Longitudinal Deceleration (DTS-SLICE), Test No. RDTCB-1 ..... 327  
Figure F-10. Longitudinal Change in Velocity (DTS-SLICE), Test No. RDTCB-1 ..... 328  
Figure F-11. Longitudinal Change in Displacement (DTS-SLICE), Test No. RDTCB-1 ..... 329  
Figure F-12. 10-ms Average Lateral Deceleration (DTS-SLICE), Test No. RDTCB-1 ..... 330  
Figure F-13. Lateral Change in Velocity (DTS-SLICE), Test No. RDTCB-1 ..... 331  
Figure F-14. Lateral Change in Displacement (DTS-SLICE), Test No. RDTCB-1 ..... 332  
Figure F-15. Vehicle Angular Displacements (DTS-SLICE), Test No. RDTCB-1 ..... 333  
Figure F-16. Acceleration Severity Index (DTS-SLICE), Test No. RDTCB-1 ..... 334  
Figure F-17. 10-ms Average Longitudinal Deceleration (EDR-3), Test No. RDTCB-1 ..... 335  
Figure F-18. Longitudinal Change in Velocity (EDR-3), Test No. RDTCB-1 ..... 336  
Figure F-19. Longitudinal Change in Displacement (EDR-3), Test No. RDTCB-1 ..... 337  
Figure F-20. 10-ms Average Lateral Deceleration (EDR-3), Test No. RDTCB-1 ..... 338  
Figure F-21. Lateral Change in Velocity (EDR-3), Test No. RDTCB-1 ..... 339  
Figure F-22. Lateral Change in Displacement (EDR-3), Test No. RDTCB-1 ..... 340  
Figure F-23. Acceleration Severity Index (EDR-3), Test No. RDTCB-1 ..... 341  
Figure G-1. 10-ms Average Longitudinal Deceleration (DTS), Test No. RDTCB-2 ..... 343  
Figure G-2. Longitudinal Change in Velocity (DTS), Test No. RDTCB-2 ..... 344

Figure G-3. Longitudinal Change in Displacement (DTS), Test No. RDTCB-2 ..... 345  
Figure G-4. 10-ms Average Lateral Deceleration (DTS), Test No. RDTCB-2..... 346  
Figure G-5. Lateral Change in Velocity (DTS), Test No. RDTCB-2..... 347  
Figure G-6. Lateral Occupant Displacement (DTS), Test No. RDTCB-2..... 348  
Figure G-7. Vehicle Angular Displacements (DTS), Test No. RDTCB-2 ..... 349  
Figure G-8. Acceleration Severity Index (DTS), Test No. RDTCB-2 ..... 350  
Figure G-9. 10-ms Average Longitudinal Deceleration (DTS-SLICE), Test No. RDTCB-2 .... 351  
Figure G-10. Longitudinal Change in Velocity (DTS-SLICE), Test No. RDTCB-2 ..... 352  
Figure G-11. Longitudinal Change in Displacement (DTS-SLICE), Test No. RDTCB-2..... 353  
Figure G-12. 10-ms Average Lateral Deceleration (DTS-SLICE), Test No. RDTCB-2 ..... 354  
Figure G-13. Lateral Change in Velocity (DTS-SLICE), Test No. RDTCB-2 ..... 355  
Figure G-14. Lateral Change in Displacement (DTS-SLICE), Test No. RDTCB-2 ..... 356  
Figure G-15. Vehicle Angular Displacements (DTS-SLICE), Test No. RDTCB-2..... 357  
Figure G-16. Acceleration Severity Index (DTS-SLICE), Test No. RDTCB-2..... 358  
Figure G-17. 10-ms Average Longitudinal Deceleration (EDR-3), Test No. RDTCB-2..... 359  
Figure G-18. Longitudinal Change in Velocity (EDR-3), Test No. RDTCB-2..... 360  
Figure G-19. Longitudinal Change in Displacement (EDR-3), Test No. RDTCB-2 ..... 361  
Figure G-20. 10-ms Average Lateral Deceleration (EDR-3), Test No. RDTCB-2 ..... 362  
Figure G-21. Lateral Change in Velocity (EDR-3), Test No. RDTCB-2..... 363  
Figure G-22. Lateral Change in Displacement (EDR-3), Test No. RDTCB-2..... 364  
Figure G-23. Acceleration Severity Index (EDR-3), Test No. RDTCB-2..... 365

## LIST OF TABLES

Table 1. Free-Standing F-shape TCB Deflections.....	5
Table 2. TCB Deflections for Free-Standing and Reduced-Deflection Applications .....	12
Table 3. Summary of Deflection-Limiting Mechanism Parametric Study.....	51
Table 4. Component Testing Results, Test Nos. TCBF-1 through TCBF-6 .....	76
Table 5. MAT_159_CSCM Input Variables.....	80
Table 6. MAT_159_CSCM Concrete Cylinder Simulation, Cases 1- 10.....	84
Table 7. MASH TL-3 Crash Test Conditions.....	110
Table 8. MASH Evaluation Criteria for Longitudinal Barrier.....	112
Table 9. Weather Conditions, Test No. RDTCB-1 .....	152
Table 10. Sequential Description of Impact Events, Test No. RDTCB-1 .....	153
Table 11. Maximum Occupant Compartment Deformations by Location, Test No. RDTCB-1	156
Table 12. Summary of OIV, ORA, THIV, PHD, and ASI Values, Test No. RDTCB-1.....	158
Table 13. Summary of Estimated Deflections for Proposed RDTCB-2 Design Modifications .	193
Table 14. Weather Conditions, Test No. RDTCB-2.....	217
Table 15. Sequential Description of Impact Events, Test No. RDTCB-2 .....	218
Table 16. Maximum Occupant Compartment Deformations by Location, Test No. RDTCB-2	222
Table 17. Summary of OIV, ORA, THIV, PHD, and ASI Values, Test No. RDTCB-2.....	223
Table 18. Summary of Safety Performance Evaluation Results.....	252
Table B-1. Summary of Material Certifications, Test No. RDTCB-1 .....	265
Table C-1. Summary of Material Certifications, Test No. RDTCB-2.....	281

## **1 INTRODUCTION**

### **1.1 Background**

Roadway construction or work zones are found along almost all Federal, State, and local highways in the United States. In most cases, these roadways often require the redirection of vehicular traffic around or through the construction zone. Typically, some form of temporary barrier is used to separate the flow of traffic within the construction area. In general, temporary barriers are segmented units which are attached end-to-end by a load-bearing connection. The segmentation of temporary concrete barriers allows them to be easily installed, repositioned, and removed from the work-zone region. The barrier system is designed to protect equipment and workers in the work zone, to prevent errant vehicles from leaving the traveled way, and to safely redirect those vehicles impacting the barrier.

Often, temporary barriers are used in applications where it is desired that their deflection during vehicular impacts be limited. During bridge construction, temporary barriers are often placed adjacent to the edge of a bridge deck in order to provide adequate lane width. Free-standing temporary barriers that are used in these types of installations pose a potential safety hazard to errant vehicles due to the risk for barrier segments to be propelled off of the bridge. In addition, most work zones are restricted in terms of the available lateral space in which to accommodate traffic and the construction activity, or temporary barriers are used to separate opposing traffic. Thus, it is desirable to minimize the deflection of temporary barriers in order to minimize the required buffer distance and maximize the space and number of lanes available for traffic. Therefore, a need exists to develop systems to reduce the deflection of temporary barriers.

A significant amount of highway safety research has been focused on methods for constraining or limiting the deflection of free-standing, temporary concrete barriers (TCB).

These designs have typically focused on tie-down applications that anchor the TCB to the roadway surface, or designs that stiffen or alter the connection between the barrier segments. However, there remain some unresolved issues with the use of current deflection-limiting mechanisms. First, tie-down systems which anchor barriers to the roadway surface have several drawbacks in that they are labor intensive, expensive, and increase worker exposure. They also pose the risk of damaging the road surface during a severe impact event. Designs that alter or stiffen the connection between the barrier segments have shown promise in limiting deflections, but their use requires additional inventory and maintenance concerns for end users as it can require alteration of the original, free-standing TCB design.

Recent crash testing of temporary concrete barriers has shown that additional structural elements can help reduce barrier deflections. The Wisconsin Department of Transportation (WisDOT) desired that a concept be developed that limited barrier deflection without the need for additional tie-down anchors and could be retrofitted to the TCB design that they currently use with minimal modification. WisDOT currently employs the F-shape TCB design previously developed by the Midwest Roadside Safety Facility (MwRSF) [1-3]. WisDOT also desired the safety performance of the new reduced-deflection TCB system meet the Test Level 3 (TL-3) safety requirements published in the American Association of State Highway and Transportation Officials' (AASHTO) *Manual for Assessing Safety Hardware* (MASH) [4].

## **1.2 Objective**

The objective of this research effort was to develop a stiffening mechanism for use in reducing the deflection of TCB installations without requiring anchorage of the barrier segments to the road surface. The stiffening mechanism was developed for use with the Midwest Pooled Fund States' 12.5-ft (3.8-m) long, F-shape, temporary concrete barrier. The TCB system with the

joint-stiffening mechanism was designed and evaluated to meet the TL-3 requirements set forth in MASH.

### **1.3 Scope**

The research objectives were accomplished through a series of several tasks. The research effort began with a literature search to review existing designs for joint stiffening and limiting deflection of temporary concrete barriers. Next, new concepts and mechanisms for limiting deflections were brainstormed to identify potential designs. Engineering analysis and LS-DYNA computer simulation were then used to evaluate and refine the concepts. Following analysis of the candidate designs and review by the sponsor, the most desirable design was detailed and fabricated for full-scale crash testing. Test designation no. 3-11 was conducted on the TCB stiffening mechanism according to the safety criteria set forth in MASH. The results from this test were documented and analyzed to provide insight into potential improvements in the stiffening mechanism with an emphasis on further minimizing barrier deflections. Improvements to the design were then evaluated through engineering analysis and LS-DYNA computer simulation. A revised design was then selected for evaluation with full-scale crash testing, and a second full-scale crash test was conducted on the revised reduced deflection design.

LS-DYNA simulations of a pickup truck impacting the stiffened barrier system at the 85<sup>th</sup> percentile impact severity were then conducted to estimate the deflection of the barrier. The predicted deflection was then used to set placement criteria for normal construction applications where the system is not installed adjacent to a drop-off.

## **2 LITERATURE REVIEW**

Prior to the development of the new TCB deflection-limiting concepts, a literature search was performed to investigate the various TCB systems relevant to this project, including the free-standing F-shape TCB that served as the basis of the design and other alternative deflection-limiting mechanisms that did not anchor the TCB system to the roadway surface.

### **2.1 MwRSF Free-Standing F-shape TCB**

The current TCB design used by WisDOT and a number of other states is the F-shape TCB design developed through the Midwest States Regional Pooled Fund [1-3]. This TCB system consists of a 32-in. (813-mm) tall x 22.5-in. (572-mm) wide x 12.5-ft (3.8-m) long F-shape concrete barrier segment with a pin-and-loop type connection. The barrier has been tested to TL-3 under both the National Cooperative Highway Research Program (NCHRP) Report No. 350 [5] and MASH safety criteria. In the NCHRP Report No. 350 testing of the system, test no. ITMP-2 demonstrated that the F-shape TCB was capable of safely redirecting a 2000P vehicle when the system was impacted at a speed of 62.3 mph (100.3 km/h) and an angle of 27.1 degrees. The maximum dynamic deflection of the TCB system in test no. ITMP-2 was 45.3 in. (1,151 mm).

Two full-scale crash tests were conducted on the F-shape TCB during the development of the MASH safety requirements in NCHRP Project 22-17. The MASH testing varied from the NCHRP Report No. 350 testing in that a 5,000-lb (2,268-kg) pickup truck was used for the MASH testing rather than the 4,409-lb (2,000 kg) pickup truck specified in NCHRP Report No. 350. In test no. TB-1, the F-shape TCB was impacted with a 2002 GMC 2500 ¾-ton, single-cab pickup truck with a mass of 5,000 lb (2,268 kg) at a speed of 61.8 mph (99.5 km/h) and at an angle of 25.7 degrees. The TCB system safely redirected the impacting vehicle with a maximum lateral dynamic barrier deflection of 56.7 in. (1,440 mm). Significant vehicle climb was observed

during test no. TB-1. It should be noted that the vehicle used in this test had a center-of-gravity (CG) lower than desired for use in MASH, and subsequent testing with a higher CG vehicle was recommended.

A second test of the F-shape TCB was then conducted using a 2002 Dodge Ram 1500 Quad Cab pickup truck with a mass of 5,000 lb (2,268 kg). Test no. TB-2 consisted of the 2270P vehicle impacting the TCB system with a speed of 62.0 mph (99.8 km/h) and at an angle of 25.4 degrees. The TCB system safely redirected the impacting vehicle with a maximum lateral dynamic barrier deflection of 79.6 in. (2,022 mm).

Free-standing TCB deflections were significantly higher when testing was conducted with the 2270P vehicle under the MASH criteria as opposed to testing conducted with the 2000P vehicle under the NCHRP Report No. 350 criteria. TCB deflections increased 25 to 76 percent when the F-shape TCB was tested under MASH impact criteria, as shown in Table 1.

Table 1. Free-Standing F-shape TCB Deflections

Test No.	Vehicle	Mass lbs (kg)	Speed mph (km/h)	Angle deg.	IS kip-ft (kJ)	Dynamic Deflection in. (mm)	Static Deflection in. (mm)
<b>ITMP-2</b>	2000P	4,420 (2,005)	62.3 (100.3)	27.1	119.1 (161.5)	45.3 (1,151)	44.9 (1,140)
<b>TB-1</b>	2270P	5,000 (2,268)	61.8 (99.5)	25.7	120.2 (163.0)	56.7 (1,440)	56.7 (1,440)
<b>TB-2</b>	2270P	5,000 (2,268)	62.0 (99.8)	25.4	118.0 (160.0)	79.6 (2,022)	73.0 (1,854)

This increase in deflection observed in the MASH TL-3 testing was believed to be due to a combination of factors. First, the 2270P vehicle used in the MASH crash tests has significantly higher mass than the 2000P vehicle. The increase in vehicle mass created increased momentum transfer to the TCB segments and increased the load on the barrier. This effect has been noted on

other MASH crash tests using the 2270P vehicle [6]. For example, test no. ITD-1 of the F-shape TCB utilizing a steel strap tie-down with the 2000P vehicle had a maximum lateral dynamic deflection of 37.8 in. (960 mm). Analysis of lateral impact loads from test no. ITD-1 found a maximum lateral barrier load of 41.5 kips (184.6 kN). Analysis of lateral impact loads from test no. TB-2 with the 2270P vehicle found a maximum lateral barrier load of 60.0 kips (266.9 kN). Thus, the 2270P vehicle impact in test no. TB-2 was found to have a 44.4 percent increase in lateral barrier loading even with over twice the amount of barrier deflection.

The second factor which affected the TCB deflections during MASH testing involved changes in the impact behavior of the 2270P vehicle as compared to the 2000P. The 2270P vehicle provided increased length, mass, and body stiffness, and the front tire and the wheel assembly of the 2270P vehicle have been shown to disengage more easily than was observed in previous 2000P testing. These two changes in the vehicle response resulted in the 2270P vehicle providing a more stable vehicle impact with the TCB segments with reduced vehicle pitch, roll, and climb. This in turn allowed the vehicle to directly load the barrier longer. Thus, the increase in the magnitude and duration of the barrier loads is believed to create increased deflection observed in the MASH testing of free-standing TCB segments.

## **2.2 Reduced-Deflection TCB Designs**

In addition to reviewing previous free-standing TCB research, the researchers also reviewed research efforts that attempted to reduce TCB deflections without anchoring the barriers to the roadway surface.

In 2000, the National Crash Analysis Center (NCAC) conducted research on limiting the deflection of TCB by simulating a series of barrier modifications using LS-DYNA [7] according to the NCHRP Report No. 350 TL-3 criteria. Three design concepts were evaluated with the F-shape TCB design previously developed by the Midwest Roadside Safety Facility:

1. A steel cover placed over the joint and bolted to the concrete segments.
2. Tapered shims placed between the pin-and-loops to reduce pin motion.
3. A separator block placed between the TCB segments and held in place with the existing joint pin to reduce the gap between the barriers.

The three simulated concepts each reduced barrier deflections to some extent. The tapered shims design reduced the deflection by approximately 13 percent. The cover plate and the separator block designs performed similarly and reduced the displacement of the TCB by approximately 38 percent. None of the modifications proposed in the study were ever implemented or further evaluated through full-scale crash testing.

MwRSF conducted a research study, in cooperation with the New York State Department of Transportation (NYSDOT), to develop, test, and evaluate a joint-stiffening method for temporary concrete barriers [8]. This study set out to evaluate the potential for reducing barrier deflections through the use of box-beam stiffening on an acceptable NYSDOT TCB design. In addition, all safety performance evaluations were to be performed using the criteria found in MASH. The systems were constructed with ten 20-ft (6.1-m) long, New Jersey shape, TCB sections utilizing a connection key between the barrier sections, with the first and last barrier sections anchored to the tarmac. Three full-scale crash tests were performed on the various temporary barrier systems.

The first full-scale crash test, test no. NYTCB-1, was performed on a stiffened version of the TCB system according to MASH test designation 3-11. This system consisted of 12-ft (3.7-m) long, box-beam stiffeners spanning each joint between barrier nos. 4 and 7. The box-beam sections were configured with 6-in. x 6-in. x  $\frac{3}{16}$ -in. (152-mm x 152-mm x 5-mm) steel tubes. The first and last barrier sections were anchored into the concrete. The test consisted of a 5,016-lb (2275-kg) pickup truck impacting the barrier system at a speed of 61.8 mph (99.5 km/h) and at

an angle of 24.6 degrees, resulting in an impact severity of 111.34 k-ft (151.0 kJ). The impact point for this test was 4 ft – 3 <sup>3</sup>/<sub>16</sub> in. (1300 mm) upstream from the downstream end of barrier no. 4. The maximum permanent set and dynamic deflections were 26 in. (660 mm) and 27.6 in. (701 mm), respectively. The test results were found to meet all of the MASH safety requirements as the pickup truck was safely redirected and brought to a controlled stop.

The second full-scale crash test, test no. NYTCB-2, was performed on an un-stiffened version of the TCB system according to MASH test designation 3-11. This system consisted of free-standing temporary concrete barriers with the first and last barrier sections anchored to the concrete. The test consisted of a 5,024-lb (2279-kg) pickup truck impacting the barrier system at a speed of 61.2 mph (98.5 km/h) and at an angle of 25.8 degrees, resulting in an impact severity of 119.2 k-ft (161.6 kJ). The impact point for this test was 4 ft – 3 <sup>3</sup>/<sub>16</sub> in. (1300 mm) upstream from the downstream end of barrier no. 4. The maximum permanent set and dynamic deflections were 39.5 in. (1,003 mm) and 40.3 in. (1,024 mm), respectively. The test results were found to meet all of the MASH safety requirements as the pickup truck was safely redirected and brought to a controlled stop.

The third full-scale crash test, test no. NYTCB-3, was performed on a stiffened version of the TCB system according to test designation 3-11 of MASH. This system consisted of 12-ft long (3.7-m), box-beam stiffeners spanning each joint between barrier nos. 2 and 8. The box-beam sections were configured with 6-in. x 8-in. x <sup>1</sup>/<sub>4</sub>-in. (152-mm x 203-mm x 6-mm) steel tubes. In addition, the system was installed with the back side of the barriers placed 12 in. (305 mm) from the edge of a bridge deck. The first and last barrier sections were anchored to the concrete. The test consisted of a 5,001-lb (2268-kg) pickup truck impacting the barrier system at a speed of 63.5 mph (102.2 km/h) and at an angle of 24.4 degrees, resulting in an impact severity of 115.0 k-ft (156.0 kJ). The impact point for this test was 4 ft – 3 <sup>3</sup>/<sub>16</sub> in. (1,300 mm) upstream

from the downstream end of barrier no. 4. The maximum permanent set and dynamic deflections were 26 in. (660 mm) and 30.9 in. (785 mm), respectively. The test results were found to meet all of the currently proposed Update to NCHRP Report No. 350 safety requirements as the pickup truck was safely redirected and brought to a controlled stop.

Upon examination of the impact severity values and maximum dynamic deflections, it was evident that the box-beam stiffening system was effective in reducing barrier deflections. In general, the box-beam system reduced dynamic deflections from 23 to 32 percent over those observed for the free-standing temporary concrete barrier. However, it should be noted that the NYDOT TCB system differed from the free-standing F-shape barrier proposed for use in this research. The NYDOT TCB was a 20-ft (6.1-m) long, New Jersey shape barrier that had a minimal joint gap and was anchored on the upstream and downstream ends of the system. These differences in connection, segment length, and anchorage led to reduced free-standing barrier deflections when compared to the F-shape TCB in this research as well as the magnitude of the barrier deflection when the box-beam stiffening was used.

The Oregon Department of Transportation (ODOT) full-scale crash tested a 32-in. (813-mm) tall, F-shape temporary concrete barrier. Each barrier section was 12.5 ft (3.8 m) in length [9]. The barrier sections were held together with a pin-and-steel bar loop assembly. However, the gap between the barrier segments for the Oregon F-shape barrier was reduced to 1 in. (25 mm). Full-scale crash testing of the Oregon F-shape TCB demonstrated safe redirection of the 2000P vehicle under the TL-3 impact conditions for NCHRP Report No. 350 test designation no. 3-11 and developed a maximum dynamic lateral barrier deflection of 30 in. (762 mm).

In 2005, the Texas A&M Transportation Institute (TTI) developed a barrier-to-barrier joint in order to limit deflections in portable concrete median barrier systems [10-11]. This joint

consisted of two bolts which crossed from the front face of one barrier to the back face of the other and vice versa. Hence, an 'X' was formed when looking down upon the joint.

Following a design and simulation effort, the new X-bolt connection was subjected to two full-scale crash tests to assess impact performance and quantify the design deflection of the cross-bolted F-shape barrier for two different segment lengths of 10 ft (3.0 m) and 30 ft. (9.1 m). Previous full-scale testing of this 30-ft (9.1 m) long F-shape barrier, with a connection consisting of a 4-in. (102-mm) wide by  $\frac{3}{16}$ -in. (5-mm) thick steel strap bolted to the face of the barrier segments across each side of the joint, limited the barrier deflection to 48 in. (1,200 mm).

In both tests of the F-shape barrier with the X-Bolt connection, the structural integrity of the barrier and its connections was maintained, and the barrier successfully contained and redirected the test vehicle in an upright manner while reducing barrier deflections. The occupant risk factors were within the preferred limits specified in NCHRP Report No. 350, and all relevant evaluation criteria were met. The crash test of the X-bolt barrier with 30-ft (9.1 m) segments used the 2000P vehicle recommended in NCHRP Report No. 350, and produced a dynamic deflection of 19 in. (483 mm). The test of the X-bolt connection with 10-ft barrier segments involved a 5,000-lb (2268-kg), 2001 Chevrolet 2500 pickup truck. Even though the impact severity was 15 percent greater than required in NCHRP Report No. 350, the dynamic deflection of the 10-ft (3.0 m) barrier segments with X-bolt connection was only 27 in. (686 mm).

### **2.3 Comparison of Previous Reduced-Deflection Designs**

Following the literature search, a comparison was made between the previously crash-tested limited-deflection systems and the free-standing barrier deflections for the F-shape TCB proposed for use in this study. The results of this comparison are summarized in Table 2.

Based on the comparisons, the researchers made some conclusions regarding reduced-deflection concrete barrier designs. First, as noted previously, the maximum lateral barrier

deflections increased significantly for MASH crash testing with 5,000 lb (2268-kg) pickup truck vehicles. This was especially evident in the free-standing barrier testing and suggested that the baseline dynamic barrier deflection for the free-standing F-shape TCB was 80 in. (2,032 mm). Second, it was apparent that modifications to stiffen or develop moment continuity over the joint between barrier segments could provide for reduced barrier deflections as evidenced by the NYDOT, Oregon, and TTI X-Bolt crash testing. However, it was noted that the NYDOT and X-bolt barrier systems had advantages in barrier design in terms of end anchorage, and/or segment length that aided in reducing overall dynamic system deflections. Thus, the review of previous reduced-deflection systems suggested that reduction in barrier deflections of 25 to 60 percent was possible depending on the design of the barrier section and connection of the reduced-deflection system.

Table 2. TCB Deflections for Free-Standing and Reduced-Deflection Applications

<b>Test No.</b>	<b>PCB System</b>	<b>Vehicle</b>	<b>Mass lb (kg)</b>	<b>Speed mph (km/h)</b>	<b>Angle deg</b>	<b>IS kip-ft (kJ)</b>	<b>Dynamic Deflection in. (mm)</b>	<b>Static Deflection in. (mm)</b>
<b>ITMP-2</b>	Iowa F-shape (free)	2000P	4,420 (2,005)	62.3 (100.3)	27.1	119.1 (161.5)	45.3 (1,151)	44.9 (1,140)
<b>TB-1</b>	Kansas F-shape (free)	2270P	5,000 (2,268)	61.8 (99.5)	25.7	120.2 (163.0)	56.7 (1,440)	56.7 (1,440)
<b>TB-2</b>	Kansas F-shape (free)	2270P	5,000 (2,268)	62.0 (99.8)	25.4	118.0 (160.0)	79.6 (2,022)	73.0 (1,854)
<b>NYTCB-1</b>	NY TCB with Box- Beam	2000P	5,016 (2,275)	61.8 (99.5)	24.6	111.1 (150.6)	27.6 (701)	26.0 (660)
<b>NYTCB-2</b>	NY TCB (free)	2270P	5,024 (2,279)	61.2 (98.5)	25.8	119.2 (161.6)	40.3 (1,024)	39.5 (1,003)
<b>NYTCB-3</b>	NY TCB with Box- Beam	2270P	5,000 (2,268)	63.5 (102.2)	24.4	115.0 (155.9)	30.9 (785)	26.0 (660)
<b>KARCO 3- 11</b>	32" Oregon F-shape	2000P	4,500 (2,041)	62.6 (100.7)	25.0	105.3 (142.8)	30.0 (762)	30.0 (762)
<b>441623-1</b>	TxDOT 30' F-shape – X- Bolt	2000P	4,535 (2,057)	62.3 (100.3)	25.7	110.7 (150.1)	19.0 (483)	18.1 (460)
<b>446924-1</b>	TxDOT 10' F-shape – X- Bolt	2000P	4,965 (2,252)	62.0 (99.8)	24.5	109.8 (148.9)	27.0 (686)	27.0 (686)

### **3 DEVELOPMENT OF DESIGN CONCEPTS**

#### **3.1 Design Criteria**

Prior to developing design concepts for the reduced-deflection TCB system, discussions were held between the researchers and the sponsor to better define the design criteria for the project. Within the overall project objective of developing a method for reducing TCB deflections without anchoring to the roadway, the following design criteria were identified:

1. WisDOT required that the dynamic deflection of the system be less than 48 in. (1,219 mm) and desired that the dynamic deflection of the system be between 24 in. and 36 in. (610 mm and 914 mm).
2. WisDOT requested that the system be developed for traffic on either side of the barrier system.
3. WisDOT desired that the design consist of a retrofit to the existing F-shape TCB design, thus requiring minimal modification to the barrier. This included no modifications to the barrier reinforcement or the pin-and-loop connection.

These criteria were noted in the project plan and considered during the development of design concepts.

#### **3.2 Design Concepts**

Following development of the design criteria, the researchers brainstormed a variety of ideas for reducing the deflection of the F-shape TCB. The concepts were grouped into four main categories based on the mechanism for limiting deflection that each concept employed. The four concept categories for reducing the deflection of TCB were as follows:

1. Composite Action – Development of tension and compression loads across the barrier joints in order to develop moment continuity in the barrier.

2. Reduced Joint Tolerance – Reduction in the tolerance or gaps in the barrier joint such that the barrier segments engage with each other more rapidly during impact.
3. Increased Barrier-to-Ground Friction – Increasing friction between barrier and roadway surface.
4. Increased Barrier Mass – Adding mass or ballast to the barrier segments in order to provide increased inertial and friction resistance to motion.

A series of design concepts were generated and drawn as schematics for further evaluation. These designs were not final representations of the design concepts, but they represented the function of the concept. The design concepts are shown in in Figure 1 through Figure 13.

The researchers reviewed the design concepts and believed that several had potential for limiting deflection through the four mechanisms described above. However, it was not clear how to quantify the effect of each mechanism for reducing TCB deflection. Thus, it was decided to conduct a parametric study using LS-DYNA computer simulation [12]. Each of the four deflection reduction mechanisms listed above was applied to an LS-DYNA model of a TCB system in order to quantify which mechanism had the greatest potential for reducing barrier deflection.

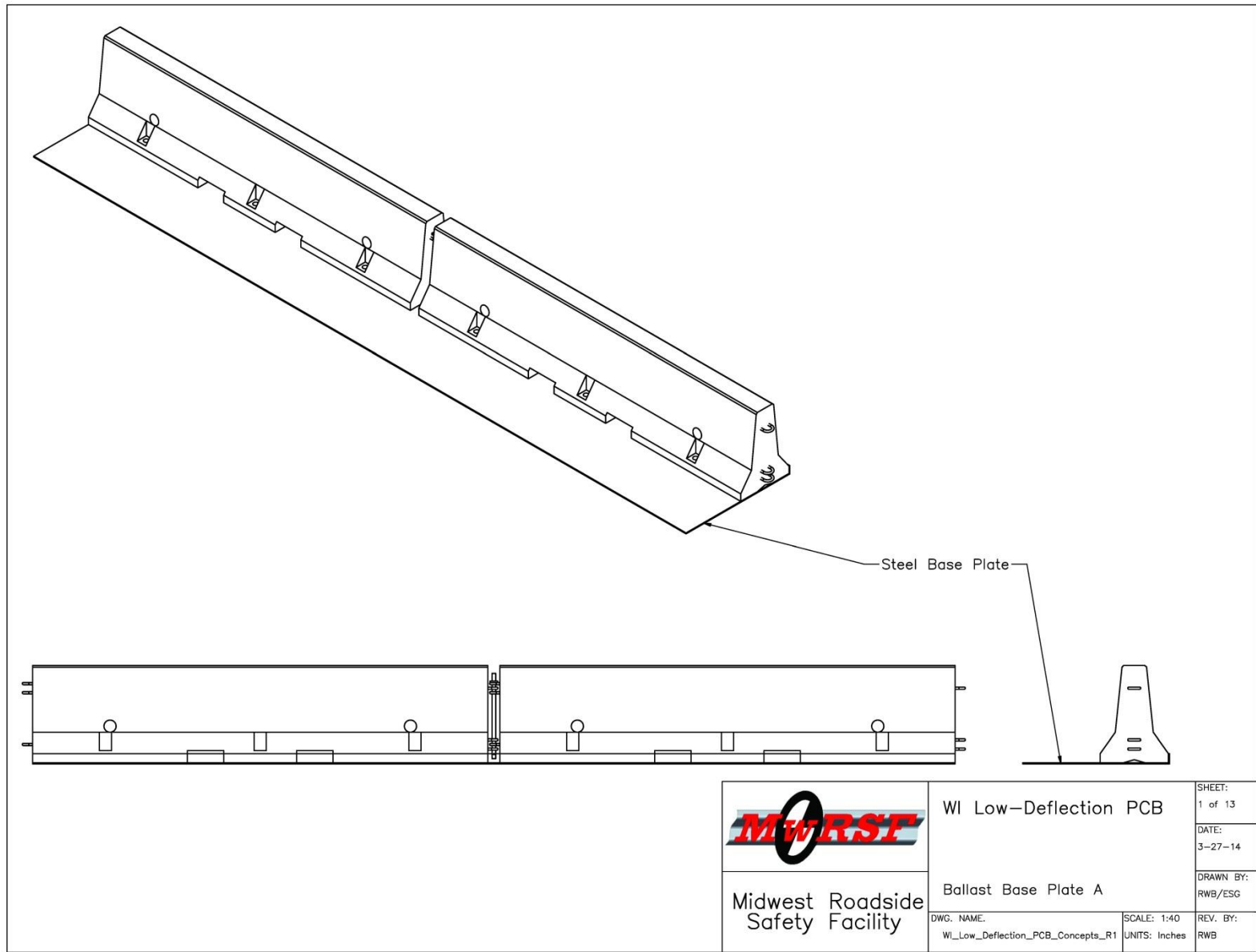


Figure 1. Ballast Base Plate A

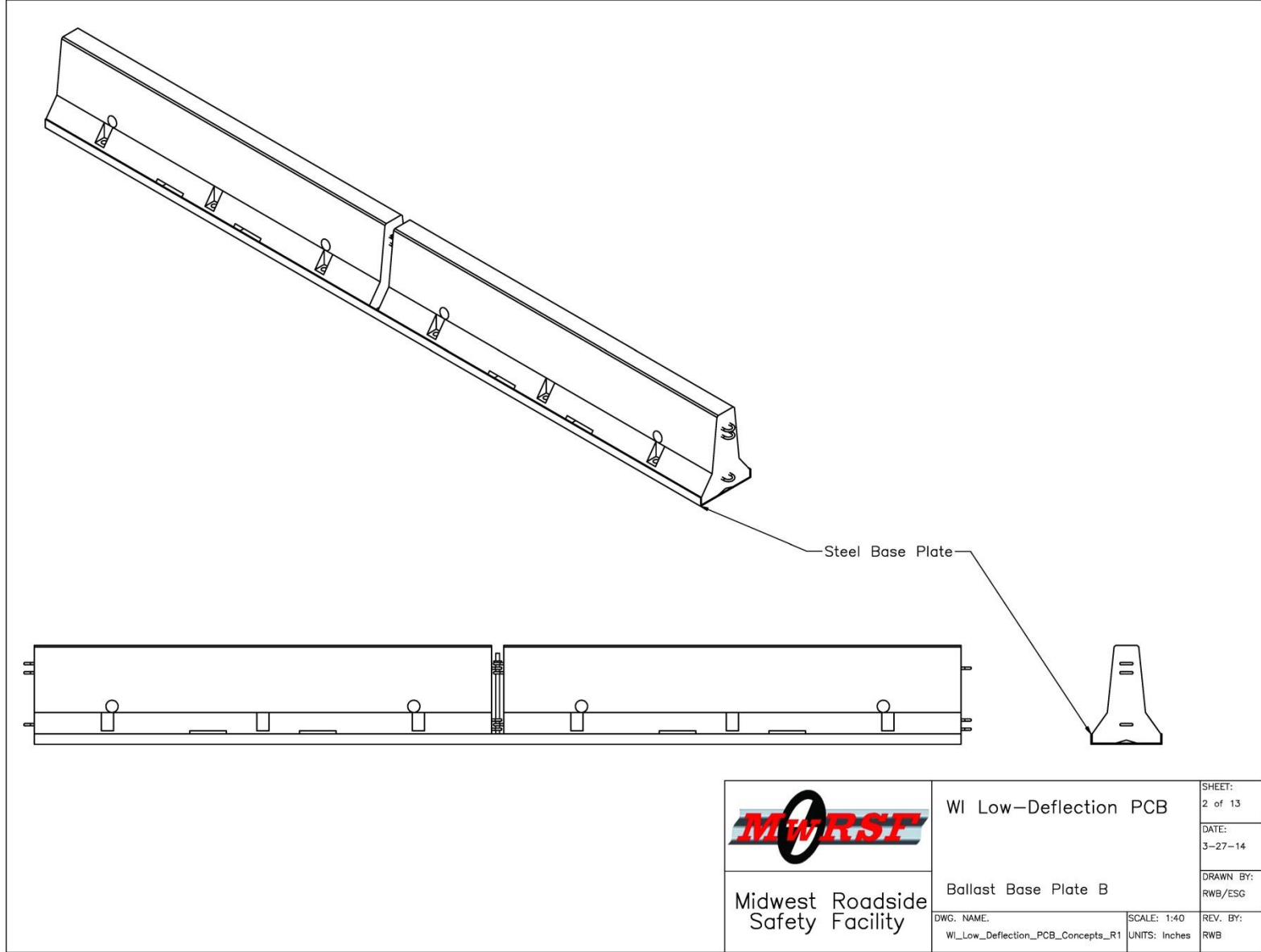
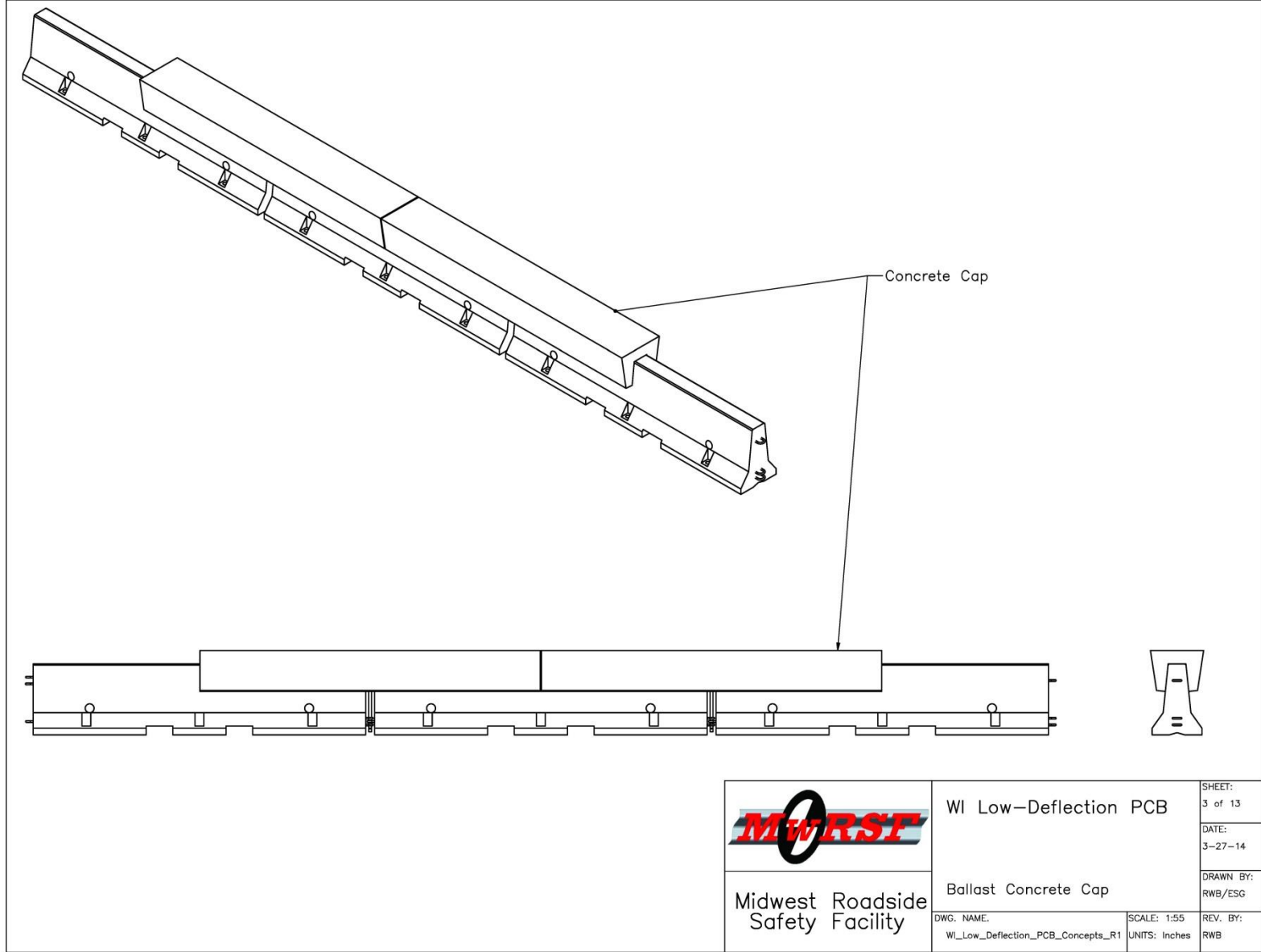


Figure 2. Ballast Base Plate B



Midwest Roadside Safety Facility

WI Low-Deflection PCB	SHEET: 3 of 13
	DATE: 3-27-14
Ballast Concrete Cap	DRAWN BY: RWB/ESG
DWG. NAME: WI_Low_Deflection_PCB_Concepts_R1	SCALE: 1:55 UNITS: Inches
	REV. BY: RWB

Figure 3. Ballast Concrete Cap

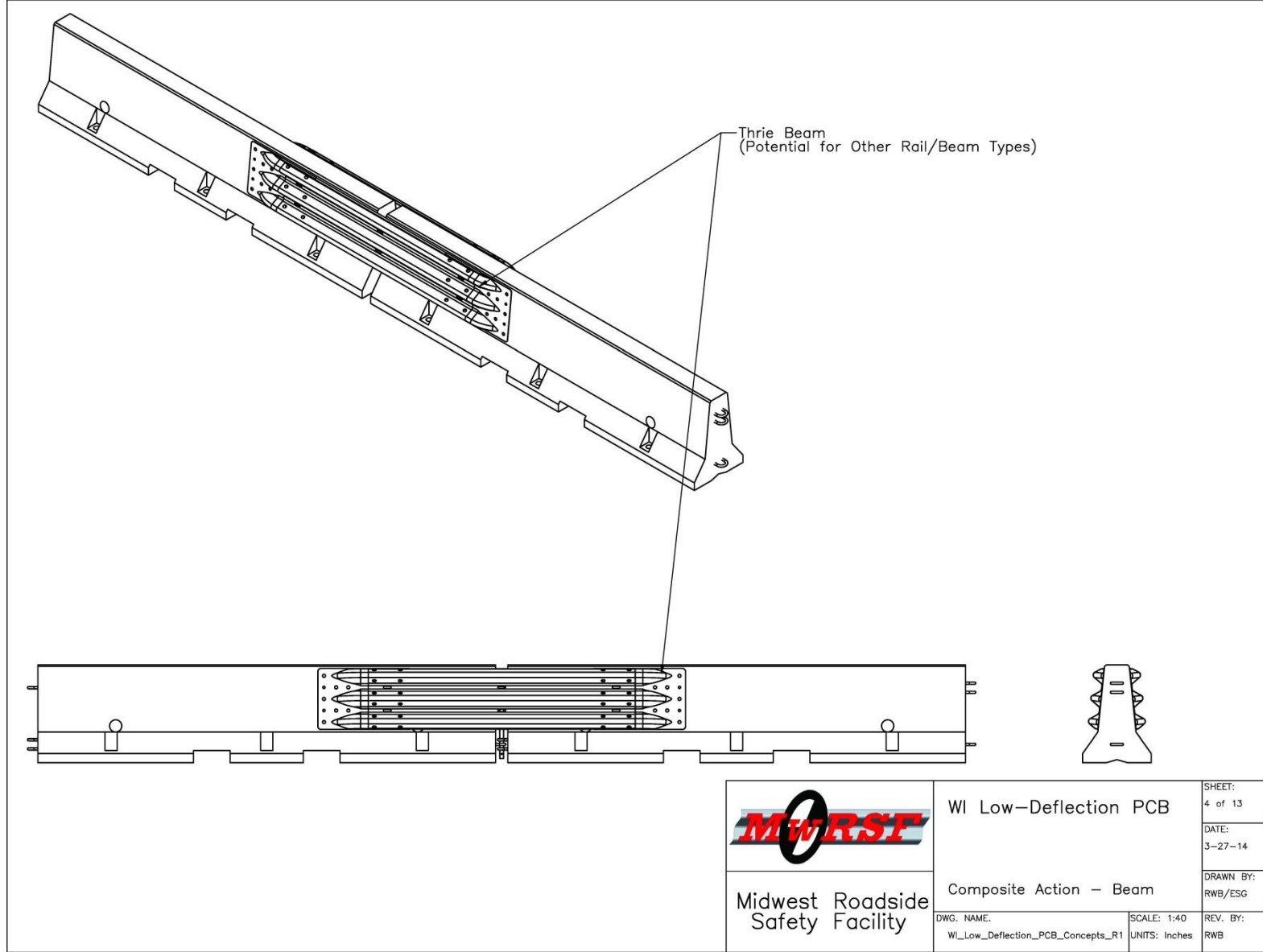


Figure 4. Composite Action - Beam

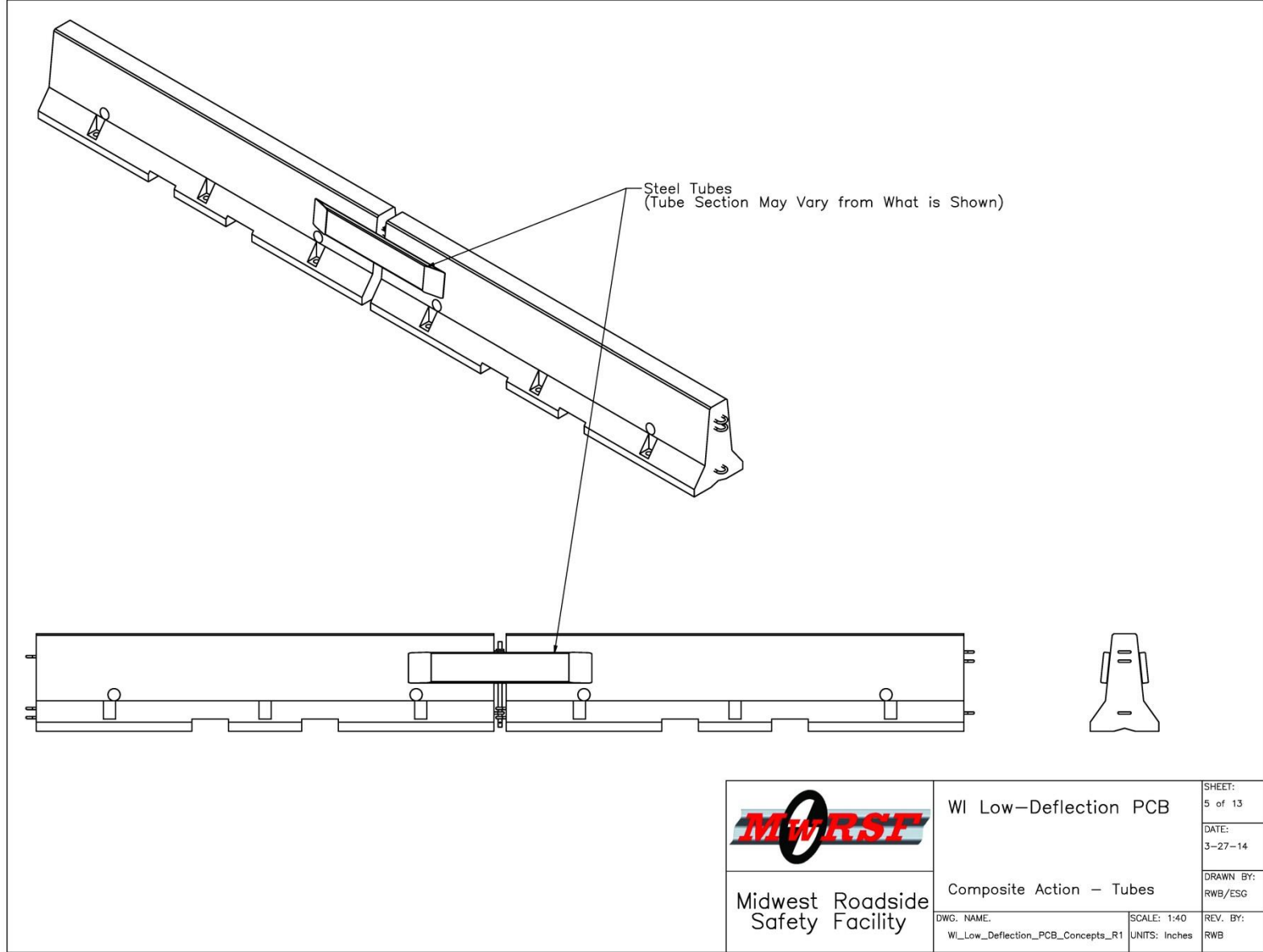


Figure 5. Composite Action – Tube

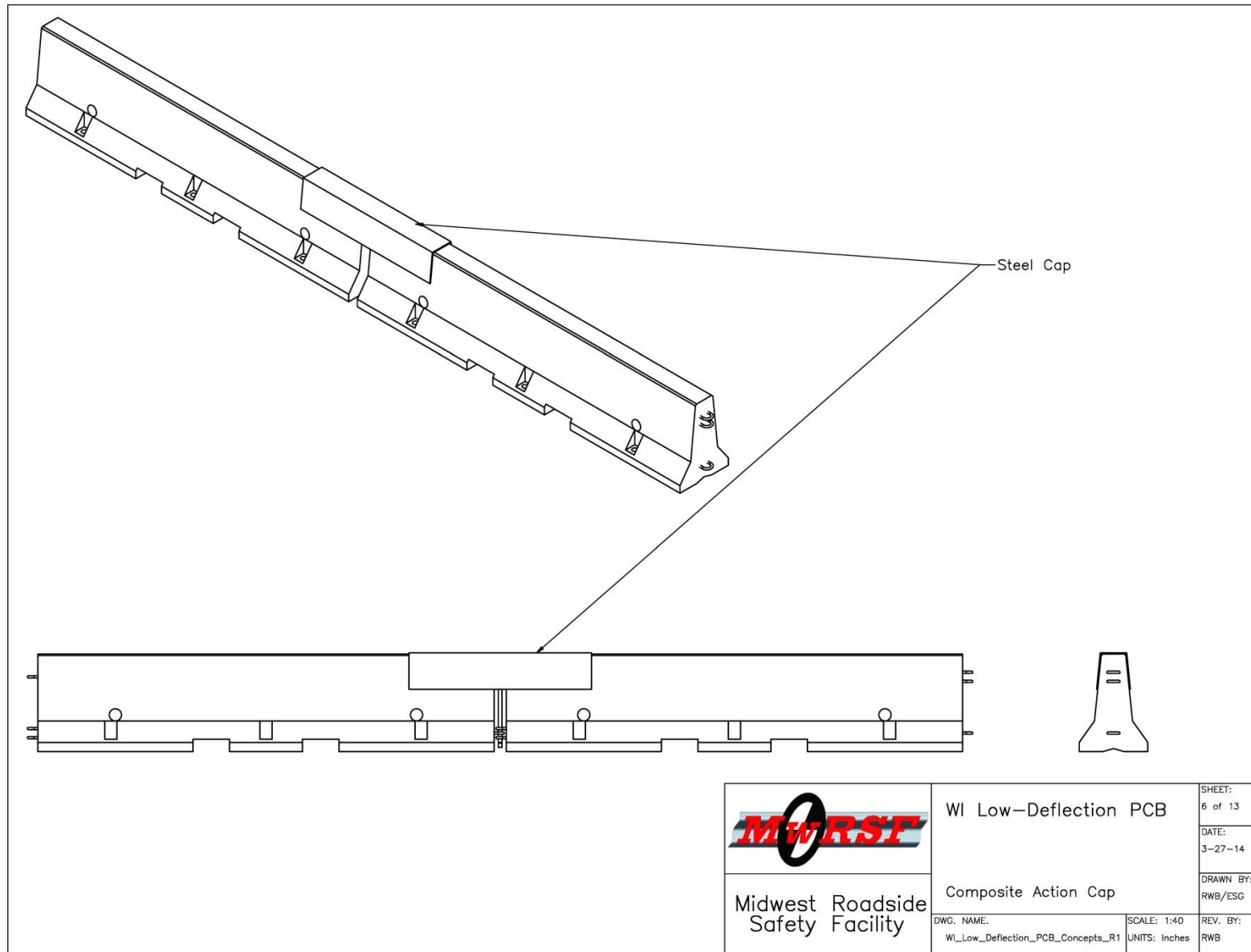


Figure 6. Composite Action – Cap

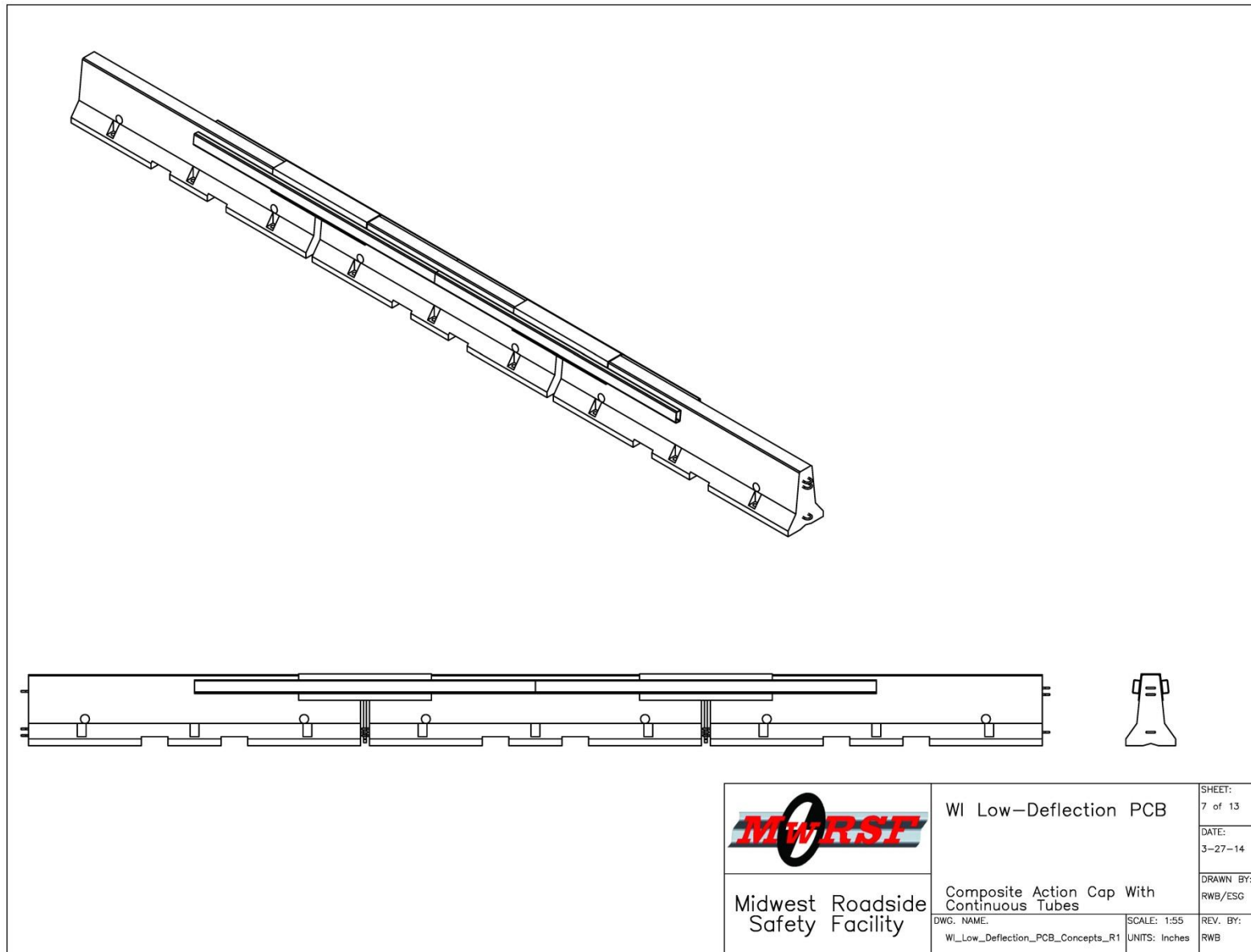


Figure 7. Composite Action – Cap with Continuous Tubes

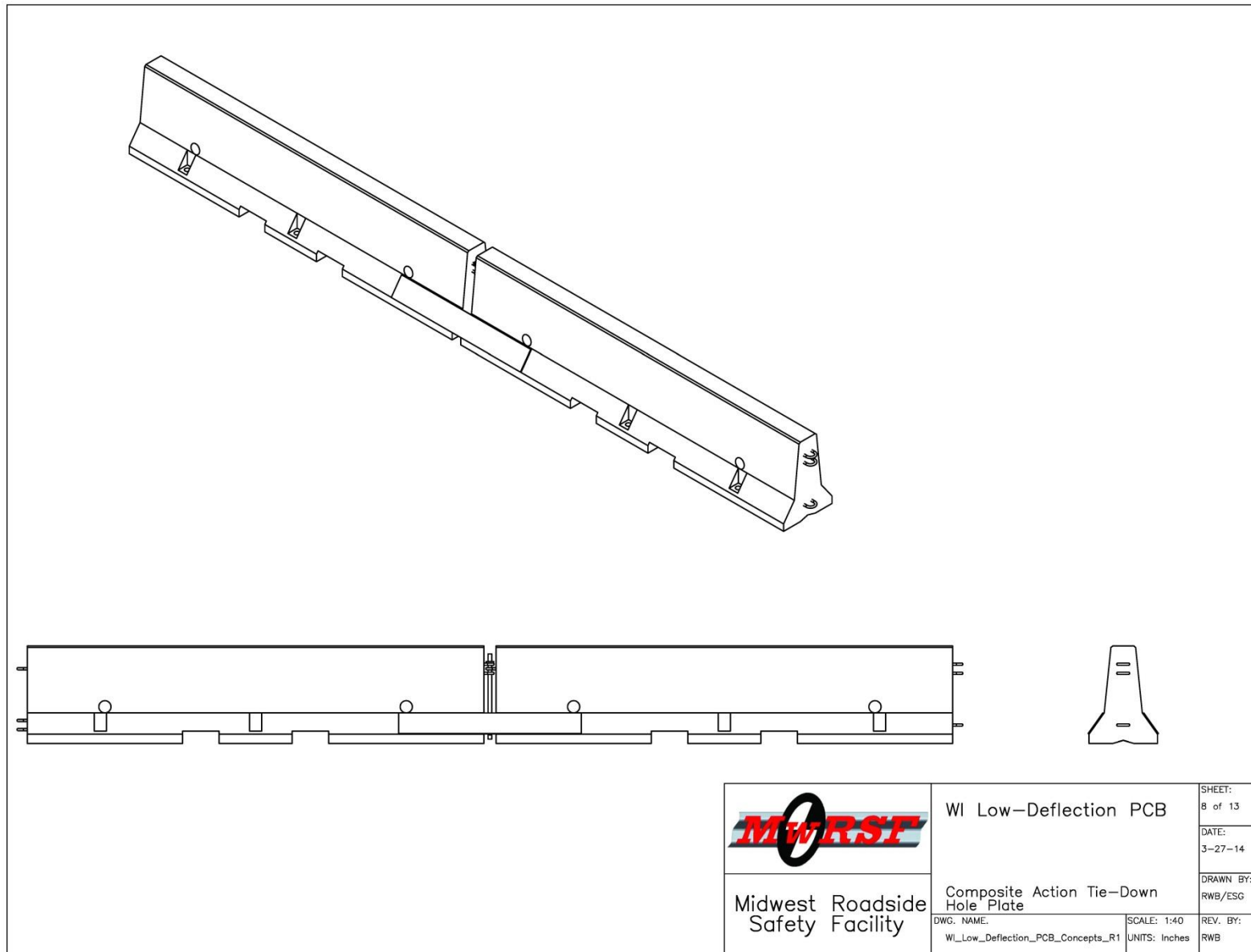


Figure 8. Composite Action – Tie-Down Hole Plate

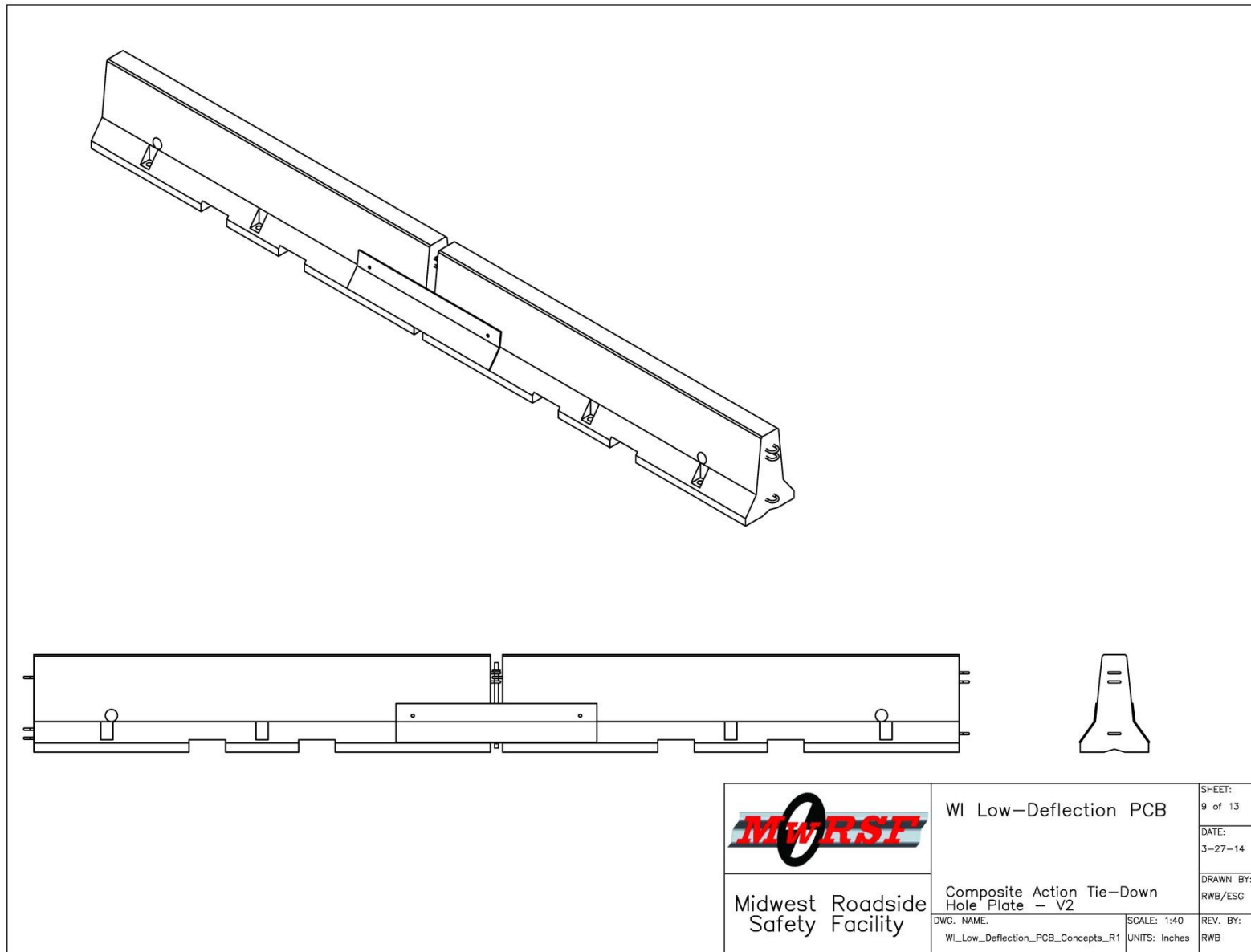


Figure 9. Composite Action – Tie-Down Hole Plate – V2

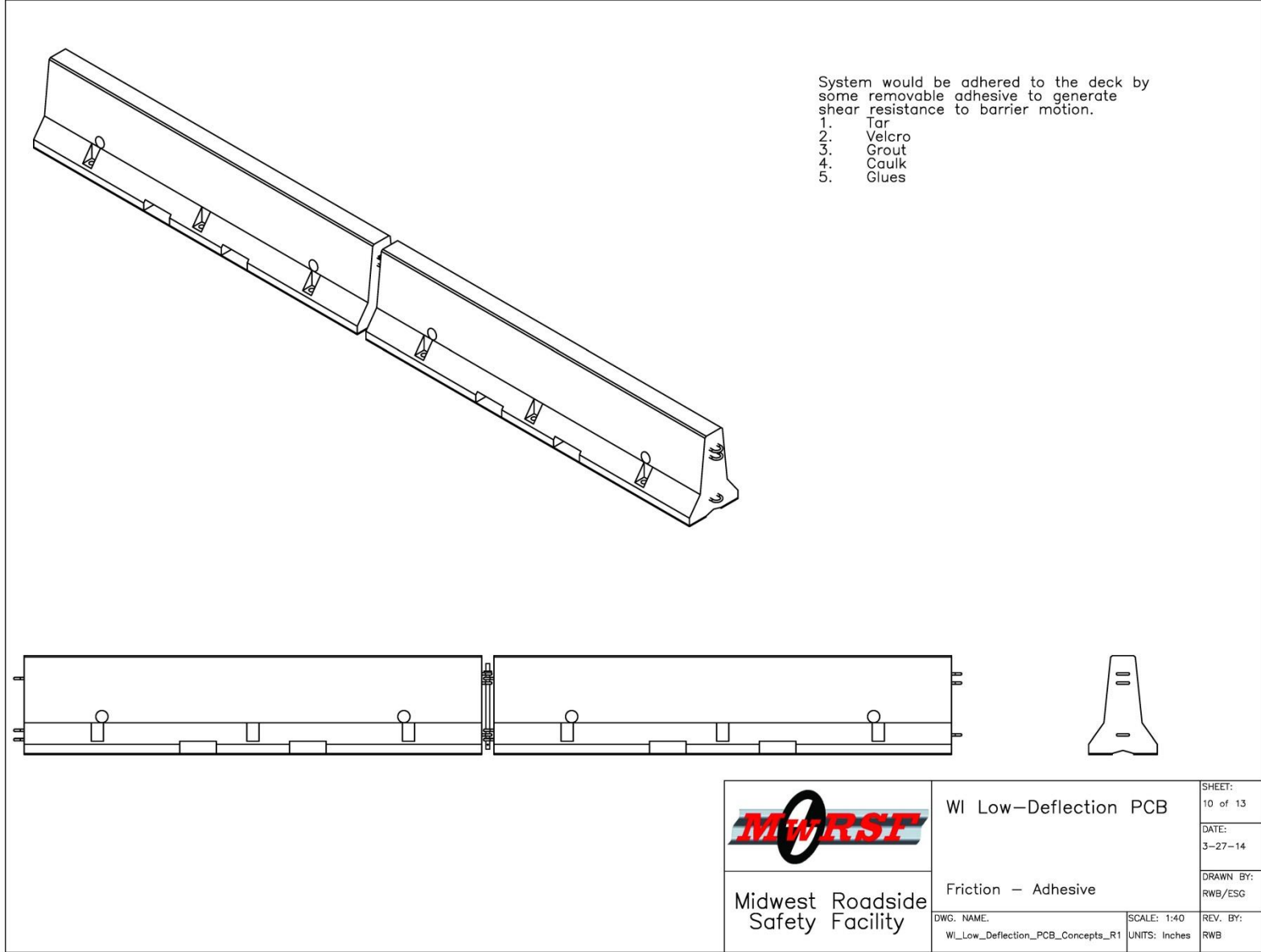


Figure 10. Friction – Adhesive

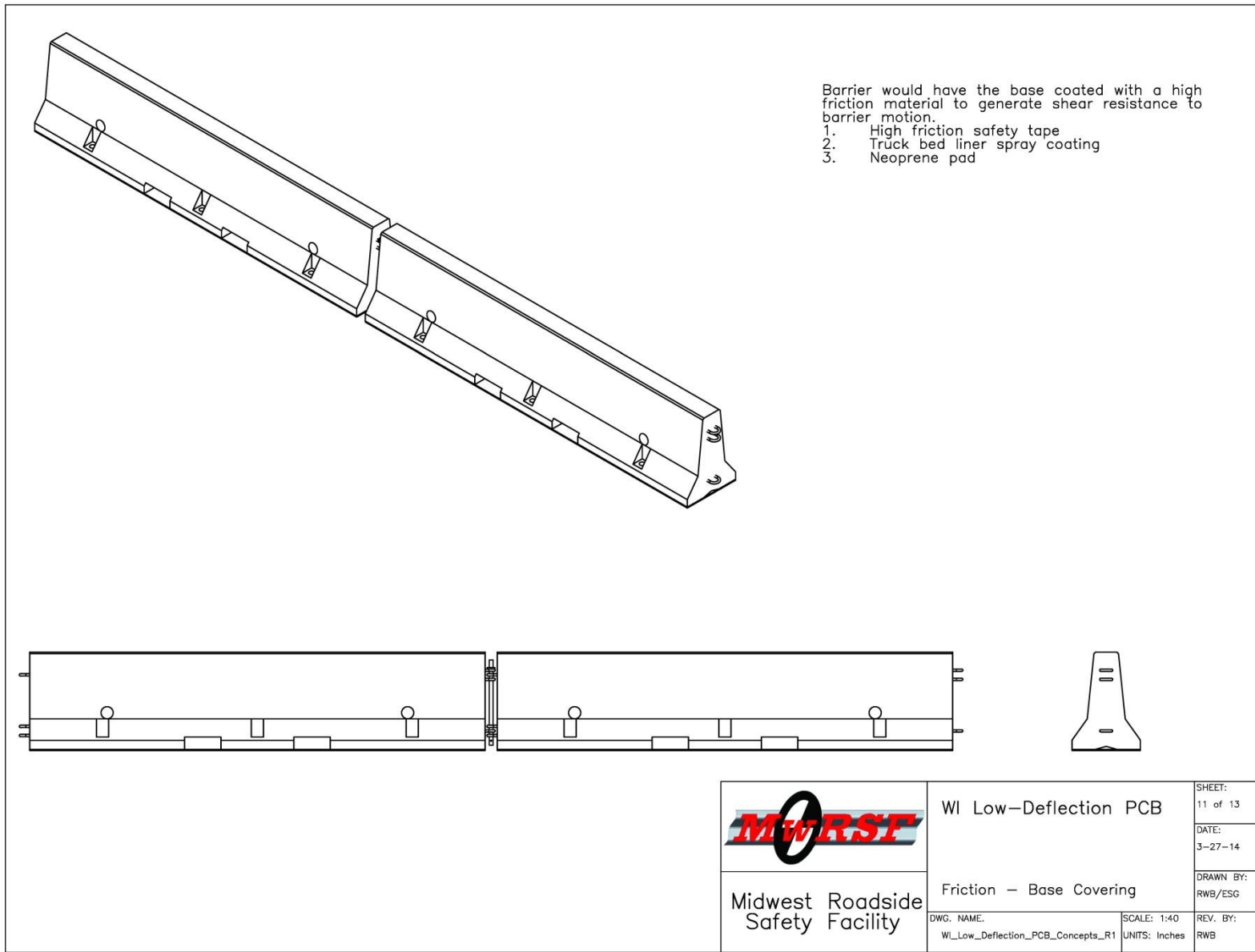


Figure 11. Friction – Base Covering

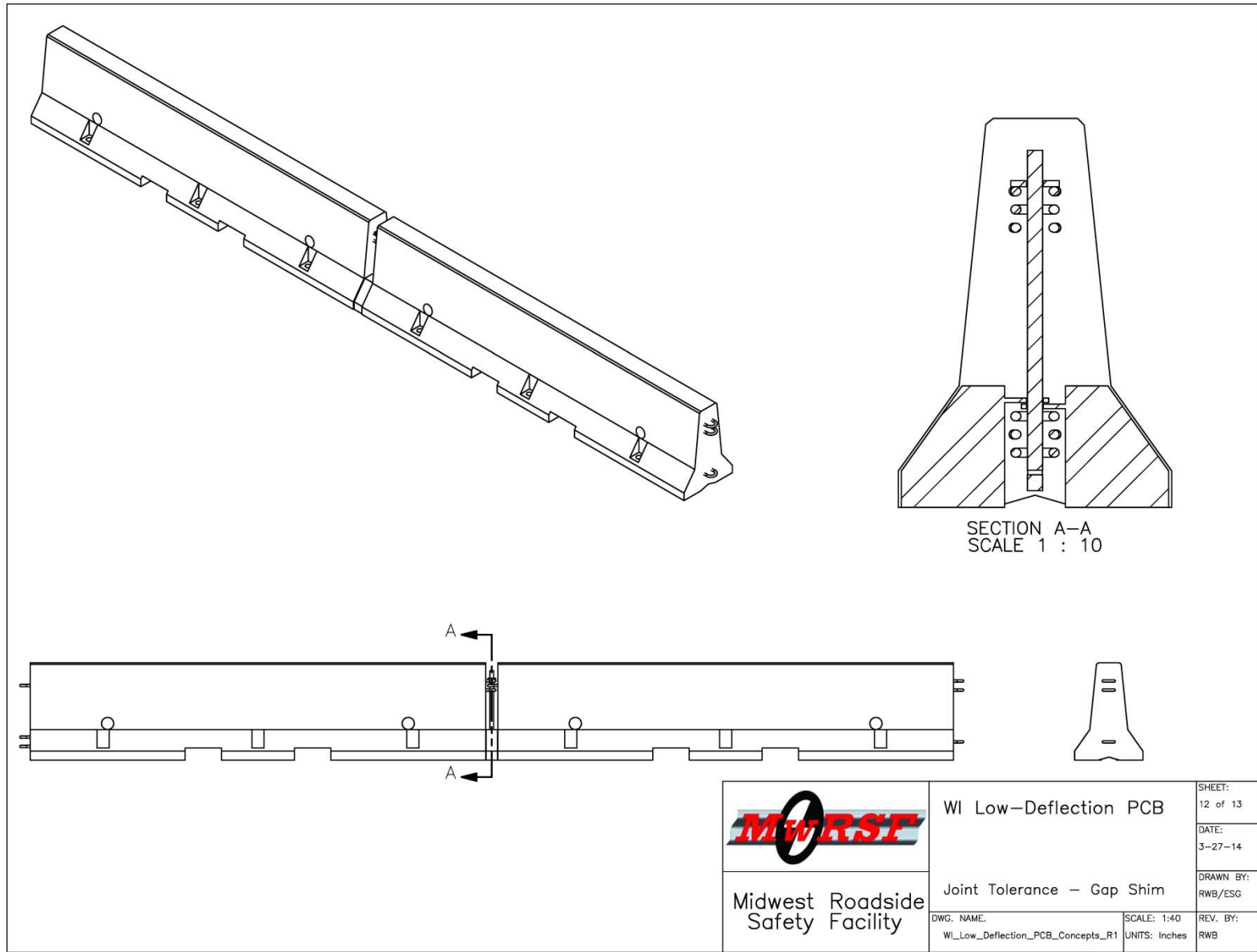


Figure 12. Joint Tolerance – Gap Shim

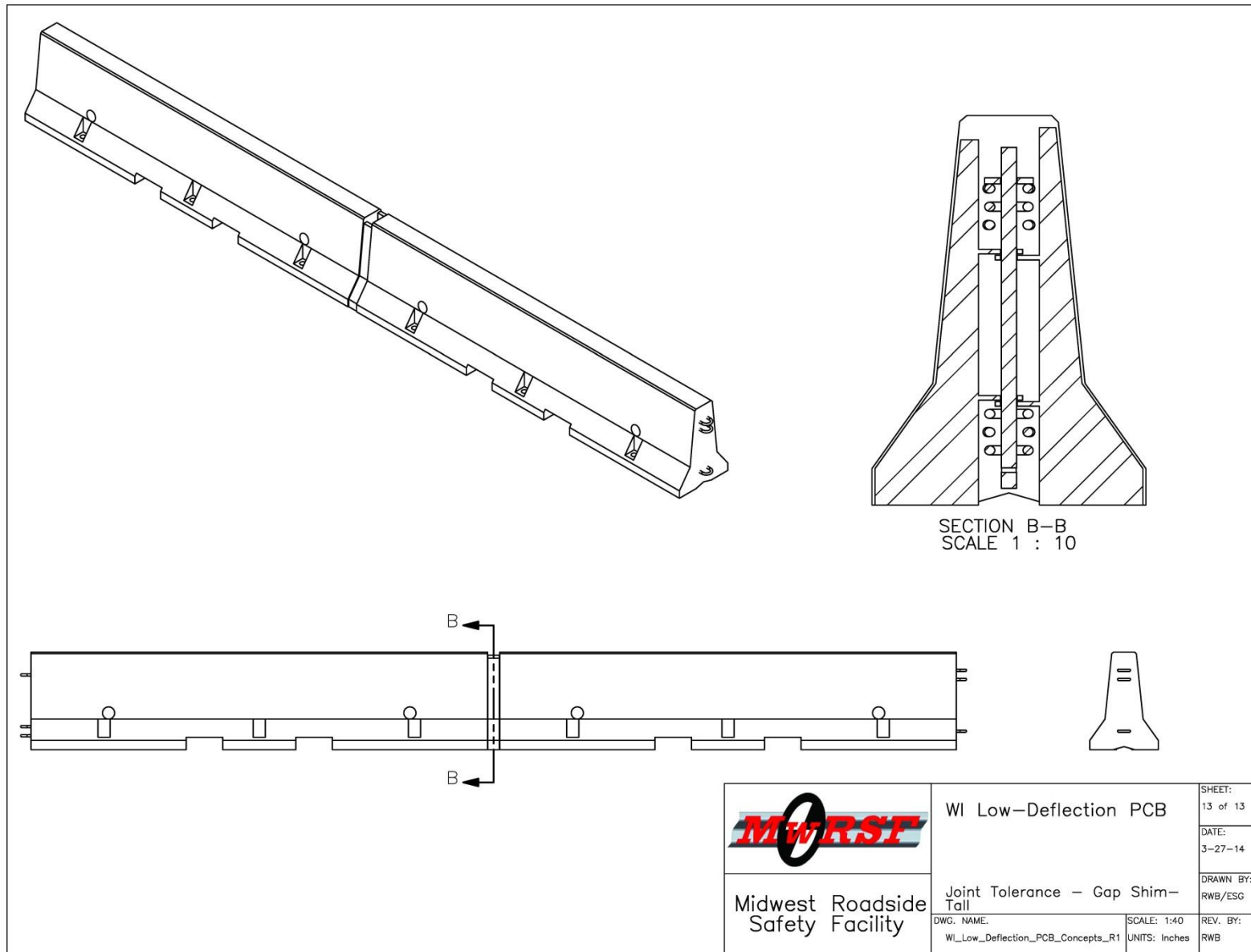


Figure 13. Joint Tolerance – Gap Shim – Tall

## **4 SIMULATION OF REDUCED-DEFLECTION MECHANISMS**

### **4.1 Methodology**

In order to evaluate and determine the potential of the proposed deflection-limiting mechanisms, a parameter study was conducted using LS-DYNA. LS-DYNA is a transient, nonlinear finite element analysis code that has been widely used in analysis and design of roadside safety hardware. The methodology for evaluating the deflection-limiting mechanisms began with development of a baseline model of the free-standing, F-shape TCB system that produced similar deflections to previous MASH TL-3 full-scale crash testing with the 2270P vehicle. Next, the baseline model was modified with simplified representations of the proposed deflection-limiting mechanisms and simulated. The results of the simulations of the various deflection-limiting mechanisms were then collected, compared, and used to select the most desired mechanism for development of a prototype system for full-scale crash testing.

### **4.2 Baseline Model**

#### **4.2.1 Baseline Model Description**

The model of the F-shape temporary concrete barrier was based on a model developed previously at MwRSF for determining the deflection of tie-down F-shape barriers [13]. The model consisted of the F-shape barrier, the end connection loops, and the connection pins, as shown in Figure 14. The main body of the F-shape barrier model was created using shell elements with a rigid material definition. The rigid material definition allowed the proper mass and rotational inertias to be defined for the barrier even though it was essentially hollow. The barrier segments were assigned a mass of 4,976 lb (2,257 kg) based on measurements taken from actual barrier segments. The rotational inertias were determined based on SolidWorks models of the TCB segment. The SolidWorks models used tended to overestimate the mass and rotational inertia of the TCB segment as the solid model included the mass of the concrete body and the

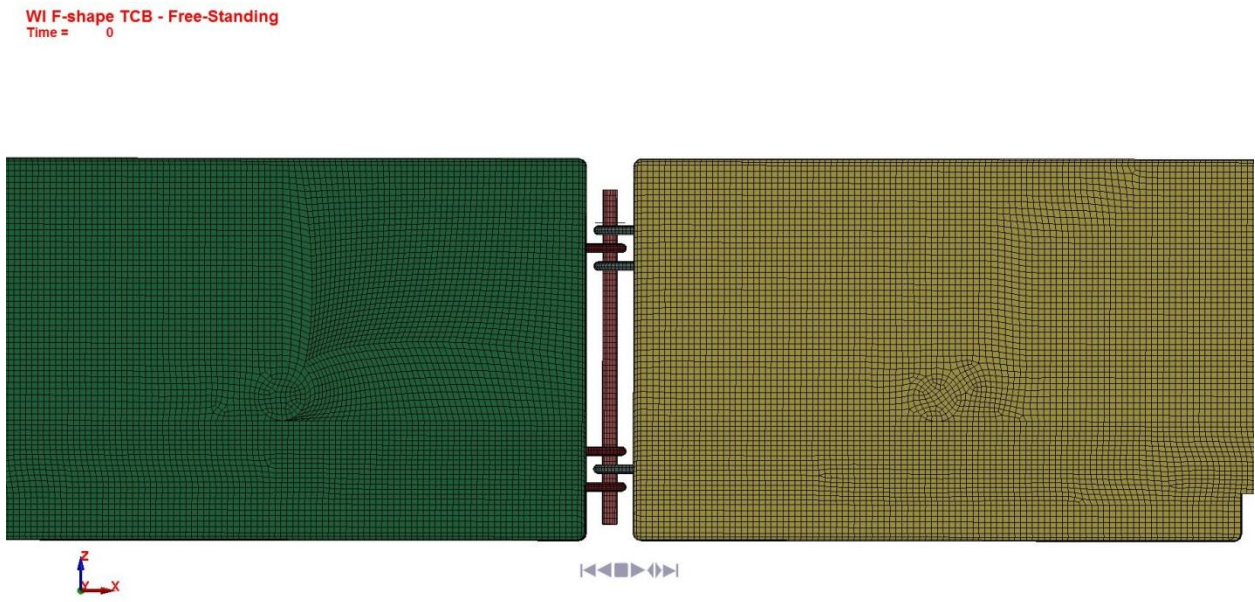
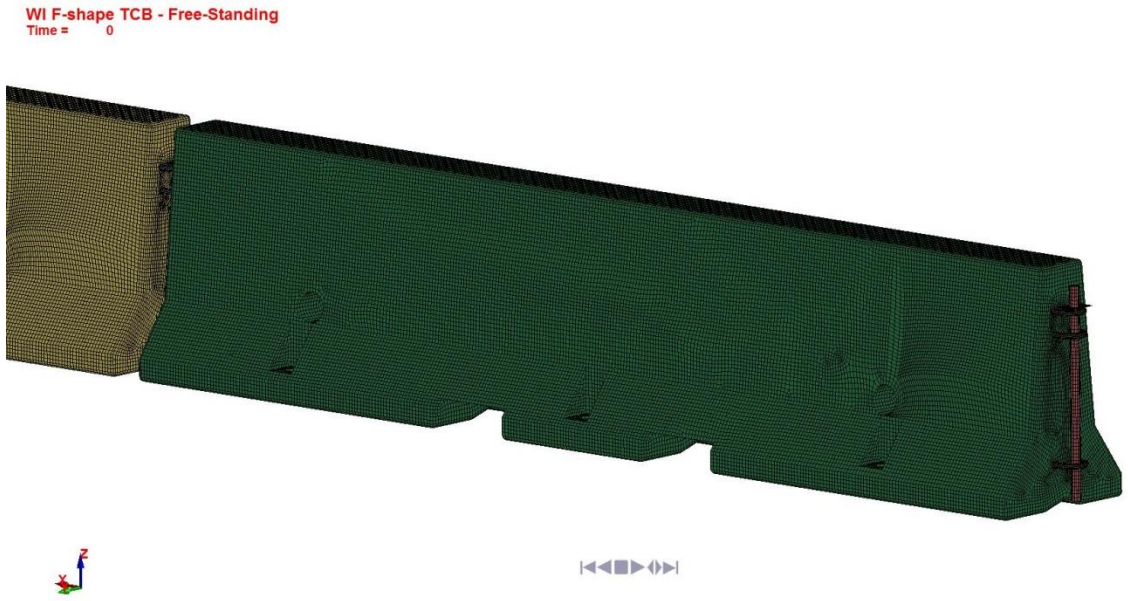


Figure 14. F-shape TCB Barrier Model

reinforcing steel, but did not account for the volume of concrete lost due to the reinforcing steel. Thus, the rotational inertias determined by the software were scaled down based on the ratio of the actual measured mass of the barrier segment to the software-estimated mass of the segment. The use of the shell elements improved the overall contact of the barrier and the vehicle. In addition, the use of shell elements made it easier to fillet the corners and edges of the barrier. By rounding off the barrier edges, the edge contacts and penetrations were reduced, thus further improving the contact interface.

The loops in the barrier model were also modified to match the current configuration which consisted of two sets of three rebar loops. The connection loops were modeled with a rigid material as previous testing of the barrier in various configurations has shown little to no deformation of the connection loops. The connection pin was modeled with the `MAT_PIECEWISE_LINEAR_PLASTICITY` material in LS-DYNA with the appropriate properties for A36 steel. The barrier system model incorporated a total of sixteen barrier segments for a total barrier length of 200 ft (61.0 m).

Another critical component of the baseline model of the free-standing, F-shape TCB was the definition of the barrier-to-ground friction. TCB systems use a combination of inertial resistance and longitudinal tension to redirect impacting vehicles. The longitudinal tension in the barrier system is largely developed by barrier-to-ground friction. Previous research at TTI measured the kinematic friction coefficient for a concrete TCB segment sliding on a concrete surface at 0.40 [10]. That friction value was applied in the LS-DYNA model of the TCB system between the barrier segments and the ground shell element. In addition to providing appropriate friction coefficients, the barrier model needed to develop the correct weight or normal forces on the ground. This was accomplished by allowing the barriers in the simulation model to reach quasi-static equilibrium on the ground prior to being impacted. Damping was used to help the

barriers reach a steady normal force on the ground and was then turned off prior to impact of the vehicle. An example of the barrier weight forces on the ground in the model is shown in Figure 15.

The F-shape barrier model described above was simulated under the MASH TL-3 impact conditions for test designation no. 3-11 and then compared with previous free-standing F-shape barrier testing in order to ensure that it was capable of providing reasonable estimates of the barrier deflection prior to modifying the model to evaluate the deflection-limiting concepts.

#### **4.2.2 Simulation of Baseline Model and Comparison with Test No. TB-2**

The baseline model of the free-standing F-shape TCB was simulated with a 2270P vehicle impacting the system at a speed of 62 mph (100 km/h) and an angle of 25 degrees. The vehicle model used for the simulation was Version 3 of the Chevy Silverado model developed at the National Crash Analysis Center (NCAC). The vehicle impacted the system 4.3 ft (1.3 m) upstream of the center of the joint between the eighth and ninth barrier segments, as shown in Figure 16.

The results of the simulation of the baseline free-standing, F-shape TCB were compared with the results from test no. TB-2. Test no. TB-2 consisted of a 2270P vehicle impacting the TCB system with a speed of 62.0 mph (99.7 km/h) and at an angle of 25.4 degrees. The TCB system safely redirected the impacting vehicle with a maximum lateral dynamic barrier deflection of 79.6 in. (2,023 mm).

Comparison of the baseline model with the full-scale crash test found that the baseline model provided good correlation with the full-scale test and was appropriate for use in evaluation of the deflection-limiting mechanisms. Graphical comparison of the baseline model and test no. TB-2, as shown in Figure 17 through Figure 20, found that the behavior of the vehicle and the barrier were very similar between the full-scale test and the baseline simulation. Some difference

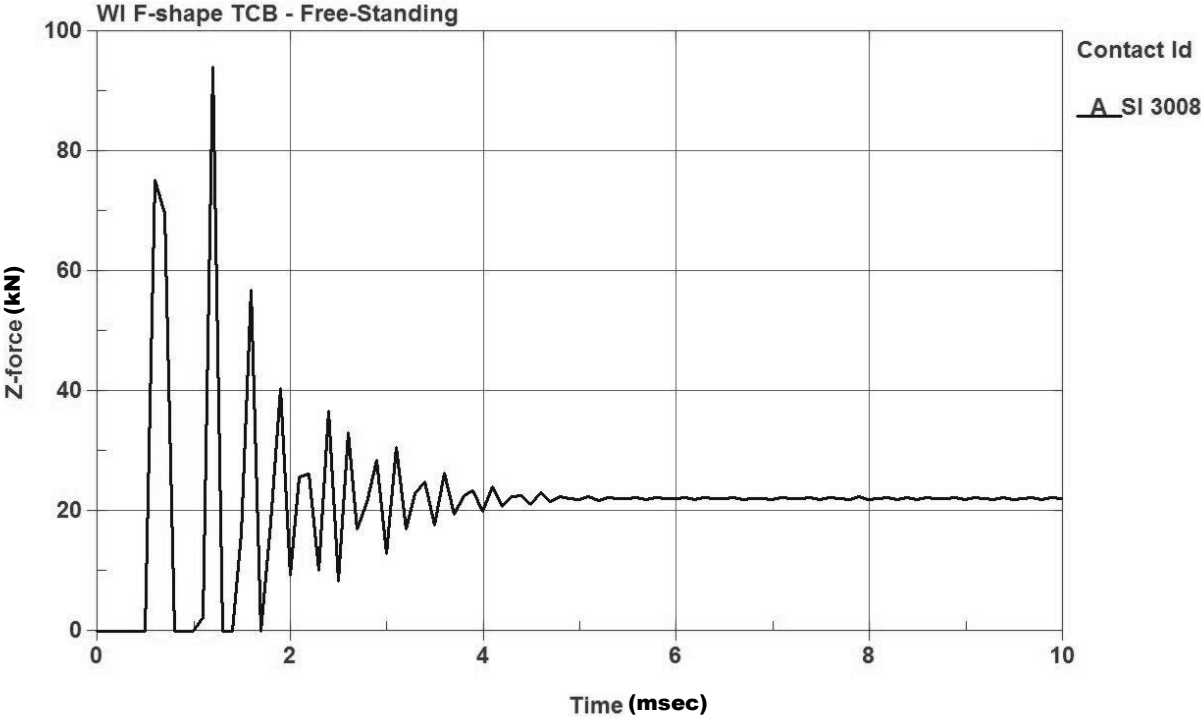


Figure 15. Barrier Segment-to-Ground Contact Forces Prior to Impact

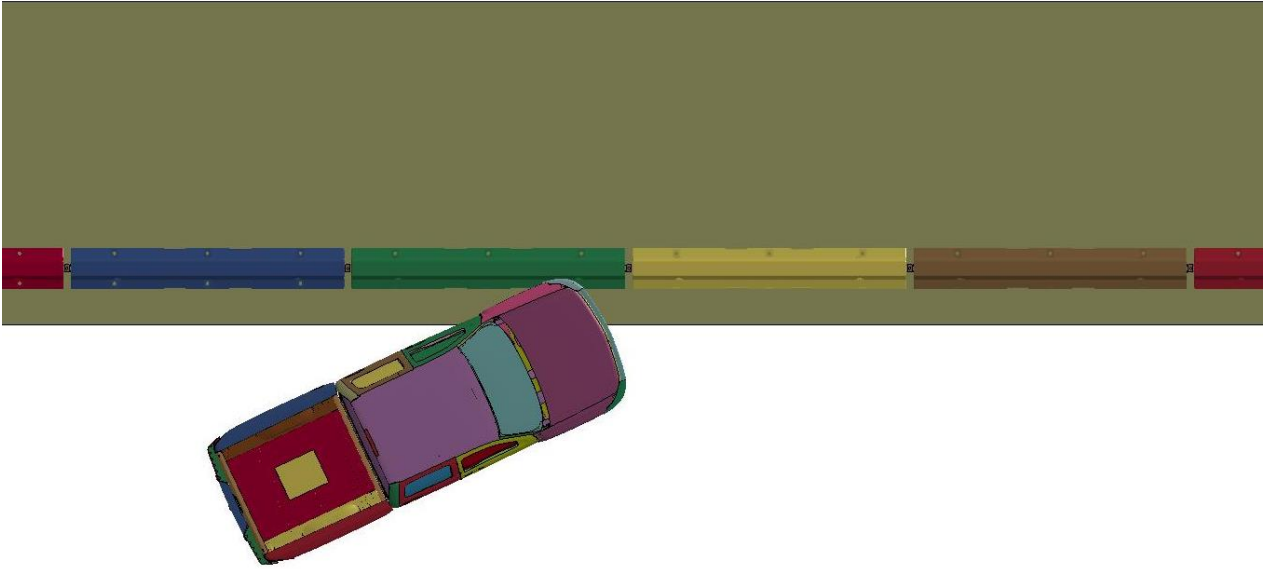
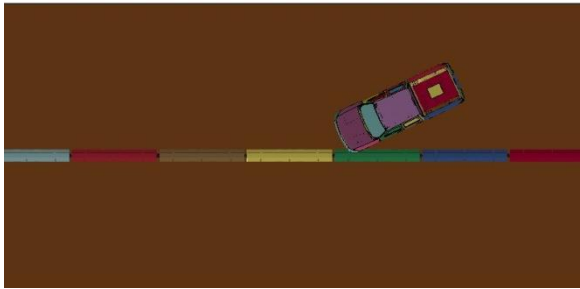


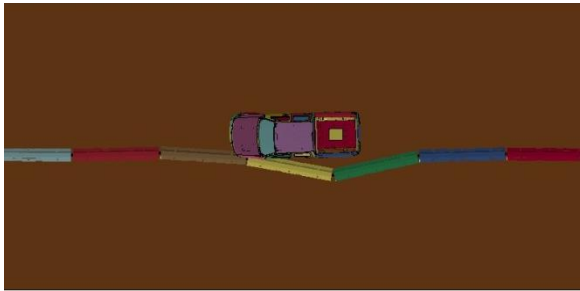
Figure 16. Baseline Model Impact Point



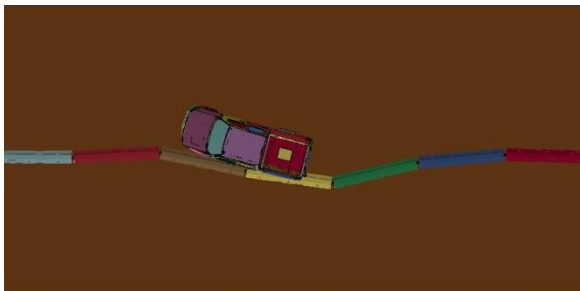
Time = 0.000 sec



Time = 0.100 sec

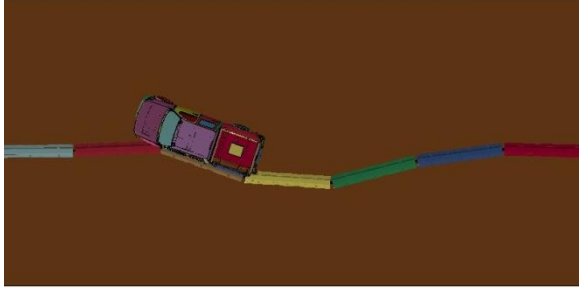


Time = 0.200 sec

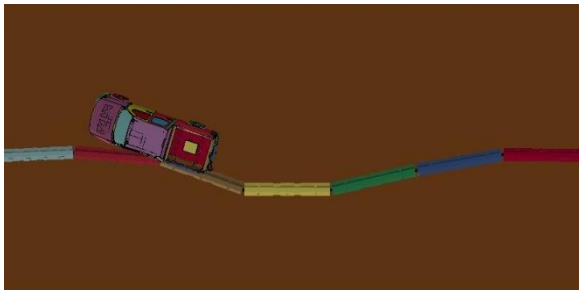


Time = 0.300 sec

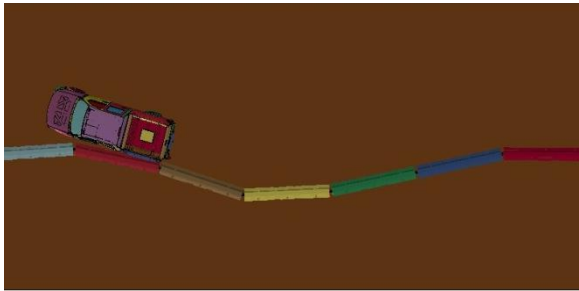
Figure 17. Overhead Sequential Views, Baseline Model and Test No. TB-2



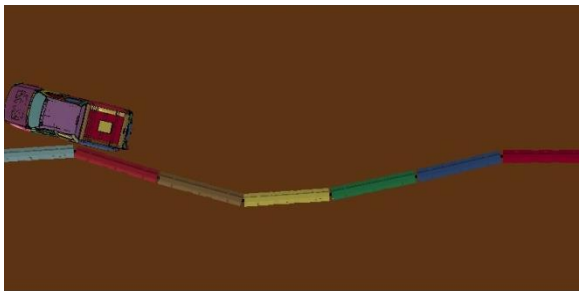
Time = 0.400 sec



Time = 0.500 sec

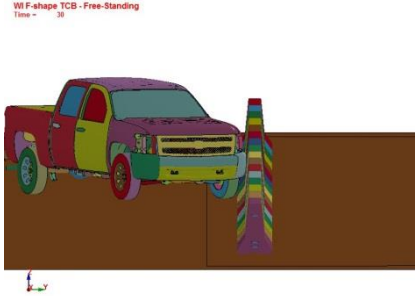


Time = 0.600 sec



Time = 0.700 sec

Figure 18. Overhead Sequential Views, Baseline Model and Test No. TB-2



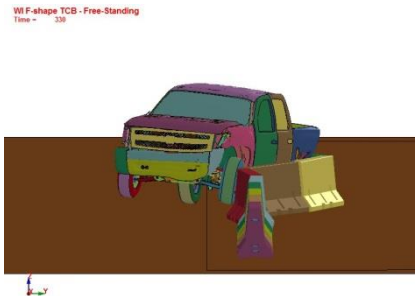
Time = 0.000 sec



Time = 0.100 sec



Time = 0.200 sec



Time = 0.300 sec

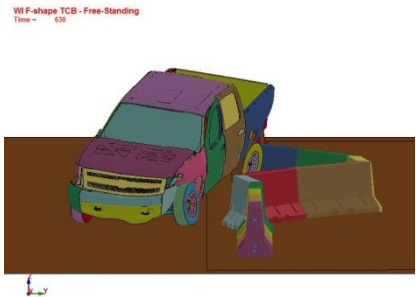
Figure 19. Downstream Sequential Views, Baseline Model and Test No. TB-2



Time = 0.400 sec



Time = 0.500 sec



Time = 0.600 sec



Time = 0.700 sec

Figure 20. Downstream Sequential Views, Baseline Model and Test No. TB-2

in the yaw and trajectory of the vehicle were observed after 300 msec due to differences in the vehicle's reaction to tail slap. However, these differences did not seem to adversely affect the redirection of the vehicle or the loading of the barriers. The dynamic deflection of the baseline model was found to be 80.5 in. (2,045 mm) at the downstream end of the ninth barrier segment. This compared very well with the dynamic deflection of test no. TB-2, which was measured from high-speed film to be 79.6 in. (2,023 mm) at the downstream end of the ninth barrier segment.

Based on this comparison, it was believed that the baseline model was providing reasonable estimates of barrier deflection under TL-3 impact conditions, and the baseline model was then applied to investigate the proposed deflection-limiting mechanisms.

#### **4.3 Parametric Study**

The functional baseline model of the F-shape TCB was then applied to investigate the various deflection-limiting mechanisms proposed previously in Chapter 3. These deflection-limiting mechanisms included:

1. Increased Barrier Mass
2. Increased Barrier-to-Ground Friction
3. Reduced Joint Tolerance
4. Composite Action

Computer simulation of each of these mechanisms and the results are discussed in the subsequent sections. It should be noted all of the simulations of the deflection-limiting mechanisms were conducted with the Chevy Silverado model at an impact point slightly upstream of the impact point used in the previous baseline model. All of the simulations of the deflection-limiting mechanisms shown herein impacted the system at the midpoint of the eighth TCB segment in the model. This impact point was chosen in order to improve the stability of the model across the

various deflection-limiting mechanism simulations because preliminary models demonstrated instabilities when impacted near the joint. Thus, rather than debug each of the individual deflection-limiting models, the impact point was changed slightly to lessen interaction with the barrier joint. It was believed that this change in the impact location would have minimal effect on the predicted barrier deflections.

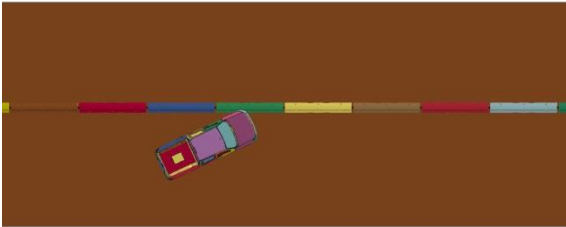
#### **4.3.1 Increased Barrier Mass**

Increasing the mass of the barrier segments was anticipated to provide both increased inertial resistance and increased frictional forces during impact with the barrier system. The effectiveness of increased TCB mass was investigated by simply increasing the mass of the barrier segments in the LS-DYNA model. In reality, increased barrier mass would need to be achieved through the mounting of additional structures on the TCB system. It was believed that simply increasing the mass of the barrier segments in the simulation would provide a reasonable estimate of the reduced deflections.

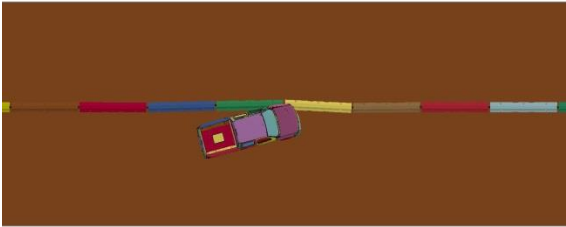
Two increased-barrier mass models were simulated. The first model increased the mass of the TCB segment to 8,366 lb (3,795 kg). Results from this simulation indicated that increased mass was effective at reducing barrier deflections as the peak dynamic lateral barrier deflection was found to be 37.3 in. (947 mm). A second increased-mass model was simulated with the mass of the TCB segment further increased to 11,155 lb (5,060 kg). The greater increased mass of the second simulation model further reduced the peak dynamic lateral barrier deflection to 24.9 in. (632 mm). Plots of the simulation results for the increased-mass TCB segments are shown in Figure 21 and Figure 22.

Simulation of increased-mass barrier segments demonstrated a clear benefit in terms of reducing the peak lateral barrier deflections. However, concerns were noted regarding

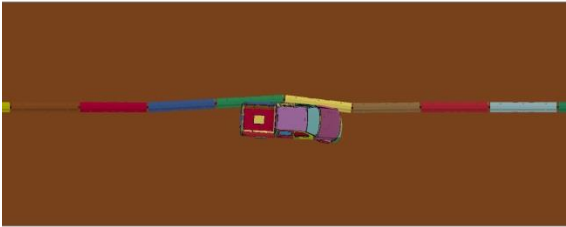
WI F-shape TCB - Free-Standing  
Time = 30



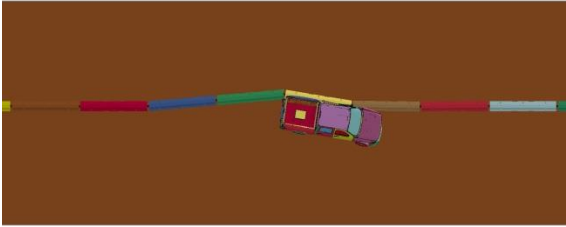
WI F-shape TCB - Free-Standing  
Time = 120



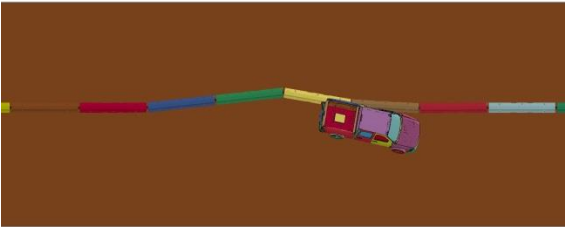
WI F-shape TCB - Free-Standing  
Time = 220



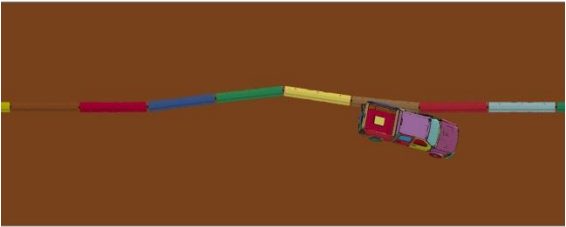
WI F-shape TCB - Free-Standing  
Time = 320



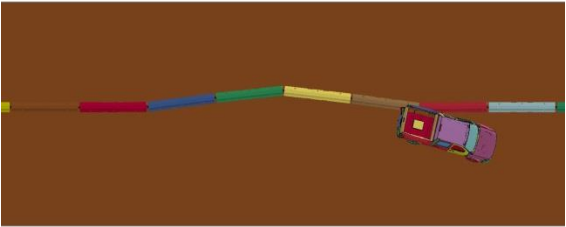
WI F-shape TCB - Free-Standing  
Time = 420



WI F-shape TCB - Free-Standing  
Time = 520



WI F-shape TCB - Free-Standing  
Time = 620



WI F-shape TCB - Free-Standing  
Time = 720

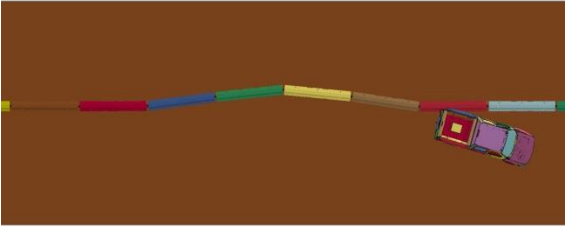
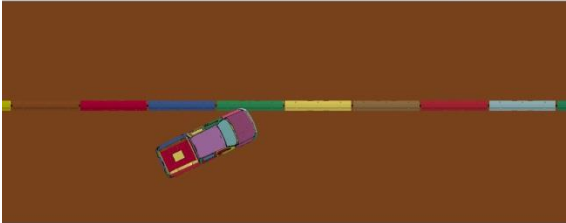
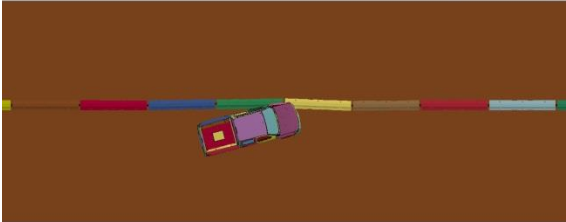


Figure 21. Low-Deflection TCB Parametric Study, Segment Mass = 8,366 lb (3,795 kg)

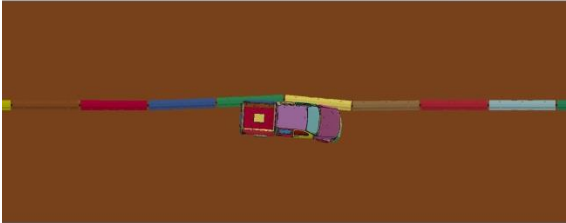
WI F-shape TCB - Free-Standing  
Time = 30



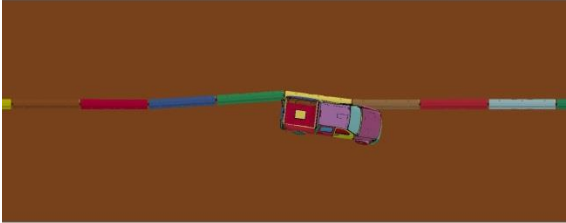
WI F-shape TCB - Free-Standing  
Time = 120



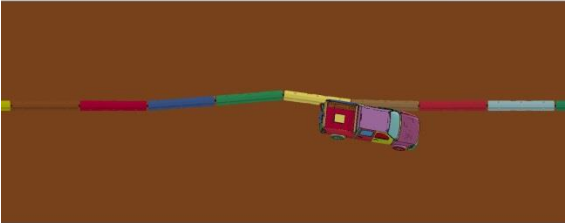
WI F-shape TCB - Free-Standing  
Time = 220



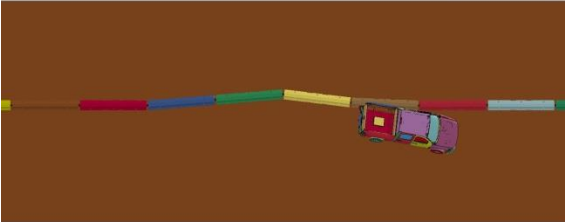
WI F-shape TCB - Free-Standing  
Time = 320



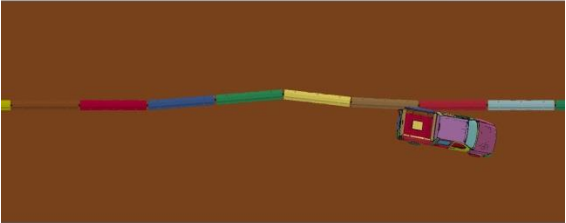
WI F-shape TCB - Free-Standing  
Time = 420



WI F-shape TCB - Free-Standing  
Time = 520



WI F-shape TCB - Free-Standing  
Time = 620



WI F-shape TCB - Free-Standing  
Time = 720

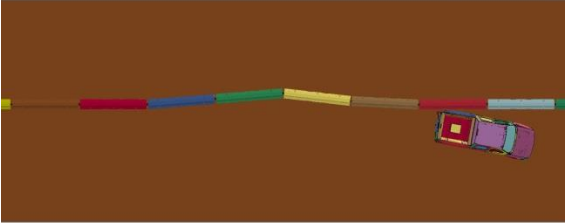


Figure 22. Low-Deflection TCB Parametric Study, Segment Mass = 11,155 lb (5,060 kg)

the use of such large increases in barrier mass on partially- and fully-constructed bridge deck edges and the feasibility of adding that magnitude of mass to the existing barrier system.

#### **4.3.2 Increased Barrier-to-Ground Friction**

Increased barrier-to-ground friction was expected to provide increased longitudinal and lateral resistive forces during impact with the barrier system. The effectiveness of increased friction was investigated by increasing the contact friction coefficients between the barrier segments and the ground in the LS-DYNA model. In reality, increased friction mass would need to be achieved through the use of high-friction surfaces on the base of the TCB segments or the road surface.

Two increased-friction models were simulated. The first model increased the friction coefficient between the TCB segments and the ground to 0.60. This represented a 50 percent increase in friction over that baseline model. Results from this simulation indicated that increased friction was effective at reducing barrier deflections as the peak dynamic lateral barrier deflection was found to be 41.5 in. (1,054 mm). A second increased-friction model was simulated with a friction coefficient between the TCB segments and the ground of 0.80. The higher friction coefficient of the second simulation model further reduced the peak dynamic lateral barrier deflection to 29.8 in. (757 mm). Simulation of increased-mass barrier segments demonstrated a clear benefit in terms of reducing the peak lateral barrier deflections. Plots of the simulation results for the increased-friction TCB segments are shown in Figure 23 and Figure 24.

#### **4.3.3 Reduced Joint Tolerance**

The third deflection-limiting mechanism investigated was reduction of the gap tolerance between the adjacent barrier segments. The F-shape TCB segment considered in this research has a gap between the barrier segments that can be as large as 4 in. (101.6 mm). The size of this gap

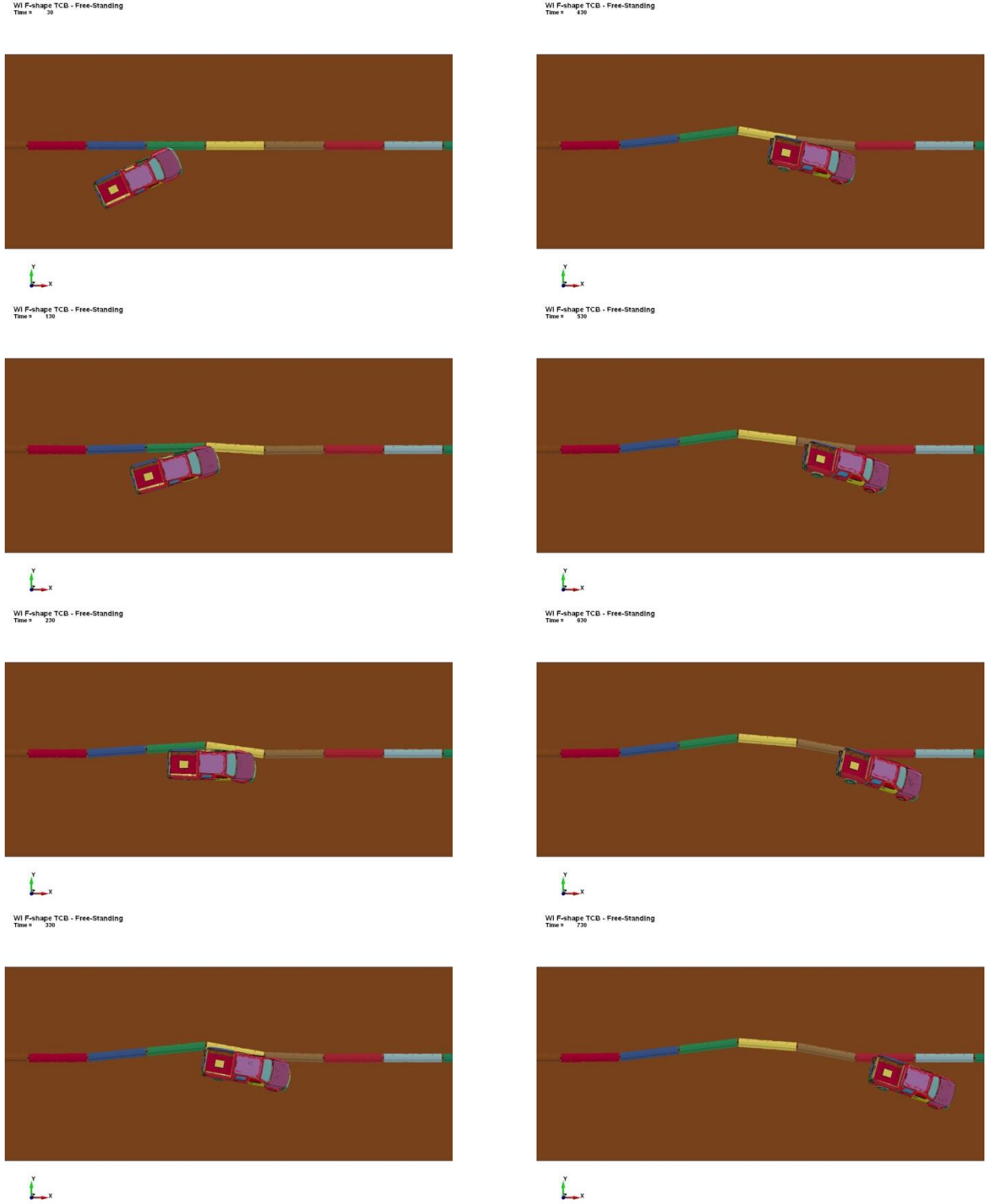
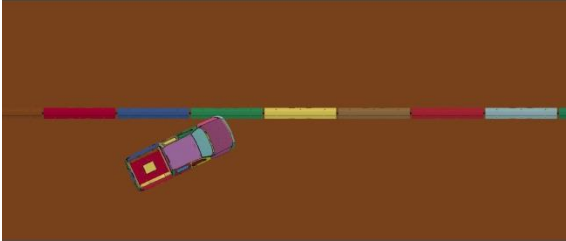
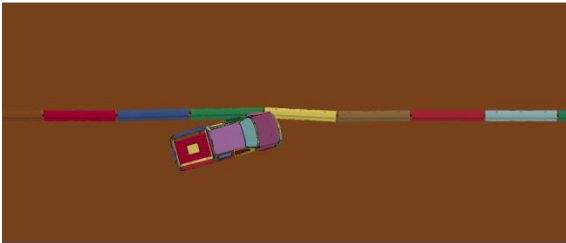


Figure 23. Low-Deflection TCB Parametric Study, Friction Coefficient = 0.6

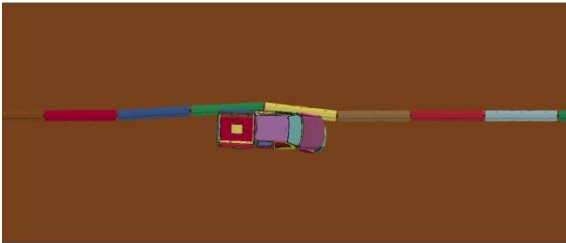
WI F-shape TCB - Free-Standing  
Time = 30



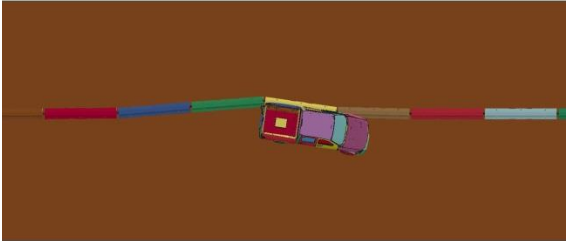
WI F-shape TCB - Free-Standing  
Time = 120



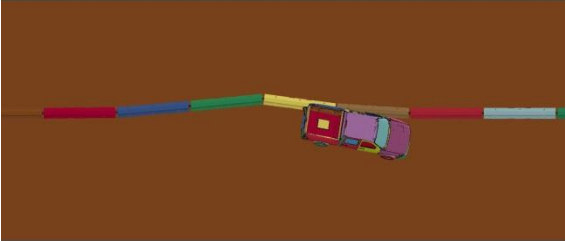
WI F-shape TCB - Free-Standing  
Time = 220



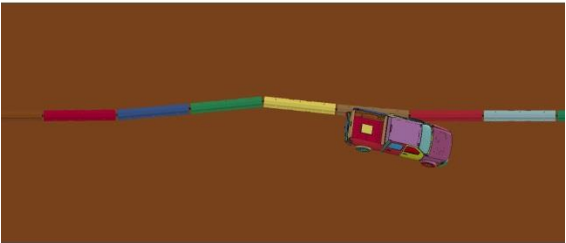
WI F-shape TCB - Free-Standing  
Time = 320



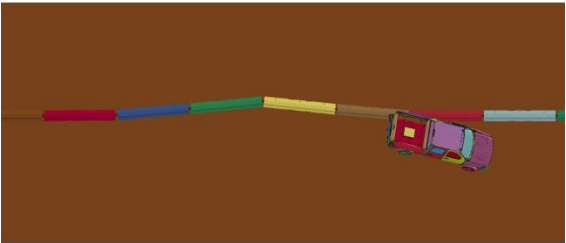
WI F-shape TCB - Free-Standing  
Time = 420



WI F-shape TCB - Free-Standing  
Time = 520



WI F-shape TCB - Free-Standing  
Time = 620



WI F-shape TCB - Free-Standing  
Time = 720

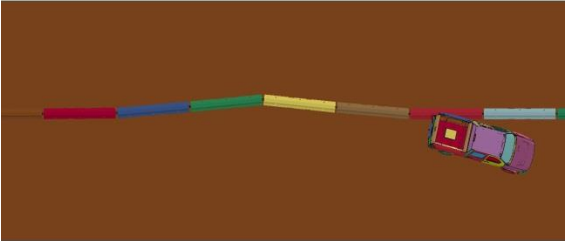


Figure 24. Low-Deflection TCB Parametric Study, Friction Coefficient = 0.8

allows for a large degree of rotation between the barrier segments prior to the toes of the barrier segments contacting and transmitting moment. Reduction of this gap between the barrier joint was expected to cause the adjacent barrier segments to engage sooner, improve transmission and distribution of the impact forces, and reduce barrier deflection. Reduction in the barrier joint gap was investigated through insertion of a steel spacer between the barrier segments that was held in place by the connection pin, as shown in Figure 25.

Results from the simulation of the TCB with the joint spacer indicated that reduction of the joint gap was effective at reducing barrier deflections as the peak dynamic lateral barrier deflection was found to be 34.1 in. (867 mm). Thus, simulation of a reduction of the gap tolerance between adjacent barrier segments demonstrated a clear benefit in terms of reducing the peak lateral barrier deflections. Plots of the simulation results for the increased-friction TCB segments are shown in Figure 26.

It should be noted that installation of the joint spacer tended to increase the loads and deformations experienced by the connection pin. The increased loads and deformations of the connection pin were not as evident in the other deflection-limiting mechanisms investigated in the parametric study.

#### **4.3.4 Composite Action**

The final deflection-limiting mechanism investigated was development of composite action between the adjacent barrier segments. Development of composite action between adjacent barrier segments would provide improved moment continuity across the barrier joint. Depending on the effectiveness, the use of composite action at the barrier joint would allow the TCB system to act as one continuous barrier section, thus reducing deflection. In order to

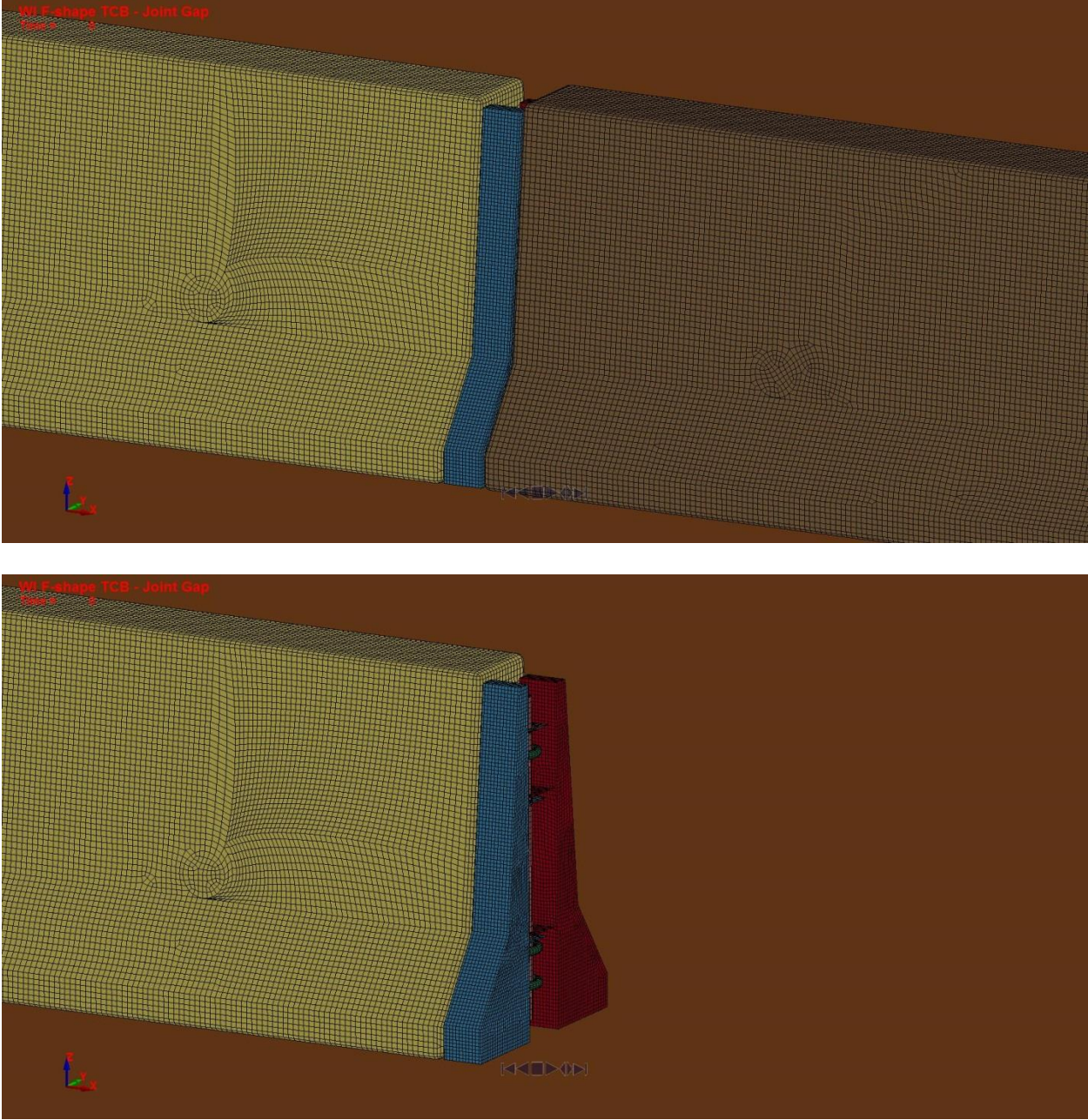


Figure 25. Low-Deflection TCB Parametric Study, Reduced Joint Gap Spacer

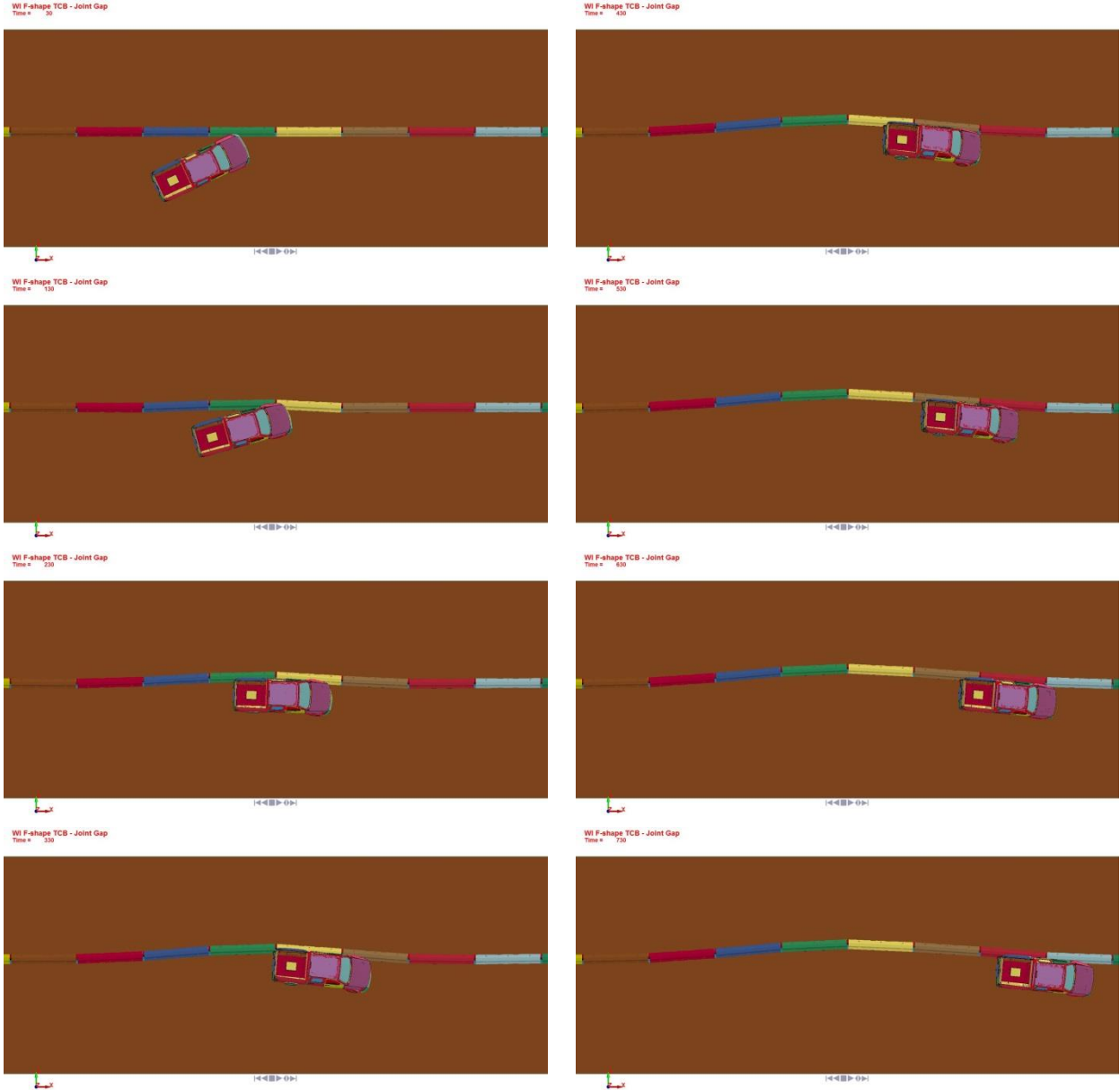


Figure 26. Low-Deflection TCB Parametric Study, Reduced Joint Gap

evaluate the use of composite action at the barrier joint, two different load-bearing members were used to span the TCB joint in the simulation model: (1) a  $\frac{3}{8}$ -in. (10-mm) thick steel plate bolted across both sides of the barrier joint; and (2) a 6-in. x 6-in. x  $\frac{3}{8}$ -in. (152-mm x 152-mm x 10-mm) steel tube bolted across both sides the barrier joint, as shown in Figure 27.

Both of the simulation models of the composite action concepts demonstrated reduced barrier deflections. The simulation of the TCB segments with the  $\frac{3}{8}$ -in. (10-mm) thick steel plate found that peak dynamic lateral barrier deflection was reduced to 26.9 in. (683-mm). Simulation of the barrier model with the 6-in. x 6-in. x  $\frac{3}{8}$ -in. (152-mm x 152-mm x 10-mm) steel tube bolted across both sides the barrier joint further reduced the peak dynamic lateral barrier deflection to 20.8 in. (528-mm). Thus, simulation of improved composite action at the barrier joints demonstrated a clear benefit in terms of reducing the peak lateral barrier deflections. Plots of the simulation results for the composite action TCB segments are shown in Figure 28 and Figure 29.

It should be noted that the composite action simulation models used simplified connections from the plate and tube sections to the barrier that provided total fixity and no tolerance or slip. In addition, no concrete failure was modeled in the barrier segments near the connection points as the extent of the concrete damage due to the attachment and loading of the additional hardware was unknown at this time. Thus, the estimated reductions in lateral barrier deflections were likely overestimated in the models. However, it was believed that the models provided a reasonable estimation of the effectiveness of composite action on the system.

#### **4.4 Discussion of Results and Concept Selection**

Simulation of the various concepts for limiting the barrier deflection were compared to determine which mechanism would be most effective for the system being developed in this study. Results from the parametric study are summarized in Table 3 for the variations of the four

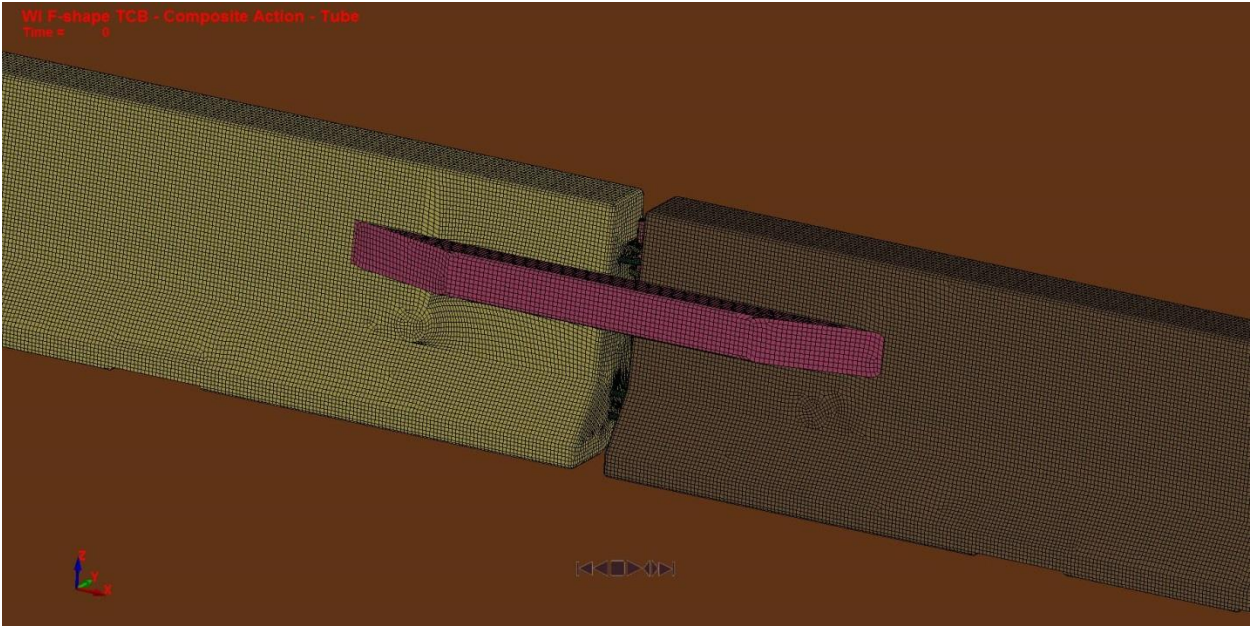
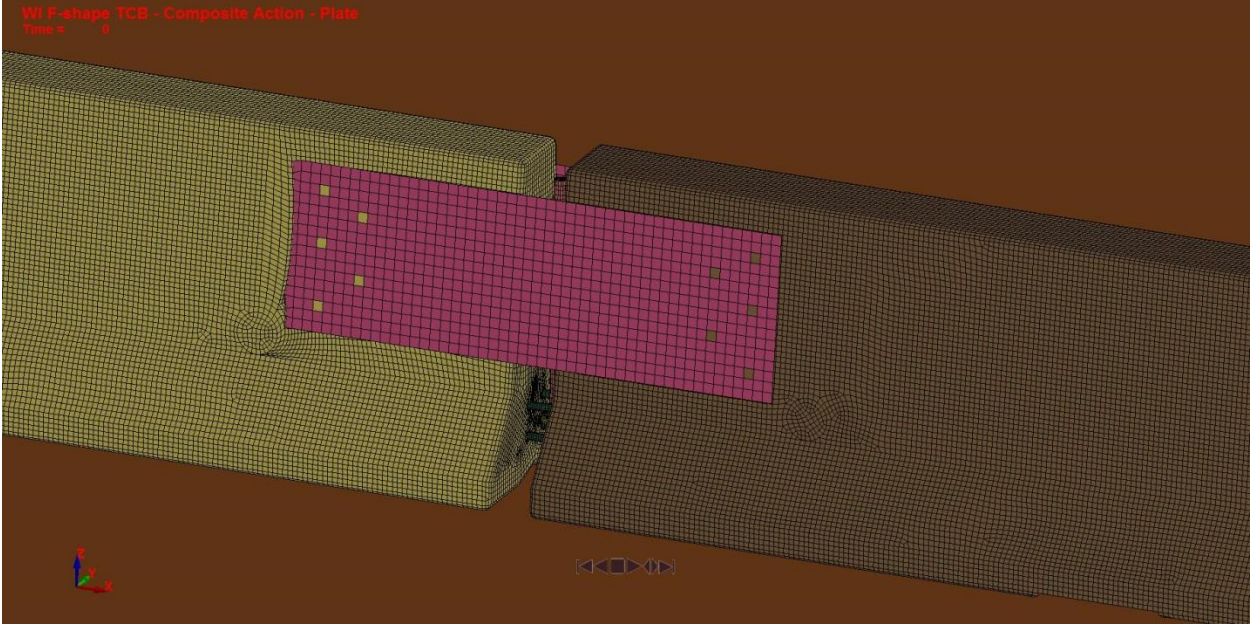


Figure 27. Low-Deflection TCB Parametric Study, Composite Action Models

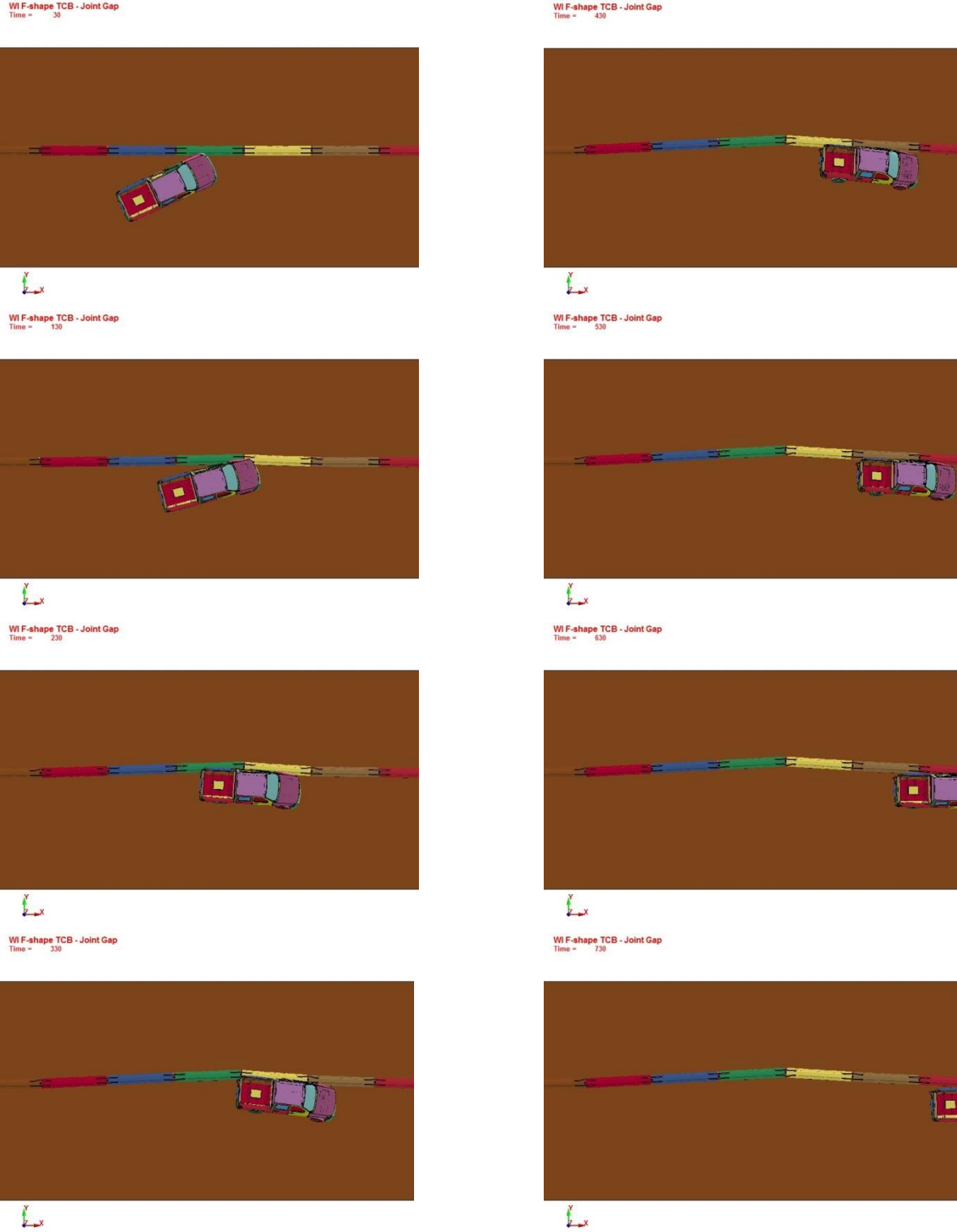


Figure 28. Low-Deflection TCB Parametric Study, Composite Action – Plate

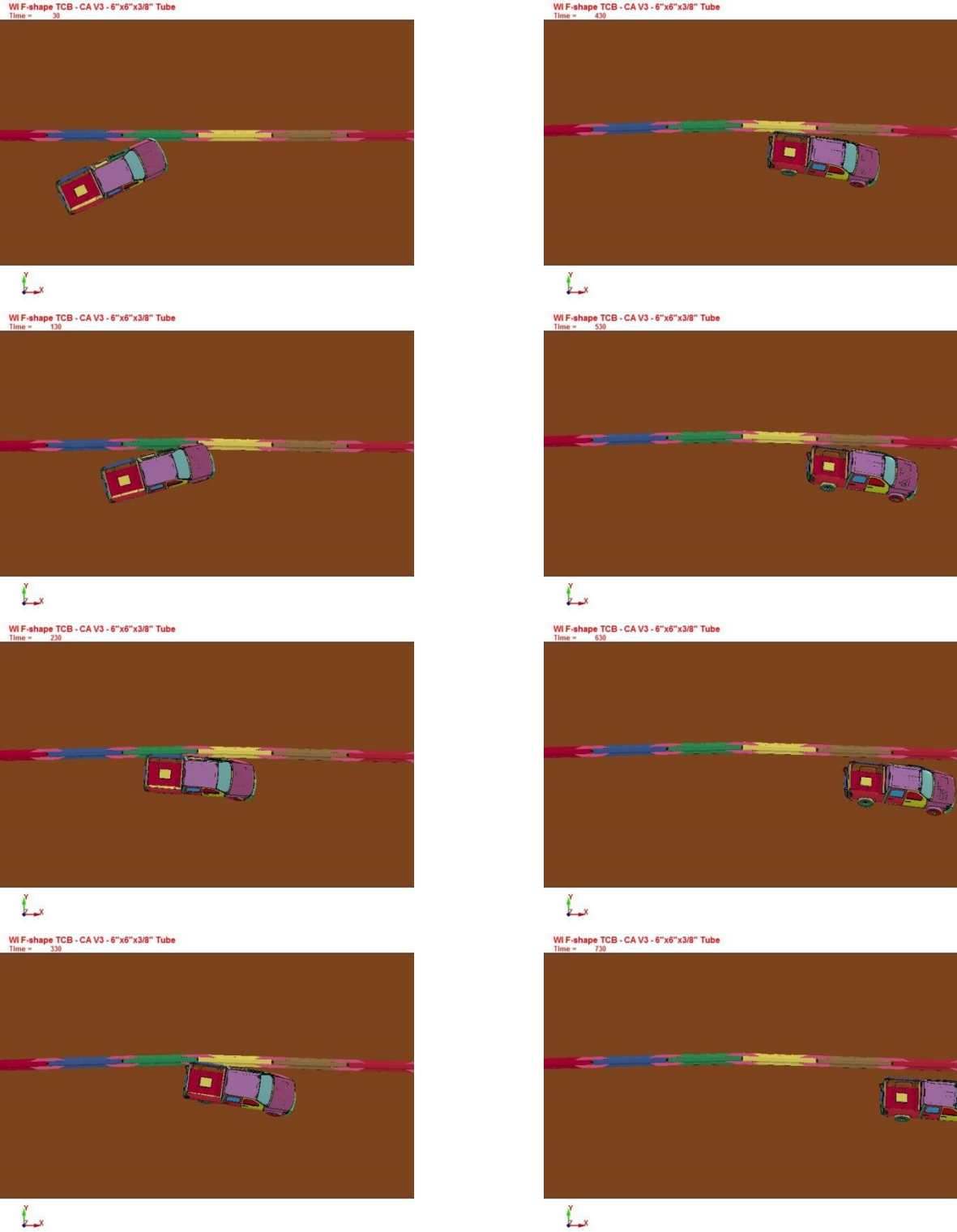


Figure 29. Low-Deflection TCB Parametric Study, Composite Action – Tube

Table 3. Summary of Deflection-Limiting Mechanism Parametric Study

<b>Comparison of Predicted Barrier Deflections</b>		
Model	Peak Lateral Deflection in. (mm)	% Reduction From Baseline
Baseline		
Free-Standing F-shape PCB – Run 18b	80.5 (2045)	NA
Increased Friction		
Friction F-shape PCB – Run 1 - $\mu = 0.6$	41.5 (1054)	48.4
Friction F-shape PCB – Run 2 - $\mu = 0.8$	29.8 (757)	63.0
Increased Mass		
Mass F-shape PCB – Run 1 – 8,366 lb	37.3 (947)	53.7
Mass F-shape PCB – Run 2 – 11,155 lb	24.9 (632)	69.0
Reduced Joint Gap		
Joint Gap F-shape PCB – Run 13	34.1 (866)	57.6
Composite Action		
Composite Action F-shape PCB – Run 2 – 3/8" Steel Plate	26.9 (683)	66.6
Composite Action F-shape PCB – V3 – Run 1 – 6"x6"x3/8" Steel Tube	20.8 (528)	74.2

main deflection-limiting techniques. Based on the simulation data, it appeared that the composite action and increased-barrier mass concepts provided the highest reductions in barrier deflection. Composite action was very effective in reduced barrier deflections. However, as noted in the previous section, the estimated deflections for that mechanism were likely overestimated to some degree. Increasing the mass of the barriers in combination with using composite action would provide further deflection reduction due to increased inertial resistance as well as increased friction loads. As such, it was believed that combining the two methods would provide the greatest reduction in barrier deflection.

MwRSF discussed the results of this parametric study with WisDOT to obtain their feedback with regards to the deflection-limiting mechanisms. WisDOT agreed that the composite action and increased-mass options provided the most effective reduction in barrier deflection. However, WisDOT noted that increased mass on the bridge decks was not desirable. As such, MwRSF proceeded to develop concepts for the initial full-scale crash test based on composite action. In order to proceed, prototype designs were submitted to WisDOT for feedback. Each design had inherent advantages and disadvantages. These designs are discussed in Chapter 10.

## **5 COMPONENT TESTING OF TCB FRICTION COEFFICIENTS**

### **5.1 Purpose**

Temporary concrete barriers rely on friction between the bottom surface of the barrier and the roadway to develop resistance to longitudinal and lateral barrier motion and limit deflection. Previous research conducted at TTI conducted basic component testing of PCB segments on flat ground to determine coefficients of friction for TCB segments [10]. The results of those component tests estimated the coefficient of friction for TCB segments on concrete to be 0.40. This value was used successfully in the previous baseline simulation model of the TCB, as described in Section 4.2.

While composite action was chosen as the primary deflection-limiting mechanism, component testing of the barrier-to-ground friction mechanism was desired to better quantify barrier-to-ground friction values and provide data for improvement of the reduced-deflection TCB design following the initial full-scale crash test. Basic tests of the concrete barrier segment on the concrete tarmac would verify the barrier-to-ground friction coefficient previously determined at TTI. In addition, testing was also conducted on some simple modifications to the base of the barrier to increase friction. These tests of modified barriers would help determine what levels of increased barrier friction were achievable. Thus, a series of pull tests were designed in order to determine the static and kinetic coefficients of friction between a concrete barrier segment and concrete roadway. Pull tests were performed with two different durometer neoprene bearing pads between the barrier and roadway to determine the effect and feasibility of implementing increased friction modifications in reduced-deflection TCB designs.

### **5.2 Scope**

Six pull tests were conducted on TCB segments with and without neoprene rubber pad adhered to the base. The test setup is shown in Figure 30 through Figure 35.

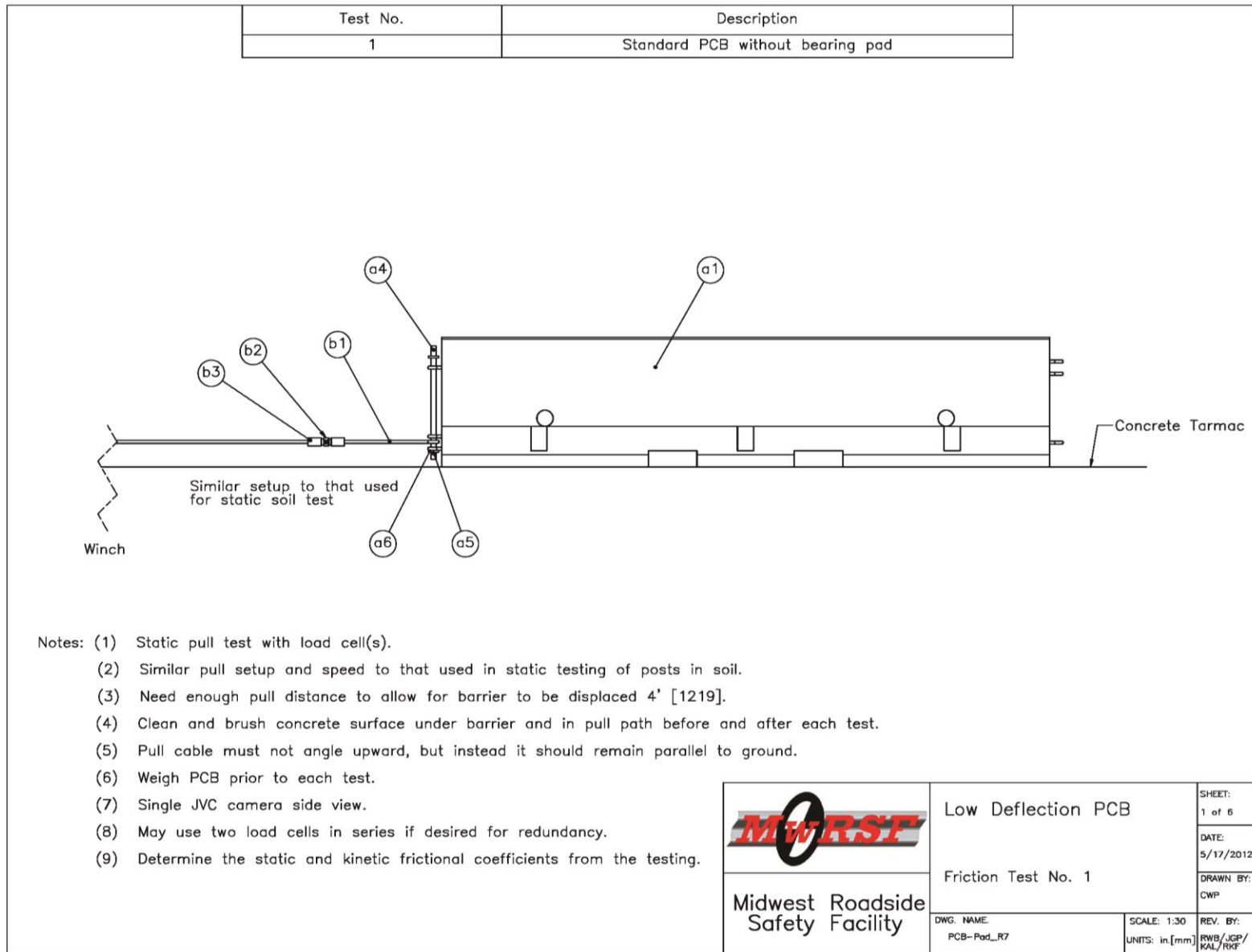
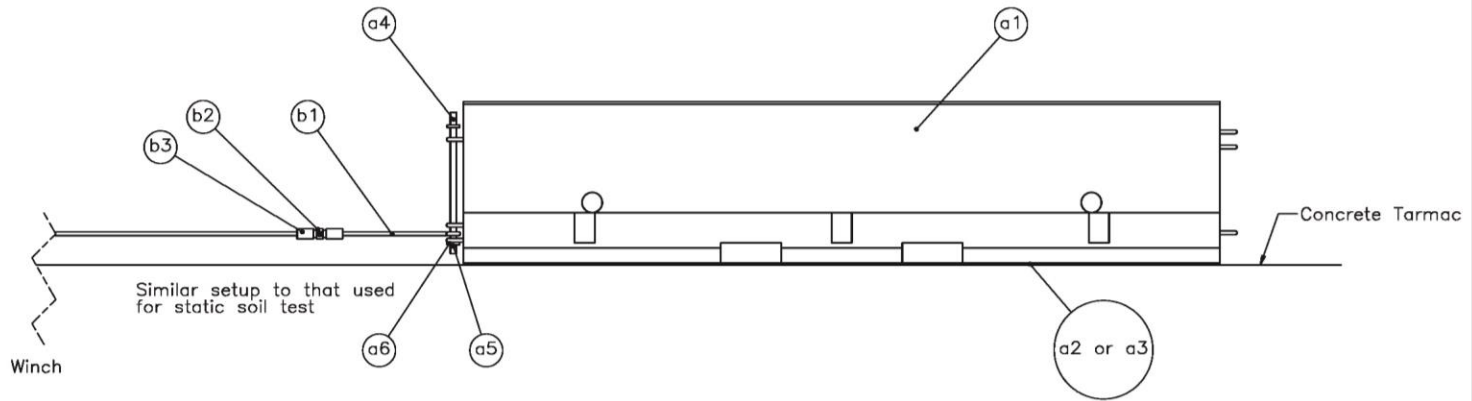


Figure 30. Friction Pull Test Setup

Test No.	Description
2	Standard PCB with 50 Durometer bearing pad
3	Standard PCB with 70 Durometer bearing pad



- Notes:
- (1) Static pull test with load cell(s).
  - (2) Similar pull setup and speed to that used in static testing of posts in soil.
  - (3) Need enough pull distance to allow for barrier to be displaced 4' [1219].
  - (4) Clean and brush concrete surface under barrier and in pull path before and after each test.
  - (5) Pull cable must not angle upward, but instead it should remain parallel to ground.
  - (6) Weigh PCB prior to each test.
  - (7) Single JVC camera side view.
  - (8) May use two load cells in series if desired for redundancy.
  - (9) Determine the static and kinetic frictional coefficients from the testing.

 <b>Midwest Roadside Safety Facility</b>	Low Deflection PCB	SHEET: 2 of 6
	Friction Test Nos. 2 and 3	DATE: 5/17/2012
DWG. NAME: PCB-Pad_R7	SCALE: 1:30 UNITS: in,[mm]	DRAWN BY: CWP
		REV. BY: RWB/JGP/ KAL/RKF

Figure 31. Friction Pull Test Setup

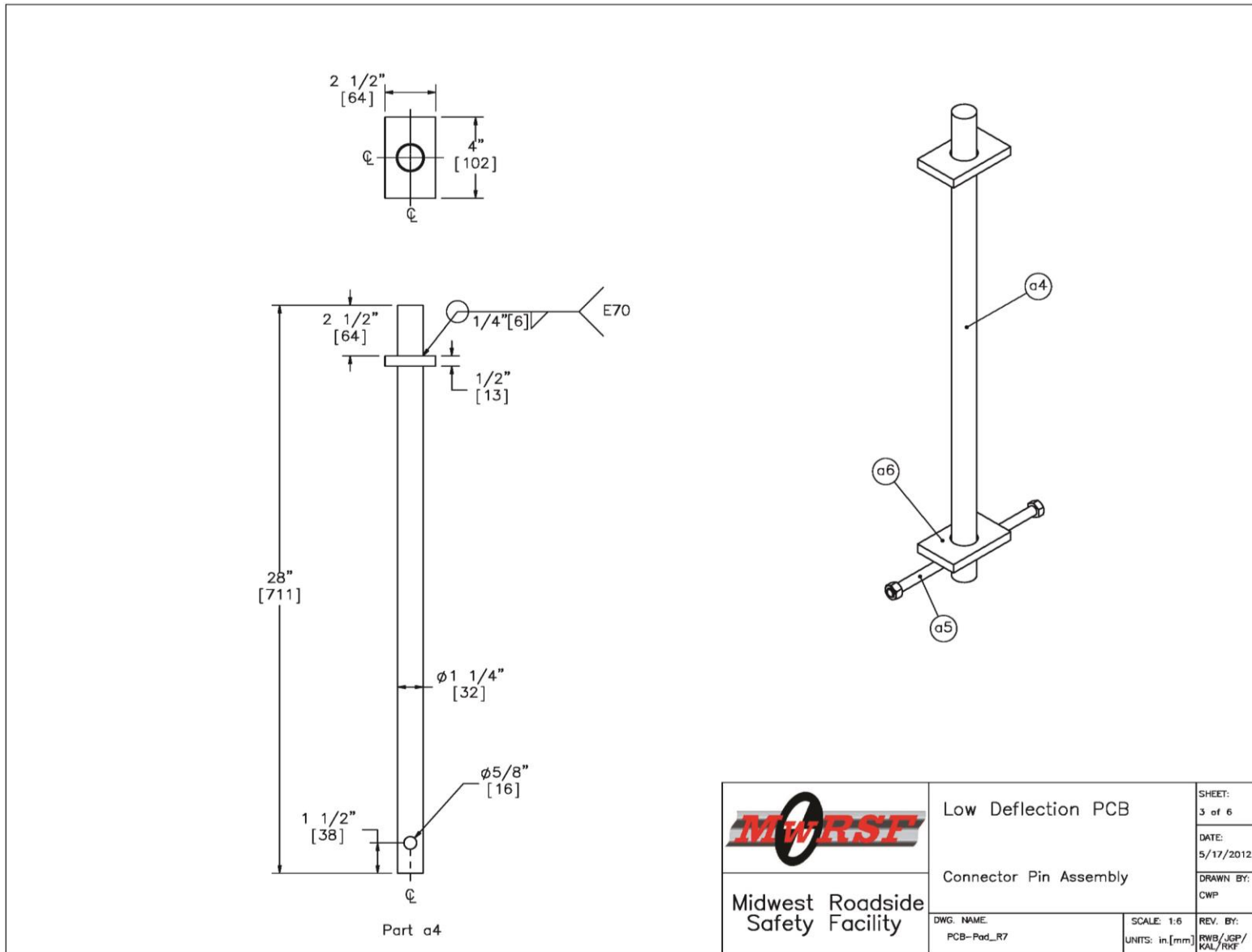


Figure 32. Friction Pull Test Setup

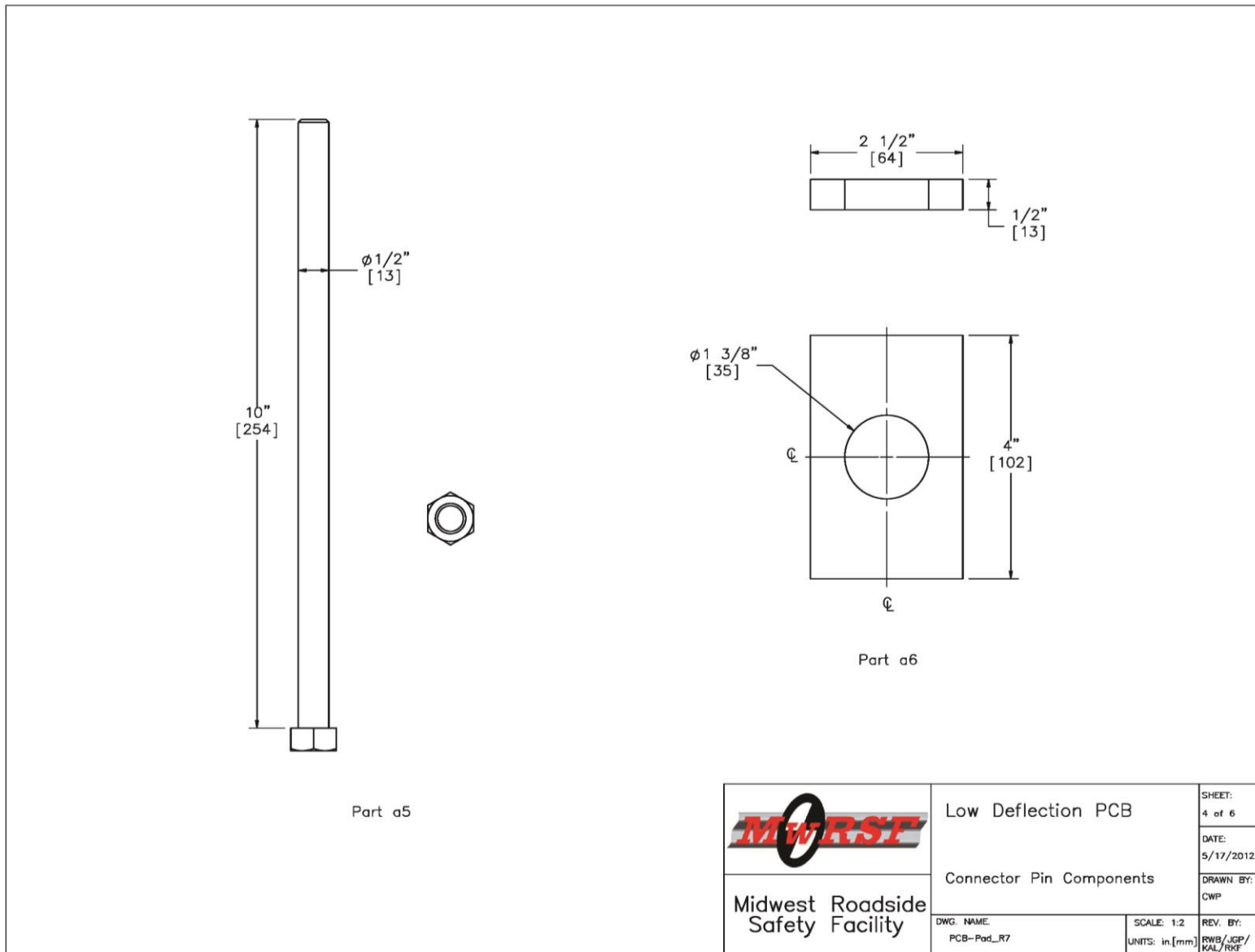


Figure 33. Friction Pull Test Setup

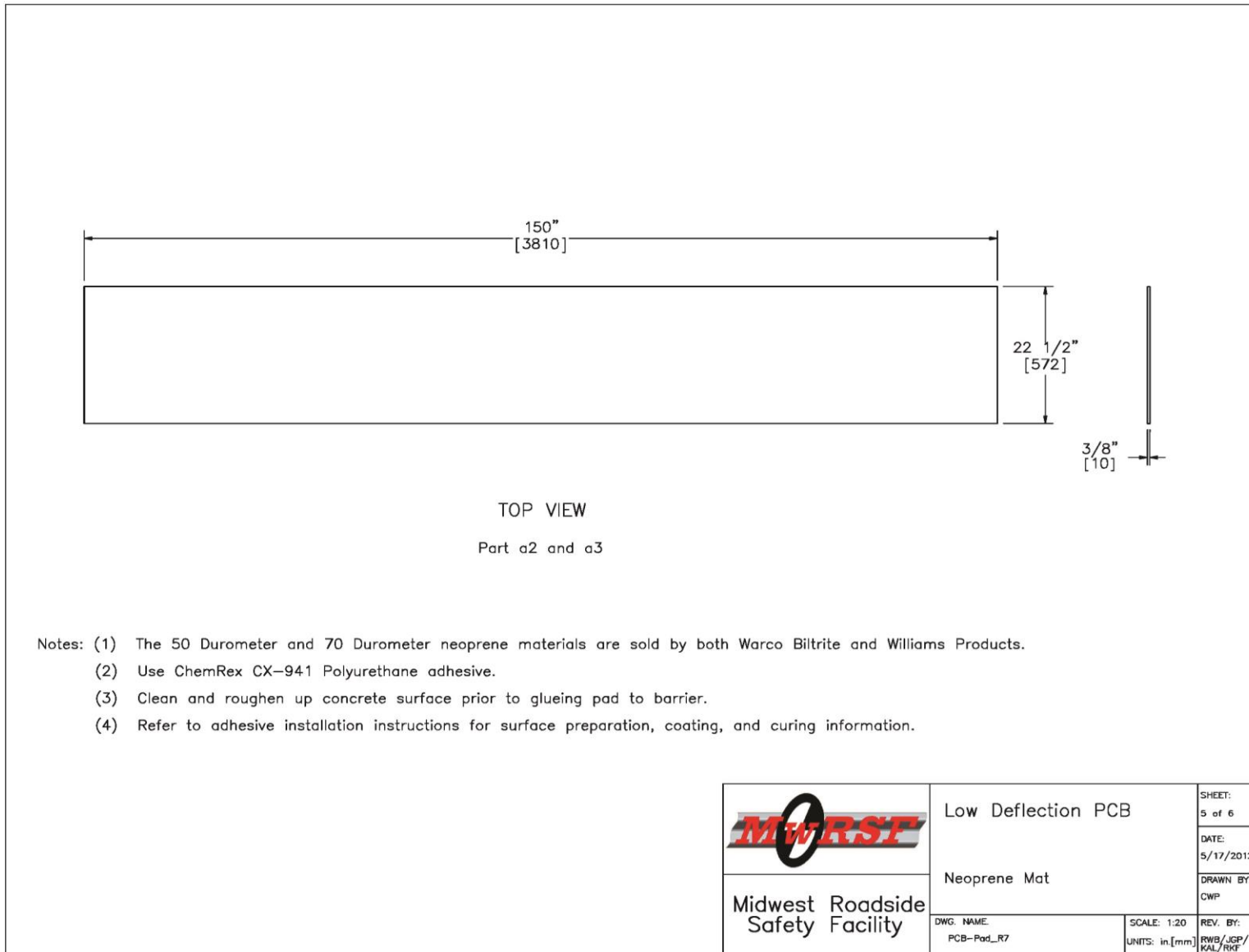


Figure 34. Friction Pull Test Setup

Item No.	QTY.	Description	Material Specification	Hardware Guide
a1	1	Portable Concrete Barrier	min f'c=5000 psi [34.5 MPa]	SWC09
a2	1	150"x22.5"x3/8" [3810x572x10] Neoprene Mat	50 Durometer AASHTO Grade 3 Bearing Pad	—
a3	1	150"x22.5"x3/8" [3810x572x10] Neoprene Mat	70 Durometer AASHTO Grade 3 Bearing Pad	—
a4	1	Connector Pin	ASTM A36	FMW02
a5	1	1/2"—13 Dia. x 10" Long [M13x254] Hex Head Bolt and Nut	ASTM A325 and ASTM A563 DH	FMW03
a6	2	2 1/2"x4"x1/2" [64x102x13] Washer	ASTM A36	FMW03
b1	2	3/4" [19] Dia. Cable	Steel	—
b2	1	50,000-lb Load Cell	N/A	—
b3	2	Load Cell Coupler	N/A	—
—	1	Polyurethane Adhesive	ChemRex CX-941	—

	Low Deflection PCB	SHEET: 6 of 6
	Bill of Materials	DATE: 5/17/2012
Midwest Roadside Safety Facility	DWG. NAME: PCB-Pad_R7	DRAWN BY: CWP
	SCALE: 1:2 UNITS: in,[mm]	REV. BY: RWB/JGP/ KAL/RKF

Figure 35. Friction Pull Test Setup

The neoprene pads used for the testing were  $\frac{3}{8}$ -in. (10-mm) thick and were attached to the underside of the TCB segment with adhesive. The neoprene material chosen was standard bearing pad material used during bridge construction for use underneath bridge girders. Two different neoprene hardness levels, 50-durometer and 70-durometer, were chosen for the testing to evaluate how the hardness of the rubber affected the friction values. Material specifications, mill certifications, and certificates of conformity are shown in Appendix A. The first three tests were conducted to determine a friction coefficient between concrete barrier segments and concrete roadways. The last three tests were to determine the friction coefficient for two durometer neoprene bearing pads.

### **5.3 Equipment and Instrumentation**

Equipment and instrumentation utilized to collect and record data during the pull tests included a skid-steer, winch, two tensile-load cells, high-speed and standard-speed digital video, and still cameras.

#### **5.3.1 Tensile-Load Cells**

Two load cells were mounted in line with the pull cable to measure the tension in the cable for test nos. TCBF-1 through TCBF-6. The positioning of the load cells is shown in Figure 36. The data from both load cells was processed and compared to ensure accuracy of the readings. The load cells were manufactured by Transducer Techniques and conformed to model no. TLL-50K with a load range up to 50 kips (222 kN). During testing, output voltage signals were sent from the load cells to a National Instruments data acquisition board, acquired with LabView software, and stored permanently on a personal computer. The data collection rate for the load cells was 1,000 samples per second (1,000 Hz).



Figure 36. Load Cell Arrangement, Test Nos. TCBF-1 through TCBF-6

### 5.3.2 Digital Photography

One AOS VITcam high-speed digital video camera and one JVC standard-speed digital video camera were used to document each test. The AOS high-speed camera had a frame rate of 500 frames per second and the JVC digital video camera had a frame rate of 29.97 frames per second. Both cameras were placed laterally from the barrier test segment, with a view perpendicular to the direction of pull. A Nikon D50 digital still camera was also used to document pre- and post-test conditions for all tests.

### 5.4 Data Processing

For test nos. TCBF-1 through TCBF-6, force data was measured with the load cell transducers and filtered using the SAE Class 60 Butterworth filter conforming to the SAE J211/1 specifications [14]. The pertinent voltage signal was extracted from the bulk of the data signal similar to the acceleration data. The filtered voltage data was converted to load using the following equation:

$$Load = \left[ \frac{1}{Gain} \right] * \left[ \frac{Filtered\ Load\ Cell\ Data}{\left( \frac{(Calibration\ Factor)(Excitation\ Voltage)}{Full - Scale\ Load} \right) * \left( \frac{1V}{1000\ mV} \right)} \right]$$

Details behind the theory and equations used for processing and filtering the load cell data are located in SAE J211/1. The gain and excitation voltage were recorded for each test. The calibration factor varied depending on the specific load cell being used. The load cell data was recorded in a data file and processed in a specifically-designed Excel spreadsheet. Force vs. time plots were created to describe the load imparted to the system.

## **6 FRICTION TESTING RESULTS AND DISCUSSION**

### **6.1 Test Results**

A series of six component tests were conducted to evaluate the barrier-to-ground friction coefficients for unmodified and modified TCB segments on concrete pavement. Three component tests, test nos. TCBF-1 through TCBF-3, were conducted on an unmodified concrete barrier segment. Three tests were conducted in order to determine the best method for loading the TCB segment at a consistent, steady rate. Following the baseline tests of the unmodified TCB segments, three tests, test nos. TCBF-4 through TCBF-6, were conducted on TCB segments with two different durometer neoprene pads adhered to the base. Further details on the individual tests are provided in subsequent sections.

The component testing of the TCB segments sliding on the concrete pavement was instrumented to estimate friction forces and coefficients. When the pulling force was initially applied to the barrier, a noticeable peak in the force vs. time graph was achieved. This peak force was used to calculate the static coefficient of friction between the surfaces by dividing the peak force by the weight of the barrier segment. Once the barrier began to slide on the pavement, the resistive force was reduced. The force readings taken when the barrier was in motion were averaged, and the average force was divided by the weight of the barrier segment to calculate the kinetic coefficient of friction. Several issues arose during testing of the concrete barrier segments due to uneven, stuttered loading of the PCB segment and significant oscillations in the measured pulling force. In some cases the test was completely rerun due to the inconsistent loading and motion of the barrier. However, if the barrier loading yielded a consistent sliding of the barrier the averaged force reading was still considered valid.

### 6.1.1 Test No. TCBF-1

In test no. TCBF-1, a 4,976 lb (2,257 kg) F-shape TCB segment with no additional rubber bearing pad was pulled on the concrete tarmac using an electric winch. The test setup is shown in Figure 37 and the corresponding force vs. time data is shown in Figure 38. During test no. TCBF-1, the barrier and winch setup did not achieve a constant-velocity pull required to establish the kinetic friction coefficient. Instead, the barrier winch loaded the barrier segment in a start-and-stop motion. The start-and-stop oscillation in the motion was observed in the video analysis and was apparent on the force vs. time graph. The motion of the barrier prevented determination of a consistent sliding force as the barrier moved, thus the data from the test was not usable for determination of friction coefficients.



Figure 37. Pull Test Setup, Test No. TCBF-1

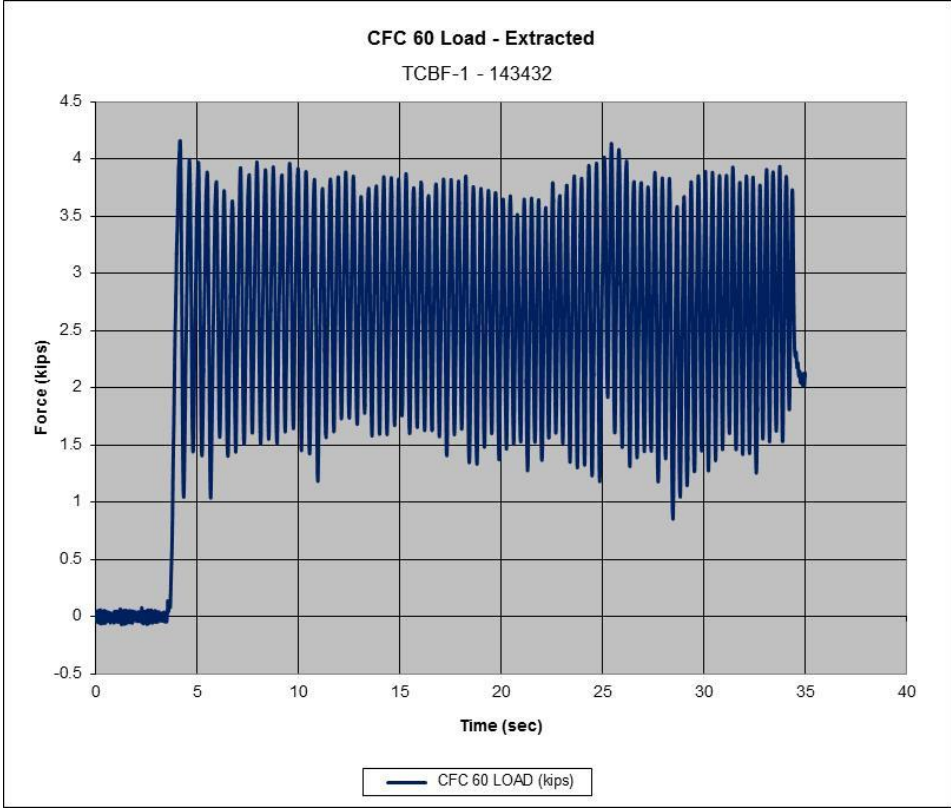
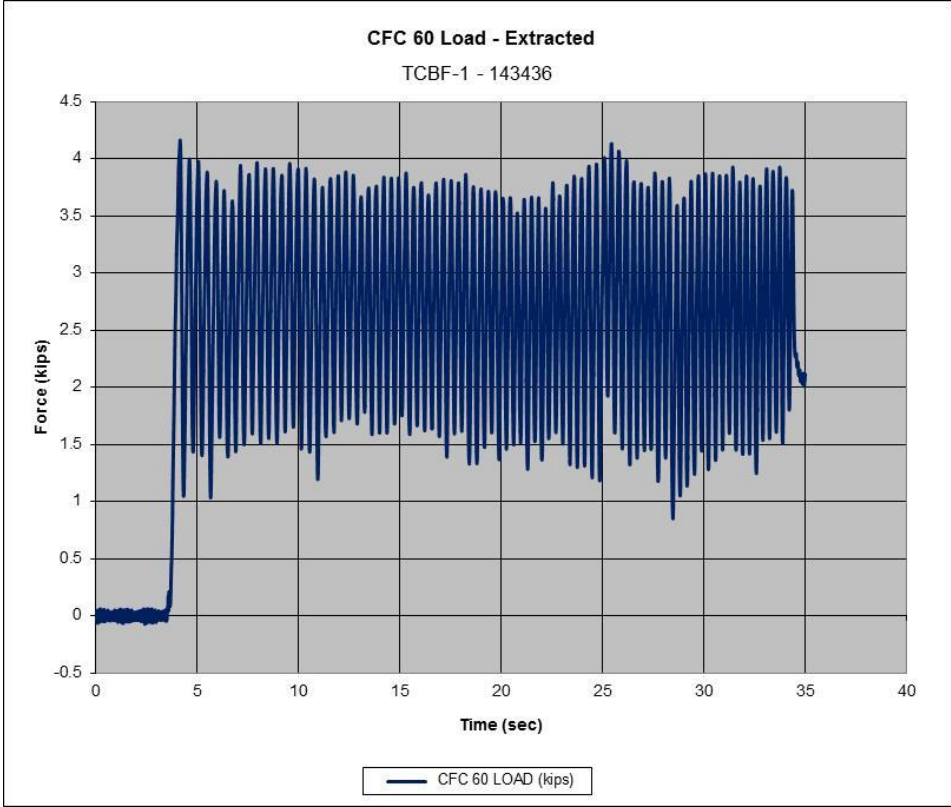


Figure 38. Force vs. Time, Test No. TCBF-1

### 6.1.2 Test No. TCBF-2

In test no. TCBF-2 the test setup was modified to address the stop and start motion observed in test no. TCBF-1. In test no. TCBF-2 the winch was replaced with a skid-steer loader in order to provide a more consistent velocity and displacement to the barrier segment. The loader was connected to the barrier segment similar to the winch setup. The operator then pulled the barrier at a constant speed for the test. The test setup is shown in Figure 39. The skid-steer was able to produce a much steadier barrier velocity throughout the test. The force vs. time graphs are shown for both load cells in Figure 40. The static and kinetic coefficients of friction between the concrete surfaces were determined to be 0.72 and 0.44, respectively.



Figure 39. Pull Test Setup, Test No. TCBF-2

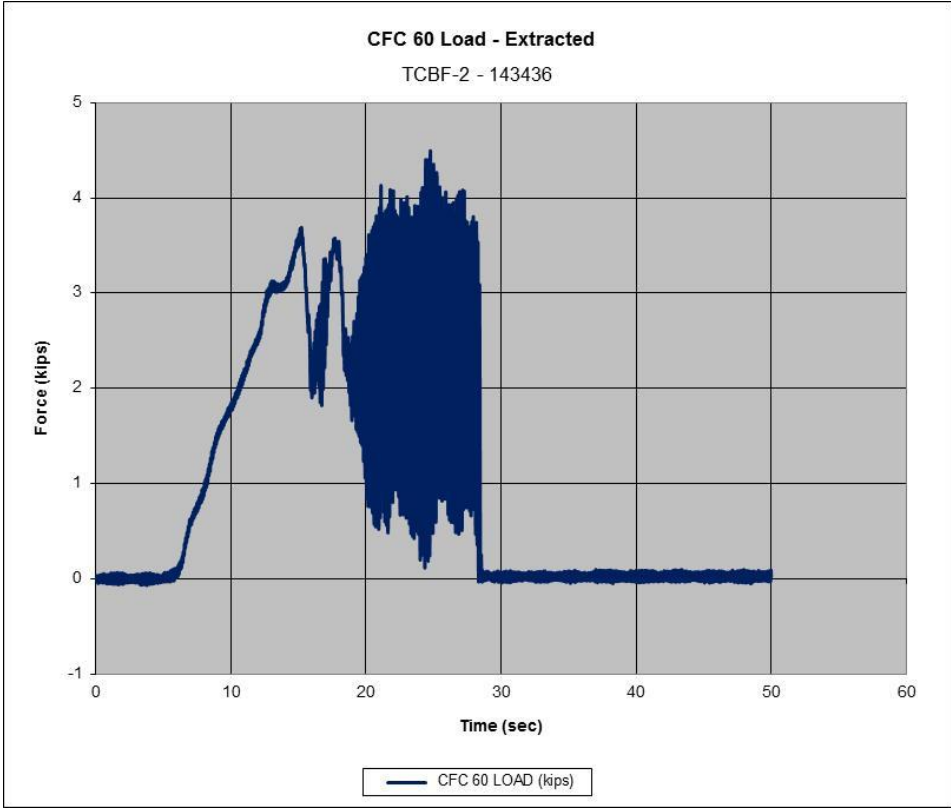
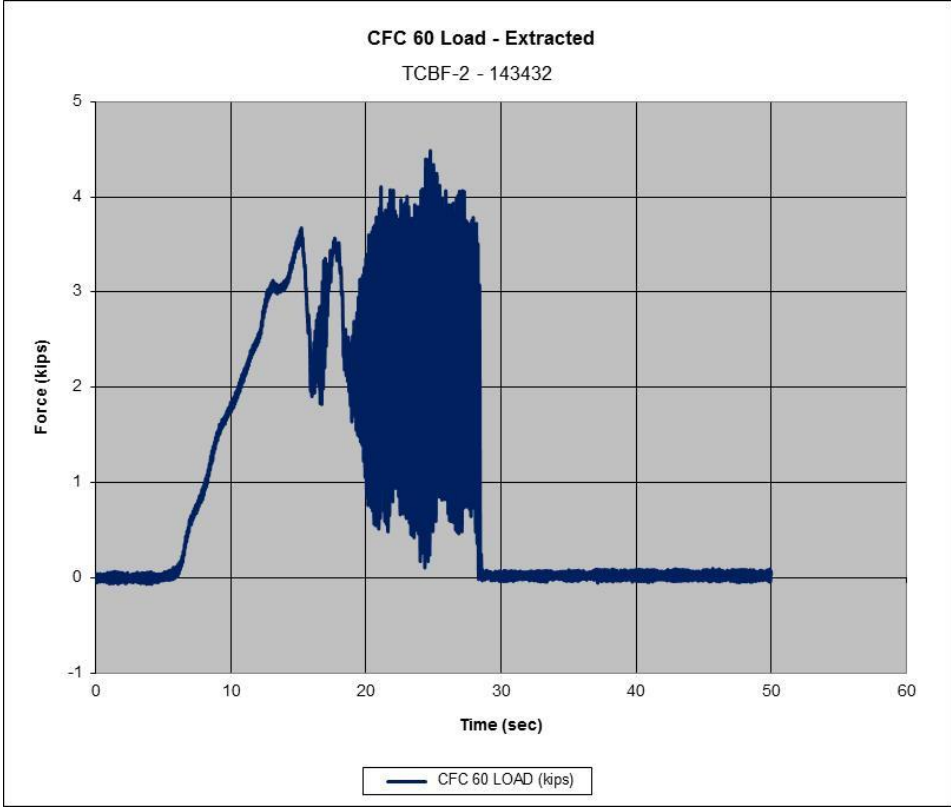


Figure 40. Force vs. Time, Test No. TCBF-2

### 6.1.3 Test No. TCBF-3

In test no. TCBF-3, a third method for pulling the TCB segment across the ground was attempted. For this test, an electric winch was again used on to pull the concrete barrier with no additional rubber bearing pad. The load cells were hooked directly to the lowest connection loop of the barrier to observe the pulling motion without the pin. The modified test setup is shown in Figure 41. During test no. TCBF-3, the barrier and winch setup did not achieve a constant velocity pull required to establish the kinetic friction coefficient. Instead the barrier winch loaded the barrier segment in a start-and-stop motion. The start-and-stop oscillation in the motion was observed in the video analysis and was apparent on the force vs. time graph. The motion of the barrier prevented determination of a consistent sliding force as the barrier moved, thus the data from the test was not usable for determination of friction coefficients.

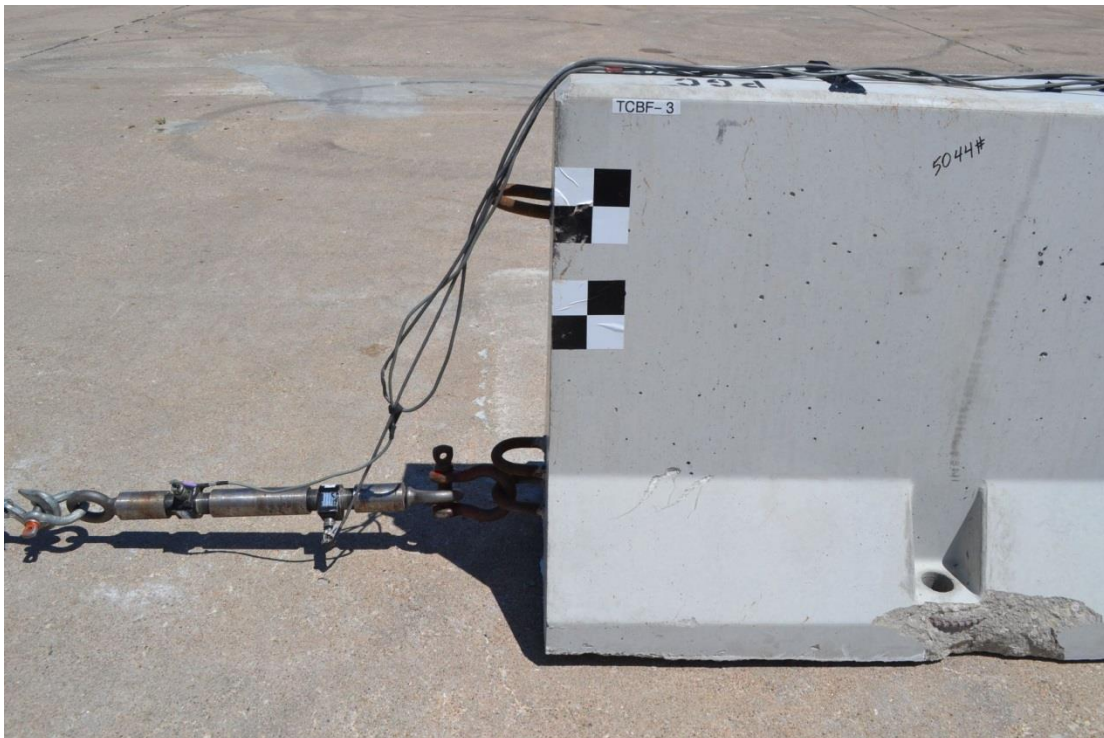


Figure 41. Pull Test Setup, Test No. TCBF-3

#### **6.1.4 Test No. TCBF-4**

In test no. TCBF-4, a  $\frac{3}{8}$ -in. (10-mm) thick rubber bearing pad was adhered to the base of the concrete barrier using a trowel-grade, polyurethane adhesive. The bearing pad had a durometer value of 70. In test no. TCBF-4, the load cell was directly hooked to the lower connection loop on the barrier as in test no. TCBF-3 and pulled with an electric winch. During the test the rubber remained bonded to the base of the barrier and the sliding motion was steady enough to allow force measurements to be taken. The force vs. time graphs for test no. TCBF-4 are shown in Figure 42. The static and kinetic friction coefficients between the 70-durometer bearing pad and the concrete tarmac were found to be 1.01 and 0.62, respectively. After the test was conducted two rubber wear marks parallel to the direction of the pull were observed on the concrete in the path of the barrier as shown in Figure 43.

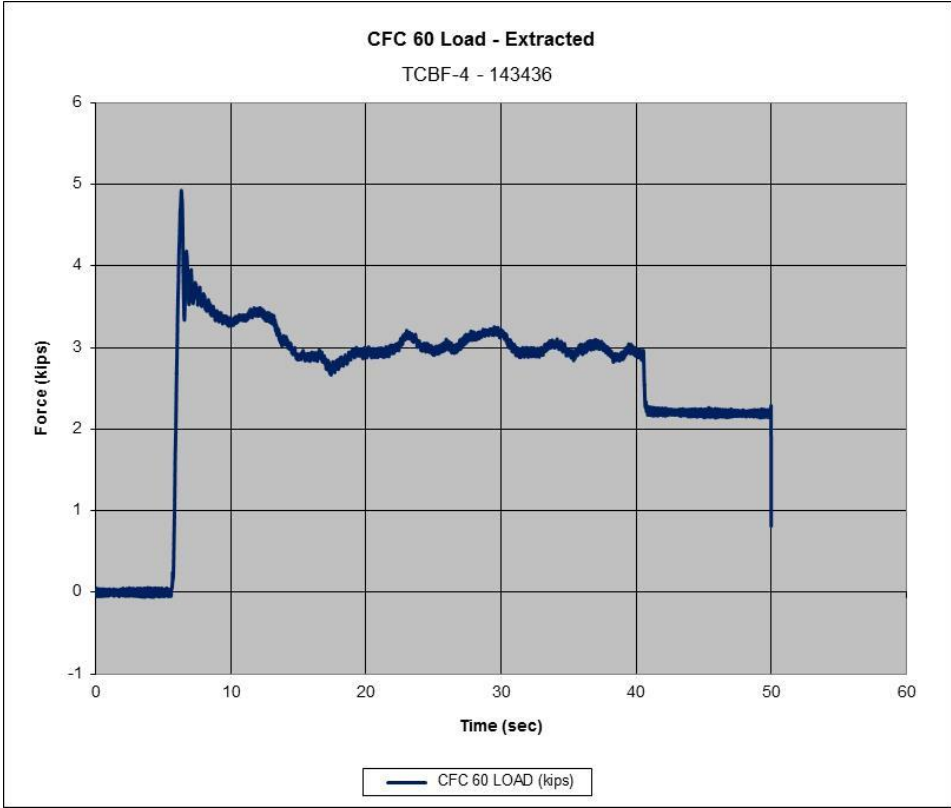
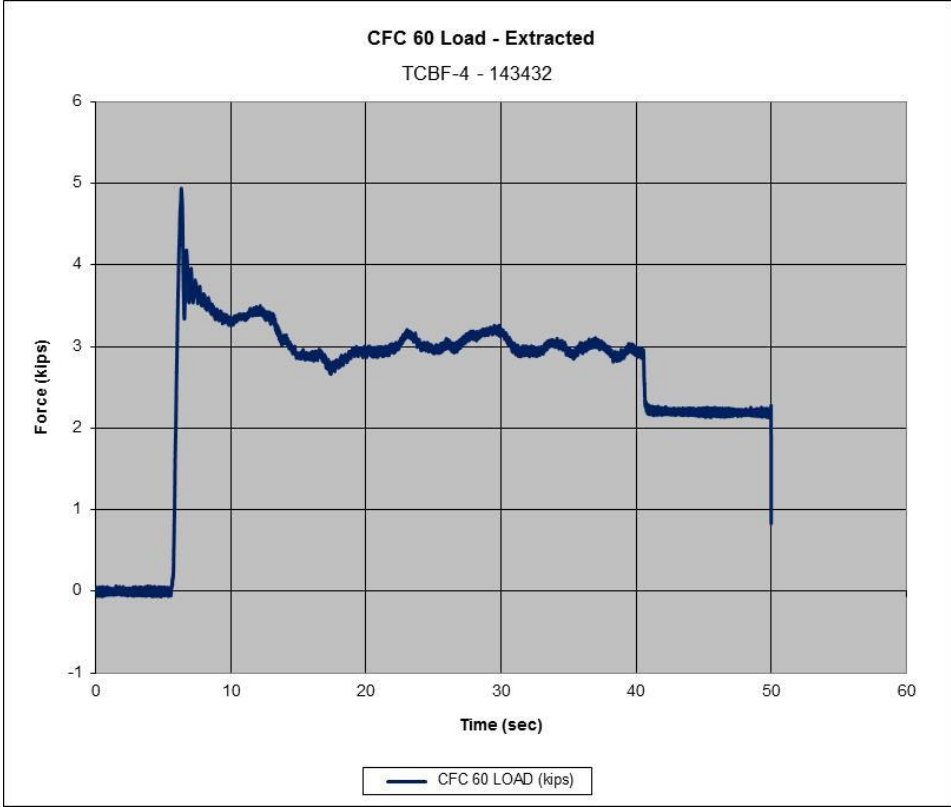


Figure 42. Force vs. Time, Test No. TCBF-4



Figure 43. Rubber Wear Marks, Test No. TCBF-4

### **6.1.5 Test No. TCBF-5**

In test no. TCBF-5, a  $\frac{3}{8}$ -in. (10-mm) thick rubber bearing pad was adhered to the base of the concrete barrier using a trowel-grade, polyurethane adhesive. The bearing pad had a durometer value of 50. In test no. TCBF-5, the load cell was directly hooked to the lower connection loop on the barrier as in test no. TCBF-3 and pulled with an electric winch. During the test the adhesive bond between the concrete and rubber failed, allowing the rubber to roll under the barrier segment. As such, the force data for TCBF-5 was not usable and the test was rerun.

### **6.1.6 Test No. TCBF-6**

In test no. TCBF-6, a  $\frac{3}{8}$ -in. (10-mm) thick rubber bearing pad was adhered to the base of the concrete barrier using a trowel-grade, polyurethane adhesive. The bearing pad had a durometer value of 50. In test no. TCBF-6, the load cell was directly hooked to the lower connection loop on the barrier as in test no. TCBF-3 and pulled with an electric winch. During the test the rubber remained bonded to the base of the barrier and the sliding motion was steady enough to allow force measurements to be taken. The static and kinetic friction coefficients between the 50-durometer bearing pad and the concrete tarmac were found to be 0.95 and 0.76, respectively. The force vs. time graphs for test no. TCBF-6 are shown in Figure 44.

## **6.2 Test Results**

The results from the component testing of the TCB friction coefficients with and without neoprene bearing pads on a concrete tarmac are summarized in

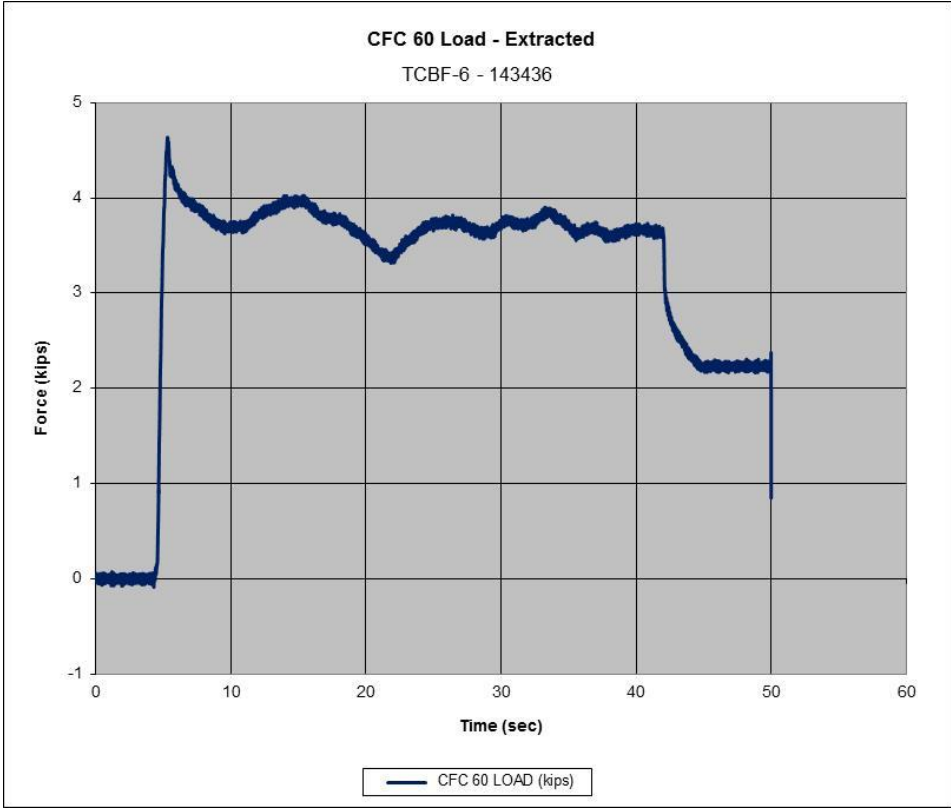
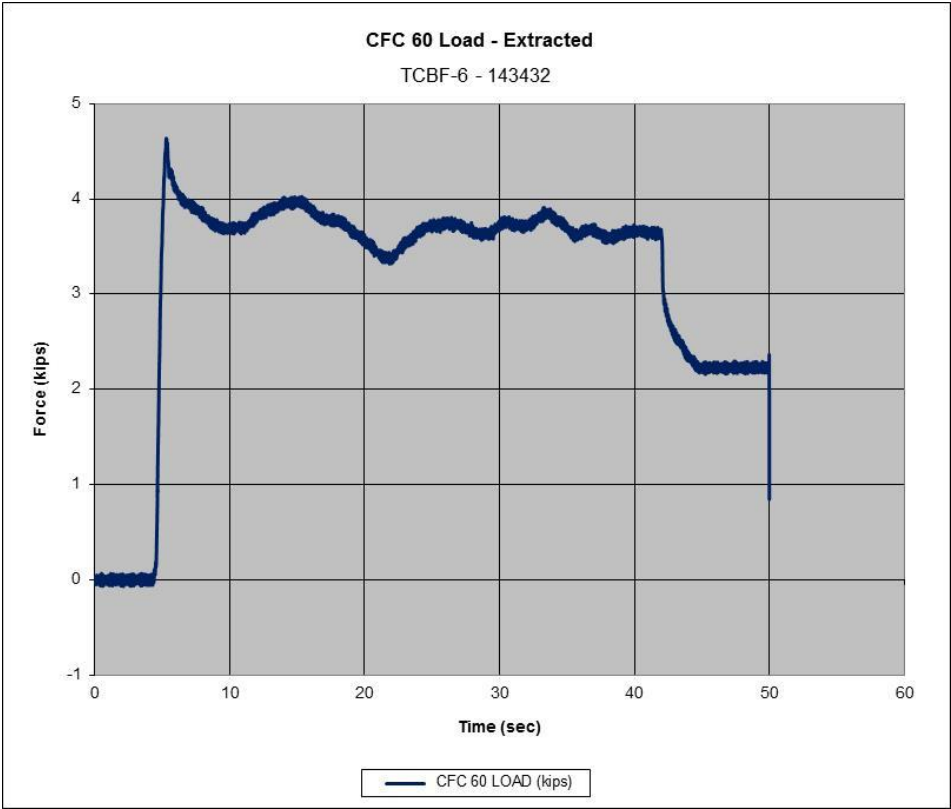


Figure 44. Force vs. Time, Test No. TCBF-6

Table 4. Note that three tests, test nos. TCBF-1, TCBF-3, and TCBF-5 were unusable due to inconsistent barrier motion or failure of the neoprene adhesion. However, the three remaining tests provided valuable friction data for the research effort.

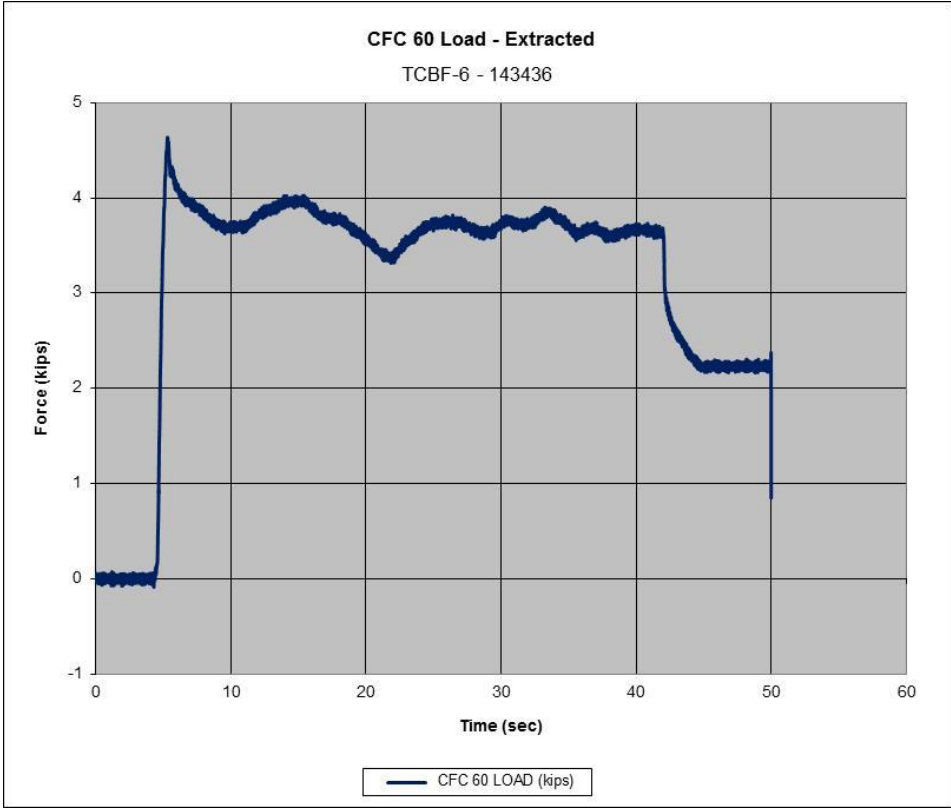
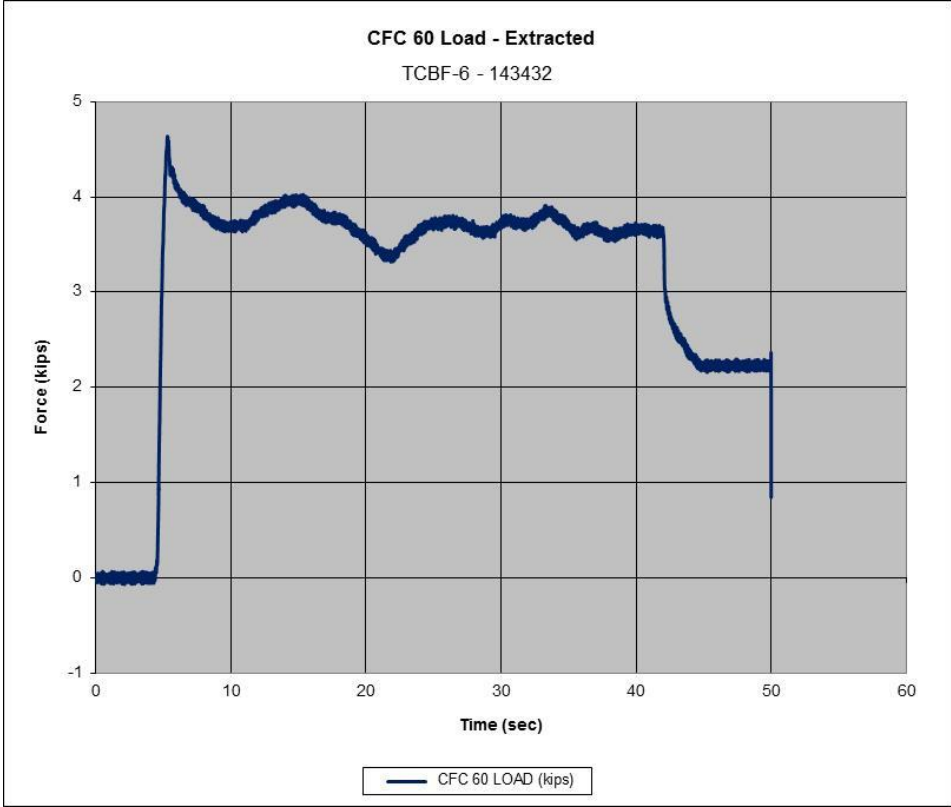


Figure 44. Force vs. Time, Test No. TCBF-6

Table 4. Component Testing Results, Test Nos. TCBF-1 through TCBF-6

Test No.	TCB Base Material	Barrier Weight lbs (N)	Peak Force lbs (N)		Average Force lbs (N)		Friction Coefficients			
			Load Cell 1	Load Cell 2	Load Cell 1	Load Cell 2	Static		Kinetic	
							Load Cell 1	Load Cell 2	Load Cell 1	Load Cell 2
TCBF-1	Concrete	4,976 (22,134)	NA	NA	NA	NA	NA	NA	NA	NA
TCBF-2	Concrete	4,976 (22,134)	3,566 (15,862)	3,579 (15,920)	2,202 (9,795)	2,210 (9,831)	0.72	0.72	0.44	0.44
TCBF-3	Concrete	4,976 (22,134)	NA	NA	NA	NA	NA	NA	NA	NA
TCBF-4	Rubber D70	4,900 (21,796)	4,939 (21,970)	4,925 (21,908)	3,034 (13,496)	3,035 (13,500)	1.01	1.01	0.62	0.62
TCBF-5	Rubber D50	4,972 (22,117)	NA	NA	NA	NA	NA	NA	NA	NA
TCBF-6	Rubber D50	4,972 (22,117)	4,635 (20,618)	4,636 (20,622)	3,705 (16,481)	3,710 (16,503)	0.95	0.95	0.76	0.76

In test no. TCBF-2, the force levels for the motion of the concrete TCB base on the concrete tarmac generated static and kinetic coefficients of friction of 0.72 and 0.44, respectively. These values corresponded well with the 0.40 kinetic coefficient of friction reported previously by TTI and the 0.40 kinetic coefficient of friction value used in the baseline modeling of the F-shape TCB.

In test nos. TCBF-4 and TCBF-6, the addition of the rubber bearing pad clearly increased the frictional resistance of the TCB segments. The addition of the 70-durometer rubber increased the static and kinetic coefficients of friction to 1.01 and 0.62, respectively, while the addition of the 50-durometer rubber increased the static and kinetic coefficients of friction to 0.95 and 0.76, respectively. The increase in the kinetic coefficient of friction was important to note because the kinetic impact energy of the vehicle during a TCB impact is largely dissipated through sliding friction of the TCB segments. Thus an increased kinetic friction coefficient would tend to produce reduced barrier deflections. There is also potential for the increased friction to promote barrier tipping due to the moment created by the friction at the base of the barrier and the vehicle impact load. However, the tipping of the barrier segment would be mitigated to some degree by

the barrier segment connections. In addition, the simulation of the TCB with increased friction indicated only minor increases in the vertical rotation of the barrier segments.

The 50-durometer neoprene used in test no. TCBF-6 increased the kinetic coefficient of friction more than the 70-durometer neoprene used in test no. TCBF-4. The 50-durometer neoprene was softer than the 70-durometer neoprene. Thus, the softer neoprene was expected to provide increased deflection and engagement of the rubber into the disparities of the concrete tarmac, thus generating increased friction. The results of test nos. TCBF-4 and TCBF-6 found that the softer neoprene had a slightly lower static coefficient of friction, which was unexpected.

The friction values determined from the testing with the neoprene bearing pads correlated closely with the assumed kinematic friction values of 0.6 and 0.8 used in the LS-DYNA simulations conducted during the parametric study of deflection-limiting mechanisms. Thus, it appeared that increased friction levels could be produced by simple barrier modifications, and that the reductions in barrier deflection observed during the parametric study simulation modeling may be feasible. As such, it may be possible for future TCB designs to incorporate rubber bearing pads as a means to help limit barrier deflection. If this method were employed, further research would need to be conducted to determine the best strategy for attaching the rubber to the concrete barrier, or to potentially investigate other mechanisms for increasing friction.

## **7 CONCRETE MATERIAL MODELING**

In addition to the investigation of deflection-limiting mechanisms for TCB systems, a portion of the research effort for this project was devoted to evaluation of concrete material modeling in LS-DYNA. In recent years, several concrete material models have been developed for LS-DYNA that can be applied for simulation of reinforced concrete structures under dynamic impact. One material model for concrete was specifically developed for use in the simulation of roadside safety devices under impact loading. MAT\_159 Continuous Surface Cap Model (CSCM) was developed by Aptek through a research project with the Federal Highway Administration (FHWA) [15-16]. This material model claims to provide for the capability to accurately model the structural response of concrete under various load conditions including capturing concrete damage and fracture.

Limited research has been conducted by TTI regarding the use of this model for roadside safety hardware [17-18], and no research to date has used the material model for analysis of TCB segments. TTI's previous evaluation of the material model found some preliminary recommended settings for the model, but noted that these settings may not be applicable for a wide range of simulations. However, the use of this material model could provide a great deal of insight into the performance and damage of TCB sections using reduced-deflection mechanisms developed in this research. As such, an effort was made to review the MAT\_159\_CSCM material model to determine its functionality and applicability to this research.

### **7.1 MAT\_159\_CSCM**

In order to evaluate the use of the MAT\_159\_CSCM material model for this research effort, the researchers reviewed the model, its input parameters, previous simulation efforts using the model published with its release, and subsequent simulation efforts by TTI. Following review of the previous research, it was decided to evaluate the material model through a series of

simulations. The first phase of the material model investigation consisted of simple models of concrete cylinders that were subjected to tension and compression. These models were reviewed and analyzed to determine best practices for using the model in more complex simulations. Next, models of a reinforced concrete beam loaded in flexure were conducted and reviewed. Results from both sets of concrete models as well as conclusions regarding the use of MAT\_159\_CSCM are discussed in more detail in subsequent sections.

MAT\_159\_CSCM functions with very basic input parameters. For the purposes of creating the initial material model, the user need only supply the concrete compressive strength, density, aggregate size, and some basic model control parameters. The model then generates a variety of material parameters for the concrete based on these inputs as well as inputs for controlling the various functions of the material model itself. If desired, these generated material model parameters can be edited by the user to control the material behavior. A summary of these material parameters is shown in Table 5.

For the purposes of this effort, concrete cylinder data and reinforced concrete beam details were obtained from component testing efforts performed at MwRSF as part of the development of the MAT\_159\_CSCM material model [19]. The concrete used in those component tests had a concrete compressive strength of 6,705 psi (0.046 GPa) and maximum aggregate size of 1 in. (25 mm). Thus, these values were used as the primary material model inputs. The remaining model parameters and their variations as part of the investigation of the material model itself will be discussed in the subsequent sections.

Table 5. MAT\_159\_CSCM Input Variables

Card No.	Variable	Description	Symbol	Origin
1	MID	material identification	-	-
	RO	mass density	$\rho$	sample properties
	NPLOT	component 7 for d3plot database	-	list
	INCRE	maximum strain increment	-	
	IRATE	rate effects option	-	list
	ERODE	element erosion for damage exceedance	-	
	RECOV	recovery modulus in compression	-	list
	ITRETRC	cap retraction option	-	list
2	PRED	pre-existing damage	-	sample properties
3	FPC	unconfined compression strength	$f'_c$	uniaxial compression test
	DAGG	maximum aggregate size	$D_{agg}$	sieve analysis
	UNITS	units options	-	list
3	G	shear modulus	G	calculate
	K	bulk modulus	K	calculate
	ALPHA	tri-axial compression surface constant	$\alpha$	TXC test curve fit
	THETA	tri-axial compression linear term	$\theta$	TXC test curve fit
	LAMBDA	tri-axial compression non-linear term	$\lambda$	TXC test curve fit
	BETA	tri-axial compression surface exponent	$\beta$	TXC test curve fit
	NH	hardening initiation	$N_H$	$0.7 < N_H < 1.0$
	CH	hardening rate	$C_H$	
4	ALPHA1	torsion surface constant term	$\alpha_1$	TXC test curve fit
	THETA1	torsion surface linear term	$\theta_1$	TXC test curve fit
	LAMBDA1	torsion surface non-linear term	$\lambda_1$	TXC test curve fit
	BETA1	torsion surface exponent term	$\beta_1$	TXC test curve fit
	ALPHA2	tri-axial extension surface constant	$\alpha_2$	TXC test curve fit
	THETA2	tri-axial extension linear term	$\theta_2$	TXC test curve fit
	LAMBDA2	tri-axial extension non-linear term	$\lambda_2$	TXC test curve fit
	BETA2	tri-axial extension surface exponent	$\beta_2$	TXC test curve fit
5	R	cap aspect ratio	R	fit to P-V strain curves
	XO	cap initial location	$X_0$	fit to P-V strain curves
	W	maximum plastic volume compaction	W	fit to P-V strain curves
	D1	linear shape parameter	$D_1$	fit to P-V strain curves
	D2	quadratic shape parameter	$D_2$	fit to P-V strain curves
6	B	ductile shape softening parameter	B	softening curve
	GFC	fracture energy in uniaxial stress	$G_{fc}$	uniaxial compression test
	D	brittle shape softening parameter	D	softening curve
	GFT	fracture energy in uniaxial tension	$G_{ft}$	uniaxial tension test
	GFS	fracture energy in pure shear stress	$G_{fs}$	direct shear test
	PWRC	shear-to-compression transition parameter	-	
	PWRT	shear-to-tension transition parameter	-	
	PMOD	moderate pressure softening parameter	-	
7	ETA0C	rate effects parameter for uniaxial compressive stress	$\eta_{0c}$	uniaxial compression test
	NC	rate effects power for uniaxial compressive stress	$N_c$	uniaxial compression test
	ETA0T	rate effects parameter for uniaxial tensile stress	$\eta_{0t}$	uniaxial tension test
	NT	rate effects power for uniaxial tensile stress	$N_t$	uniaxial tension test
	OVERC	maximum overstress allowed in compression	-	
	OVERT	maximum overstress allowed in tension	-	
	SRATE	ratio of effective shear stress to tensile stress	-	direct shear test
	REPOW	power which increases fracture energy with rate effects	-	

## 7.2 Concrete Cylinder Models

The first task in reviewing and evaluating the MAT\_159\_CSCM material model consisted of analysis of simple models of concrete cylinders to determine the models' behavior when loaded in compression and tension. The focus of these models was to gauge the performance of the model under basic loading conditions and to determine material input parameters. As noted in a previous section, TTI performed previous evaluations of the material model and had determined some basic guidance regarding the modifications to the default parameters that improved the material model behavior. The implementation guidance from the research performed by TTI was used as a starting point in these models and was then modified to further investigate the performance of the material model.

The first step in the analysis of the material model was the determination of proper inputs for the model. As noted previous, MAT\_159\_CSCM can be used with a very basic set of input parameters. The material model then generates the data for the extended input parameters. Thus, for this study, the MAT\_159\_CSCM model was first run by entering only the compressive strength and aggregate size to generate the extended model input. The extended model input was then taken from this initial LS-DYNA model and used to create the extended impact card that was used in the remainder of the analysis. The extended input for MAT\_159\_CSCM used in this study is shown in Figure 45.

Following generation of the extended material model input, it was decided to simulate both compression and tension models using MAT\_159\_CSCM. The material parameters would generally follow the guidance previously provided by the model creator and TTI regarding its use. The simulation effort then modified critical model parameters, mesh size, and boundary conditions to evaluate the model performance. TTI had noted that the value of the REPOW parameter, which increases fracture energy with rate effects, and the ratio of the fracture energy

in shear and tension (Gfs/Gft) were critical to proper model behavior. It was also noted that the value of ERODE, which determines the element erosion criteria, should be set greater than 1 and that the value given for the ERODE parameter had a significant effect on performance. The values for IRATE, which activates strain rate effects, and RECOV, which defines the recovery modulus in compression, were also utilized for adjusting material model performance. Boundary conditions were varied and two mesh sizes were examined as well. More complete details of the simulation of compression and tension loading of concrete cylinders is discussed in the subsequent section.

\*MAT\_CSCM\_(TITLE) (159) ( 10 )

---

**TITLE**

1 **MID**      **RO**      **NPLOT**      **INCR**      **IRATE**      **ERODE**      **RECOV**      **ITRETRC**

2 **PRED**

3 **G**      **K**      **ALPHA**      **THETA**      **LAMDA**      **BETA**      **NH**      **CH**

4 **ALPHA1**      **THETA1**      **LAMDA1**      **BETA1**      **ALPHA2**      **THETA2**      **LAMDA2**      **BETA2**

5 **R**      **XD**      **W**      **D1**      **D2**

6 **B**      **GFC**      **D**      **GFI**      **GFS**      **PWRC**      **PWRT**      **PMOD**

7 **ETA0C**      **NC**      **ETA0T**      **NT**      **OVERC**      **OVERT**      **SRATE**      **REPOW**

**COMMENT:**

---

Figure 45. MAT\_159\_CSCM Extended Input

### 7.2.1 Compression Cylinder Simulations

In order to evaluate the performance of MAT\_159\_CSCM for simulation of concrete compression, a model was created with ten 6-in. diameter x 12-in. tall (152-mm diameter x 305-mm tall) concrete cylinders. Ten cylinders were placed in each model such that several variations on the model parameters could be varied and compared in a single model run more easily. The model used a 1 in. (25 mm) mesh size for the initial simulations that was later reduced to ½ in. (13 mm). The basic model setup is shown in Figure 46. For the initial model of the concrete cylinder compression, ten variations of the model parameters were run to vary the REPOW, ERODE, and  $G_{fs}/G_{ft}$  values as well as to vary the constraints on the cylinder ends. The remaining material model parameters were left at the default values. The ten cases evaluated are shown in Table 6. The cylinders were loaded in compression by placing a fixed rigid wall at the base of the cylinders and compressing each cylinder with a moving rigid wall at the top. Forces and displacements were measured using cross-sections, rigid wall forces, rigid wall displacements, and nodal displacements.

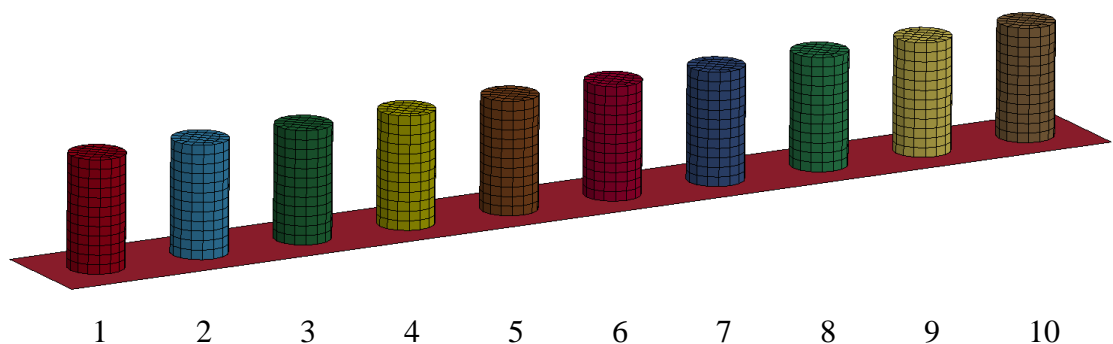


Figure 46. Concrete Cylinder Compression Model Setup

Table 6. MAT\_159\_CSCM Concrete Cylinder Simulation, Cases 1- 10

Case No.	ERODE	REPOW	$G_{fs}/G_{ft}$	Boundary Conditions
1	0.0	1.0	1.0	Top and bottom nodes of the cylinder are constrained from moving in x and y direction
2	0.0	1.0	0.5	Top and bottom nodes of the cylinder are constrained from moving in x and y direction
3	1.05	1.0	0.5	Top and bottom nodes of the cylinder are constrained from moving in x and y direction
4	1.10	1.0	0.5	Top and bottom nodes of the cylinder are constrained from moving in x and y direction
5	0.0	0.0	0.5	Top and bottom nodes of the cylinder are constrained from moving in x and y direction
6	0.0	1.0	1.0	Top and bottom nodes of the cylinder are unconstrained
7	0.0	1.0	0.5	Top and bottom nodes of the cylinder are unconstrained
8	1.05	1.0	0.5	Top and bottom nodes of the cylinder are unconstrained
9	1.10	1.0	0.5	Top and bottom nodes of the cylinder are unconstrained
10	0.0	0.0	0.5	Top and bottom nodes of the cylinder are unconstrained

The first simulation run of the concrete cylinder compression, Run 1, used the material parameter data in Table 6 and the 1 in. (25 mm) mesh size. Results from that model found that the MAT\_159\_CSCM produced consistent and accurate compressive strengths for all ten of the simulation cases. The simulation model returned a maximum compression strength of 6,360 psi (0.044 GPa) which corresponded well with the input compressive strength of 6,705 psi (0.046 GPa). It was noted that the variation of the constraints on the cylinder had no effect on peak compressive load, but did affect the post-peak loading and overall internal energy of the cylinder, as shown in Figure 47. Deformation and element erosion of the cylinder models were not as consistent or predictable. None of the elements in the models eroded as would be expected once the peak compressive stress was reached, and deformation appeared to be unstable after the peak

compressive loads were reached, as shown in Figure 48. Hourglass energies were reasonable even with the observed unstable deformation. Thus, initial simulation of the concrete cylinder compression showed some promise based on compressive loading, but gross material behavior in terms of fracture and deformation was not as expected.

A second simulation model of the ten cylinder compressions, Run 2, was conducted using  $IRATE = 1$  and  $RECOV = 10$ . Previous  $MAT\_159\_CSCM$  modeling by TTI suggested that these values could improve the model response.  $IRATE$  would turn on rate effects in the material model and  $RECOV$  would alter the recovery modulus in compression. Results from the second simulation found that all ten cases provided reasonable and accurate compression strengths. The maximum compressive stress varied from 7,079 psi to 7,194 psi (0.049 to 0.050 GPa). These values were close to the input compressive strength of 6,705 psi (0.046 GPa) and were expected to be slightly increased due to the inclusion of rate effects in this simulation. Variation of the constraints on the cylinder had a minor effect on peak compressive load in these models, and it did not affect the post-peak loading and overall internal energy of the cylinder to the degree observed in the previous model, as shown in Figure 49. Deformation of the concrete cylinders seemed to be slightly improved in this simulation and element erosion was observed in some of the cases, as shown in Figure 50. However, the deformation of the cylinders still showed instability, and high hourglass energies were observed in case nos. 2 and 5.

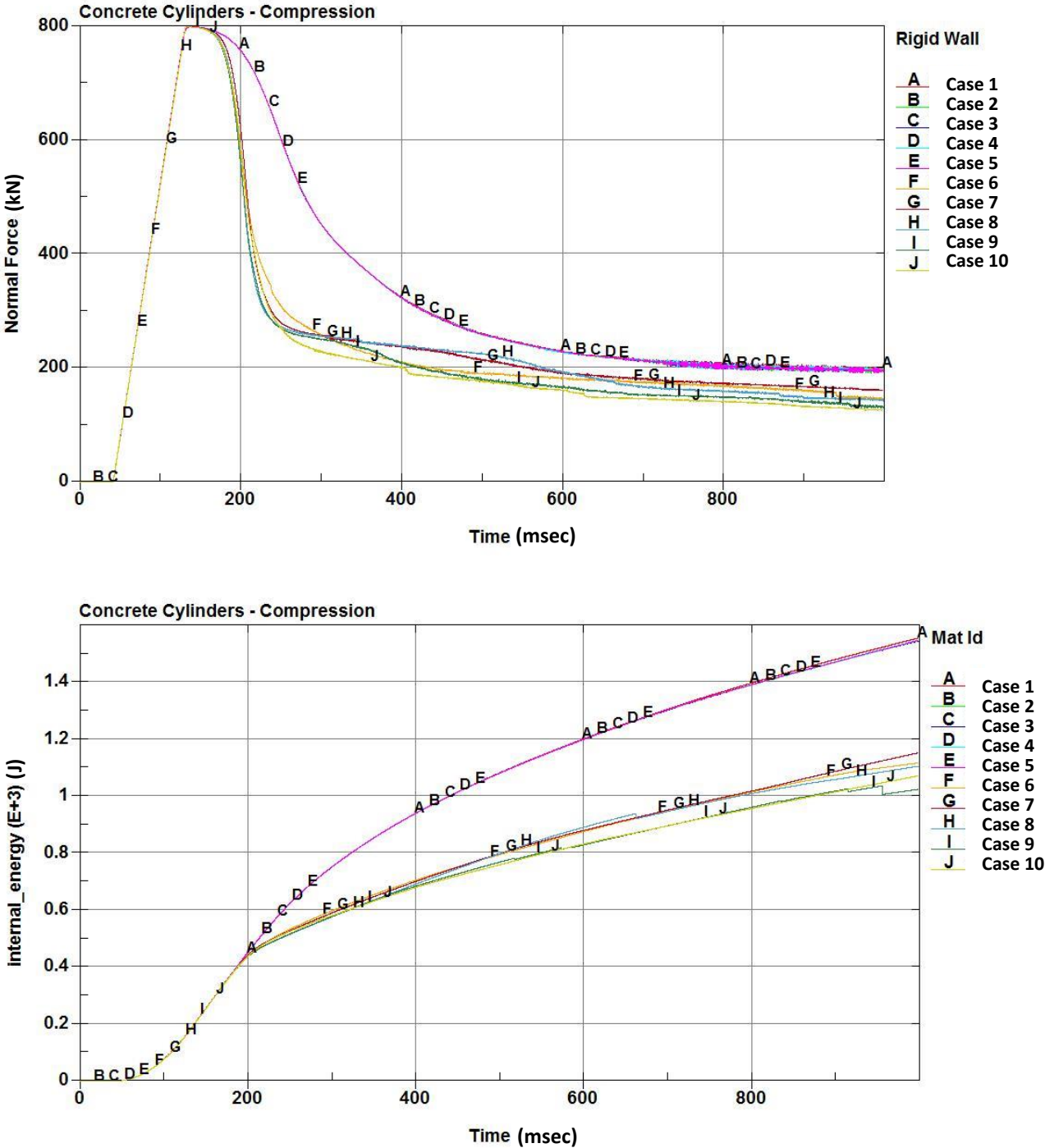
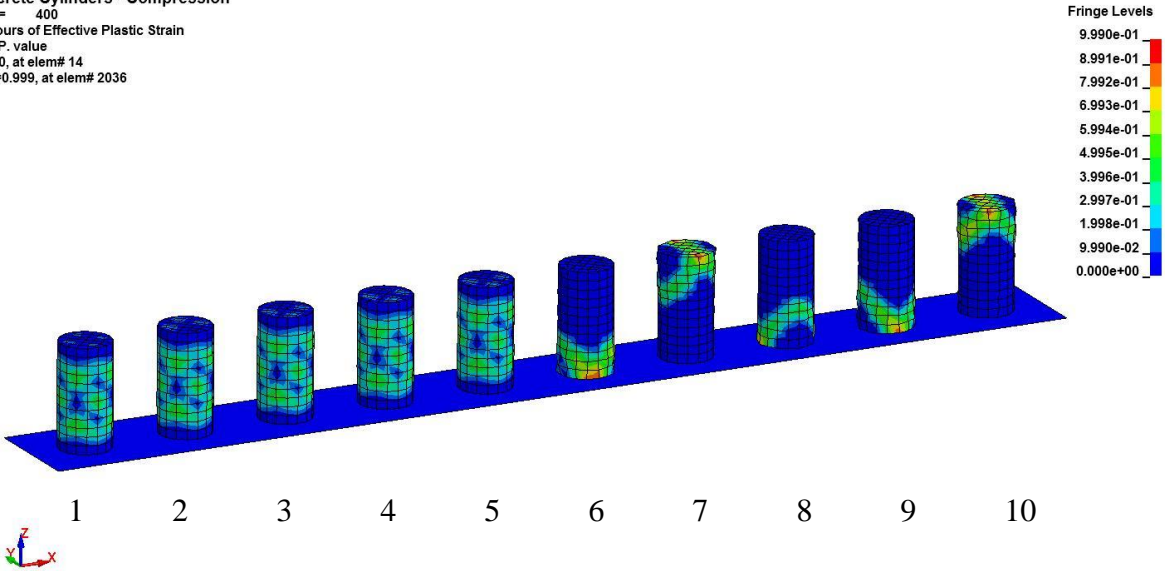


Figure 47. Force and Internal Energy Vs. Time, Concrete Cylinder Compression – Run 1

Concrete Cylinders - Compression  
Time = 400  
Contours of Effective Plastic Strain  
max IP. value  
min=0, at elem# 14  
max=0.999, at elem# 2036



Concrete Cylinders - Compression  
Time = 1000  
Contours of Effective Plastic Strain  
max IP. value  
min=0, at elem# 14  
max=0.999, at elem# 2036

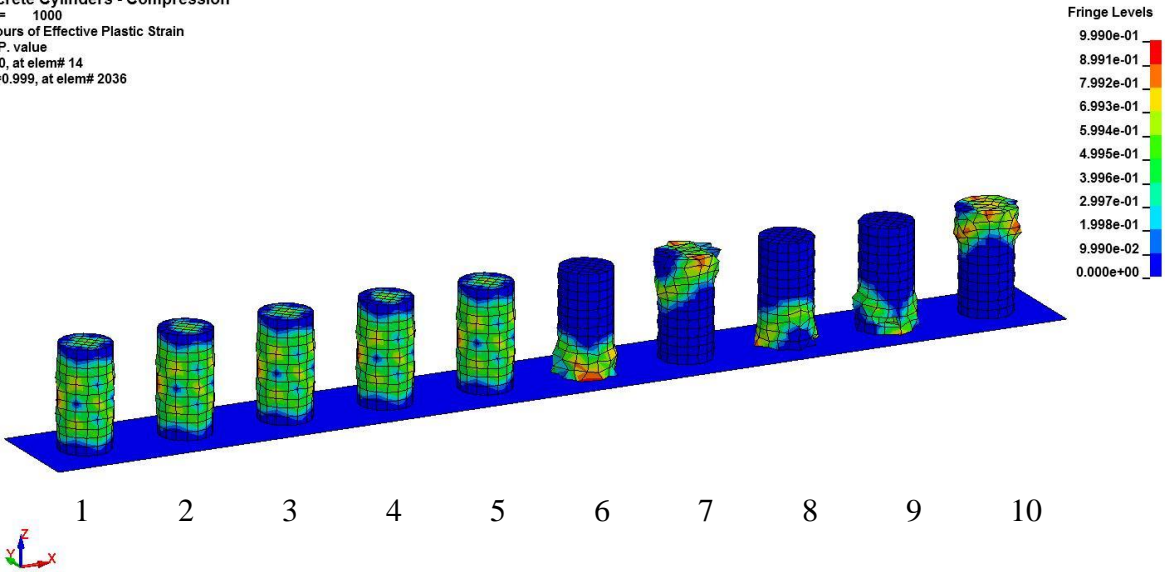


Figure 48. Deformation and Damage, Concrete Cylinder Compression – Run 1

Two additional simulation runs were conducted by repeating the first two simulation runs described above, with the mesh size reduced by one half. Thus, Run 3 was a repeat of Run 1 and Run 4 was a repeat of Run 2. The results from Run 3 found that reduced mesh size improved the model response somewhat. The compressive strength for all ten cylinder models in Run 3 was found to be an average of 6,498 psi (0.045 GPa), which was closer to the input compressive strength of 6,705 psi (0.046 GPa) than the value observed in Run 1. This suggested that reduction of the mesh size improved the compression strength response. Variation of the cylinder constraints had similar effects on the material response in Runs 1 and 3. The deformation of the cylinders still appeared to be somewhat unstable, but hourglass energies remained low, as shown in Figure 51. Element erosion was not observed in any of the ten cylinders in the simulation. The damage of the concrete cylinders in the model did appear to improve in displaying the characteristic “X” bands of damage to the material that are expected for the cylinders with constrained ends [16]. These bands were not evident at the larger mesh sizes.

The results from Run 4 also showed that reduced mesh size affected the material model response. Mesh size appeared to affect compression strength slightly as the compressive strength of the concrete cylinders increased to 7,321 psi (0.051 GPa) as compared to the range of 7,079 psi to 7,194 psi (0.049 to 0.045 GPa) observed in Run 2. Deformation of the concrete cylinders seemed to be slightly improved with reduced mesh size and element erosion was observed in some of the cases, as shown in Figure 52. However, the deformation of the cylinders still showed instability, and high hourglass energies were observed in case nos. 3 and 5. The concrete cylinders with reduced mesh size in Run 4 demonstrated a much different post-peak force reduction from previous models, as shown in Figure 53. This resulted in significantly higher energy levels for Run 4 as compared to the previous models.

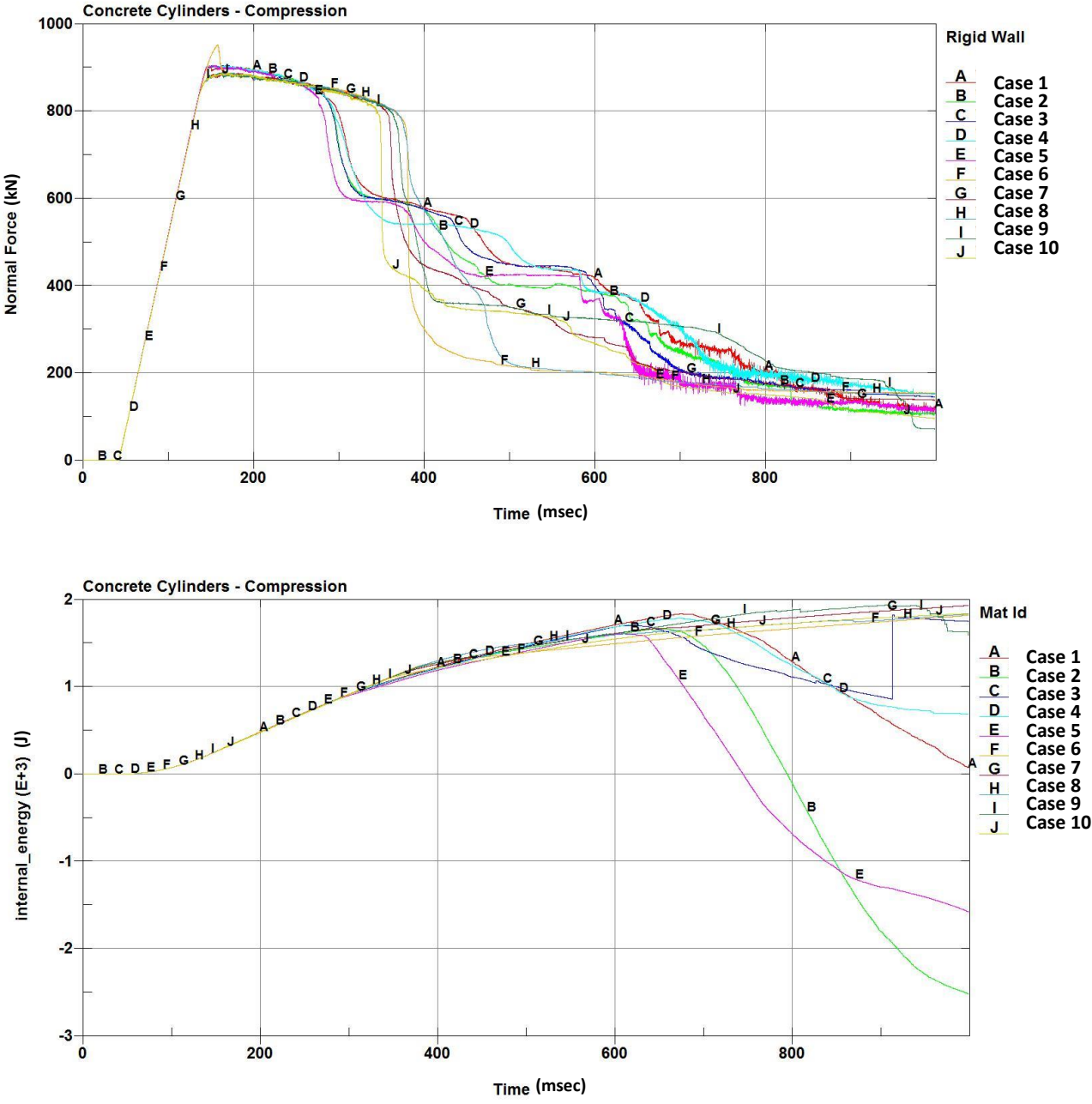
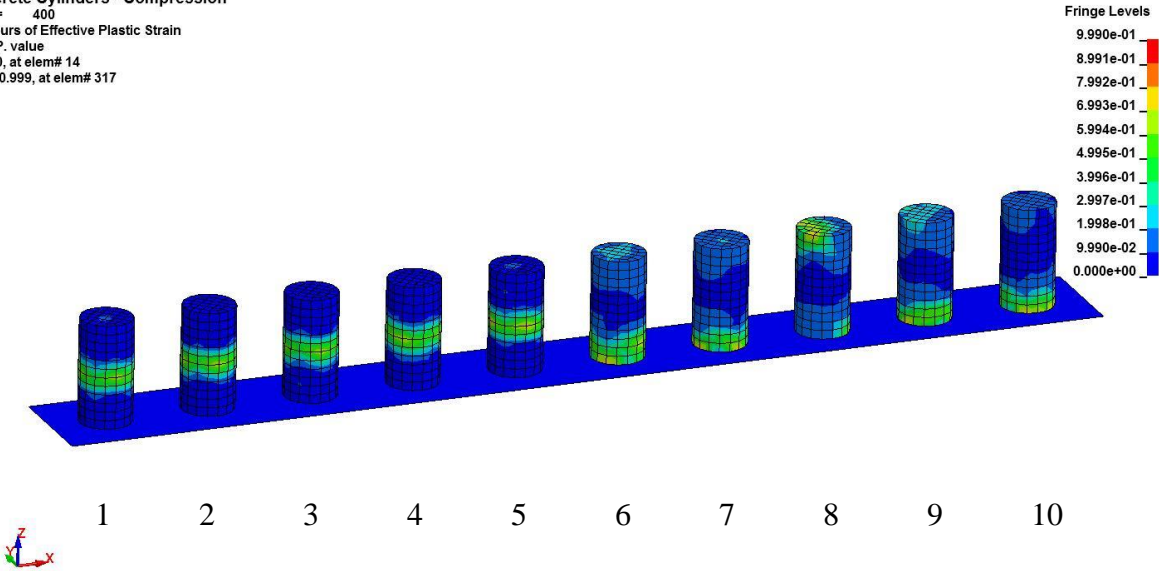


Figure 49. Force and Internal Energy Vs. Time, Concrete Cylinder Compression – Run 2

Concrete Cylinders - Compression  
Time = 400  
Contours of Effective Plastic Strain  
max IP. value  
min=0, at elem# 14  
max=0.999, at elem# 317



Concrete Cylinders - Compression  
Time = 1000  
Contours of Effective Plastic Strain  
max IP. value  
min=0, at elem# 21  
max=0.999001, at elem# 260

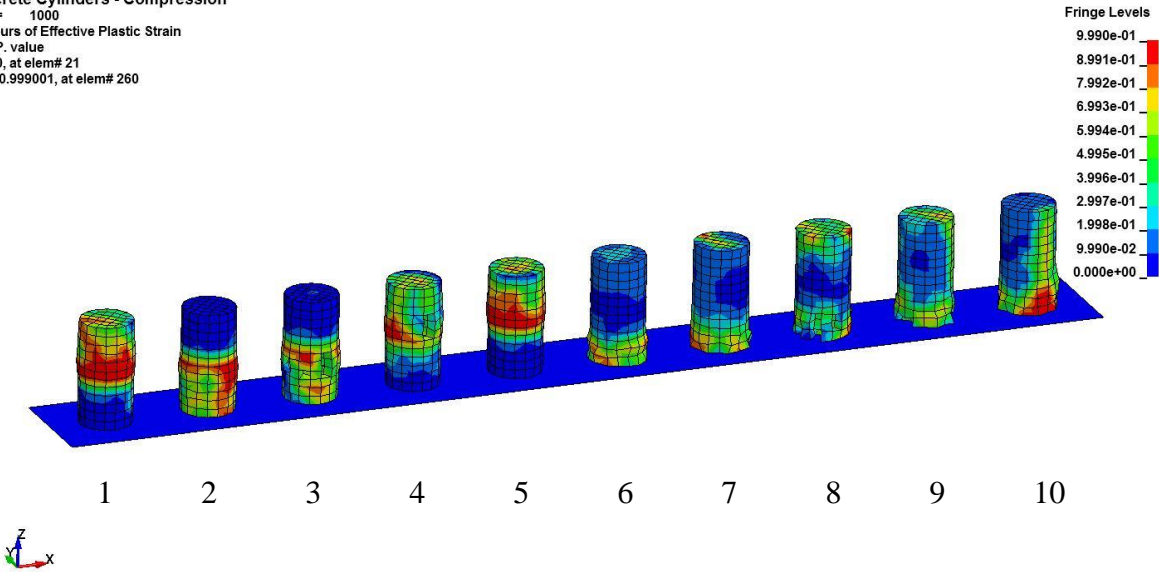
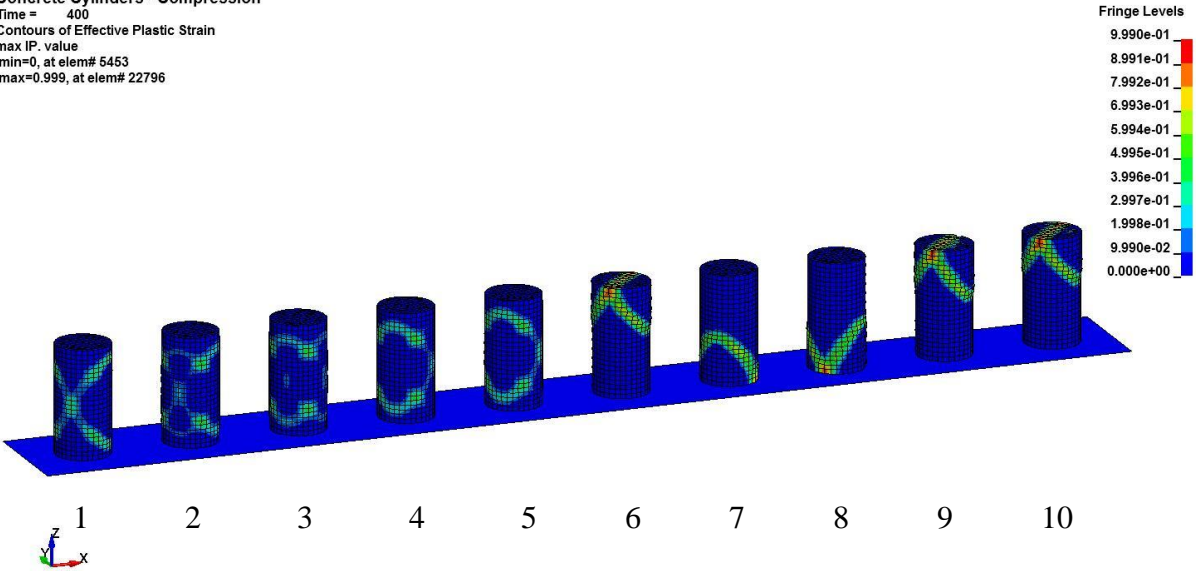


Figure 50. Deformation and Damage, Concrete Cylinder Compression – Run 2

Concrete Cylinders - Compression  
Time = 400  
Contours of Effective Plastic Strain  
max IP. value  
min=0, at elem# 5453  
max=0.999, at elem# 22796



Concrete Cylinders - Compression  
Time = 1000  
Contours of Effective Plastic Strain  
max IP. value  
min=0, at elem# 5453  
max=0.999, at elem# 6494

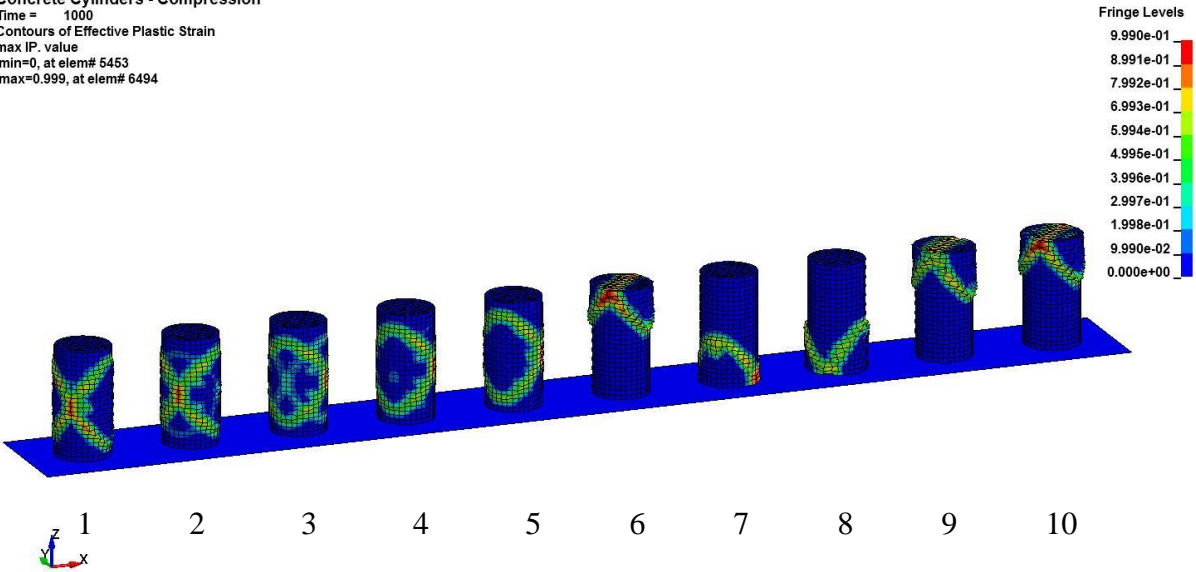


Figure 51. Deformation and Damage, Concrete Cylinder Compression – Run 3

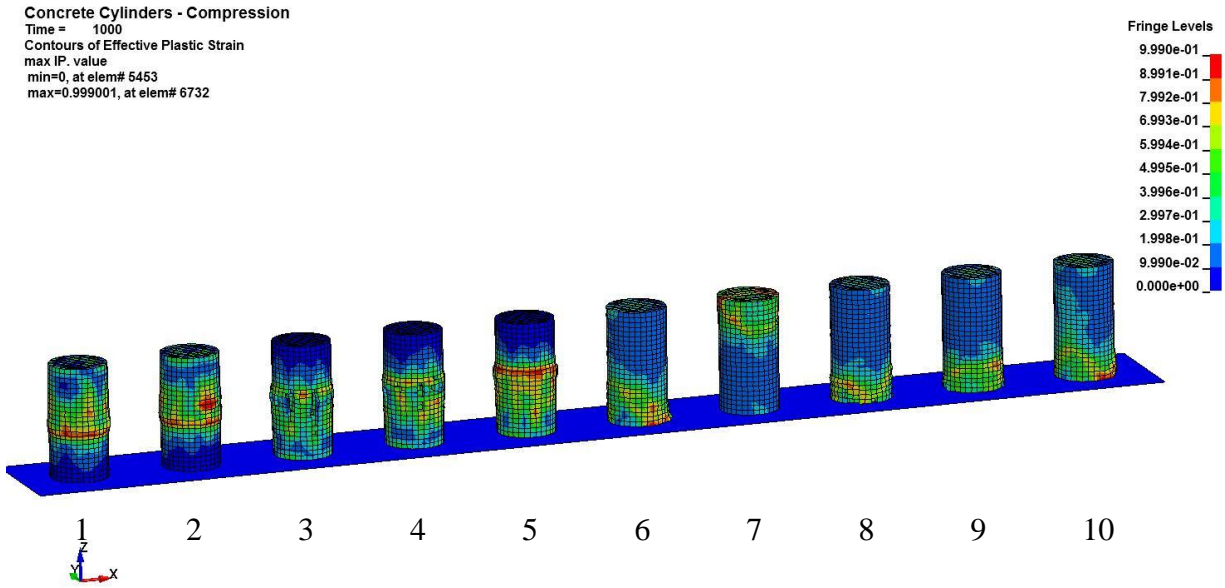
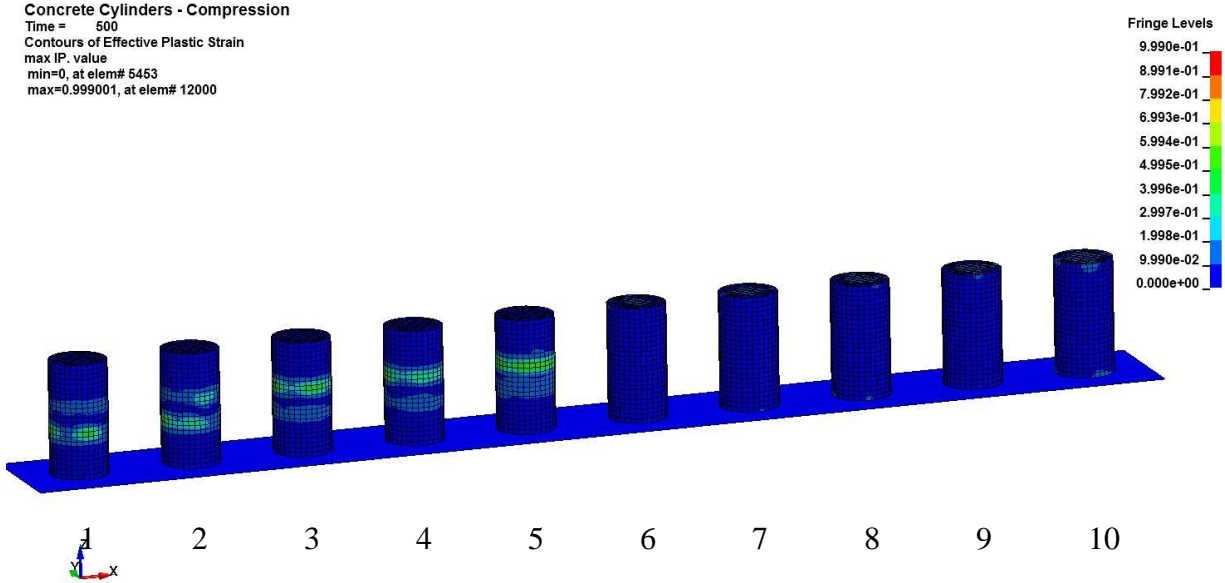


Figure 52. Deformation and Damage, Concrete Cylinder Compression – Run 4

### 7.2.2 Tension Cylinder Simulations

Following the simulation of the concrete cylinders in compression, simulations were conducted which loaded the cylinders in tension to evaluate the performance of MAT\_159\_CSCM under a different load condition. For the tension cylinder simulations, the parameters from case nos. 1 through 5 in the compression models were again simulated with both the 1 in. (25 mm) and ½ in. (13 mm) mesh sizes, as shown in Figure 54. The tension models were run using  $IRATE = 1$  and  $RECOV = 10$  because those parameters had demonstrated improved model response in the compression cylinder simulations. The model was loaded by constraining the base of the cylinder and applying a displacement to the top of the cylinder.

The simulation run of the tension cylinder models, Run 5, found that the MAT\_159\_CSCM material model provided reasonable results for the tensile capacity of the cylinders. Tensile capacity for concrete is typically found to be 8 to 15 percent of the peak compressive strength. Thus, one would expect peak tensile stresses in the 536 psi to 1,006 psi range (0.0037 GPa to 0.0070 GPa). Results from the tensile simulations returned lower-than-expected peak tensile stress values between 461 psi to 473 psi range (0.0032 GPa to 0.0033 GPa), as shown in Figure 55. Cylinder deformations appeared reasonable and similar erosion of the elements was observed for both mesh sizes, as shown in Figure 56. The smaller mesh size did demonstrate more consistent results and higher internal energies while providing reduced hourglass energies. Case no. 5 with  $REPOW = 0$  demonstrated high hourglass energy and very low internal energy.

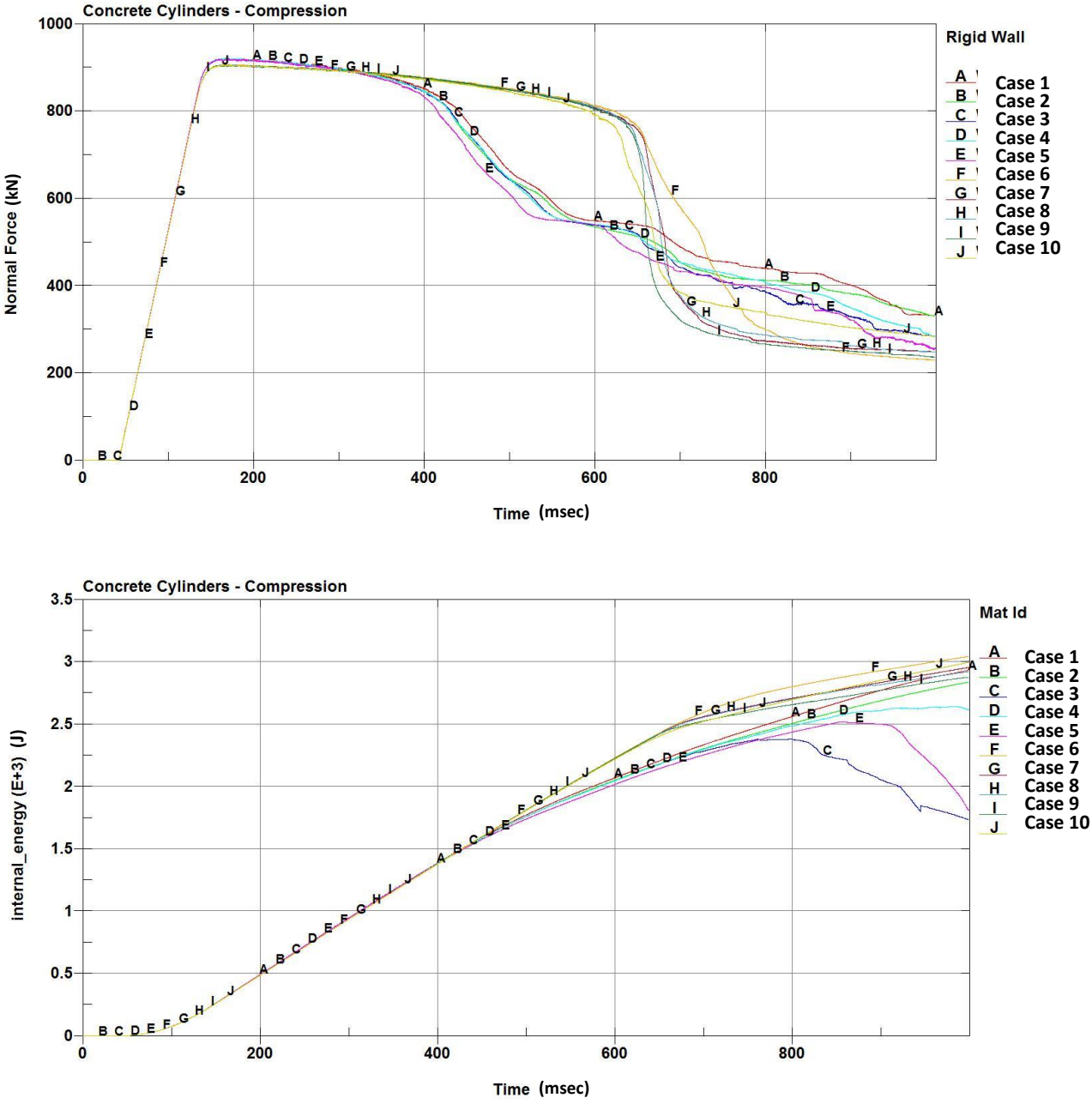


Figure 53. Force and Internal Energy Vs. Time, Concrete Cylinder Compression – Run 4

Concrete Cylinders - Tension  
Time = 0

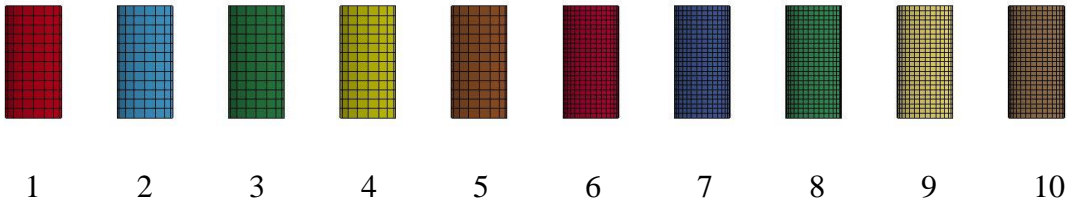


Figure 54. Concrete Cylinder Tension Model Setup

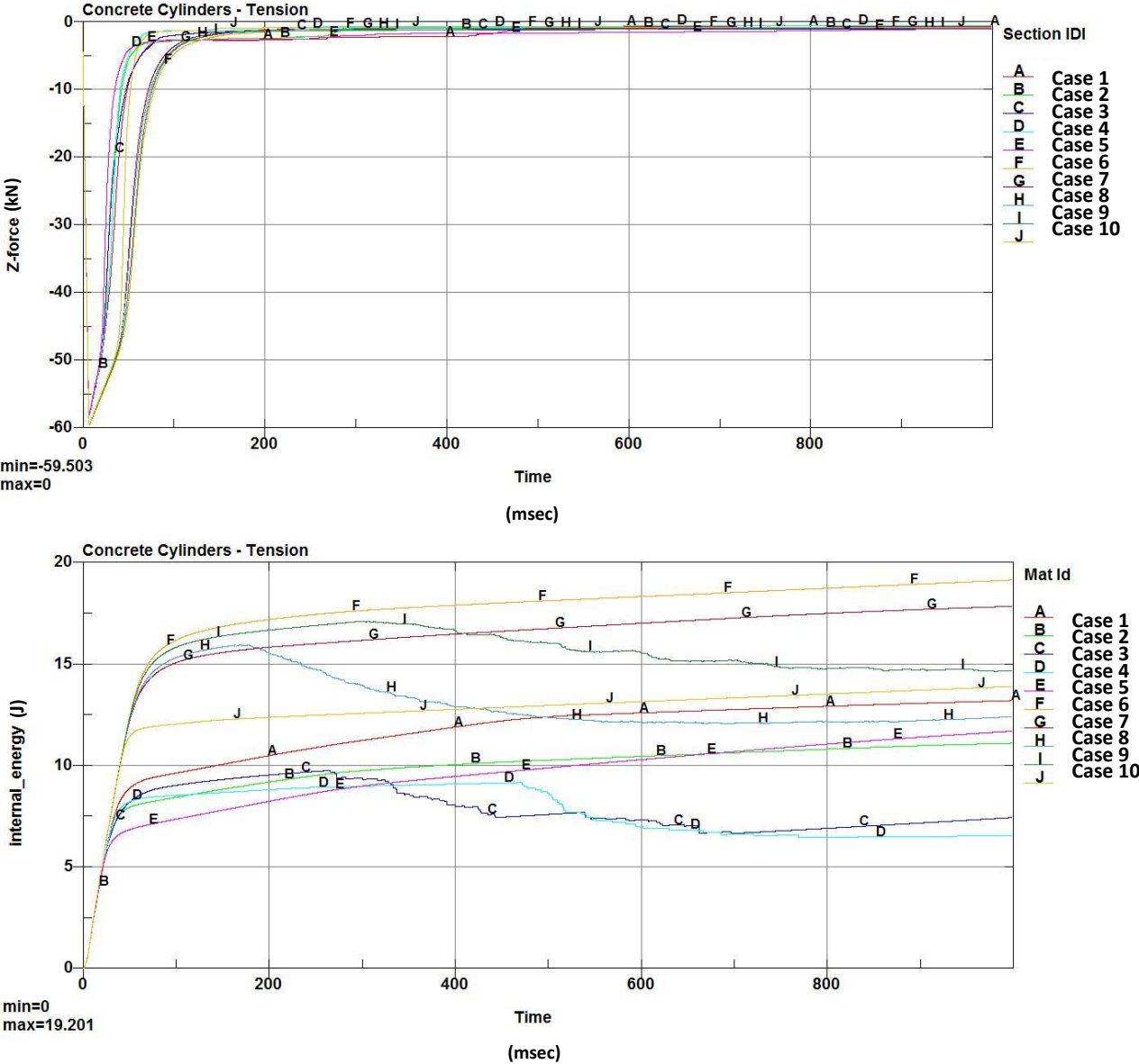
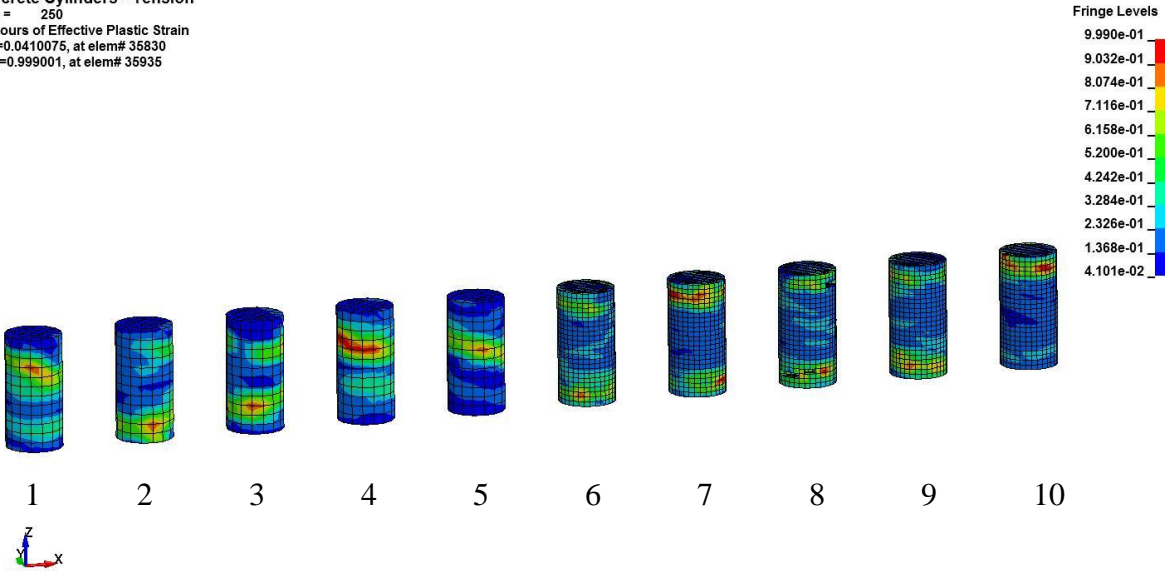


Figure 55. Force and Internal Energy Vs. Time, Concrete Cylinder Tension – Run 6

Concrete Cylinders - Tension  
Time = 250  
Contours of Effective Plastic Strain  
min=0.0410075, at elem# 35830  
max=0.999001, at elem# 35935



Concrete Cylinders - Tension  
Time = 1000  
Contours of Effective Plastic Strain  
min=0.0410075, at elem# 35830  
max=0.999001, at elem# 35927

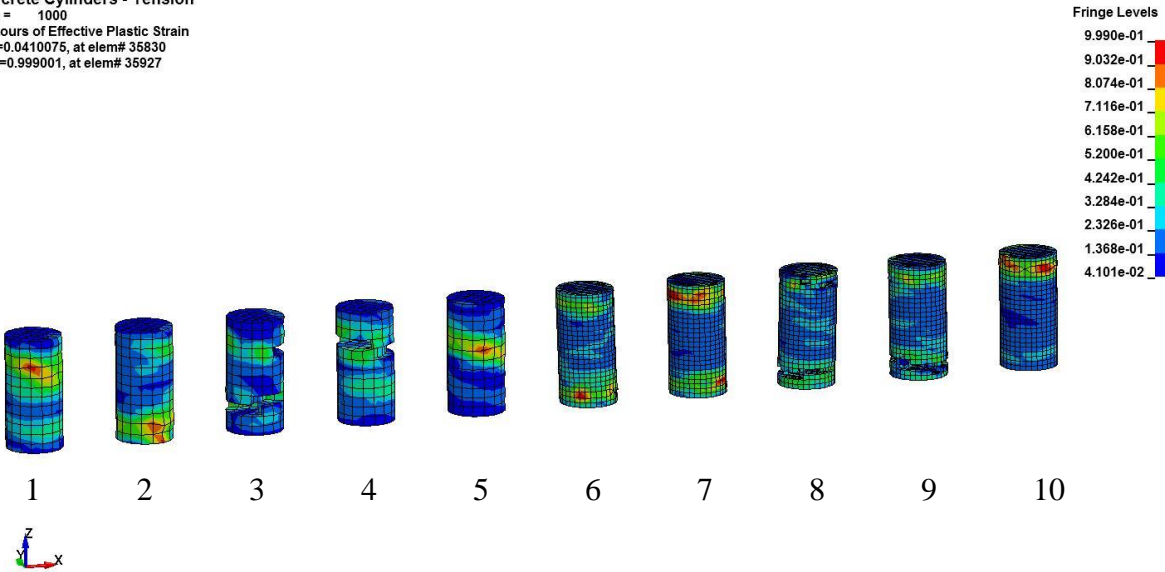


Figure 56. Deformation and Damage, Concrete Cylinder Tension – Run 5

### **7.2.1 Concrete Cylinder Simulation Discussion**

Simulation of the concrete cylinders led to several observations regarding the performance of the MAT\_159\_CSCM material model. First, it appears that the material model captures peak compression and tensile capacity reasonably well. Deformation of the elements in the models was often unstable and hourglass energies appeared to be an issue as well, especially if the value of REPOW was low. Erosion of the elements after peak loading was not observed in any of the models unless the rate effects in the model were activated. However, erosion should have been active with or without the rate effects. Setting the REPOW value equal to zero tended to generate higher hourglass energies and would not be recommended when using the material model. Post-peak load behavior of the material model seemed to be dependent on mesh size and the RECOV parameter. However, it was not known which of the post-peak behaviors was more accurate. Thus, the material model appeared to capture the strength of the concrete well, but the response of the model was sensitive to constraints and parameter variation.

### **7.3 Concrete Beam Models**

Based on the observations made regarding the MAT\_159\_CSCM material model simulations of tension and compression cylinders, the researchers decided to apply the best material model settings determined previously to a model of a dynamic impact of a reinforced concrete beam. As part of the original development of the MAT\_159\_CSCM material model, MwRSF conducted dynamic component testing of reinforced concrete beam specimens, as shown in Figure 57. Full details on this testing and the results can be found in the MwRSF research report detailing the tests [19].

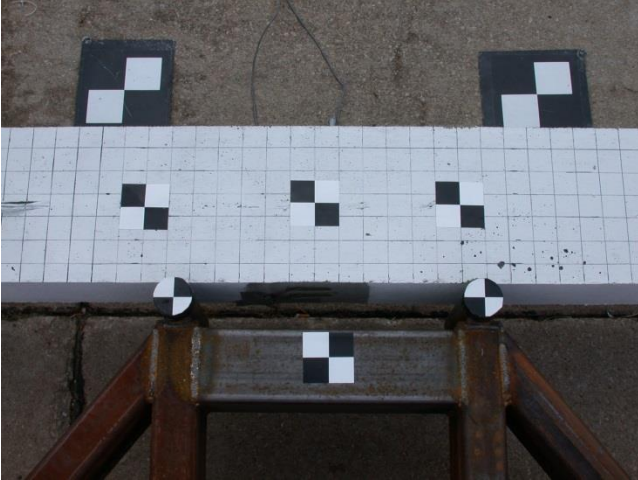
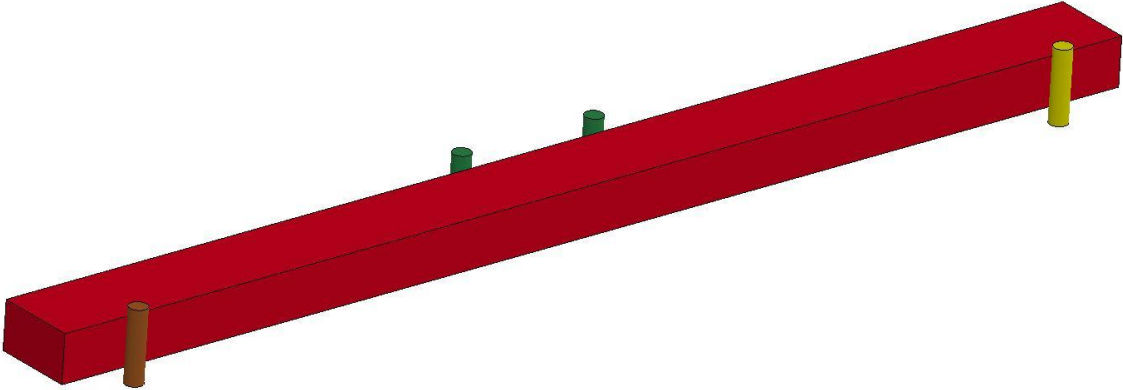


Figure 57. Reinforced Concrete Beam Test Setup

The simulation effort focused on the modeling of two of the concrete beam tests using the MAT\_159\_CSCM material model and the concrete beam geometry, reinforcement, and material data from test nos. ABC-2 and ABC-3. Test no. ABC-2 consisted of a 4,819-lb (2,186-kg) bogie impacting the reinforced concrete beam specimen at a speed of 20.6 mph (33.2 km/h). The high-velocity impact in this test caused failure of the beam due to shear cracks on both sides of the beam. Test no. ABC-3 consisted of the 4,819-lb (2,186-kg) bogie impacting the reinforced concrete beam specimen at a speed of 5.3 mph (8.5 km/h). The results from this test showed that the beam failed in pure bending. Fracture of the beam occurred due to tension cracks in the constant moment region of the beam. Peak reaction loads at the east and west load frames were measured to be 7.45 kips and 9.24 kips (33.13 kN and 41.11 kN), respectively. Analysis of the loading of the beam found a peak moment of 665.6 kip-in. (75,210.7 kN-mm). Review of the data from the tests demonstrated that the reinforced concrete beams displayed significantly different failure modes depending on the velocity of the impact. At the highest impact speed, the presence of inclined shear cracking and a predominantly shear failure mode was observed in the specimens. At the lowest impact speed, the expected bending failure mode was observed.

The simulation model of the reinforced concrete beam specimens used the MAT\_159\_CSCM material model with the basic input parameters for compressive strength and aggregate size from the concrete cylinder simulations. The concrete beam was modeled with solid elements and the reinforcing steel was modeled with beam elements that were constrained in the beam using the CONSTRAINED\_LANGRANGE\_IN\_SOLID keyword. The reinforcing steel was modeled with material properties for ASTM A615 Grade 60 steel. The simulation model used fixed supports at each end of the beam. Two supports with the mass and velocity of the impacting bogie vehicle from the physical test were used to load the beam specimen. The setup of the simulation model is shown in Figure 58.

Aptek Beam  
Time = 0



Aptek Beam  
Time = 0

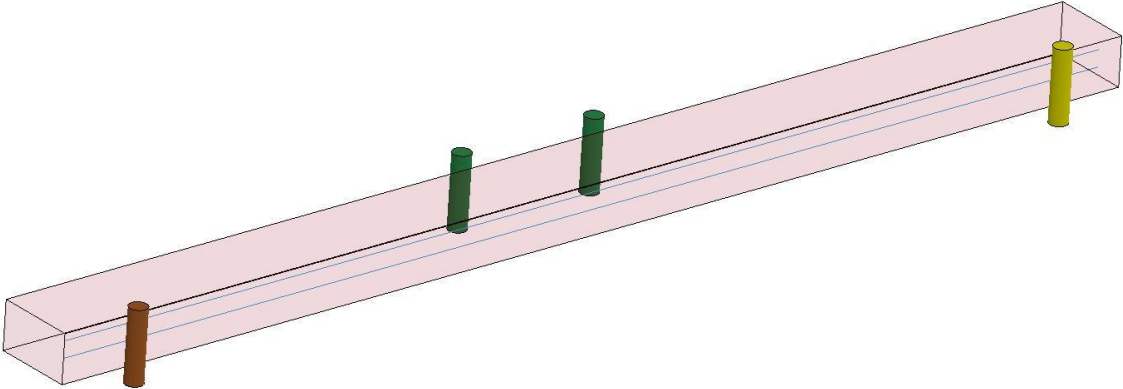


Figure 58. Reinforced Concrete Beam Simulation Model

In order to determine the best combination of model parameters for the beam simulation, the following parameters were varied.

1.  $G_{ft}/G_{fs}$  – The ratio of the tensile and shear fracture energies was varied between 0.5 and 1.0. Previous analysis by TTI during the development of the model found that ratios in this range worked best, but it may be problem-dependent.
2. REPOW – REPOW defines the power for the equation-defining increase in fracture energy with rate effects. In addition, modeling of the concrete cylinders seemed to demonstrate that REPOW had an effect on hourglass energies in the model. Thus, REPOW was varied from 0.5 to 1.0 to determine the optimal setting.
3. RECOV – RECOV defines the recovery modulus in compression for the material model. If RECOV is set to zero, then the modulus is recovered in compression. If RECOV is set between 0 and 1, recovery is based on the sign of the pressure invariant only. If RECOV is set between 10 and 11, recovery is based on the sign of the pressure invariant and the volumetric strain. Thus, values of RECOV between 0 and 1 and 10 and 11 were simulated.
4. ERODE – ERODE defines deformation of the element when damage exceeds 0.99 and the maximum principal strain exceeds ERODE-1.0. The MAT\_159\_CSCM material model evaluation manual noted that values of ERODE between 1.05 and 1.10 produced reasonable damage and element erosion in reinforced concrete structures. Values of 1 tended to produce excessive erosion at low damage levels. Thus, ERODE was varied between 1.05 and 1.10 for the reinforced beam simulations.
5. Hourglass control formulation – Hourglass energies were a noted issue in the concrete cylinder modeling described previously, and it was an overriding problem in the initial simulation models of the reinforced concrete beams. As such, various

hourglass controls for solid elements were applied to the simulations to determine a reasonable hourglass control that managed the hourglass energy levels without affecting the material model response. Hourglass control types 3, 5, and 6 were considered with hourglass coefficients between 0.05 and 0.10.

A series of simulation models of the concrete beam tests was conducted to evaluate the performance of the MAT\_159\_CSCM material model by varying the parameters noted above. The models were analyzed based on the load developed by the concrete beam; the damage of the concrete material; the failure mode; and fracture, stability, and proper energy levels. From these models, a set of optimized parameters was developed as a starting point for use in future reinforced concrete models. These parameters may require modification for accurate simulation of other reinforced concrete structures, but they should provide a reasonable starting point for future models. The basic model setup is described in the following steps:

1. Create the extended material model input data using the MAT\_159\_CSCM short input setting with the appropriate compressive strength and aggregate size.
2. Alter the MAT\_159\_CSCM extended input settings to the following values. Other extended input parameters can be left at the defaults.
  - a.  $IRATE = 1$ 
    - i. This activates strain rate effects and appeared to provide better damage and element erosion.
  - b.  $REPOW = 0.5$ 
    - i.  $REPOW = 0$  yielded high hourglass energies in all models.
    - ii.  $REPOW = 0.5$  worked best for the reinforced beam model; however,  $REPOW = 1.0$  may be appropriate as well.
  - c.  $G_{fs}/G_{ft} = 0.5$

- i. This ratio of shear and tensile fracture energies provided the best correlation for the reinforced concrete beam simulated here. Values closer to 1.0 provided more tensile damage and less shear and compression damage. Thus, modeling of different structures or types of load may require modification of this value.
- d.  $ERODE = 1.05$
- i. Setting  $ERODE$  greater than 1 provided for erosion of an element only after damage and plastic strain thresholds were exceeded, which provided for a less brittle response and prevented excessive element erosion. This parameter may also need to be modified depending on the structure and loading being simulated and the mesh size. However, values greater than 1 are recommended.
- e.  $RECOV = 1$
- i.  $RECOV$  equal to 1 was required for providing stable material energies.  $RECOV$  equal to 11 should provide a similar response.
3. The hourglass control is required when using the material model. All models had excessive hourglass levels without it. For the models described herein, hourglass control type 6 with an hourglass coefficient of 0.05 provided adequate control of hourglass energies by reducing hourglassing without affecting model response.

The  $MAT_{159\_CSCM}$  material model recommendations were applied to the simulation of test nos. ABC-2 and ABC-3. Test no. ABC-3, the lower speed impact, was simulated first to verify that the material model was capable of developing accurate bending capacity and displaying the appropriate damage and failure modes. The results from the simulation of test no. ABC-3 demonstrated good correlation with the physical test. Comparison of the damage and

deflection of the concrete beam in both the simulation and physical test are shown in Figure 59. The simulation showed similar deflection and damage to the physical test. The damage observed in the simulation was primarily due to tensile cracking in the constant moment region on the back side of the beam, and no large scale failure of the beam material was found. The simulation also captured tension cracking on the impact side face of the beam specimen during rebound. The dynamic beam deflection of the simulation model was slightly higher than the physical test, as shown in Figure 60. The predicted beam moment based on the end support load from test no. ABC-2, and the simulation model are shown in Figure 61. The simulation predicted slightly higher moments than the physical testing but the overall moment capacities were similar. Thus, simulation of test no. ABC-3 provided reasonable correlation with the physical test as the observed beam damage, dynamic beam deflection, and beam moment capacity were similar. Further refinement of the results might be possible through adjustment of the model parameters, but the focus of this effort was to develop general input settings for the material model that yielded reasonable results.

A simulation of test no. ABC-2 was also performed to determine if the MAT\_159\_CSCM material model was capable of capturing the alternate shear failure mode observed at increased impact velocity. Graphical comparison of the simulation and test no. ABC-2 is shown in Figure 62. The comparison shows that the simulation model captured the change in the failure mode as the impact velocity increased. Both the simulation and the model displayed shear cracking and damage which led to fracture of the reinforced concrete beam. The simulation demonstrated initial damage and cracking along the 45 degree shear planes similar to the test. As the simulation continued, the damage resulted in erosion of the elements in a lateral crack in beam rather than a 45 degree angle crack. It was believed that the element erosion did not proceed in the same angle due to the size and direction of the reinforced concrete beam finite element mesh.

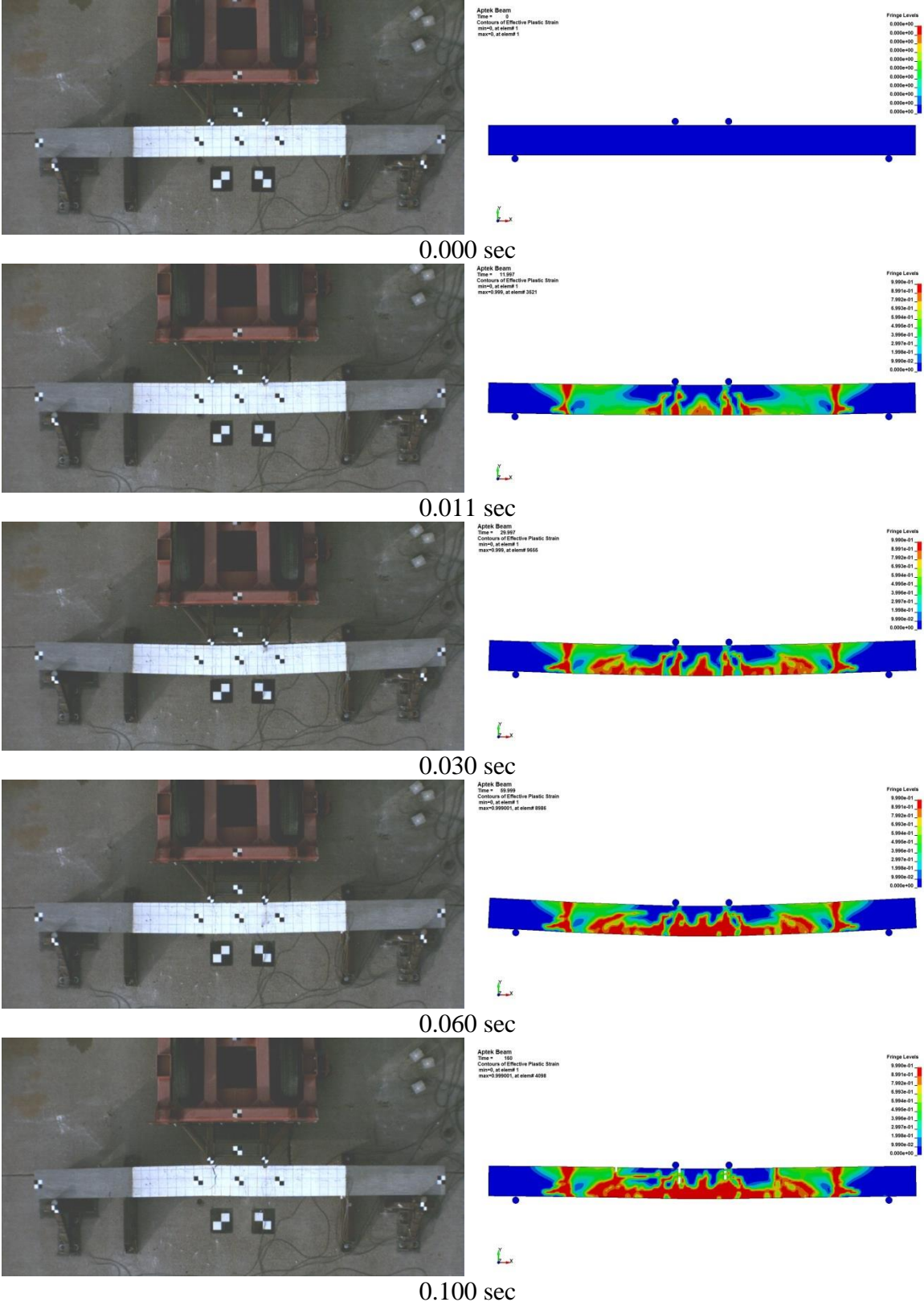


Figure 59. Deformation and Damage, Simulation and Test No. ABC-3

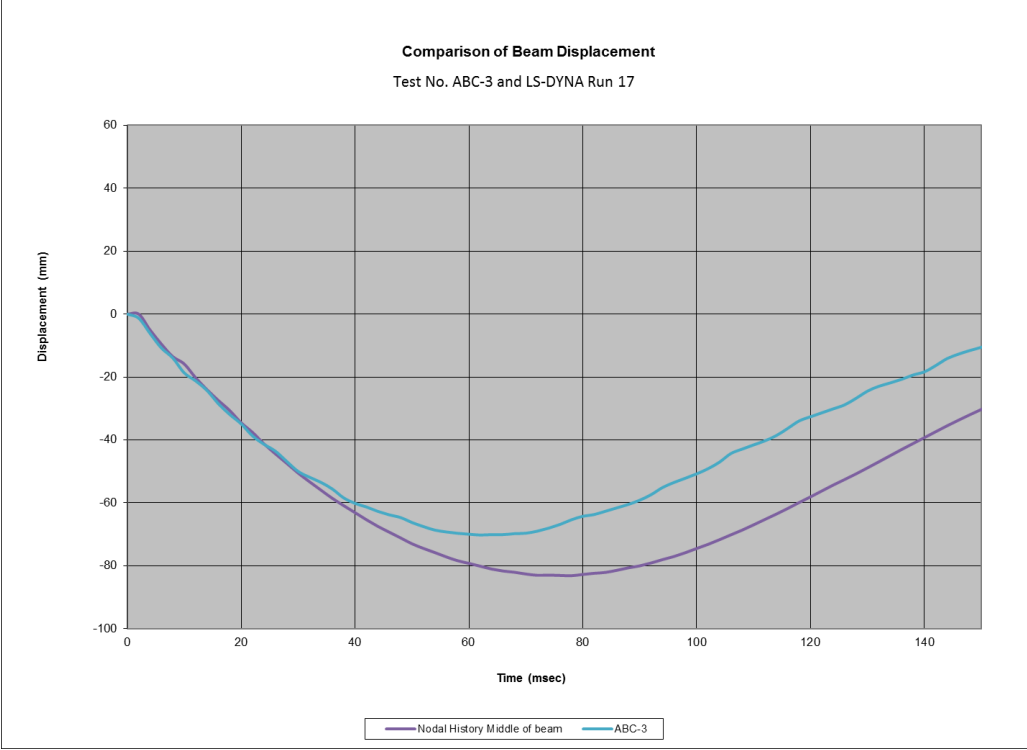


Figure 60. Beam Deflection, Simulation and Test No. ABC-3

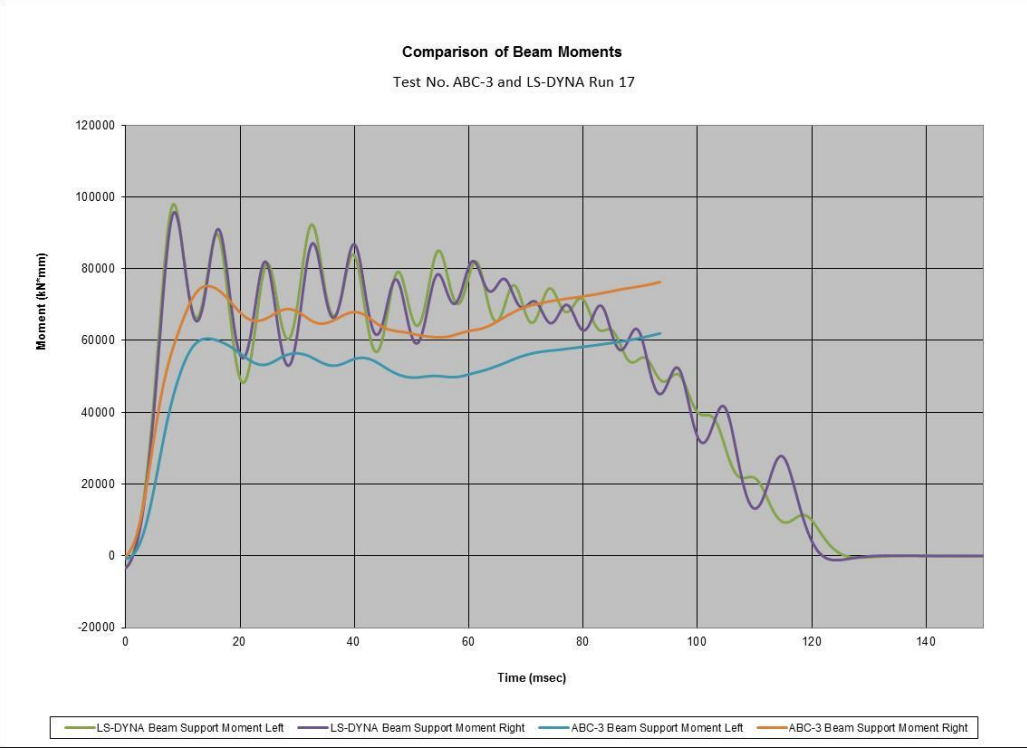


Figure 61. Beam Moment, Simulation and Test No. ABC-3

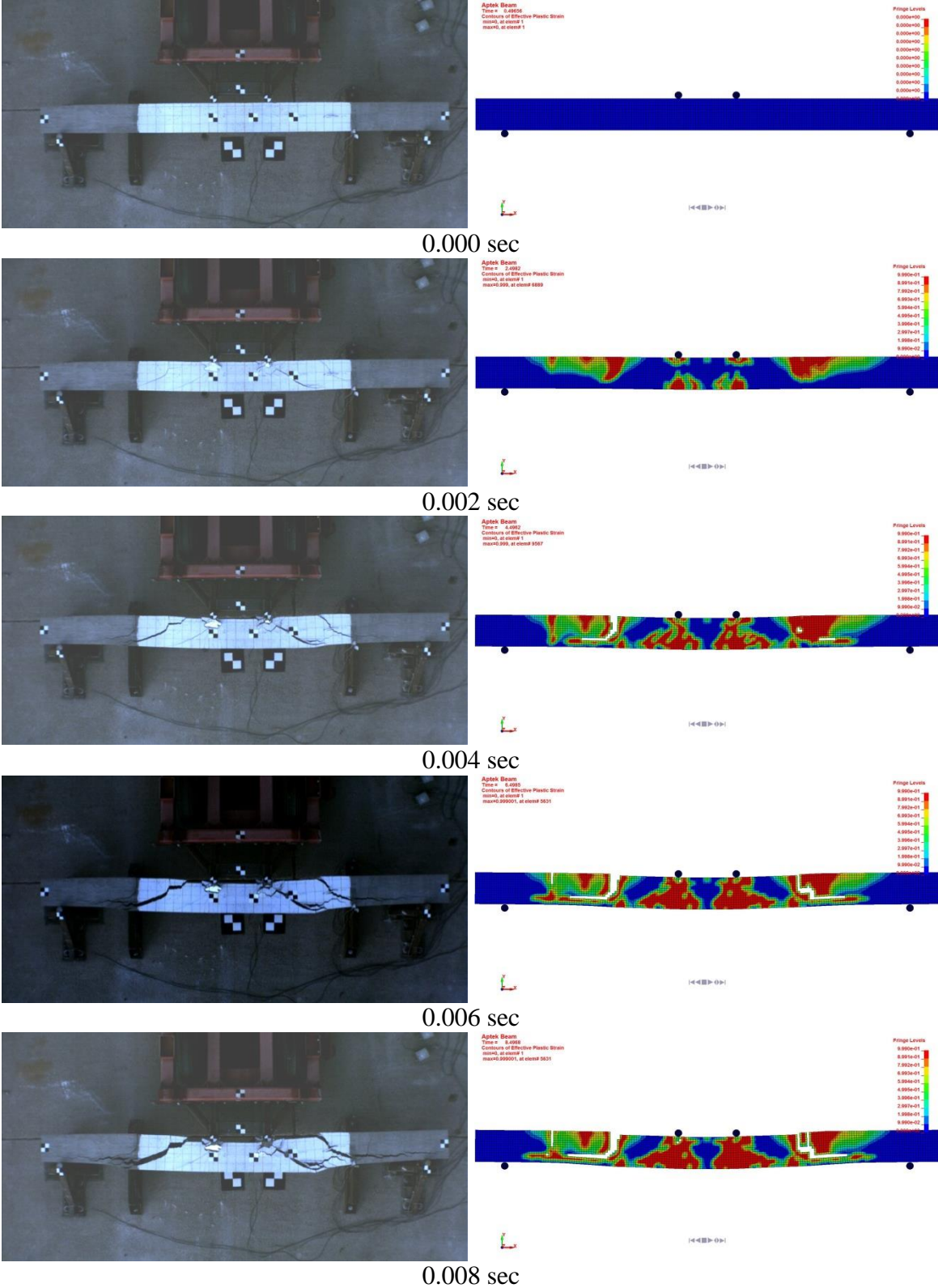


Figure 62. Deformation and Damage, Simulation and Test No. ABC-2

Thus, while the model did not completely replicate the failure mode observed in test no. ABC-2, the failure modes were similar, and the model did predict the change in the failure mode. Accurate impact loads and moments were not obtained for ABC-2 simulation due to the short duration of the impact event and thus were not compared.

#### **7.4 Concrete Material Model Recommendations**

The analysis of the MAT\_159\_CSCM material model through the concrete cylinder and reinforced concrete beam simulation models allowed the researchers to develop a reasonable set of preliminary input parameters for concrete material modeling. The MAT\_159\_CSCM material model proved capable of predicting reasonable compressive, tensile, and flexural capacities in simple cylinder and more complex reinforced-beam simulations. These results also correlated well with previous research done with the MAT\_159\_CSCM material model by TTI. Currently, the model was only evaluated for a simple beam under flexural loading, and other factors, such as shear reinforcement, compression reinforcement, and additional loading modes were not evaluated. However, it was noted that the material model performance was sensitive to the model input parameters, mesh size, and the hourglass controls used. Thus, further research with the model was recommended to build confidence in its performance and extend its use.

At this time, it is not clear how well the material model parameters would extend to more complex structures and loadings, but it provides a valuable starting point for further analysis of reinforced concrete structures. Further research and experience with the material model would likely be required to address these issues. With regards to the development of the low-deflection TCB system, the researchers noted that the MAT\_159\_CSCM material model would be used if deemed necessary during the analysis, but it would not initially be applied to simplify and speed the analysis of the design concepts.

## 8 TEST REQUIREMENTS AND EVALUATION CRITERIA

### 8.1 Test Requirements

Longitudinal barriers must satisfy impact safety standards in order to be accepted by the Federal Highway Administration (FHWA) for use on the National Highway System (NHS). For new hardware, these safety standards consist of the guidelines and procedures published in MASH [1]. According to TL-3 of MASH, longitudinal barrier systems must be subjected to two full-scale vehicle crash tests. The two full-scale crash tests are noted below:

1. Test Designation No. 3-10 consists of a 2,425-lb (1,100-kg) passenger car impacting the system at a nominal speed and angle of 62 mph (100 km/h) and 25 degrees, respectively.
2. Test Designation No. 3-11 consists of a 5,000-lb (2,268-kg) pickup truck impacting the system at a nominal speed and angle of 62 mph (100 km/h) and 25 degrees, respectively.

The test conditions of TL-3 longitudinal barriers are summarized in Table 7.

Table 7. MASH TL-3 Crash Test Conditions

Test Article	Test Designation No.	Test Vehicle	Impact Conditions			Evaluation Criteria <sup>1</sup>
			Speed		Angle (deg)	
			mph	km/h		
Longitudinal Barrier	3-10	1100C	62	100	25	A,D,F,H,I
	3-11	2270P	62	100	25	A,D,F,H,I

<sup>1</sup> Evaluation criteria explained in Table 8.

A rigid, F-shape bridge rail was successfully impacted by a small car weighing 1,800 lb (816 kg) at 60.1 mph (96.7 km/h) and 21.4 degrees according to the American Association of State Highway and Transportation Officials (AASHTO) *Guide Specifications for Bridge Railings* [20-21]. In the same manner, rigid New Jersey safety shape barriers struck by small cars have

been shown to meet safety performance standards [22-23]. In addition, a New Jersey safety shape barrier was impacted by a passenger car weighing 2,579 lb (1,170 kg) at 60.8 mph (97.8 km/h) and 26.1 degrees according to the TL-3 standards set forth in MASH. Furthermore, temporary New Jersey safety shape concrete median barriers have experienced only slight barrier deflections when impacted by small cars and behave similarly to rigid barriers [24]. As such, the 1100C passenger car test was deemed unnecessary for this project.

## **8.2 Evaluation Criteria**

Evaluation criteria for full-scale vehicle crash testing are based on three appraisal areas: (1) structural adequacy, (2) occupant risk, and (3) vehicle trajectory after collision. Criteria for structural adequacy are intended to evaluate the ability of the temporary concrete barrier to contain and redirect impacting vehicles. In addition, controlled lateral deflection of the test article is acceptable. Occupant risk evaluates the degree of hazard to occupants in the impacting vehicle. Post-impact vehicle trajectory is a measure of the potential of the vehicle to result in a secondary collision with other vehicles and/or fixed objects, thereby increasing the risk of injury to the occupants of the impacting vehicle and/or other vehicles. These evaluation criteria are summarized in Table 8 and are defined in greater detail in MASH. The full-scale vehicle crash test was conducted and reported in accordance with the procedures provided in MASH.

In addition to the standard occupant risk measures, the Post-Impact Head Deceleration (PHD), the Theoretical Head Impact Velocity (THIV), and the Acceleration Severity Index (ASI) were determined and reported on the test summary sheet. Additional discussion on PHD, THIV and ASI is provided in MASH.

Table 8. MASH Evaluation Criteria for Longitudinal Barrier

Structural Adequacy	A. The test article should contain and redirect the vehicle or bring the vehicle to a controlled stop; the vehicle should not penetrate, underride, or override the installation, although controlled lateral deflection of the test article is acceptable.		
Occupant Risk	D. Detached elements, fragments or other debris from the test article should not penetrate or show potential for penetrating the occupant compartment; or present an undue hazard to other traffic, pedestrians, or personnel in a work zone. Deformations of, or intrusions into, the occupant compartment should not exceed limits set forth in Section 5.3 and Appendix E of MASH.		
	F. The vehicle should remain upright during and after collision. The maximum roll and pitch angles are not to exceed 75 degrees.		
	H. Occupant Impact Velocity (OIV) (see Appendix A, Section A5.3 of MASH for calculation procedure) should satisfy the following limits:		
	Occupant Impact Velocity Limits		
	Component	Preferred	Maximum
Longitudinal and Lateral	30 ft/s (9.1 m/s)	40 ft/s (12.2 m/s)	
I. The Occupant Ridedown Acceleration (ORA) (see Appendix A, Section A5.3 of MASH for calculation procedure) should satisfy the following limits:	Occupant Ridedown Acceleration Limits		
Component	Preferred	Maximum	
Longitudinal and Lateral	15.0 g's	20.49 g's	

## **9 TEST CONDITIONS**

### **9.1 Test Facility**

The testing facility is located at the Lincoln Air Park on the northwest side of the Lincoln Municipal Airport, and is approximately 5 miles (8.0 km) northwest of the University of Nebraska-Lincoln.

### **9.2 Vehicle Tow and Guidance System**

A reverse cable tow system with a 1:2 mechanical advantage was used to propel the test vehicle. The distance traveled and the speed of the tow vehicle were one-half that of the test vehicle. The test vehicle was released from the tow cable before impact with the barrier system. A digital speedometer on the tow vehicle increased the accuracy of the test vehicle impact speed.

A vehicle guidance system developed by Hinch [25] was used to steer the test vehicle. A guide flag, attached to the left-front wheel and the guide cable, was sheared off before impact with the barrier system. The  $\frac{3}{8}$ -in. (10-mm) diameter guide cable was tensioned to approximately 3,500 lb (15.6 kN) and was supported both laterally and vertically every 100 ft (30.5 m) by hinged stanchions. The hinged stanchions stood upright while holding up the guide cable, but as the vehicle was towed down the line, the guide flag struck and knocked each stanchion to the ground.

### **9.3 Test Vehicles**

For test no. RDTCB-1, a 2003 Dodge Ram 1500 Quad Cab was used as the test vehicle. The curb, test inertial, and gross static vehicle weights were 4,991 lb (2,264 kg), 4,998 lb (2,267 kg), and 5,163 lb (2,342 kg), respectively. The test vehicle is shown in Figure 63, and vehicle dimensions are shown in Figure 64.

For test no. RDTCB-2, a 2005 Dodge Ram 1500 Quad Cab was used as the test vehicle. The curb, test inertial, and gross static vehicle weights were 4,887 lb (2,217 kg), 4,978 lb (2,258



Figure 63. Test Vehicle, Test No. RDTCB-1

Date: 9/5/2012 Test Number: RDTCB-1 Model: 2270P  
Make: Dodge Ram 1500 QC Vehicle I.D.#: 1D7HA18N43J587071  
Tire Size: 265/70 R17 Year: 2003 Odometer: 126094  
Tire Inflation Pressure: 35 psi  
\*(All Measurements Refer to Impacting Side)

Vehicle Geometry -- in. (mm)

a	<u>78</u>	<u>(1981)</u>	b	<u>75</u>	<u>(1905)</u>
c	<u>227 1/2</u>	<u>(5779)</u>	d	<u>47</u>	<u>(1194)</u>
e	<u>140 1/4</u>	<u>(3562)</u>	f	<u>40 1/4</u>	<u>(1022)</u>
g	<u>28 1/7</u>	<u>(715)</u>	h	<u>63 1/6</u>	<u>(1604)</u>
i	<u>15</u>	<u>(381)</u>	j	<u>27</u>	<u>(686)</u>
k	<u>20 1/2</u>	<u>(521)</u>	l	<u>29 1/2</u>	<u>(749)</u>
m	<u>68 1/4</u>	<u>(1734)</u>	n	<u>67 5/8</u>	<u>(1718)</u>
o	<u>45</u>	<u>(1143)</u>	p	<u>3 1/4</u>	<u>(83)</u>
q	<u>31 1/4</u>	<u>(794)</u>	r	<u>18 1/2</u>	<u>(470)</u>
s	<u>15 1/4</u>	<u>(387)</u>	t	<u>75</u>	<u>(1905)</u>

Wheel Center Height Front 15 (381)  
Wheel Center Height Rear 15 1/4 (387)  
Wheel Well Clearance (F) 35 (889)  
Wheel Well Clearance (R) 38 (965)  
Frame Height (F) 17 1/2 (445)  
Frame Height (R) 25 (635)  
Engine Type 8 cyl. Gas  
Engine Size 4.7L  
Transmission Type:  
Automatic  Manual   
FWD  RWD  4WD

Mass Distribution lb (kg)

Gross Static	LF	<u>1430</u>	<u>(649)</u>	RF	<u>1417</u>	<u>(643)</u>
	LR	<u>1138</u>	<u>(516)</u>	RR	<u>1178</u>	<u>(534)</u>

Weights lb (kg)

	Curb	Test Inertial	Gross Static			
W-front	<u>2772</u>	<u>(1257)</u>	<u>2747</u>	<u>(1246)</u>	<u>2847</u>	<u>(1291)</u>
W-rear	<u>2219</u>	<u>(1007)</u>	<u>2251</u>	<u>(1021)</u>	<u>2316</u>	<u>(1051)</u>
W-total	<u>4991</u>	<u>(2264)</u>	<u>4998</u>	<u>(2267)</u>	<u>5163</u>	<u>(2342)</u>

GVWR Ratings

Front	<u>3650</u>
Rear	<u>2240</u>
Total	<u>5023</u>

Dummy Data

Type: Hybrid II  
Mass: 165 lbs  
Seat Position: passenger

Note any damage prior to test: none

Figure 64. Vehicle Dimensions, Test No. RDTCB-1

kg), and 5,143 lb (2,333 kg), respectively. The test vehicle is shown in Figure 65, and vehicle dimensions are shown in Figure 66.

The longitudinal component of the center of gravity (c.g.) was determined using the measured axle weights. The Suspension Method [26] was used to determine the vertical component of the c.g. for the pickup truck. This method is based on the principle that the c.g. of any freely suspended body is in the vertical plane through the point of suspension. The vehicle was suspended successively in three positions, and the respective planes containing the c.g. were established. The intersection of these planes pinpointed the final c.g. location for the test inertial condition. The final location of the c.g. is shown in Figures 64 and 66 for RDTCB-1 and RDTCB-2, respectively. Data used to calculate the location of the c.g. and ballast information are shown in Appendix D. Square, black and white-checked targets shown in Figures 67 and 68 for RDTCB-1 and RDTCB-2, respectively, were placed on the vehicle for reference to be viewed from the high-speed digital video cameras and to aid in the video analysis. Round, checked targets were placed on the center of gravity on the left-side door, the right-side door, and the roof of the vehicle.

The front wheels of the test vehicle were aligned to vehicle standards except the toe-in value was adjusted to zero so that the vehicles would track properly along the guide cable. A 5B flash bulb was mounted on the right side of the vehicle's dash and was fired by a pressure tape switch mounted at the impact corner of the bumper. The flash bulb was fired upon initial impact with the test article to create a visual indicator of the precise time of impact on the high-speed videos. A remote-controlled brake system was installed in the test vehicle so the vehicle could be brought safely to a stop after the test.



Figure 65. Test Vehicle, Test No. RDTCB-2

Date: 8/8/2013 Test Number: RDTCB-2 Model: Ram 1500  
 Make: Dodge Vehicle I.D.#: 1D7HA18K85J591455  
 Tire Size: 265/70 R17 Year: 2005 Odometer: 226453  
 Tire Inflation Pressure: 35 psi  
 \*(All Measurements Refer to Impacting Side)

**Vehicle Geometry -- in. (mm)**

a <u>77 1/2 (1969)</u>	b <u>74 1/2 (1892)</u>
c <u>227 1/2 (5779)</u>	d <u>40 1/4 (1022)</u>
e <u>140 1/4 (3562)</u>	f <u>47 (1194)</u>
g <u>28 (711)</u>	h <u>64 3/5 (1641)</u>
i <u>14 3/4 (375)</u>	j <u>27 1/4 (692)</u>
k <u>20 1/4 (514)</u>	l <u>29 (737)</u>
m <u>67 7/8 (1724)</u>	n <u>67 1/2 (1715)</u>
o <u>46 (1168)</u>	p <u>3 1/2 (89)</u>
q <u>31 1/2 (800)</u>	r <u>17 (432)</u>
s <u>14 3/4 (375)</u>	t <u>74 7/8 (1902)</u>

Wheel Center Height Front 14 3/4 (375)  
 Wheel Center Height Rear 14 3/4 (375)  
 Wheel Well Clearance (F) 35 1/4 (895)  
 Wheel Well Clearance (R) 37 1/4 (946)  
 Frame Height (F) 17 1/2 (445)  
 Frame Height (R) 24 1/2 (622)  
 Engine Type V-6 gas  
 Engine Size 3.7L  
 Transmission Type: Automatic Manual  
 FWD RWD 4WD

**Mass Distribution lb (kg)**

Gross Static	LF <u>1410 (640)</u>	RF <u>1377 (625)</u>
	LR <u>1160 (526)</u>	RR <u>1196 (542)</u>

**Weights lb (kg)**

	Curb	Test Inertial	Gross Static
W-front	<u>2702 (1226)</u>	<u>2685 (1218)</u>	<u>2787 (1264)</u>
W-rear	<u>2185 (991)</u>	<u>2293 (1040)</u>	<u>2356 (1069)</u>
W-total	<u>4887 (2217)</u>	<u>4978 (2258)</u>	<u>5143 (2333)</u>

**GVWR Ratings**

Front	<u>3700</u>
Rear	<u>3900</u>
Total	<u>6650</u>

**Dummy Data**

Type: Hybrid II  
 Mass: 170 lbs  
 Seat Position: Passenger

Note any damage prior to test: none

Figure 66. Vehicle Dimensions, Test No. RDTCB-2

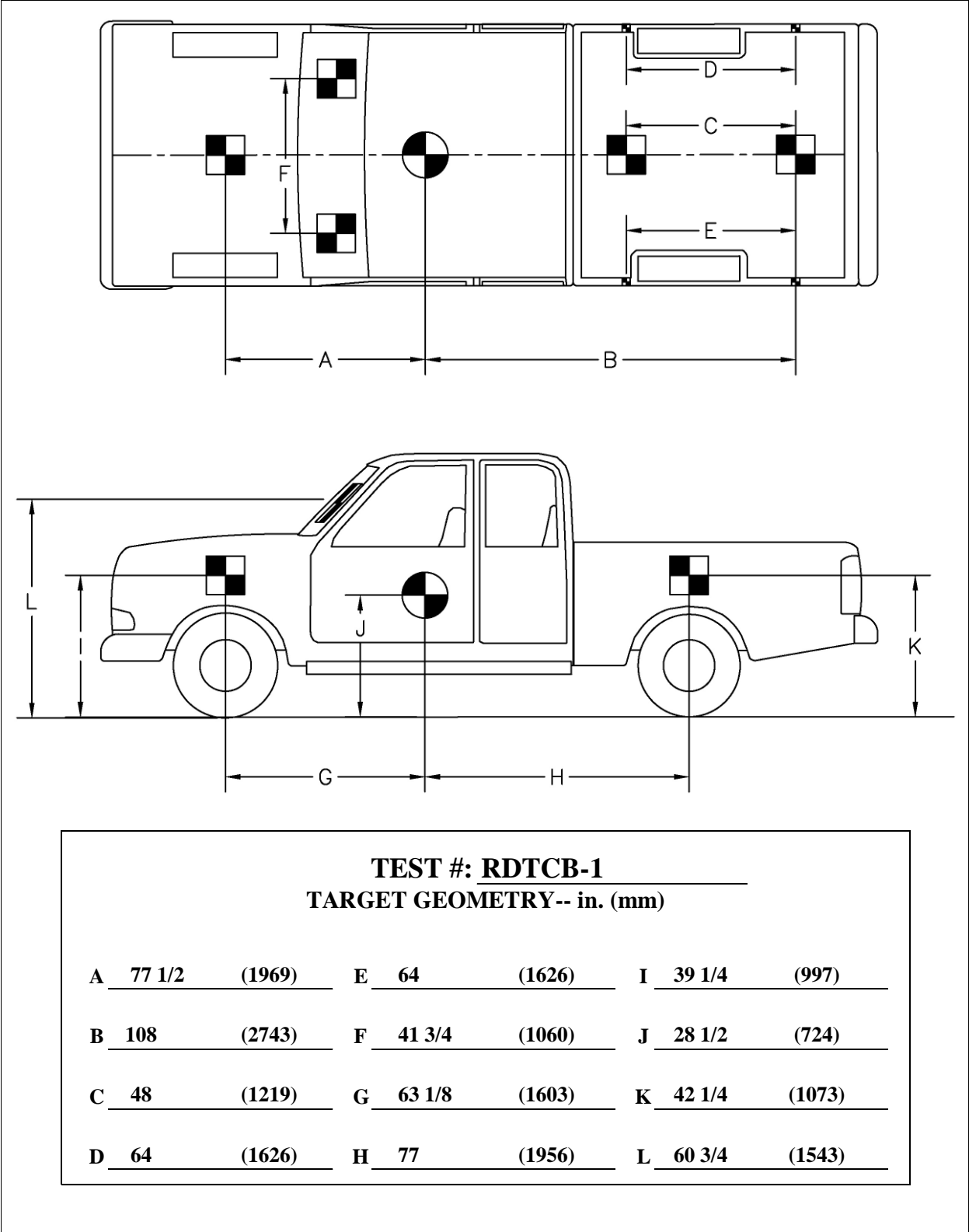


Figure 67. Target Geometry, Test No. RDTCB-1

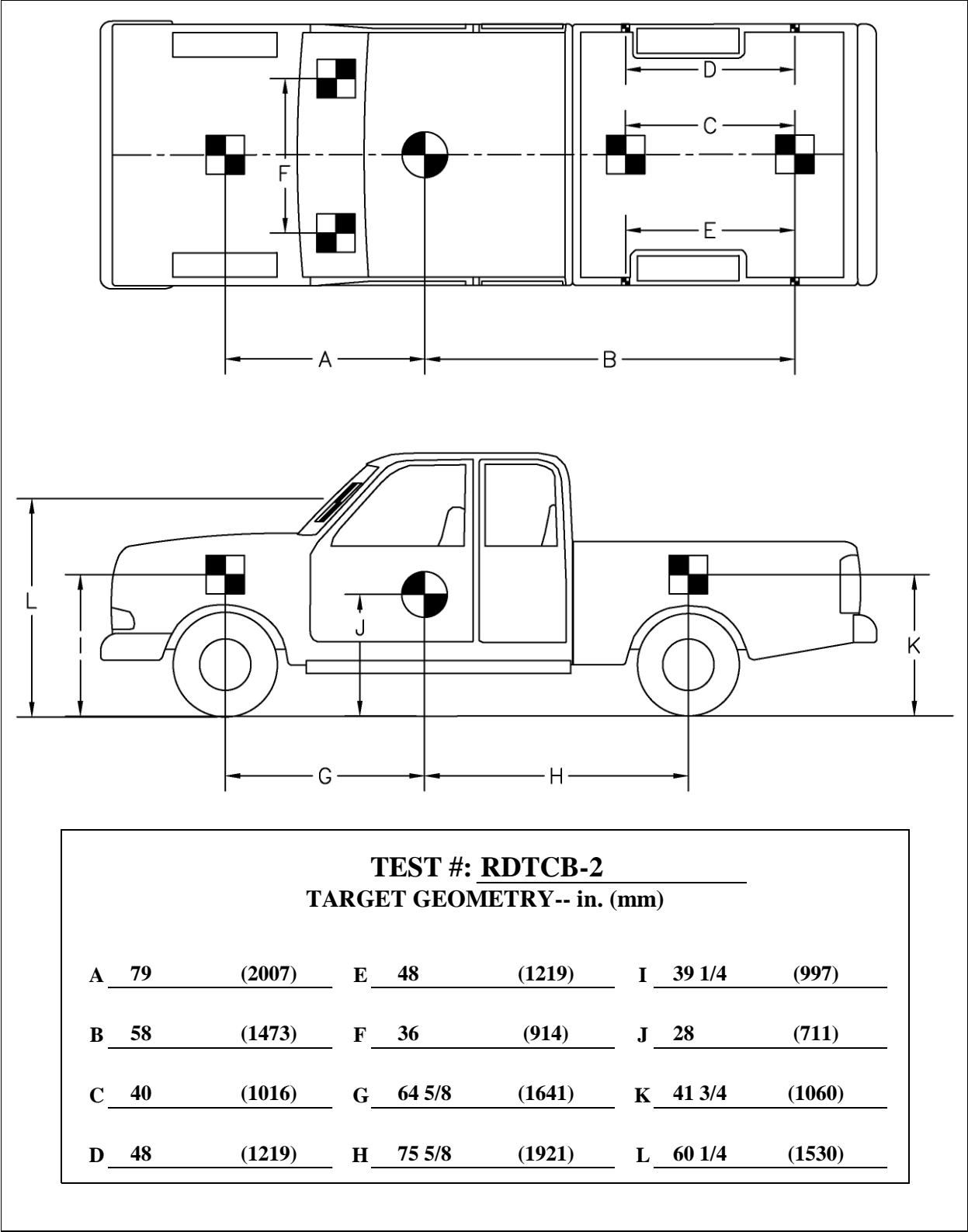


Figure 68. Target Geometry, Test No. RDTCB-2

## **9.4 Simulated Occupant**

For test nos. RDTCB-1 and RDTCB-2, a Hybrid II 50<sup>th</sup>-Percentile, Adult Male Dummy, equipped with clothing and footwear, was placed in the right-front seat of the test vehicle with the seat belt fastened. The dummy, which had a final weight of 170 lb (77 kg), was represented by model no. 572, serial no. 451, and was manufactured by Android Systems of Carson, California. As recommended by MASH, the dummy was not included in calculating the center of gravity location.

## **9.5 Data Acquisition Systems**

### **9.5.1 Accelerometers**

Three environmental shock and vibration sensor/recorder systems were used to measure the accelerations in the longitudinal, lateral, and vertical directions. All of the accelerometers were mounted near the center of gravity of the test vehicles. The electronic accelerometer data obtained in dynamic testing was filtered using the SAE Class 60 and the SAE Class 180 Butterworth filters conforming to the SAE J211/1 specifications [14].

The first accelerometer system was a two-arm piezoresistive accelerometer system manufactured by Endevco of San Juan Capistrano, California. Three accelerometers were used to measure each of the longitudinal, lateral, and vertical accelerations independently at a sample rate of 10,000 Hz. The accelerometers were configured and controlled using a system developed and manufactured by Diversified Technical Systems, Inc. (DTS) of Seal Beach, California. More specifically, data was collected using a DTS Sensor Input Module (SIM), Model TDAS3-SIM-16M. The SIM was configured with 16 MB SRAM and 8 sensor input channels with 250 kB SRAM/channel. The SIM was mounted on a TDAS3-R4 module rack. The module rack was configured with isolated power/event/communications, 10BaseT Ethernet and RS232 communication, and an internal backup battery. Both the SIM and module rack were

crashworthy. The “DTS TDAS Control” computer software program and a customized Microsoft Excel worksheet were used to analyze and plot the accelerometer data.

The second system, SLICE 6DX, was a modular data acquisition system manufactured by DTS of Seal Beach, California. The acceleration sensors were mounted inside the body of the custom built SLICE 6DX event data recorder and recorded data at 10,000 Hz to the onboard microprocessor. The SLICE 6DX was configured with 7 GB of non-volatile flash memory, a range of  $\pm 500$  g's, a sample rate of 10,000 Hz, and a 1,650 Hz (CFC 1000) anti-aliasing filter. The “SLICEWare” computer software programs and a customized Microsoft Excel worksheet were used to analyze and plot the accelerometer data.

The third system, Model EDR-3, was a triaxial piezoresistive accelerometer system manufactured by IST of Okemos, Michigan. The EDR-3 was configured with 256 kB of RAM, a range of  $\pm 200$  g's, a sample rate of 3,200 Hz, and a 1,120 Hz low-pass filter. The “DynaMax 1 (DM-1)” computer software program and a customized Microsoft Excel worksheet were used to analyze and plot the accelerometer data.

### **9.5.2 Rate Transducers**

An angle rate sensor, the ARS-1500, with a range of 1,500 degrees/sec in each of the three directions (roll, pitch, and yaw) was used to measure the rates of rotation of the test vehicles. The angular-rate sensor was mounted on an aluminum block inside the test vehicle near the center of gravity and recorded data at 10,000 Hz to the SIM. The raw data measurements were then downloaded, converted to the proper Euler angles for analysis, and plotted. The “DTS TDAS Control” computer software program and a customized Microsoft Excel worksheet were used to analyze and plot the angular-rate sensor data.

A second angular-rate sensor system, the SLICE MICRO Triax ARS, with a range of 1,500 degrees/sec in each of the three directions (roll, pitch, and yaw) was used to measure the

rates of rotation of the test vehicles. The angular-rate sensors were mounted inside the body of the custom built SLICE 6DX event data recorder and recorded data at 10,000 Hz to the onboard microprocessor. The raw data measurements were then downloaded, converted to the proper Euler angles for analysis, and plotted. The “SLICEWare” computer software program and a customized Microsoft Excel worksheet were used to analyze and plot the angular-rate sensor data.

### **9.5.3 Speed Trap**

For test no. RDTCB-1, three pressure-activated tape switches, spaced at approximately 6.0-ft (1.8-m) intervals, were used to determine the speed of the vehicle before impact. Each tape switch fired a strobe light which sent an electronic timing signal to the data-acquisition system as the right-front tire of the test vehicle passed over it. Test vehicle speeds were determined from electronic timing mark data recorded using TestPoint and LabVIEW computer software programs. A retro optical sensor triggered by targets on the side of the vehicle was used as a backup in test no. RDTCB-1. The targets triggered an electronic timing signal recorded by the data-acquisition system, allowing the test vehicle speed to be determined. Strobe lights and high-speed video analysis are used only in the event that vehicle speed cannot be determined from the electronic data.

For test no. RDTCB-2, a retro reflective optical sensor was used to determine the speed of the vehicle before impact. There were five targets spaced at 18-in. (457-mm) intervals along the side of the vehicle. Each target triggered an electronic timing signal to the data-acquisition system later used to calculate the vehicle speed. In test no. RDTCB-2, a second optical sensor using the same targets on the vehicle was used as a backup. High-speed video analysis is used only in the event that vehicle speed cannot be determined from the optical sensors.

#### **9.5.4 Digital Photography**

Three AOS VITcam high-speed digital video cameras, three AOS X-PRI high-speed digital video cameras, four JVC standard-speed digital video cameras, and one Canon standard-speed digital video camera were utilized to film test no. RDTCB-1. Three AOS VITcam high-speed digital video cameras, two AOS X-PRI high-speed digital video cameras, four JVC standard-speed digital video cameras, one Canon standard-speed digital video camera, and two GoPro standard-speed digital video cameras were utilized to film test no. RDTCB-2. Camera details, camera operating speeds, lens information, and a schematic of the camera locations relative to the system are shown in Figure 69 for test no. RDTCB-1 and Figure 70 for test no. RDTCB-2.

The high-speed videos were analyzed using ImageExpress MotionPlus and RedLake MotionScope software programs. Actual camera speed and camera divergence factors were considered in the analysis of the high-speed videos. A Nikon D50 digital still camera was also used to document pre- and post-test conditions for all tests.

	No.	Type	Operating Speed (frames/sec)	Lens	Lens Setting
High-Speed Video	2	AOS Vitcam	500	Cosmicar 12.5mm Fixed	-
	3	AOS Vitcam	500	Nikkor 28mm Fixed	-
	4	AOS X-PRI	500	Sigma 50mm Fixed	-
	5	AOS X-PRI	500	Canon 17-102	102
	6	AOS X-PRI	500	Nikkor 20mm Fixed	-
	7	AOS S-VIT 1531	500	Fujinon 50mm Fixed	-
	Digital Video	1	JVC – GZ-MC500 (Everio)	29.97	
2		JVC – GZ-MG27u (Everio)	29.97		
3		JVC – GZ-MG27u (Everio)	29.97		
4		JVC – GZ-MG27u (Everio)	29.97		
2		Canon ZR90	29.97		

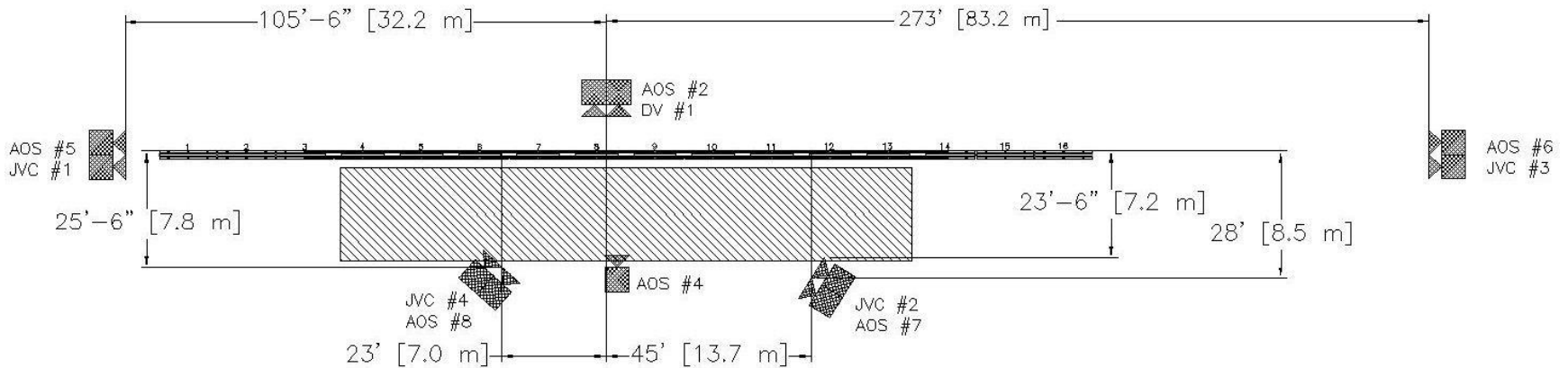


Figure 69. Camera Locations, Speeds, and Lens Settings, Test No. RDTCB-1

	No.	Type	Operating Speed (frames/sec)	Lens	Lens Setting
High-Speed Video	1	Vitcam CTM	500	Nikkor 28mm Fixed	-
	2	AOS Vitcam	500	Cosmicar 12.5mm Fixed	-
	6	AOS X-PRI	500	Fujinon 50mm Fixed	-
	7	AOS X-PRI	500	Canon 17-102	75
	8	AOS S-VIT 1531	500	Telesar Fixed 135mm	-
Digital Video	1	JVC – GZ-MC500 (Everio)	29.97		
	2	JVC – GZ-MG27u (Everio)	29.97		
	3	JVC – GZ-MG27u (Everio)	29.97		
	4	JVC – GZ-MG27u (Everio)	29.97		
	1	Canon ZR90	29.97		
	1	GoPro Hero 3	120		
	2	GoPro Hero 3	120		

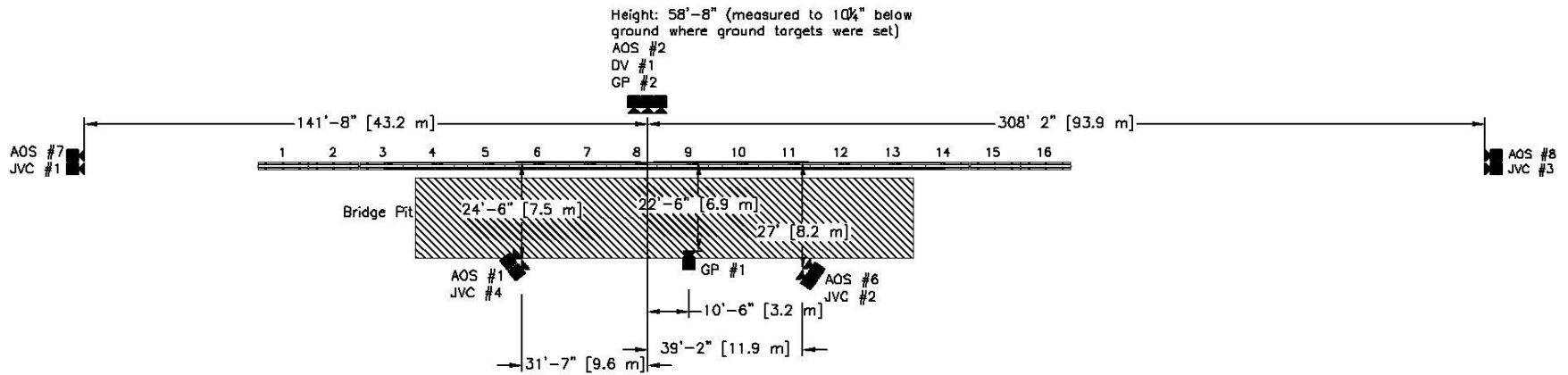


Figure 70. Camera Locations, Speeds, and Lens Settings, Test No. RDTCB-2

## 10 DESIGN DETAILS FOR TEST NO. RDTCB-1

### 10.1 Design Considerations

WisDOT worked with MwRSF to select a relatively conservative design for full-scale testing. The basic design consisted of a cap plate bolted across the TCB joint and continuous tubes running along the sides of the barriers. It was anticipated that a combination of the steel cap and the tubes would be effective at limiting barrier deflection through composite action, and the continuous tubes would provide for increased vehicle stability by presenting a more vertical face for the impacting vehicle to interact with. Various continuous tube sections were evaluated and an HSS 5-in. x 5-in. x  $\frac{3}{16}$ -in. (127-mm x 127-mm x 5-mm) square tube section was selected for the design based on several factors, including weight, mitigation of tube damage during impact, vehicle interaction, and moment capacity.

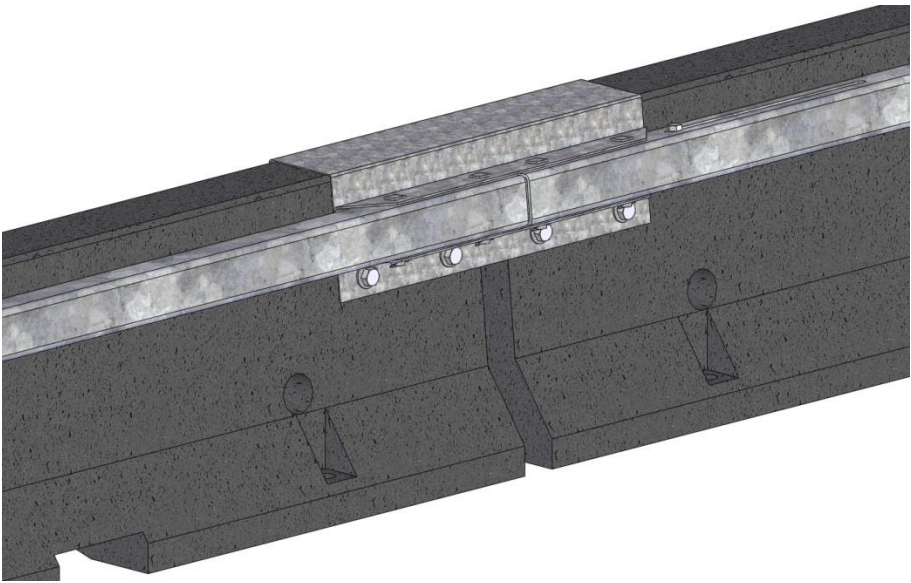
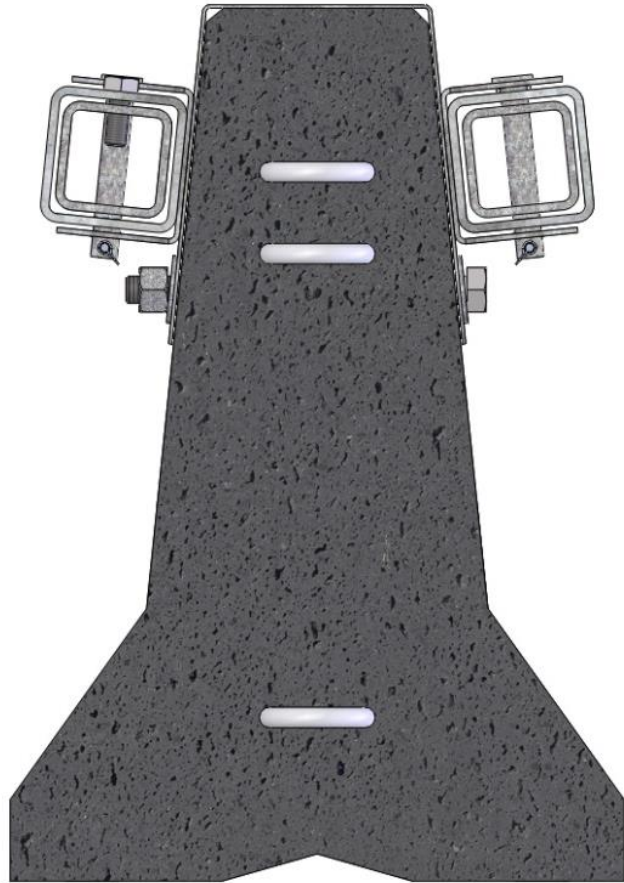
The mounting height of the tubes was also a consideration in the design. Previous MASH full-scale crash testing was conducted on the G3 box-beam guardrail system and New York's box-beam terminal design [27-28] found that box-beam systems with top mounting heights of 27 in. (685.6 mm) were capable of safely redirecting a 2270P vehicle under TL-3 impact conditions. Thus, 27 in. (685.6 mm) was selected as the minimum top mounting height for the tubes. This height was later increased to 29 in. (736.6 mm) due to interference with the connection of the cap and the barrier reinforcing steel.

MwRSF proposed several variations on the basic design of the low-deflection TCB system with variations on joints and connection details. Discussions with the sponsor and internal review narrowed the design down to three main prototypes. The three versions of the prototype varied in the attachment between the tubes and the steel cap, and the method for splicing and connecting the tube sections. These variations were made to address concerns regarding transport of the design, worker exposure, and ease of installation:

1. Version 3 – This design combined the location of the tube splice and the attachment of the tubes to the steel cap plate at the barrier joint using drop-in joint pins, as shown in Figure 71. It utilized a tube splice between tube sections and a mounting bracket located on the cap plate to hold the tubes at the correct height. This design was totally modular and allowed for splicing and mounting of the tubes using only drop pins. This design would be installed by placing the steel cap plate and bracket on the barrier and then installing the tubes and the splices.
2. Version 5 – This design was the same as Version 3 except that the tube splices were moved to the midspan of the TCB, away from the TCB joint and the steel cap plate bracket, as shown in Figure 72. This system was also modular, but allowed the tubes to be installed on a mounting bracket on the steel cap plate prior to lifting the entire assembly into place on the barrier.
3. Version 6 – This design welded the tubes directly to the mounting plate, with the tube splices located at the midspan, as shown in Figure 73. This design was not as modular or as easy to transport to the job site, but it was perceived as faster and easier to install.

WisDOT preferred Version 6 of the design prototypes due to the ease and speed of installation, and this design was carried forward into the first full-scale crash test.

A few remaining design considerations were deliberated for the low-deflection TCB system. First, it was noted that the design would need to account for construction tolerances and variability in the gap between the barrier segments as well as the barrier segment geometry. Thus, slotted holes were included in the various connection pieces and slight oversizing of the steel cap plate were included in the design to accommodate these variations. Second, the system was not designed for use on small-radius curvatures at this time. It was anticipated that the



129

Figure 71. Low-Deflection TCB Prototype, Version 3

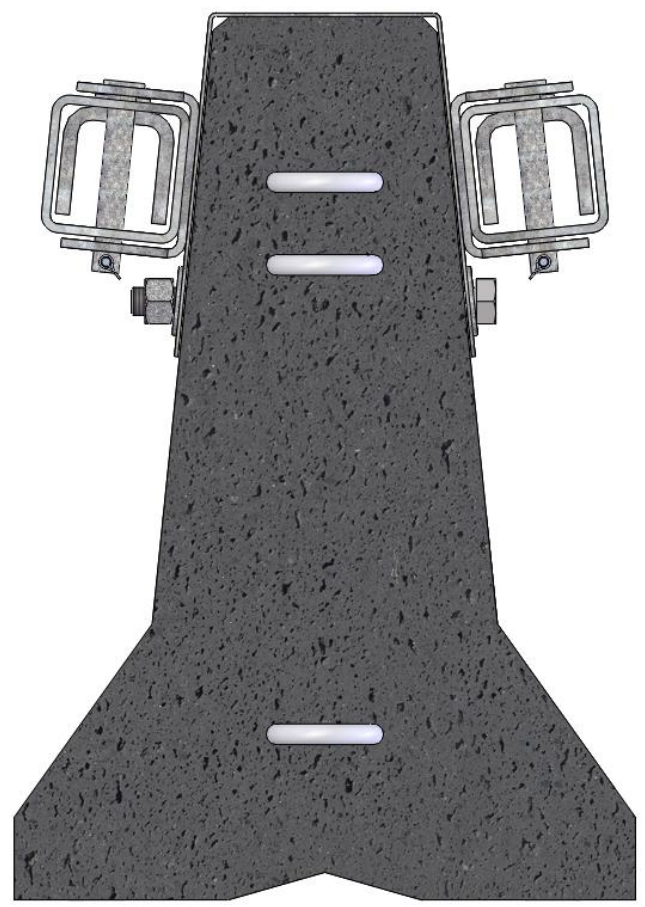
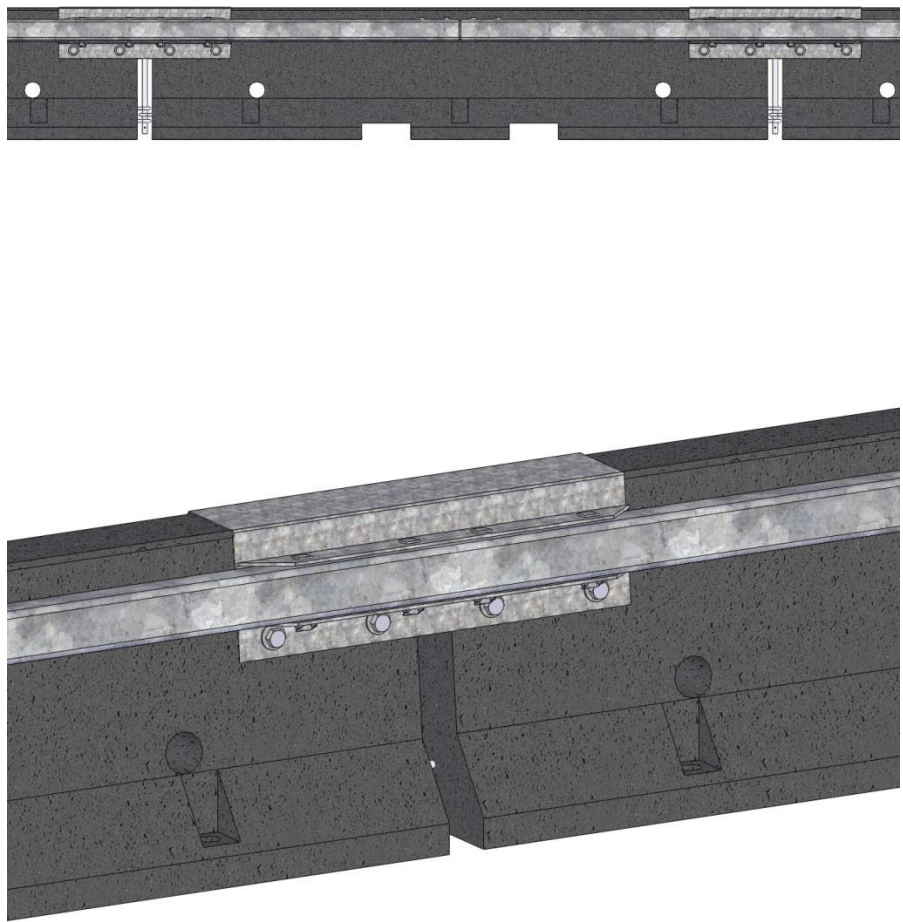
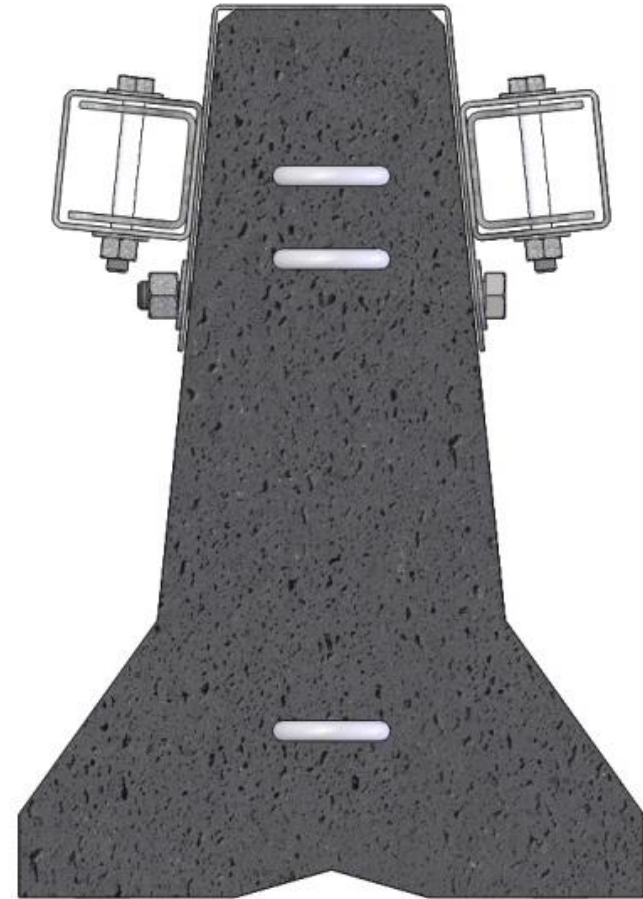


Figure 72. Low-Deflection TCB Prototype, Version 5



131

Figure 73. Low-Deflection TCB Prototype, Version 6

system would be used primarily in installations with very large curve radii that could be accommodated by the construction tolerance features described previously, and it was noted that design for smaller curve radii would require further design. Finally, end sections were not considered as part of the design. The testing described herein was conducted to evaluate the performance of the length-of-need of the barrier system. Thus, determination of adequate end termination and/or connection to other barrier systems was left for future research after the performance of the length-of-need was defined.

## 10.2 Design Details

The barrier system test installation was comprised of F-shape TCB segments joined with pins and stiffened by attachment of a steel cap across each joint of the barrier system and the addition of tubular beams on both faces of the barrier, as shown in Figure 74 through Figure 89. Photographs of the test installation are shown in Figure 90 and Figure 91. Material specifications, mill certifications, and certificates of conformity for the system materials are shown in Appendix B.

The system was composed of 16 F-shaped temporary concrete barriers 12.5-ft (3.81-m) long with a 5000 psi (34.5 MPa) compressive strength. Each of the barrier segments were connected by a 1 ¼-in. (32-mm) diameter A36 steel pin placed between ¾-in. (19-mm) diameter reinforcing bar loops extending from the end of the barrier sections. The connection loop bar material was A709 Grade 70 or A706 Grade 60 steel. The connection pin details are shown in Figure 82. All sections of the barrier were set on top of the concrete tarmac at the MwRSF outdoor test facility.

At the TCB segment connections, a 10 gauge ASTM A1011 Grade 50 formed sheet metal connection bracket was placed over the barrier and bolted to the concrete segments. Threaded rods with nuts and washers on both sides of the barrier were used rather than the nut and bolt

connection originally specified. Both bolts and threaded rods made from ASTM A449 or equivalent materials were considered acceptable for the connection of the metal bracket to the barrier as long as the threaded ends of the connection hardware did not extend more than ½ in. (12.7 mm) past the end of the nut. The connection brackets were 42 in. (1,067 mm) long and were centered on the barrier joint. It should be noted that the TCB segments were fabricated slightly wider than the 8-in. (203 mm) width specified for the cap. As such, the concrete on several of the TCB segments near the cap was ground down to allow the caps to fit, and it was anticipated that future versions of the cap would be widened slightly to allow for fabrication tolerances. Typical system installations would use galvanized hardware for the plate and tube sections. However, the tested system used painted steel to reduce costs.

The stiffness of the barrier was further increased by the addition of 5-in. x 5-in. x  $\frac{3}{16}$ -in. (127-mm x 127-mm x 5-mm) steel tubes to both faces of the barrier. Tubular beams were welded to the sheet metal connection bracket in order to complete the barrier-stiffening assembly. The square tubes were made of A500 Grade B steel. The beams used slotted holes at the connections with one slot substantially longer. The single increased slot length allowed for the splice inserts to be inserted and aligned with the next beam section and then moved back to the final position. Beam splices were placed at the center of each concrete barrier segment. Each splice contained a 22-in. (559-mm) long insert bolted to the inside of the box-beam on each side of the splice. The inserts were 4 ½-in. x 4 ½-in. x ½-in. (114-mm by 114-mm x 13-mm) U-shaped bent plates. The bent plates were made from grade A36 steel rather than ASTM 572 Grade 50 as specified in the bill of materials. Either material grade would be acceptable for actual field installations. The beam splices were bolted together on both the front and back beams with four Grade 5,  $\frac{3}{4}$ -in. (19-mm) diameter bolts.

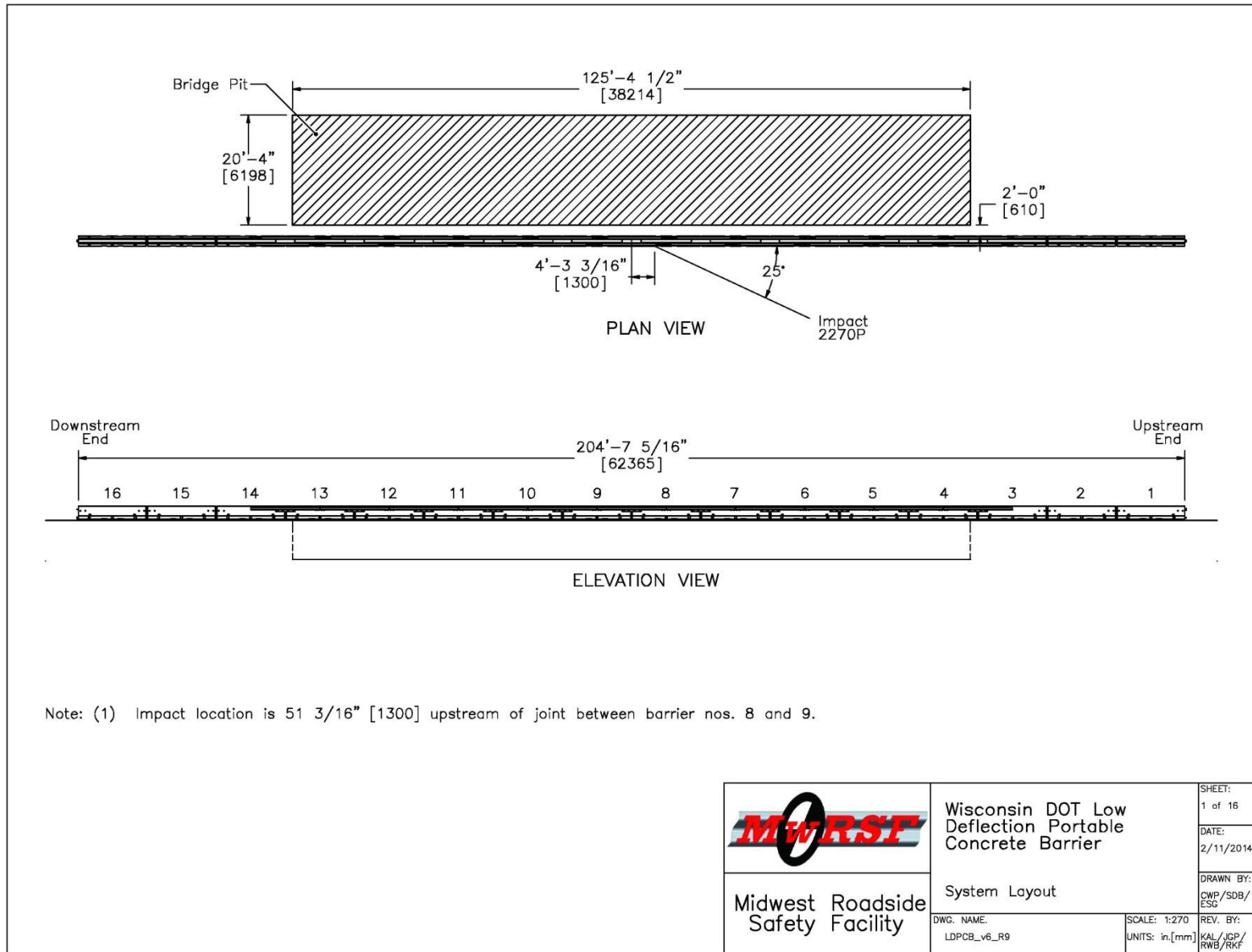


Figure 74. Test Installation Layout, Test No. RDTCB-1

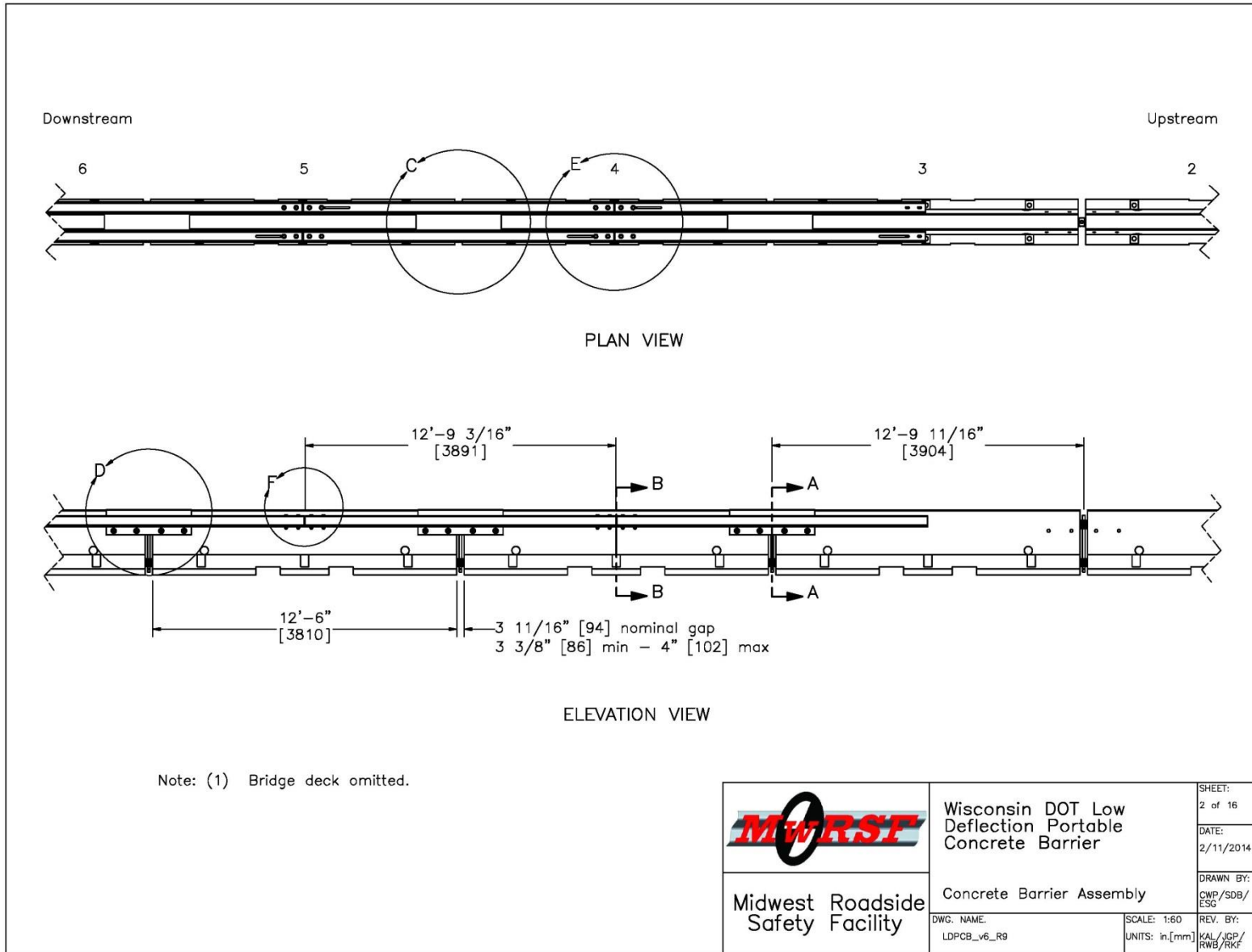


Figure 75. Test Installation Layout, Test No. RDTCB-1

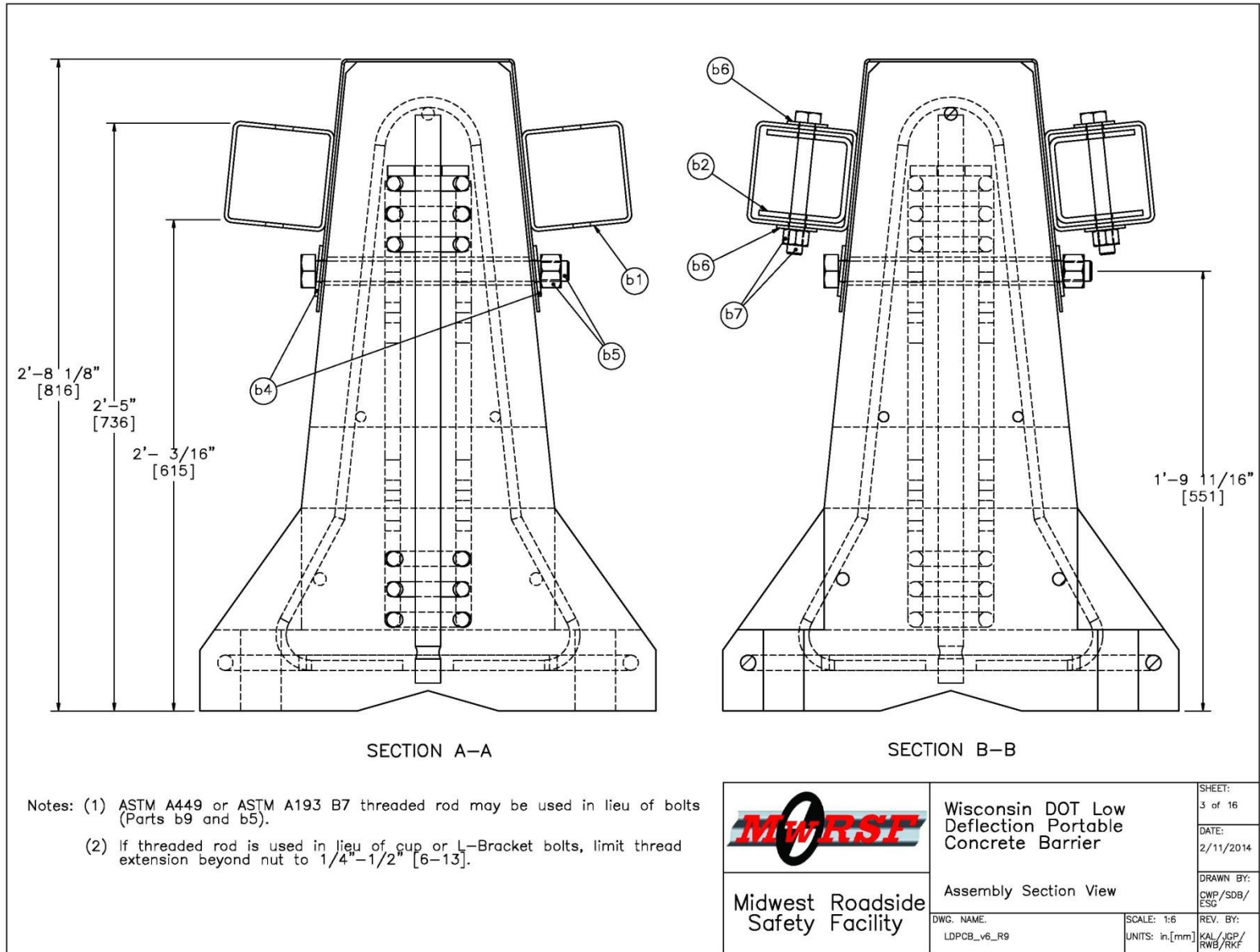


Figure 76. Test Installation Layout, Test No. RDTCB-1

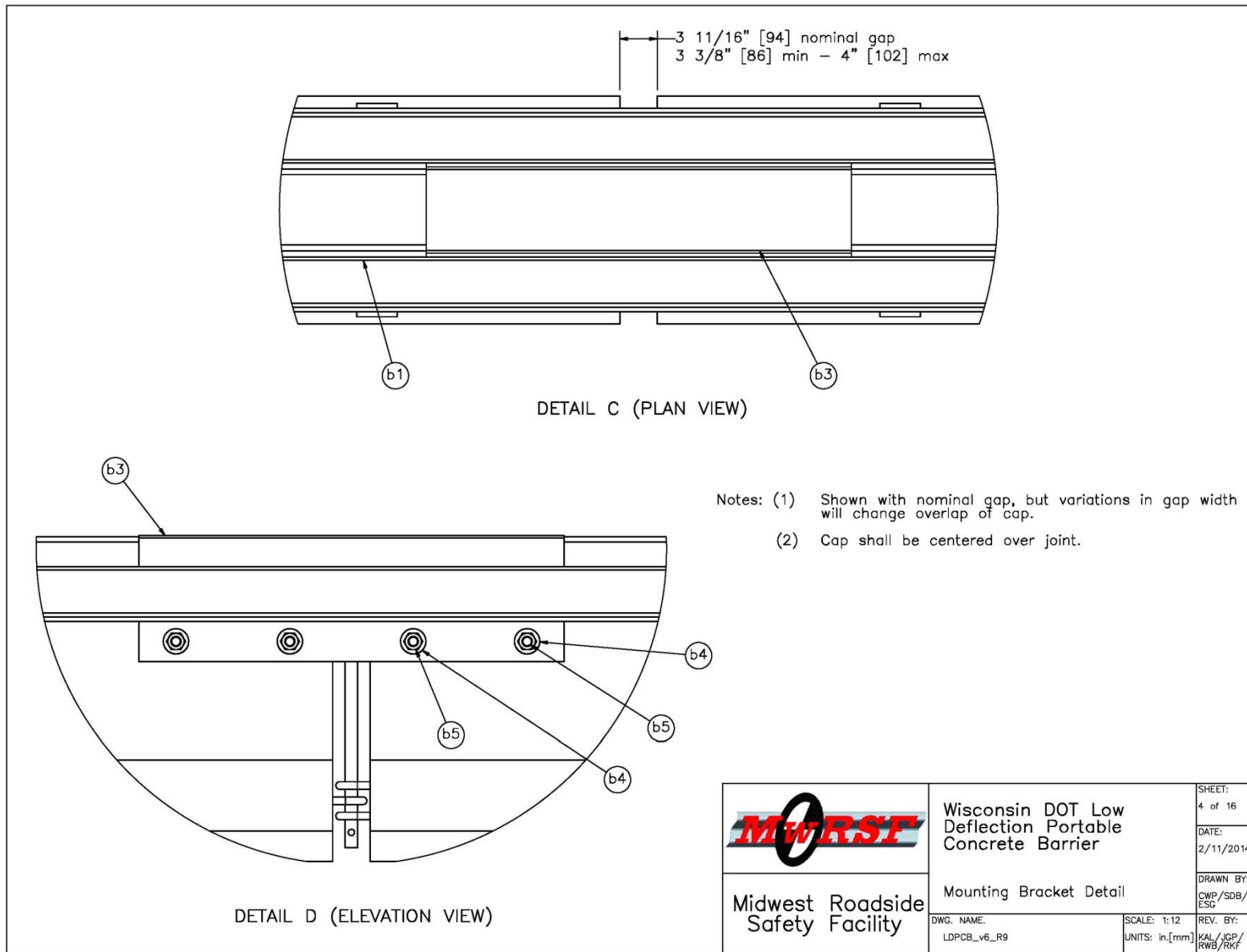


Figure 77. Test Installation Layout, Test No. RDTCB-1

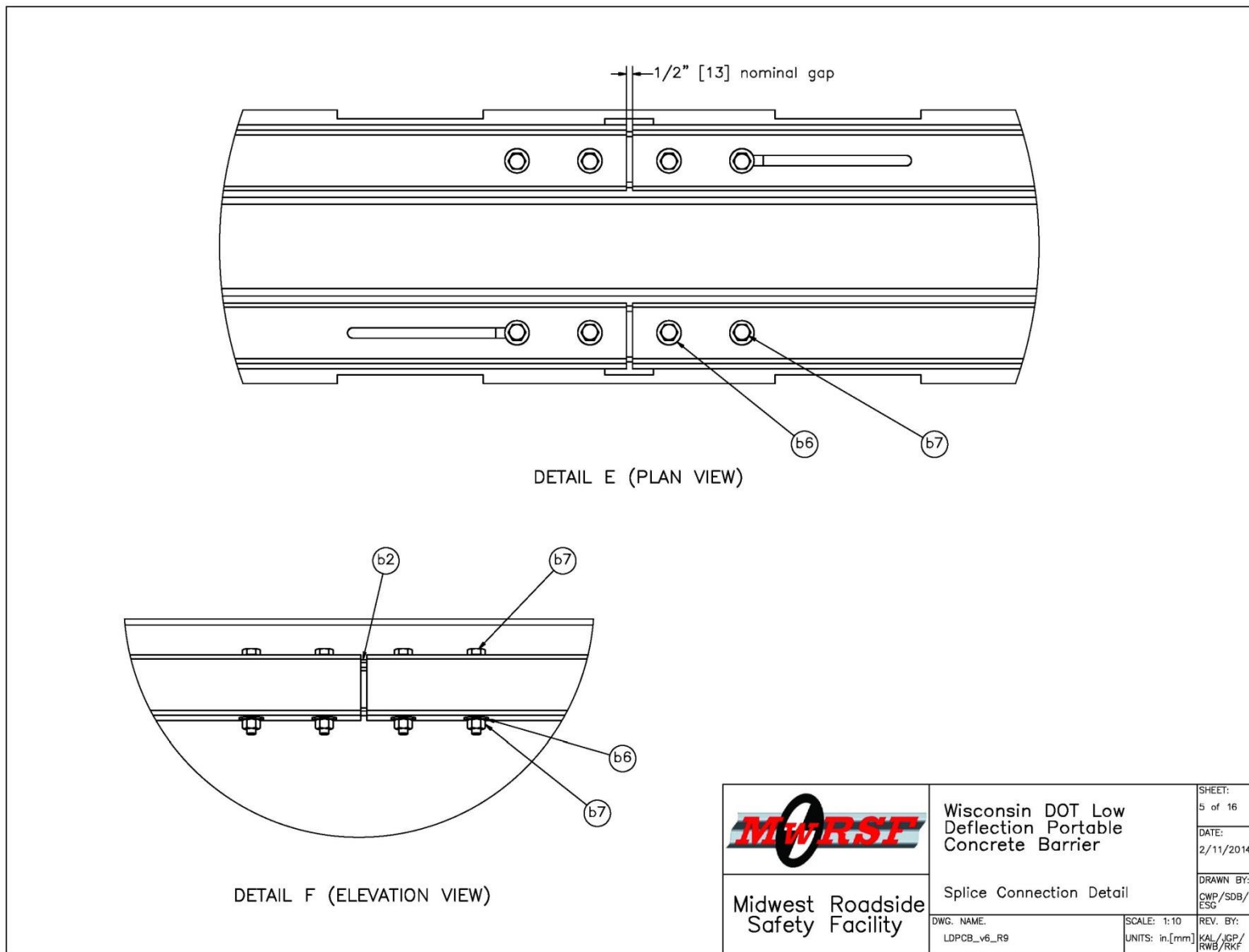


Figure 78. Test Installation Layout, Test No. RDTCB-1

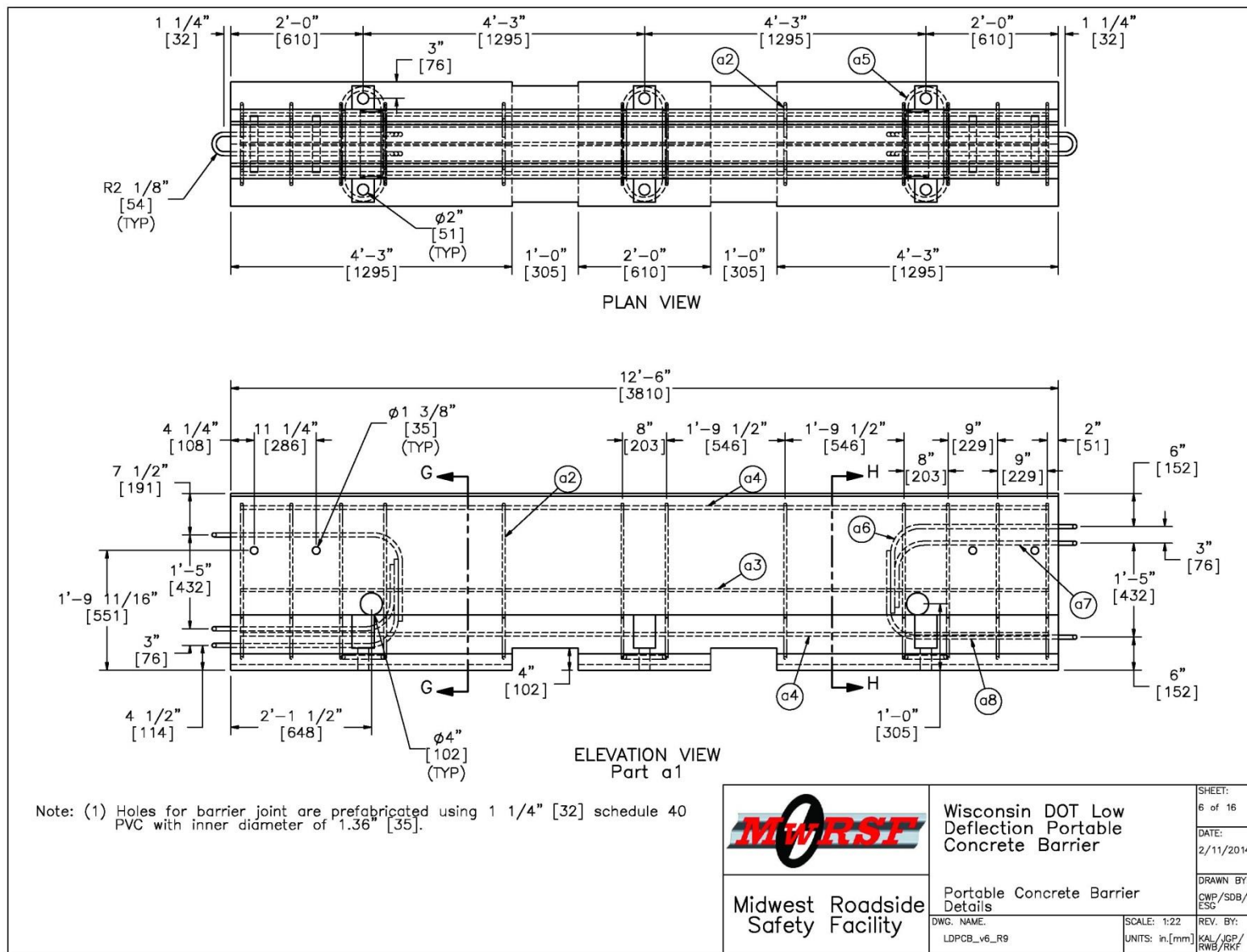


Figure 79. Test Installation Layout, Test No. RDTCB-1

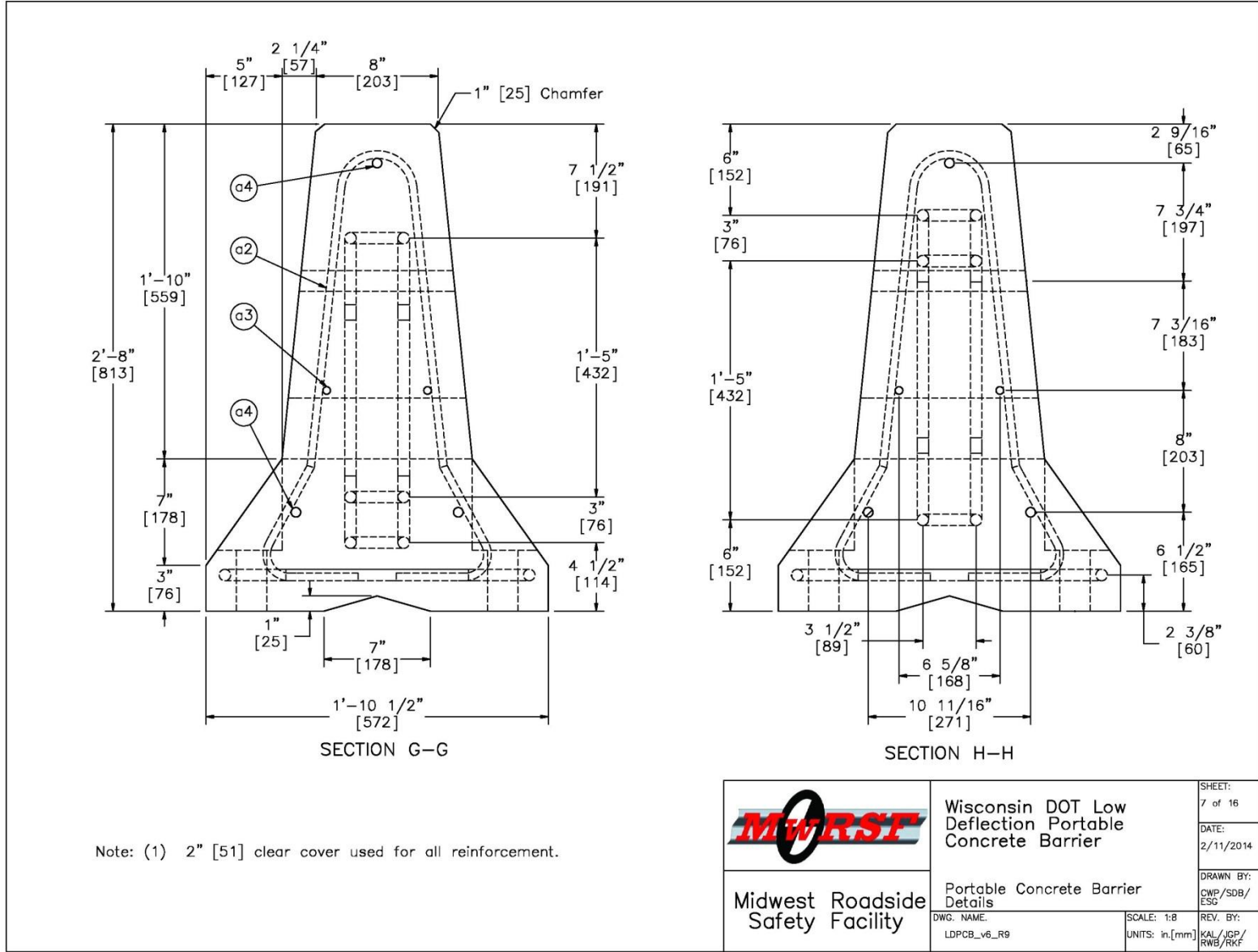


Figure 80. Test Installation Layout, Test No. RDTCB-1

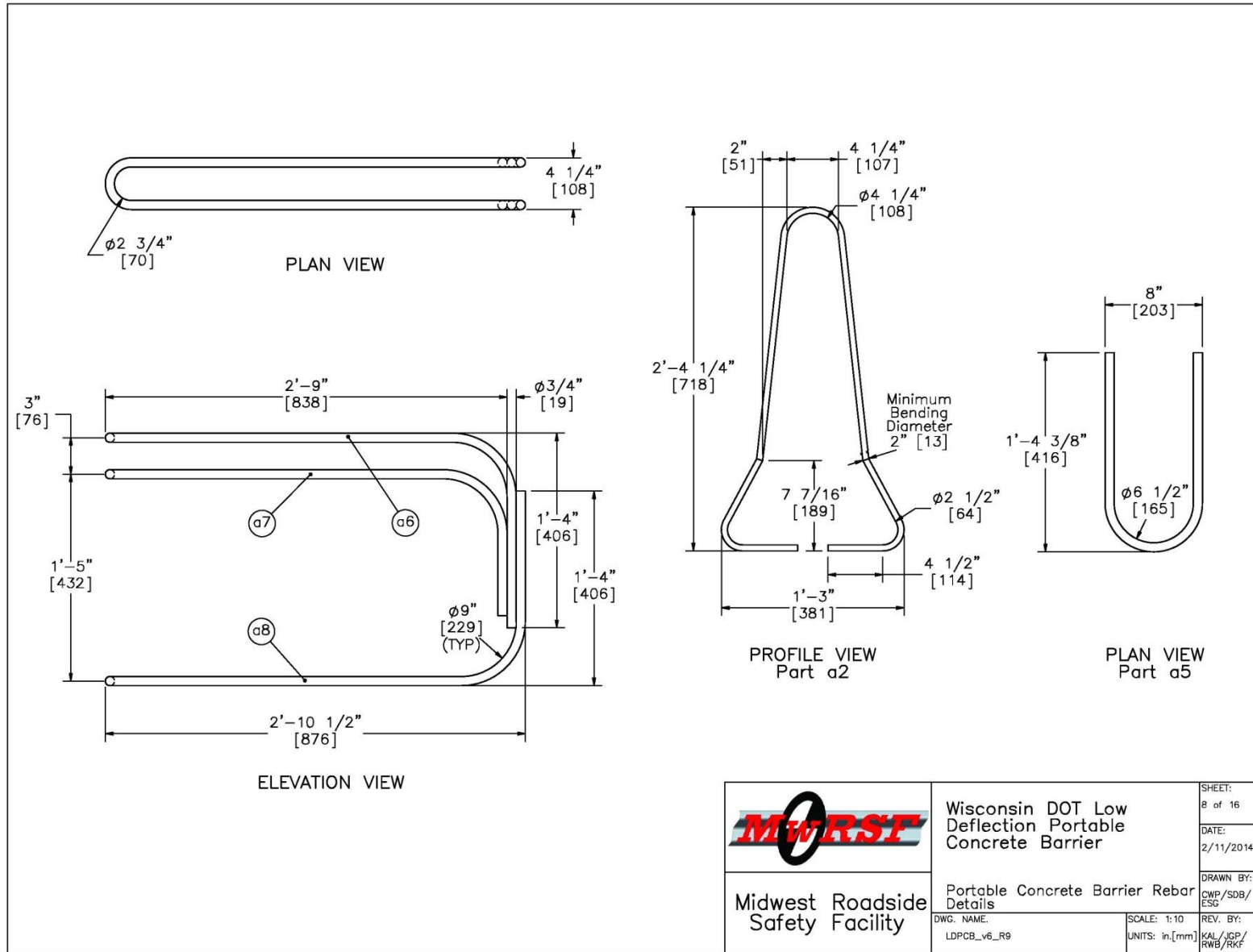


Figure 81. Test Installation Layout, Test No. RDTCB-1

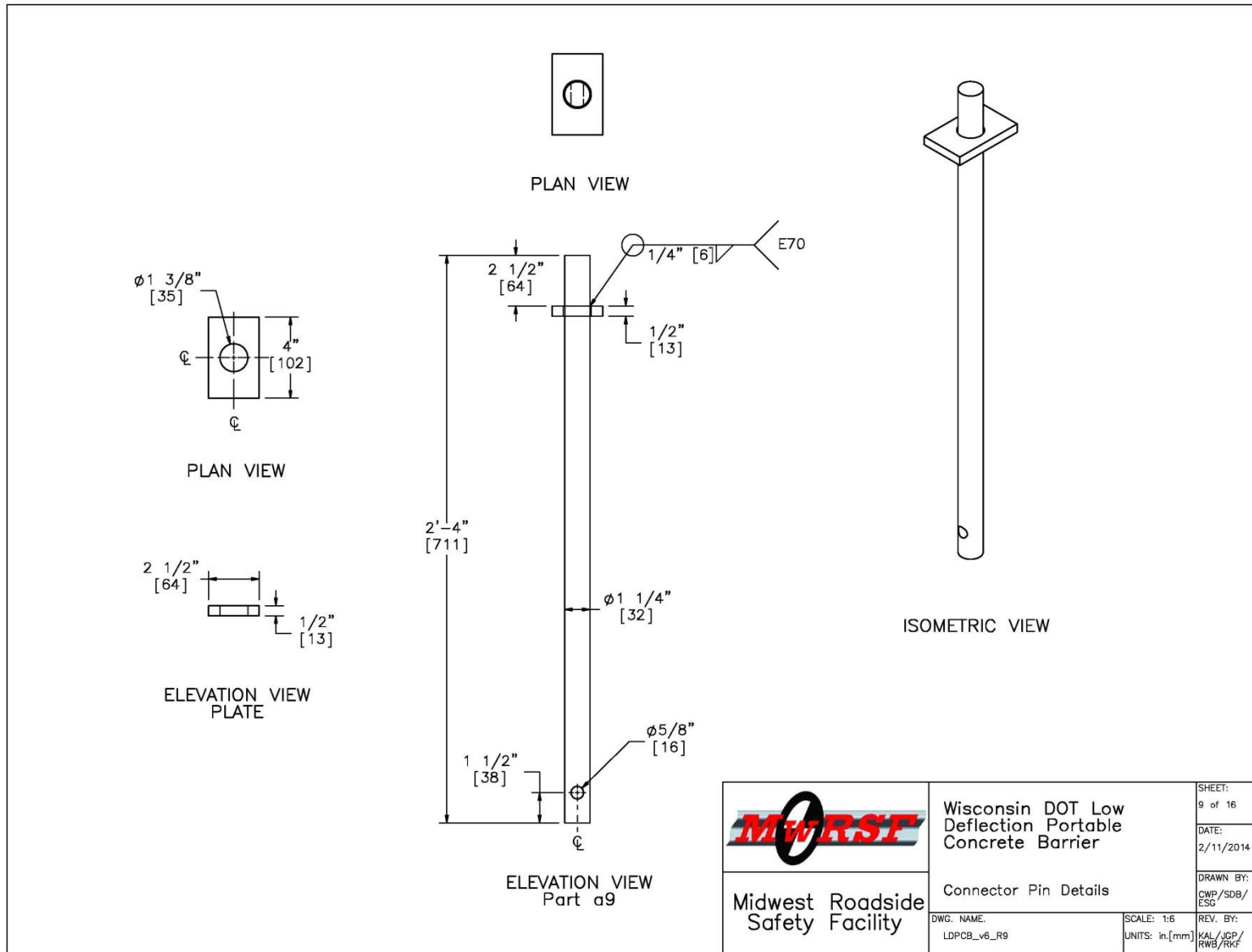


Figure 82. Test Installation Layout, Test No. RDTCB-1

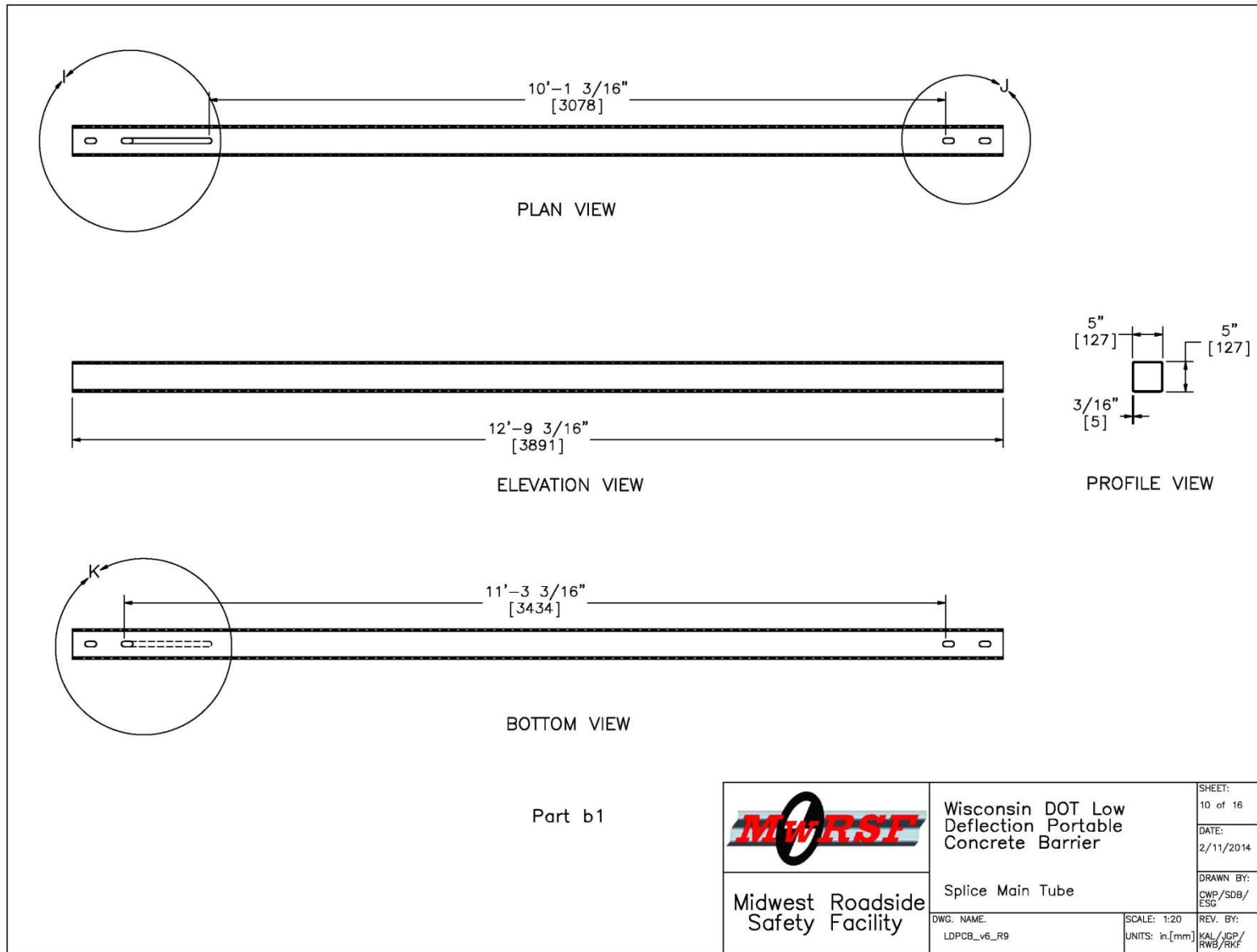


Figure 83. Test Installation Layout, Test No. RDTCB-1

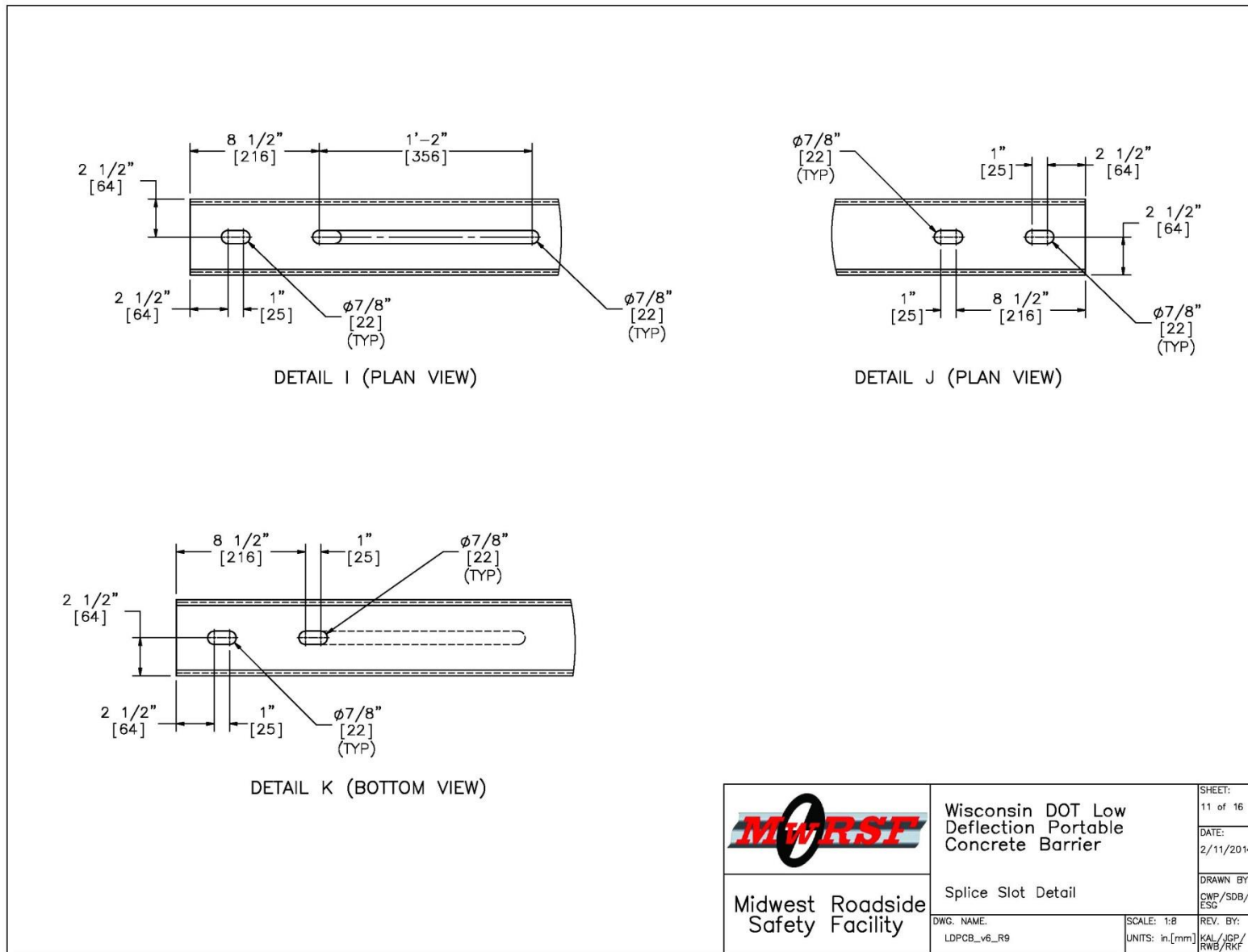


Figure 84. Test Installation Layout, Test No. RDTCB-1

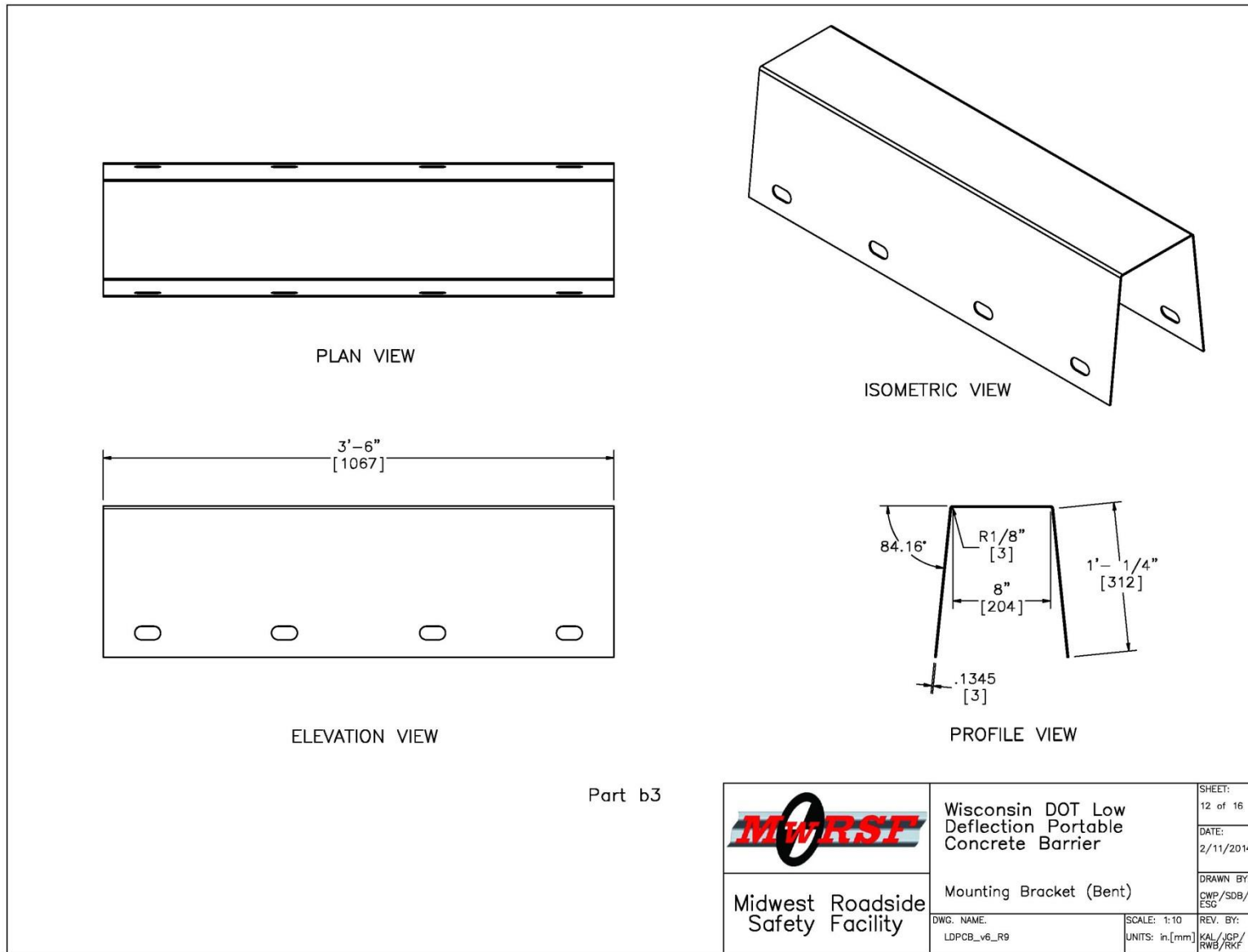


Figure 85. Test Installation Layout, Test No. RDTCB-1

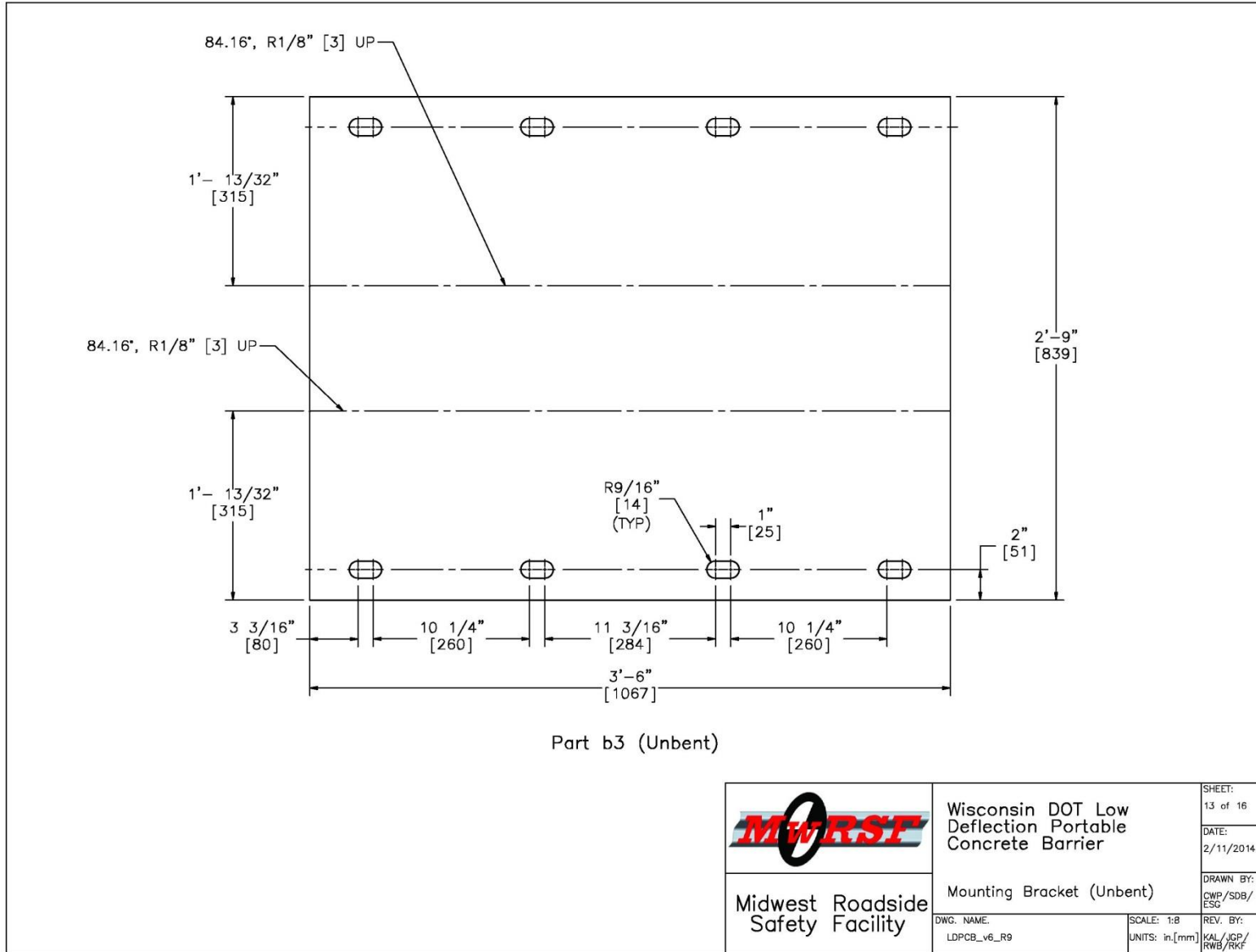


Figure 86. Test Installation Layout, Test No. RDTCB-1

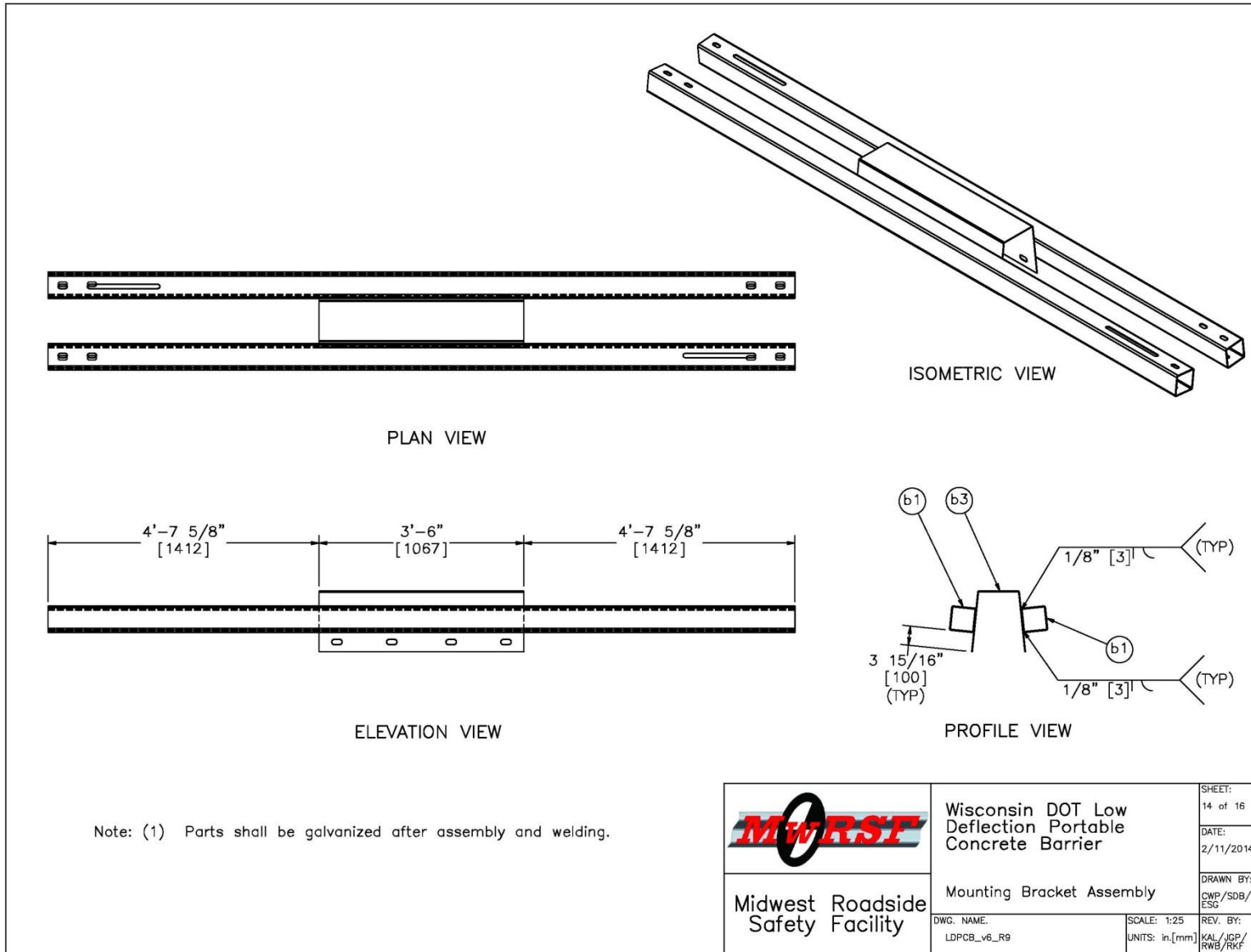


Figure 87. Test Installation Layout, Test No. RDTCB-1

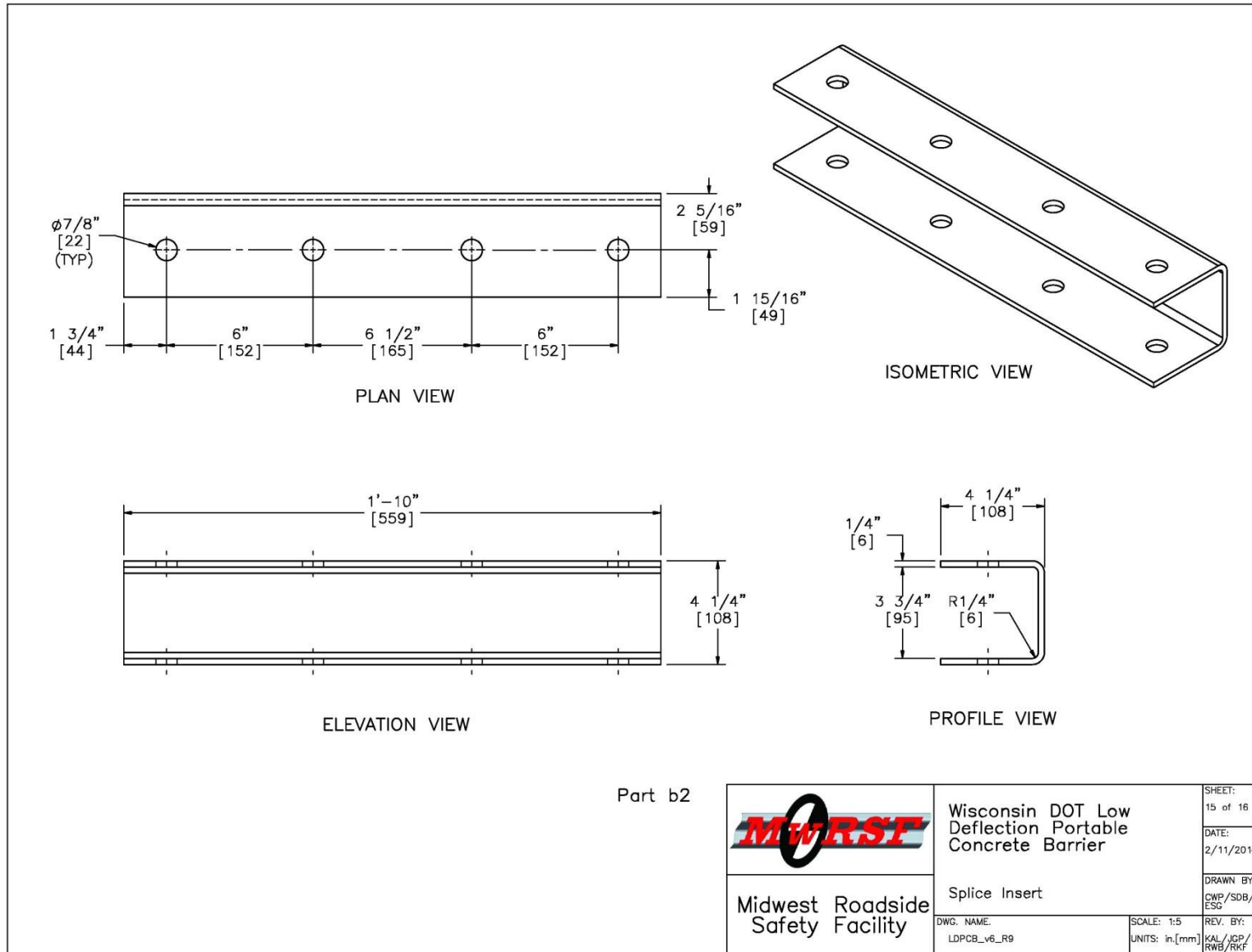


Figure 88. Test Installation Layout, Test No. RDTCB-1

Item No.	QTY.	Description	Material Specifications	Hardware
a1	16	Portable Concrete Barrier	min f'c=5000 psi [34.5 MPa]	SWC09
a2	192	1/2" [13] Dia., 72" [1829] Long Form Bar	ASTM A615 Grade 60	SWC09
a3	32	1/2" [13] Dia., 146" [3708] Long Longitudinal Bar	ASTM A615 Grade 60	SWC09
a4	48	5/8" [16] Dia., 146" [3708] Long Longitudinal Bar	ASTM A615 Grade 60	SWC09
a5	96	3/4" [19] Dia., 36" [914] Long Anchor Loop Bar	ASTM A615 Grade 60	SWC09
a6	32	3/4" [19] Dia., 101" [2565] Long Connection Loop Bar	ASTM A709 Grade 70 or A706 Grade 60	SWC09
a7	32	3/4" [19] Dia., 91" [2311] Long Connection Loop Bar	ASTM A709 Grade 70 or A706 Grade 60	SWC09
a8	32	3/4" [19] Dia., 102" [2591] Long Connection Loop Bar	ASTM A709 Grade 70 or A706 Grade 60	SWC09
a9	15	1 1/4" [32] Dia., 28" [711] Long Connector Pin	ASTM A36 Galvanized	FMW02
b1	22	5"x5"x3/16" [127x127x5], 12'-9 3/16" [3891] Long Splice Main Tube	ASTM A500 Grade B Galvanized after Welding	-
b2	20	4 1/2"x4 1/2"x1/4" [114x114x6], 22" [559] Long Splice Insert	ASTM 572 Grade 50 Galvanized	-
b3	11	42"x33" [1067x838] 10 Gage Mounting Bracket Plate	ASTM A1011 Grade 50 Galvanized after Welding	-
b4	88	1" [25] Dia. Washer	ASTM F844 Galvanized	-
b5	44	1" [25] Dia. UNC, 12 1/2" [318] Long Heavy Hex Bolt and Nut	Bolt ASTM A325/A449 Type 1 Galvanized, Nut ASTM A563DH Galvanized	-
b6	160	3/4" [19] Dia. Washer	ASTM F844 Galvanized	-
b7	80	3/4" [19] Dia. UNC, 6 1/2" [165] Long, 2" [51] Threaded Hex Bolt and Nut	Bolt ASTM A325/A449/SAE Grade 5 Galvanized, Nut ASTM A563DH Grade 5 Galvanized	-
			Wisconsin DOT Low Deflection Portable Concrete Barrier	
			Bill of Materials	
Midwest Roadside Safety Facility			DWG. NAME: LDPcb_v6_R9	SCALE: NONE UNITS: in.[mm]
			REV. BY: KAL/jgp/ RWB/Rkf	
			SHEET: 16 of 16	
			DATE: 2/11/2014	
			DRAWN BY: CWP/SDB/ ESG	

Figure 89. Test Installation Layout, Test No. RDTCB-1



Figure 90. Stiffened TCB Test Installation, Test No. RDTCB-1

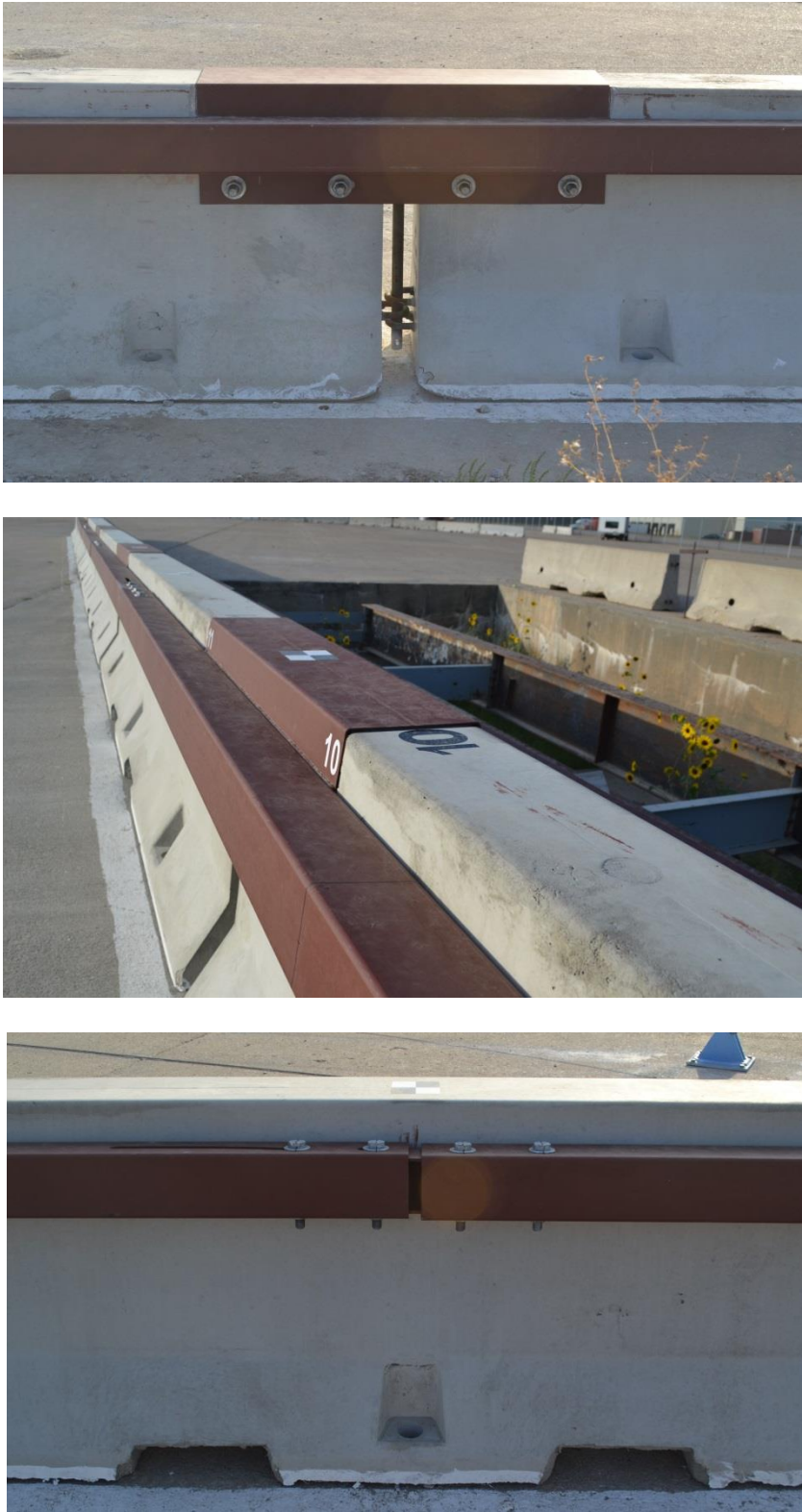


Figure 91. Barrier Segment Connection Designs, Test No. RDTCB-1

## **11 FULL-SCALE CRASH TEST NO. RDTCB-1**

### **11.1 Test No. RDTCB-1**

The 4,998-lb (2,267-kg) pickup truck impacted the low-deflection TCB system at a speed of 63.6 mph (102.4 km/h) and at an angle of 24.9 degrees. A summary of the test results and sequential photographs are shown in Figure 92. Additional sequential photographs are shown in Figures 93 through 94. Documentary photographs of the crash test are shown in Figure 95.

### **11.2 Weather Conditions**

Test no. RDTCB-1 was conducted on September 5<sup>th</sup>, 2012 at approximately 1:50 pm. The weather conditions as per the National Oceanic and Atmospheric Administration (station 14939/LNK) were reported and are shown in Table 9.

Table 9. Weather Conditions, Test No. RDTCB-1

Temperature	89° F
Humidity	23%
Wind Speed	13 mph
Wind Direction	20° from True North
Sky Conditions	Clear
Visibility	10 Statute Miles
Pavement Surface	Dry
Previous 3-Day Precipitation	0 in.
Previous 7-Day Precipitation	0 in.

### **11.3 Test Description**

Initial vehicle impact was to occur  $51\frac{3}{16}$  in. (1.3 m) upstream of the center of the joint between barrier nos. 8 and 9, as shown in Figure 96, which was selected using the CIP guidance found in Section 2.3 of MASH or Table 2.6 of MASH. The actual point of impact was 10 in. (254 mm) upstream of the target impact point. A sequential description of the impact events is contained in Table 10. The vehicle came to rest approximately 153 ft (46.6 m) past the

downstream end on the traffic side of the barrier with a slight yaw angle toward the barrier. The vehicle trajectory and final position are shown in Figures 92 and 97.

Table 10. Sequential Description of Impact Events, Test No. RDTCB-1

TIME (sec)	EVENT
0.000	Right-front bumper of vehicle impacted barrier $61\frac{3}{16}$ in. (1,554 mm) upstream of joint between barrier nos. 8 and 9
0.005	Vehicle right-side fender was deflecting upward and backward
0.014	Cracks began to form on backside of barrier no. 8
0.018	Barrier no. 8 began to deflect backward
0.020	Vehicle hood began to deflect upward and backward
0.032	Barrier no. 9 began to deflect backward
0.038	Vehicle headlight had shattered
0.044	Vehicle began to yaw away from barrier
0.048	Barrier no. 7 was deflecting downstream
0.054	Vehicle front right-side door was ajar
0.058	Upstream end of barrier no. 10 was deflecting forward
0.060	Cracks began to form on backside of barrier 9
0.070	Vehicle was rolling toward barrier
0.072	Vehicle roof was deformed
0.110	Vehicle was pitching upward
0.114	Upstream end of barrier no. 6 was deflecting backward
0.114	Vehicle left front tire was airborne
0.118	Downstream end of barrier no. 11 was deflecting backward
0.138	Rear-left tire became airborne
0.144	Spalling occurred on lower downstream edge of barrier no. 9
0.190	Vehicle was rolling toward barrier
0.202	Vehicle was parallel to system
0.258	Back edge of system reached edge of simulated bridge deck
0.270	Spalling occurred on lower downstream edge of barrier no. 10
0.282	Vehicle rear bumper was deformed
0.324	Vehicle was pitching downward
0.354	Downstream end of barrier no. 5 was deflecting backward

0.590	Vehicle exited system
0.614	Vehicle began to roll away from barrier
0.664	Barrier segments stopped moving
0.776	Front left tire made contact with ground
0.912	Vehicle was yawing toward system
1.20	Vehicle continued to move downstream from system

#### 11.4 Barrier Damage

Damage to the barrier was moderate, as shown in Figure 99 through Figure 101. Barrier damage consisted of contact marks on the front face of the concrete segments, spalling of the concrete, concrete cracking and failure, and permanent deformation of the steel tube rails. The length of vehicle contact along the barrier was approximately 36.7 ft (11.2 m) which spanned from 5.1 ft (1.6 m) upstream from the center of the joint between barrier nos. 8 and 9, to 5.8 ft (1.8 m) downstream from the center of the joint between barrier nos. 10 and 11.

Barrier nos. 5 through 12 all sustained permanent lateral deflection. Barrier nos. 7 through 10 had portions of their bases suspended over the simulated roadway edge, but showed no drop in barrier height. Tire marks were visible on the concrete faces of barrier nos. 8 and 9, and the steel tubes on the front of barrier nos. 8 through 11 showed tire and scuff marks. Barrier no. 8 had significant spalling on the front downstream toe which resulted in a 22-in. x 5-in. x 3-in. (559-mm x 127-mm x 76-mm) piece of concrete separating from the barrier. The backside of barrier no. 8 showed two vertical cracks which spanned from the top edge to the downstream lifting recess slot. Barrier no. 9 showed three vertical cracks that spanned from the top edge to the lifting recesses. The cracks were observed to have penetrated about halfway through the barrier. The downstream toe on the backside of barrier no. 9 also exhibited significant spalling. Barrier nos. 7, 10, 11, and 12 had cracks on the front of the concrete originating near the lifting recesses.

Deformation of the steel hardware components was observed following the full-scale crash test. The tubular steel rails did not tear or crush inward at any point in the system. However, permanent deformation due to flexure of the tube section was observed in the tube rails on the front and back sides of the system at the joint between barrier segment nos. 8 and 9. The rail splices remained connected, but were expanded or contracted due to bolt slippage. The back rail splice at the middle of barrier no. 8 was separated from the concrete about 2 in. (51 mm). The back rail splice at the middle of barrier no. 9 was separated from the concrete about 2 ½ in. (64 mm). The front rail splice at the middle of barrier nos. 11 and 12 was separated from the concrete about ¾ in. (19 mm) and 1 in. (25 mm), respectively. Separation of the tubes from the face of the barrier segments was noted to a lesser extent at several additional splice locations along the deformed length of the barrier system. Deformation of the steel plate cap at the joint between barrier segment nos. 8 and 9 was observed as well. No damage was noted to the splice bolts or steel cap connection bolts.

Barrier segment gap widths were recorded before and after the test at the front and back top edge. The barrier gaps were initially equal before the test was conducted. The gaps after the test were found to be different in the front and back due to curvature of the system. The maximum expansion of the joint gap was limited to 1<sup>1</sup>/<sub>16</sub> in. (27 mm) at the back edge between barrier nos. 8 and 9, and the maximum contraction was also found to be 1<sup>3</sup>/<sub>16</sub> in. (30 mm) at this joint.

The permanent set deflection of the barrier system was 41 ½ in. (1,054 mm), which occurred at the upstream end of barrier no. 9, as measured in the field. This level of barrier deflection created a maximum extent of the TCB segment past the edge of the bridge deck of 17½ in. (445 mm). However, there was no indication of the barriers disengaging or tipping off of the bridge deck, and the entire system remained stable and upright on the road surface. The

maximum lateral dynamic barrier deflection, including tipping of the barrier along the top surface, was 43.0 in. (1,092 mm) at the upstream end of barrier no. 9, as determined from high-speed digital video analysis. The working width of the system was found to be 55.1 in. (1,400 mm), also determined from high-speed digital video analysis.

### 11.5 Vehicle Damage

The damage to the vehicle was moderate, as shown in Figure 102 and Figure 103. The maximum occupant compartment deformations are listed in Table 11 along with the deformation limits established in MASH for various areas of the occupant compartment. Note that none of the MASH-established deformation limits were violated. Complete occupant compartment and vehicle deformations and the corresponding locations are provided in Appendix E.

Table 11. Maximum Occupant Compartment Deformations by Location, Test No. RDTCB-1

LOCATION	MAXIMUM DEFORMATION in. (mm)	MASH ALLOWABLE DEFORMATION in. (mm)
Wheel Well & Toe Pan	$\frac{3}{8}$ (10)	$\leq 9$ (229)
Floor Pan & Transmission Tunnel	$\frac{1}{2}$ (13)	$\leq 12$ (305)
Side Front Panel (in Front of A-Pillar)	$\frac{1}{2}$ (13)	$\leq 12$ (305)
Side Door (Above Seat)	$\frac{1}{4}$ (8)	$\leq 9$ (229)
Side Door (Below Seat)	$1\frac{1}{4}$ (32)	$\leq 12$ (305)
Roof	0 (0)	$\leq 4$ (102)
Windshield	0 (0)	$\leq 3$ (76)

The majority of the damage was concentrated on the right-front corner and right side of the vehicle where the impact occurred. The right side of the bumper was crushed inward and back. The right-front fender was deformed inward in front of the right-front wheel and was dented and torn behind the right-front wheel. A 4½-in. (114-mm) gap was measured between the right-front fender and hood near the front of the vehicle. The right-front steel rim was severely

deformed with tears and significant crushing. An 11-in. (279-mm) tear was observed in the right-front tire sidewall. The right side headlight was removed from the vehicle. Denting and scraping were observed on the right side including a 5½-in. (140-mm) wide gouge that extended the entire length of the vehicle. The right-front upper control arm was fractured, but the right-front wheel was upright and not completely disengaged. The right-rear bumper was folded and torn at the corner and buckled inward. The right-rear taillight was removed. The left side of the front bumper separated from the left-front fender 3½ in. (89 mm). The front of the hood had a 2½-in. (64-mm) gap on the left side. The left-front fender was dented in at the top. There was a 2-in. (51-mm) gap between the left-front fender and the left-front door. The roof and window glass remained undamaged during the impact. No visible sign of deformation occurred on the vehicle interior and floor pan, but measurements revealed slight deformation. The maximum deformation in the interior was found at the bottom of the side door to be only 1¼ in. (32 mm).

### **11.6 Occupant Risk**

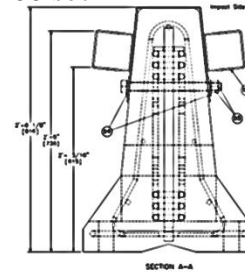
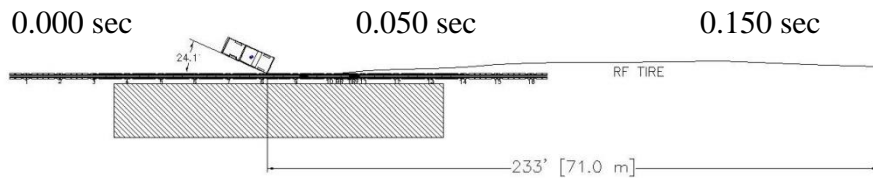
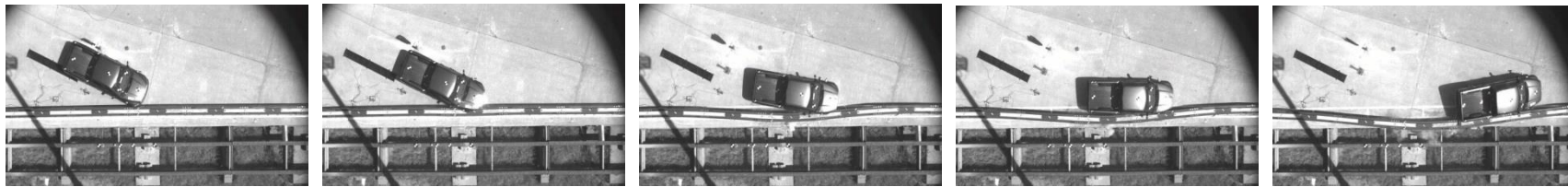
The calculated occupant impact velocities (OIVs) and maximum 0.010-sec occupant ridedown accelerations (ORAs) in both the longitudinal and lateral directions are shown in Table 12. Note that the OIVs and ORAs were within the suggested limits provided in MASH. The calculated THIV, PHD, and ASI values are also shown in Table 12. The results of the occupant risk analysis, as determined from the accelerometer data, are also summarized in Figure 92. The recorded data from the accelerometers and the rate transducers are shown graphically in Appendix F.

Table 12. Summary of OIV, ORA, THIV, PHD, and ASI Values, Test No. RDTCB-1

Evaluation Criteria		Transducer			MASH Limits
		EDR-3	DTS	DTS-SLICE	
OIV ft/s (m/s)	Longitudinal	14.42 (4.39)	13.65 (4.16)	13.95 (4.25)	≤ 40 (12.2)
	Lateral	18.31 (5.58)	19.14 (5.83)	20.42 (6.22)	≤40 (12.2)
ORA g's	Longitudinal	4.58	4.06	4.54	≤ 20.49
	Lateral	7.55	7.67	7.22	≤ 20.49
THIV ft/s (m/s)		NA	22.93 (6.99)	23.98 (7.31)	not required
PHD g's		NA	7.68	7.78	not required
ASI		1.31	1.29	1.36	not required

### 11.7 Discussion

The analysis of the test results for test no. RDTCB-1 showed that the TCB system adequately contained and redirected the 2270P vehicle with controlled lateral displacements of the barrier. There were no detached elements or fragments that showed potential for penetrating the occupant compartment, or that presented undue hazard to other traffic. Deformations of, or intrusions into, the occupant compartment that could have caused serious injury did not occur. The test vehicle did not penetrate or ride over the barrier and remained upright during and after the collision. Vehicle roll, pitch, and yaw angular displacements, as shown in Appendix F, were deemed acceptable because they did not adversely influence occupant risk safety criteria or cause a rollover. After impact, the vehicle exited the barrier and its trajectory did not violate the bounds of the exit box. Therefore, test no. RDTCB-1 conducted on the low-deflection TCB system was determined to be acceptable according to the MASH safety performance criteria for test designation no. 3-11.



- Test Agency.....MwRSF
- Test Number.....RDTCB-1
- Date ..... September 5, 2012
- MASH Test Designation.....3-11
- Test Article..... Stiffened Temporary Concrete Barrier
- Total Length .....204 ft 7<sup>5</sup>/<sub>16</sub> in. (62.4 m)
- Key Component – Concrete Barrier
  - Length..... 12 ft (3.81 m)
  - Base Width.....22.5 in. (572 mm)
  - Height.....32 in. (813 mm)
- Key Component – Box-Beam
  - Length..... 153<sup>3</sup>/<sub>16</sub> in. (3,891 mm)
  - Dimensions .....5 in. x 5 in. (127 mm x 127 mm)
  - Wall Thickness .....<sup>3</sup>/<sub>16</sub> in. (5mm)
- Soil Type ..... NA
- Vehicle Make /Model .....Dodge Ram 1500 Quad Cab
  - Curb .....4,991 lb (2264 kg)
  - Test Inertial.....4,998 lb (2267 kg)
  - Gross Static.....5,163 lb (2342 kg)
- Impact Conditions
  - Speed .....63.6 mph (102.4 km/h)
  - Angle ..... 24.9 deg
  - Impact Location ..... 61<sup>3</sup>/<sub>16</sub> in. (1554 mm) US of barrier 8 and 9 joint
- Exit Conditions
  - Speed ..... NA
  - Angle ..... NA
- Exit Box Criterion .....Pass
- Vehicle Stability ..... Satisfactory
- Vehicle Stopping Distance..... 153 ft (46.6 m)
- Vehicle Damage
  - VDS<sup>[29]</sup>..... 1-RFQ-3
  - CDC<sup>[30]</sup>..... 1-RYEN2
  - Maximum Interior Deformation..... 1/4 in. (32 mm)

- Maximum Test Article Deflections
  - Permanent Set..... 41 1/2 in. (1,054 mm)
  - Dynamic .....43.0 in. (1,092 mm)
  - Working Width .....55.1 in. (1,400 mm)
- Maximum Angular Displacements
  - Roll..... 22.5 ° < 75°
  - Pitch.....-3.6° < 75°
  - Yaw .....-36.6 °
- Impact Severity (IS) ..... 119.8 kip-ft (162.4 kJ) > 106 kip-ft (144 kJ)
- Transducer Data

Evaluation Criteria		Transducer			MASH Limit
		EDR-3	EDR-4	DTS	
OIV ft/s (m/s)	Longitudinal	14.42 (4.39)	13.65 (4.16)	13.95 (4.25)	≤ 40 (12.2)
	Lateral	18.31 (5.58)	19.14 (5.83)	20.42 (6.22)	≤ 40 (12.2)
ORA g's	Longitudinal	4.58	4.06	4.54	≤ 20.49
	Lateral	7.55	7.67	7.22	≤ 20.49
THIV – ft/s (m/s)		NA	22.93 (6.99)	23.98 (7.31)	not required
PHD – g's		NA	7.68	7.78	not required
ASI		1.31	1.29	1.36	not required

Figure 92. Summary of Test Results and Sequential Photographs, Test No. RDTCB-1



0.000 sec



0.026 sec



0.050 sec



0.086 sec



0.122 sec



0.170 sec



0.000 sec



0.100 sec



0.200 sec



0.300 sec



0.400 sec



0.500 sec

Figure 93. Additional Sequential Photographs, Test No. RDTCB-1



0.000 sec



0.050 sec



0.124 sec



0.192 sec



0.276 sec



.350 sec



0.000 sec



0.124 sec



0.192 sec



0.350 sec



0.580 sec



0.750 sec

Figure 94. Additional Sequential Photographs, Test No. RDTCB-1



Figure 95. Documentary Photographs, Test No. RDTCB-1



Figure 96. Impact Location, Test No. RDTCB-1



Figure 97. Vehicle Final Position and Trajectory Marks, Test No. RDTCB-1



Figure 98. Overall System Damage, Test No. RDTCB-1



Figure 99. System Damage at Barrier Nos. 8 and 9, Test No. RDTCB-1



Figure 100. Rail Splice at Barrier Nos. 8 and 9, Test No. RDTCB-1



Figure 101. Permanent Barrier Deflection, Test No. RDTCB-1



Figure 102. Vehicle Damage, Test No. RDTCB-1



Figure 103. Vehicle Damage, Test No. RDTCB-1

## **12 ANALYSIS AND REFINEMENT OF LOW-DEFLECTION TCB DESIGN**

Following test no. RDTCB-1, a review of the test results and system damage was conducted to identify potential areas for improvement in the design of the low-deflection TCB system. In test no. RDTCB-1, the barrier system exhibited a dynamic deflection of 43.0 in. (1,092 mm). This dynamic deflection was larger than the deflections estimated during the parameter study performed prior to the full-scale crash test. Review of the full-scale crash test identified several areas that contributed to the increased system deflection.

First, the system evaluated in test no. RDTCB-1 was constructed with slotted holes, slightly oversized part geometry, and other construction tolerances required in order to allow for installation of the retrofit stiffening system on TCB segments that may vary in elevation, joint gap, overall length, and other critical dimensions. These tolerances built into the system prevent the stiffening hardware from developing load as quickly or as effectively as the simplified, fixed attachments used for the parameter study models. Thus, the increased tolerances and gaps in the tested system allowed for additional system deflection.

Second, the tubes used in the low-deflection TCB system evaluated in test no. RDTCB-1 displayed permanent deformation and bending that was not observed in the simulation model. However, the simulation model utilized a significantly larger tube section which did not display that degree of damage. The continuous tubes in the tested low-deflection design also appeared to flex away from the barrier due to the distance from their attachment to the steel cap plate and opening of the splice connection in the tubes at the midspan of the TCB segment. The deformation and deflection of the steel tubes in test no. RDTCB-1 is shown in Figure 104. It was believed that the combination of the tube deformation and the displacement/flex of the tubes away from the side of the TCB further added to the dynamic deflection of the tested system.



Figure 104. Steel Tube Deformation and Deflection, Test No. RDTCB-1

Finally, deformation of the steel cap plate that was mounted across the barrier joint was observed, as shown in Figure 105. The deformation of this component was also a contributor to the deflections observed in the test.

Based on the observation of the mechanisms that allowed additional deflection in the first full-scale crash test, and review of the deflection-limiting mechanisms evaluated in the initial parametric study, the researchers proposed several potential design improvements to further reduce system deflections. First, increasing the thickness of the steel tubes used in the design was proposed. Increased tube thickness would reduce the deformation of the tubes and the tendency of the tubes to pull away from the face of the TCB, as observed during the full-scale test. Second, increasing the thickness of the steel cap mounted at the barrier joint was proposed to further stiffen the barrier joint and reduce deflections. Third, the application of additional attachment points between the steel tubes and the TCB segment was proposed. Finally two deflection-limiting mechanisms were carried over from the original parameter study. These mechanisms were increased barrier-to-ground friction and reduction of the joint gap tolerance.

In order to investigate these proposed improvements, a simulation model of test no. RDTCB-1 was developed and validated against the full-scale crash test. This model was then modified with each of the proposed modifications to determine which concepts were most effective.

### **12.1 Simulation and Validation of Test No. RDTCB-1**

A simulation model of test no. RDTCB-1 was constructed to serve as a baseline for comparison of proposed design modifications for further reducing the deflections of the TCB system. The simulation model of test no. RDTCB-1 was constructed using the same TCB model developed as part of the original parametric study. The steel cap across the barrier joint and the

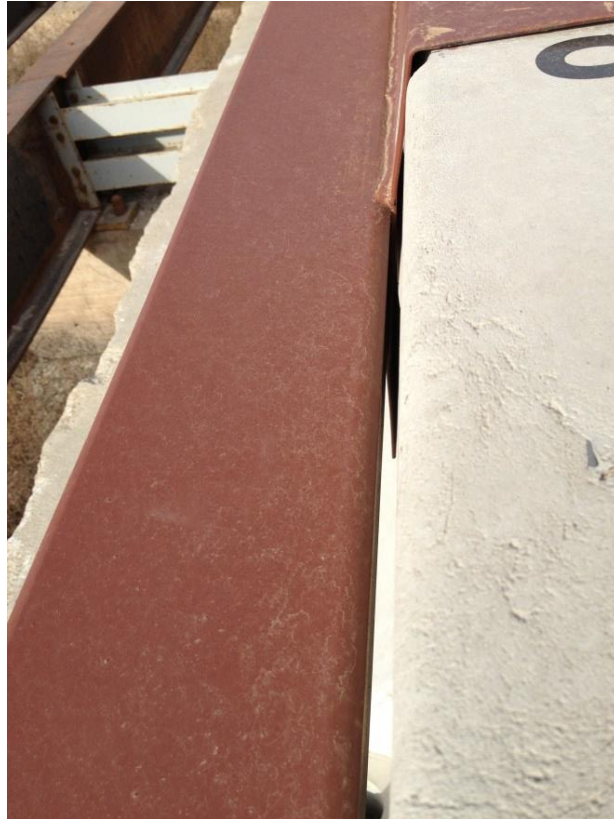


Figure 105. Steel Cap Deformation, Test No. RDTCB-1

steel tubes on the side of the barrier were added using shell elements. MAT\_24\_PIECEWISE\_LINEAR\_PLASTICITY was used to define the steel material properties for these components. The tubes were welded to the cap using constrained nodal rigid bodies to create a simplified weld. The connection hardware, including the bolts, nuts, and splice plates were modeled explicitly in the model. Bolt preload was achieved using the INITIAL\_STRESS\_SECTION command in LS-DYNA. Details of the model of the barrier system evaluated in test no. RDTCB-1 are shown in Figure 106.

The baseline model was simulated for a 2270P vehicle impacting the system with the same impact conditions as test no. RDTCB-1. Thus, the Chevy Silverado model impacted the barrier system at a speed of 63.6 mph (102.4 km/h) and an angle of 24.9 degrees. The vehicle model used for the simulation was the Version 3 Chevy Silverado model developed at the National Crash Analysis Center (NCAC). The vehicle impacted the system 4.3 ft (1.3 m) upstream of the center of the joint between the eighth and ninth barrier segments.

Comparison of the simulation results with the full-scale crash test no. RDTCB-1 found that the model provided good correlation with the full-scale test and was appropriate for use in evaluation of the deflection-limiting mechanisms. Graphical comparison of the simulation model and test no. RDTCB-1, as shown in Figure 107 through Figure 110, found that the behavior of the vehicle and the barrier were very similar. The dynamic deflection of the simulation model was found to be 35.9 in. (912 mm) at the upstream end of the ninth barrier segment. This compared reasonably well with the dynamic deflection of test no. RDTCB-1, which was measured from high-speed film to be 43.0 in. (1,092 mm) at the upstream end of the ninth barrier segment. The decreased deflection in the simulation model was believed to be due largely to concrete damage in the physical test that was not reproducible in the simulation. However, the peak system deflections in the simulation and test were still within 16.7

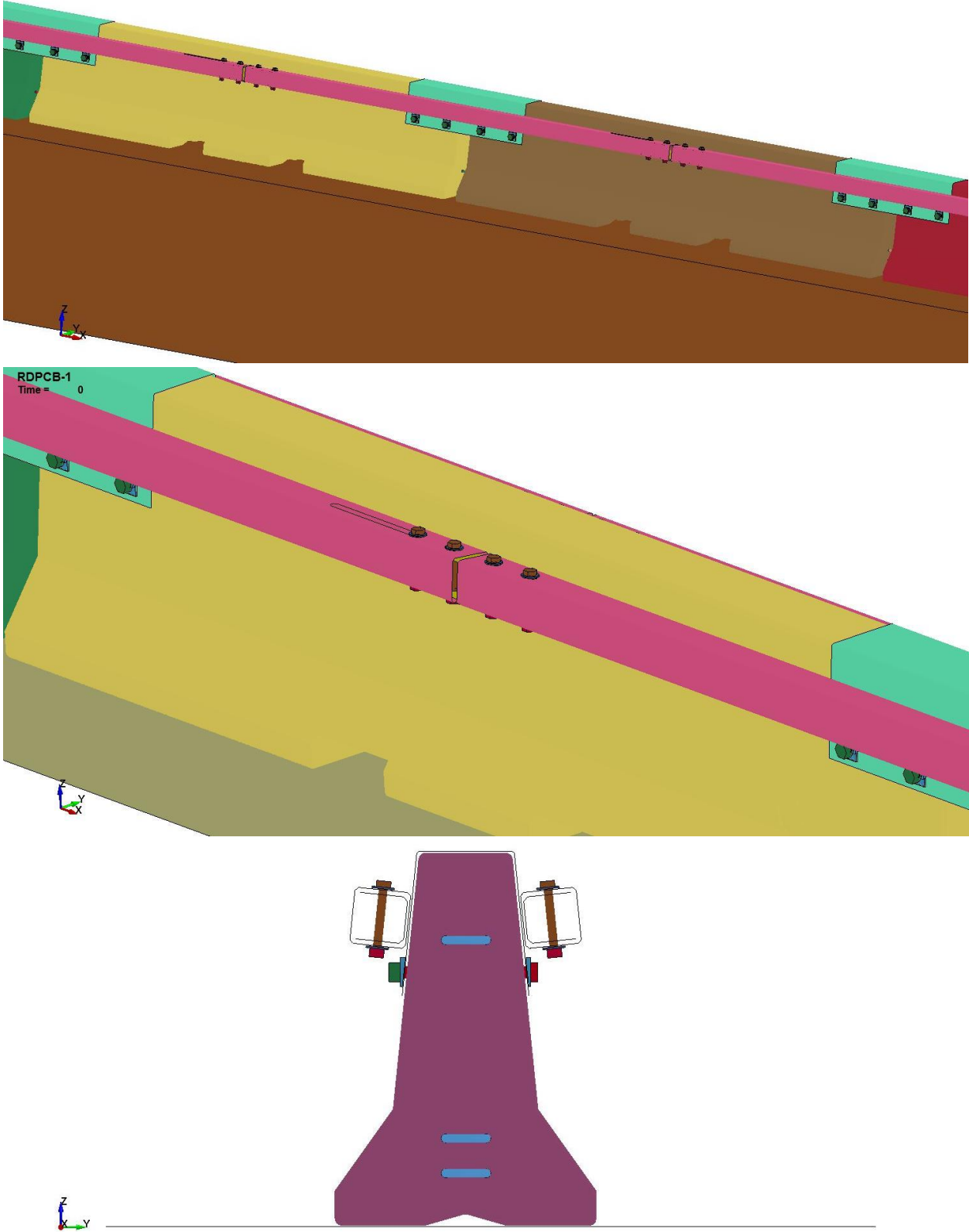
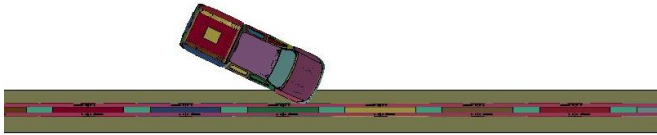
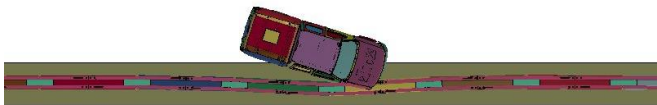


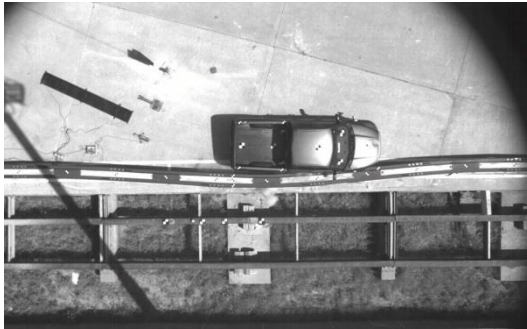
Figure 106. RDTCB-1 Baseline Model



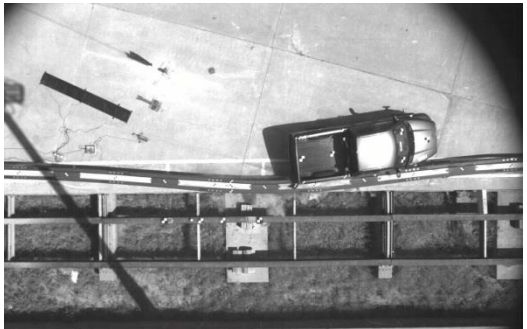
Time = 0.000 sec



Time = 0.100 sec

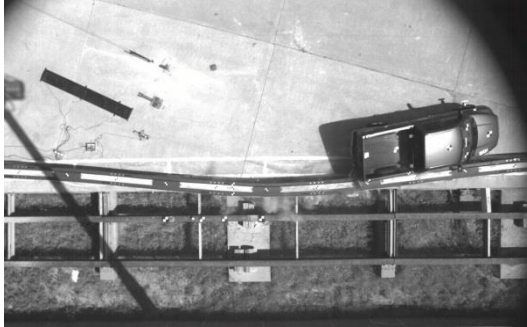


Time = 0.200 sec

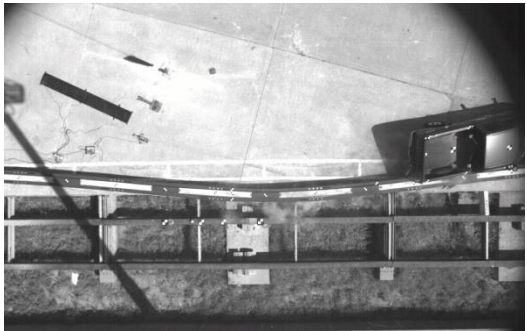


Time = 0.300 sec

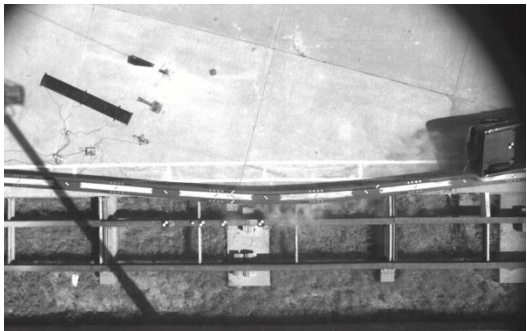
Figure 107. Overhead Sequential Views, Simulation Model and Test No. RDTCB-1



Time = 0.400 sec

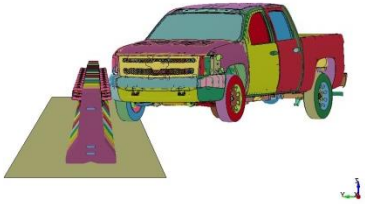


Time = 0.500 sec

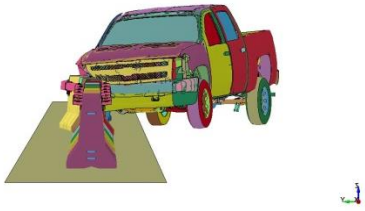


Time = 0.600 sec

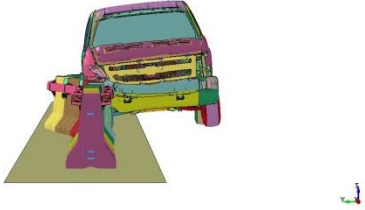
Figure 108. Overhead Sequential Views, Simulation Model and Test No. RDTCB-1



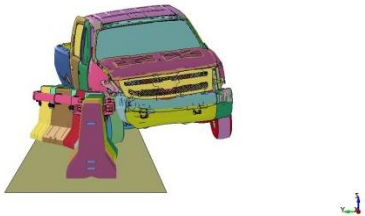
Time = 0.000 sec



Time = 0.100 sec



Time = 0.200 sec

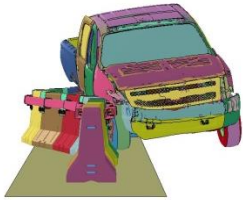


Time = 0.300 sec

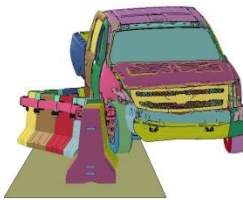
Figure 109. Downstream Sequential Views, Simulation Model and Test No. RDTCB-1



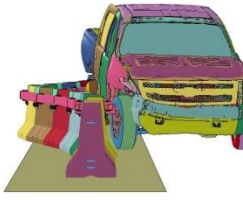
Time = 0.400 sec



Time = 0.500 sec



Time = 0.600 sec



Time = 0.700 sec

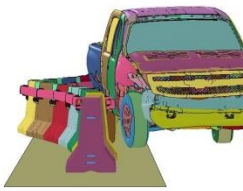


Figure 110. Downstream Sequential Views, Simulation Model and Test No. RDTCB-1

percent. The simulation also replicated several of the critical system behaviors that were observed in test no. RDTCB-1, including opening of the tube splices, deformation of the steel tubes and cap plate, and the pulling away of the steel tubes from the face of the barrier. Comparison of these system behaviors is shown in Figure 111.

The simulation and full-scale crash test were also compared using the RSVVP program [31]. RSVVP was used to compare the acceleration and rotational behaviors of the vehicle in the test and the simulation. The results from the RSVVP comparison are shown in Figure 112 through Figure 116. The RSVVP analysis found that the longitudinal and lateral accelerations and the vehicle yaw predicted by the simulation model were very close to the full-scale crash test. Roll and pitch behavior did not display the same degree of correlation. Differences in the roll and pitch of the vehicle were likely due to several factors, including the lack of suspension failure in the model, and differences in the body style of the Chevy Silverado truck used in the simulation and the Dodge Ram truck used in the physical test. Thus, the discrepancies in roll and pitch were not considered to a significant source of error in the simulation model. The combined multi-channel RSVVP metrics also indicated that the simulation correlated well with the full-scale test, as shown in Figure 117.

Based on this comparison, it was believed that the simulation model was providing a valid representation of the system behavior in test no. RDTCB-1. Thus, the simulation model was used to investigate the proposed system modifications. It should be noted that for evaluation of the system modifications, all of the models, including the baseline simulation of the design evaluated in test no. RDTCB-1, were simulated with the standard MASH TL-3 impact conditions of 62.1 mph (100.0 km/h) and an angle of 25 degrees in order to provide a consistent comparison basis. The baseline model simulation with these impact conditions resulted in a peak dynamic lateral barrier deflection of 34.1 in. (866 mm).

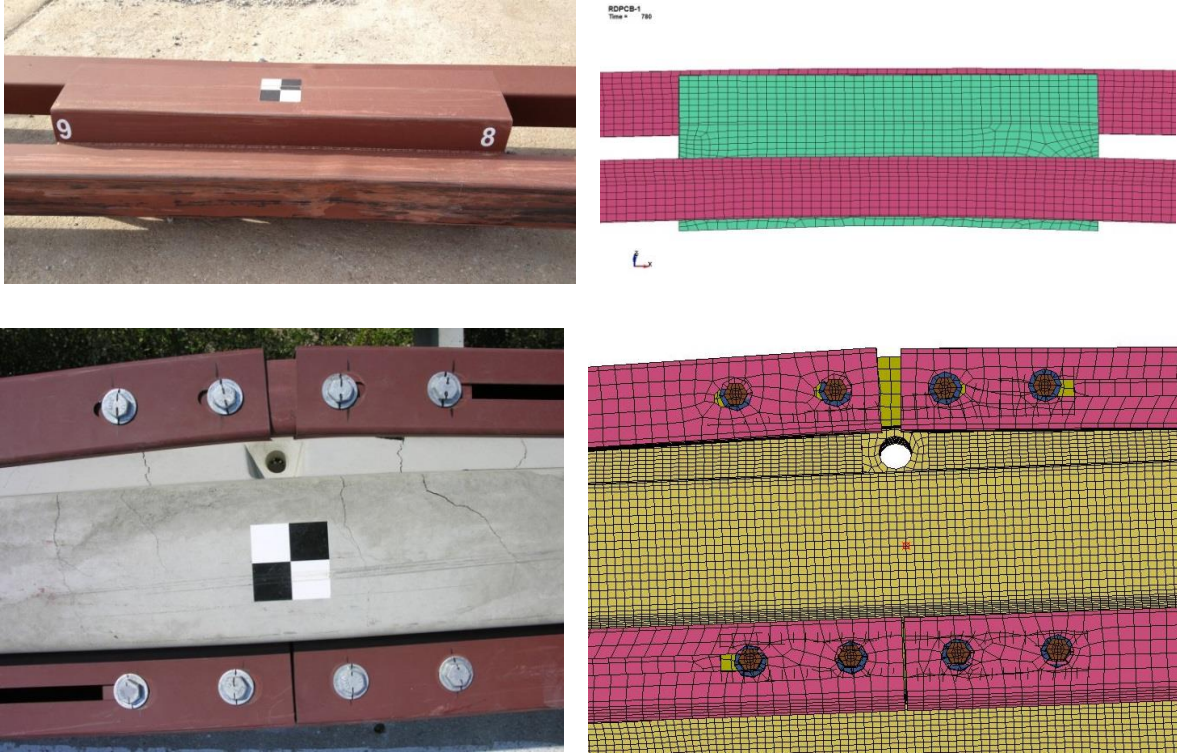


Figure 111. System Damage and Deformation, Simulation Model and Test No. RDTCB-1

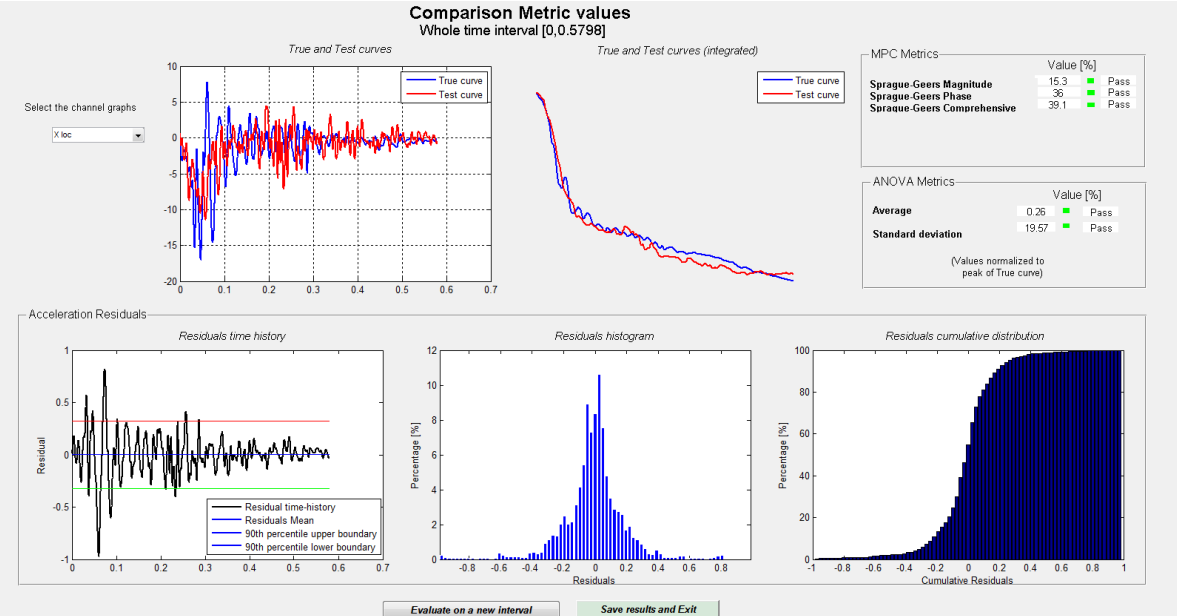


Figure 112. RSVVP, X-Acceleration, Simulation Model and Test No. RDTCB-1

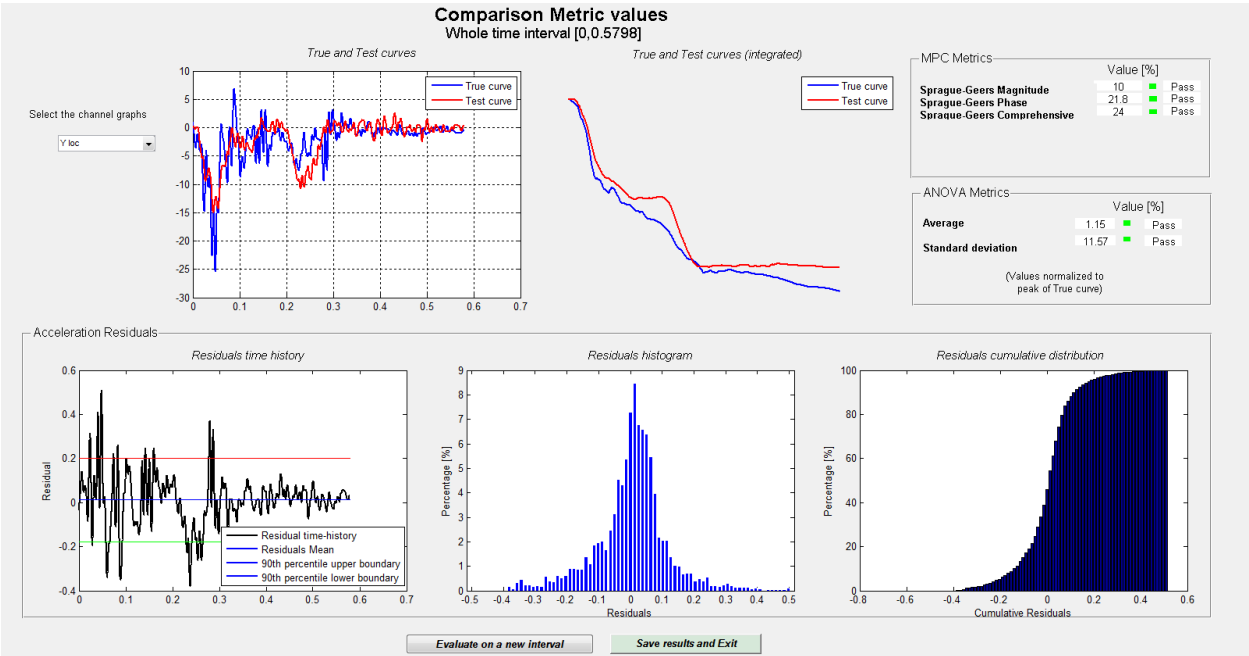


Figure 113. RSVVP, Y-Acceleration, Simulation Model and Test No. RDTCB-1

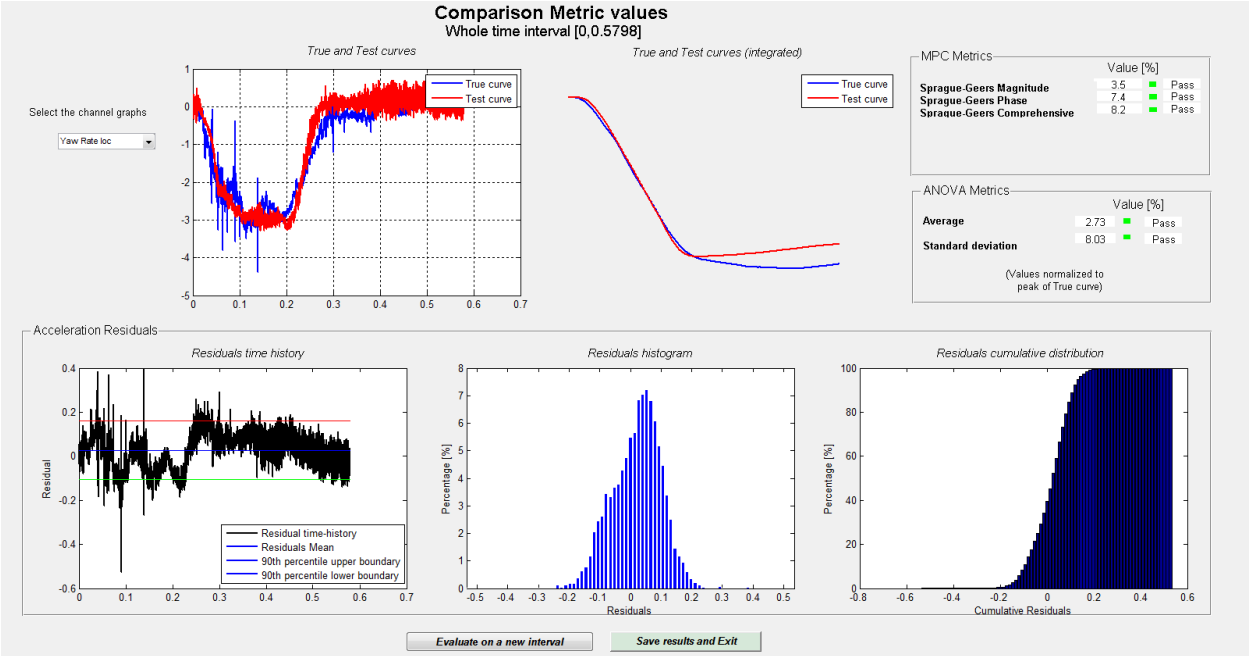


Figure 114. RSVVP, Yaw, Simulation Model and Test No. RDTCB-1

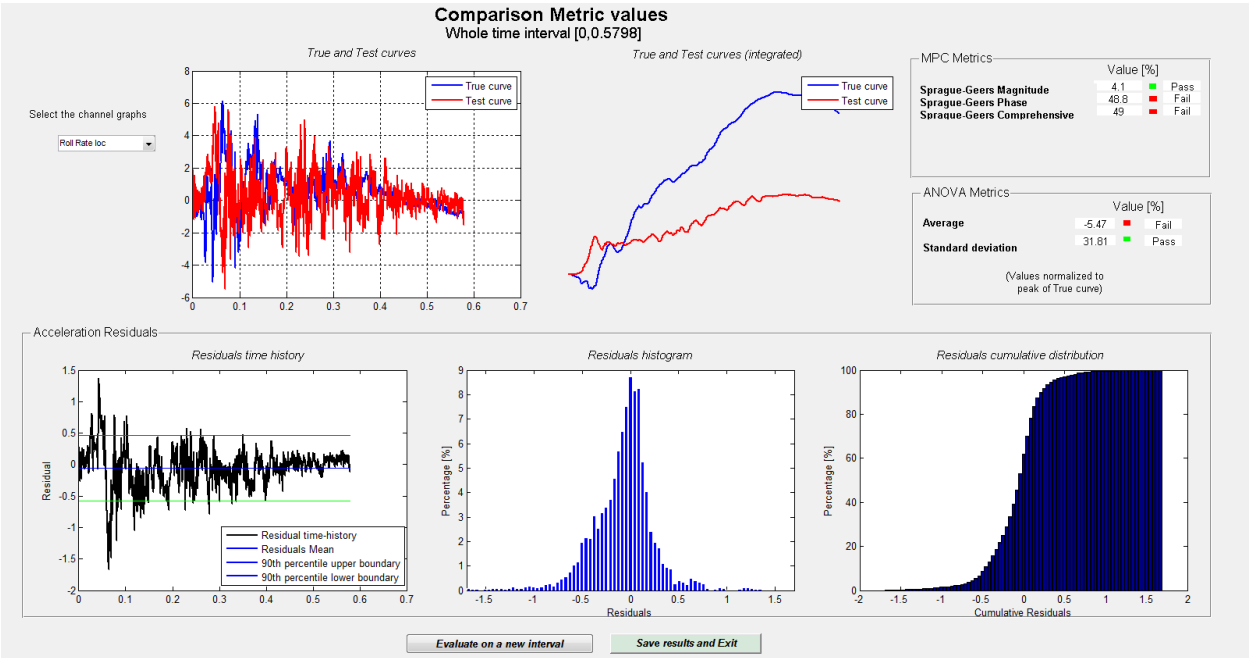


Figure 115. RSVVP, Roll, Simulation Model and Test No. RDTCB-1

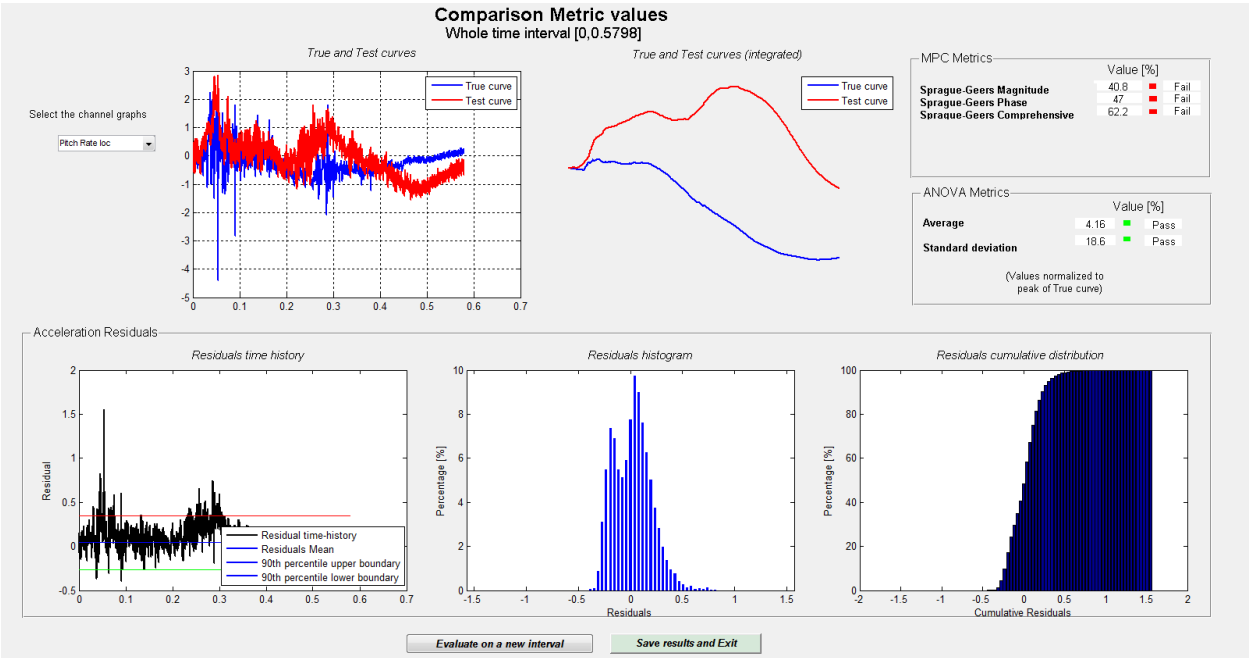


Figure 116. RSVVP, Pitch, Simulation Model and Test No. RDTCB-1

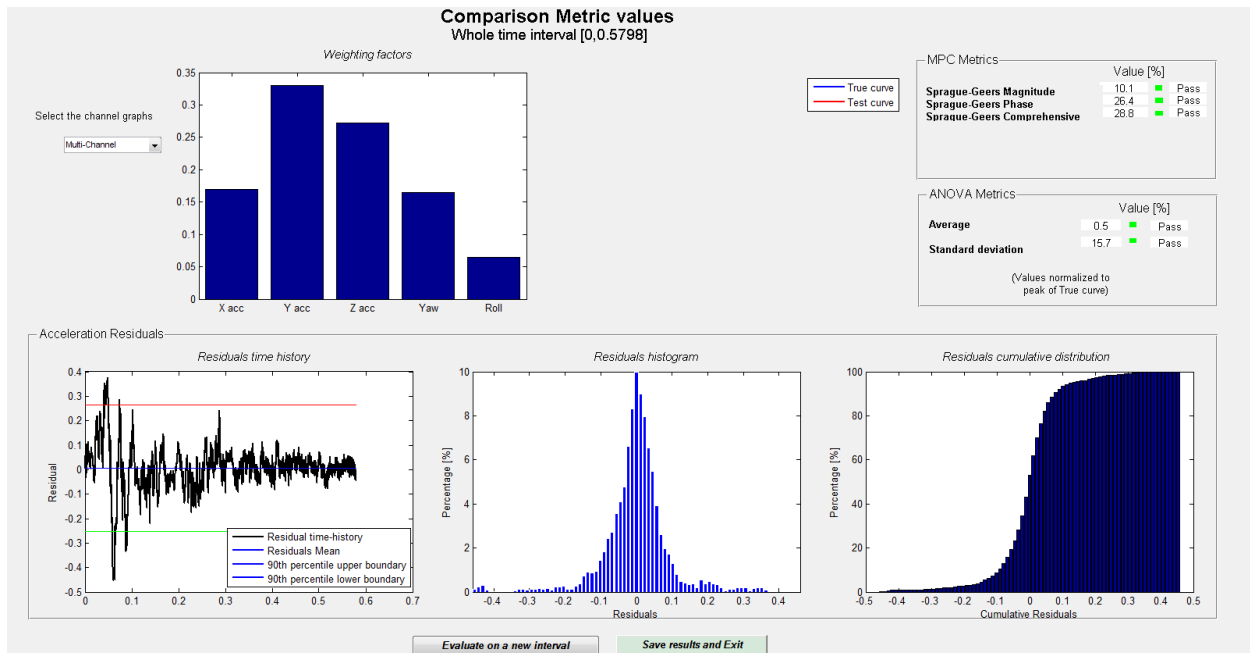


Figure 117. RSVVP, Multi-Channel Comparison, Simulation Model and Test No. RDTCB-1

## 12.2 Simulation of Proposed Design Modifications

The simulation model of the low-deflection TCB system was used to investigate the various design modifications proposed after the review of the test results from test no. RDTCB-

1. The proposed modifications included:

1. Increased barrier-to-ground friction
2. Increased tube thickness
3. Increased cap thickness
4. Reduced Joint Tolerance
5. Additional attachment points for the tubes on the TCB

Computer simulation of each of these proposed modifications and the results are discussed in the subsequent sections.

### **12.2.1 Increased Barrier-to-Ground Friction**

Increased friction was expected to provide increased longitudinal and lateral resistive forces during impact with the barrier system. The effectiveness of increased friction was investigated by increasing the contact friction coefficients between the barrier segments and the ground in the LS-DYNA model. The friction coefficients evaluated were selected based on the friction data obtained during the component testing of barriers with neoprene base pads in Chapter 6.

Two increased-friction models were simulated by increasing the friction coefficient of the baseline simulation model. The first model increased the friction coefficient between the TCB segments and the ground to 0.62, which represented the friction coefficient determined previously in the study for the 70-durometer neoprene pad. Results from this simulation indicated that increased friction was effective at reducing barrier deflections as the peak dynamic lateral barrier deflection was found to be 26.7 in. (678 mm). A second increased friction model was simulated with a friction coefficient between the TCB segments and the ground of 0.76, which represented the friction coefficient determined previously in the study for the 50-durometer neoprene pad. The higher friction coefficient of the second simulation model further reduced the peak dynamic lateral barrier deflection to 23.5 in. (597 mm). Thus, simulation of increased barrier-to-ground friction demonstrated a clear benefit in terms of reducing the peak lateral barrier deflections.

### **12.2.2 Tube Thickness**

Increased steel tube thickness was expected to increase the bending strength of the tubes, thus reducing system deflections. In order to determine the effectiveness of increased tube thickness, the baseline simulation model was modified by doubling the thickness of the steel tubes to  $\frac{3}{8}$  in. (10 mm).

Results from the simulation with increased tube thickness indicated that the modification was effective at reducing barrier deflections, as the peak dynamic lateral barrier deflection was found to be 24.0 in. (610 mm). Tube deformation and deflection at the TCB joint and the pull-away of the steel tubes from the side of the barrier were still observed, but the magnitude of the deformation was reduced.

### **12.2.3 Cap Thickness**

Increased steel cap thickness was expected to increase the bending strength of the barrier joint, thus reducing system deflections. In order to determine the effectiveness of increased cap thickness, the baseline simulation model was modified by increasing the thickness of the steel cap to ¼ in. (6 mm).

Results from the simulation with increased steel cap thickness indicated that the modification was effective at reducing barrier deflections, as the peak dynamic lateral barrier deflection was found to be 31.6 in. (803 mm). An increase in the steel cap thickness reduced joint deflections, but not to the same degree as increasing the steel tube thickness.

### **12.2.4 Reduced Joint Gap Tolerance**

The F-shape TCB segment considered in this research has a gap between the adjacent barrier segments that can be as large as 4 in. (102 mm). Reduction of this gap at the barrier joint was expected to cause the adjacent barrier segments to engage sooner, improve transmission and distribution of the impact forces, and reduce barrier deflection. Reduction in the barrier joint gap was investigated with the insertion of a steel spacer between the barrier segments. The steel spacer was the same spacer used in the parametric study of deflection-limiting mechanisms documented previously in Chapter 4.

Results from the simulation of the model with the joint spacer installed indicated that reduction of the joint gap was effective at reducing barrier deflections, as the peak dynamic

lateral barrier deflection was found to be 28.0 in. (711 mm). The original simulation of the steel spacer during the parametric study without the additional cap and tube constraints yielded a peak dynamic lateral barrier deflection of 34.1 in. (866 mm). Thus, the combination of the reduced spacing and the low-deflection system from test no. RDTCB-1 did not reduce deflections significantly more than when these mechanisms were used individually.

#### **12.2.5 Additional Tube Attachments**

The final deflection-limiting mechanism investigated was the incorporation of additional, intermediate attachments between the steel tubes and the TCB segments. The use of additional attachments between the tube and the barrier would serve to reduce deflections by increasing the stiffness of the barrier system, reducing the pull-away of the steel tubes from the barrier face, reducing slip of the splice joint between the tubes, and forcing the TCB segments to move as a continuous section of barrier.

The first simulation of additional attachment points modified the baseline model with ¼-in. (6-mm) thick, L-shaped steel brackets that were welded on the top and bottom of the steel tubes at  $\frac{1}{3}$  and  $\frac{2}{3}$  of the length of the TCB segment. These plates were then attached to the barrier with fixed attachments to simulate bolting the brackets to the barrier with a concrete anchor, as shown in Figure 118. The results of this simulation found that peak dynamic lateral barrier deflection was reduced to 25.6 in. (650 mm). Thus, attachment of the tubes was effective at reducing deflection. However, it was found that the use of upper and lower brackets on the tubes was impractical, as the anchor bolts would have insufficient concrete cover and would interfere with the longitudinal reinforcement in the barrier.

In order to address this issue, a second simulation model was created that used single L-angles beneath the tubes. The L-angles were increased in thickness and length in order to create a similar level of restraint as the previous simulation's upper and lower brackets. Thus, the L-angle

in the simulation was made  $\frac{3}{8}$ -in. (10-mm) thick and 12-in. (305-mm) long and connected to the barrier with two simulated anchors, as shown in Figure 119. The anchor brackets were also moved closer to the center of the barrier segment adjacent to the tube splice joint. Simulation of the revised tube attachment found that peak dynamic lateral barrier deflection was reduced to 22.2 in. (564 mm). The revised tube anchor brackets displayed low levels of permanent deformation in the TL-3 impact, and were very effective at maintaining the tubes alongside the face of the TCB segment.

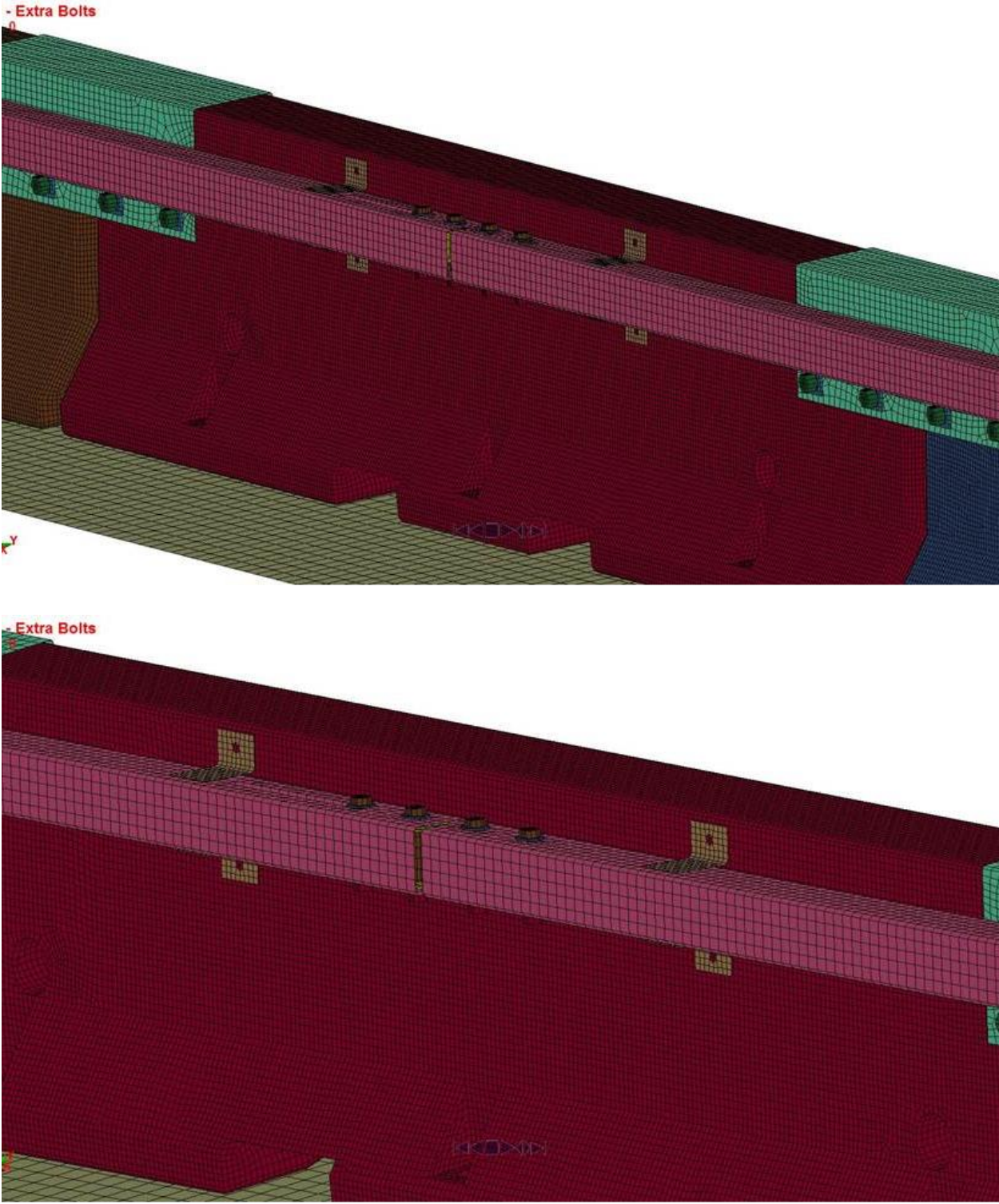


Figure 118. Additional Tube Attachments – Run 1

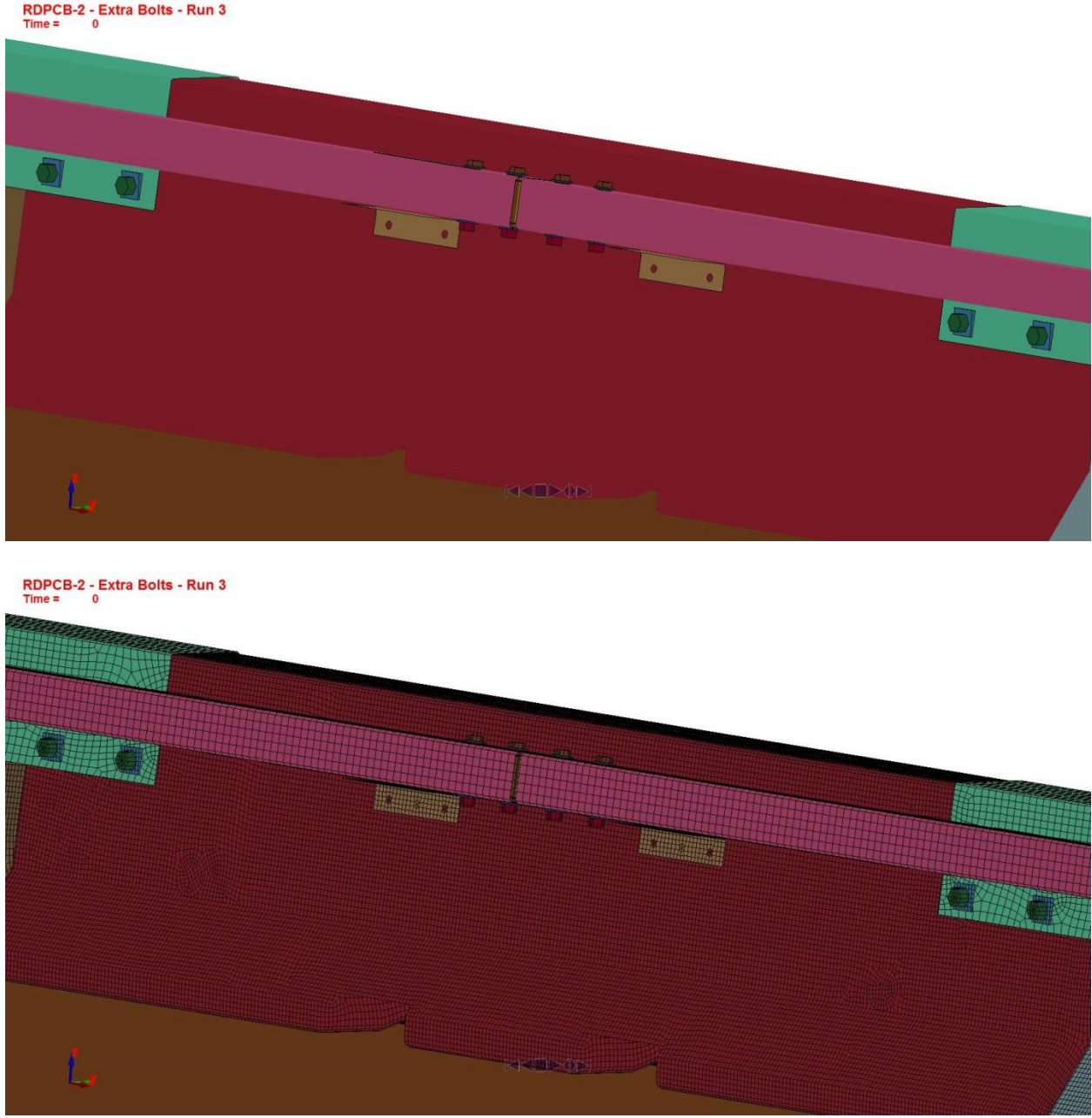


Figure 119. Additional Tube Attachments – Run 3b

### **12.3 Discussion of Results and Selection of Design Modification**

Following the completed simulation of all five proposed design modifications, the model results were further evaluated to estimate potential reductions in barrier deflection, as well as to compare the alternatives. In order to provide a better estimate of barrier deflection, the dynamic deflections from the simulation models were scaled to better correspond to the full-scale test data from test no. RDTCB-1. As noted previously, the simulation model of test no. RDTCB-1 underestimated the dynamic lateral deflection of the system by 16.7 percent. In order to account for the reduced deflection of the simulation model as compared to the full-scale test, the simulations of the proposed design modifications were compared to the baseline simulation under the standard MASH TL-3 impact conditions, which had a predicted dynamic deflection of 34.1 in. (867 mm). This allowed for the predicted percent reduction in deflection for the design modification to be determined. The predicted percent reduction for each modification was then applied to the full-scale test deflection from test no. RDTCB-1 of 43.0 in. (1,092 mm) in order to determine an estimate of the actual barrier deflection.

The estimated deflections for each of the modifications simulated are shown in Table 13. Based on the simulation data, it appeared several of the proposed modifications demonstrated the ability to further reduce the system deflections. The modifications that showed the most promise were increased friction, thicker steel tubes, and extra attachments for anchoring the tubes along the TCB segments. The other options did not appear to be as effective. In reviewing the modifications with the highest deflection reductions, friction and thicker tubes appeared to have some drawbacks. Friction pads adhered to the barrier would likely work, but might be difficult to install and would permanently alter the function of the barrier from its typical free-standing configuration. Thus, it would not be the most desirable path from the WisDOT perspective. Thicker tubes also worked well in reducing deflections, but would be a very expensive option in

terms of the additional steel cost. Based on these factors, incorporating additional anchorage for the tubes along the side of the barriers seemed to be the best option as it provided reduced deflection at a reasonable cost and installation effort.

Table 13. Summary of Estimated Deflections for Proposed RDTCB-2 Design Modifications

<b>RDTCB-2 Design Modification Comparisons</b>			
Test/Run No.	LS-DYNA Predicted Deflection in. (mm)	% Difference from MASH TL-3 Simulation (Deflection = 34.1 in.)	Estimated Actual Deflection in. (mm)
Test No. RDTCB-1	NA	-20.7	43.0 (1,093)
RDTCB-2 Friction – Run 1 - $\mu = 0.76$	23.5 (597)	-31.2	29.6 (752)
RDTCB-2 Friction – Run 2 - $\mu = 0.62$	26.7 (678)	-21.8	33.7 (856)
RDTCB-2 Tube – Run 1 - $t = 0.375$ "	24.0 (611)	-29.6	30.3 (770)
RDTCB-2 Cap – Run 1 - $t = 0.25$ "	31.6 (803)	-7.4	39.9 (1,013)
RDTCB-2 Joint Gap – Run 1	28.1 (713)	-17.8	35.4 (899)
RDTCB-2 Additional Attachments – Run 1	25.6 (650)	-25.1	32.3 (820)
RDTCB-2 Additional Attachments – Run 3b	22.2 (564)	-35.0	28.0 (711)

### **13 DESIGN DETAILS FOR TEST NO. RDTCB-2**

The barrier system design for test no. RDTCB-2 was comprised of the same hardware and layout as in RDTCB-1 with the addition of hardware for attachment of the steel tubes to the concrete barrier near the midspan of the TCB segments. The additional attachment points were achieved using 4-in. x 3-in. x  $\frac{3}{8}$ -in. (102-mm x 76-mm x 10-mm) L-angle brackets that were welded to the underside of the steel tubes and then through-bolted to the barrier with  $\frac{3}{4}$ -in. (19-mm) diameter ASTM A449 bolts. Through-bolting was used in lieu of other types of anchors as the sponsor felt that it would provide for the easiest and most consistent connection. For the full-scale test, the bolts were replaced with threaded rods with less than  $\frac{1}{2}$  in. (13 mm) of length exposed past the end of the nut to minimize the potential for vehicle snag. The L-angle brackets were located  $13\frac{1}{2}$  in. (343 mm) from the ends of the steel tubes.

Two adjustments were also made for the tested system to deal with fabrication tolerance issues. First, the steel cap top width was increased from 8 in. (203 mm) to  $8\frac{1}{4}$  in. (210 mm) to accommodate variation in the width of the fabricated TCB segments. Second, due to fabrication issues with the TCB segments, hole location tolerances for the attachment of the steel cap were often between  $\frac{1}{4}$  in. to  $\frac{1}{2}$  in. (6 mm to 13 mm) off in vertical and longitudinal directions. Thus, for test no. RDTCB-2, the PVC pipe used to create the attachment holes was removed from inside the barrier segment to increase hole diameters to 1.66 in. (42 mm) and allow for bolt installation. It was believed that this modification would represent a worst-case scenario for the bolt hole tolerances. The nominal hole size of  $1\frac{3}{8}$  in. (35 mm) should be used for actual installations.

The design details for test no. RDTCB-2 are shown in Figure 120 through Figure 138. Photographs of the test installation are shown in Figures 139 and 140. Material specifications,

mill certifications, and certificates of conformity for the system materials are shown in Appendix C.

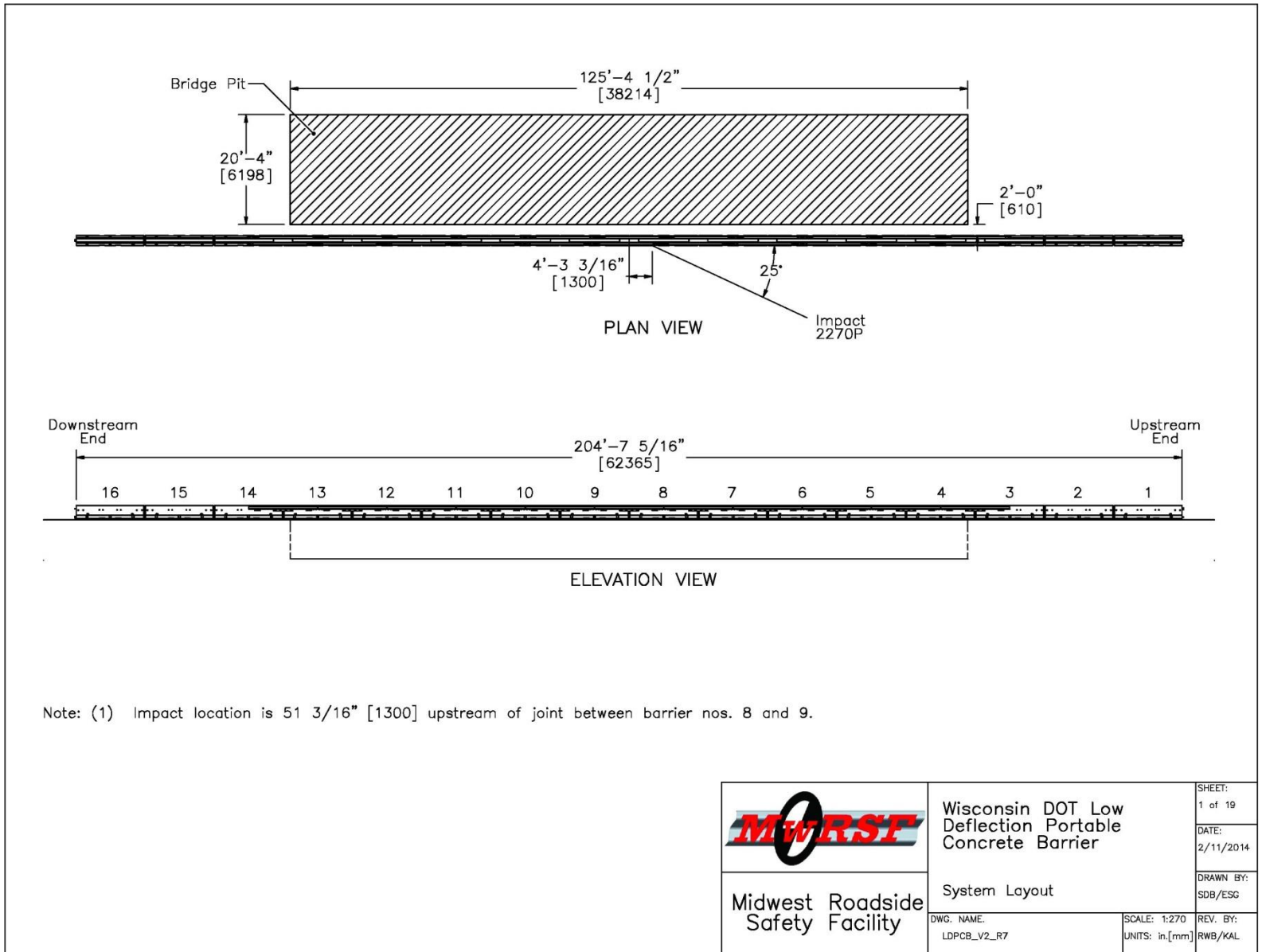


Figure 120. Test Installation Layout, Test No. RDTCB-2

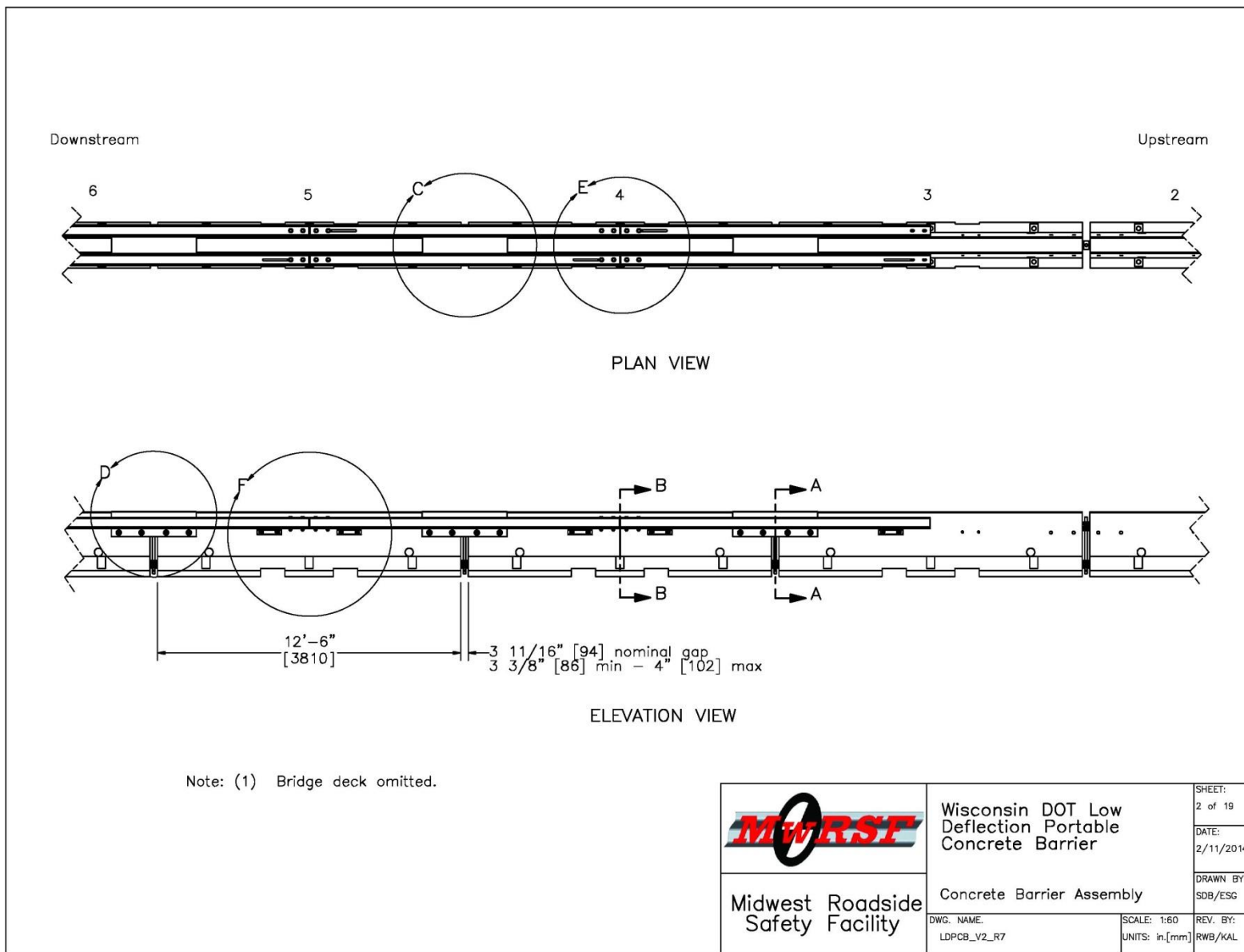


Figure 121. Design Details, Test No. RDTCB-2

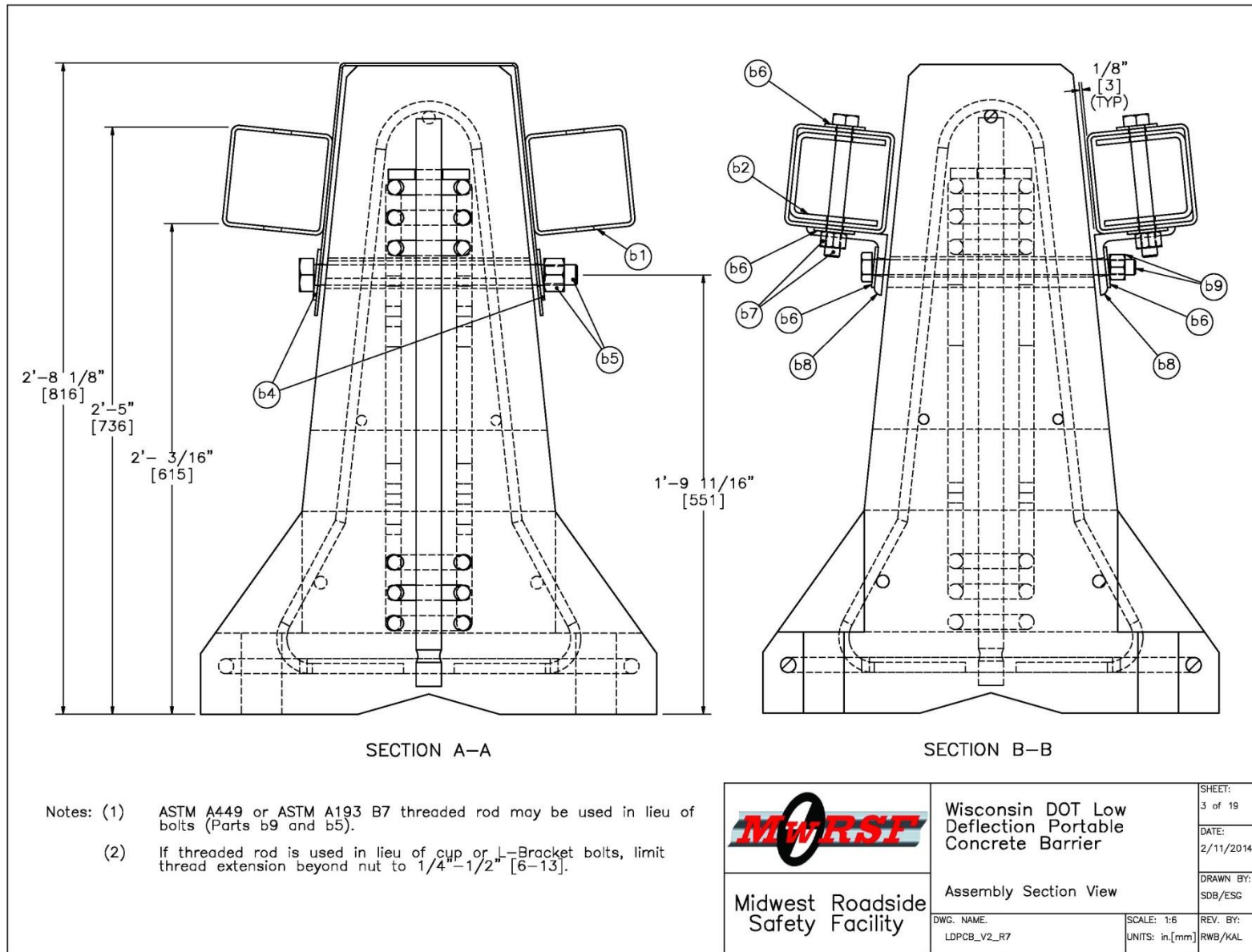


Figure 122. Design Details, Test No. RDTCB-2

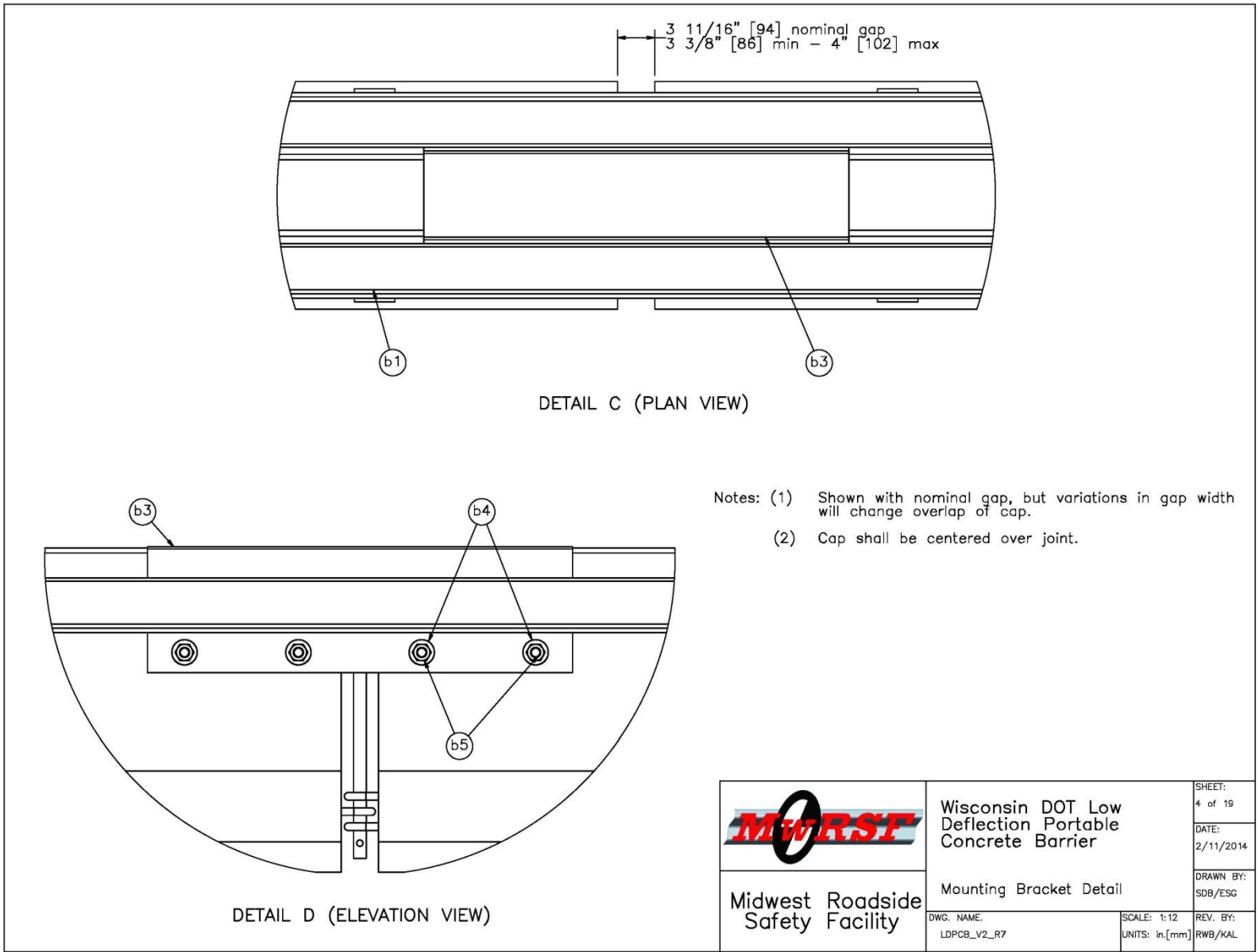
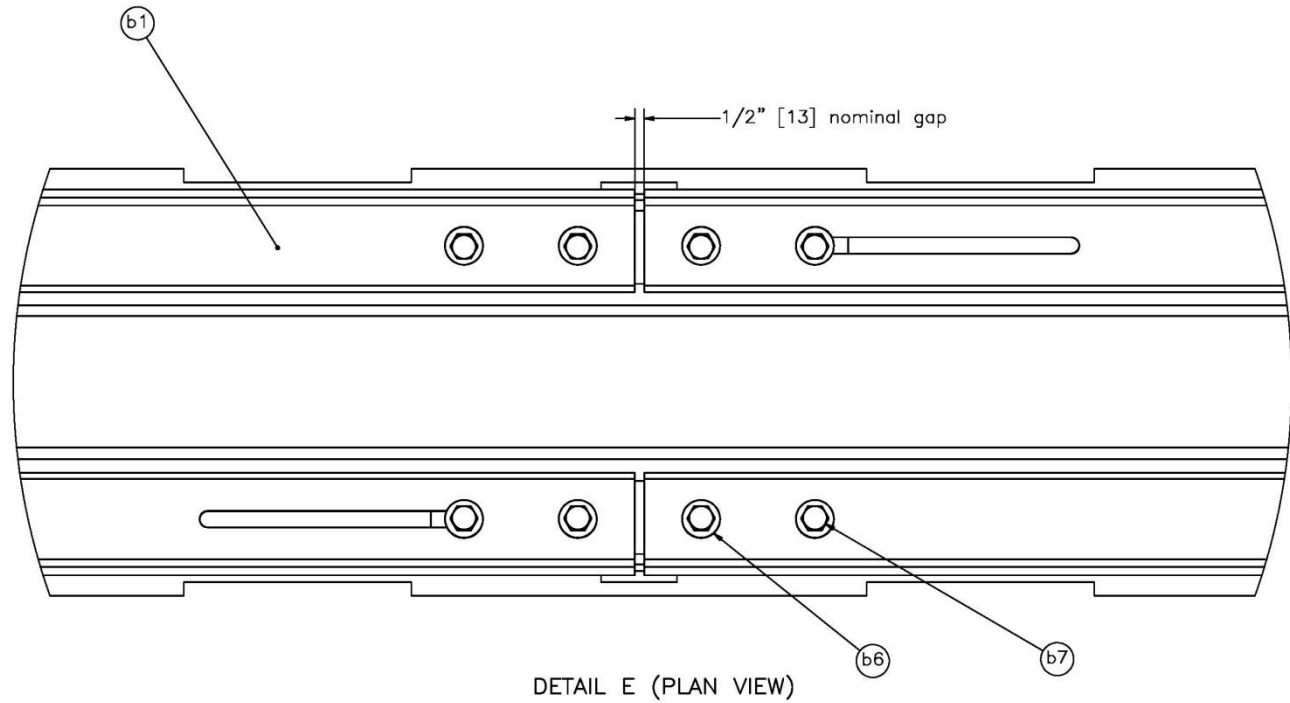


Figure 123. Design Details, Test No. RDTCB-2

200



DETAIL E (PLAN VIEW)

 Midwest Roadside Safety Facility	Wisconsin DOT Low Deflection Portable Concrete Barrier	SHEET: 5 of 19
	Splice Connection Detail	DATE: 2/11/2014
DWG. NAME: LDPCB_V2_R7	SCALE: 1:8 UNITS: in.[mm]	DRAWN BY: SDB/ESG
		REV. BY: RWB/KAL

Figure 124. Design Details, Test No. RDTCB-2

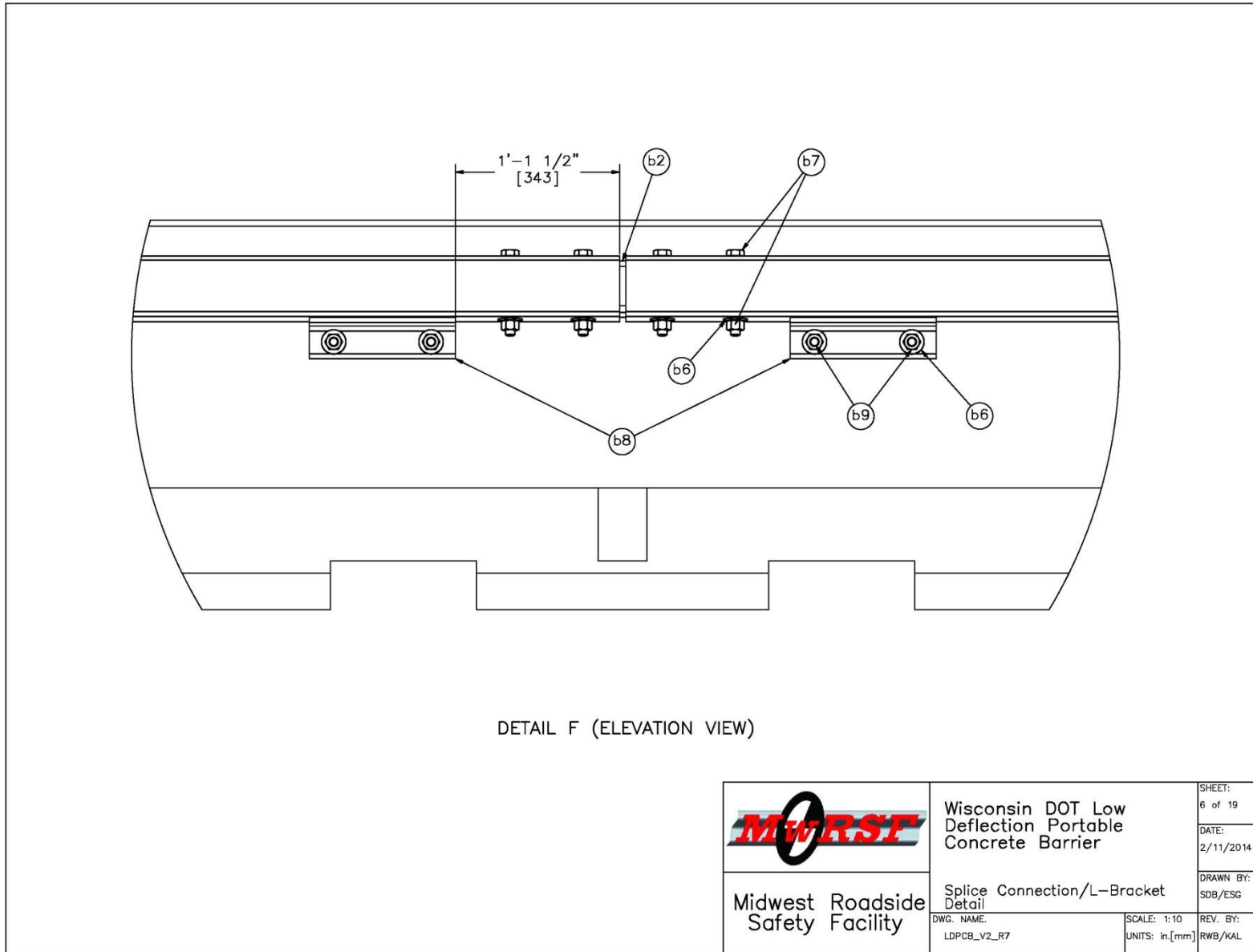


Figure 125. Design Details, Test No. RDTCB-2

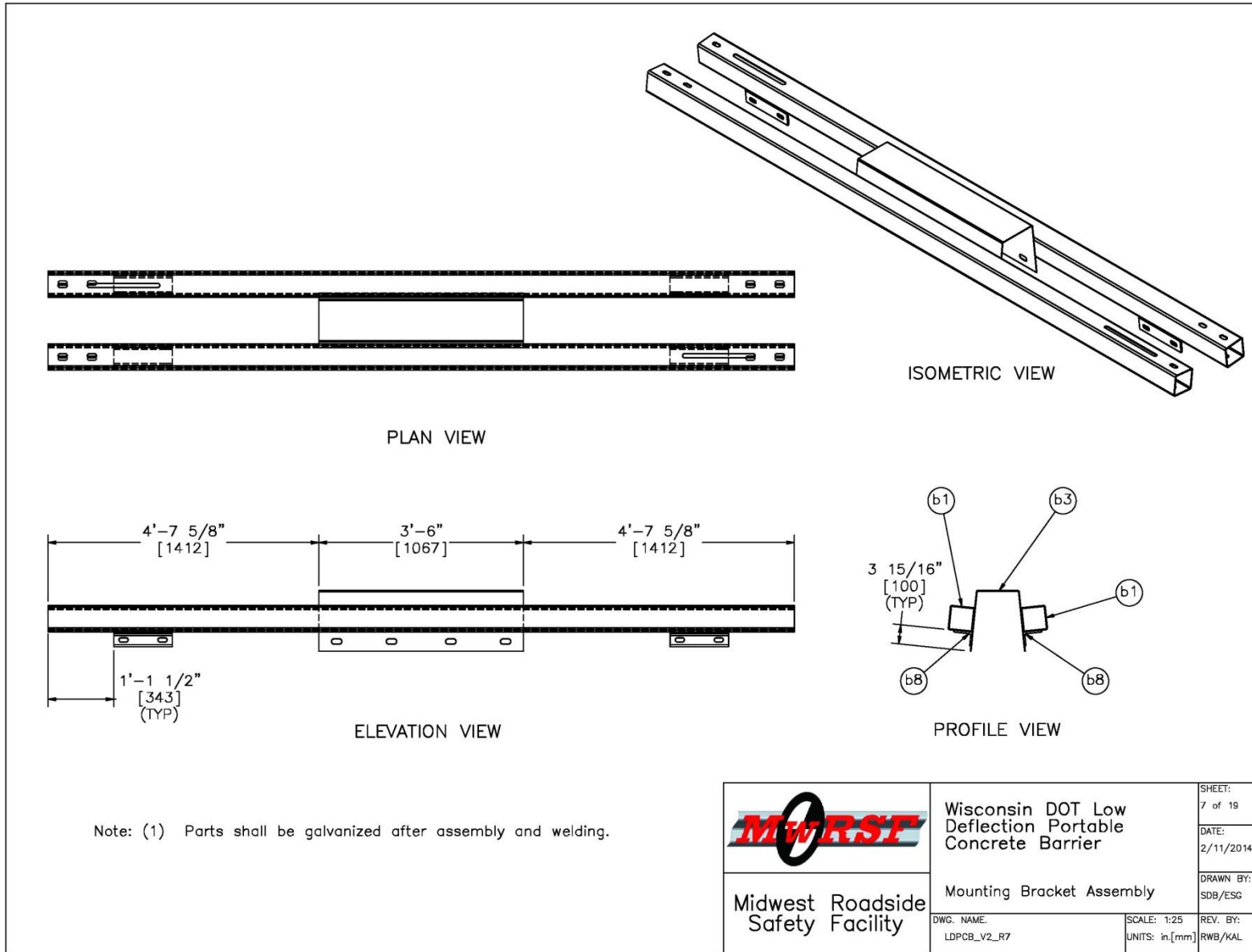


Figure 126. Design Details, Test No. RDTCB-2

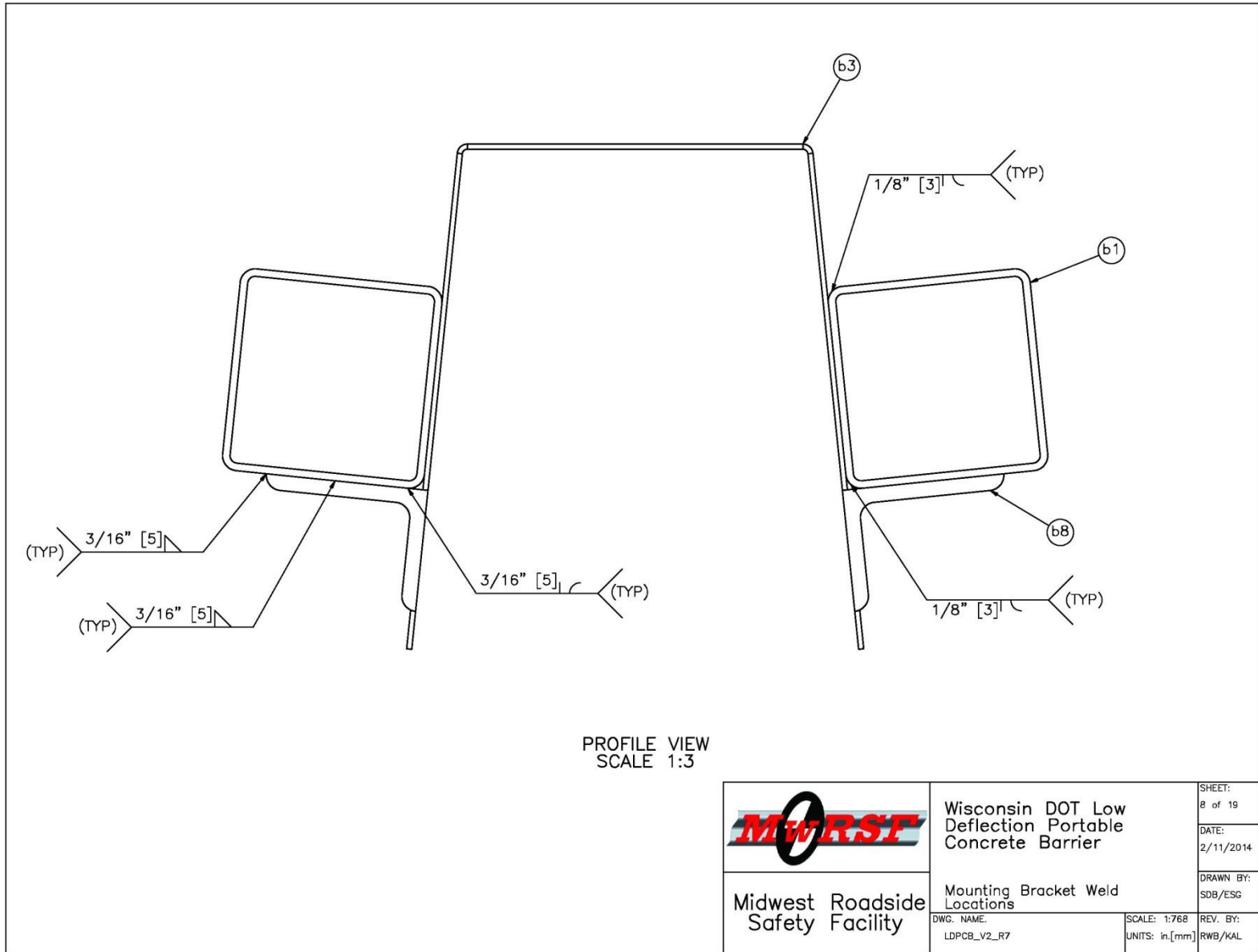


Figure 127. Design Details, Test No. RDTCB-2

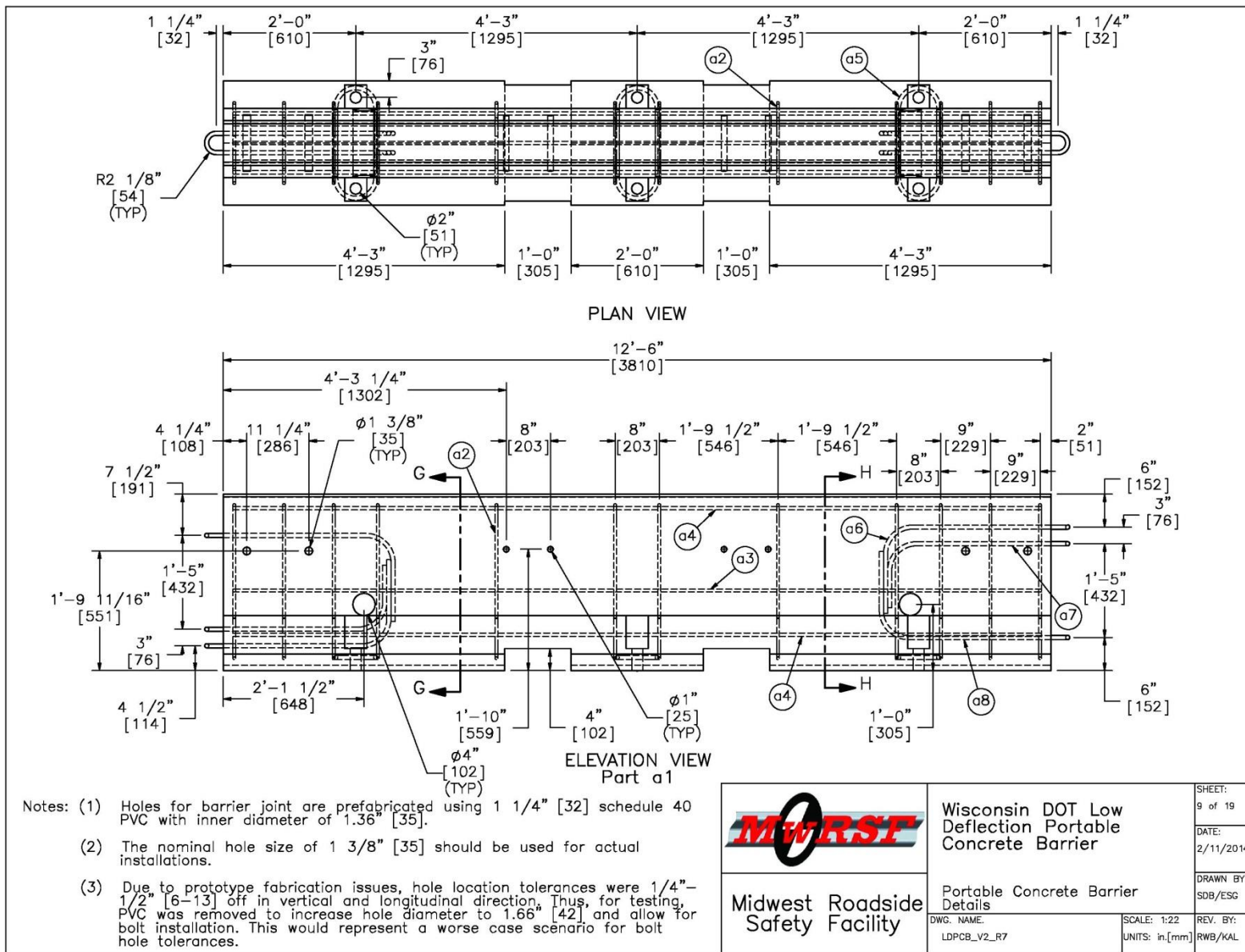


Figure 128. Design Details, Test No. RDTCB-2

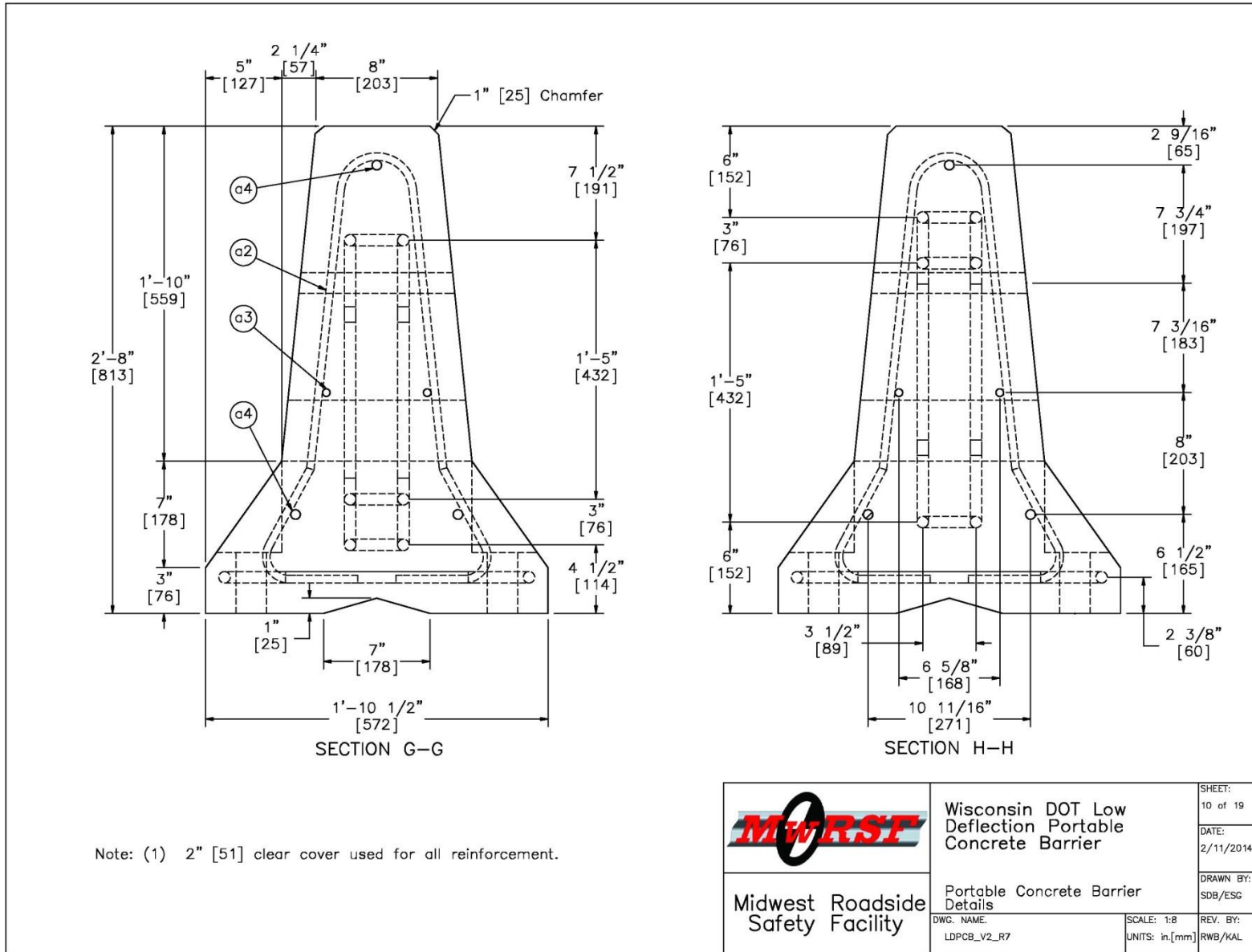


Figure 129. Design Details, Test No. RDTCB-2

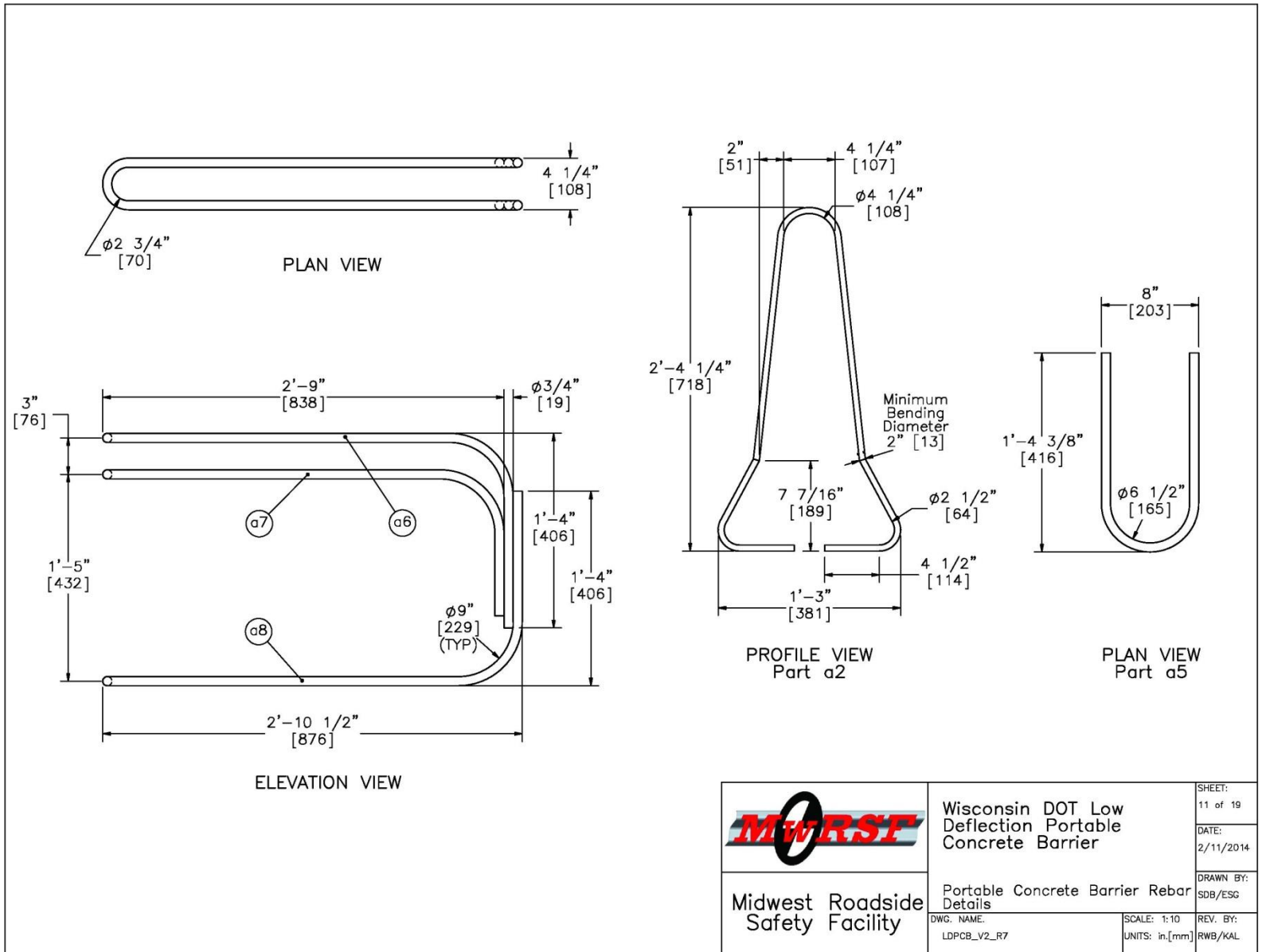


Figure 130. Design Details, Test No. RDTCB-2

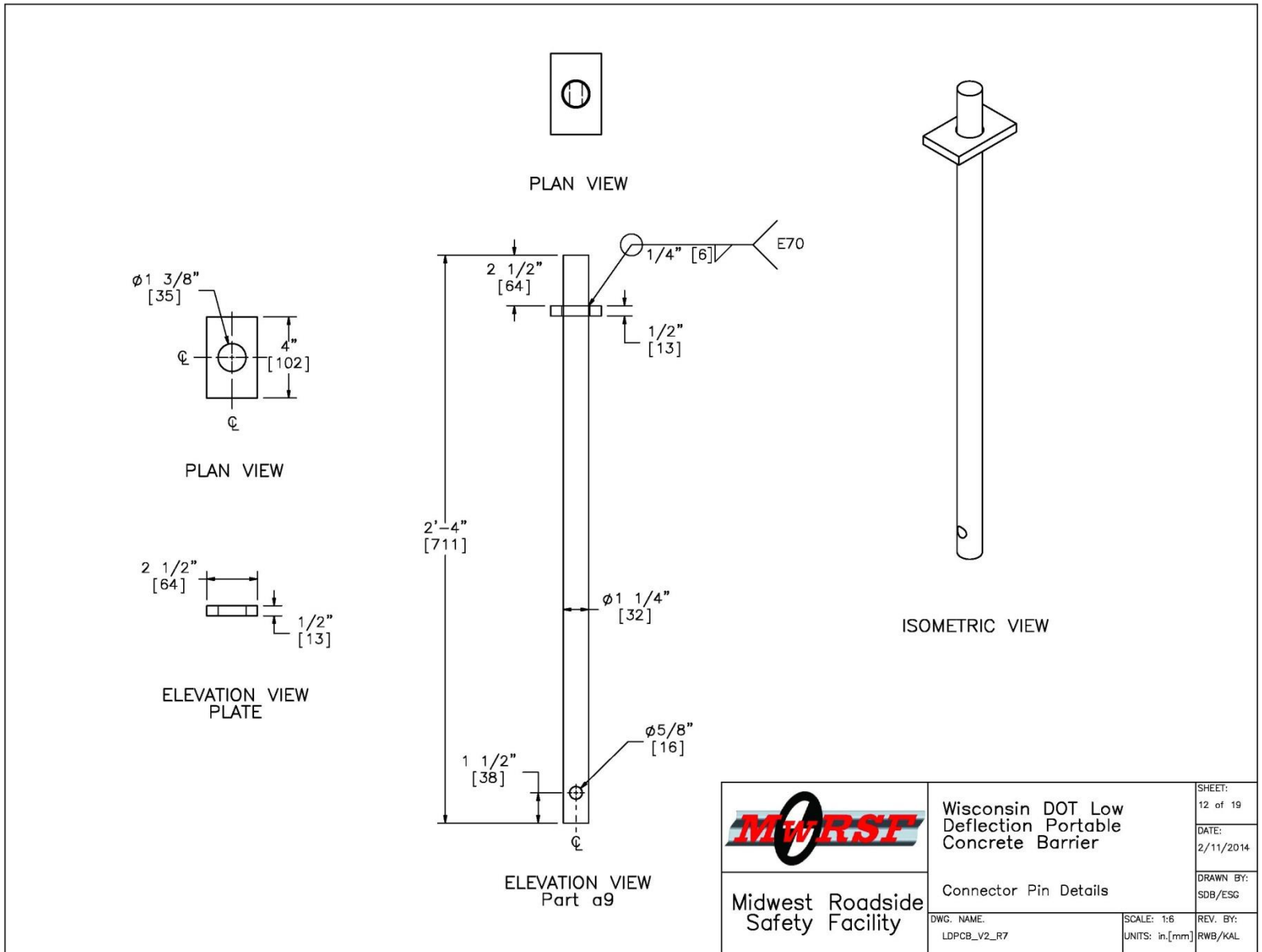


Figure 131. Design Details, Test No. RDTCB-2

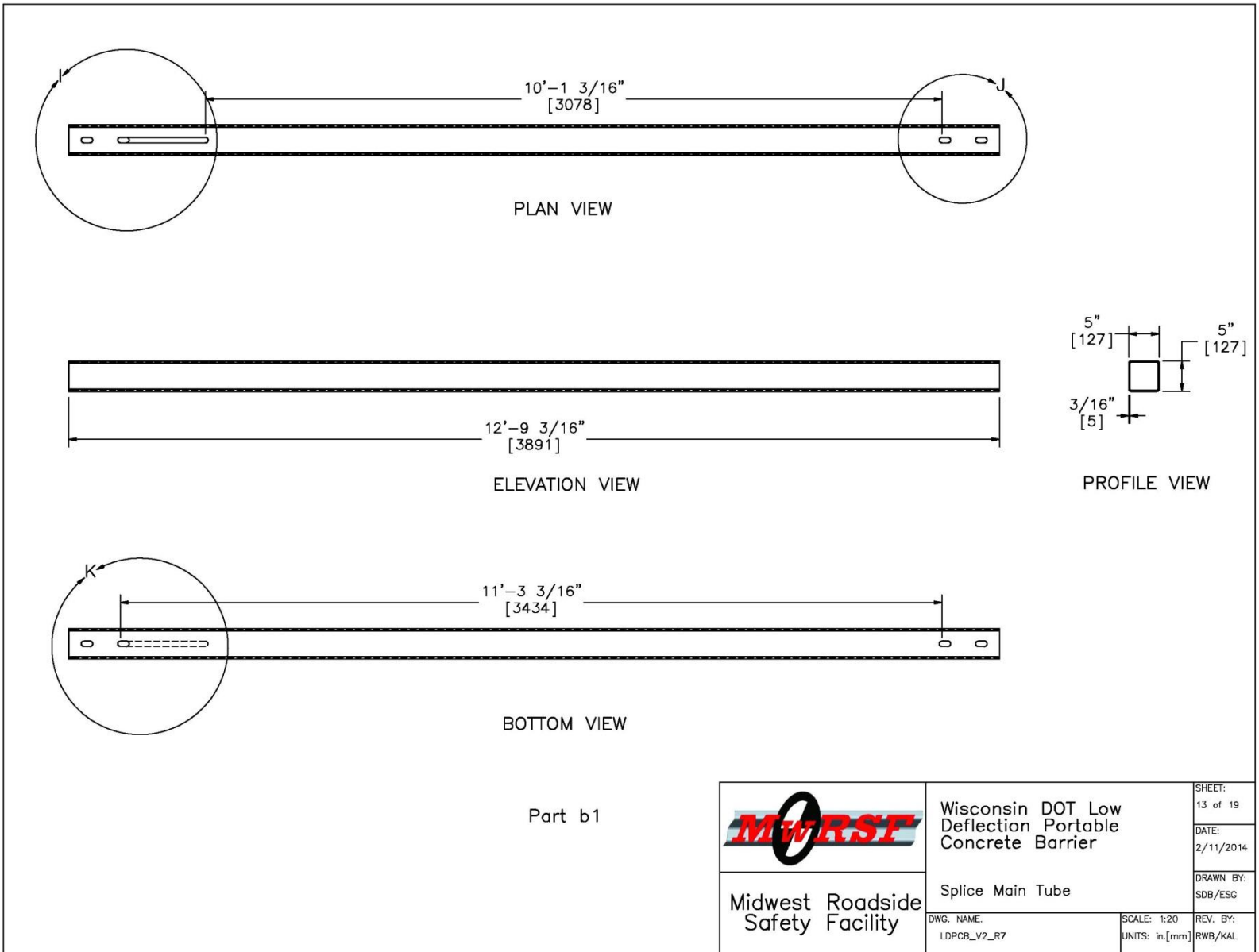


Figure 132. Design Details, Test No. RDTCB-2

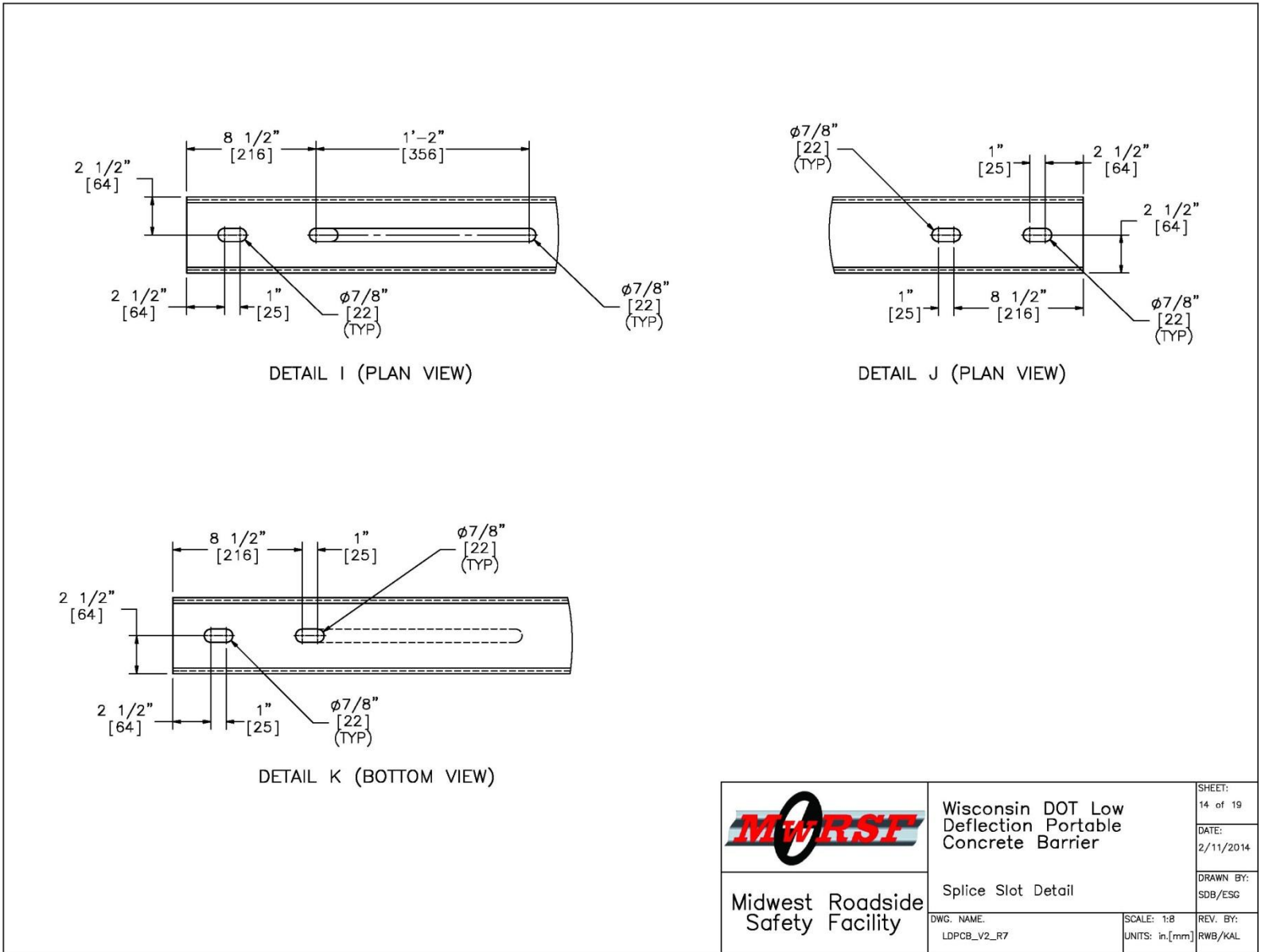


Figure 133. Design Details, Test No. RDTCB-2

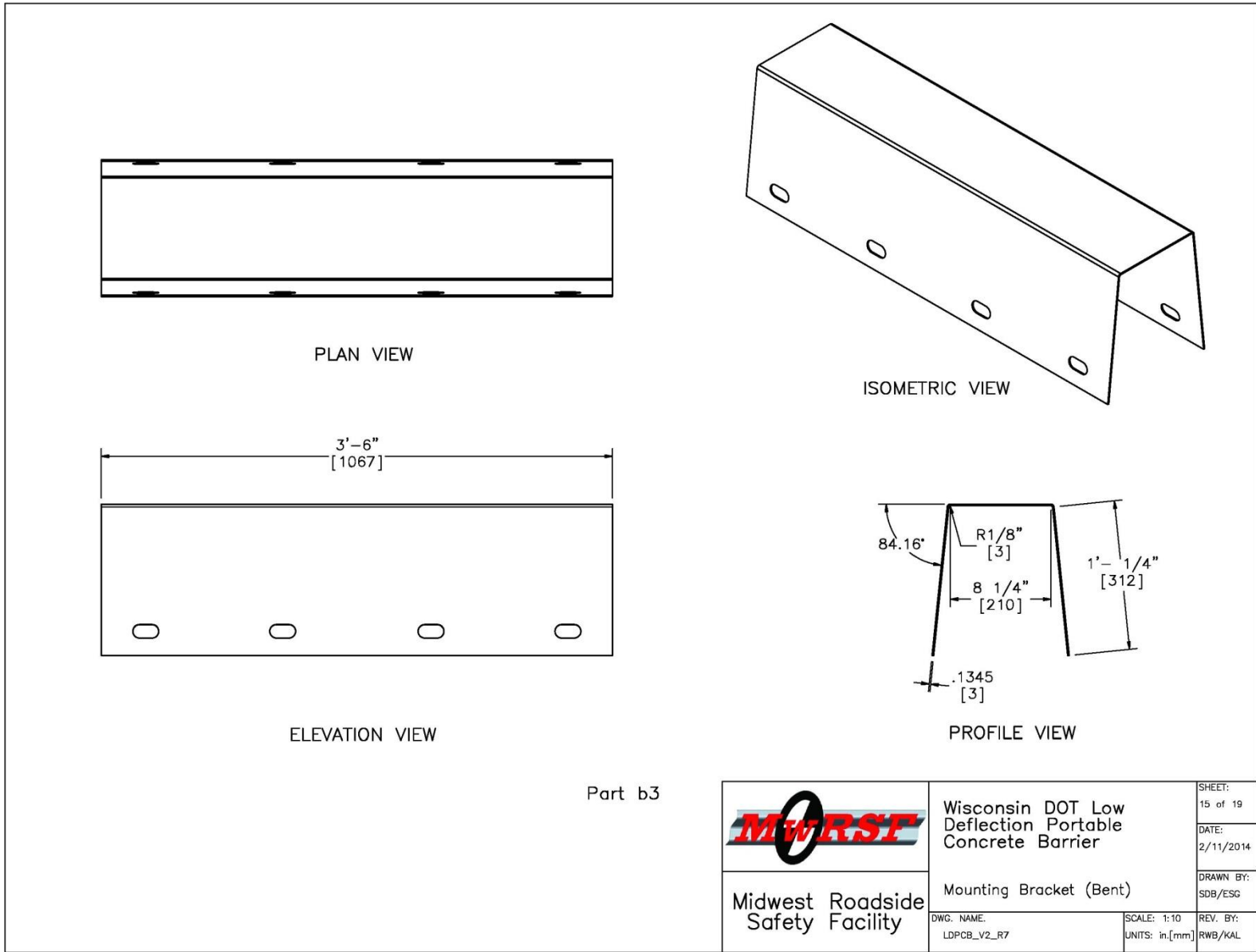


Figure 134. Design Details, Test No. RDTCB-2

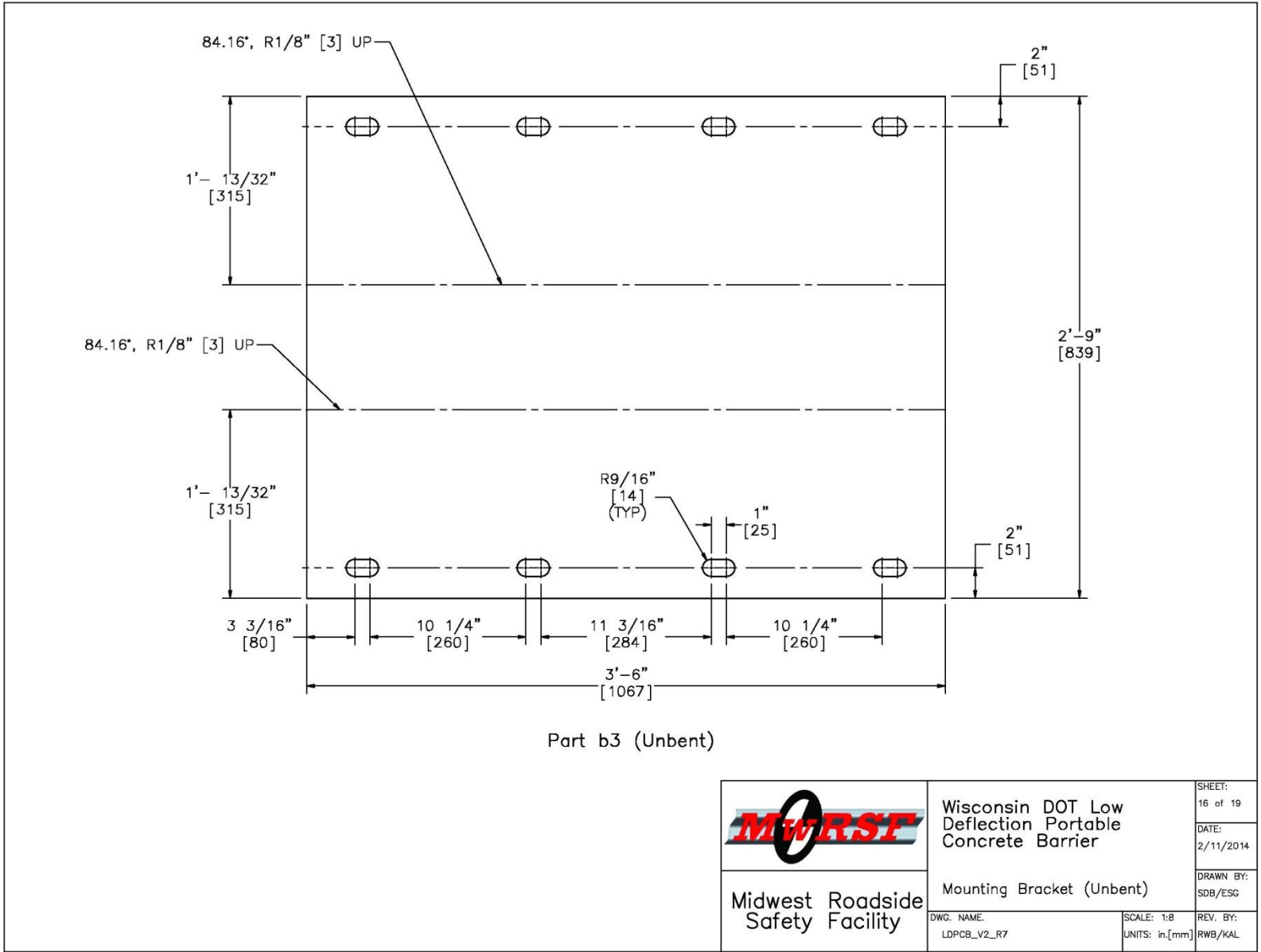


Figure 135. Design Details, Test No. RDTCB-2

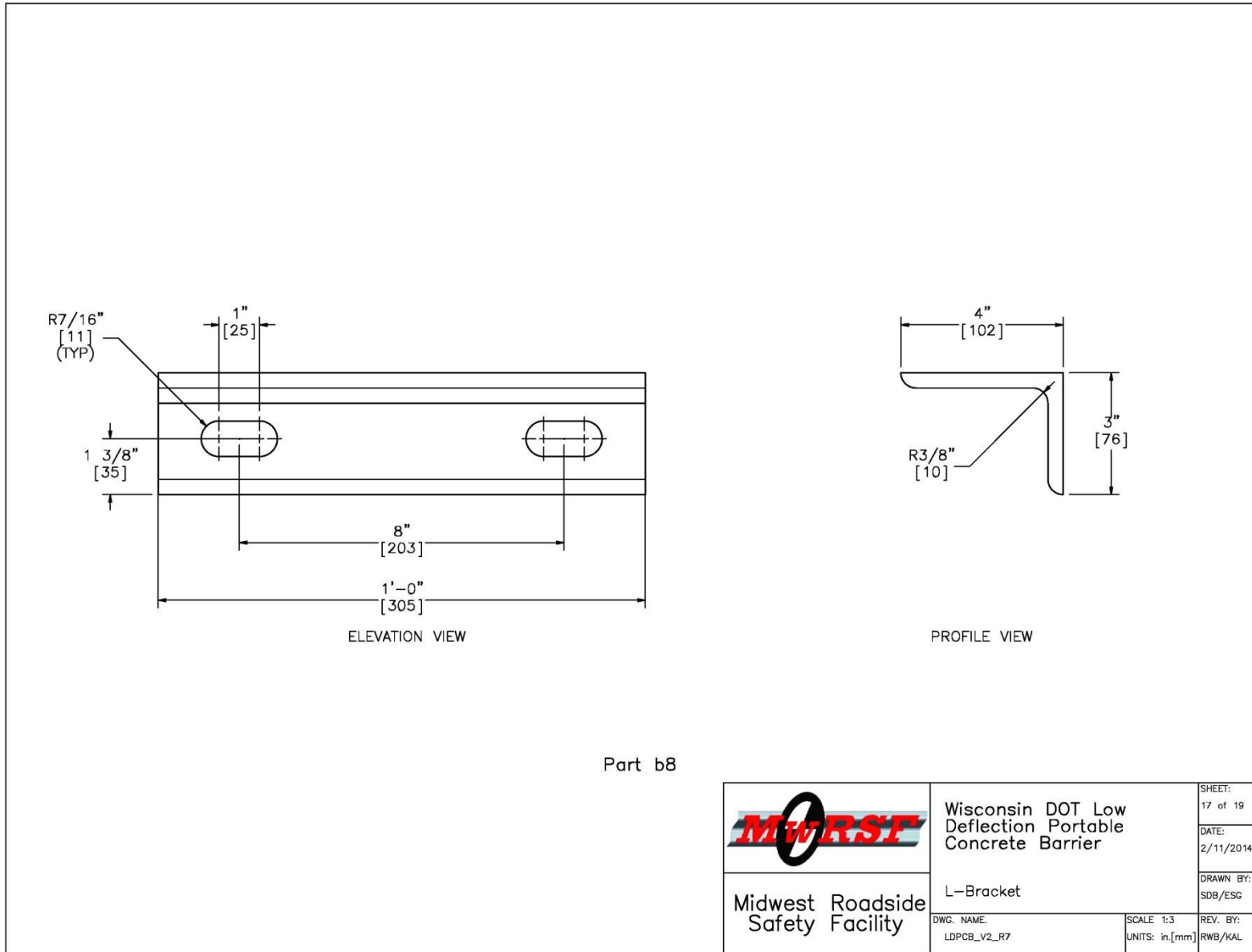


Figure 136. Design Details, Test No. RDTCB-2

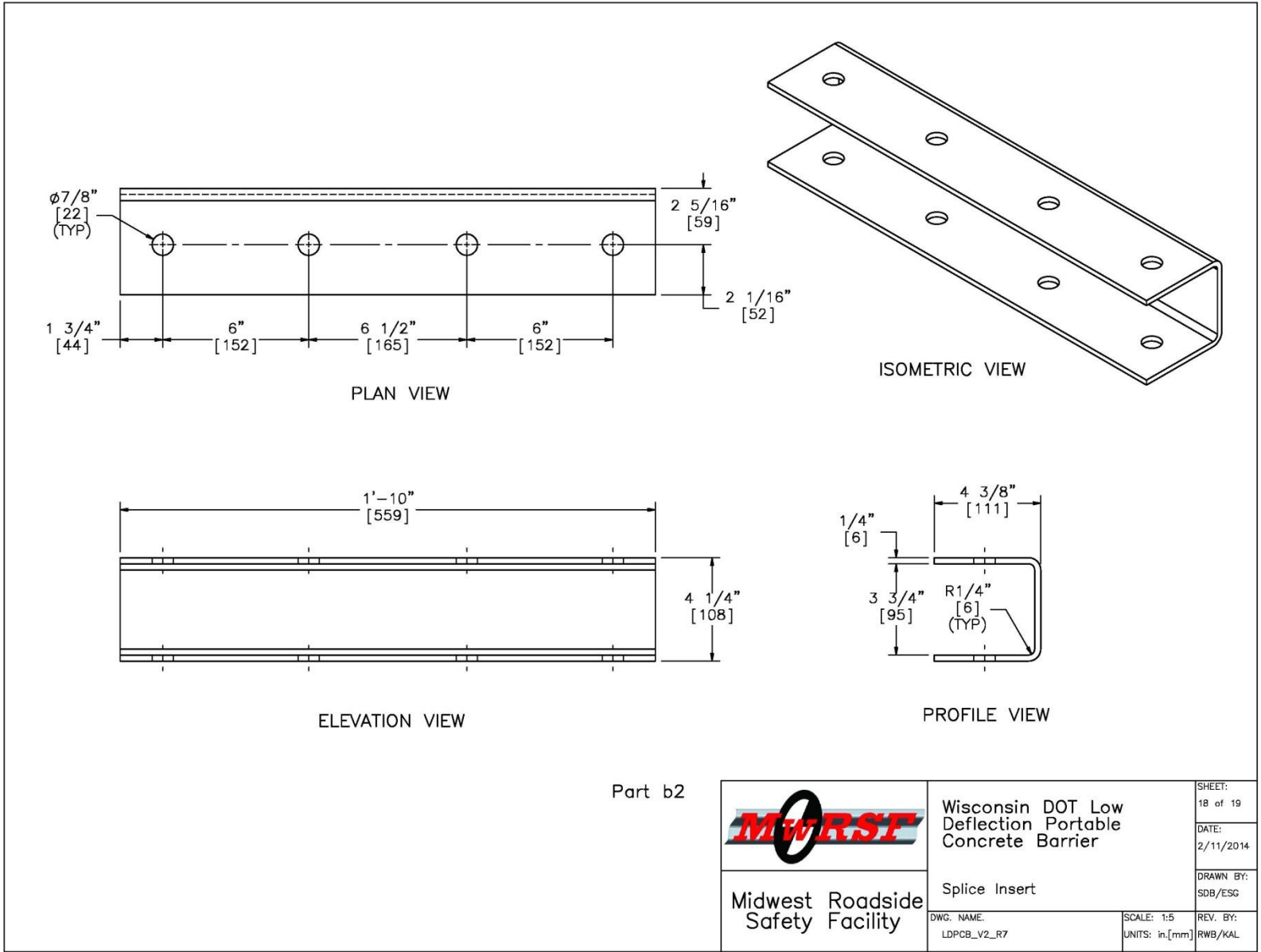


Figure 137. Design Details, Test No. RDTCB-2

Item No.	QTY.	Description	Material Specifications	Hardware								
a1	16	Portable Concrete Barrier	min f'c=5000 psi [34.5 MPa]	SWC09								
a2	192	1/2" [13] Dia., 72" [1829] Long Form Bar	ASTM A615 Grade 60	SWC09								
a3	32	1/2" [13] Dia., 146" [3708] Long Longitudinal Bar	ASTM A615 Grade 60	SWC09								
a4	48	5/8" [16] Dia., 146" [3708] Long Longitudinal Bar	ASTM A615 Grade 60	SWC09								
a5	96	3/4" [19] Dia., 36" [914] Long Anchor Loop Bar	ASTM A615 Grade 60	SWC09								
a6	32	3/4" [19] Dia., 101" [2565] Long Connection Loop Bar	ASTM A709 Grade 70 or A706 Grade 60	SWC09								
a7	32	3/4" [19] Dia., 91" [2311] Long Connection Loop Bar	ASTM A709 Grade 70 or A706 Grade 60	SWC09								
a8	32	3/4" [19] Dia., 102" [2591] Long Connection Loop Bar	ASTM A709 Grade 70 or A706 Grade 60	SWC09								
a9	15	1 1/4" [32] Dia., 28" [711] Long Connector Pin	ASTM A36 Galvanized	FMW02								
b1	22	5"x5"x3/16" [127x127x5], 12'-9 3/16" [3891] Long Splice Main Tube	ASTM A500 Grade B Galvanized after Welding	-								
b2	20	4 1/2"x4 1/2"x1/4" [114x114x6], 22" [559] Long Splice Insert	ASTM 572 Grade 50 Galvanized	-								
b3	11	42"x33" [1067x838] 10 Gage Mounting Bracket Plate	ASTM A1011 Grade 50 Galvanized after Welding	-								
b4	88	1" [25] Dia. Washer	ASTM F844 Galvanized	-								
b5	44	1" [25] Dia. UNC, 12 3/4" [324] Long Heavy Hex Bolt and Nut	Bolt ASTM A325/A449 Type 1 Galvanized, Nut ASTM A563 Galvanized	-								
b6	248	3/4" [19] Dia. Washer	ASTM F844 Galvanized	-								
b7	80	3/4" [19] Dia. UNC, 6 1/2" [165] Long, 2" [51] Threaded Hex Bolt and Nut	Bolt ASTM A325/A449/SAE Grade 5 Galvanized, Nut ASTM A563DH Grade 5 Galvanized	-								
b8	44	4"x3"x3/8" [102x76x10], 12" [305] Long L-Bracket	ASTM A529 Grade 50 Galvanized	-								
b9	44	3/4" [19] Dia. UNC, 13" [330] Long, 2" [51] Threaded Hex Bolt and Nut	Bolt ASTM A325/A449/SAE Grade 5 Galvanized, Nut ASTM A563DH Grade 5 Galvanized	-								
<table border="1" style="width: 100%; border-collapse: collapse;"> <tr> <td rowspan="2" style="text-align: center; vertical-align: middle;">   <b>Midwest Roadside Safety Facility</b> </td> <td style="text-align: center;"> <b>Wisconsin DOT Low Deflection Portable Concrete Barrier</b> </td> <td style="font-size: small;">                 SHEET: 19 of 19             </td> </tr> <tr> <td style="text-align: center;">                 Bill of Materials             </td> <td style="font-size: small;">                 DATE: 2/11/2014             </td> </tr> <tr> <td style="font-size: x-small;">                 DWG. NAME: LDPCB_V2_R7             </td> <td style="font-size: x-small;">                 SCALE: NONE UNITS: in.[mm]             </td> <td style="font-size: x-small;">                 DRAWN BY: SDB/ESG                   REV. BY: RWB/KAL             </td> </tr> </table>					 <b>Midwest Roadside Safety Facility</b>	<b>Wisconsin DOT Low Deflection Portable Concrete Barrier</b>	SHEET: 19 of 19	Bill of Materials	DATE: 2/11/2014	DWG. NAME: LDPCB_V2_R7	SCALE: NONE UNITS: in.[mm]	DRAWN BY: SDB/ESG  REV. BY: RWB/KAL
 <b>Midwest Roadside Safety Facility</b>	<b>Wisconsin DOT Low Deflection Portable Concrete Barrier</b>	SHEET: 19 of 19										
	Bill of Materials	DATE: 2/11/2014										
DWG. NAME: LDPCB_V2_R7	SCALE: NONE UNITS: in.[mm]	DRAWN BY: SDB/ESG  REV. BY: RWB/KAL										

Figure 138. Design Details, Test No. RDTCB-2



Figure 139. Test Installation, Test No. RDTCB-2



Figure 140. Barrier Segment Connection Designs, Test No. RDTCB-2

## 14 FULL-SCALE CRASH TEST NO. RDTCB-2

### 14.1 Test No. RDTCB-2

The 4,978-lb (2,258-kg) pickup truck impacted the low-deflection TCB system at a speed of 64.8 mph (104.3 km/h) and at an angle of 25.4 degrees. A summary of the test results and sequential photographs are shown in Figure 141. Additional sequential photographs are shown in Figure 142 and Figure 143. Documentary photographs of the crash test are shown in Figure 144.

### 14.2 Weather Conditions

Test no. RDTCB-2 was conducted on August 8<sup>th</sup>, 2013 at approximately 2:45 pm. The weather conditions as per the National Oceanic and Atmospheric Administration (station 14939/LNK) were reported and are shown in Table 14.

Table 14. Weather Conditions, Test No. RDTCB-2

Temperature	67° F
Humidity	81%
Wind Speed	3 mph
Wind Direction	40° from True North
Sky Conditions	Clear
Visibility	10 Statute Miles
Pavement Surface	Dry
Previous 3-Day Precipitation	0 in.
Previous 7-Day Precipitation	.06 in.

### 14.3 Test Description

Initial vehicle impact was to occur  $51\frac{3}{16}$  in. (1,300 mm) upstream of the joint between barrier nos. 8 and 9, as shown in Figure 145, which was selected using the CIP plots found in Section 2.3 or Table 2.6 of MASH. The actual point of impact was  $2\frac{1}{4}$  in. (57 mm) upstream of the target impact point. A sequential description of the impact events is contained in Table 15. The vehicle came to rest approximately 164 ft (50.0 m) past the downstream end on the back side

of the barrier with a yaw angle toward the barrier. The vehicle trajectory and final position are shown in Figures 141 and 146.

Table 15. Sequential Description of Impact Events, Test No. RDTCB-2

TIME (sec)	EVENT
0.000	Impact
0.000	Barrier nos. 8 & 9 began to deflect backward
0.000	Vehicle right-front bumper began to deform
0.002	Vehicle hood was deflecting upward
0.008	Vehicle right-front headlight began to override box-beam
0.012	Vehicle right-front fender began to deform
0.018	Vehicle grill began to deform
0.026	Vehicle right-front door began to open
0.034	Vehicle right headlight shattered
0.048	Vehicle began to roll toward barrier
0.056	Steel cap between barrier nos. 8 & 9 began to deform
0.066	Barrier nos. 7 & 10 began to deflect backward
0.078	Barrier no. 9 concrete began to crack
0.086	Barrier no. 8 concrete began to crack
0.112	Barrier no. 11 began to deflect forward
0.128	Vehicle left-rear tire became airborne
0.130	Vehicle left-front tire became airborne
0.132	Barrier no. 12 began to deflect forward
0.138	Barrier no. 6 began to deflect backward
0.144	Downstream end of barrier no. 5 began to deflect forward
0.162	Barrier no. 11 began to deflect backward
0.186	Vehicle right-rear quarter panel contacted steel tube
0.186	Barrier no. 4 was deflecting forward
0.192	Vehicle was parallel to system
0.212	Barrier no. 3 began to deflect backward
0.226	Barrier no. 9 began to spall on backside toe
0.236	Barrier no. 12 began to deflect backward
0.264	Joint between barrier nos. 2 & 3 was deflecting backward

0.276	Vehicle right taillight was completely detached
0.278	Downstream end of barrier no. 3 began to deflect forward
0.288	Vehicle began to pitch down
0.304	Barrier no. 5 was deflecting backward
0.414	Front-left tire made contact with ground
0.470	Barrier no. 4 was deflecting backward
0.668	Joint between barrier nos. 15 & 16 was deflecting backward
0.684	Vehicle lost contact with barrier
0.760	Vehicle was parallel to system
0.936	Vehicle right-front bumper made contact with barrier no. 13
1.368	Vehicle right-front bumper contacted barrier no. 16
1.494	Vehicle right-front tire lost contact with barrier no. 16
1.712	System came to rest
1.914	Vehicle continued to move downstream

#### 14.4 Barrier Damage

Damage to the system was moderate, as shown in Figures 147 through 151. Barrier damage consisted of contact marks on the front face of the concrete segments and box-beams, spalling of the concrete, and concrete cracking. The vehicle initially came into contact with barrier no. 8 a distance of 2 1/4 in. (57 mm) upstream from the target impact point and maintained contact until separating from the barrier at the downstream end of barrier no. 11. The vehicle then began to yaw toward the barrier and again made contact with barrier nos. 13 through 16.

Barrier nos. 5 through 16 showed significant lateral deflection upon post-impact examination. Barrier nos. 7 through 10 had portions of their bases suspended over the simulated roadway edge, but showed no drop in barrier height or potential for disengaging from the simulated bridge deck. Tire marks were visible on the concrete face of barrier nos. 8 through 10 and barrier nos. 13 through 16. The steel tubes on the front of barrier nos. 8 through 11 and barrier nos. 13 and 14 showed tire and scuff marks.

Several of the TCB segments displayed cracking and damage following the test. Barrier nos. 4 through 7 had vertical cracks on the impact side of the TCB segments near the midspan due to reverse bending loads generated during the impact event. Barrier nos. 8 through 10 had significant vertical cracks on the backside of the barrier segments. Barrier no. 8 developed three vertical cracks extending from lifting pockets on the back side of the barrier. Barrier no. 9 showed four vertical cracks on the backside which extended from the lifting pockets and extended to the top and through the width of the barrier, as shown in Figure 148. The cracking of barrier no. 9 was sufficient to permanently deform the barrier segment. Barrier no. 9 also had significant spalling on the front downstream toe between the lifting pockets and minor spalling on the backside. Barrier nos. 10 and 11 showed vertical cracks on the front and back of the barriers that nearly penetrated the width of the barriers. Barrier no. 12 showed vertical cracks on the front face of the barrier from reverse bending that were sufficient to form a permanent bend in the TCB segment, as shown in Figure 150. Spalling occurred along 12 ½ in. (318 mm) of the downstream backside toe of barrier no. 12 along with vertical cracks near the middle of the barrier.

The steel tubes did not tear or flatten at any point in the system. However, permanent deformation due to flexure of the tube section was observed in the tube rails on the front and back sides of the system at the joint between barrier segment nos. 8 and 9. The steel tube splices remained connected, but several of the splices were expanded or contracted during the impact. Expansion of the steel tube splices as large as 1 ¾ in. (44 mm) was observed at the back of barrier no. 9. Contraction of the tube splices to ¼ in. (6 mm) was observed on the front of barrier no. 9. Barrier segment gap widths were recorded after the test at the base of the front and back edge of the barrier segments. The barrier gaps were initially equal before the test was conducted. The gaps after the test were found to be different in the front and back due to curvature of the

system, but the recorded difference between the gaps on the front and the back of the barriers was limited to 1 ¼ in. (32 mm) or less. The steel tube rails did not show any significant separation from the concrete at any point in the system. No damage was noted to the splice bolts or steel cap connection bolts.

The permanent set of the barrier system was 39 ½ in. (1,003 mm), which occurred at the upstream end of barrier no. 9, as measured in the field. This level of barrier deflection created a maximum extent of the TCB segment past the edge of the bridge deck of 15 ½ in. (394 mm). However, there was no indication of the barriers disengaging or tipping off of the bridge deck, and the entire system remained stable and upright on the road surface. The maximum lateral dynamic barrier deflection, including tipping of the barrier along the top surface, was 40.7 in. (1,034 mm) at the upstream end of barrier no. 9, as determined from high-speed digital video analysis. The working width of the system was found to be 51.9 in. (1,318 mm), also determined from high-speed digital video analysis.

#### **14.5 Vehicle Damage**

The damage to the vehicle was moderate, as shown in Figures 152 and 153. The maximum occupant compartment deformations are listed in Table 16 along with the deformation limits established in MASH for various areas of the occupant compartment. Note that none of the MASH-established deformation limits were violated. Complete occupant compartment and vehicle deformations and the corresponding locations are provided in Appendix E.

The majority of the damage was concentrated on the right-front corner and right side of the vehicle where the impact occurred. The right side of the front bumper was crushed inward and back while the right-front fender was pushed downward. A 3 ½-in. (89-mm) gap was formed between the front of the hood and fender. The right-front steel rim was dented and deformed and a 2 ½-in. (64-mm) square hole was gouged through the tire sidewall. The front-right upper and

lower ball joints failed and the control arms were deformed. The grill was fractured around the right-side headlight assembly which, along with the fog light, was fractured and nearly removed from the vehicle. Denting and scraping were observed on the entire right side of the vehicle due to contact with the steel tubes. The right-side doors were ajar, but were inoperable due to the vehicle deformation. The right taillight was disengaged. The rear bumper was dented inward and scraped on the right side. The tailgate was shifted, but remained upright and attached. The front of the hood had a 2 ¼-in. (57-mm) gap on the left side. The lower left side of the windshield had spider-web cracking in an area measuring 6 ½ in. x 14 in. (165 mm x 356 mm). The roof and remaining window glass remained undamaged.

Table 16. Maximum Occupant Compartment Deformations by Location, Test No. RDTCB-2

LOCATION	MAXIMUM DEFORMATION in. (mm)	MASH ALLOWABLE DEFORMATION in. (mm)
Wheel Well & Toe Pan	1 (25)	≤ 9 (229)
Floor Pan & Transmission Tunnel	½ (13)	≤ 12 (305)
Side Front Panel (in Front of A-Pillar)	1 (25)	≤ 12 (305)
Side Door (Above Seat)	½ (13)	≤ 9 (229)
Side Door (Below Seat)	1 (25)	≤ 12 (305)
Roof	0 (0)	≤ 4 (102)
Windshield	0 (0)	≤ 3 (76)

#### 14.6 Occupant Risk

The calculated occupant impact velocities (OIVs) and maximum 0.010-sec occupant ridedown accelerations (ORAs) in both the longitudinal and lateral directions are shown in Table 17. Note that the OIVs and ORAs were within the suggested limits provided in MASH. The calculated THIV, PHD, and ASI values are also shown in Table 17. The results of the occupant risk analysis, as determined from the accelerometer data, are also summarized in Figure 141. The

recorded data from the accelerometers and the rate transducers are shown graphically in Appendix G.

Table 17. Summary of OIV, ORA, THIV, PHD, and ASI Values, Test No. RDTCB-2

Evaluation Criteria		Transducer			MASH Limits
		EDR-3	DTS	DTS-SLICE	
OIV ft/s (m/s)	Longitudinal	12.11 (3.69)	12.30 (3.75)	12.99 (3.96)	≤ 40 (12.2)
	Lateral	21.05(6.42)	21.41 (6.53)	23.06 (7.03)	≤40 (12.2)
ORA g's	Longitudinal	4.85	5.56	5.66	≤ 20.49
	Lateral	7.68	8.52	7.04	≤ 20.49
THIV ft/s (m/s)		NA	23.92 (7.29)	25.56 (7.79)	not required
PHD g's		NA	9.23	8.31	not required
ASI		1.34	1.32	1.42	not required

#### 14.7 Discussion

The analysis of the test results for test no. RDTCB-2 showed that the TCB system adequately contained and redirected the 2270P vehicle with controlled lateral displacements of the barrier. There were no detached elements or fragments which showed potential for penetrating the occupant compartment or presenting undue hazard to other traffic. Deformations of, or intrusions into, the occupant compartment that could have caused serious injury did not occur. The test vehicle did not penetrate or ride over the barrier, and it remained upright during and after the collision. Vehicle roll, pitch, and yaw angular displacements, as shown in Appendix G, were deemed acceptable because they did not adversely influence occupant risk safety criteria or cause rollover. After impact, the vehicle exited the barrier at an angle of 7.2 degrees away from the barrier and its trajectory did not violate the bounds of the exit box. Therefore, test no.

RDTCB-2 conducted on the box-beam-reinforced TCB system was determined to be acceptable according to the MASH safety performance criteria for test designation no. 3-11.

Review of the results of test no. RDTCB-2 revealed several insights into the performance of the revised low-deflection TCB design as compared to the test no. RDTCB-1 system design and the computer simulation models. It was apparent that the additional steel tube attachments were successful at constraining the steel tubes to the sides of the TCB segments and further reducing lateral system deflections. The modification transmitted impact loads more effectively to adjacent barrier segments and engaged more of the barrier system. This was evident in the increased number of displaced barrier segments upstream and downstream of impact. However, the reduction in lateral system deflection was not as significant as predicted during the simulation of the proposed design alternatives.

The inability of the design modification to reduce the lateral barrier deflections to the predicted levels was believed to be largely due to the increased TCB segment damage observed in test no. RDTCB-2. Flexural cracking and damage due to the primary vehicle impact and reverse bending upstream and downstream of impact was significantly greater in test no. RDTCB-1 as compared to test no. RDTCB-2. Barrier segment nos. 9 and 12 were permanently deformed due to the concrete cracking and fracture, and as many as eight additional barrier segments displayed cracking and damage due to flexural loading. This barrier damage in both standard and reverse bending was not accounted for in the simulation model and allowed for higher system deflections than anticipated. It was believed that the additional attachment points for the steel tubes successfully stiffened the TCB system, but that the loads imparted to the TCB by the additional connections exceeded the capacity of the barrier segment.

A secondary factor in the increased deflections observed in test no. RDTCB-2 was the impact velocity and angle of the crash test. The simulation effort used impact conditions of 62.1

mph (100.0 km/h) and an angle of 25 degrees, while test no RDTCB-1 had a speed and angle of 64.8 mph (104.3 km/h) and 25.4 degrees, respectively. This resulted in a 12.2 percent increase in impact severity for the full-scale crash test as compared to the simulation model. The increased speed and angle in the full-scale crash test would have tended to further increase the observed barrier deflections over those predicted by computer simulation. The increased impact severity for test no. RDTCB-2 also potentially contributed to a limited decrease in dynamic deflection for that test as compared to test no. RDTCB-1.

These results suggested that the current design was limited by the TCB segment capacity, and that further redesign of composite action retrofits to the TCB system would have negligible benefit. It appeared that the current system exceeded the TCB flexural capacity, and further stiffening would not be likely to reduce deflections as the TCB reinforcement would limit their effectiveness. Thus, other options would need to be investigated to further reduce deflection of the TCB system. These options would include increased reinforcement of the TCB segment, redesign of the TCB connection, and/or the use of additional deflection-reducing mechanisms.



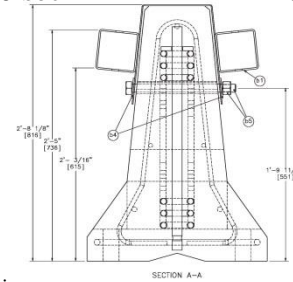
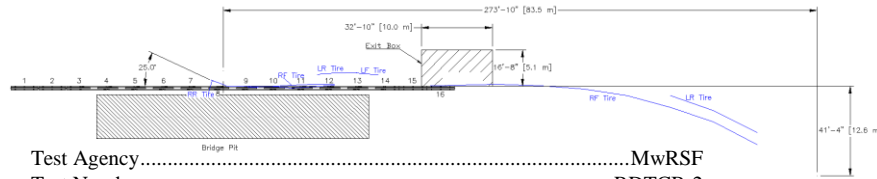
0.000 sec

0.150 sec

0.300 sec

0.450 sec

0.600 sec



- Test Agency .....MwRSF
- Test Number .....RDTCB-2
- Date ..... August 8, 2013
- MASH Test Designation..... 3-11
- Test Article.....Stiffened Temporary Concrete Barrier
- Total Length .....204 ft 7<sup>5</sup>/<sub>16</sub> in. (62.4 m)
- Key Component – Concrete Barrier
  - Length..... 150 in. (3,810 mm)
  - Base Width.....22.5 in. (572 mm)
  - Height.....32 in. (813 mm)
- Key Component – Box-Beam
  - Length..... 153<sup>3</sup>/<sub>16</sub> in. (3,891mm)
  - Dimension..... 5 in. x 5 in. (127 mm x 127 mm)
  - Wall Thickness .....<sup>3</sup>/<sub>16</sub> in. (5 mm)
- Soil Type ..... N/A
- Vehicle Make /Model .....Dodge Ram 1500 Quad Cab
  - Curb .....4,887 lb (2,217 kg)
  - Test Inertial.....4,978 lb (2,258 kg)
  - Gross Static.....5,143 lb (2,333 kg)
- Impact Conditions
  - Speed .....64.8 mph (104.3 km/h)
  - Angle ..... 25.4 deg
  - Impact Location ..... 53<sup>7</sup>/<sub>16</sub> in. (1359 mm) US of barriers 8 and 9 joint
- Exit Conditions
  - Speed .....56.7 mph (91.2 km/h)
  - Angle ..... -7.2 deg
- Exit Box Criterion ..... Pass
- Vehicle Stability..... Satisfactory
- Vehicle Stopping Distance..... 164 ft (50.0 m)
- Vehicle Damage .....
  - VDS<sup>[29]</sup>..... 1-RFQ-3
  - CDC<sup>[30]</sup>..... 1-RYEN2
  - Maximum Interior Deformation..... 1 in. (25 mm)

- Maximum Test Article Deflections
  - Permanent Set..... 39.5 in. (1,003 mm)
  - Dynamic ..... 40.7 in. (1,034 mm)
  - Working Width..... 51.9 in. (1,318 mm)
- Maximum Angular Displacements
  - Roll ..... 14.95° < 75°
  - Pitch..... -5.92° < 75°
  - Yaw ..... -35.07°
- Impact Severity (IS)..... 128.6 kip-ft (174.4 kJ) > 106 kip-ft (144 kJ)
- Transducer Data

Evaluation Criteria		Transducer			MASH Limit
		EDR-3	EDR-4	DTS	
OIV ft/s (m/s)	Longitudinal	12.11 (3.69)	12.30 (3.75)	12.99 (3.96)	≤ 40 (12.2)
	Lateral	21.05 (6.42)	21.41 (6.53)	23.06 (7.03)	≤ 40 (12.2)
ORA g <sup>2</sup> s	Longitudinal	4.85	5.56	5.66	≤ 20.49
	Lateral	7.68	8.52	7.04	≤ 20.49
THIV – ft/s (m/s)		NA	23.92 (7.29)	25.56 (7.79)	not required
PHD – g’s		NA	9.23	8.31	not required
ASI		1.34	1.32	1.42	not required

Figure 141. Summary of Test Results and Sequential Photographs, Test No. RDTCB-2



0.000 sec



0.050 sec



0.090 sec



0.140 sec



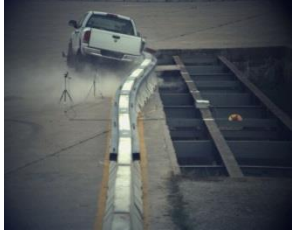
0.200 sec



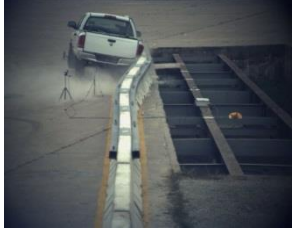
0.240 sec



0.000 sec



0.140 sec



0.226



0.600 sec



0.800 sec



1.000 sec

Figure 142. Additional Sequential Photographs, Test No. RDTCB-2



0.000 sec



0.038 sec



0.100 sec



0.200 sec



0.250 sec



.312 sec



0.000 sec



0.100 sec



0.250 sec



0.700 sec



1.000 sec



1.350 sec

Figure 143. Additional Sequential Photographs, Test No. RDTCB-2

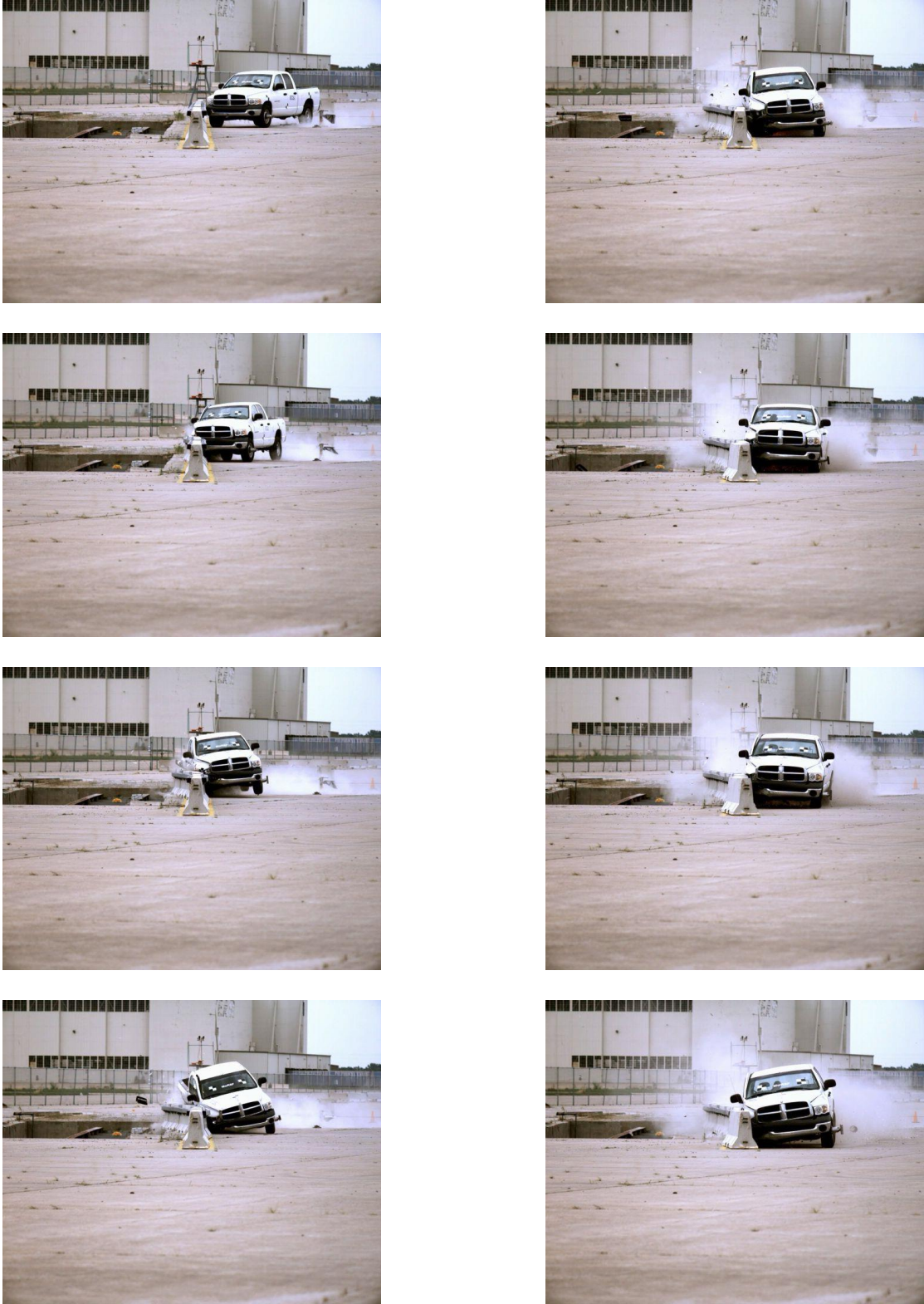


Figure 144. Documentary Photographs, Test No. RDTCB-2

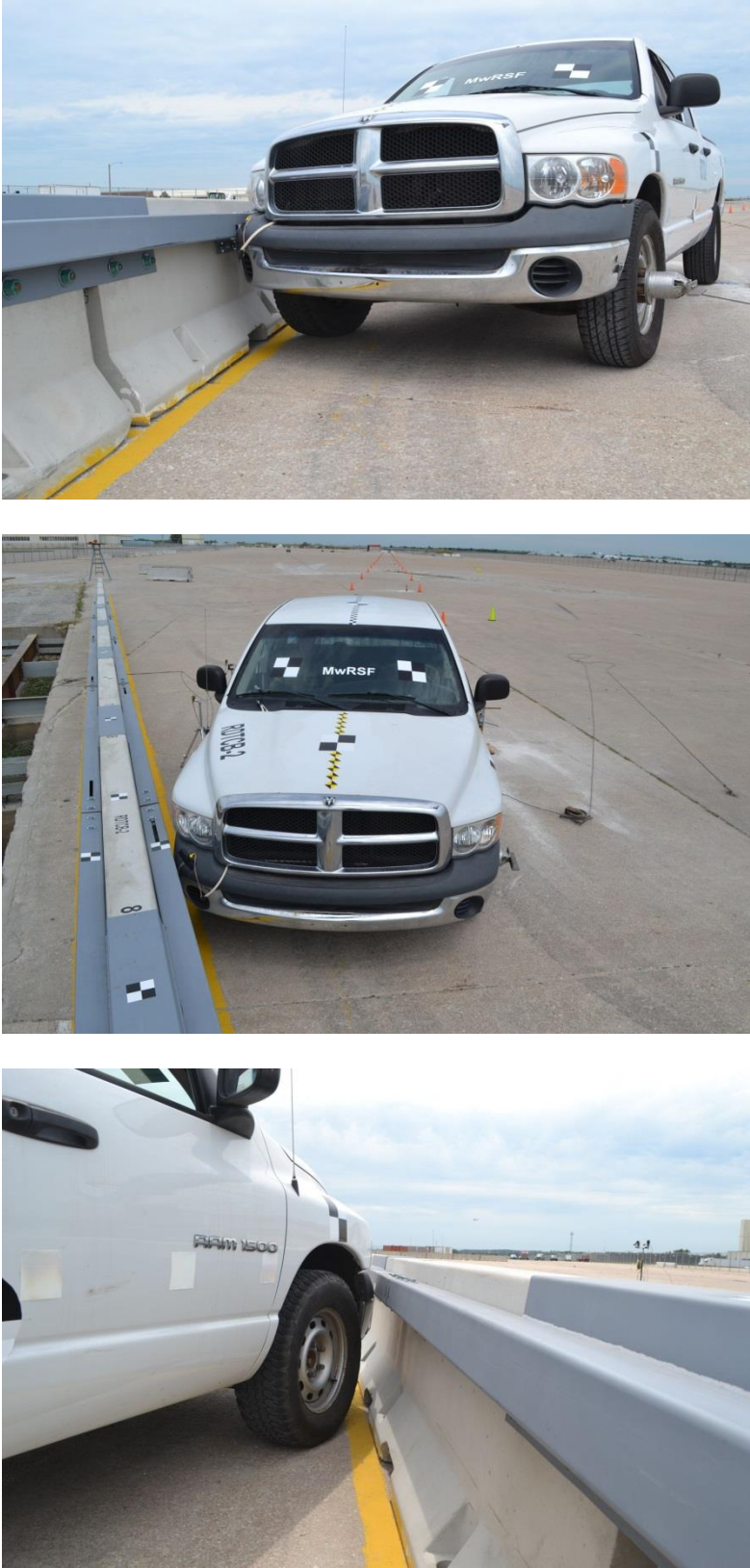


Figure 145. Impact Location, Test No. RDTCB-2



Figure 146. Vehicle Final Position and Trajectory Marks, Test No. RDTCB-2



Figure 147. Overall System Damage, Test No. RDTCB-2



Figure 148. System Damage at Barrier Nos. 8 and 9, Test No. RDTCB-2



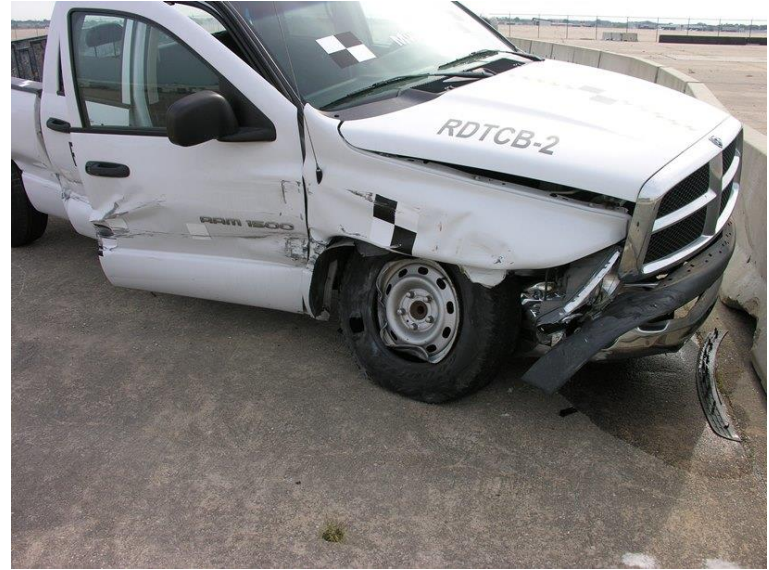
Figure 149. Rail Splices at Barrier Nos. 8 and 9, Test No. RDTCB-2



Figure 150. Barrier Segment Damage Due to Reverse Bending, Test No. RDTCB-2



Figure 151. Permanent System Deflection, Test No. RDTCB-2



237

Figure 152. Vehicle Damage, Test No. RDTCB-2



Figure 153. Vehicle Damage, Test No. RDTCB-2

## 15 EVALUATION OF DEFLECTION LIMITS

Previous research at MwRSF investigated the TCB deflection limits for less critical TCB installations [0]. This research argued that when temporary concrete barriers are used on the edge of a bridge, the risk of the entire line of barriers falling off the deck requires that deflection limits be selected to preclude such behavior in almost all impact scenarios. Hence, it was recommended that at the edge of a bridge deck, design deflection limits should be selected to contain more than 95 percent of all crashes. In all other barrier applications, the consequences of a barrier exceeding the design deflection criteria are not severe. In these situations, a more modest deflection limit criterion based on an 85<sup>th</sup> percentile impact severity was deemed more appropriate. The sponsor of this research effort requested that a similar analysis be performed on the low-deflection TCB system developed herein in order to provide deflection limits for less critical installations.

A number of research studies have shown that the Impact Severity (IS), as defined below, is a good indicator of the degree of loading and the lateral deflections of longitudinal barriers [33-35].

$$\frac{1}{2}m(v \sin \theta)^2$$

where:

m = mass of impacting vehicle  
v = velocity of impacting vehicle  
 $\theta$  = angle of impact.

IS incorporates the effect of the mass of the impacting vehicle to provide a good measure of the severity of impact and the magnitude of the resulting barrier deflections. In order to determine appropriate IS values for this study, data was taken from the results of the NCHRP 22-17 project [36]. NCHRP 22-17 was used to generate the impact conditions for MASH and

represented the most applicable data set from which to draw. While the NCHRP 22-17 data was biased toward severe and fatal crashes, it was believed that the dataset would provide a conservative basis for the analysis that correlated with the impact conditions specified in MASH.

Figure 154 shows the IS distribution for freeways from NCHRP 22-17. As shown in Figure 154, the 95<sup>th</sup> percentile IS value was 127.6 kip-ft (173.0 kJ). This value was greater than the IS value associated with the TL-3 strength test of 115.4 kip-ft (156.5 kJ), but it was almost equivalent to the IS value of test no. RDTCB-2, which was 128.6 kip-ft (174.4 kJ). Therefore, it was reasonable to utilize the deflections measured during full-scale crash testing no. RDTCB-2 when selecting barrier deflection limits for use on the edge of a bridge deck or drop-off. However, the 85<sup>th</sup> percentile IS value, which is more appropriate for all other applications of temporary concrete barriers, was 78.3 kip-ft (106.2 kJ). An IS value of 78.3 kip-ft (106.2 kJ) would correspond to an impact velocity of 51.2 mph (82.4 km/h) for 5,000-lb (2,268-kg) pickup truck impacting the barrier at an angle of 25 degrees. Barrier deflections under this impact condition would be much less than those observed under the MASH TL-3 criteria.

Although additional crash tests could be conducted to determine the deflection of the low-deflection TCB system at this reduced impact condition, the cost would be extremely high. Instead, computer simulation of the reduced impact condition was used to estimate the deflection of barriers impacted under the 85<sup>th</sup> percentile impact severity. This process involved using LS-DYNA to model the behavior of the barrier system when subjected to full-scale crash testing. After the model was calibrated to accurately predict barrier deflections for the high energy crash test conditions, the impact conditions were revised and the barrier deflections were estimated for the lower energy crash.

## Distribution of IS Values at Road Departure

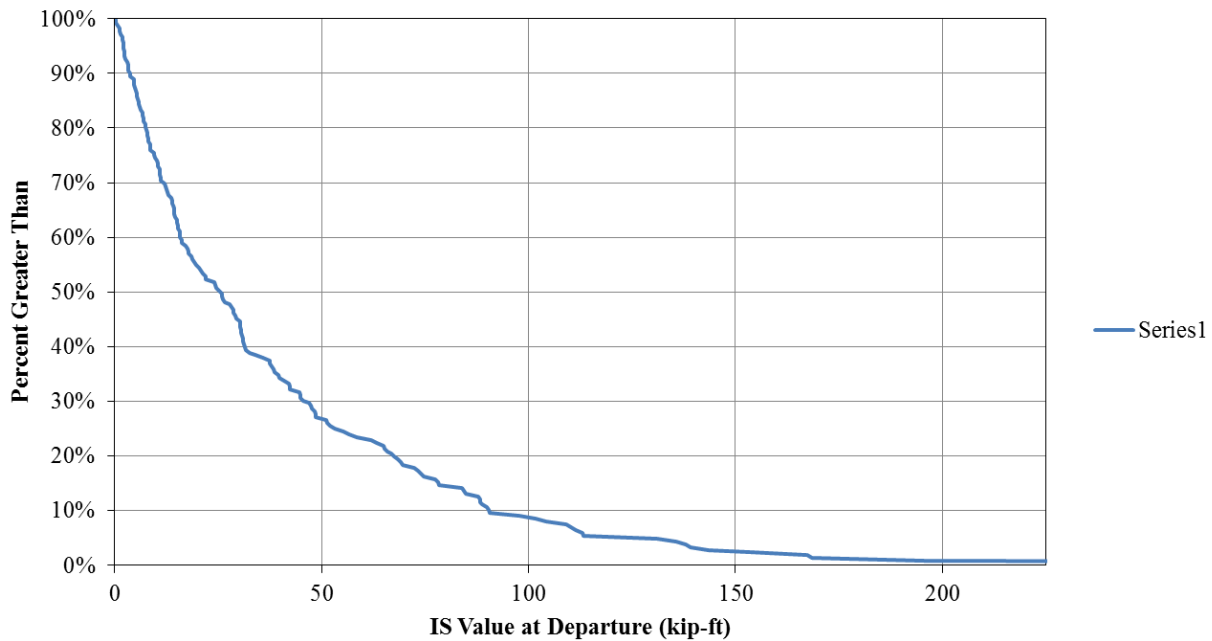


Figure 154. NCHRP 22-17 IS Distribution for Freeways

In order to simulate test no. RDTCB-2 in LS-DYNA, a simulation model of the barrier system in that test was created and simulated under the test impact conditions, as shown in Figure 155. The model of the reduced-deflection TCB system was modeled similarly to the reduced-deflection models created for the original parametric study and the models of the potential design modifications. Thus, the simulation model used rigid barriers and explicit models of the steel hardware and bolted connections. Initial simulations of test no. RDTCB-2 demonstrated significantly lower deflections than the full-scale test. The discrepancy between the physical test and the model was attributed largely to the concrete damage and fracture observed in the test which was not reproduced in the rigid TCB model.

The researchers discussed applying the concrete material model investigated in Chapter 7 in order to capture the concrete damage seen in the physical test. However, this was rejected for two reasons. First, the researchers' confidence in the ability of the concrete material model to capture the damage in the full-scale test was limited due to the difficulties encountered in

modeling of a simple concrete beam specimen and the lack of any previous experience in application of the material model to the simulation of TCB segments. As such, a significant amount of additional component level simulation and modeling would have been required to accurately model a TCB segment using the concrete material model. Second, the concrete damage that contributed to the deflections in test no. RDTCB-2 was distributed through many of the barrier segments in the system. Thus, capturing the damage would require modeling of fully reinforced TCB segments with the concrete material model for most if not all of the TCB segments in the simulation. It was believed that this would be very computationally expensive. Based on these considerations it was decided to attempt to model the reduced-deflection TCB system deflection without the concrete material model.

As a compromise, the simulation model of test no. RDTCB-2 was modified to reduce the barrier-to-ground friction level until the simulation model reproduced the dynamic barrier deflections observed in the full-scale test. While this was not the optimal solution, it provided a conservative baseline with which to create simulations using the reduced impact conditions. It was believed that the reduction in barrier friction would produce conservative estimates of the deflection of the barrier system for the 85<sup>th</sup> percentile IS impact. The concrete damage that the reduced friction was acting as a surrogate for in the simulation model would not be as large of a factor for reduced-severity impacts where lower levels of concrete damage were expected. Thus, the reduction in friction would likely generate larger estimated deflections at reduced IS levels than explicit modeling of concrete damage and provide a conservative response.

Thus, a simulation model of the reduced-deflection TCB system tested in test no. RDTCB-2 was simulated using a reduced barrier-to-ground friction coefficient of 0.24. The results from this model estimated a dynamic lateral barrier deflection of 41.1 in. (1,044 mm).

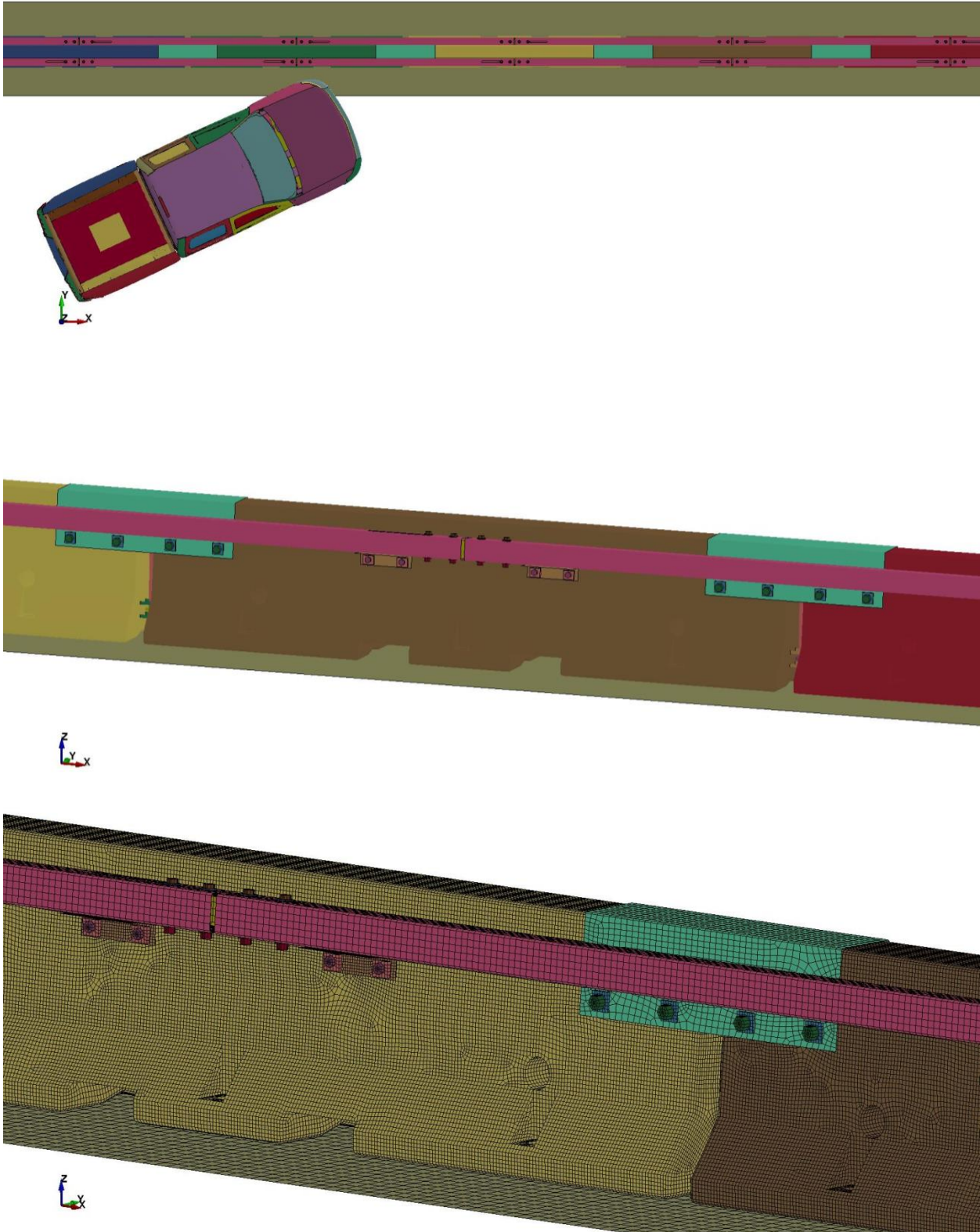


Figure 155. Simulation Model of System, Test No. RDTCB-2

This value correlated very well with the 39.5 in. (1,003 mm) permanent set deflection and 40.7 in. (1,034 mm) dynamic lateral barrier deflection from test no. RDTCB-2.

Two simulation models were then run to bracket the expected deflection of the low-deflection TCB system under the 85<sup>th</sup> percentile impact condition by simulating the barrier at normal and reduced friction values. First, a model of the system evaluated in test no. RDTCB-2 was simulated with an impact speed of 51.2 mph (82.4 km/h), an angle of 25 degrees, and a barrier-to-ground friction coefficient of 0.24. This model would serve as the upper bound of the expected lateral barrier deflection for an 85<sup>th</sup> percentile IS impact. The results from the simulation found a peak dynamic lateral barrier deflection of 23.6 in. (599 mm).

Next, a model of the system evaluated in test no. RDTCB-2 was simulated with an impact speed of 51.2 mph (82.4 km/h), an angle of 25 degrees, and a barrier-to-ground friction coefficient of 0.40. This model used the appropriate barrier-to-ground friction coefficient determined for the TCB segments and would represent the lower bound of estimated lateral barrier deflection for a barrier system where no concrete damage occurred. The results from the simulation found a peak dynamic lateral barrier deflection of 18.2 in. (462 mm).

Based on these results, the computer simulations indicated that dynamic deflections for the low-deflection TCB system would range between 18.2 in. (462 mm) and 23.6 in. (599 mm) at the 85<sup>th</sup> percentile impact condition. In order to be conservative, it is recommended that installations in non-critical locations use an estimated dynamic deflection value of 24 in. (610 mm) until further full-scale crash testing at reduced IS values or in-service evaluation of system damage for lower-severity impacts indicate that lower deflection estimates are more appropriate. This deflection value would correspond to a working width of 46.5 in. (1181 mm). For critical installations adjacent to drop-off or bridge deck edges, the full-scale crash-tested system deflection should be applied.

## **16 SUMMARY, CONCLUSIONS, AND RECOMMENDATIONS**

The research effort described herein detailed the design, analysis, and testing of a new, low-deflection TCB system that was designed to be retrofitted to existing F-shape TCB designs and did not require anchoring to the roadway surface. The effort began with a review of existing low-deflection TCB systems and determination of the design criteria for the new design. The researchers developed a variety of design concepts centered on four main deflection-limiting mechanisms: (1) increased barrier mass; (2) increased barrier-to-ground friction; (3) reduction of the joint gap between adjacent barrier segments; and (4) development of composite action across the TCB joint.

In order to evaluate these deflection-limiting mechanisms, a parametric study was conducted using LS-DYNA computer simulation to gauge their potential. The simulation effort began with development of a baseline model based on previous MASH full-scale crash testing of the free-standing F-shape TCB system that was to be used in the design. Following development of the baseline model, a series of models of the deflection-limiting mechanisms were simulated and analyzed. The results of the parametric study found that all of the mechanisms were effective at limiting barrier deflections. However, input from the project sponsor and further review of the parametric study results led to a decision to focus on the composite action mechanism for further development.

Two additional research efforts were conducted in parallel with the parametric study. First, a series of tests were conducted on TCB segments sliding on a concrete tarmac to further investigate the effects of friction on barrier deflection. The testing measured the barrier-to-ground friction for the standard TCB segment as well as two modified TCB segments with 50- and 70-durometer neoprene bearing pads mounted on their bases. The results from the testing found a kinetic friction coefficient for the standard TCB segment of 0.44. This value correlated

well with previous research and the simulation models. Testing of the TCB segments with the neoprene bearing pads found that the pads increased the friction significantly. The 70-durometer neoprene developed a kinetic friction coefficient of 0.62, while the 50-durometer neoprene developed a kinetic friction coefficient of 0.76. These results suggested that increased barrier-to-ground friction was attainable.

Investigation of concrete material modeling in LS-DYNA was also conducted to a limited extent as part of the research effort as it related to the modeling of the TCB segments and potential barrier damage. The simulation effort focused on MAT\_159\_CSCM in LS-DYNA. Simulation models of concrete cylinders and simple reinforced concrete beams were used to determine best practices and inputs for use with the material model. However, it was noted that the material model performance was sensitive to the model inputs, mesh size, and the hourglass controls used. Thus, further research with the model was recommended to build confidence in its performance and extend its use.

The research effort continued with development of an initial low-deflection TCB system design and evaluation of that design through full-scale crash testing. The initial system design consisted of a cap plate bolted across the TCB joint and continuous tubes running along the sides of the barriers. It was anticipated that the combination of the steel cap and tubes would be effective at limiting barrier deflection through composite action, and that the continuous tubes would provide for increased vehicle stability by presenting a more vertical face to the impacting vehicle. Full-scale crash test no. RDTCB-1 was conducted on the initial low-deflection TCB design, with the back of the TCB system offset 24 in. (610 mm) from the edge of a simulated bridge deck. Test no. RDTCB-1 consisted of a 4,998-lb (2,267-kg) pickup truck impacting the low-deflection TCB system at a speed of 63.6 mph (102.4 km/h) and at an angle of 24.9 degrees. The impacting vehicle was safely and smoothly redirected in the test and all of the barrier

segments were safely retained on the edge of the bridge deck. The peak dynamic lateral deflection of the barrier system was 43.0 in. (1,092 mm), which represented a 46 percent reduction in deflection as compared to the free-standing F-shape TCB MASH crash testing.

Following the crash test of the initial low-deflection TCB system, design modifications were proposed and investigated to further reduce dynamic system deflections. The proposed design modifications included: (1) increased barrier-to-ground friction, (2) increased tube thickness, (3) increased cap thickness, (4) reduced joint gap tolerance, and (5) additional attachment points for the tubes to the TCB segments. An LS-DYNA model of the low-deflection TCB system in test no. RDTCB-1 was created and validated, and this model was used to evaluate the proposed design modifications. The simulation results and input from the sponsor led to the selection of additional attachment points between the tubes and the TCB to further stiffen the barrier system. Test no. RDTCB-2 was conducted to evaluate the revised barrier system.

Full-scale crash test no. RDTCB-2 was conducted on the revised low-deflection TCB design with the back of the TCB system offset 24 in. (610 mm) from the edge of a simulated bridge deck. Test no. RDTCB-2 consisted of a 4,978-lb (2,258-kg) pickup truck impacting the low-deflection TCB system at a speed of 64.8 mph (104.3 km/h) and at an angle of 25.4 degrees. The impacting vehicle was safely and smoothly redirected in the test and all of the barrier segments were safely retained on the edge of the bridge deck. The peak dynamic lateral deflection of the barrier system was 40.7 in. (1,034 mm), which represented a 49 percent reduction in deflection as compared to the free-standing F-shape TCB MASH crash testing.

Review of the results of test no. RDTCB-2 noted that the additional steel tube attachments were successful at constraining the steel tubes to the sides of the TCB segments and further reducing dynamic lateral system deflections, but the reduction in deflection was not as large as those predicted during computer simulations. The higher-than-expected deflections were

attributed to a combination of damage and fracture observed in the concrete barrier segments in the test and an increased impact severity level in the test as compared to the LS-DYNA simulation. The barrier damage observed in the full-scale test suggested that the low-deflection TCB design was limited by the TCB segment capacity, and that further redesign of the retrofit deflection-reducing system would have negligible benefit with additional deflection-limiting mechanisms or barrier reinforcement changes.

The final task undertaken in this research was the evaluation of the displacement of the low-deflection TCB system designed in the study under less severe impacts. Previous research at MwRSF had suggested that it was feasible to use deflection limits for TCB systems in non-critical areas based on the estimated deflection of the TCB system when impacted at the 85<sup>th</sup> percentile IS value, as determined from accident data. A similar analysis was performed on the barrier system developed herein, which found that the dynamic deflection of the low-deflection TCB system at the 85<sup>th</sup> percentile IS was in the range between 18.2 in. (462 mm) and 23.6 in. (599 mm). It was conservatively recommended that installation in non-critical locations utilize an estimated dynamic deflection of 24 in. (610 mm) until further data regarding lower severity impacts was collected. This deflection value would correspond to a working with of 46.5 in. (1181 mm). For critical installations adjacent to drop-off or bridge deck edges, the full-scale crash-tested system deflection was recommended.

This research to develop a low-deflection TCB system that did not anchor to the roadway surface led to the design of a retrofit system capable of reducing deflections almost 50 percent under the most severe impacts. It was believed that these deflections could have been further reduced if additional reinforcement were added to the F-shape TCB to limit or prevent the concrete damage observed during test no. RDTCB-2. Comparison of the computer simulation models and the full-scale test data suggested that increasing the barrier reinforcement to prevent

concrete damage would conservatively restrict system deflections to less than 36 in. (914 mm) and may produce barrier deflections near 30 in. (762 mm). Additionally, it was believed that the TCB system deflections could have been further reduced if the design constraints in this study were relaxed to allow more modifications to the standard free-standing barrier. It was believed that the F-shape barrier used in this study was not optimized in terms of barrier geometry, reinforcement, and connection design, and that a new, optimized TCB segment design could potentially achieve similar or reduced deflections to those achieved in this research without the need for additional retrofit hardware.

### **16.1 Recommendations**

As noted previously, the researchers concluded that the low-deflection TCB design evaluated in this study exceeded the flexural capacity of the TCB section which limited its effectiveness in reducing barrier deflections. Thus, it would be recommended that users wishing to implement the design consider the use of additional barrier-reinforcing steel in order to limit barrier damage and further reduce system deflections. However, additional research would be needed to quantify the exact nature of the additional reinforcement and the actual dynamic system deflections with the increased-capacity TCB segments.

The research detailed herein focused on the design and evaluation of the length-of-need of a new, low-deflection TCB system. However, as with any barrier system, additional considerations must be taken into account when dealing with the barrier system outside the length-of-need, such as transitions to other barrier systems and end termination. The design of end termination and transitions for the new barrier system were outside the scope of this study and would require further research to design and evaluate. Similarly, the system detailed herein was designed for use in TCB segments placed in a straight line or large-radius curves where the

existing design tolerances can accommodate the small angles between adjacent barrier segments. Design of the system for use on smaller curve radii would require additional research.

Recommendations were made regarding the displacement of the low-deflection TCB system designed in the study under less severe impacts. These recommendations were based on the barrier system evaluated in test no. RDTCB-2. However, the first iteration of the reduced-deflection TCB system evaluated in test no. RDTCB-1 also met the MASH safety requirements. Thus, either system would be acceptable for installations requiring reduced TCB deflection. However, the estimated deflections for less severe impacts would only apply to the barrier design in test no. RDTCB-2.

Finally, there may be a desire to adapt the low-deflection TCB system developed in this research to other TCB designs. It is believed that this design could be adapted to other systems with some additional considerations. First, the reinforcement of the alternative TCB design would need to provide equal or greater capacity to the barrier segment used in this research. Second, there is potential for different TCB segment connections to be used with the design as the design of the steel cap and tubes in the low-deflection hardware provides the majority of the load transfer across the TCB joints. However, barriers with different joint constraints and joint gap tolerances may result in slightly different performance, and differences in joint design should be considered. Third, barrier geometry may affect the performance of the system. Barrier height should be maintained at the 32 in. (813 mm) height of the barrier evaluated herein in order to maintain the position of the continuous steel tubes in the as-tested design. In addition, different barrier shapes, such as single slope or New Jersey shape TCBs may affect the performance of the system, but the horizontal tubes used in the design would be expected to provide a more vertical profile regardless of the barrier shape and would tend to increase vehicle stability. Finally, variations in specific TCB designs, like those noted here, may affect the extent of the reduced

lateral deflections when using the low-deflection retrofit design. Thus, the reduction in barrier deflection may vary from those observed in this study and should be further investigated on an individual basis.

Table 18. Summary of Safety Performance Evaluation Results

Evaluation Factors	Evaluation Criteria	Test No. RDTCB-1	Test No. RDTCB-2	
Structural Adequacy	A. Test article should contain and redirect the vehicle or bring the vehicle to a controlled stop; the vehicle should not penetrate, underide, or override the installation, although controlled lateral deflection of the test article is acceptable.	S	S	
Occupant Risk	D. Detached elements, fragments or other debris from the test article should not penetrate or show potential for penetrating the occupant compartment, or present an undue hazard to other traffic, pedestrians, or personnel in a work zone. Deformations of, or intrusions into, the occupant compartment should not exceed limits set forth in Section 5.3 and Appendix E of MASH.	S	S	
	F. The vehicle should remain upright during and after collision. The maximum roll and pitch angles are not to exceed 75 degrees.	S	S	
	H. Occupant Impact Velocity (OIV) (see Appendix A, Section A5.3 of MASH for calculation procedure) should satisfy the following limits:	S	S	
	Occupant Impact Velocity Limits			
	Component			Preferred
Longitudinal and Lateral	30 ft/s (9.1 m/s)	40 ft/s (12.2 m/s)		
I. The Occupant Ridedown Acceleration (ORA) (see Appendix A, Section A5.3 of MASH for calculation procedure) should satisfy the following limits:	S	S		
Occupant Ridedown Acceleration Limits				
Component			Preferred	Maximum
Longitudinal and Lateral	15.0 g's	20.49 g's		

S – Satisfactory      U – Unsatisfactory      NA – Not Applicable

## 17 REFERENCES

1. Faller, R. K., Rohde, J. R., Rosson, B. T., Smith, R. P., and Addink, K. H., *Development of a TL-3 F-Shape Temporary Concrete Median Barrier*, Final Report to the Iowa Department of Transportation, Project SPR 3(017), Transportation Research Report No. TRP-03-64-96, Midwest Roadside Safety Facility, University of Nebraska Lincoln, December 1996.
2. Polivka, K. A., Faller, R. K., Sicking, D. L., Rohde, J. R., Bielenberg, B. W., Reid, J. D., and Coon, B. A., *Performance Evaluation of the Free-Standing Temporary Barrier – Update to NCHRP 350 Test No. 3-11 (2214TB-1)*, Final Report to the National Cooperative Highway Research Program (NCHRP), Transportation Research Board, Transportation Research Report No. TRP-03-173-06, Midwest Roadside Safety Facility, University of Nebraska Lincoln, October 11, 2006.
3. Polivka, K. A., Faller, R. K., Sicking, D. L., Rohde, J. R., Bielenberg, B. W., Reid, J. D., and Coon, B. A., *Performance Evaluation of the Free-Standing Temporary Barrier – Update to NCHRP 350 Test No. 3-11 with 28" C.G. Height (2214TB-2)*, Final Report to the National Cooperative Highway Research Program (NCHRP), Transportation Research Board, Transportation Research Report No. TRP-03-174-06, Midwest Roadside Safety Facility, University of Nebraska Lincoln, October 12, 2006.
4. *Manual for Assessing Safety Hardware (MASH)*, American Association of State Highway and Transportation Officials (AASHTO), Washington, D.C., 2009.
5. Ross, H. E., Sicking, D. L., Zimmer, R. A., and Michie, J. D., *Recommended Procedures for the Safety Performance Evaluation of Highway Features*, National Cooperative Highway Research Program (NCHRP) Report 350, Transportation Research Board, Washington, D.C., 1993.
6. Eller, C. M., *Determination of Impact Forces from Vehicle-to-Barrier Crashes*, University of Nebraska Honors Thesis, Midwest Roadside Safety Facility, University of Nebraska Lincoln, April 23, 2007.
7. Marzougui, D., Bahouth, G., Eskandarian, A., Meczkowski, L., and Taylor, H., *Evaluation Of Portable Concrete Barriers Using Finite Element Simulation*, Paper No. 00-0501, Transportation Research Record 1720, pages 1-6, Washington, D.C., 2000.
8. Stolle, C. J., Polivka, K. A., Faller, R. K., Sicking, D. L., Bielenberg, R. W., Reid, J. D., Rohde, J. R., Allison, E. M., Terpsma, R. J., *Evaluation of Box-Beam Stiffening of Unanchored Temporary Concrete Barriers*, Final Report to the New York State Department of Transportation, Transportation Research Report No. TRP-03-202-08, Midwest Roadside Safety Facility, University of Nebraska-Lincoln, March 14, 2008.
9. MacDonald, D. J. and Kirk, A. R., *Precast Concrete Barrier Crash Testing*, Final Report SPR 330, Oregon Department of Transportation Research Group, December 2001.

10. Bligh, R. P., Sheikh, N. M., Menges, W. L., and Haug, R. R., *Development of Low-Deflection Precast Concrete Barrier*, Report 0-4162-3, Texas Transportation Institute, College Station, TX, January 2005.
11. Bligh, R. P., Sheikh, N. M., Menges, W. L., and Haug, R. R., *Portable Concrete Traffic Barrier for Maintenance Operations*. Report 0-4692-1, Texas Transportation Institute, College Station, TX, May 2005.
12. Hallquist, J. O. *LS-DYNA Keyword User's Manual*, Livermore Software Technology Corporation, Livermore, California, 2007.
13. Bielenberg, B. W., Faller, R. K., Rohde, J. R., Reid, J. D., Sicking, D. L., and Holloway, J. C., *Development of Tie-Down and Transition Systems for Temporary Concrete Barrier on Asphalt Road Surfaces*, Final Report to the Midwest States Regional Pooled Fund Program, Transportation Research Report No. TRP-03-180-06, Midwest Roadside Safety Facility, University of Nebraska Lincoln, February 23, 2007.
14. Society of Automotive Engineers (SAE), *Instrumentation for Impact Test – Part 1 – Electronic Instrumentation*, SAE J211/1 MAR95, New York City, NY, July, 2007.
15. Murray, Y. D., *Users Manual for LS-DYNA Concrete Material Model 159*, Report No. FHWA-HRT-05-062, Federal Highway Administration, 2007.
16. Murray, Y. D., *Evaluation of LS-DYNA Concrete Material Model 159*, Report No. FHWA-HRT-05-063, Federal Highway Administration, 2007.
17. Abu-Odeh, A., *Application of New Concrete Model to Roadside Safety Barriers*, 9th International LS-DYNA Users Conference, pg. 1-8.
18. Abu-Odeh, A., *Modeling and Simulation of Bogie Impacts on Concrete Bridge Rails using LS-DYNA*, 10th International LS-DYNA Users Conference, pg. 9-20.
19. Bielenberg, B. W., Faller, R. K., Reid, J. D., Holloway, J. C., Rohde, J. R., and Sicking, D. L., *Impact Analysis of Three Reinforced Concrete Beam Specimens*, Midwest Roadside Safety Facility, University of Nebraska, Transportation Research Report No. TRP-03-130-03, submitted to APTEK, Inc., March 2003.
20. Buth, C. E., Hirsch, T. J., and McDevitt, C. F., *Performance Level 2 Bridge Railings*, Transportation Research Record No. 1258, Transportation Research Board, National Research Council, Washington, D.C., 1990.
21. *Guide Specifications for Bridge Railings*, American Association of State Highway and Transportation Officials (AASHTO), Washington, D.C., 1989
22. Bronstad, M. E., Calcote, L. R., and Kimball Jr, C. E., *Concrete Median Barrier Research-Vol.2 Research Report*, Report No. FHWA-RD-77-4, Submitted to the Office of Research and Development, Federal Highway Administration, Performed by Southwest Research Institute, San Antonio, TX, March 1976.

23. Buth, C. E., Campise, W. L., Griffin III, L. I., Love, M. L., and Sicking, D. L., *Performance Limits of Longitudinal Barrier Systems-Volume I: Summary Report*, FHWA/RD-86/153, Final Report to the Federal Highway Administration, Office of Safety and Traffic Operations R&D, Performed by Texas Transportation Institute, Texas A&M University, College Station, TX, May 1986.
24. Fortuniewicz, J. S., Bryden, J. E., and Phillips, R. G., *Crash Tests of Portable Concrete Median Barrier for Maintenance Zones*, Report No. FHWA/NY/RR-82/102, Final Report to the Office of Research, Development, and Technology, Federal Highway Administration, Performed by the Engineering Research and Development Bureau, New York State Department of Transportation, December 1982.
25. Hinch, J., Yang, T. L., and Owings, R., *Guidance Systems for Vehicle Testing*, ENSCO, Inc., Springfield, Virginia, 1986.
26. *Center of Gravity Test Code – SAE J874 March 1981*, SAE Handbook Vol. 4, Society of Automotive Engineers, Inc., Warrendale, Pennsylvania, 1986.
27. Stolle, C. J., Zhu, L., Lechtenberg, K. A., Bielenberg, R. W., Faller, R. K., Sicking, D. L., Reid, J. D., and Rohde, J. R., *Performance Evaluation of Type II and Type IIA Box-Beam End Terminals – Volume I: Research Results and Discussion*, Final Report to the New York State Department of Transportation, Transportation Research Report No. TRP-03-203-10, Project No.: C-06-16 Phase I, C-06-16 Phase II, SPR-3(017) Supplement #56, TPF-5(193), Supplement #9, Midwest Roadside Safety Facility, University of Nebraska-Lincoln, January 20, 2010.
28. Bullard, L. D., Bligh, R. P., Menges, W. L., and Haug, R. R., *NCHRP No. 157: Volume I: Evaluation of Existing Roadside Hardware Using Updated Criteria – Technical Report*, Final Report, for NCHRP Project 22-14(03), Texas Transportation Institute, College Station, TX, March, 2010.
29. *Vehicle Damage Scale for Traffic Investigators*, Second Edition, Technical Bulletin No. 1, Traffic Accident Data (TAD) Project, National Safety Council, Chicago, Illinois, 1971.
30. *Collision Deformation Classification – Recommended Practice J224 March 1980*, Handbook Volume 4, Society of Automotive Engineers (SAE), Warrendale, Pennsylvania, 1985.
31. Mongiardini, M., Ray, M. H., Plaxico, C. A., and Anghileri, M., *Procedures for Verification and Validation of Computer Simulations Used for Roadside Safety Applications*, Final Report to the National Cooperative Highway Research Program (NCHRP) Report No. W179, Project No. 22-24, Worcester Polytechnic Institute, March 2010.

32. Polivka, K. A., Sicking, D. L., and Reid, J. D., *Deflections Limits for Temporary Concrete Barriers*, Revised Final Report to the Midwest State's Regional Pooled Fund Program, Transportation Research Report No. TRP-03-113-02, Project No. SPR-3(017)-Year 9, Midwest Roadside Safety Facility, University of Nebraska Lincoln, June 18, 2003.
33. Bronstad, M. E. and Michie, J. D., *Multiple-Service-Level Highway Bridge Railing Selection Procedures*, National Cooperative Highway Research Program (NCHRP) Report No. 239, Transportation Research Board, Washington, D.C., November 1981.
34. Sicking, D. L., *Guidelines for Positive Barrier Use in Construction Zones*, Transportation Research Record No. 1035, Transportation Research Board, National Research Council, Washington, D.C., 1985.
35. Mak, K. K. and Sicking, D. L., *Evaluation of Performance Level Selection Criteria for Bridge Railings*, Final Report, NCHRP Project 22-8, Texas Transportation Institute, Texas A&M University, September 1993.
36. Mak, K. M., Sicking, D. L., Benicio, F. D., and Coon, B. A., *NCHRP Report 665 – Identification of Vehicular Impact Conditions Associated with Serious Run-Off-Road Crashes*, Final Report to the National Cooperative Highway Research Program (NCHRP) Report No. 665, Project No. 17-22, University of Nebraska, 2010.

## **18 APPENDICES**

## **Appendix A. Component Test Material Specifications**

Figure No.	Item No.	QTY.	Description in. [mm]	Material Specification	Reference
Figure A-1	a2	1	150" x 22.5" x 3.8" [3810 x 572 x 10] Neoprene Mat	50 Durometer AASHTO Grade 3 Bearing Pad	Z5310-0375-22.5IN-150IN-50D
Figure A-2	a3	1	150" x 22.5" x 3.8" [3810 x 572 x 10] Neoprene Mat	70 Durometer AASHTO Grade 3 Bearing Pad	Z5410-0375-22.5IN-150IN-70D
Figure A-3 A-5	-	1	Polyurethane Adhesive	ChemRex CX-941	

Figure A-1. Summary of Material Certifications, Test Nos. TCBF-1 through TCBF-6

# Certificate of Compliance

*We hereby certify that all material, physical and chemical, and/or work performed, with all subsequent processes, are in accordance with all specifications, drawings and all other purchase order requirements. Test and/or inspection reports indicating conformance are on file with Abbott Rubber Company Inc. or our suppliers for your examination.  
 We also certify that the material supplied is in compliance with RoHS Directive 2002/95/EC*

MOTION INDUSTRIES	NEO2-00047429	1 EACH
Company Name	Purchase Order Number	Quantity
PO BOX 1655	3090686	139 LBS
Address	Invoice Number	Weight
BIRMINGHAM, AL 35201	Z5310-0375-22.5IN-150IN-50D	2 BOXES
City, State and Zip Code	Part Number	Number of Packages

3/8 TH X 22-1/2 IN WIDE X 150 IN LONG  
 50D NEOPRENE RUBBER STRIP



*John McEwen* 06/15/2012  
 Quality Control Manager Date

**Abbott Rubber Company Inc.**  
 1700 Nicholas Blvd  
 Elk Grove Village, IL 60007

Additional Comments

Figure A-2. 50-Durometer Rubber Bearing Pad, Test Nos. TCBF-5 and TCBF-6

# Certificate of Compliance

*We hereby certify that all material, physical and chemical, and/or work performed, with all subsequent processes, are in accordance with all specifications, drawings and all other purchase order requirements. Test and/or inspection reports indicating conformance are on file with Abbott Rubber Company Inc. or our suppliers for your examination.  
 We also certify that the material supplied is in compliance with RoHS Directive 2002/95/EC*

MOTION INDUSTRIES	NEO2-00047429	1 EACH
Company Name	Purchase Order Number	Quantity
PO BOX 1655	3090686	139 LBS
Address	Invoice Number	Weight
BIRMINGHAM, AL 35201	Z5410-0375-22.5IN-150IN-70D	2 BOXES
City, State and Zip Code	Part Number	Number of Packages

3/8 TH X 22-1/2 IN WIDE X 150 IN LONG  
 70D BUNA RUBBER STRIP



*John McEwen* 06/15/2012  
 Quality Control Manager Date

**Abbott Rubber Company Inc.**  
 1700 Nicholas Blvd  
 Elk Grove Village, IL 60007

Additional Comments

Figure A-3. 70-Durometer Rubber Bearing Pad, Test No. TCBF-4



## CHEMREX® CX-941

Trowel-grade polyurethane adhesive  
for wood flooring

PRODUCT DATA

7 07200

**Thermal  
Protection**

### Description

CHEMREX® CX-941 is a one-component, polyurethane-based trowel-grade, waterproof structural adhesive with vapor reducing characteristics. Its elastomeric properties enable it to move with wood as it expands and contracts. The patented formula is VOC compliant and it contains no solvents or water, so it will not cause wood to expand. CHEMREX® CX-941 provides excellent initial green strength and outstanding bond strength. It is formulated for indoor and outdoor applications.

### Yield

See page 3 for chart.

### Packaging

2 gallon (7.6 L) pails, 80 pails per pallet

5 gallon (18.95 L) pails, 36 pails per pallet

### Color

Light brown

### Shelf Life

1 year when properly stored

### Storage

Store at 75° F (24° C) and 50% relative humidity. Protect unopened containers from heat and direct sunshine. In cool weather, store containers at room temperature for at least 24 hours before using.

### Features

- Patented formula
- VOC compliant
- No chlorinated solvents, nonflammable
- No water
- Suitable for indoor or outdoor applications
- Eligible for Lead's Points, South Coast Bay compliant
- Non-ozone depleting solvents

### Where to Use

#### APPLICATION

- Recycled rubber tiles
- Laminated hardwood flooring
- Solid hardwood planks
- Parquet flooring
- Rubber tiles
- Cork flooring and underlayment
- Stair treads
- Stair nosing
- Transitions
- Code-approved subfloor application
- Underlayment grade OSB

#### LOCATION

- Interior and exterior

#### SUBSTRATE

- Concrete
- Plywood
- Particle or chip board or scarify
- Cement and gypsum underlayment
- Radiant heat flooring
- Asphalt

### Benefits

Contains no solvents or water, wood will not expand

Extremely low odor

Improves worker safety

Freeze/thaw stable

Single adhesive required

Suitable for use in all 50 states

Environmentally friendly

### How to Apply

#### Surface Preparation

1. Ensure that floors are structurally sound and fully cured a minimum of 28 days. Test floor for vapor drive in accordance with anhydrous calcium chloride test. Vapor drive should not exceed the industry standard of less than 3.0 lbs per 1,000 ft<sup>2</sup> in 24 hours.
2. When test results are greater than 3.0 but less than 12 lbs per 1,000 ft<sup>2</sup> in 24 hours, refer to the product data sheet for CHEMREX® Concrete Floor Primer (Form No. 1C19775).
3. Repair concrete and install joint sealants and fillers as necessary. Use patching materials as appropriate.
4. Low spots must be filled with CHEMREX® Self-Leveling Underlayment or LevelPrep™.
5. Mechanical surface profiling is the preferred floor preparation method. It is the only acceptable preparation method where warranties are issued. Acid etching is not recommended. Shotblast the floor to medium-grit sandpaper texture, to remove curing and parting compounds and other surface hardeners and floor coatings.
6. Clean floors of oil, grease, and other bond-inhibiting materials not removed by shotblasting or other mechanical means with a commercial degreaser.



www.DegussaBuildingSystems.com

Figure A-4. Polyurethane Adhesive Specifications, Test Nos. TCBF-4 through TCBF-6

CHEMREX® PRODUCT DATA  
CHEMREX® CX-941

**Technical Data**

**Composition**

CHEMREX® CX-941 is a one-component, polyurethane-based, waterproof structural adhesive.

**Compliances**

- ASTM E 84-95B; NFPN, class A and UBC, Class 1
- USDA compliant for use in meat and poultry areas

**Typical Properties**

PROPERTY	VALUE
<b>Polymer type</b>	Polyurethane
<b>Viscosity</b>	Creamy, trowelable
<b>Working time, min</b>	45 – 60
<b>Freeze-thaw stability</b>	Unlimited cycles
<b>Service temp., ° F (° C)</b>	-40 – 150 (-40 – 66)
<b>Slab temp., ° F (° C)</b>	50 – 100 (10 – 38)

**Test Data**

PROPERTY	RESULTS	TEST METHODS
<b>Solids, %</b>	95 ±2	ASTM D 1259
<b>Specific gravity</b>	1.25±0.10	ASTM D 1475
<b>Tensile strength, psi</b>		
Hardwood/concrete	300	ASTM D 412
Plywood/concrete	120	ASTM D 412
<b>Elongation, %</b>	50 ±5	ASTM D 412
<b>Flame spread*</b>		
1/8 x 1/8" trowel-applied thickness	5 flame spread	15 smoke density
1/4 x 1/4" trowel-applied thickness	10 flame spread	30 smoke density
<b>Perm Ratings and Water Vapor Transmission (WVT)</b>		
	<b>WVT (per 24 hours)</b>	<b>US Perms</b>
1/4 x 1/4" trowel at 35 ft/gallon	2.67 lbs/1,000 ft²	1.88
1/8 x 1/8" trowel at 90 ft/gallon	3.05 lbs/1,000 ft²	2.15

\* Meets flame spread requirement at both NFPA, Class A, and UBC, Class 1.

**Application**

1. Ensure that starter rows are firmly in place by wedging or face nailing. Once initial rows are secure, use CHEMREX® CX-941 in a wet-lay or walk-on-work method of installation.
2. Wet-lay method: Apply adhesive to substrate with an appropriate trowel. Immediately place flooring into the wet adhesive. No flashing required.  
NOTE: Do not apply more adhesive than can be covered in 30 minutes or the adhesive transfer could be jeopardized.
3. A 100 lb roller must be used in the wet-lay method during all installations. It must be rolled again within 30 minutes. Uneven flooring should be tacked, weighted or rolled to ensure good contact between the flooring and the substrate.
4. Clean up tip: Before troweling CHEMREX® CX-941, cover the unused portions of the trowel with duct tape. After troweling, tear off the tape before the material cures.

**Special Installation Requirements**

- NWFA INSTALLATION GUIDELINES SEC. III, DEC. 99
1. Radiant Heat Installations
    - Check for subfloor moisture
    - The heating system must be turned off 24 hours before installation to prevent accelerated curing
    - Maximum surface temperature is 85° F (29° C)
    - Expect some heating season shrinkage

2. Sound control products

- Cork underlayment use 1/8 by 1/8" (3 by 3 mm) v-notched trowel
- 3. Stair treads and nosings
  - Lightly water mist the CHEMREX® CX-941 to accelerate cure
  - Depending on manufacturer, treads and nosings may require solvent wipe to remove residual mold release

**Glue Down of 3/4" Subfloor Underlayment**

- NWFA INSTALLATION GUIDELINES SEC. II, CH. 3-4, DEC. 99
1. Properly moisture test according to NWFA standards
  2. Add moisture barrier before applying underlayment
  3. 3/4" (19.05 mm) CDX grade plywood underlayment
  4. 2 by 8" (51 by 203 mm) or 4 by 4" (102 by 102 mm) sections scored on the back 3/8" (9.5 mm) deep on a 12 by 12" (305 by 305 mm) grid laid in a staggered joint pattern in CHEMREX® CX-941 using 1/4 by 1/4" (6 by 6 mm) notched trowel
  5. 1/8 - 1/4" (3 by 6 mm) spacing between sheets
  6. 3/4" (19 mm) expansion space at all vertical obstructions

**Curing**

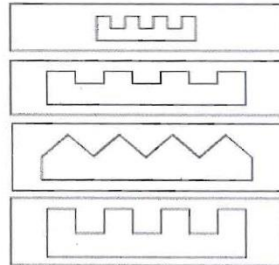
Cure time is dependent on temperature and humidity. Times are based on 75° F (57° C) and 50% relative humidity.  
Firm set: 1 – 2 hours  
Light foot traffic: 8 – 10 hours  
Normal traffic: 24 hours  
Higher temperatures and humidity shorten the cure rate, while lower temperatures and humidity lengthen the time.

**Clean Up**

Clean all tools and excess CHEMREX® CX-941 immediately after use with mineral spirits. Use proper precautions when handling solvents. Cured adhesive can be removed by cutting with a mechanical tool.  
NOTE: Do not clean up with water. It will accelerate the cure of the adhesive.

Figure A-5. Polyurethane Adhesive Specifications, Test Nos. TCBF-4 through TCBF-6

CHEMREX® PRODUCT DATA  
CHEMREX® CX-941



TROWEL SIZE (INCHES)	YIELD (FT <sup>2</sup> /GALLON)	TYPICAL USES
1/8 by 1/8 square notch	80 – 90 ft <sup>2</sup>	Smooth surface tiles, finger block parquet or cork
1/4 by 1/8 square notch	40 – 50 ft <sup>2</sup>	Rough surface tiles, laminated planks greater than 1/2" and 3/4" parquet
3/16 by 5/32 V-notch	60 – 70 ft <sup>2</sup>	Semi-smooth tiles, 3- and 5-ply laminated planks and 3/4" parquet
1/4 by 1/4 square notch	35 – 40 ft <sup>2</sup>	Plywood to concrete, solid planks, flat milled solids and shorts
1/16 V-notch	75 ft <sup>2</sup>	Recycled rubber interior
1/8 V-notch	60 ft <sup>2</sup>	Recycled rubber exterior

The trowel sizes suggested will maximize adhesive coverage. The coverage required for laminated plank is 80% for solid woods, 95%. Check periodically during installation. If subflooring is uneven, use a leveling or patching material beforehand or use a large notched trowel to provide the appropriate coverage. If insufficient transfer occurs, additional CHEMREX® CX-941 will need to be applied.

**For Best Performance**

- Wear gloves during application; CHEMREX® CX-941 is difficult to remove from skin and clothing. If adhesive gets on skin, immediately wipe it off with a dry cloth.
- Do not apply on frozen surfaces or standing water.
- Avoid contact with water or alcohol before use and before complete cure.
- Do not use in areas subject to hydrostatic head pressure.
- Do not use on wet, contaminated, or friable substrates.
- The maximum acceptable floor variation is 3/16" (4.76 mm) in 10 feet (3 m) or 1/8" (3.75 mm) in 6 feet (1.8 m).
- Do not use as a leveling agent.
- Do not set flooring into an adhesive that has a dry skin.
- Make certain the most current versions of product data sheet and MSDS are being used; call Customer Service (1-800-433-9517) to verify the most current version.
- Proper application is the responsibility of the user. Field visits by Degussa personnel are for the purpose of making technical recommendations only and are not for supervising or providing quality control on the jobsite.

**Health and Safety**

CHEMREX® CX-941

**Caution**

CHEMREX® CX-941 contains methylene bisphenyl diisocyanate; Talc; Hydrotreated light petroleum distillate; Polymethylene polyphenol isocyanate; Silica and crystalline quartz.

**Risks**

May cause skin and eye irritation. May cause dermatitis and allergic responses. Potential skin and/or respiratory sensitizer. Inhalation of vapors may cause irritation and intoxication with headaches, dizziness and nausea. Ingestion may cause irritation. Reports have associated repeated or prolonged occupational overexposure to solvents with permanent brain, nervous system, liver and kidney damage. Contains crystalline silica. NTP and IARC recognize respirable crystalline silica as a human carcinogen. The exposure to crystalline silica during the normal use of this product will be little or none. INTENTIONAL MISUSE BY DELIBERATELY INHALING THE CONTENTS MAY BE HARMFUL OR FATAL.

**Precautions**

Avoid contact with skin, eyes and clothing. Wash thoroughly after handling. Avoid breathing vapors. Use only with adequate ventilation. Use impervious gloves, eye protection and if the TLV is exceeded or if used in a poorly ventilated area, use NIOSH/MSHA approved respiratory protection in accordance with applicable Federal, state and local regulations. DO NOT take internally. Keep container closed. Empty container may contain hazardous residues. All label warnings must be observed until container is commercially cleaned or reconditioned.

**First Aid**

In case of eye contact, flush thoroughly with water for at least 15 minutes. SEEK IMMEDIATE MEDICAL ATTENTION. In case of skin contact, wash affected areas with soap and water. If irritation persists, SEEK MEDICAL ATTENTION. Remove and wash contaminated clothing. If inhalation causes physical discomfort, remove to fresh air. If discomfort persists or any breathing difficulty occurs, or if swallowed, SEEK IMMEDIATE MEDICAL ATTENTION.

Refer to Material Safety Data Sheet (MSDS) for further information.

**VOC Content**

45 g/L or 0.38 lbs/gal less water and exempt solvents.

Figure A-6. Polyurethane Adhesive Specifications, Test Nos. TCBF-4 through TCBF-6

**Appendix B. Material Specifications, Test No. RDTCB-1**

Table B-1. Summary of Material Certifications, Test No. RDTCB-1

Figure	Item No.	QTY.	Description in. [mm]	Material Specifications	Reference
Figure B-1	a1	16	Portable Concrete Barrier	min f <sub>c</sub> =5000 psi [34.5 MPa]	5000 psi Mix 7156475101
Figure B-2	a2	192	1/2" [13] Dia., 72" [1829] Long Form Bar	A615 Grade 60	H# K120760
Figure B-2	a3	32	1/2" [13] Dia., 146" [3708] Long Longitudinal Bar	A615 Grade 60	H# K120760
Figure B-4	a4	48	5/8" [16] Dia., 146" [3708] Long Longitudinal Bar	A615 Grade 60	H# K122397
Figure B-3	a5	96	3/4" [19] Dia., 36" [914] Long Anchor Loop Bar	A615 Grade 60	H# M674348/49
Figure B-3	a6	32	3/4" [19] Dia., 101" [2565] Long Connection Loop Bar	A709 Grade 70 or A706 Grade 60	H# M674348/49
Figure B-3	a7	32	3/4" [19] Dia., 91" [2311] Long Connection Loop Bar	A709 Grade 70 or A706 Grade 60	H# M674348/49
Figure B-3	a8	32	3/4" [19] Dia., 102" [2591] Long Connection Loop Bar	A709 Grade 70 or A706 Grade 60	H# M674348/49
Figure B-5	a9	15	1 1/4" [32] Dia., 28" [711] Long Connector Pin	ASTM A36 Galvanized	R# B160600
Figure B-6	b1	22	5"x5"x3/16" [127 x 127 x 5], 12'-9 3/16" [3891] Long Splice Main Tube	A500 Grade B Galvanized after Welding	H# 411120
Figure B-7	b2	20	4 1/2"x4 1/2"x1/4" [114 x 114 x 6], 22" [559] Long Splice Insert	ASTM 572 Grade 50 Galvanized	H# 060157
Figure B-8	b3	11	42"x33" [1067 x 838] 10 Gage Mounting Bracket Plate	ASTM A1011 Grade 50 Galvanized after Welding	H# 530487
Figure B-9	b4	88	1" [25] Dia. Washer	F844 Galvanized	33188
Figure B-10 and B-11	b5	44	1" [25] Dia. UNC, 12 1/2" [318] Long Heavy Hex Bolt and Nut	Bolt ASTM A325/A449 Type 1 Galvanized, Nut ASTM A563 Galvanized	H# DL1210218902 / 36719
Figure B-12	b6	160	3/4" [19] Dia. Washer	F844 Galvanized	33186
Figure B-13 and B-14	b7	80	3/4" [19] Dia. UNC, 6 1/2" [165] Long, 2" [51] Threaded Hex Bolt and Nut	Bolt ASTM A325/A449/SAE Grade 5 Galvanized, Nut ASTM A563DH Grade 5 Galvanized	19736 / 36715

# WIESER CONCRETE PRODUCTS, INC.

W3716 U.S. HWY 10 • MAIDEN ROCK, WI 54750  
(715) 647-2311 800-325-8456 Fax (715) 647-5181  
E-mail: wieserpc@wieserconcrete.com Website: www.wieserconcrete.com

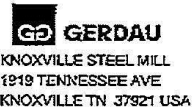
## 5000 psi MIX DESIGN

### WEIGHTS PER CUBIC YARD

Coarse Aggregate, 3/4"minus	(ASTM C 33/#67)	1527 pounds
Fine Aggregate; sand	(ASTM C 33)	1527 pounds
Cement	(ASTM C 150/Type III)	517 pounds
Fly Ash		192 pounds
Axim CATEXOL™ A.E. 260		7.0+/- ounces
Axim CATEXOL™ SUPERFLUX 2100pc		49 ounces
Water		237 pounds

*Material variations may require mixture adjustments to maintain strength, water-cement ratio, slump, air, and yield.*

Figure B-1. Concrete Barrier Mix Specifications



Chemical and Physical Test Report  
MADE IN UNITED STATES

*PO*  
*5/3/12*  
*BARRIER*  
*STEEL*

CUSTOMER: WIESER

PROJECT: MAIDEN ROCK BARRIER REL. 965

SHAPE + SIZE	GRADE	SPECIFICATION	SALES ORDER	CUST P.O. NUMBER
X19MM REBAR (# 6)	420 (60)	ASTM A615/A615M-09B THERMEX TREATED		
HEAT I.D.	C Mn P S Si Cu Ni Cr Mo V Nb Sn C Eqv			
K118257	.28 .67 .033 .059 .16 .33 .13 .17 .020 .005 .002 .003 .433			

Mechanical Test: Yield 85050 PSI, 586.4 MPA Tensile: 102680 PSI, 707.95 MPA %EL: 12.5/8in, 12.5/200MM Bend: OK Def HT: .045, 1.14MM Def Cap: .111, 2.82MM Def SP: .461, 11.71MM %WR 4.4L

Customer Requirements CASTING: STRAND CAST

SHAPE + SIZE	GRADE	SPECIFICATION	SALES ORDER	CUST P.O. NUMBER
X13MM REBAR (# 4)	420 (60)	ASTM A615/A615M-09B THERMEX TREATED		
HEAT I.D.	C Mn P S Si Cu Ni Cr Mo V Nb Sn C Eqv			
K120760	.28 .60 .009 .072 .18 .33 .22 .07 .029 .003 .002 .003 .405			

Mechanical Test: Yield 87960 PSI, 606.46 MPA Tensile: 105040 PSI, 724.23 MPA %EL: 12.5/8in, 12.5/200MM Bend: OK Def HT: .03, .76MM Def Gap: .116, 2.95MM Def SP: .332, 8.43MM %WR 3.7L

Customer Requirements CASTING: STRAND CAST

WIESER CONCRETE

This material, including the billets, was melted and manufactured in the United States of America

*Mhasakay*

Bhaswar Yalamanchili  
Quality Director  
Gerdau

THE ABOVE FIGURES ARE CERTIFIED CHEMICAL AND PHYSICAL TEST RECORDS AS CONTAINED IN THE PERMANENT RECORDS OF COMPANY.

*Jess Chaudhri*

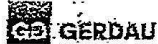
Metallurgical Services Manager  
KNOXVILLE STEEL MILL

Seller warrants that all material furnished shall comply with specifications subject to standard published manufacturing variations. NO OTHER WARRANTIES, EXPRESSED OR IMPLIED, ARE MADE BY THE SELLER, AND SPECIFICALLY EXCLUDED ARE WARRANTIES OF MERCHANTABILITY AND FITNESS FOR A PARTICULAR PURPOSE. In no event shall seller be liable for indirect, consequential or punitive damages arising out of or related to the materials furnished by seller. Any claim for damages for materials that do not conform to specifications must be made from buyer to seller immediately after delivery of same in order to allow the seller the opportunity to inspect the material in question.

7156475181  
00:13:00  
2012/02/08

Figure B-2. Reinforcement Bar Specifications

END Loops



ST PAUL STEEL MILL  
1678 RED ROCK ROAD  
ST PAUL, MN 55119 USA  
(651) 731-5800

Chemical and Physical Test Report  
MADE IN UNITED STATES

RJ  
6/4/12  
PO# 72732

M-110802

SHIP TO WIESER CONCRETE W3716 HWY 10 RED 715-647-2311 MAIDEN ROCK, WI 54750	INVOICE TO GERDAU SC 4224 W BOY SCOUT BLVD. ST-600 TAMPA, FL 33607	SHIP DATE 05/31/12  CUST. ACCOUNT NO 10000008
---	---	---

PRODUCED IN: ST PAUL

SHAPE + SIZE	GRADE	SPECIFICATION	SALES ORDER	CUST P.O. NUMBER
R34	A588M1-A	A6/A6M-10a A566/A588M-05	2035280-01	72732-01
HEAT ID. M674348	C Mn P S Si Cu Ni Cr Mo V Nb N Sn Al Ti Ca Zn Co			

Mechanical Test: Yield 63200 PSI, 435.75 MPA Tensile: 89200 PSI, 615.01 MPA %E: 20.6/in, 20.6/203.2mm Red R 69.24 Idl Diam: 1.1 Corrosion Index: 6.3  
 Customer Requirements SOURCE: GA-STP CASTING: STRAND CAST  
 Mechanical Test: Yield 63400 PSI, 437.13 MPA Tensile: 89300 PSI, 606.81 MPA %E: 20.0/in, 20.0/203.2mm Red R 69.24 Idl Diam: 1.1 Corrosion Index: 6.3  
 Customer Requirements SOURCE: GA-STP CASTING: STRAND CAST

PRODUCED IN: ST PAUL

SHAPE + SIZE	GRADE	SPECIFICATION	SALES ORDER	CUST P.O. NUMBER
R34	A588M1-A	A6/A6M-10a A503/A588M-05	2035280-01	72732-01
HEAT ID. M074349	C Mn P S Si Cu Ni Cr Mo V Nb N Sn Al Ti Ca Zn Co			

Mechanical Test: Yield 66500 PSI, 458.5 MPA Tensile: 87600 PSI, 603.98 MPA %E: 19.4/in, 19.4/203.2mm Red R 69.24 Idl Diam: 1.16 Corrosion Index: 6.2  
 Customer Requirements SOURCE: GA-STP CASTING: STRAND CAST  
 Mechanical Test: Yield 65600 PSI, 452.3 MPA Tensile: 88700 PSI, 611.56 MPA %E: 18.8/in, 18.8/203.2mm Red R 69.24 Idl Diam: 1.16 Corrosion Index: 6.2  
 Customer Requirements SOURCE: GA-STP CASTING: STRAND CAST

Customer Notes

NO WELD REPAIRMENT PERFORMED. STEEL NOT EXPOSED TO MERCURY.  
This material, including the billets, was melted and manufactured in the United States of America

THE ABOVE FIGURES ARE CERTIFIED CHEMICAL AND PHYSICAL TEST RECORDS AS CONTAINED IN THE PERMANENT RECORDS OF COMPANY.

*Shankar*

Bhaskar Yalamanchili  
Quality Director  
Gerdau

*[Signature]*

Metallurgical Services Manager  
ST PAUL STEEL MILL

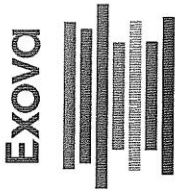
\*Seller warrants that all material furnished shall conform with specifications subject to standard published manufacturing variations. NO OTHER WARRANTIES, EXPRESSED OR IMPLIED, ARE MADE BY THE SELLER, AND SPECIFICALLY EXCLUDED ARE WARRANTIES OF MERCHANTABILITY AND FITNESS FOR A PARTICULAR PURPOSE.  
In no event shall seller be liable for indirect, consequential or punitive damages arising out of or related to the materials furnished by seller.  
Any claim for damages for materials that do not conform to specifications must be made from buyer to seller immediately after delivery of same in order to allow the seller the opportunity to inspect the material in question.

Figure B-3. Loop Connection Bar Specifications



Exova  
1440 Graham's Lane, Unit #9  
Burlington  
Ontario  
Canada  
L7S 1W3

T: +1 (905) 631-7785  
F: +1 (905) 631-7786  
E: sales@exova.com  
W: www.exova.com



**Test Certificate**

Salit Steel  
Division of Myer Salit Ltd.  
7771 Stanley Av.  
P.O. Box 837  
Niagara Falls, Ontario  
L2E 6V6  
Attn: Dan Potter

REF No B 160600 : Issue 1  
Page 1 of 1  
Ord No NA  
Date Tested 08/05/11  
Date Reported 08/05/11

Item - Parent Tag#: 4  
Round Bar 1-1/4"

Specification - ASTM A36/CSA G40.21 44W

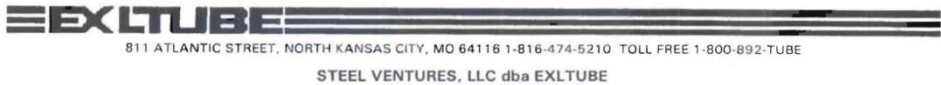
Tensile Test - ASTM A 370-10								
	Dimensions [in]	Area [in <sup>2</sup> ]	GL [in]	0.20%YS [psi]	UTS [psi]	%E1	%RA	Comments
001: Parent	0.4970	0.1940	2.00	49100	73700	34	62	Nil
002: Parent	0.4970	0.1940	2.00	48100	73500	34	62	Nil

Tested by Exova Burlington Laboratory

  
Mohinder Singh  
Chemical Lab. Manager  
Signed for and on behalf of  
Exova Burlington Laboratory

The recording of false, fictitious or fraudulent statements or entries may be punished as a felony under federal law.  
This document may not be reproduced other than in full, except with the prior written approval of the issuing laboratory.  
These results pertain only to the item(s) tested as sampled by the client unless otherwise indicated.

Figure B-5. Connector Pin Specifications



**Certification - Purchased Material**

Customer: SPS - New Century 401 New Century Parkway New Century KS 66031	Size: 05.00X05.00	Spec No: ASTM-A500	Date: 07/02/2012
	Gauge: 3/16	Grade: B	Customer Order No: 4500183805
			BA No: 81936401

Heat No	Yield P.S.I.	Tensile P.S.I.	Elongation % 2 inch
411120	52,000	62,000	25.00

Heat No	C.	MN.	P.	S.	Si.
411120	.0800	.3507	.0129	.0166	

\*\*\*\* THIS IS NOT THE ORIGINAL MILL TEST REPORT \*\*\*\*  
 EXLTUBE hereby certifies that all test results shown in this report are correct as contained in the records of our company. Furthermore, the material was produced by another manufacturer to the specifications denoted above.

Figure B-6. Long Splice Main Tube Specifications

SPS Coil Processing Tulsa  
 5275 Bird Creek Ave.  
 Port of Catoosa, OK 74015



# METALLURGICAL TEST REPORT

PAGE 1 of 1  
 DATE 05/31/2012  
 TIME 10:46:18  
 USER GIANGRER

S  
O  
L  
D  
T  
O

S  
H  
I  
P  
T  
O  
13716  
 Warehouse 0040  
 401 New Century Parkway  
 New Century KS 66031

Order	Material No.	Description	Quantity	Weight	Customer Part	Customer PO	Ship Date
40180308-0010	70872120TM	1/4 72 X 120 A36 TEMPERPASS STPMLPL	15	9,189			05/31/2012

### Chemical Analysis

Heat No.	Vendor	MILL THYSSENKRUPP STEEL USA-LLC													
060157	THYSSENKRUPP STEEL USA-LLC														
Batch 0001698169	15 EA	9,189 LB													
Carbon	Manganese	Phosphorus	Sulphur	Silicon	Nickel	Chromium	Molybdenum	Boron	Copper	Aluminum	Titanium	Vanadium	Columbium	Nitrogen	Tin
0.2020	0.8540	0.0110	0.0082	0.0140	0.0100	0.0170	0.0000	0.0001	0.0110	0.0350	0.0010	0.0030	0.0000	0.0028	0.0000

### Mechanical/ Physical Properties

Mill Coil No.	Tensile	Yield	Elong	Rckwl	Grain	Charpy	Charpy Dr	Charpy Sz	Temperature	Olsen
1111373490	68800.000	43800.000	29.60	0	0.000	0	NA	0		
	71400.000	45900.000	27.15	0	0.000	0	NA			
	70000.000	52000.000	27.87	0	0.000	0	NA			
	70100.000	51100.000	29.02	0	0.000	0	NA			

THE CHEMICAL, PHYSICAL, OR MECHANICAL TESTS REPORTED ABOVE ACCURATELY REFLECT INFORMATION AS CONTAINED IN THE RECORDS OF THE CORPORATION.

272

Figure B-7. Long Splice Insert Specifications

SPS Coil Processing Houston  
 1550 North Witter Rd  
 Pasadena, TX 77506



# METALLURGICAL TEST REPORT

PAGE 1 of 1  
 DATE 11/30/2011  
 TIME 09:32:42  
 USER 065SHIP2

**S**  
**O**  
**L**  
**D**  
**T**  
**O**

11953  
 Great Plains Steel, Inc.  
 2916  
 Lubbock TX 79408

**S**  
**H**  
**I**  
**P**  
**T**  
**O**

11953  
 Great Plains Steel, Inc.  
 5001 Clovis Road  
 Lubbock TX 79416

Order	Material No.	Description	Quantity	Weight	Customer Part	Customer PO	Ship Date
1322022-0090	801072120TM	10GA 72 X 120 A1011-CS-TYB TEMPERED	20,000	6,750.000		26497	11/30/2011

### Chemical Analysis

Heat No. 530487 Vendor THYSSENKRUPP STEEL USA-LLC Mill

Batch 0001337725 15 EA 5,062,500 LB

Carbon	Manganese	Phosphorus	Sulphur	Silicon	Nickel	Chromium	Molybdenum	Boron	Copper	Aluminum	Titanium	Vanadium	Columbium	Nitrogen	Tin
0.0660	0.3870	0.0160	0.0078	0.0190	0.0160	0.0240	0.0010	0.0001	0.0210	0.0410	0.0170	0.0020	0.0000	0.0041	0.0050

### Mechanical/ Physical Properties

Mill Coil No. 1102768400

Tensile	Yield	Elong	Rckwl	Grain	Charpy	Charpy Dr	Charpy Sz	Olsen

THE CHEMICAL, PHYSICAL, OR MECHANICAL TESTS REPORTED ABOVE ACCURATELY REFLECT INFORMATION AS CONTAINED IN THE RECORDS OF THE CORPORATION.

273

Figure B-8. 10 Gauge Mounting Bracket Plate Specifications



[View more images](#)

**1" Hot Dipped Galvanized Finish USS Flat Washer**

**FASTENAL**

Wholesale Price: \$1.44

<b>Fastenal Part No. (SKU):</b>	33188	<b>Package Quantity:</b>	1 (EA)
<b>UNSPSC:</b>	31161807		
<b>Manufacturer:</b>	FASTENAL		
<b>Category:</b>	Fasteners > Washers > Flat Washers		

Web Store: Usually ships in 1 day  
Not available at Beatrice, NE Store  
Check another store for availability

**Quantity 1**  
x 1 (EA)

<b>Product Details</b>	Catalog	Product Standards	CAD Drawings
------------------------	---------	-------------------	--------------

<b>Finish:</b>	Hot Dipped Galvanized
<b>Inner Diameter:</b>	1.062"
<b>Material:</b>	Steel
<b>Outer Diameter:</b>	2.500"
<b>Style:</b>	USS
<b>Type:</b>	Flat Washer
<b>Nominal Size:</b>	1"
<b>Nominal Thickness:</b>	0.165"
<b>Product Weight:</b>	0.1655 lbs.
<b>Notes:</b>	Flat washers are used typically under the head of a bolt or a nut to distribute the forces applied when tightening. USS and SAE washers are designed for cap screws and other threaded products. Galvanized plating protects the bolt from corrosion; typically used in outdoor applications.

Copyright © 2012 Fastenal Company. All Rights Reserved.

<http://www.fastenal.com/web/products/detail.ex?sku=33188>

8/17/2012

Figure B-9. 1-in. Flat Washer Specifications



**CAVALIER, INC.**  
1493 LONDON BRIDGE ROAD  
VIRGINIA BEACH, VA 23453  
ADMIN 757-427-6588  
ADMIN 757-427-2658 FAX  
SALES 757-427-6405

\* C E R T I F I C A T E \*  
\* O F T E S T \*

To: UNIVERSITY OF NEBRASKA  
4800 N.W. 35TH ST.  
LINCOLN, NE 68524

Customer P/O # VERBAL KEN  
Our Order # 054443

Line	Qty	UOM	Description	LOT	
1	46	EA	1-8 x 14 O/A ALL THREAD STUD ASTM A449	033422	
ASTM A449-07B MELTED & MANUFACTURED IN USA					
			CARBON	PHOSPHORUS	
			.45	.005	
Heat No.	HARDNESS (HB)	TENSILE (PSI)	SULFUR	MANGANESE	SILICON
DL1210218902	262	129300	.010	.80	.24
YIELD (PSI)	ELONGATION	RED. OF AREA	CHROMIUM	MOLY.	ALUM
108800	20	55	.08	.01	
PROOF LOAD					

Date: 08/27/12

We hereby certify that the forgoing data is a true copy of the data furnished to us by the producing mill.

CAVALIER, INC.

By: *[Signature]*  
Authorized Test Clerk

Figure B-10. 1 in.-8 x 14 in. Bolt Specifications



[View more images](#)

**1"-8 Hot Dip Galvanized Finish Grade A Finished Hex Nut**

**FASTENAL** Wholesale Price: \$2.26

<b>Fastenal Part No. (SKU):</b>	36719	<b>Package Quantity:</b>
<b>UNSPSC:</b>	31161727	
<b>Manufacturer:</b>	FASTENAL	
<b>Category:</b>	Fasteners > Web Store: Usually ships Nuts > Hex Nuts > Hex Nuts 1 day Not available at Beatrice, NE Store Check another store for availability	

**Quantity 1**  
x 1 (EA)

<a href="#">Product Details</a>	<a href="#">Catalog</a>	<a href="#">Product Standards</a>	<a href="#">CAD Drawings</a>
---------------------------------	-------------------------	-----------------------------------	------------------------------

<b>Diameter:</b>	1"
<b>Finish:</b>	Hot Dip Galvanized
<b>Grade:</b>	A
<b>Material:</b>	Steel
<b>Specification:</b>	ASTM A563
<b>Thickness:</b>	0.875"
<b>Thread:</b>	Coarse
<b>Thread Size:</b>	8
<b>Type:</b>	Finished Hex Nut
<b>Wrench Size:</b>	1-1/2"
<b>System of Measurement:</b>	Imperial (Inch)
<b>Product Weight:</b>	0.2651 lbs.
<b>Notes:</b>	The most versatile and widely used nut, it should be used with any low carbon bolt or screw that is not heat-treated. Galvanized plating protects the bolt from corrosion; typically used in outdoor applications.

<http://www.fastenal.com/web/products/detail.ex?sku=36719>

8/17/2012

Figure B-11. 1 in.-8 Hex Nut Specifications



[View more images](#)

**3/4" Hot Dipped Galvanized Finish  
USS Flat Washer**

<b>FASTENAL</b>	Wholesale Price: \$0.9305
<b>Fastenal Part No. (SKU):</b> 33186	<b>Package Quantity:</b> 1 (EA)
<b>UNSPSC:</b> 31161807	<b>Manufacturer:</b> FASTENAL
<b>Category:</b>	Fasteners > Washers > Flat Washers

Web Store: Usually ships in 1 day  
Not available at Beatrice, NE Store

[Check another store for availability](#)

Quantity 1  
x 1 (EA)

[Add to Cart](#)

- [Product Details](#)
- [Catalog](#)
- [Product Standards](#)
- [CAD Drawings](#)

**Related Items**

<b>Finish:</b>	Hot Dipped Galvanized
<b>Inner Diameter:</b>	0.812"
<b>Material:</b>	Steel
<b>Outer Diameter:</b>	2.000"
<b>Style:</b>	USS
<b>Type:</b>	Flat Washer
<b>Nominal Size:</b>	3/4"
<b>Nominal Thickness:</b>	0.148"
<b>Product Weight:</b>	0.1101 lbs.
<b>Notes:</b>	Flat washers are used typically under the head of a bolt or a nut to distribute the forces applied when tightening. USS and SAE washers are designed for cap screws and other threaded products. Galvanized plating protects the bolt from corrosion; typically used in outdoor applications.

Copyright © 2012 Fastenal Company. All Rights Reserved.

<http://www.fastenal.com/web/products/detail.ex?sku=33186>

8/17/2012

Figure B-12. 3/4 in. Flat Washer Specifications



[View more images](#)

**3/4"-10 x 6-1/2" ASTM A325  
Galvanized USA Structural Bolt w/o  
Nut**

**Fastenal Approved  
Vendor**

Wholesale Price:  
\$7.06

<b>Fastenal Part No. (SKU):</b>	19736	<b>Package Quantity:</b>	1 (EA)
<b>UNSPSC:</b>	31161614		
<b>Manufacturer:</b>	Fastenal Approved Vendor	Web Store: Usually ships in 1 day	Not available at Lincoln, NE Store
<b>Category:</b>	Fasteners > Bolts > Structural Bolts	Check another store for availability	

**Quantity 1**  
x 1 (EA)

[Add to Cart](#)

**Product Details** | **Catalog** | **Product Standards** | **CAD Drawings**

<b>Diameter:</b>	3/4"
<b>Finish:</b>	Hot Dipped Galvanized
<b>Head:</b>	Hex
<b>Length:</b>	6-1/2"
<b>Material:</b>	Steel
<b>Specification:</b>	ASTM A325
<b>Style:</b>	Without Nut
<b>Thread:</b>	Coarse
<b>Thread Size:</b>	10
<b>Type:</b>	Structural Bolt
<b>Wrench Size:</b>	1-1/4"
<b>System of Measurement:</b>	Imperial (Inch)
<b>Product Weight:</b>	0.93 lbs.
<b>Notes:</b>	Structural Bolts are a specialized heavy type of hex bolt intended for use in large structures, such as buildings and bridges. This bolt is designed to withstand the loads of steel-to-steel structural connections. They contain a flat, washer-faced bearing surface and a chamfered thread point. Galvanized plating protects the bolt from corrosion; typically used in outdoor applications.

<http://www.fastenal.com/web/products/detail.ex?sku=19736>

8/17/2012

Figure B-13. 3/4 in.-10 x 6 1/2 in. Bolt Specifications



[View more images](#)

**3/4"-10 Hot Dip Galvanized Finish Grade A Finished Hex Nut**

**FASTENAL**

Wholesale Price:  
\$0.8864

**Fastenal Part No. (SKU):** 36715

**UNSPSC:** 31161727

**Package Quantity:**  
1 (EA)

**Manufacturer:** FASTENAL

**Category:** Fasteners > Nuts > Hex Nuts  
Web Store: Usually ships 1 day  
Available at Beatrice, NE Store  
Check another store for availability

**Quantity** 1  
x 1 (EA)

[Add to Cart](#)

<a href="#">Product Details</a>	<a href="#">Catalog</a>	<a href="#">Product Standards</a>	<a href="#">CAD Drawings</a>
---------------------------------	-------------------------	-----------------------------------	------------------------------

<b>Diameter:</b>	3/4"
<b>Finish:</b>	Hot Dip Galvanized
<b>Material:</b>	Steel
<b>Specification:</b>	ASTM A563
<b>Thickness:</b>	0.656"
<b>Thread:</b>	Coarse
<b>Thread Size:</b>	10
<b>Type:</b>	Finished Hex Nut
<b>Wrench Size:</b>	1-1/8"
<b>System of Measurement:</b>	Imperial (Inch)
<b>Product Weight:</b>	0.1105 lbs.
<b>Notes:</b>	The most versatile and widely used nut, it should be used with any low carbon bolt or screw that is not heat-treated. Galvanized plating protects the bolt from corrosion; typically used in outdoor applications.

Copyright © 2012 Fastenal Company. All Rights Reserved.

<http://www.fastenal.com/web/products/detail.ex?sku=36715>

8/17/2012

Figure B-14. 3/4 in.-10 Hex Nut Specifications

**Appendix C. Material Specifications, Test No. RDTCB-2**

Table C-1. Summary of Material Certifications, Test No. RDTCB-2

Figure	Item No.	QTY.	Description	Material Specifications	Reference
Figure C-1	a1	16	Portable Concrete Barrier	min f <sub>c</sub> =5000 psi [34.5 MPa]	5000 psi Mix 7156475101
Figure C-2	a2	192	1/2" [13] Dia., 72" [1829] Long Form Bar	A615 Grade 60	H# K120760
Figure C-2	a3	32	1/2" [13] Dia., 146" [3708] Long Longitudinal Bar	A615 Grade 60	H# K120760
Figure C-4	a4	48	5/8" [16] Dia., 146" [3708] Long Longitudinal Bar	A615 Grade 60	H# K122397
Figure C-3	a5	96	3/4" [19] Dia., 36" [914] Long Anchor Loop Bar	A615 Grade 60	H# M674348/49
Figure C-3	a6	32	3/4" [19] Dia., 101" [2565] Long Connection Loop Bar	A709 Grade 70 or A706 Grade 60	H# M674348/49
Figure C-3	a7	32	3/4" [19] Dia., 91" [2311] Long Connection Loop Bar	A709 Grade 70 or A706 Grade 60	H# M674348/49
Figure C-3	a8	32	3/4" [19] Dia., 102" [2591] Long Connection Loop Bar	A709 Grade 70 or A706 Grade 60	H# M674348/49
Figure C-5	a9	15	1 1/4" [32] Dia., 28" [711] Long Connector Pin	ASTM A36 Galvanized	R# B160600
Figure C-6	b1	22	5"x5"x3/16" [127x127x5], 12'-9 3/16" [3891] Long Splice Main Tube	A500 Grade B Galvanized after Welding	R# 14-0005 H# A66860
Figure C-7	b2	20	4 1/2"x4 1/2"x1/4" [114x114x6], 22" [559] Long Splice Insert	ASTM 572 Grade 50 Galvanized	R# 14-0005 H# 63130212/02
Figure C-8	b3	11	42"x33" [1067x838] 10 Gage Mounting Bracket Plate	ASTM A1011 Grade 50 Galvanized after Welding	R# 14-0005 H# A211424
Figure C-9	b4	88	1" [25] Dia. Washer	ASTM F436 Galvanized	L# C4816D H# 0124225
Figure C-10 - C-12	b5	44	1" [25] Dia. UNC, 12 3/4" [324] Long Heavy Hex Bolt and Nut	Bolt ASTM A325/A449 Type 1 Galvanized, Nut ASTM A563 Galvanized	L# 033422 / H# DL12104575
Figure C-13	b6	248	3/4" [19] Dia. Washer	ASTM F436 Galvanized	H# 211887 / L# C6542D
Figure C-14 - C-17	b7	80	3/4" [19] Dia. UNC, 6 1/2" [165] Long, 2" [51] Threaded Hex Bolt and Nut	Bolt ASTM A325/A449/SAE Grade 5 Galvanized, Nut ASTM A563DH Grade 5 Galvanized	Structural Bolt Co: L#305965A
Figure C-7	b8	44	4"x3"x3/8" [102x76x10], 12" [305] Long L-Bracket	ASTM A529 Grade 50 Galvanized	R# 14-0005 H# 63130212/02
Figure C-18 - C-20	b9	44	3/4" [19] Dia. UNC, 13" [330] Long, 2" [51] Threaded Hex Bolt and Nut	Bolt ASTM A325/A449/SAE Grade 5 Galvanized, Nut ASTM A563DH Grade 5 Galvanized	Structural Bolt Co: H# M49050 L# 308

# WIESER CONCRETE PRODUCTS, INC.

W3716 U.S. HWY 10 • MAIDEN ROCK, WI 54750  
(715) 647-2311 800-325-8456 Fax (715) 647-5181  
E-mail: wieserpc@wieserconcrete.com Website: www.wieserconcrete.com

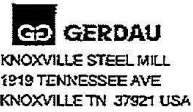
## 5000 psi MIX DESIGN

### WEIGHTS PER CUBIC YARD

Coarse Aggregate, 3/4"minus	(ASTM C 33/#67)	1527 pounds
Fine Aggregate; sand	(ASTM C 33)	1527 pounds
Cement	(ASTM C 150/Type III)	517 pounds
Fly Ash		192 pounds
Axim CATEXOL™ A.E. 260		7.0+/- ounces
Axim CATEXOL™ SUPERFLUX 2100pc		49 ounces
Water		237 pounds

*Material variations may require mixture adjustments to maintain strength, water-cement ratio, slump, air, and yield.*

Figure C-1. Concrete Barrier Mix Specifications



Chemical and Physical Test Report  
MADE IN UNITED STATES

*PO*  
*5/3/12*  
*BARRIER*  
*STEEL*

CUSTOMER: WIESER

PROJECT: MAIDEN ROCK BARRIER REL. 965

SHAPE + SIZE	GRADE	SPECIFICATION	SALES ORDER	CUST P.O. NUMBER
X19MM REBAR (# 6)	420 (60)	ASTM A615/A615M-09B THERMEX TREATED		
HEAT I.D.	C Mn P S Si Cu Ni Cr Mo V Nb Sn C Eqv			
K118257	.28 .67 .033 .059 .16 .33 .13 .17 .020 .005 .002 .003 .433			

Mechanical Test: Yield 85050 PSI, 586.4 MPA Tensile: 102680 PSI, 707.95 MPA %EL: 12.5/8in, 12.5/200MM Bend: OK Def HT: .045, 1.14MM Def Cap: .111, 2.82MM Def SP: .461, 11.71MM %HR 4.4L

Customer Requirements CASTING: STRAND CAST

SHAPE + SIZE	GRADE	SPECIFICATION	SALES ORDER	CUST P.O. NUMBER
X13MM REBAR (# 4)	420 (60)	ASTM A615/A615M-09B THERMEX TREATED		
HEAT I.D.	C Mn P S Si Cu Ni Cr Mo V Nb Sn C Eqv			
K120760	.28 .60 .009 .072 .18 .33 .22 .07 .029 .003 .002 .003 .405			

Mechanical Test: Yield 87960 PSI, 606.46 MPA Tensile: 105040 PSI, 724.23 MPA %EL: 12.5/8in, 12.5/200MM Bend: OK Def HT: .03, .76MM Def Gap: .116, 2.95MM Def SP: .332, 8.43MM %HR 3.7L

Customer Requirements CASTING: STRAND CAST

WIESER CONCRETE

This material, including the billets, was melted and manufactured in the United States of America

*Mhasakay*

Bhaswar Yalamanchili  
Quality Director  
Gerdau

THE ABOVE FIGURES ARE CERTIFIED CHEMICAL AND PHYSICAL TEST RECORDS AS CONTAINED IN THE PERMANENT RECORDS OF COMPANY.

*Jess Chaudhri*

Metallurgical Services Manager  
KNOXVILLE STEEL MILL

Seller warrants that all material furnished shall comply with specifications subject to standard published manufacturing variations. NO OTHER WARRANTIES, EXPRESSED OR IMPLIED, ARE MADE BY THE SELLER, AND SPECIFICALLY EXCLUDED ARE WARRANTIES OF MERCHANTABILITY AND FITNESS FOR A PARTICULAR PURPOSE. In no event shall seller be liable for indirect, consequential or punitive damages arising out of or related to the materials furnished by seller. Any claim for damages for materials that do not conform to specifications must be made from buyer to seller immediately after delivery of same in order to allow the seller the opportunity to inspect the material in question.

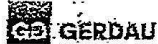
7156475181

13:00 08/20/2012

283

Figure C-2. Reinforcement Bar Specifications

END Loops



ST PAUL STEEL MILL  
1678 RED ROCK ROAD  
ST PAUL, MN 55119 USA  
(651) 731-5800

Chemical and Physical Test Report  
MADE IN UNITED STATES

RJ  
6/4/12  
PO# 72732

M-110802

SHIP TO WIESER CONCRETE W3716 HWY 10 RED 715-647-2311 MAIDEN ROCK, WI 54750	INVOICE TO GERDAU SC 4224 W BOY SCOUT BLVD. ST-600 TAMPA, FL 33607	SHIP DATE 05/31/12  CUST. ACCOUNT NO 10000008
---	---	---

PRODUCED IN: ST PAUL

SHAPE + SIZE	GRADE	SPECIFICATION	SALES ORDER	CUST P.O. NUMBER
R34	A588M1-A	A6/A6M-10a A566/A588M-05	2035280-01	72732-01
HEAT ID. M674348	C Mn P S Si Cu Ni Cr Mo V Nb N Sn Al Ti Ca Zn Co			

Mechanical Test: Yield 63200 PSI, 435.75 MPA Tensile: 89200 PSI, 615.01 MPA %E: 20.0/8in, 20.0/203.2mm Red R 69.24 Idl Diam: 1.1 Corrosion Index: 6.3  
 Customer Requirements SOURCE: GA-STP CASTING: STRAND CAST  
 Mechanical Test: Yield 63400 PSI, 437.13 MPA Tensile: 89300 PSI, 606.81 MPA %E: 20.0/8in, 20.0/203.2mm Red R 69.24 Idl Diam: 1.1 Corrosion Index: 6.3  
 Customer Requirements SOURCE: GA-STP CASTING: STRAND CAST

PRODUCED IN: ST PAUL

SHAPE + SIZE	GRADE	SPECIFICATION	SALES ORDER	CUST P.O. NUMBER
R34	A588M1-A	A6/A6M-10a A503/A588M-05	2035280-01	72732-01
HEAT ID. M074349	C Mn P S Si Cu Ni Cr Mo V Nb N Sn Al Ti Ca Zn Co			

Mechanical Test: Yield 66500 PSI, 458.5 MPA Tensile: 87600 PSI, 603.98 MPA %E: 19.4/8in, 19.4/203.2mm Red R 69.24 Idl Diam: 1.16 Corrosion Index: 6.2  
 Customer Requirements SOURCE: GA-STP CASTING: STRAND CAST  
 Mechanical Test: Yield 65600 PSI, 452.3 MPA Tensile: 88700 PSI, 611.56 MPA %E: 18.8/8in, 18.8/203.2mm Red R 69.24 Idl Diam: 1.16 Corrosion Index: 6.2  
 Customer Requirements SOURCE: GA-STP CASTING: STRAND CAST

Customer Notes

NO WELD REPAIRMENT PERFORMED. STEEL NOT EXPOSED TO MERCURY.  
This material, including the billets, was melted and manufactured in the United States of America

THE ABOVE FIGURES ARE CERTIFIED CHEMICAL AND PHYSICAL TEST RECORDS AS CONTAINED IN THE PERMANENT RECORDS OF COMPANY.

*Shankar*

Shankar Yalamanchili  
Quality Director  
Gerdau

*[Signature]*

Metallurgical Services Manager  
ST PAUL STEEL MILL

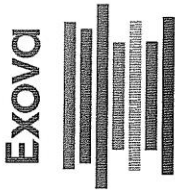
\*Seller warrants that all material furnished shall conform with specifications subject to standard published manufacturing variations. NO OTHER WARRANTIES, EXPRESSED OR IMPLIED, ARE MADE BY THE SELLER, AND SPECIFICALLY EXCLUDED ARE WARRANTIES OF MERCHANTABILITY AND FITNESS FOR A PARTICULAR PURPOSE.  
In no event shall seller be liable for indirect, consequential or punitive damages arising out of or related to the materials furnished by seller.  
Any claim for damages for materials that do not conform to specifications must be made from buyer to seller immediately after delivery of same in order to allow the seller the opportunity to inspect the material in question.

Figure C-3. Loop Connection Bar Specifications



Exova  
1440 Graham's Lane, Unit #9  
Burlington  
Ontario  
Canada  
L7S 1W3

T: +1 (905) 631-7785  
F: +1 (905) 631-7786  
E: sales@exova.com  
W: www.exova.com



**Test Certificate**

Salit Steel  
Division of Myer Salit Ltd.  
7771 Stanley Av.  
P.O. Box 837  
Niagara Falls, Ontario  
L2E 6V6  
Attn: Dan Potter

REF No            B 160600     : Issue   1  
Page                1 of 1  
Ord No              NA  
Date Tested        08/05/11  
Date Reported     08/05/11

Item                - Parent Tag#: 4  
                          Round Bar 1-1/4"

Specification     - ASTM A36/CSA G40.21 44W

Tensile Test - ASTM A 370-10								
	Dimensions [in]	Area [in <sup>2</sup> ]	GL [in]	0.20%YS [psi]	UTS [psi]	%E1	%RA	Comments
001: Parent	0.4970	0.1940	2.00	49100	73700	34	62	Nil
002: Parent	0.4970	0.1940	2.00	48100	73500	34	62	Nil

Tested by            Exova Burlington Laboratory

  
Mohinder Singh  
Chemical Lab. Manager  
Signed for and on behalf of  
Exova Burlington Laboratory

The recording of false, fictitious or fraudulent statements or entries may be punished as a felony under federal law.  
This document may not be reproduced other than in full, except with the prior written approval of the issuing laboratory.  
These results pertain only to the item(s) tested as sampled by the client unless otherwise indicated.

Figure C-5. Connector Pin Specifications

**EXLTUBE**  
811 ATLANTIC STREET, NORTH KANSAS CITY, MO 64116 1-816-474-5210 TOLL FREE 1-800-892-TUBE  
STEEL VENTURES, LLC dba EXLTUBE

### Certified Test Report

Customer: SPS - New Century 401 New Century Parkway NEW CENTURY KS 66031 USA	Size: 05.00X05.00	Spec No: ASTM <b>A500-07</b>	Date: 05/24/2013
	Gauge: 3/16	Grade: <b>B</b>	Customer Order No: 4500202438
			Bl. No: 82142445

Heat No	Yield P.S.I.	Tensile P.S.I.	Elongation % 2 Inch
<b>A6880</b>	57,500	64,100	29.70

Heat No	C	MN	P	S	SI
<b>A6880</b>	0.0600	0.7600	0.0180	0.0040	0.0300

Long Splice Main Tube

This material was melted & manufactured in the U.S.A.  
We hereby certify that all test results shown in this report are correct as contained in the records of our company. All testing and manufacturing is in accordance to A.S.T.M. parameters encompassed within the scope of the specifications denoted in the specification and grade files above. This product was manufactured in accordance with your purchase order requirements.

This material has not come into direct contact with mercury, any of its compounds, or any mercury bearing devices during our manufacturing process, testing, or inspections.

This material is in compliance with EN 10204 Section 4.1 Inspection Certificate Type 3.1

STEEL VENTURES, LLC dba EXLTUBE

*Jonathan Wolfe*

Jonathan Wolfe  
Quality Assurance Manager

Figure C-6. Long Splice Main Tube Specifications



**GERDAU**

US-ML-JACKSON TN  
801 GERDAU AMERISTEEL ROAD  
JACKSON, TN 38305  
USA

**CERTIFIED MATERIAL TEST REPORT**

CUSTOMER SHIP TO STEEL & PIPE SUPPLY CO INC 4750 W MARSHALL AVE LONGVIEW, TX 75604-4817 USA		CUSTOMER BILL TO STEEL & PIPE SUPPLY CO INC MANHATTAN, KS 66505-1688 USA		GRADE A36/A529-50	SHAPE / SIZE Angle / 4X3X3/8	
SALES ORDER 322239/000020		LENGTH 40'00"	WEIGHT 19,040 LB	HEAT / BATCH 63130212/02		
CUSTOMER PURCHASE ORDER NUMBER G450010292		BILL OF LADING 1333-0000002256	DATE 03/25/2013	SPECIFICATION / DATE or REVISION 1-ASTM A6-11, A36-08, A572-50-07 2-A529-09(2009), A709-11 3-CSA-G40.21-44W/50W-04(2009) 4-AASHTO M270-36/50-11		

CHEMICAL COMPOSITION											
C %	Mn %	P %	S %	Si %	Cu %	Ni %	Cr %	Mo %	V %	Nb %	Al %
0.15	0.72	0.013	0.032	0.20	0.27	0.13	0.09	0.030	0.021	0.001	0.001

MECHANICAL PROPERTIES						
Elong. %	G/L Inch	G/L mm	UTS PSI	UTS MPa	YS PSI	YS MPa
32.00	8.000	200.0	71900	496	52070	3380
30.00	8.000	200.0	71900	496	52120	3380

MECHANICAL PROPERTIES	
YS MPa	359
YS MPa	359

COMMENTS / NOTES

\*\*\*\*\*KILLED STEEL\*\*\*\*\*

Long Splice Insert/ Long L-Bracket

The above figures are certified chemical and physical test records as contained in the permanent records of company. This material, including the billets, was melted and manufactured in the USA. We certify that these data are correct and in compliance with specified requirements. CMTR complies with EN 10204 3.1.

*Bhaskar*  
BHASKAR YALAMANCHILI  
QUALITY DIRECTOR

*Prasann*  
PRASANN JINTURKAR  
QUALITY ASSURANCE MGR

288

Figure C-7. Long Splice Insert and Long L-Bracket Specifications

LDPCB Project R# 14-0005

SPS Coil Processing Tulsa  
5275 Bird Creek Ave.  
Port of Catoosa, OK 74015



# METALLURGICAL TEST REPORT

PAGE 1 of 2  
DATE 10/29/2012  
TIME 22:01:54  
USER MEHEULAL

**SOLD TO** 10G Mounting Bracket Plate

**SHIP TO** 13713  
Warehouse 0020  
1050 Fort Gibson Rd  
CATOOSA OK 74015

Order	Material No.	Description	Quantity	Weight	Customer Part	Customer PO	Ship Date
40190652-0140	801072120TM	10GA 72 X 120 A1011-CS-TYB TEMPERED	30	10,125			10/29/2012

### Chemical Analysis

Heat No.	Vendor	Melted and Manufactured in the USA													
A211424	SEVERSTAL COLUMBUS	DOMESTIC Mill SEVERSTAL COLUMBUS													
Batch 0002007505	30 EA	10,125 LB													
Carbon	Manganese	Phosphorus	Sulphur	Silicon	Nickel	Chromium	Molybdenum	Boron	Copper	Aluminum	Titanium	Vanadium	Columbium	Nitrogen	Tin
0.0600	0.3700	0.0090	0.0020	0.0400	0.0500	0.0500	0.0100	0.0001	0.1200	0.0310	0.0010	0.0010	0.0010	0.0064	0.0070

### Mechanical/ Physical Properties

Mill Coil No.	Tensile	Yield	Elong	Rckwl	Grain	Charpy	Charpy Dr	Charpy Sz	Temperature	Olsen
A211424-09										

### Chemical Analysis

Heat No.	Vendor	Melted and Manufactured in the USA													
A211424	SEVERSTAL COLUMBUS	DOMESTIC Mill SEVERSTAL COLUMBUS													
Batch 0002007507	30 EA	10,125 LB													
Carbon	Manganese	Phosphorus	Sulphur	Silicon	Nickel	Chromium	Molybdenum	Boron	Copper	Aluminum	Titanium	Vanadium	Columbium	Nitrogen	Tin
0.0600	0.3700	0.0090	0.0020	0.0400	0.0500	0.0500	0.0100	0.0001	0.1200	0.0310	0.0010	0.0010	0.0010	0.0064	0.0070

### Mechanical/ Physical Properties

Mill Coil No.	Tensile	Yield	Elong	Rckwl	Grain	Charpy	Charpy Dr	Charpy Sz	Temperature	Olsen
A211424-09										

### Chemical Analysis

Heat No.	Vendor	Melted and Manufactured in the USA													
A211424	SEVERSTAL COLUMBUS	DOMESTIC Mill SEVERSTAL COLUMBUS													
Batch 0002007510	30 EA	10,125 LB													
Carbon	Manganese	Phosphorus	Sulphur	Silicon	Nickel	Chromium	Molybdenum	Boron	Copper	Aluminum	Titanium	Vanadium	Columbium	Nitrogen	Tin
0.0600	0.3700	0.0090	0.0020	0.0400	0.0500	0.0500	0.0100	0.0001	0.1200	0.0310	0.0010	0.0010	0.0010	0.0064	0.0070

### Mechanical/ Physical Properties

Mill Coil No.	Tensile	Yield	Elong	Rckwl	Grain	Charpy	Charpy Dr	Charpy Sz	Temperature	Olsen
A211424-09										

THE CHEMICAL, PHYSICAL, OR MECHANICAL TESTS REPORTED ABOVE ACCURATELY REFLECT INFORMATION AS CONTAINED IN THE RECORDS OF THE CORPORATION.

289

Figure C-8. 10 Gauge Mounting Bracket Plate Specifications

LDPCB R#14-0029



23513 Grossbeck Highway  
Warren, Michigan 48089  
(586) 773-2700 \* Fax (586) 773-2298  
www.PrestigeStamping.com

**PRODUCT CERTIFICATION**  
CERTIFICATION NUMBER  
**98972**

THIS IS TO CERTIFY THE PRODUCT STATED BELOW WAS FABRICATED AND PROCESSED TO THE ORDER AS INDICATED AND CONFORMS TO THE APPLICABLE SPECIFICATIONS AND STANDARDS.

<b>Customer:</b> THE STRUCTURAL BOLT CO 2140 CORNHUSKER HWY LINCOLN, NE 68521	
<b>Customer Part:</b> 1" F436 H/DIP	<b>Steel Supplier:</b> KENWAL STEEL CORP.
<b>Prestige Part:</b> P1900HP300	<b>Grade:</b> CF436IGRADE STEEL
<b>Part Name:</b> 1" F436 H/DIP	<b>Lot:</b> C4816D
<b>Purchase Order:</b> 13373-1	<b>Heat:</b> 0124225
<b>Shipment BOL:</b> B157876	<b>Carbon:</b> .46 (.32 - .93)
<b>Shipment ID:</b> A0167347	<b>Manganese:</b> .75 (.6 - 1.65)
<b>Quantity:</b> 600	<b>Phosphorous:</b> .009 (.03 Max.)
<b>Manufacturers Marking:</b> "P"	<b>Sulfur:</b> .003 (.05 Max.)
	<b>Silicon:</b> .18 (.15 - .3)

<u>SPECIFICATIONS</u>	<u>TEST RESULTS</u>
<b>HARDNESS:</b> TEST METHOD: ASTM E18 HRC 38 - 45 ASTM F606	<b>HARDNESS:</b> HRC 41 - 43
<b>PLATING:</b> TEST METHOD: ASTM B499 0.0017" Min. HOT DIP GALV ASTM F-2329	<b>PLATING:</b> 0.0020" - 0.0027"

Chemistry is as reported from raw material certification and does not fall under Prestige Stamping's accreditation.  
This product was produced under an ISO/TS 16949 Quality Assurance System.  
ISO/TS 16949 Certification No: 0062933.  
Material was melted and manufactured in the U.S.A.  
This product was manufactured in Warren, Michigan U.S.A.  
This product conforms to all requirements for washers as produced according to A.S.T.M. F-436-10.  
Sampling Plan per P.S.I W.I. # 5.4.18.016.  
The test results only apply to the items tested.  
This test report must not be reproduced except in full without prior written approval.  
Materials used to manufacture these products are mercury, asbestos and radio activity free.  
No weld repairs made to material.

  
**FRANK SCHUBERT**  
 Quality Assurance Manager

Figure C-9. 1-in. Flat Washer Specifications



**CAVALIER, INC.**  
 1493 LONDON BRIDGE ROAD  
 VIRGINIA BEACH, VA 23453  
 ADMIN 757-427-6588  
 ADMIN 757-427-2658 FAX  
 SALES 757-427-6405

\* C E R T I F I C A T E \*  
 \* O F T E S T \*

To: UNIVERSITY OF NEBRASKA  
 4800 N.W. 35TH ST.  
 LINCOLN, NE 68524

Customer P/O # VERBAL KEN  
 Our Order # 054443

Line	Qty	UOM	Description	LOT
1	46	EA	1-8 x 14 O/A ALL THREAD STUD ASTM A449	033422
ASTM A449-07B MELTED & MANUFACTURED IN USA				
			CARBON	PHOSPHORUS
			.45	.005
Heat No. DL1210218902	HARDNESS (HB) 262	TENSILE (PSI) 129300	SULFUR .010	MANGANESE .80
YIELD (PSI) 108800	ELONGATION 20	RED. OF AREA 55	CHROMIUM .08	MOLY. .01
ALUM	PROOF LOAD			

Date: 08/27/12

We hereby certify that the forgoing data is a true copy of the data furnished to us by the producing mill.

CAVALIER, INC.

By: *[Signature]*  
 Authorized Test Clerk

Figure C-10. 1 in.-8 x 14 in. Bolt Specifications

1"-8 Nuts LDPCB R#14-0029

**NUCOR**  
**FASTENER DIVISION**

LOT NO.  
315776B

Post Office Box 6100  
Saint Joe, Indiana 46785  
Telephone 260/337-1800

CUSTOMER NO/NAME  
8061 STRUCTURAL BOLT CO LLC NUCOR ORDER # 815618  
TEST REPORT SERIAL# F8397386 CUST PART #  
TEST REPORT ISSUE DATE 11/19/12  
DATE SHIPPED 3/28/13 CUSTOMER P.O. # 14186  
NAME OF LAB SAMPLER: BRUCE DELAUDER, LAB TECHNICIAN  
\*\*\*\*\*CERTIFIED MATERIAL TEST REPORT\*\*\*\*\*  
NUCOR PART NO QUANTITY LOT NO. DESCRIPTION  
175647 3600 315776B 1-8 GR LH HV H.D.G.  
MANUFACTURE DATE 9/24/12 HEX NUT H.D.G.



--CHEMISTRY MATERIAL GRADE -1045L  
MATERIAL HEAT \*\*CHEMISTRY COMPOSITION (WT% HEAT ANALYSIS) BY MATERIAL SUPPLIER  
NUMBER NUMBER C MN P S SI NUCOR STEEL - SOUTH CAROL  
RM027762 DL12104575 .43 .65 .008 .014 .20  
MIN .20 .60  
MAX .55 .040 .050

--MECHANICAL PROPERTIES IN ACCORDANCE WITH ASTM A563-07a  
SURFACE CORE PROOF LOAD TENSILE STRENGTH  
HARDNESS HARDNESS 90900 LBS DEG-WEDGE  
(R50N) (RC) (LBS) STRESS (PSI)  
N/A 28.5 PASS N/A N/A  
N/A 26.5 PASS N/A N/A  
N/A 27.4 PASS N/A N/A  
N/A 27.8 PASS N/A N/A  
N/A 28.4 PASS N/A N/A  
AVERAGE VALUES FROM TESTS PRODUCTION LOT SIZE 45000 PCS  
27.7

ROTATIONAL CAPACITY TESTED IN ACCORDANCE WITH A325-10, A563-07a  
SAMPLE #1 PASSED SAMPLE #2 PASSED

--VISUAL INSPECTION IN ACCORDANCE WITH ASTM A563-07a 80 PCS. SAMPLED LOT PASSED

--COATING - HOT DIP GALVANIZED TO ASTM F2329-11 - GALVANIZING PERFORMED IN THE U.S.A.  
1. 0.00235 2. 0.00378 3. 0.00490 4. 0.00346 5. 0.00383 6. 0.00400 7. 0.00231  
8. 0.00446 9. 0.00317 10. 0.00319 11. 0.00326 12. 0.00505 13. 0.00444 14. 0.00590  
15. 0.00329  
AVERAGE THICKNESS FROM 15 TESTS .00383  
HEAT TREATMENT - AUSTENITIZED, OIL QUENCHED & TEMPERED (MIN 800 DEG F)

--DIMENSIONS PER ASME B18.2.4-2006  
CHARACTERISTIC #SAMPLES TESTED MINIMUM MAXIMUM  
Width Across Corners 8 1.8200 1.8390  
Thickness 32 0.9740 0.9970

ALL TESTS ARE IN ACCORDANCE WITH THE LATEST REVISIONS OF THE METHODS PRESCRIBED IN THE APPLICABLE SAE AND ASTM SPECIFICATIONS. THE SAMPLES TESTED CONFORM TO THE SPECIFICATIONS AS DESCRIBED/LISTED ABOVE AND WERE MANUFACTURED FREE OF MERCURY CONTAMINATION. NO INTENTIONAL ADDITIONS OF BISMUTH, SELENIUM, TELLURIUM, OR LEAD WERE USED IN THE STEEL USED TO PRODUCE THIS PRODUCT.  
THE STEEL WAS MELTED AND MANUFACTURED IN THE U.S.A. AND THE PRODUCT WAS MANUFACTURED AND TESTED IN THE U.S.A. PRODUCT COMPLIES WITH DFARS 252.225-7014. WE CERTIFY THAT THIS DATA IS A TRUE REPRESENTATION OF INFORMATION PROVIDED BY THE MATERIAL SUPPLIER AND OUR TESTING LABORATORY. THIS CERTIFIED MATERIAL TEST REPORT RELATES ONLY TO THE ITEMS LISTED ON THIS DOCUMENT AND MAY NOT BE REPRODUCED EXCEPT IN FULL.



MECHANICAL FASTENER  
CERTIFICATE NO. A2LA 0139.01  
EXPIRATION DATE 12/31/13

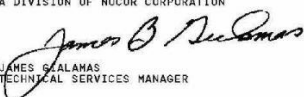
NUCOR FASTENER  
A DIVISION OF NUCOR CORPORATION  
  
JAMES SCALAMAS  
TECHNICAL SERVICES MANAGER

Figure C-11. 1 in.-8 Hex Nut Specifications

Raw Material Cert for Lot 315776B  
Nucor Steel 8/23/2012 5:30:29 AM PAGE 2/002 Fax Server

**NUCOR**  
NUCOR CORPORATION  
NUCOR STEEL SOUTH CAROLINA

Mill Certification  
8/23/2012

27762  
300 Steel Mill Road  
DARLINGTON, SC 29540  
(843) 393-5941  
Fax: (843) 395-8701

Sold To: NUCOR FASTENER INDIANA  
PO BOX 6100  
ST JOE, IN 46785-0000  
(800) 855-8826  
Fax: (219) 337-1728

Ship To: NUCOR FASTENER  
6730 COUNTY ROAD 60  
ST JOE, IN 46785  
(800) 855-8826  
Fax: (219) 337-1722

Customer P.O.	131898	Sales Order	161814.3
Product Group	Special Bar Quality	Part Number	30001261480V760
Grade	1045L	Lot #	DL1210457502
Size	1-9/32" (1.2813) Round	Heat #	DL12104575
Product	1-9/32" (1.2813) Round 40' 1045L	B.L. Number	C1-586928
Description	1045L	Load Number	C1-269954
Customer Spec		Customer Part #	025016

I hereby certify that the material described herein has been manufactured in accordance with the specifications and standards listed above and that it satisfies these requirements.

C	Mn	V	Si	S	P	Cu	Cr	Ni	Mo	Al	Cb
0.43%	0.65%	0.004%	0.20%	0.014%	0.008%	0.16%	0.09%	0.05%	0.01%	0.003%	0.003%
Pb	Sn	Ca	B	Ti	NICUMO						
0.003%	0.031%	0.0012%	0.0002%	0.001%	0.23						

NICUMO: Cu+Ni+Mo

Reduction Ratio 38 :1

ASTM E361  
Surface: 2 Mid Radius: 2 Center: 2

Specification Comments: CHEMICAL ANALYSIS WAS PERFORMED BY NUCOR NE L.A.B. ACREDITIED CHEMICAL TESTING. CERT L-2232 EXPIRES 12-15-2012 ALL MATERIAL PRODUCED BY NUCOR SC IS EAF MELTED MATERIAL TESTED IN CONFORMANCE WITH ASTM A29-05, AND E4-15-08

1. WELDING OR WELD REPAIR WAS NOT PERFORMED ON THIS MATERIAL  
2. MELTED AND MANUFACTURED IN THE USA  
3. MERCURY, RADIUM, OR ALPHA SOURCE MATERIALS IN ANY FORM HAVE NOT BEEN USED IN THE PRODUCTION OF THIS MATERIAL

**Chemistry Verification Checks**

Part# 5016 RM# 27762

Checked By \_\_\_\_\_ Date \_\_\_\_\_

Receiving OK: 397 8-23-12

Certifications OK: 375 8-23-12

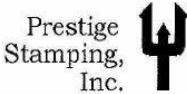
*James H. Blew*

James H. Blew  
Division Metallurgist

NBMG-10 January 1, 2012 Page 2 of 2

Figure C-12. 1 in.-8 Hex Nut Specifications

3/4" Washer LDPCB R#14-0029



23513 Grossbeck Highway  
Warren, Michigan 48089  
(586)773-2700 \* Fax (586)773-2298  
www.PrestigeStamping.com

**PRODUCT CERTIFICATION**  
CERTIFICATION NUMBER

107789

THIS IS TO CERTIFY THE PRODUCT STATED BELOW WAS FABRICATED AND PROCESSED TO THE ORDER AS INDICATED AND CONFORMS TO THE APPLICABLE SPECIFICATIONS AND STANDARDS.

<b>Customer:</b> THE STRUCTURAL BOLT CO ACCTS PAYABLE DEPT 2140 CORNHUSKER HWY LINCOLN, NE 68521	
<b>Customer Part:</b> 3/4" F436 H/DIP	<b>Steel Supplier:</b> MID STATE INDUSTRIES
<b>Prestige Part:</b> P1480HP300	<b>Grade:</b> CF436 GRADE STEEL
<b>Part Name:</b> 3/4" F436 H/DIP	<b>Lot:</b> 06542D
<b>Purchase Order:</b> 14276-1	<b>Heat:</b> 211887
<b>Shipment BOL:</b> B164844	<b>Carbon:</b> .297 (.21 - .93)
<b>Shipment ID:</b> A0174899	<b>Manganese:</b> 1.151 (.43 - 1.6)
<b>Quantity:</b> 4200	<b>Phosphorous:</b> .006 (.03 Max.)
<b>Manufacturers Marking:</b> "P"	<b>Sulfur:</b> .002 (.05 Max.)
	<b>Silicon:</b> .22

<u>SPECIFICATIONS</u>	<u>TEST RESULTS</u>
<b>HARDNESS:</b> TEST METHOD: ASTM E18 HRC 38 - 45 CHECK TO ASTM F606	<b>HARDNESS:</b> HRC 41 - 43
<b>PLATING:</b> TEST METHOD: ASTM B499 0.0017" Min. HOT DIP GALV TO ASTM F-2329	<b>PLATING:</b> 0.0020" - 0.0026"

Chemistry is as reported from raw material certification and does not fall under Prestige Stamping's accreditation.  
This product was produced under an ISO/TS 16949 Quality Assurance System.  
ISO/TS 16949 Certification No: 0062933.  
Material was melted and manufactured in the U.S.A.  
This product was manufactured in Warren, Michigan U.S.A.  
This product conforms to all requirements for washers as produced according to A.S.T.M. F-436-10.  
Sampling Plan per F.S.J W.I. # 5.4.18.018.  
The test results only apply to the items tested.  
This test report must not be reproduced except in full without prior written approval.  
Materials used to manufacture these products are mercury, asbestos and radio activity free.  
No weld repairs made to material.

  
**FRANK SCHUBERT**  
 Quality Assurance Manager

Figure C-13. 3/4 in. Flat Washer Specifications

3/4-10x6.5bolt LDPCB R#14-0029

**NUCOR**  
**FASTENER DIVISION**

LOT NO.  
305965A

Post Office Box 6100  
Saint Joe, Indiana 46785  
Telephone 260/337-1600

TEST REPORT SERIAL# F3385098  
TEST REPORT ISSUE DATE 4/30/12  
MANUFACTURE DATE 4/03/12  
NAME OF LAB SAMPLER: ROBERTA COMMENT, LAB TECHNICIAN

\*\*\*\*\*CERTIFIED MATERIAL TEST REPORT\*\*\*\*\*

PART NO. 160747  
**LOT NO. 305965A**  
**DESCRIPTION 3/4-10 X 6 1/2 A325 H.D.G.**  
STRUC SCREW H.D.G.



--CHEMISTRY MATERIAL GRADE -1039ML1  
MATERIAL HEAT \*\*CHEMISTRY COMPOSITION (WT% HEAT ANALYSIS) BY MATERIAL SUPPLIER  
NUMBER NUMBER C MN P S SI NUCOR STEEL - NEBRASKA  
RM027275 NF12201156 .41 .88 .010 .015 .25  
MIN .30 .60 .040 .050 .30  
MAX .52 .040 .050 .30

--MECHANICAL PROPERTIES IN ACCORDANCE WITH ASTM A325-10  
SURFACE CORE PROOF LOAD TENSILE STRENGTH  
HARDNESS HARDNESS 28400 LBS 10 DEG-WEDGE  
(R50N) (RC) (LBS) STRESS (PSI)  
N/A 28.7 PASS 49270 147515  
N/A 26.7 PASS 48450 145060  
N/A 27.1 PASS 48480 145150  
N/A 27.8  
AVERAGE VALUES FROM TESTS PRODUCTION LOT SIZE 9500 PCS  
27.6 48733 145908

--VISUAL INSPECTION IN ACCORDANCE WITH ASTM A325-10 6 PCS. SAMPLED LOT PASSED

--COATING - HOT DIP GALVANIZED TO ASTM F2329-11 - GALVANIZING PERFORMED IN THE U.S.A.  
1. 0.00358 2. 0.00377 3. 0.00295 4. 0.00387 5. 0.00416 6. 0.00396 7. 0.00375  
8. 0.00348 9. 0.00407 10. 0.00340 11. 0.00351 12. 0.00393 13. 0.00526 14. 0.00426  
15. 0.00375  
AVERAGE THICKNESS FROM 15 TESTS .00383  
HEAT TREATMENT - AUSTENITIZED, OIL QUENCHED & TEMPERED (MIN 800 DEG F)

--DIMENSIONS PER ASME B18.2.6-2006  
CHARACTERISTIC #SAMPLES TESTED MINIMUM MAXIMUM  
Width Across Corners 8 1.4020 1.4090  
Grip Length 8 5.0400 5.1000  
Head Height 8 0.4590 0.4710  
Threads 8 PASS PASS

ALL TESTS ARE IN ACCORDANCE WITH THE LATEST REVISIONS OF THE METHODS PRESCRIBED IN THE APPLICABLE SAE AND ASTM SPECIFICATIONS. THE SAMPLES TESTED CONFORM TO THE SPECIFICATIONS AS DESCRIBED/LISTED ABOVE AND WERE MANUFACTURED FREE OF MERCURY CONTAMINATION. NO HEATS TO WHICH BISMUTH, SELENIUM, TELLURIUM, OR LEAD WAS INTENTIONALLY ADDED HAVE BEEN USED TO PRODUCE THE BOLTS. THE STEEL WAS MELTED AND MANUFACTURED IN THE U.S.A. AND THE PRODUCT WAS MANUFACTURED AND TESTED IN THE U.S.A. PRODUCT COMPLIES WITH DFARS 252.225-7014. WE CERTIFY THAT THIS DATA IS A TRUE REPRESENTATION OF INFORMATION PROVIDED BY THE MATERIAL SUPPLIER AND OUR TESTING LABORATORY. THIS CERTIFIED MATERIAL TEST REPORT RELATES ONLY TO THE ITEMS LISTED ON THIS DOCUMENT AND MAY NOT BE REPRODUCED EXCEPT IN FULL.



MECHANICAL FASTENER  
CERTIFICATE NO. ACLA 0139.01  
EXPIRATION DATE 12/31/13

NUCOR FASTENER  
A DIVISION OF NUCOR CORPORATION

*James B. Sealamas*  
JAMES SEALAMAS  
TECHNICAL SERVICES MANAGER

Figure C-14. 3/4 in.-10 x 6 1/2 in. Bolt Specifications

 <b>UNYTITE INC.</b> <small>INNOVATIVE FASTENING SYSTEMS</small>	Unytite, Inc. 3/4" Nuts LDPCB R# 14-0029 One Unytite Drive Peru, IL 61354 Tel 815-224-2221 Fax 815-224-3434	<h1>INSPECTION CERTIFICATE</h1>																												
	<b>Job Information</b>																													
<b>Job No:</b> 16124		<b>Certified Date:</b> 7/1/13																												
<b>Customer:</b> Customer Part No: Customer PO No: Order No: Note: Lot Number: 16124-NF13201523		<b>Ship To:</b>  <b>Shipped Qty:</b> Line No:																												
<b>Part Information</b>																														
<b>Part No:</b> A563 3/4-10 +0.020 DH HHN HDG BLUE DYE																														
<b>Description:</b> ASTM A563 Heavy Hex Nut, Grade DH, Hot Dipped Galv, Blue Dye <b>Manufactured Quantity:</b> 112,289 pcs																														
<b>Applicable Specifications</b>																														
<table border="1"> <thead> <tr> <th>Specification</th> <th>Amend</th> <th>Specification</th> <th>Amend</th> </tr> </thead> <tbody> <tr> <td>ASME B1.1</td> <td></td> <td>ASME B18.2.2</td> <td></td> </tr> <tr> <td>ASME B18.2.6</td> <td></td> <td>ASTM A563</td> <td></td> </tr> <tr> <td>ASTM F2329</td> <td></td> <td>ASTM F606/F606M</td> <td></td> </tr> <tr> <td>ASTM F812/F812M</td> <td></td> <td></td> <td></td> </tr> </tbody> </table>	Specification	Amend	Specification	Amend	ASME B1.1		ASME B18.2.2		ASME B18.2.6		ASTM A563		ASTM F2329		ASTM F606/F606M		ASTM F812/F812M													
Specification	Amend	Specification	Amend																											
ASME B1.1		ASME B18.2.2																												
ASME B18.2.6		ASTM A563																												
ASTM F2329		ASTM F606/F606M																												
ASTM F812/F812M																														
<b>Test Results</b>																														
<b>Test No:</b> 1308 <b>Test:</b> A563 DH Mechanical Properties																														
<table border="1"> <thead> <tr> <th>Description</th> <th>Hardness (HRC)</th> <th>Tempering (800 degree F Min)</th> <th>Proof Load (Pass/Fail)</th> <th>Shape &amp; Dimension ASME B18.2.2</th> <th>Thread Precision ASME B18.1.1</th> <th>Visual ASTM F812</th> </tr> </thead> <tbody> <tr> <td>Sample Inspection</td> <td>28.3</td> <td>1,049</td> <td>Pass</td> <td>Pass</td> <td>Pass</td> <td>Pass</td> </tr> </tbody> </table>	Description	Hardness (HRC)	Tempering (800 degree F Min)	Proof Load (Pass/Fail)	Shape & Dimension ASME B18.2.2	Thread Precision ASME B18.1.1	Visual ASTM F812	Sample Inspection	28.3	1,049	Pass	Pass	Pass	Pass																
Description	Hardness (HRC)	Tempering (800 degree F Min)	Proof Load (Pass/Fail)	Shape & Dimension ASME B18.2.2	Thread Precision ASME B18.1.1	Visual ASTM F812																								
Sample Inspection	28.3	1,049	Pass	Pass	Pass	Pass																								
<b>Certified Chemical Analysis</b>																														
<table border="1"> <thead> <tr> <th>Heat No</th> <th>Grade</th> <th>Manufacturer</th> <th>Origin</th> <th>C</th> <th>Mn</th> <th>P</th> <th>S</th> <th>Si</th> <th>Cr</th> <th>Ni</th> <th>Cu</th> </tr> </thead> <tbody> <tr> <td>NF13201623</td> <td>1045</td> <td>Shinsho American Corporation</td> <td>USA</td> <td>0.4600</td> <td>0.8100</td> <td>0.010</td> <td>0.020</td> <td>0.2100</td> <td>0.0700</td> <td>0.0500</td> <td>0.0900</td> </tr> </tbody> </table>	Heat No	Grade	Manufacturer	Origin	C	Mn	P	S	Si	Cr	Ni	Cu	NF13201623	1045	Shinsho American Corporation	USA	0.4600	0.8100	0.010	0.020	0.2100	0.0700	0.0500	0.0900						
Heat No	Grade	Manufacturer	Origin	C	Mn	P	S	Si	Cr	Ni	Cu																			
NF13201623	1045	Shinsho American Corporation	USA	0.4600	0.8100	0.010	0.020	0.2100	0.0700	0.0500	0.0900																			
<b>Notes</b>																														
<p>All tests are in accordance with the latest revisions of the methods prescribed in the applicable SAE and ASTM Specifications. The samples tested conform the specifications as described/listed above and were manufactured free of mercury contamination. No heats to which Bismuth, Selenium, Tellurium, or Lead was intentionally added have been used to produce products. The steel was melted and manufactured in the U.S.A. and the product was manufactured and tested in the U.S.A. We certify that this data is true representation of information provided by the material supplier and our testing laboratory. This certified material test report relates only to the items listed on this document and may not be reproduced except in full.</p>																														
				 Savage, Dan - Supervisor, Quality																										
				7/1/13 Date																										

Plex Online 7/1/13 6:50 AM DSAVAGE Page 1

Figure C-15. 3/4 in.-10 Hex Nut Specifications

**NUCOR**  
NUCOR CORPORATION  
NUCOR STEEL NEBRASKA

**Mill Certification**  
4/3/2013

2911 East Nucor Road  
NORFOLK, NE 68701  
(402) 644-0200  
Fax: (402) 644-0329

Sold To: SHINSHO AMERICAN CORP  
26200 TOWN CENTER DR  
NOVI, MI 48375  
(866) 793-1232  
Fax: (248) 675-5575

Ship To: UNYTITE, INC  
ONE UNYTITE DRIVE  
PERU, IL 61354  
(815) 224-2221

Customer P.O.	SD7973	Sales Order	127732.1
Product Group	Special Bar Quality	Part Number	30001000300XHL0
Grade	1045MLAT Magnetic Flux Leakage Test	Lot #	NF1310103351
Size	1" (1.0000) Round	Heat #	NF13101033
Product	1" (1.0000) Round 25' 0" 1045MLAT	B.L. Number	N1-251486
Description	1045MLAT	Load Number	N1-187288
Customer Spec		Customer Part #	

I hereby certify that the material described herein has been manufactured in accordance with the specifications and standards listed above and that it satisfies those requirements.

Roll Date: 3/21/2013 Melt Date: 3/13/2013 Qty Shipped LBS: 29,905 Qty Shipped Pcs: 448

C	Mn	V	Si	S	P	Cu	Cr	Ni	Mo	Al	Cb
0.44%	0.84%	0.004%	0.23%	0.029%	0.008%	0.10%	0.08%	0.05%	0.01%	0.032%	0.003%
Pb	Sn	Ca	As	N	NICR						
0.000%	0.006%	0.0010%	0.0000%	82 ppm	0.13						

NICR: Ni+Cr

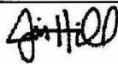
Yield 1: 62239psi (429MPa) Tensile 1: 101232psi (698MPa) Elongation 17% in 8" (in 203.3mm)  
Decarb depth 0.0033in Magnetic Flux Leakage OK Machined Straightened OK  
Austenitic Grain Size: 8.000 per ASTM E112-96 Reduction Ratio 56 :1

ASTM E381  
Surface: 1 Mid Radius: 1 Center: 1

ASTM E45 Method A (Worst)  
Sulfides: T: 1.5 H: 1.0 Alumina: T: 1.0 H: 0.0 Silicates: T: 0.5 H: 0.0 Globular: T: 1.0 H: 0.5

Specification Comments:

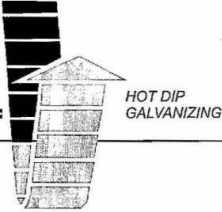
1. All manufacturing processes of the steel materials in this product, including melting, have been performed in the United States.
2. All products produced are weld free.
3. Mercury, in any form, has not been used in the production or testing of this material.
4. Test conform to ASTM A29-12, ASTM E415 and ASTM E1019-resulphurized grades or applicable customer requirements.
5. All material melted at Nucor Steel Nebraska is produced in an Electric Arc Furnace
6. Strand Cast
7. ISO-17025 LAB accreditation cert. available upon request



Jim Hill  
Division Metallurgist

Figure C-16. 3/4 in.-10 Hex Nut Specifications

# ROGERS BROTHERS INC.



June 18, 2013

Unytite, Inc.  
Unytite Quality Department  
One Unytite Drive  
Peru, IL 61354

To Whom It May Concern:

This is to certify that the hot dip galvanizing of the following material on your Purchase Order number 4677 conforms to specification ASTM A-153. The following sizes and lot numbers comply with the coating, workmanship, finish, and appearance requirements of ASTM F2329 specifications. The hot dip galvanizing is ROHS compliant. The galvanizing process was conducted in a temperature range of 830F to 850F.

108,397 Pieces	3/4"-10 A563 DH HHN	Lot#16124-NF13201523	4.53 Avg. Mils.
86,786 Pieces	3/4"-10 A194 2H HHN	Lot#16123-m50081	5.04 Avg. Mils.

This certification in no way implies anything other than the quality of our hot dip galvanizing as it pertains to your order.

This product was galvanized in Rockford, IL USA

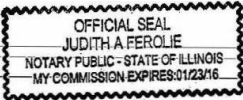
Yours very truly,

ROGERS BROTHERS INC.

Lorraine P. Shelburne  
Vice President

LPS:pd

SUBSCRIBED AND SWORN  
BEFORE ME THIS 18TH DAY  
OF JUNE 2013, AD

  
NOTARY PUBLIC

ROGERS BROTHERS, INC. 1925 KISHWAUKEE STREET, ROCKFORD, ILLINOIS 61104-5197 PHONE: 815/965-5132 FAX: 815/965-3765  
E-MAIL: rogersbros@tds.net

Figure C-17. 3/4 in.-10 Hex Nut Specifications

GAFFNEY BOLT COMPANY  
6100 MATERIAL AVENUE  
ROCKFORD, IL 61111

**FASTENER TEST REPORT**

<b>DATE SHIPPED:</b>	July 26, 2013	<b>LOT NO:</b>	308
<b>CUSTOMER:</b>	THE STRUCTURAL BOLT COMPANY		
<b>P.O. NO:</b>	14587	<b>QUANTITY:</b>	45
<b>DESCRIPTION:</b>	3/4-10 X 13 A325 HVYHEX HDG	<b>HEAT NO:</b>	M49050

HEAT CHEMICAL ANALYSIS ATTACHED

<b>MATERIAL:</b>	1045	<b>ROCKWELL:</b>	30-31
<b>TENSILE:</b>	44,160 LBS	<b>PROOFLOAD:</b>	28,400 LBS

**PASSED VISUAL INSPECTION**

ALL TEST ARE IN ACCORDANCE WITH THE METHODS PRESCRIBED IN THE APPLICABLE SAE AND ASTM SPECIFICATIONS. PRODUCT MEETS ASME B18.2.6 DIMENSIONAL SPECIFICATION AND THREADS MEET ANSI B1.1 CLASS 2A. WE CERTIFY THAT THIS DATA IS TRUE REPRESENTATION OF INFORMATION PROVIDED BY THE MATERIAL SUPPLIER AND OUR TESTING LABORATORY.

THESE PARTS WERE MANUFACTURED BY GAFFNEY BOLT COMPANY FROM STEEL MELTED AND MANUFACTURED IN THE USA.

GAFFNEY BOLT COMPANY  
  
MARY P. GAFFNEY  
SECRETARY

Figure C-18. 3/4 in.-10 x 13 in. Bolt Specifications

**KREHER STEEL COMPANY, LLC.**

GAFFNEY BOLT COMPANY  
 HOT ROLLED ROUNDS 1045  
 7500 X 20"  
 PART NO.

PO/Ret V/O- MIKE G  
 I hereby certify that this data is correct as  
 contained in the records of this company.  
 I hereby certify that no mercury came in contact

**Certificate of Mill Test Results**

SO 1 -243949-001  
 with or no weld repair was done to this product  
 while in our possession.  
 1Mar13  
 Pg 1/2  
 Attn:



GERDAU SPECIAL STEEL NORTH AMERICA  
 5591 MORRILL ROAD  
 JACKSON, MICHIGAN 49201

**CERTIFIED MATERIAL TEST REPORT**

CUSTOMER ORDER NUMBER	CUSTOMER PART NUMBER	HEAT NUMBER	WORK ORDER NUMBER	DATE
34903		M49050	276976 101	2/08/13

REPORT TO: KREHER STEEL  
 1550 N. 25TH AVE  
 MELROSE PARK, IL 60160

SHIP TO: KREHER - CUSTOMER PICK UP

*MB*

**ORDERED**

GRADE	SIZE	LENGTH
1045	0 3/4" RND	20'

CUSTOMER SPECIFICATIONS  
 ASTM A29/A29-12; A576-90B

**CHEMICAL ANALYSIS**

C	Mn	P	S	Si	Ni	Cr	Mo	Cu	Sn	Al
0.50	0.70	0.015	0.027	0.24	0.24	0.17	0.05	0.16	0.008	0.001
V	Nb									
0.055	0.001									

GRAIN SIZE: SPECIFICATION ASTM E112 FINE GRAIN 5-8

HARDNESS: SPECIFICATION ASTM E10 AS ROLLED

SURFACE AVERAGE  
 265.0  
 262.0  
 AS ROLLED AVERAGE: 263.5 BHN

PHYSICALS: SPECIFICATION ASTM E8/A370 AS ROLLED

08.0 IN

TENSILE (KSI) YIELD (KSI) % ELONGATION REDUCTION OF AREA

PAGE 1

We certify that these data are correct and in compliance with specified requirements.

Gerdau Monroe  
 3000 East Front Street  
 Monroe, MI 48161

*Wendy J. Craig*  
 Wendy J. Craig  
 Quality Assurance Representative

CONTINUED ON PAGE 2

Figure C-19. 3/4 in.-10 x 13 in. Bolt Specifications

**KREHER STEEL COMPANY, LLC.**

GAFFNEY BOLT COMPANY  
HOT ROLLED ROUNDS 1045  
7500 X 20"  
PART NO.

PO/Rel V/O- MIKE G  
I hereby certify that this data is correct as  
contained in the records of this company.  
I hereby certify that no mercury came in contact

**Certificate of Mill Test Results**

SO 1 -243949-001  
with or no weld repair was done to this product  
while in our possession.  
1Mar13  
Pg 2/2  
Attn:



GERDAU SPECIAL STEEL NORTH AMERICA  
5591 MORRILL ROAD  
JACKSON, MICHIGAN 49201

**CERTIFIED MATERIAL TEST REPORT**

CUSTOMER ORDER NUMBER	CUSTOMER PART NUMBER	HEAT NUMBER	WORK ORDER NUMBER	DATE
34903		M49050	276976 101	2/08/13

REPORT TO

KREHER STEEL  
1550 N. 25TH AVE  
MELROSE PARK , IL 60160

SHIP TO

KREHER - CUSTOMER PICK UP

**ORDERED**

GRADE	SIZE	LENGTH
1045	0 3/4" RND	20'

CUSTOMER SPECIFICATIONS  
ASTM A29/A29-12; A576-90B

127.0                      88.1                      12.5                      38.3

REDUCTION RATIO

RATIO= 81.5 TO 1.0

MADE AND MANUFACTURED IN USA

\*\* MATERIAL 100% MELTED AND MANUFACTURED IN THE U.S.A. BY THE ELECTRIC ARC FURNACE AND CONTINUOUS CASTING METHOD. THE PRODUCT HAS NOT BEEN REPAIRED BY WELDING AND THIS MATERIAL HAS NOT BEEN EXPOSED TO MERCURY OR TO ANY OTHER METAL ALLOY THAT IS LIQUID AT AMBIENT TEMPERATURES DURING PROCESSING OR WHILE IN OUR POSSESSION. GERDAU MONITORS ALL INCOMING SCRAP AND ALL HEATS OF STEEL TO ENSURE THAT PRODUCTS SHIPPED ARE FREE OF RADIOACTIVE MATERIAL.

PAGE 2 OF 2

We certify that these data are correct and in compliance with specified requirements.

Gerdau Monroe  
3000 East Front Street  
Monroe, MI 48161

*Wendy J. Craig*  
Wendy J. Craig  
Quality Assurance Representative

Figure C-20. 3/4 in.-10 x 13 in. Bolt Specifications

## **Appendix D. Vehicle Center of Gravity Determination**

Test: RDTCB-1

Vehicle: 2270P

**Vehicle CG Determination**

VEHICLE	Equipment	Weight (lb)	Vert CG (in.)	Vert M (lb-in.)
+	Unbalasted Truck (Curb)	4991	28.20691	140780.69
+	Brake receivers/wires	6	53	318
+	Brake Frame	6	26	156
+	Brake Cylinder (Nitrogen)	22	27	594
+	Strobe/Brake Battery	6	32	192
+	Hub	27	14.9375	403.3125
+	CG Plate (EDRs)	14	32	448
-	Battery	-37	41	-1517
-	Oil	-10	15.5	-155
-	Interior	-47	23	-1081
-	Fuel	-163	20	-3260
-	Coolant	-10	31	-310
-	Washer fluid	-6	34.5	-207
BALLAST	Water	174	20	3480
	DTS	17.5	32	560
	Misc.			0
				140402

Estimated Total Weight (lb)	4990.5
Vertical CG Location (in.)	28.13385

wheel base (in.) 140.25

MASH Targets	Targets	Test Inertial	Difference
Test Inertial Weight (lb)	5000 ± 110	4998	-2.0
Long CG (in.)	63 ± 4	63.17	0.16582
Lat CG (in.)	NA	-0.46216	NA
Vert CG (in.) ≥	28	28.13	0.13385

Note: Long. CG is measured from front axle of test vehicle

Note: Lateral CG measured from centerline - positive to vehicle right (passenger) side

CURB WEIGHT (lb)		
	Left	Right
Front	1430	1342
Rear	1117	1102
FRONT	2772 lb	
REAR	2219 lb	
TOTAL	4991 lb	

TEST INERTIAL WEIGHT (lb)		
(from scales)		
	Left	Right
Front	1415	1332
Rear	1118	1133
FRONT	2747 lb	
REAR	2251 lb	
TOTAL	4998 lb	

Figure D-1. Vehicle Mass Distribution, Test No. RDTCB-1

Test: RDTCB-2

Vehicle: Ram 1500

**Vehicle CG Determination**

VEHICLE	Equipment	Weight (lb)	Vert CG (in.)	Vert M (lb-in.)
+	Unbalasted Truck (Curb)	4887	28.02182	136942.63
+	Brake receivers/wires	6	54	324
+	Brake Frame	6	28	168
+	Brake Cylinder (Nitrogen)	22	28	616
+	Strobe/Brake Battery	6	31	186
+	Hub	27	15.0625	406.6875
+	CG Plate (EDRs)	8	32	256
-	Battery	-47	42	-1974
-	Oil	-6	17	-102
-	Interior	-35	22	-770
-	Fuel	-165	21	-3465
-	Coolant	-14	36	-504
-	Washer fluid	0	41	0
BALLAST	Water	170	21	3570
	DTS	17	28	476
	Ballast (steel)	99	34	3366
				139496.31

Estimated Total Weight (lb)	4981
Vertical CG Location (in.)	28.00568

wheel base (in.) 140.25

MASH Targets	Targets	Test Inertial	Difference
Test Inertial Weight (lb)	5000 ± 110	4978	-22.0
Long CG (in.)	63 ± 4	64.60	1.60290
Lat CG (in.)	NA	-0.62548	NA
Vert CG (in.) ≥	28	28.01	0.00568

Note: Long. CG is measured from front axle of test vehicle

Note: Lateral CG measured from centerline - positive to vehicle right (passenger) side

CURB WEIGHT (lb)		
	Left	Right
Front	1401	1301
Rear	1080	1105
FRONT	2702 lb	
REAR	2185 lb	
TOTAL	4887 lb	

TEST INERTIAL WEIGHT (lb)		
(from scales)		
	Left	Right
Front	1394	1291
Rear	1141	1152
FRONT	2685 lb	
REAR	2293 lb	
TOTAL	4978 lb	

Figure D-2. Vehicle Mass Distribution, Test No. RDTCB-2

## **Appendix E. Vehicle Deformation Records**

VEHICLE PRE/POST CRUSH  
FLOORPAN - SET 1

TEST: RDTCB-1  
VEHICLE: 2270P

Note: If impact is on driver side need to enter negative number for Y

POINT	X (in.)	Y (in.)	Z (in.)	X' (in.)	Y' (in.)	Z' (in.)	ΔX (in.)	ΔY (in.)	ΔZ (in.)
1	25	17	-1 1/2	25	16 1/2	-1 1/4	0	- 1/2	1/4
2	26	20 1/4	-5 1/4	26 1/4	20 1/4	-5	1/4	0	1/4
3	26	24 1/2	-5 1/4	26	24	-5	0	- 1/2	1/4
4	26	29 3/4	-5 1/4	26	29 1/2	-5	0	- 1/4	1/4
5	21 1/2	15	-2 1/2	21 1/2	14 1/2	-2 1/4	0	- 1/2	1/4
6	23	19 1/4	-6 3/4	23 1/4	19 1/4	-6 3/4	1/4	0	0
7	23	24 3/4	-6 3/4	23 1/4	24 1/4	-6 3/4	1/4	- 1/2	0
8	23 1/4	30 3/4	-6 3/4	23 1/4	30 1/2	-6 3/4	0	- 1/4	0
9	18	10	-1 1/2	18	9 3/4	-1	0	- 1/4	1/2
10	18 3/4	14 1/4	-4 1/4	18 3/4	13 3/4	-4	0	- 1/2	1/4
11	20	19 3/4	-8 1/2	20	19 3/4	-8 1/4	0	0	1/4
12	20	24 3/4	-8 1/2	20	24 3/4	-8 1/4	0	0	1/4
13	20	29 1/2	-8 1/2	20	30	-8 1/2	0	1/2	0
14	13 3/4	8 1/4	-1 1/2	14	8 3/4	-1	1/4	1/2	1/2
15	17	16 1/4	-8 1/4	17	16 1/4	-8 1/4	0	0	0
16	16 1/2	23 3/4	-8 1/4	16 1/2	23 3/4	-8 1/4	0	0	0
17	16 1/2	30	-8 1/2	16 1/4	30	-8 1/2	- 1/4	0	0
18	10	8 1/2	-2	10 1/4	8 1/2	-1 3/4	1/4	0	1/4
19	10	13 3/4	-8 1/4	10	14	-8	0	1/4	1/4
20	10	18 3/4	-8 1/4	10	18 1/2	-8	0	- 1/4	1/4
21	10	24 1/2	-8 1/4	10	24 1/4	-8	0	- 1/4	1/4
22	10	29 1/2	-8 1/4	10	29 1/2	-8 1/4	0	0	0
23	1 1/2	8 1/2	-1 3/4	1 1/2	8 1/2	-1 1/4	0	0	1/2
24	1	14	-4 1/4	1	14	-4	0	0	1/4
25	3/4	19 1/2	-4 1/4	3/4	19	-4 1/4	0	- 1/2	0
26	3/4	24 3/4	-4 1/4	1	24 1/2	-4 1/4	1/4	- 1/4	0
27	1	29 1/4	-4 1/4	1	29	-4 1/4	0	- 1/4	0
28							0	0	0
29							0	0	0
30							0	0	0
31							0	0	0

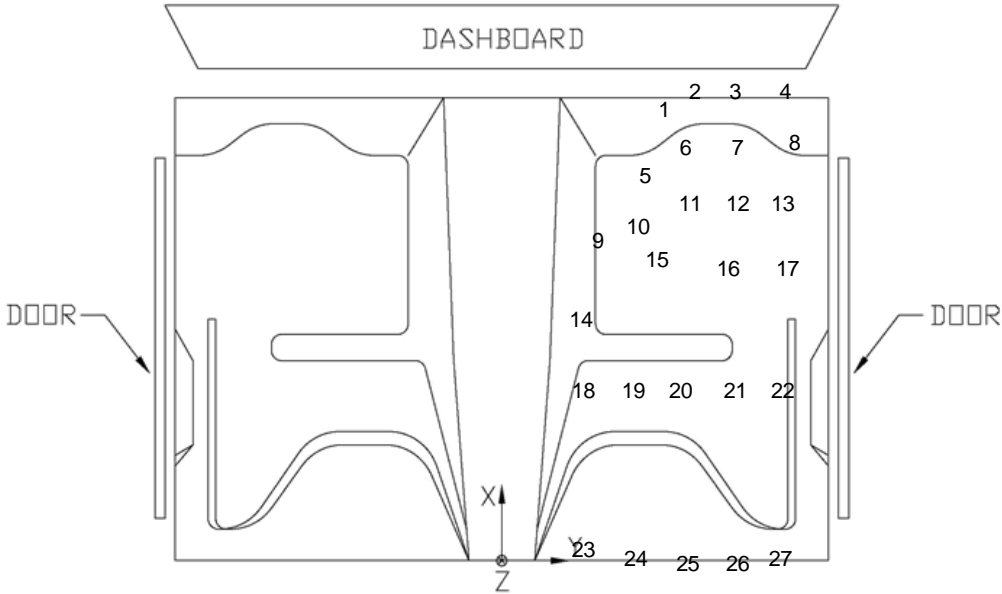


Figure E-1. Floor Pan Deformation Data – Set 1, Test No. RDTCB-1

VEHICLE PRE/POST CRUSH  
FLOORPAN - SET 2

TEST: RDTCB-1  
VEHICLE: 2270P

Note: If impact is on driver side need to enter negative number for Y

POINT	X (in.)	Y (in.)	Z (in.)	X' (in.)	Y' (in.)	Z' (in.)	ΔX (in.)	ΔY (in.)	ΔZ (in.)
1	41	21	-1	40 3/4	21	- 3/4	- 1/4	0	1/4
2	42 1/4	24 1/2	-4 1/2	42 1/4	24 1/4	-4 3/4	0	- 1/4	- 1/4
3	42 1/2	28 3/4	-4 3/4	42 1/4	28 3/4	-4 1/2	- 1/4	0	1/4
4	42 1/2	34	-4 3/4	42 1/4	34	-4 3/4	- 1/4	0	0
5	37 1/2	19	-2	37 1/4	19 1/2	-1 3/4	- 1/4	1/2	1/4
6	39 1/4	23 1/2	-6 1/4	39 1/2	24	-6 1/4	1/4	1/2	0
7	39 1/2	29 1/4	-6 1/4	39 1/2	29 1/4	-6 1/4	0	0	0
8	39 3/4	35 3/4	-6 1/2	39 1/2	35 1/2	-6 1/4	- 1/4	- 1/4	1/4
9	34	15	-1	33 3/4	14 1/2	- 3/4	- 1/4	- 1/2	1/4
10	35	19	-3 1/2	34 3/4	18 1/2	-3 1/2	- 1/4	- 1/2	0
11	36 1/4	24 1/2	-7 3/4	36 1/4	24	-7 3/4	0	- 1/2	0
12	36 1/2	29 1/4	-7 3/4	36 1/2	29 1/4	-7 3/4	0	0	0
13	36 1/2	34 1/4	-8	36 1/2	34 1/2	-8	0	1/4	0
14	29 3/4	13	-1	29 3/4	13	- 3/4	0	0	1/4
15	33 1/4	20 3/4	-7 3/4	33 1/4	20 3/4	-7 3/4	0	0	0
16	33	28 1/2	-7 3/4	32 3/4	28 3/4	-7 3/4	- 1/4	1/4	0
17	32 3/4	34 1/2	-8	32 3/4	34 1/2	-8	0	0	0
18	26	13 1/4	-1 1/2	26	13 1/4	-1 1/4	0	0	1/4
19	27	18 1/2	-7 3/4	27	18 1/4	-7 3/4	0	- 1/4	0
20	27	23 3/4	-7 3/4	27	23 1/4	-7 3/4	0	- 1/2	0
21	27	29	-7 3/4	27	29	-7 3/4	0	0	0
22	27	34 1/4	-7 3/4	27	34 1/4	-7 3/4	0	0	0
23	17 1/4	13	-1 1/4	17	13	-1	- 1/4	0	1/4
24	17	19	-4	17	18 1/2	-3 3/4	0	- 1/2	1/4
25	17	24 1/4	-4	17	23 3/4	-3 3/4	0	- 1/2	1/4
26	17	29 1/2	-4	17	29	-4	0	- 1/2	0
27	17	34 1/4	-4	17 1/4	33 3/4	-4	1/4	- 1/2	0
28							0	0	0
29							0	0	0
30							0	0	0
31							0	0	0

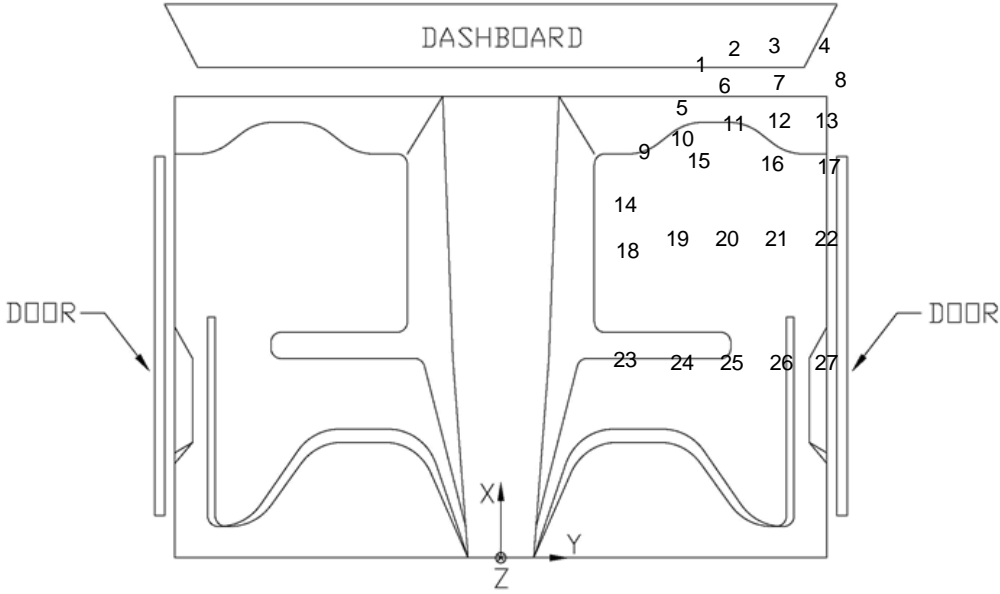


Figure E-2. Floor Pan Deformation Data – Set 2, Test No. RDTCB-1

VEHICLE PRE/POST CRUSH  
INTERIOR CRUSH - SET 1

TEST: RDTCB-1  
VEHICLE: 2270P

Note: If impact is on driver side need to enter negative number for Y

	POINT	X (in.)	Y (in.)	Z (in.)	X' (in.)	Y' (in.)	Z' (in.)	ΔX (in.)	ΔY (in.)	ΔZ (in.)	
DASH	A1	40 3/4	33 3/4	24 1/2	40 3/4	33 3/4	25	0	0	1/2	
	A2	39 1/4	46 3/4	22 1/4	39 1/2	47	22 3/4	1/4	1/4	1/2	
	A3	38 3/4	57	22 1/4	39	57	22	1/4	0	- 1/4	
	A4	32	37 1/2	14 1/4	32	37 1/2	14 1/2	0	0	1/4	
	A5	34	48	16	34	48 1/4	16 1/4	0	1/4	1/4	
	A6	34	58 1/2	16	34	58 3/4	16 1/4	0	1/4	1/4	
SIDE PANEL	B1	23 1/2	28	-3	23 1/2	27 3/4	-2 3/4	0	- 1/4	1/4	
	B2	21	27 1/2	- 1/4	21	27 1/4	- 1/4	0	- 1/4	0	
	B3	19 1/4	27 3/4	-2 3/4	19 1/2	27 1/4	-3	1/4	- 1/2	- 1/4	
IMPACT SIDE DOOR	C1	24	40 1/4	19	23 1/2	40	19	- 1/2	- 1/4	0	
	C2	14 1/2	41	19	14	41	19 1/2	- 1/2	0	1/2	
	C3	5 1/2	40 1/2	17 3/4	5	40 1/2	18	- 1/2	0	1/4	
	C4	23 1/4	34 1/4	3 1/4	23	35	3 1/2	- 1/4	3/4	1/4	
	C5	15 1/4	35 1/4	3 3/4	15	36 1/4	4	- 1/4	1	1/4	
	C6	7	35 1/2	3 3/4	6 3/4	36 1/4	4	- 1/4	3/4	1/4	
ROOF	D1							0	0	0	
	D2							0	0	0	
	D3							0	0	0	
	D4							0	0	0	
	D5							0	0	0	
	D6	Omitted due to low probability of damage							0	0	0
	D7							0	0	0	
	D8							0	0	0	
	D9							0	0	0	
	D10							0	0	0	
	D11							0	0	0	
	D12							0	0	0	
	D13							0	0	0	
	D14							0	0	0	
	D15							0	0	0	

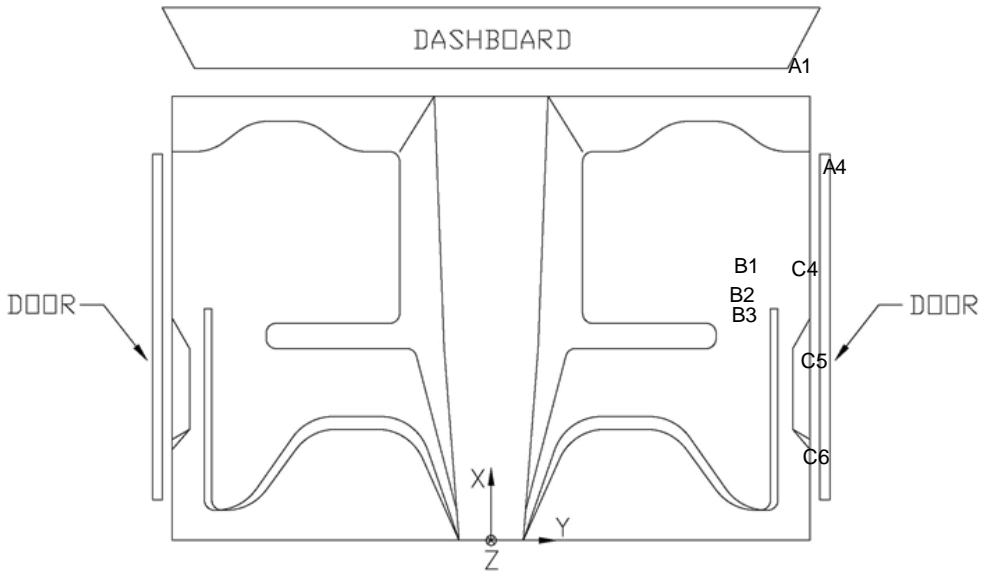


Figure E-3. Occupant Compartment Deformation Data – Set 1, Test No. RDTCB-1

VEHICLE PRE/POST CRUSH  
INTERIOR CRUSH - SET 2

TEST: RDTCB-1  
VEHICLE: 2270P

Note: If impact is on driver side need to enter negative number for Y

	POINT	X (in.)	Y (in.)	Z (in.)	X' (in.)	Y' (in.)	Z' (in.)	ΔX (in.)	ΔY (in.)	ΔZ (in.)	
DASH	A1	50 1/2	34 1/2	25	51	34 1/2	25	1/2	0	0	
	A2	52 3/4	47	23	52 1/2	47 1/4	23	- 1/4	1/4	0	
	A3	55 1/2	57	22 1/4	55 1/2	57	22 1/2	0	0	1/4	
	A4	43 1/2	38 3/4	15	43 1/2	38 3/4	14 3/4	0	0	- 1/4	
	A5	48 1/2	48 3/4	16 1/2	48 1/4	48 3/4	16 1/2	- 1/4	0	0	
	A6	51 1/2	59	16 1/2	51 3/4	59	16 1/2	1/4	0	0	
SIDE PANEL	B1	40 1/2	30	-2 1/4	40 1/4	29 3/4	-2 1/2	- 1/4	- 1/4	- 1/4	
	B2	37 3/4	29 1/4	0	37 3/4	29	0	0	- 1/4	0	
	B3	36 1/4	29	-2 1/4	36 1/4	28 3/4	-2 1/4	0	- 1/4	0	
IMPACT SIDE DOOR	C1	27 1/2	45 1/2	19 1/2	27 1/4	45 1/4	19 1/2	- 1/4	- 1/4	0	
	C2	18 1/4	45 3/4	19 1/2	18	46	19 3/4	- 1/4	1/4	1/4	
	C3	8 1/4	45 1/4	18 1/4	8 1/2	45 1/4	18 1/2	1/4	0	1/4	
	C4	28 1/2	40 1/2	3 3/4	28	41 1/4	3 3/4	- 1/2	3/4	0	
	C5	20 1/2	40 3/4	4	20 1/4	42	4 1/4	- 1/4	1 1/4	1/4	
	C6	12 1/4	40 3/4	4 1/4	11 3/4	41 1/2	4 1/2	- 1/2	3/4	1/4	
ROOF	D1							0	0	0	
	D2							0	0	0	
	D3							0	0	0	
	D4							0	0	0	
	D5							0	0	0	
	D6	Omitted due to low probability of damage.							0	0	0
	D7							0	0	0	
	D8							0	0	0	
	D9							0	0	0	
	D10							0	0	0	
	D11							0	0	0	
	D12							0	0	0	
	D13							0	0	0	
	D14							0	0	0	
	D15							0	0	0	

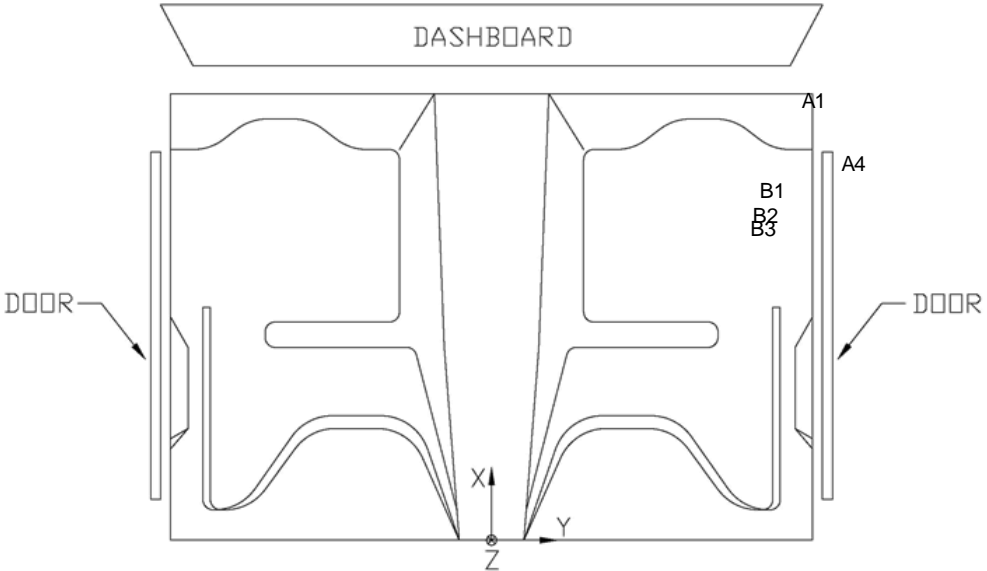


Figure E-4. Occupant Compartment Deformation Data – Set 2, Test No. RDTCB-1

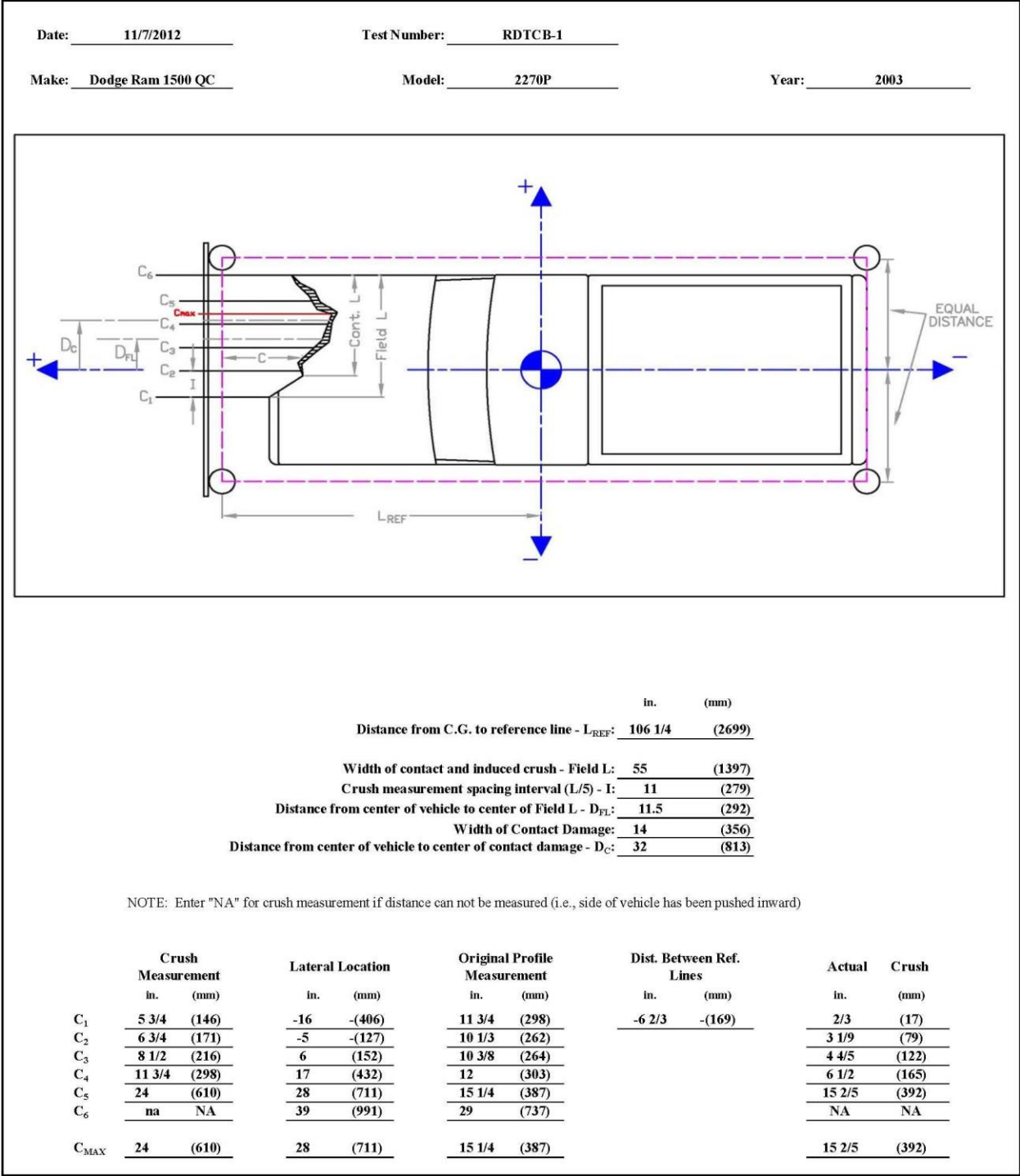


Figure E-5. Exterior Vehicle Crush (NASS) – Front, Test No. RDTCB-1

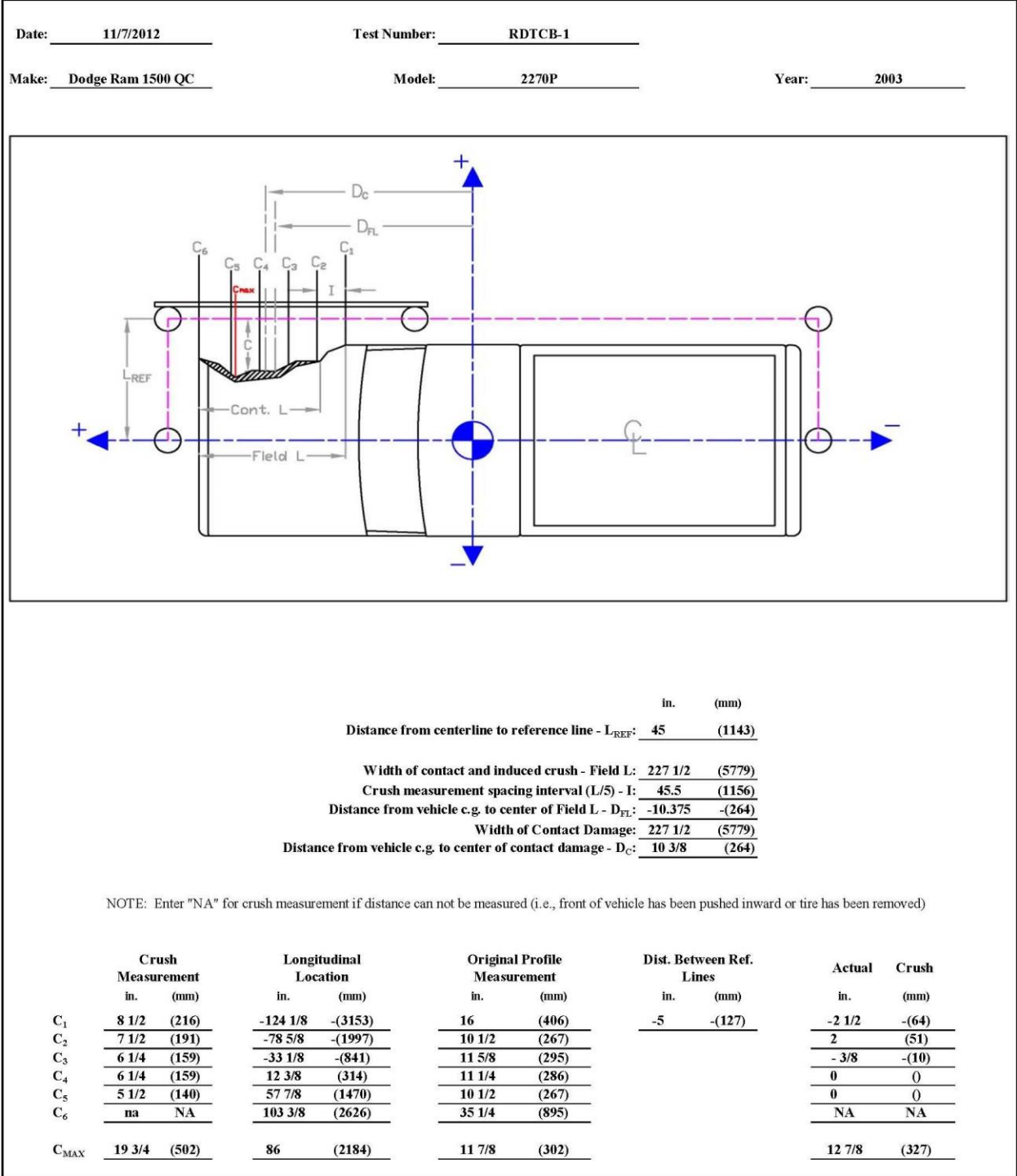


Figure E-6. Exterior Vehicle Crush (NASS) – Side, Test No. RDTCB-1

VEHICLE PRE/POST CRUSH  
FLOORPAN - SET 1

TEST: RDTCB-2  
VEHICLE: Ram 1500

Note: If impact is on driver side need to enter negative number for Y

POINT	X (in.)	Y (in.)	Z (in.)	X' (in.)	Y' (in.)	Z' (in.)	ΔX (in.)	ΔY (in.)	ΔZ (in.)
1	24 1/2	14 1/4	0	24 1/4	14 1/2	1/2	- 1/4	1/4	1/2
2	25	17 1/2	-2 1/4	24 3/4	17 1/4	-1 3/4	- 1/4	- 1/4	1/2
3	26 1/2	22	-4 3/4	26 1/2	21 1/4	-4 1/2	0	- 3/4	1/4
4	26	28 1/2	-5 1/2	26	28	-5	0	- 1/2	1/2
5	21 1/4	13 1/4	-1 1/2	21	13 1/2	- 3/4	- 1/4	1/4	3/4
6	22	17 1/4	-4 1/4	22	16 3/4	-4	0	- 1/2	1/4
7	23 1/4	21 1/4	-6 1/2	23 1/2	21	-6 1/4	1/4	- 1/4	1/4
8	23 1/2	29 1/4	-6 3/4	23 1/2	29	-6 1/2	0	- 1/4	1/4
9	12 3/4	5	- 3/4	13	5	- 1/2	1/4	0	1/4
10	15 1/4	11 3/4	-4 1/4	15 1/4	11 1/4	-4	0	- 1/2	1/4
11	17	16 1/2	-8	17	15 1/2	-7 3/4	0	-1	1/4
12	16 3/4	21 3/4	-8 1/4	17	21 1/2	-8	1/4	- 1/4	1/4
13	17	26 1/4	-8 1/2	17	26	-8	0	- 1/4	1/2
14	16 3/4	30 1/2	-8 3/4	17	30	-8 1/2	1/4	- 1/2	1/4
15	9 1/2	4 1/4	-1 1/4	9 1/2	4 1/4	-1	0	0	1/4
16	13	14 1/4	-8	13	13 1/4	-7 3/4	0	-1	1/4
17	13 1/4	20 3/4	-8 1/4	13 1/4	20 1/4	-8	0	- 1/2	1/4
18	14	28 1/2	-8 3/4	14	28 1/4	-8 1/2	0	- 1/4	1/4
19	6 1/2	5	-1 1/4	6 1/2	5	-1	0	0	1/4
20	7	14	-7 3/4	7	13 1/4	-7 1/2	0	- 3/4	1/4
21	7 1/4	19 3/4	-8	7 1/4	19	-7 3/4	0	- 3/4	1/4
22	7 1/4	25 1/2	-8 1/4	7	25	-8 1/4	- 1/4	- 1/2	0
23	10 1/4	28 3/4	-8 1/2	10	30	-8 1/4	- 1/4	1 1/4	1/4
24	1 1/2	3 1/4	- 3/4	1 1/4	3 1/4	- 1/2	- 1/4	0	1/4
25	1 1/4	8 3/4	-1	1 1/4	8 3/4	- 1/2	0	0	1/2
26	3/4	14 3/4	-3 3/4	3/4	14 1/4	-3 1/2	0	- 1/2	1/4
27	3/4	22	-4	3/4	22	-3 3/4	0	0	1/4
28	1	29	-4 1/2	1	29	-4 1/4	0	0	1/4
29							0	0	0
30							0	0	0
31							0	0	0

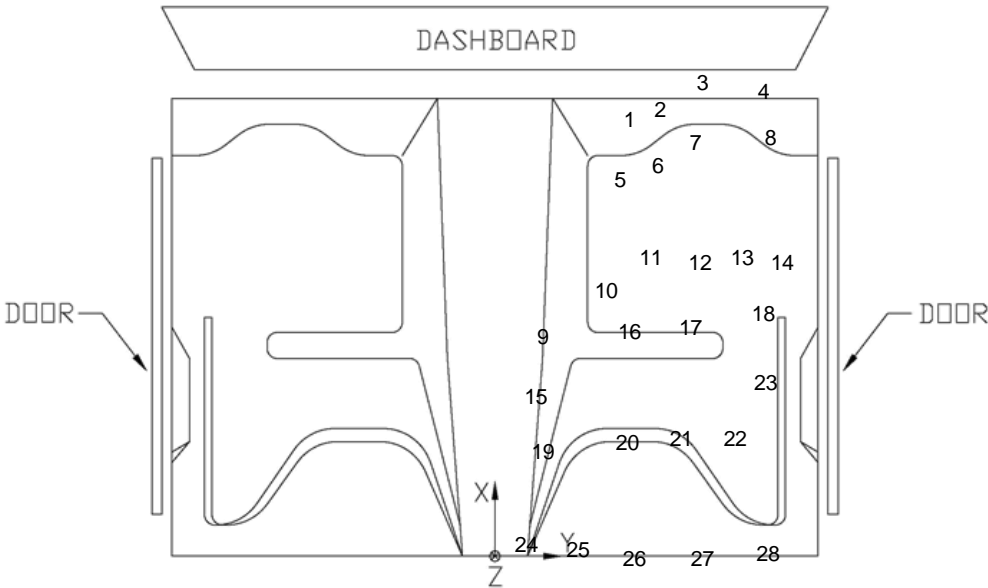


Figure E-7. Floor Pan Deformation Data – Set 1, Test No. RDTCB-2

VEHICLE PRE/POST CRUSH  
FLOORPAN - SET 2

TEST: RDTCB-2  
VEHICLE: Ram 1500

Note: If impact is on driver side need to enter negative number for Y

POINT	X (in.)	Y (in.)	Z (in.)	X' (in.)	Y' (in.)	Z' (in.)	ΔX (in.)	ΔY (in.)	ΔZ (in.)
1	40 1/2	19 1/2	- 1/4	40 1/4	19 1/2	3/4	- 1/4	0	1
2	41	22 3/4	-2 1/4	41	22 1/4	-1 3/4	0	- 1/2	1/2
3	42 3/4	27	-4 3/4	42 3/4	26	-4 1/4	0	-1	1/2
4	42 1/4	33 1/2	-5 1/4	42 1/4	32 3/4	-4 3/4	0	- 3/4	1/2
5	37 1/4	18 3/4	-1 1/2	37	18 1/2	-1	- 1/4	- 1/4	1/2
6	38 1/4	22 1/4	-4 1/4	38	22	-3 3/4	- 1/4	- 1/4	1/2
7	39 3/4	26 3/4	-6 1/2	39 3/4	26	-6	0	- 3/4	1/2
8	39 3/4	34 1/2	-6 1/2	39 3/4	33 1/4	-6 1/4	0	-1 1/4	1/4
9	29	10 1/4	-1	29	10	- 3/4	0	- 1/4	1/4
10	31 3/4	17	-4 1/2	31 1/2	16 1/4	-4	- 1/4	- 3/4	1/2
11	33 1/4	21 3/4	-8	33 1/4	21 1/4	-7 3/4	0	- 1/2	1/4
12	33 1/4	27	-8 1/4	33 1/4	26 1/4	-7 3/4	0	- 3/4	1/2
13	33 1/4	31 1/4	-8 1/4	33 1/4	30 3/4	-8	0	- 1/2	1/4
14	33 1/4	35 1/2	-8 1/2	33 1/4	35	-8 1/4	0	- 1/2	1/4
15	25 3/4	9 1/2	-1 3/4	25 3/4	9 1/2	-1 1/2	0	0	1/4
16	29 1/4	19	-8 1/4	29 1/4	18 1/2	-7 3/4	0	- 1/2	1/2
17	29 1/2	25 3/4	-8 1/4	29 1/2	25 1/4	-8	0	- 1/2	1/4
18	30 1/4	33 1/4	-8 1/2	30	33 1/4	-8 1/4	- 1/4	0	1/4
19	22 3/4	10	-1 3/4	22 3/4	10	-1 1/4	0	0	1/2
20	23 1/2	19	-8	23 1/4	18 3/4	-7 3/4	- 1/4	- 1/4	1/4
21	23 1/2	24 3/4	-8 1/4	23 1/2	24	-8	0	- 3/4	1/4
22	23 1/2	30 1/2	-8 1/4	23 1/4	30 1/4	-8 1/4	- 1/4	- 1/4	0
23	26 3/4	36 1/4	-8 1/2	26 1/2	35 1/2	-8 1/4	- 1/4	- 3/4	1/4
24	17 1/2	8 1/2	-1 1/2	17 1/2	8 1/2	-1	0	0	1/2
25	17 1/2	14	-1 1/2	17 1/2	14	- 3/4	0	0	3/4
26	17	19 3/4	-4	17	19 3/4	-3 1/2	0	0	1/2
27	17	27 1/4	-4	17	27 1/4	-4	0	0	0
28	17	34	-4 1/2	17	33 3/4	-4 1/4	0	- 1/4	1/4
29							0	0	0
30							0	0	0
31							0	0	0

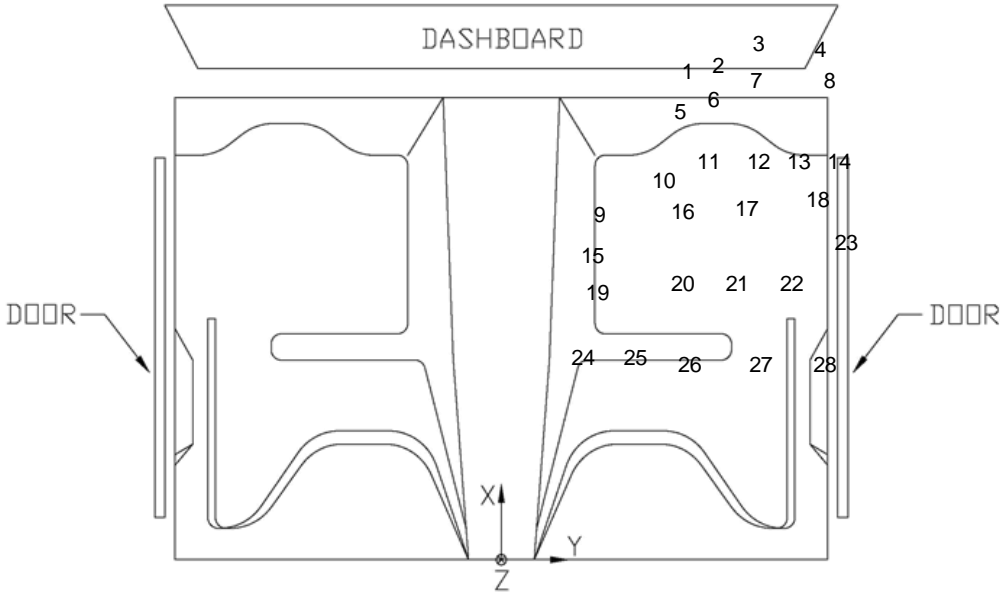


Figure E-8. Floor Pan Deformation Data – Set 2, Test No. RDTCB-2

VEHICLE PRE/POST CRUSH  
INTERIOR CRUSH - SET 1

TEST: RDTCB-2  
VEHICLE: Ram 1500

Note: If impact is on driver side need to enter negative number for Y

	POINT	X (in.)	Y (in.)	Z (in.)	X' (in.)	Y' (in.)	Z' (in.)	ΔX (in.)	ΔY (in.)	ΔZ (in.)
DASH	A1	40	30 1/2	25 3/4	40 1/4	30 1/2	25 3/4	1/4	0	0
	A2	40	43 1/2	22 3/4	40	43 1/2	23 1/2	0	0	3/4
	A3	40 1/4	56 1/4	22 1/4	40 3/4	56 1/4	22 3/4	1/2	0	1/2
	A4	35 1/2	32	20	35 1/2	31 3/4	20	0	- 1/4	0
	A5	34 1/4	46 1/2	16 1/2	34 1/2	46 1/4	16 3/4	1/4	- 1/4	1/4
	A6	34 1/2	58 1/2	16	34 3/4	58 1/4	16 1/4	1/4	- 1/4	1/4
SIDE PANEL	B1	23 3/4	26 1/2	-2 1/4	23 3/4	25 3/4	-2	0	- 3/4	1/4
	B2	20 3/4	26	-1 3/4	20 1/2	25	-1 1/2	- 1/4	-1	1/4
	B3	21 1/4	26 1/4	-4 3/4	21	25 1/2	-4 1/2	- 1/4	- 3/4	1/4
IMPACT SIDE DOOR	C1	24 1/4	40	18 3/4	23 1/2	40	18 3/4	- 3/4	0	0
	C2	16 3/4	36 1/2	18 3/4	16	37	19	- 3/4	1/2	1/4
	C3	8 1/4	38	19 1/2	7 1/4	38	19 1/2	-1	0	0
	C4	22 1/4	33 3/4	3	21 3/4	34 1/4	3 1/4	- 1/2	1/2	1/4
	C5	18 1/4	30 3/4	5	17 1/4	31 1/2	5 1/4	-1	3/4	1/4
	C6	7 1/2	31	3 3/4	6 1/2	32	4	-1	1	1/4
ROOF	D1							0	0	0
	D2							0	0	0
	D3							0	0	0
	D4							0	0	0
	D5							0	0	0
	D6							0	0	0
	D7							0	0	0
	D8							0	0	0
	D9							0	0	0
	D10							0	0	0
	D11							0	0	0
	D12							0	0	0
	D13							0	0	0
	D14							0	0	0
	D15							0	0	0

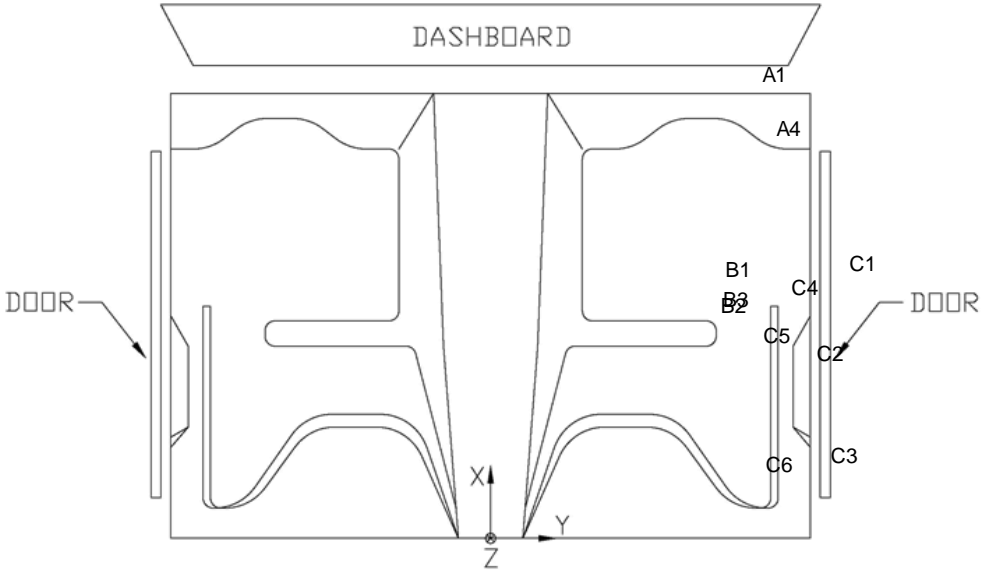


Figure E-9. Occupant Compartment Deformation Data – Set 1, Test No. RDTCB-2

VEHICLE PRE/POST CRUSH  
INTERIOR CRUSH - SET 2

TEST: RDTCB-2  
VEHICLE: Ram 1500

Note: If impact is on driver side need to enter negative number for Y

	POINT	X (in.)	Y (in.)	Z (in.)	X' (in.)	Y' (in.)	Z' (in.)	ΔX (in.)	ΔY (in.)	ΔZ (in.)
DASH	A1	49 1/2	29 1/2	25 1/4	49 3/4	29 1/2	25	1/4	0	- 1/4
	A2	53	42 3/4	23	53	42 1/2	23	0	- 1/4	0
	A3	56 1/2	56 1/4	22 1/2	56 1/2	56	23	0	- 1/4	1/2
	A4	45 3/4	30 3/4	19 1/2	46	30 1/2	19 3/4	1/4	- 1/4	1/4
	A5	48 1/2	45 1/2	16 1/4	48 1/2	45 1/2	16 1/2	0	0	1/4
	A6	51 3/4	58	16 1/4	51 3/4	58	16 1/2	0	0	1/4
SIDE PANEL	B1	40 1/4	31 1/4	-2	40	30 1/2	-1 3/4	- 1/4	- 3/4	1/4
	B2	37	30 1/4	-1 3/4	37	29 1/4	-1 1/4	0	-1	1/2
	B3	37 3/4	30	-4 1/2	37 3/4	30	-4 1/4	0	0	1/4
IMPACT SIDE DOOR	C1	27 3/4	46	18 1/2	27	46	19 1/2	- 3/4	0	1
	C2	20 1/4	46 1/4	18 3/4	19 1/2	46 1/2	19 1/2	- 3/4	1/4	3/4
	C3	11 3/4	46 1/2	19 1/4	10 3/4	47	19 1/2	-1	1/2	1/4
	C4	27 3/4	41	3	27	41 1/2	4	- 3/4	1/2	1
	C5	23 1/4	41 1/2	5	23	42 1/2	5 3/4	- 1/4	1	3/4
	C6	12 3/4	41 1/2	3 3/4	12 1/4	42 1/2	4	- 1/2	1	1/4
ROOF	D1							0	0	0
	D2							0	0	0
	D3							0	0	0
	D4							0	0	0
	D5							0	0	0
	D6							0	0	0
	D7							0	0	0
	D8							0	0	0
	D9							0	0	0
	D10							0	0	0
	D11							0	0	0
	D12							0	0	0
	D13							0	0	0
	D14							0	0	0
	D15							0	0	0

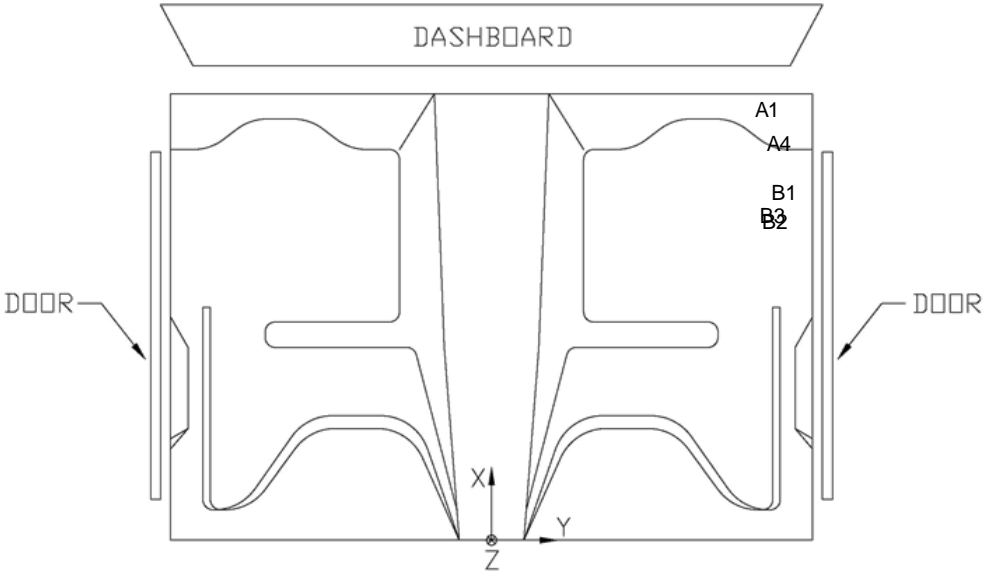


Figure E-10. Occupant Compartment Deformation Data – Set 2, Test No. RDTCB-2

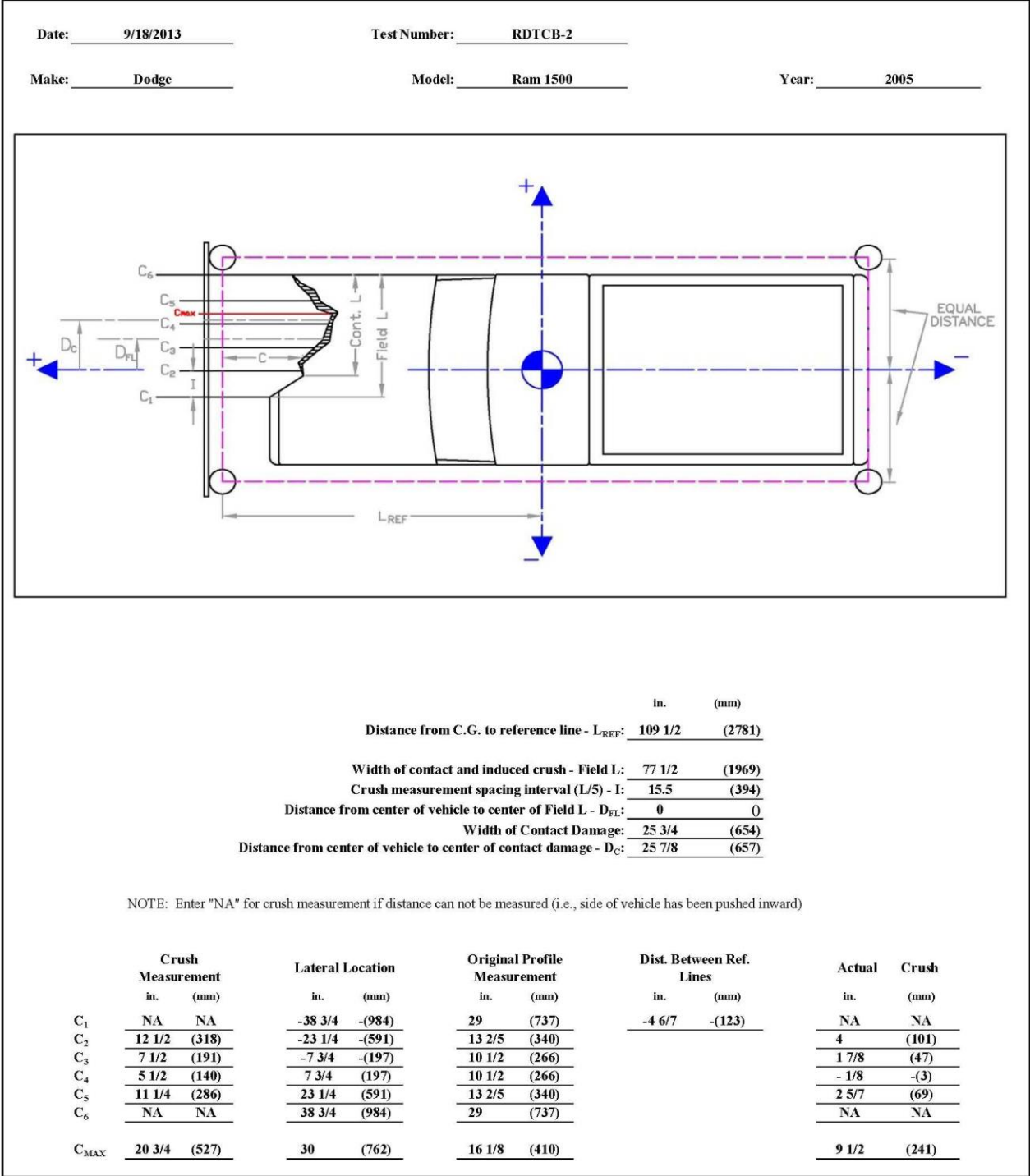


Figure E-11. Exterior Vehicle Crush (NASS) – Front, Test No. RDTCB-2

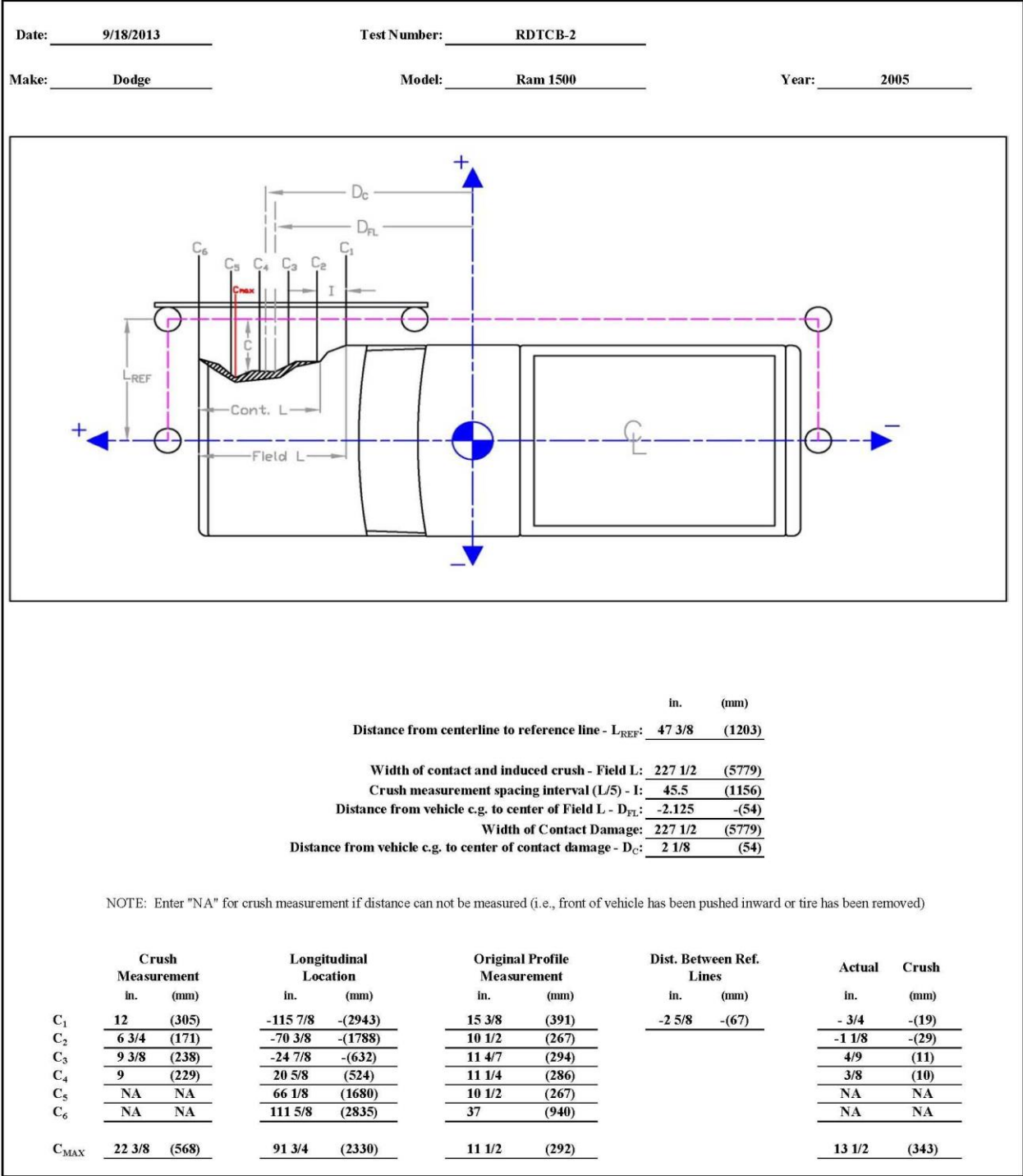


Figure E-12. Exterior Vehicle Crush (NASS) – Side, Test No. RDTCB-2

**Appendix F. Accelerometer and Rate Transducer Data Plots, Test No. RDTCB-1**

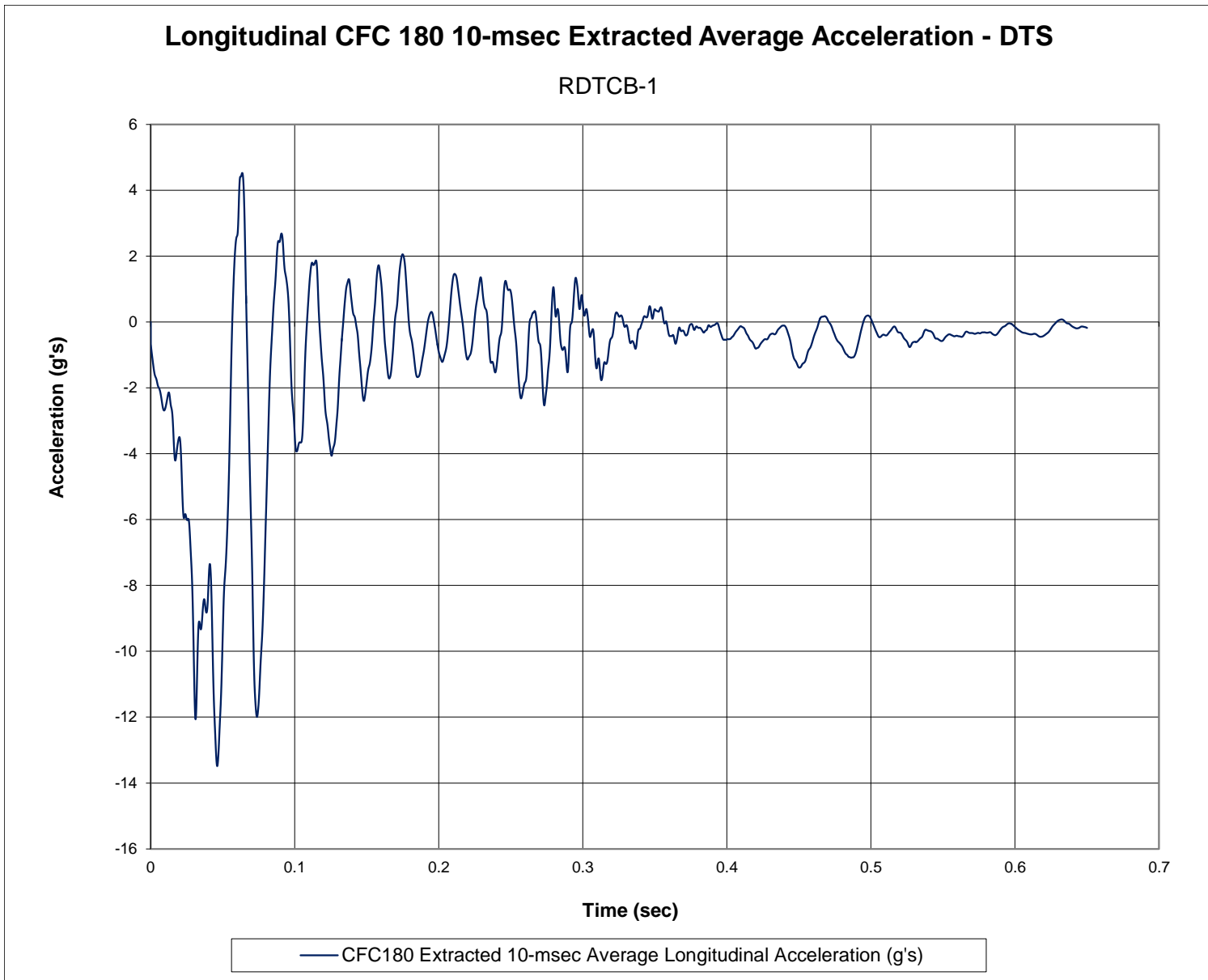


Figure F-1. 10-ms Average Longitudinal Deceleration (DTS), Test No. RDTCB-1

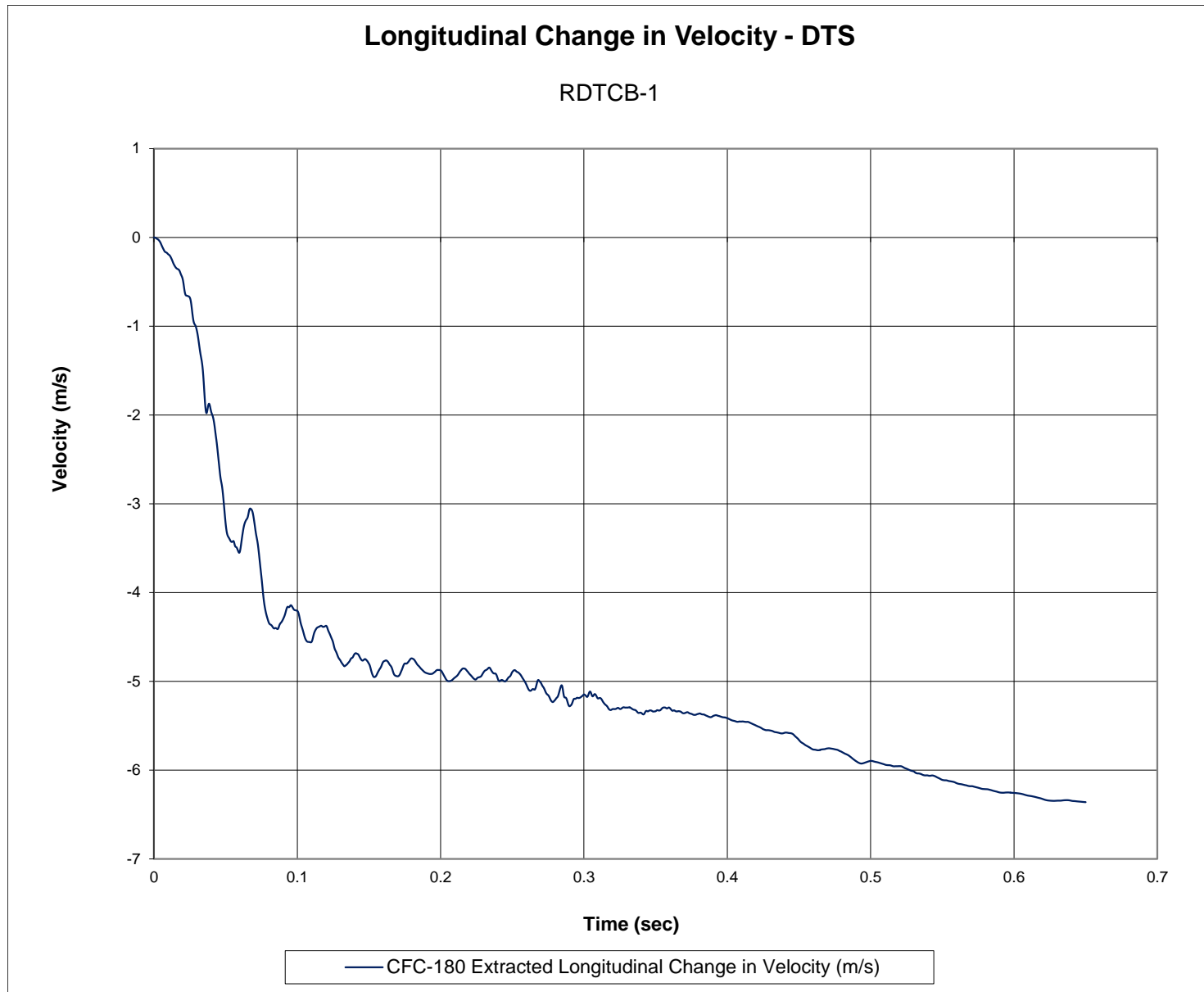


Figure F-2. Longitudinal Change in Velocity (DTS), Test No. RDTCB-1

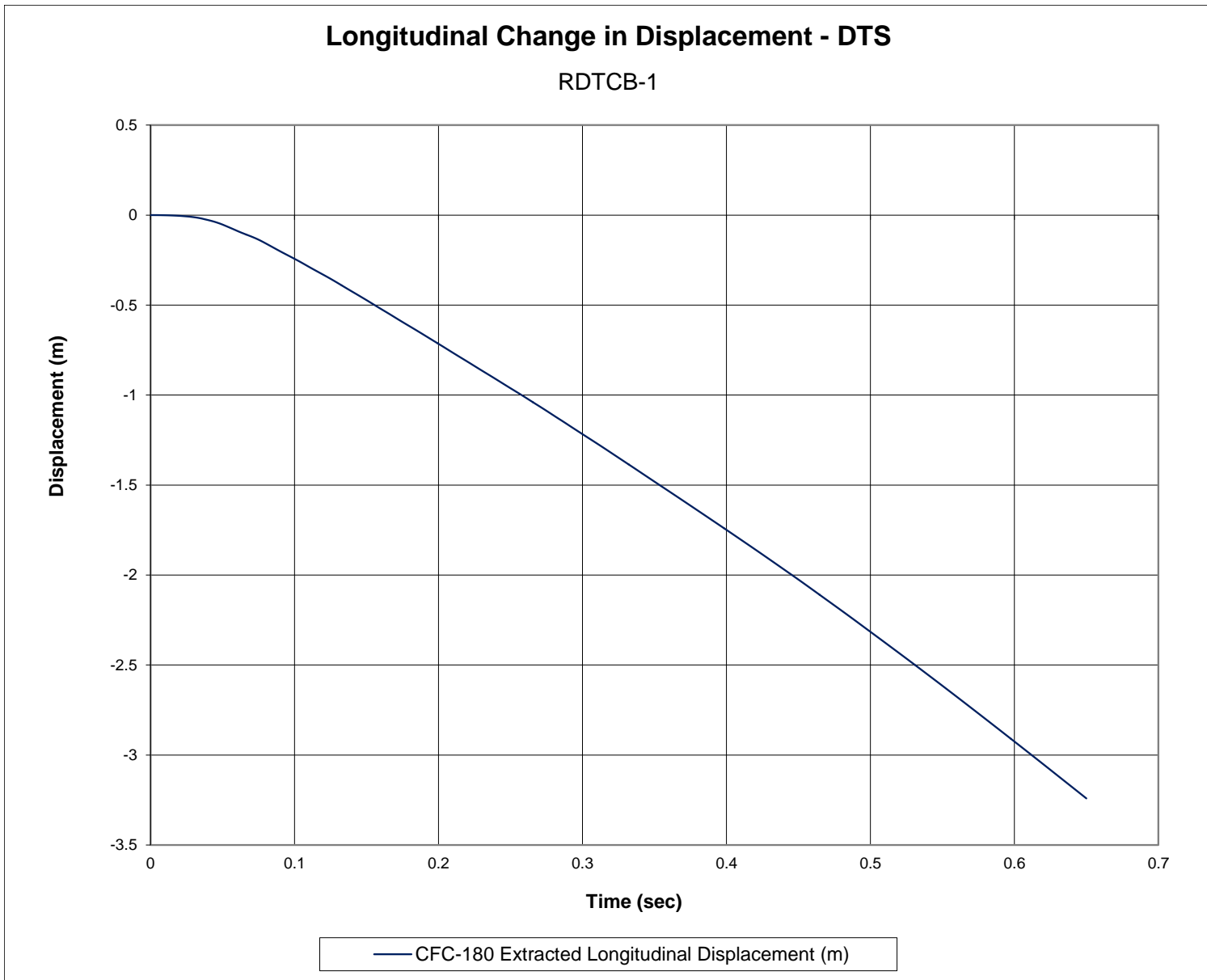


Figure F-3. Longitudinal Change in Displacement (DTS), Test No. RDTCB-1

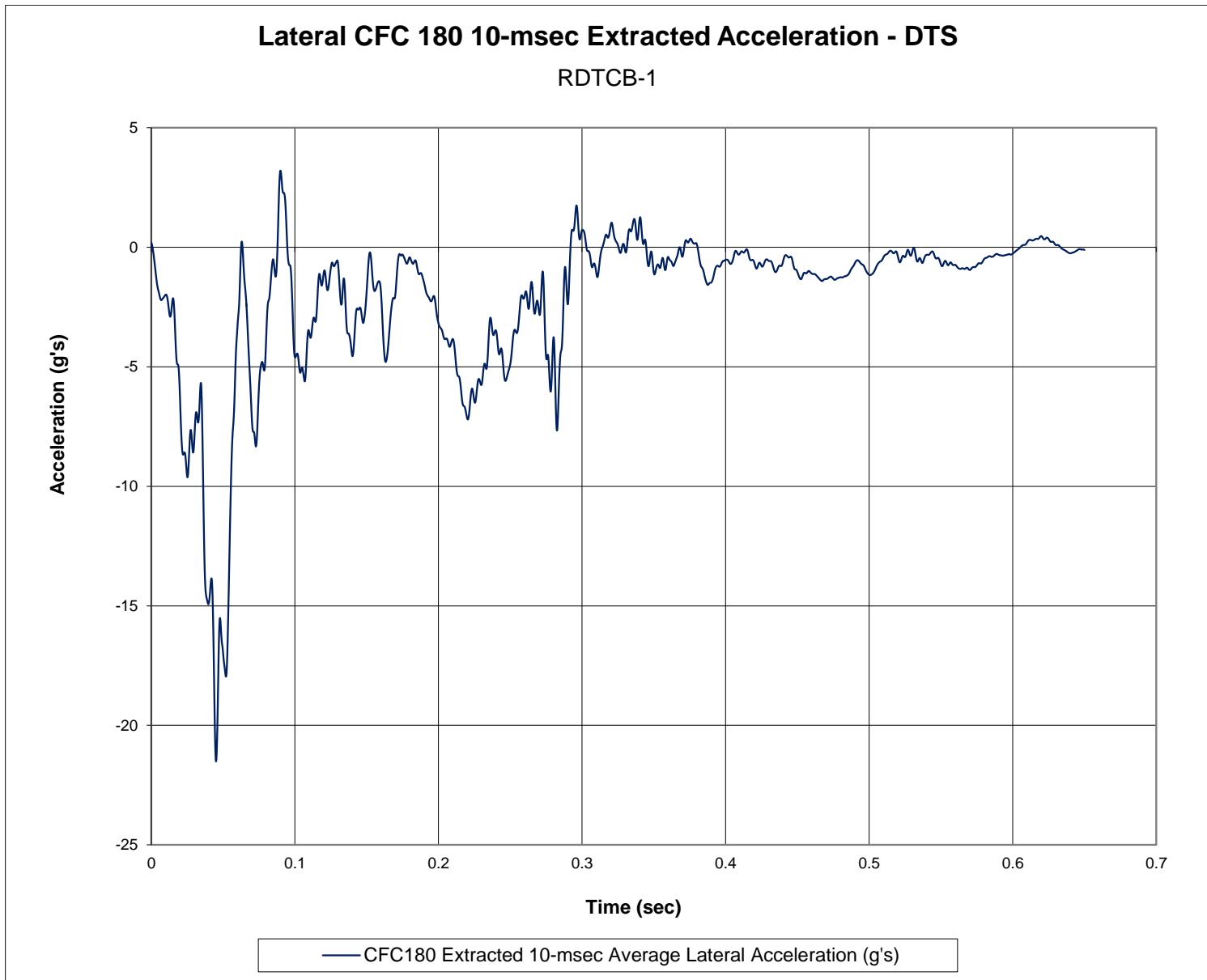


Figure F-4. 10-ms Average Lateral Deceleration (DTS), Test No. RDTCB-1

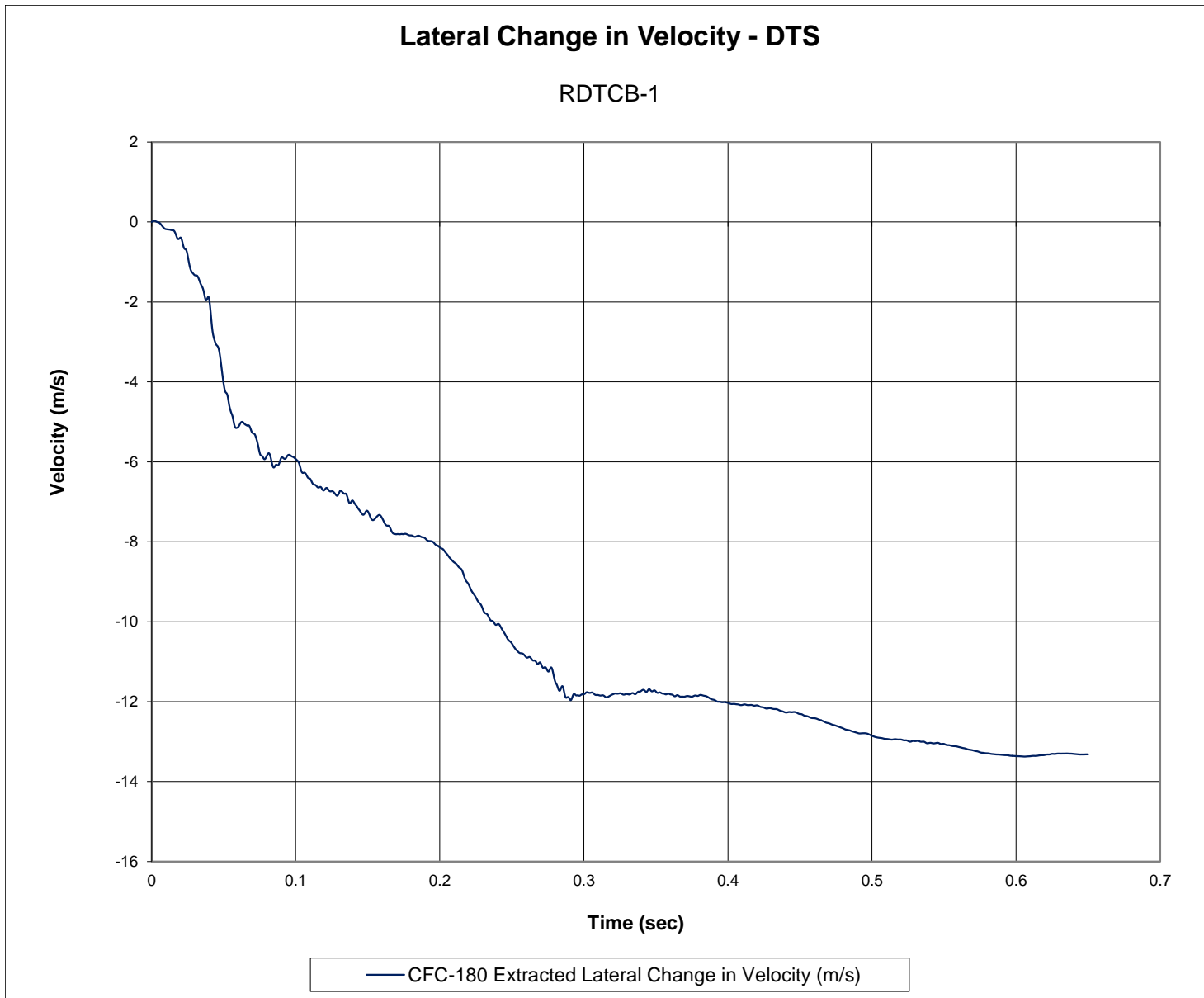


Figure F-5. Lateral Change in Velocity (DTS), Test No. RDTCB-1

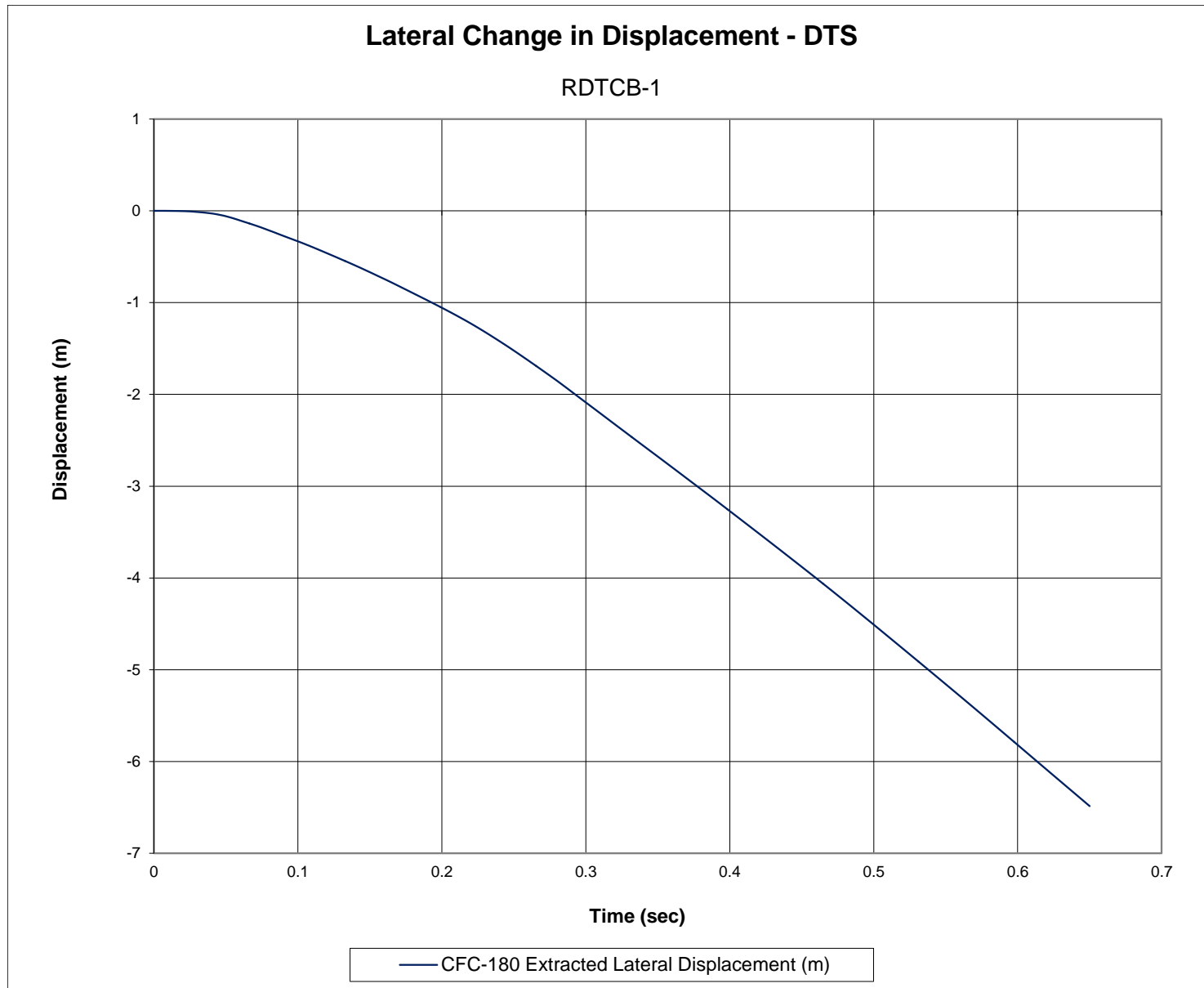


Figure F-6. Lateral Occupant Displacement (DTS), Test No. RDTCB-1

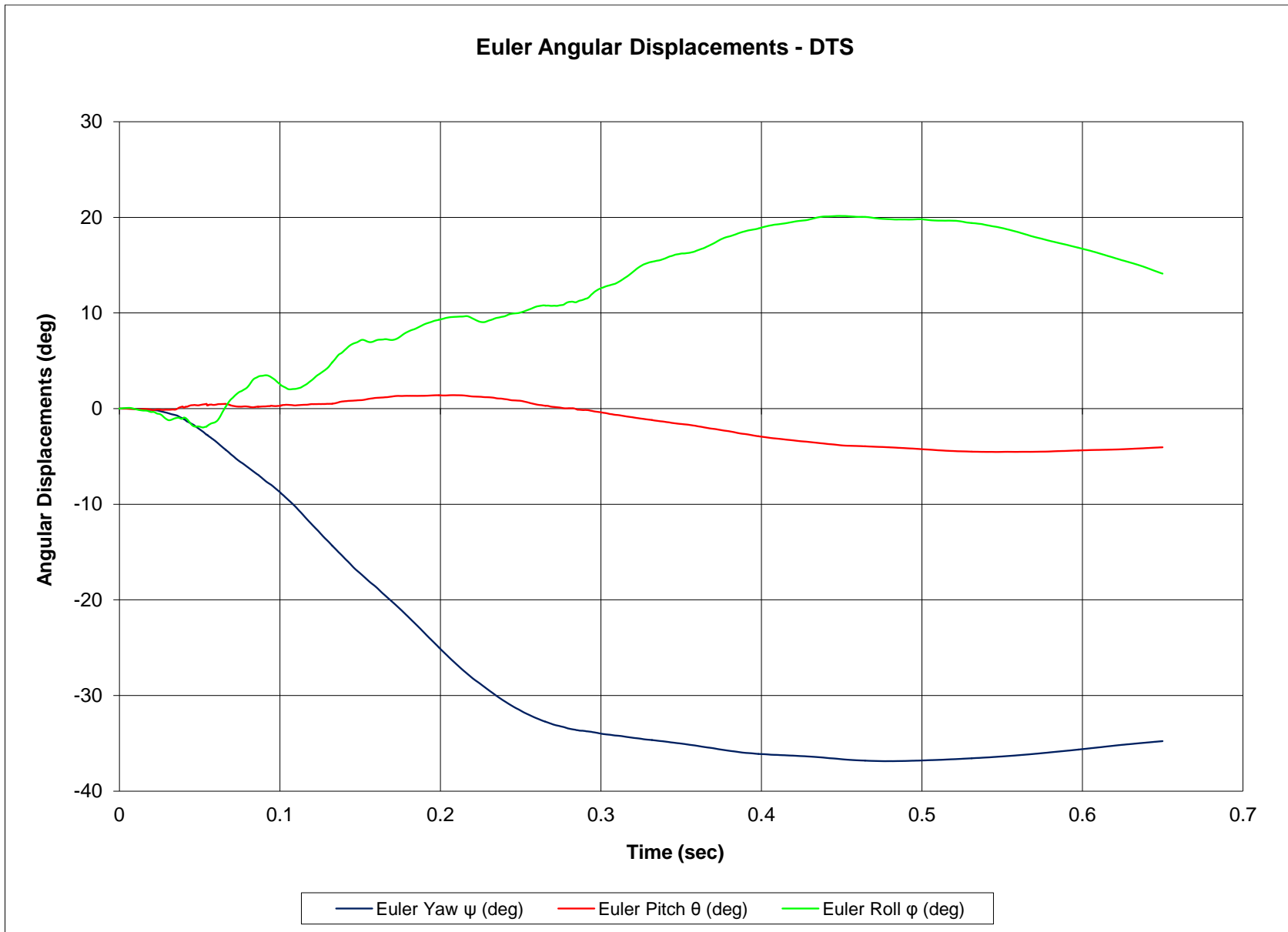


Figure F-7. Vehicle Angular Displacements (DTS), Test No. RDTCB-1

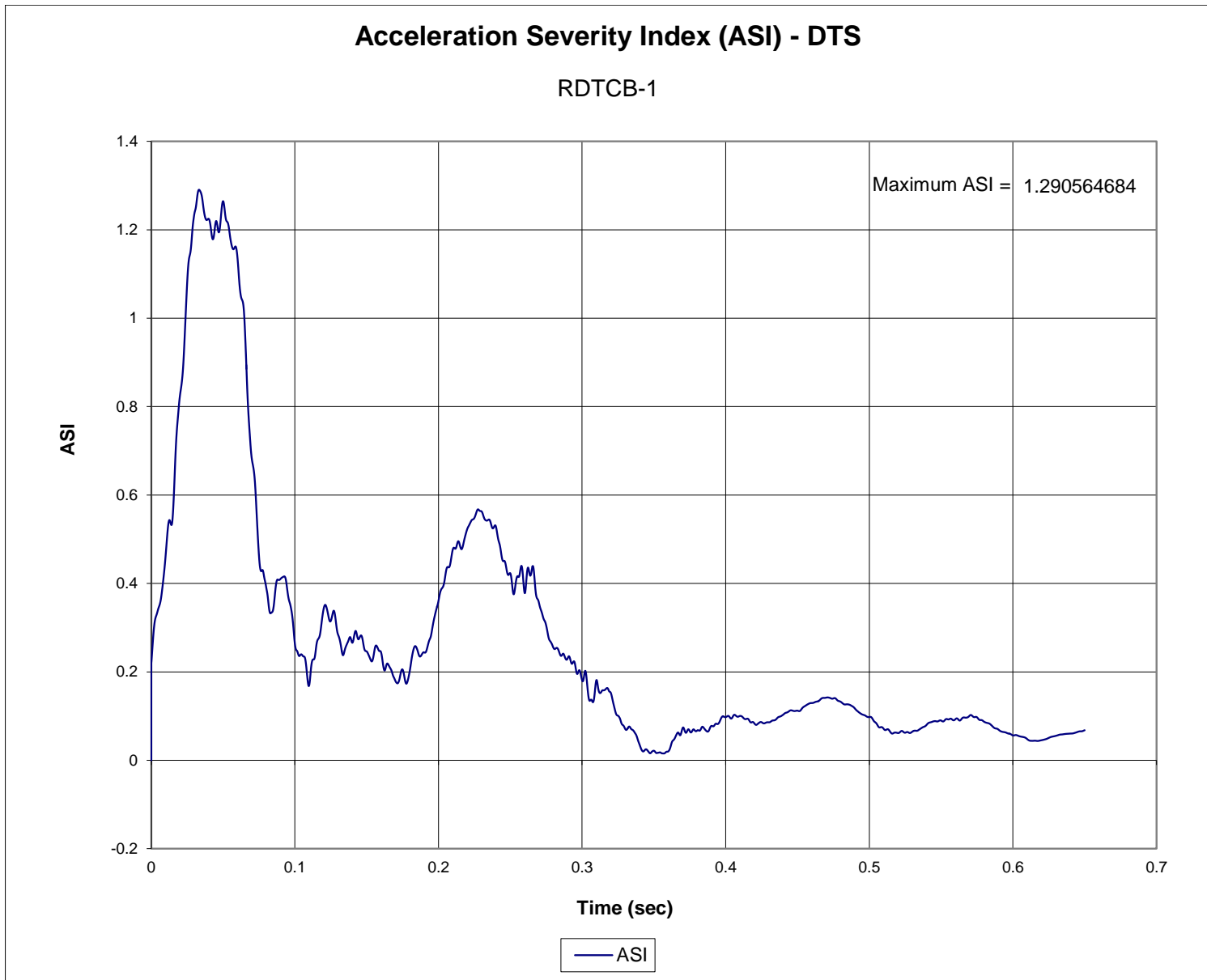


Figure F-8. Acceleration Severity Index (DTS), Test No. RDTCB-1

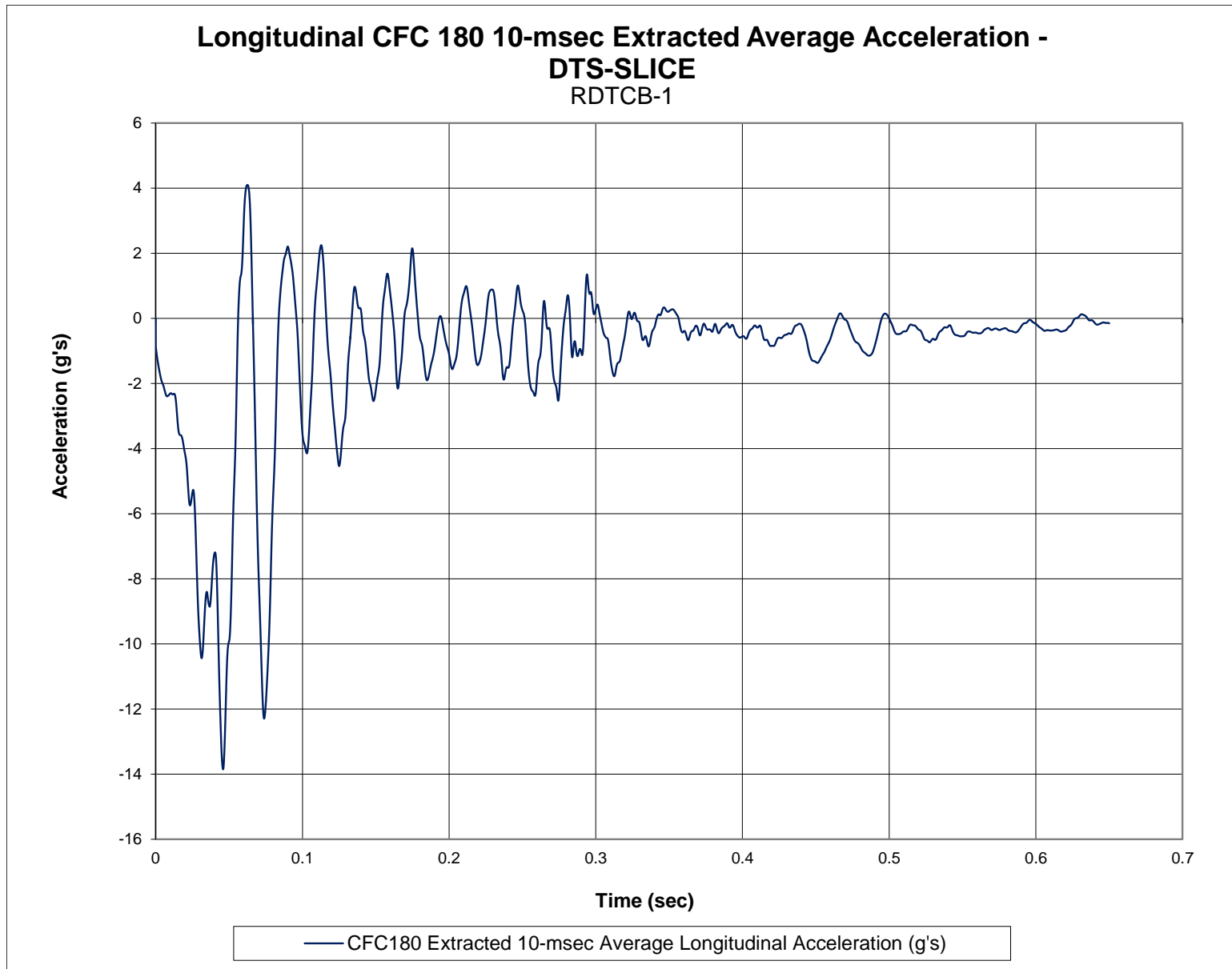


Figure F-9. 10-ms Average Longitudinal Deceleration (DTS-SLICE), Test No. RDTCB-1

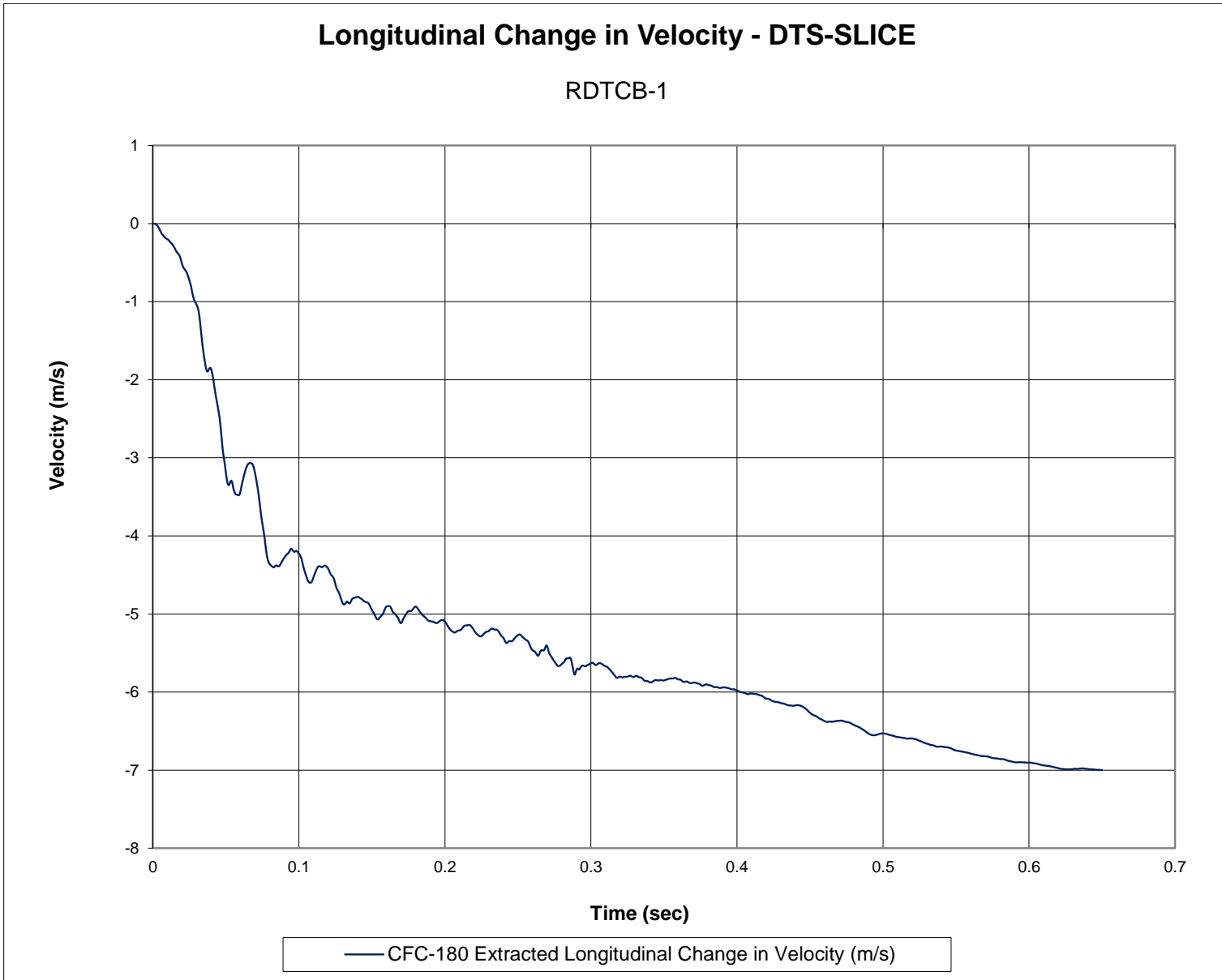


Figure F-10. Longitudinal Change in Velocity (DTS-SLICE), Test No. RDTCB-1

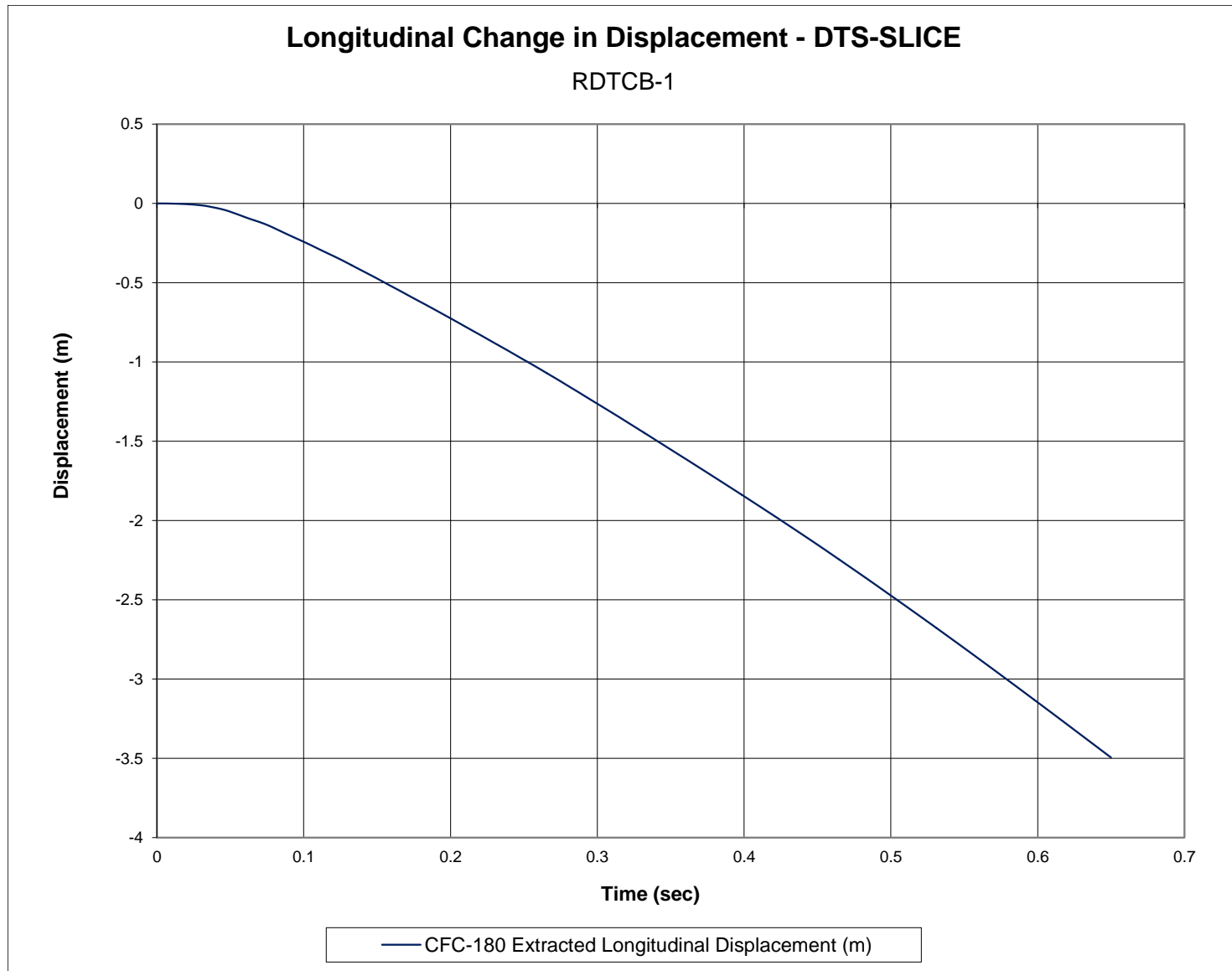


Figure F-11. Longitudinal Change in Displacement (DTS-SLICE), Test No. RDTCB-1

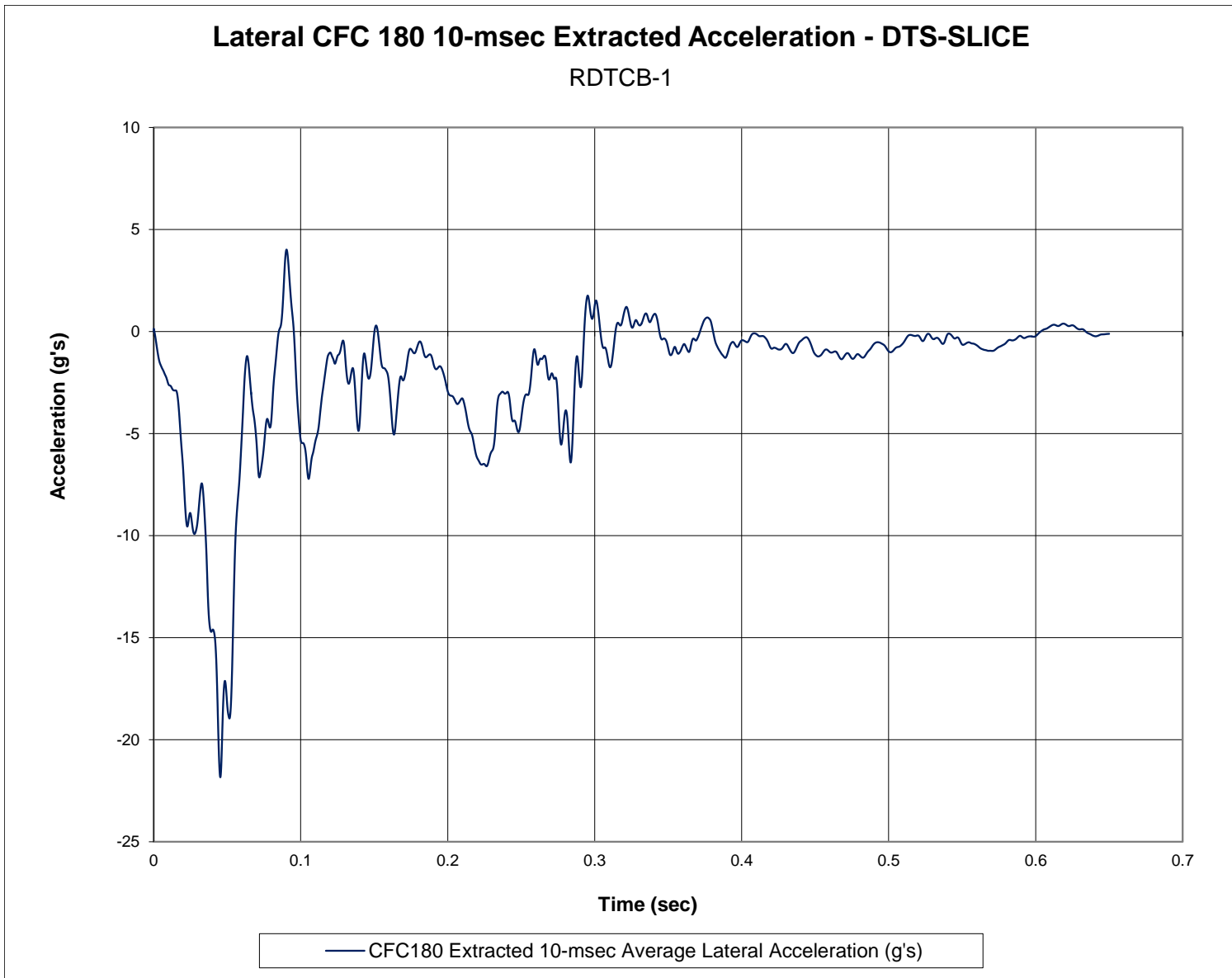


Figure F-12. 10-ms Average Lateral Deceleration (DTS-SLICE), Test No. RDTCB-1

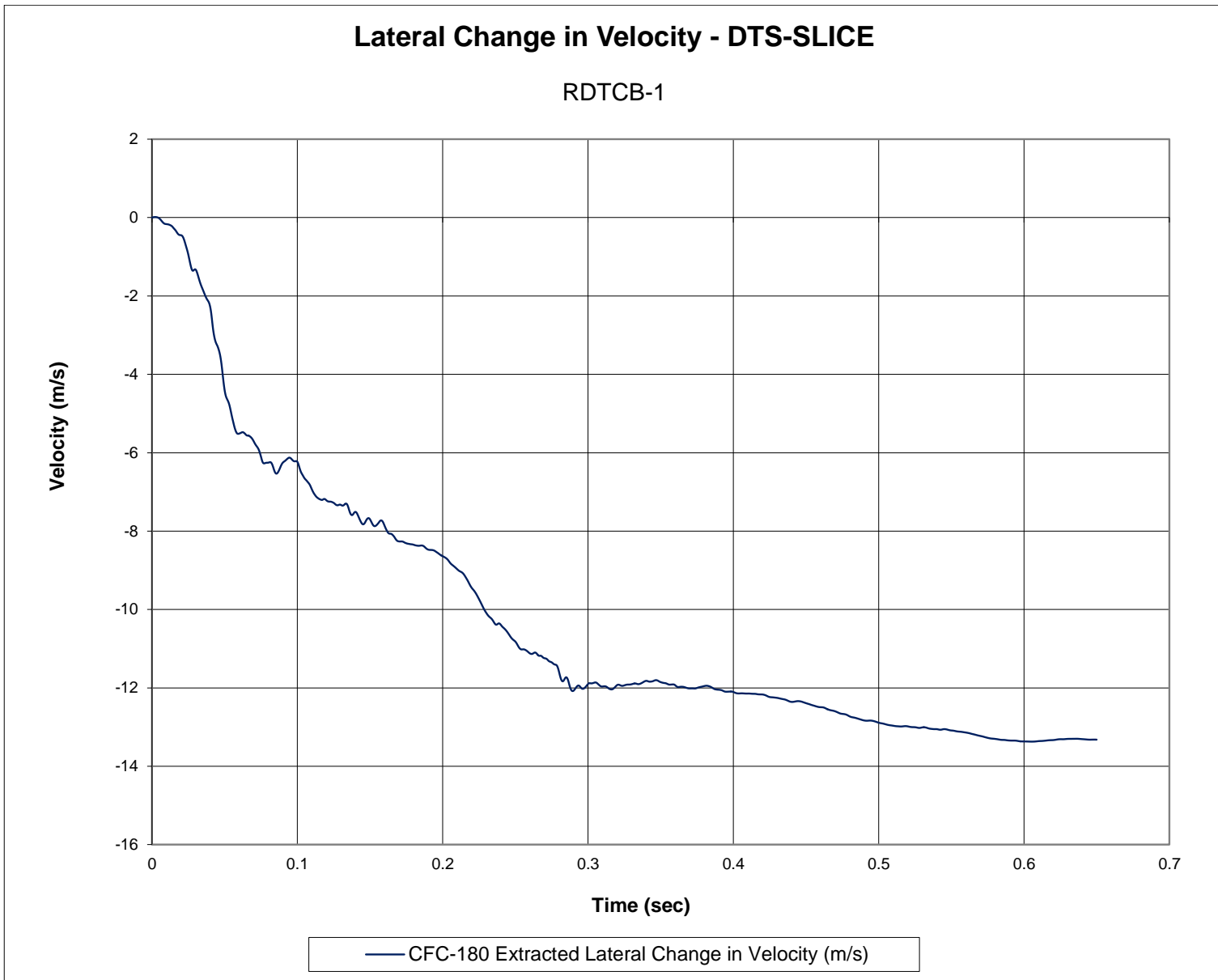


Figure F-13. Lateral Change in Velocity (DTS-SLICE), Test No. RDTCB-1

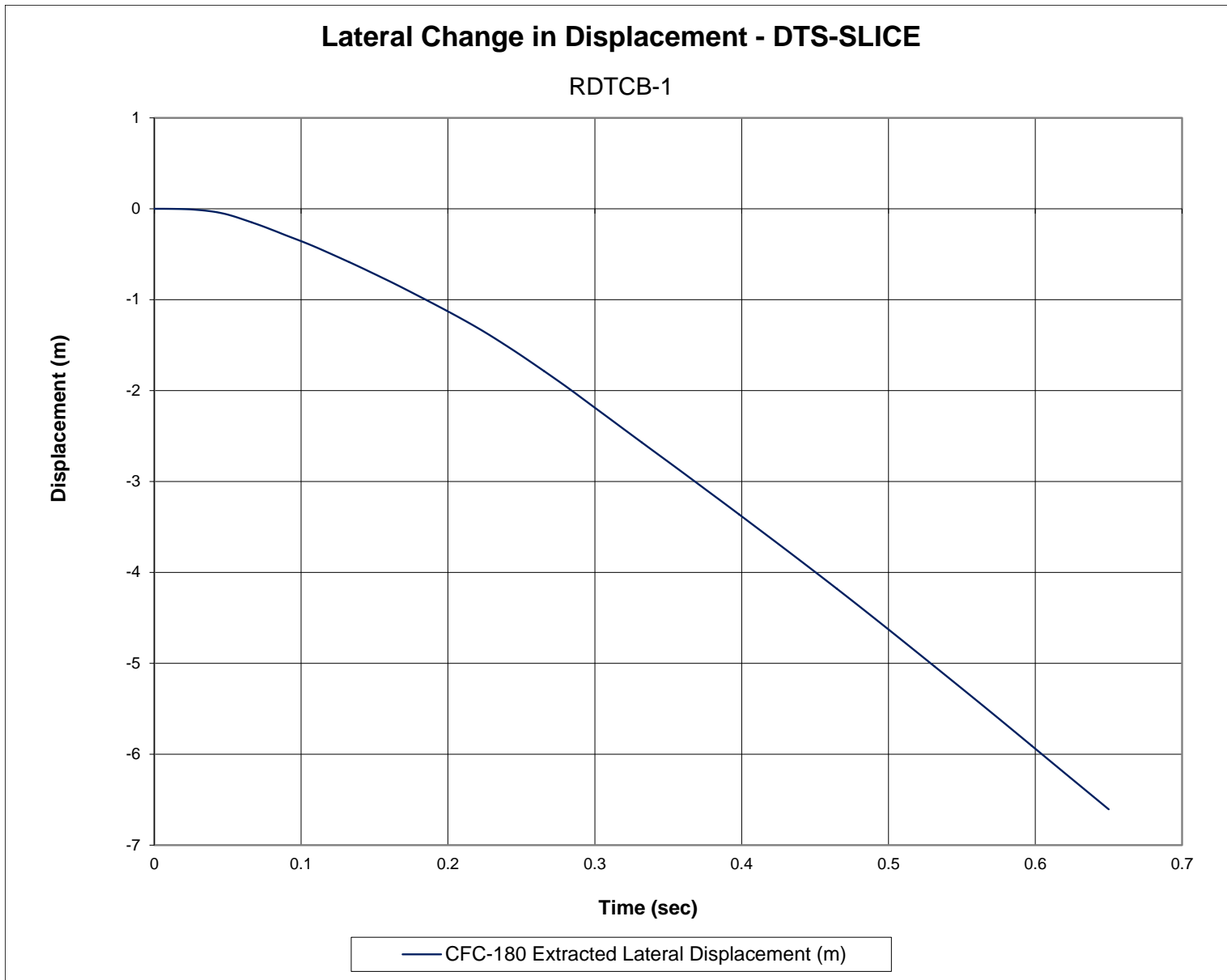


Figure F-14. Lateral Change in Displacement (DTS-SLICE), Test No. RDTCB-1

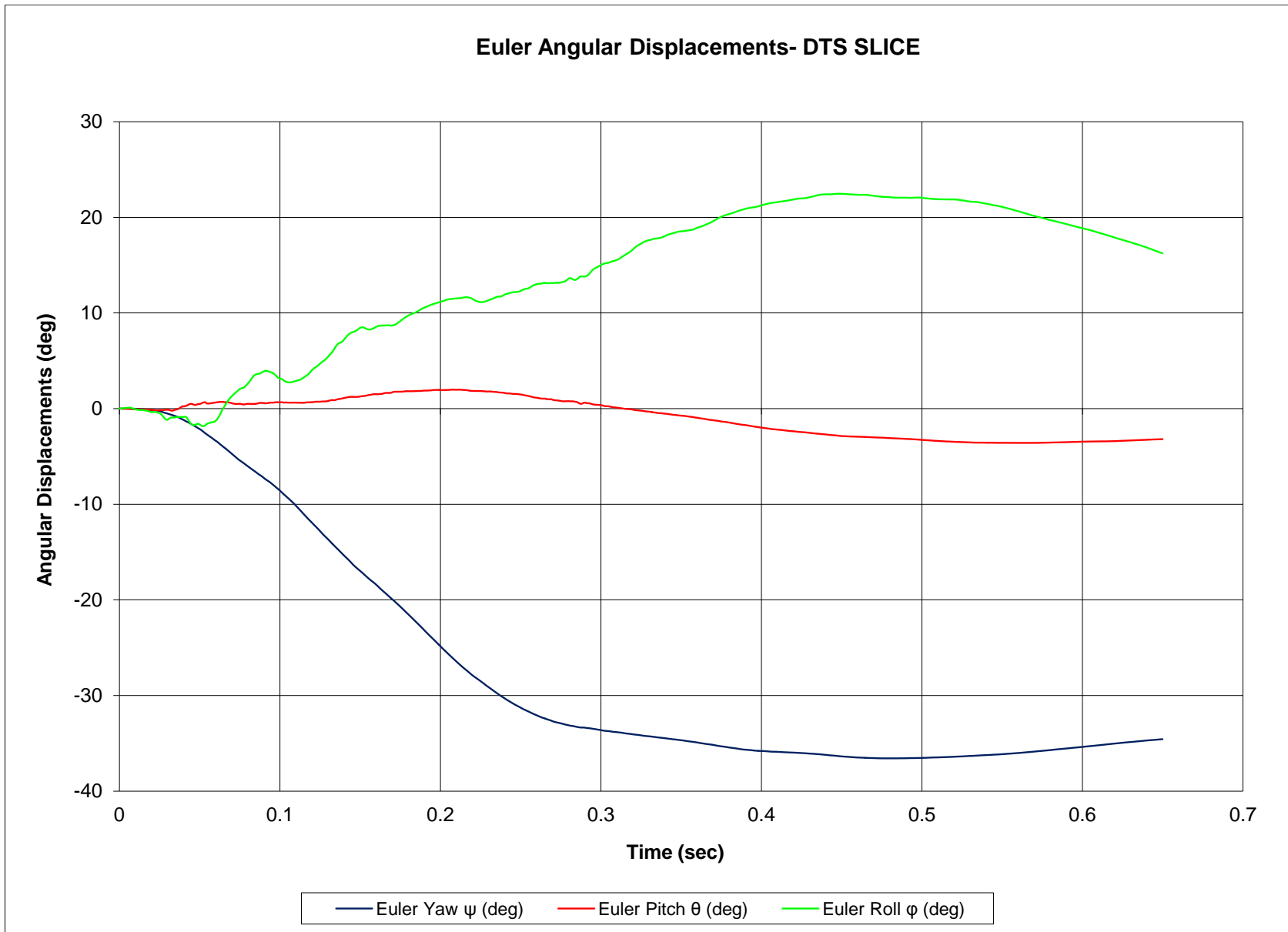


Figure F-15. Vehicle Angular Displacements (DTS-SLICE), Test No. RDTCB-1

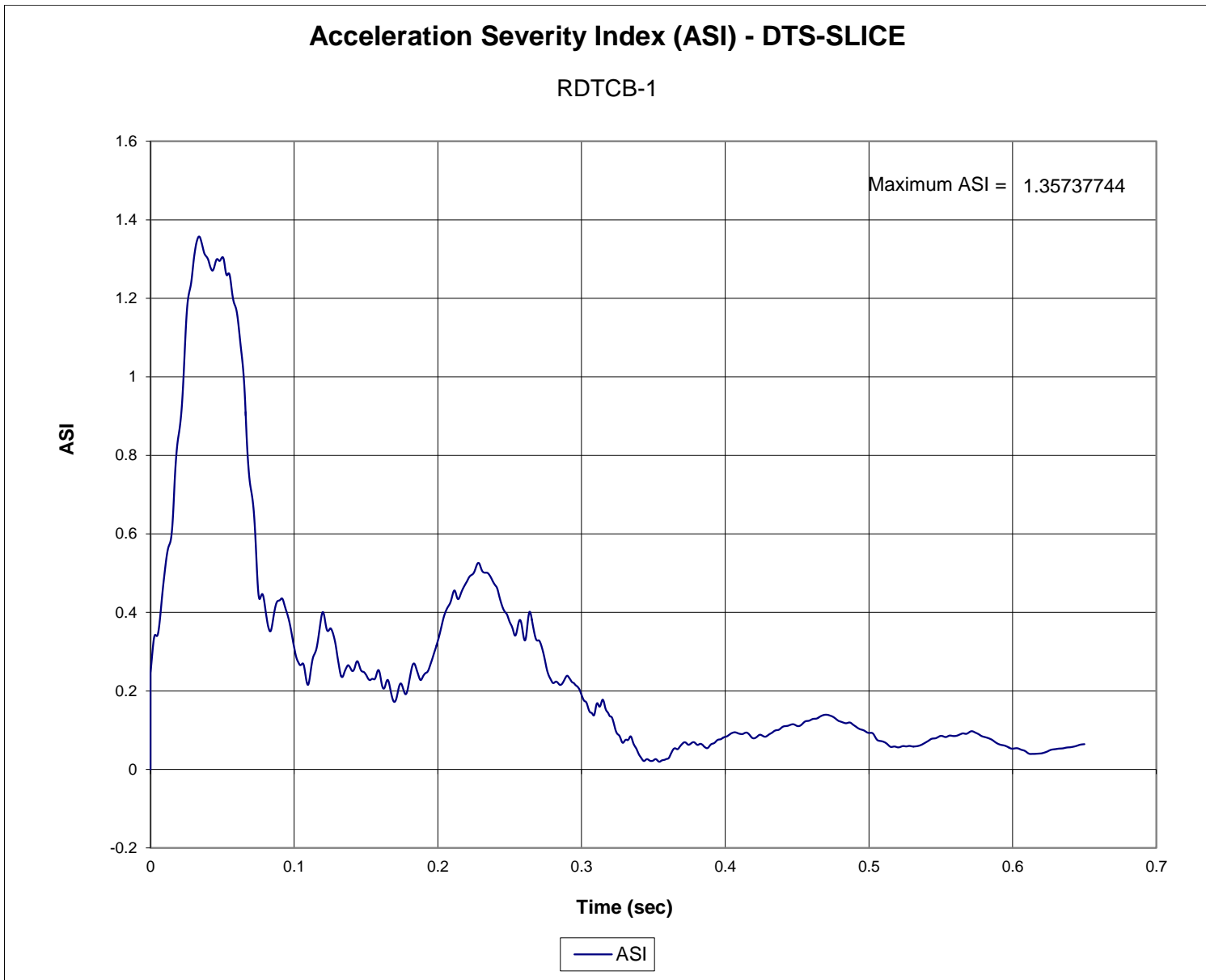


Figure F-16. Acceleration Severity Index (DTS-SLICE), Test No. RDTCB-1

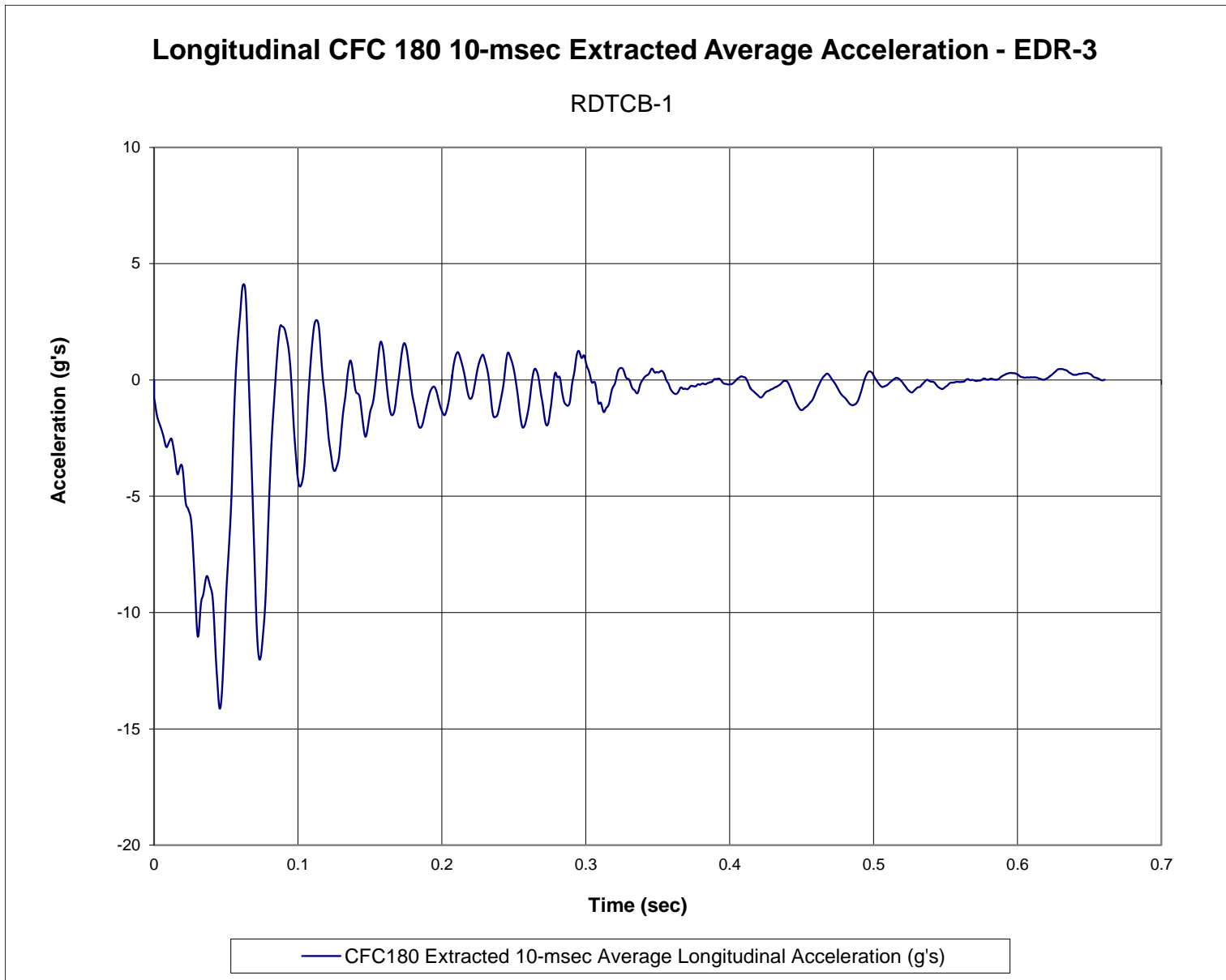


Figure F-17. 10-ms Average Longitudinal Deceleration (EDR-3), Test No. RDTCB-1

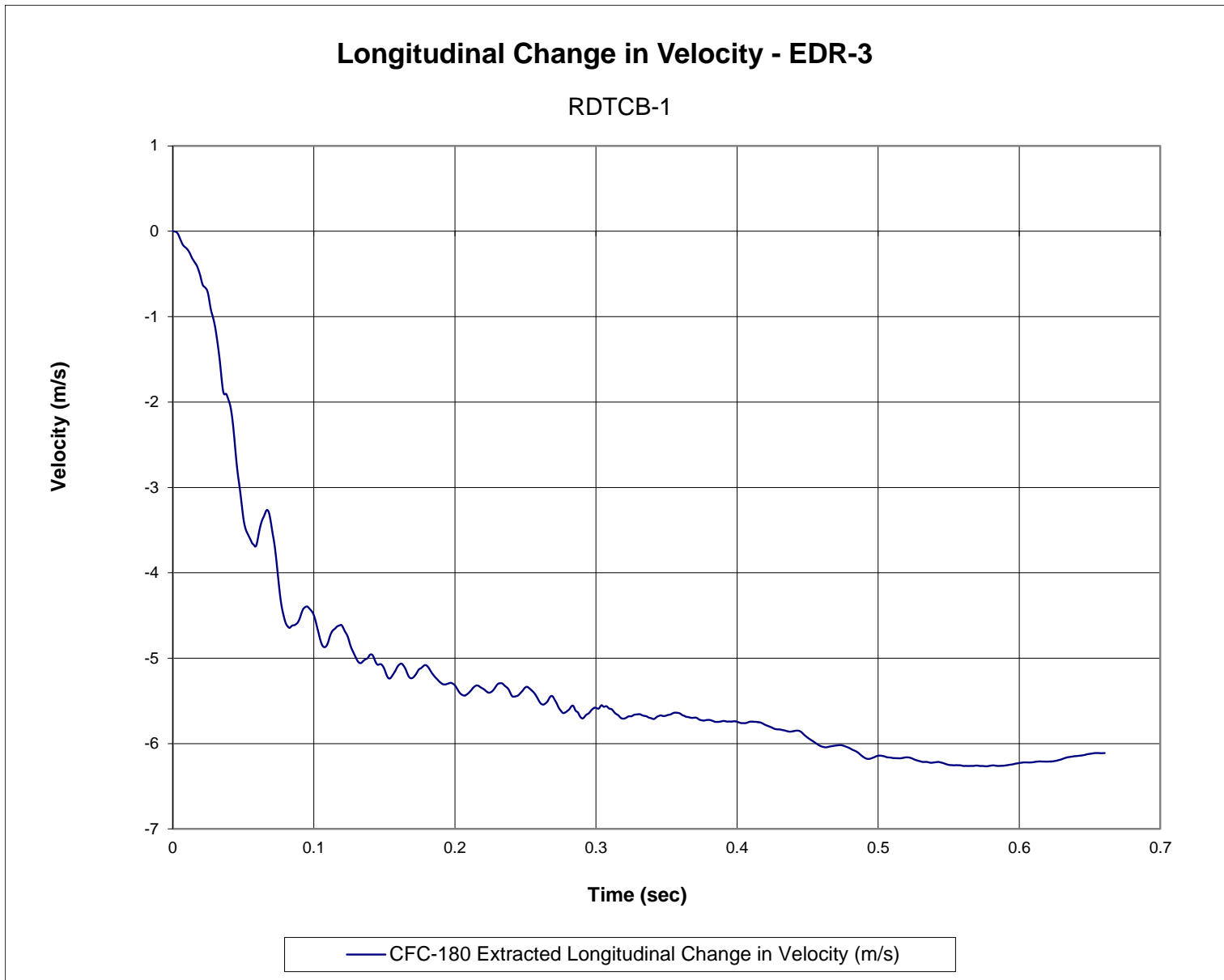


Figure F-18. Longitudinal Change in Velocity (EDR-3), Test No. RDTCB-1



Figure F-19. Longitudinal Change in Displacement (EDR-3), Test No. RDTCB-1

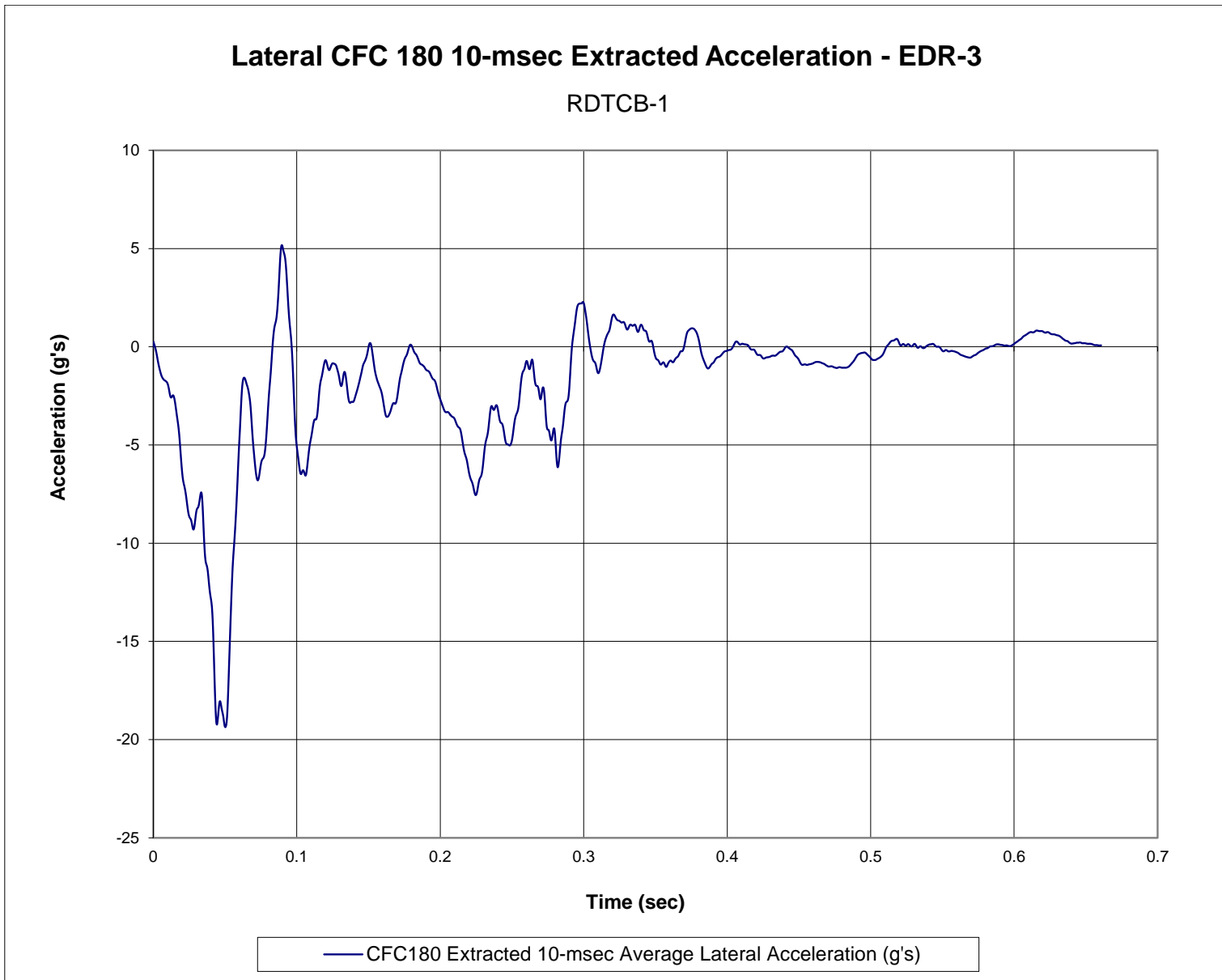


Figure F-20. 10-ms Average Lateral Deceleration (EDR-3), Test No. RDTCB-1

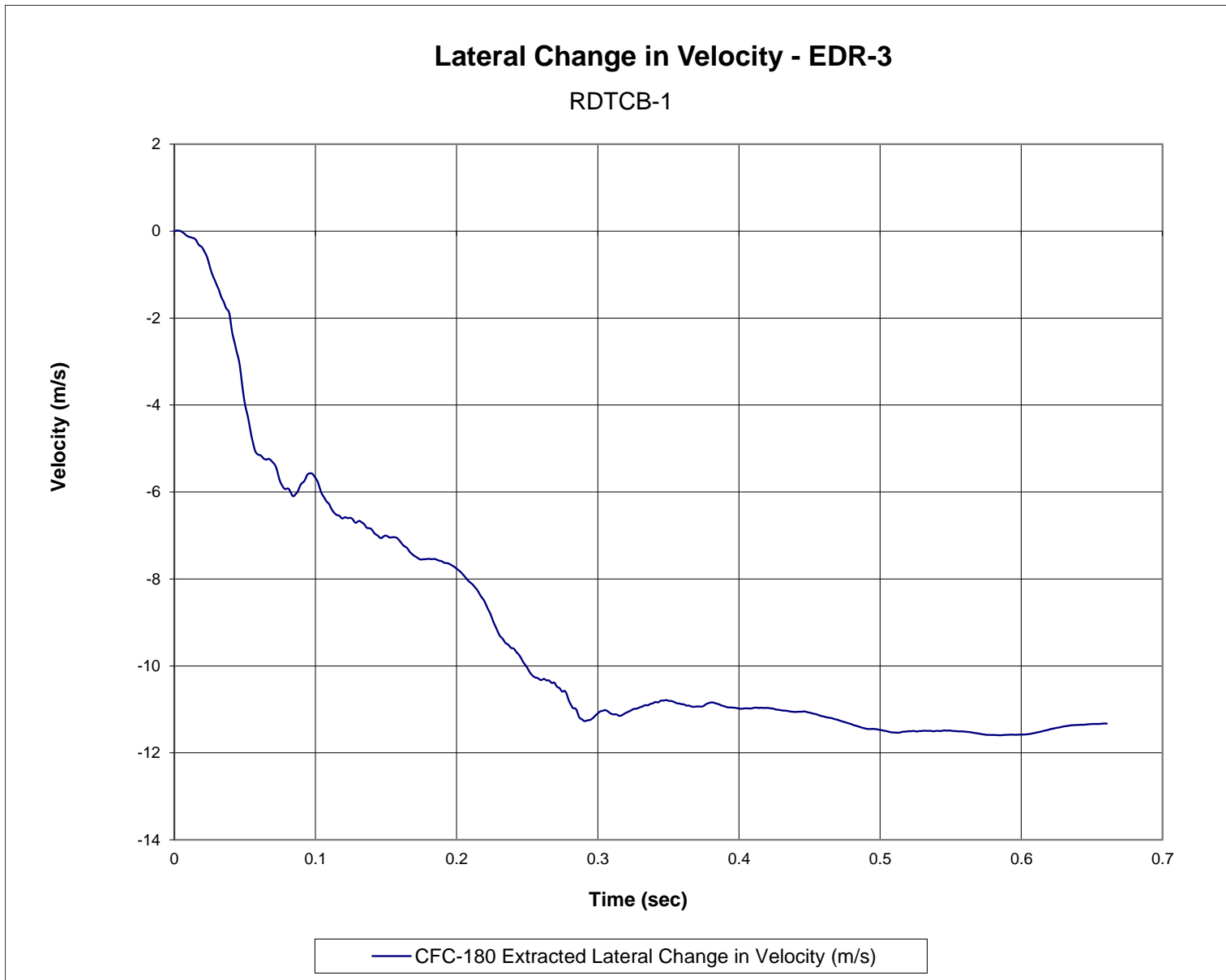


Figure F-21. Lateral Change in Velocity (EDR-3), Test No. RDTCB-1

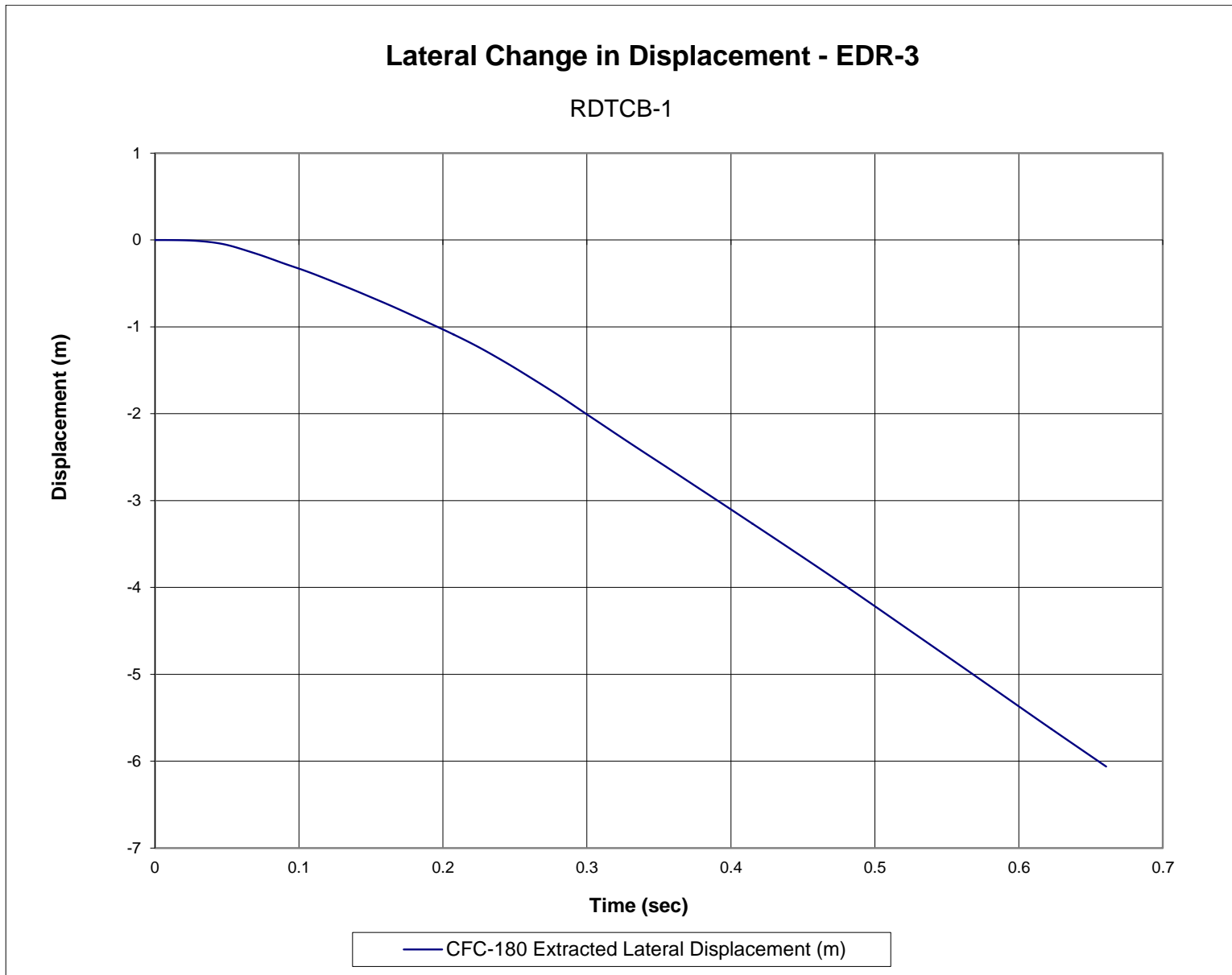


Figure F-22. Lateral Change in Displacement (EDR-3), Test No. RDTCB-1

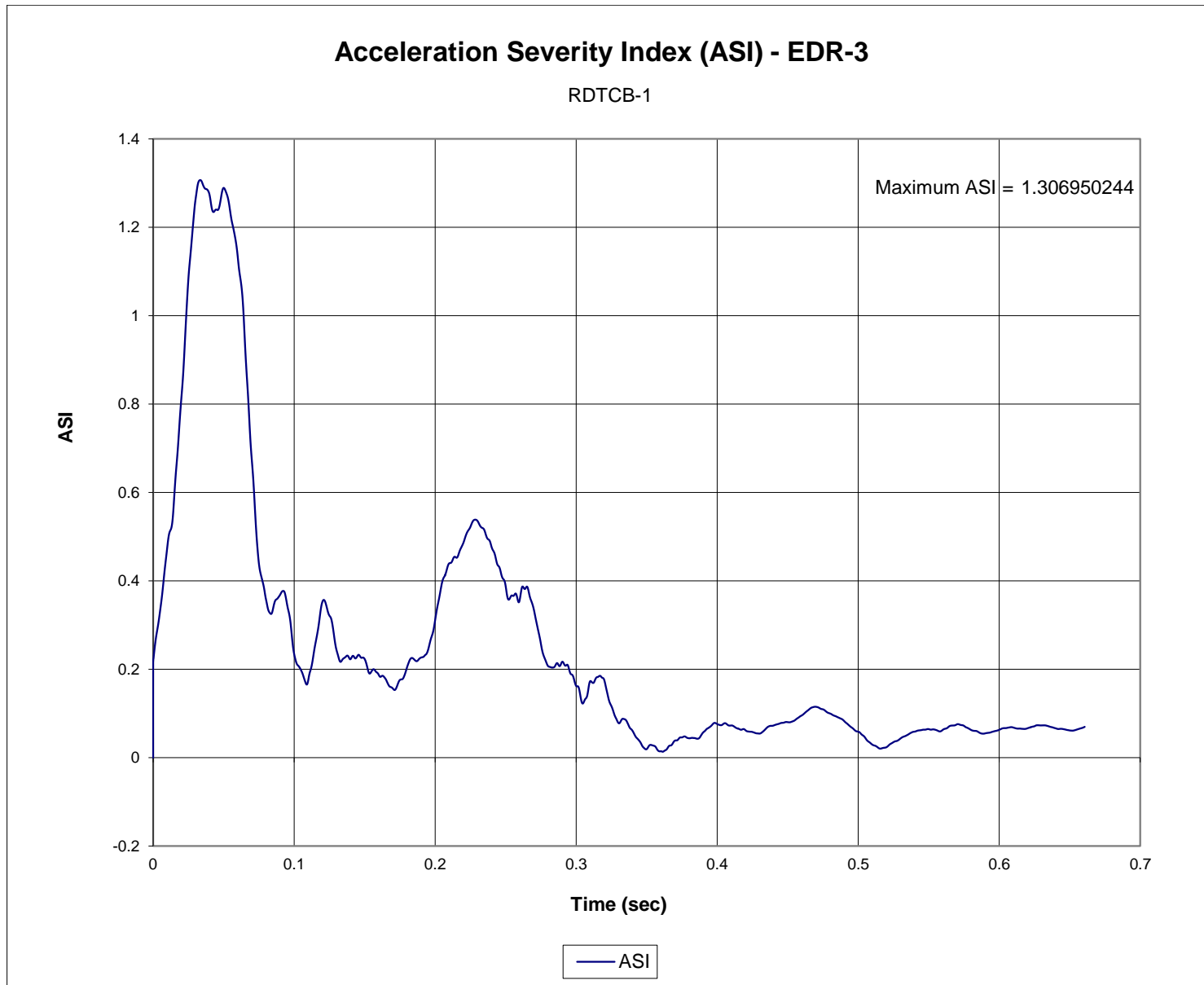


Figure F-23. Acceleration Severity Index (EDR-3), Test No. RDTCB-1

**Appendix G. Accelerometer and Rate Transducer Data Plots, Test No. RDTCB-2**

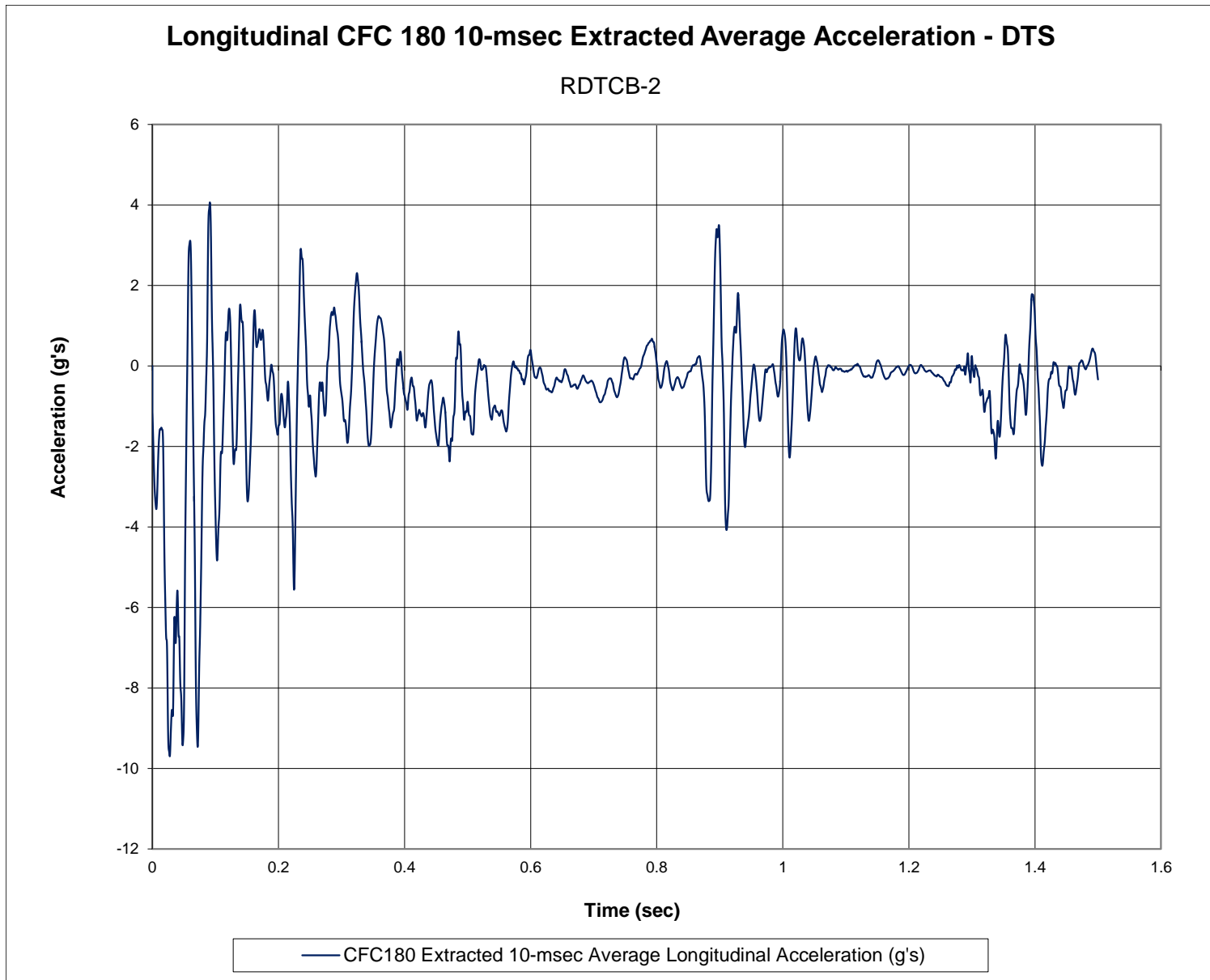


Figure G-1. 10-ms Average Longitudinal Deceleration (DTS), Test No. RDTCB-2

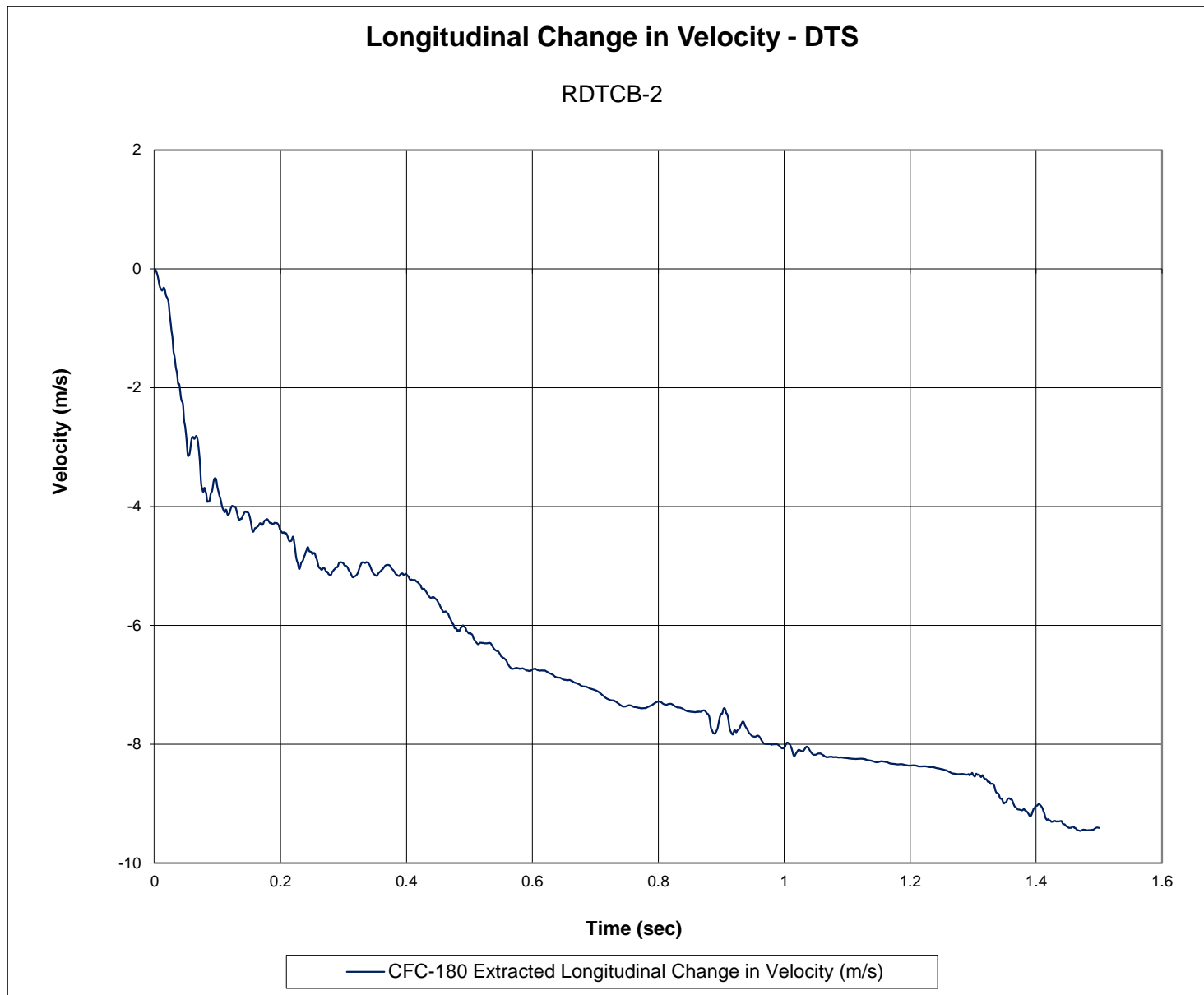


Figure G-2. Longitudinal Change in Velocity (DTS), Test No. RDTCB-2

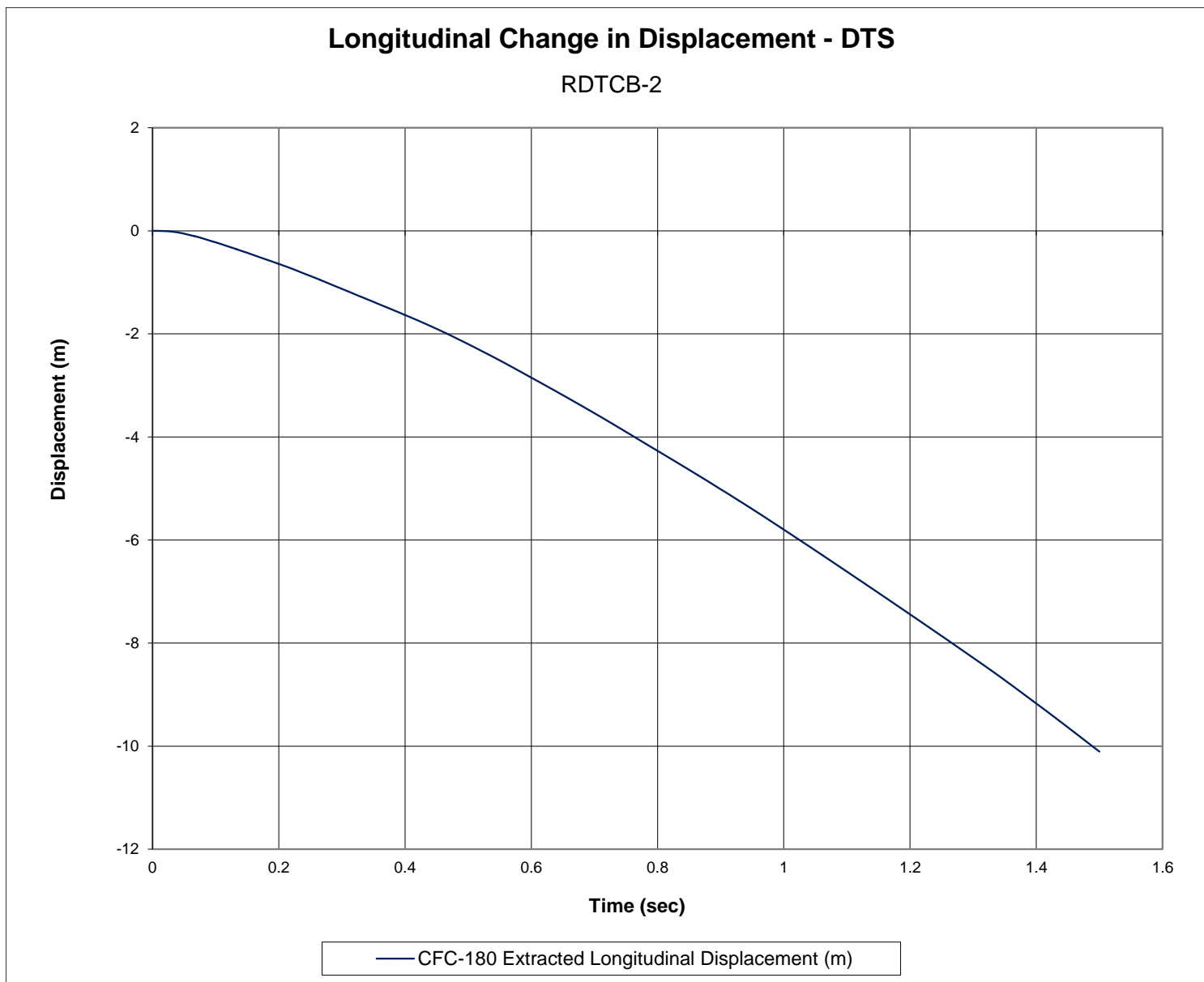


Figure G-3. Longitudinal Change in Displacement (DTS), Test No. RDTCB-2

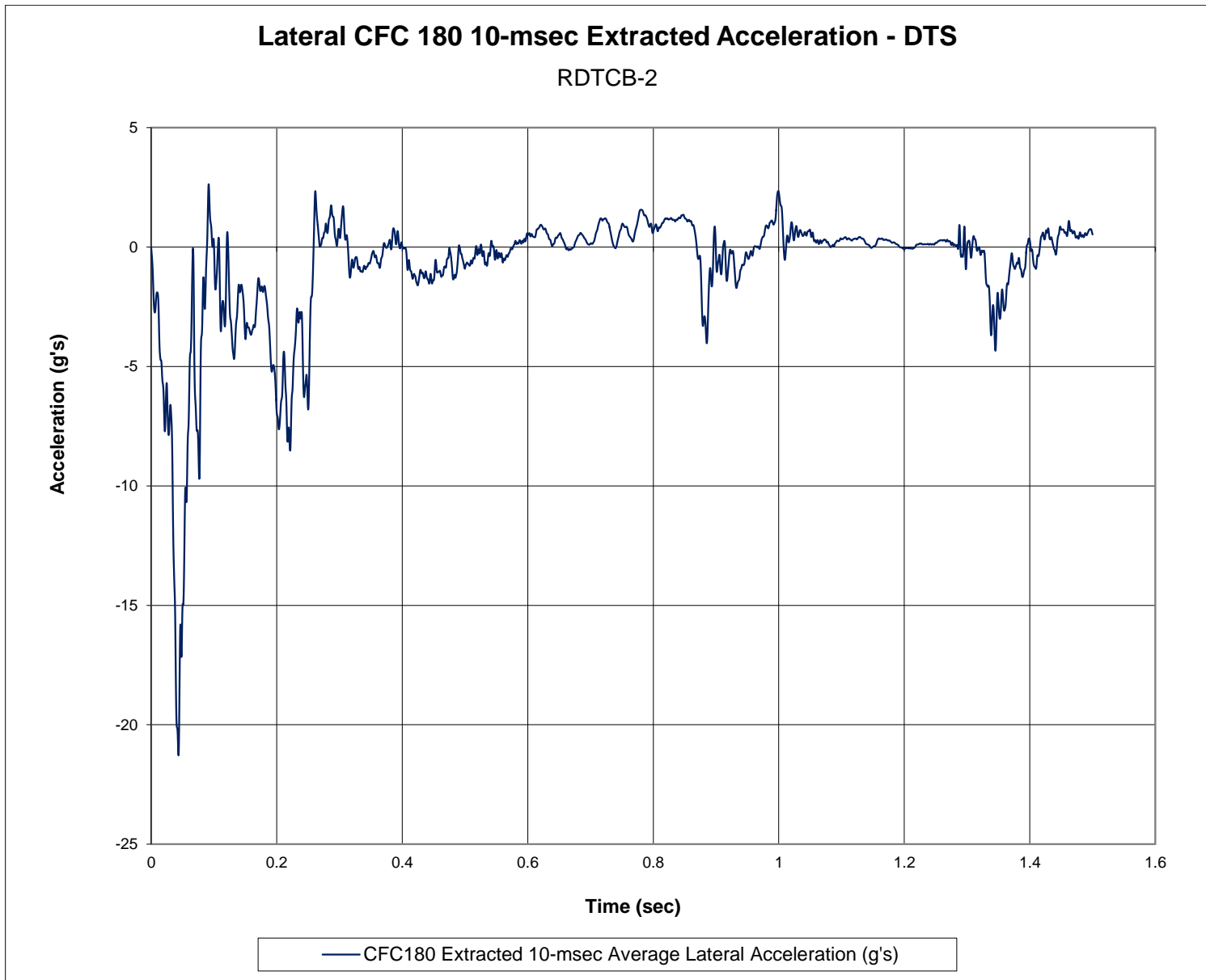


Figure G-4. 10-ms Average Lateral Deceleration (DTS), Test No. RDTCB-2

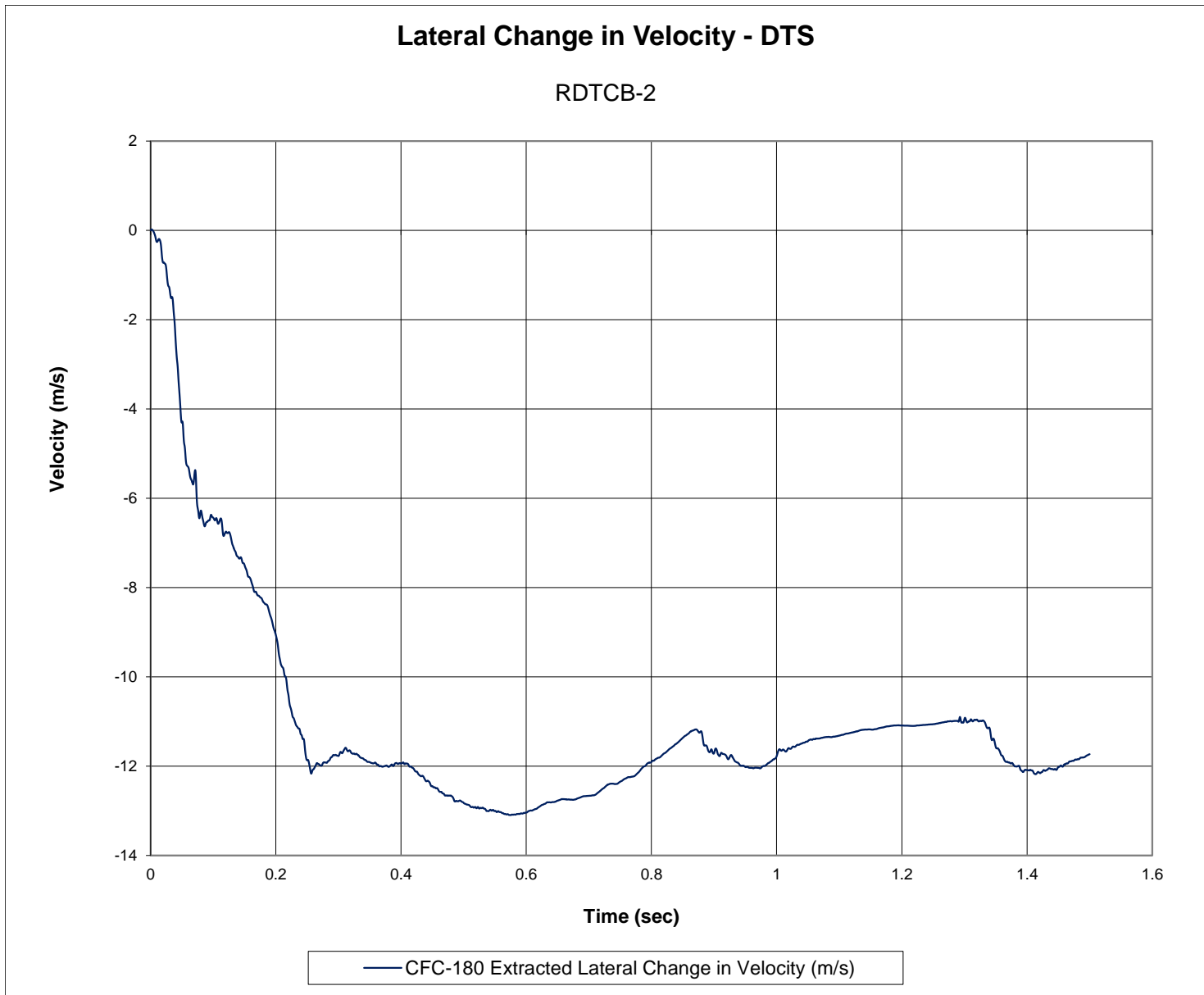


Figure G-5. Lateral Change in Velocity (DTS), Test No. RDTCB-2

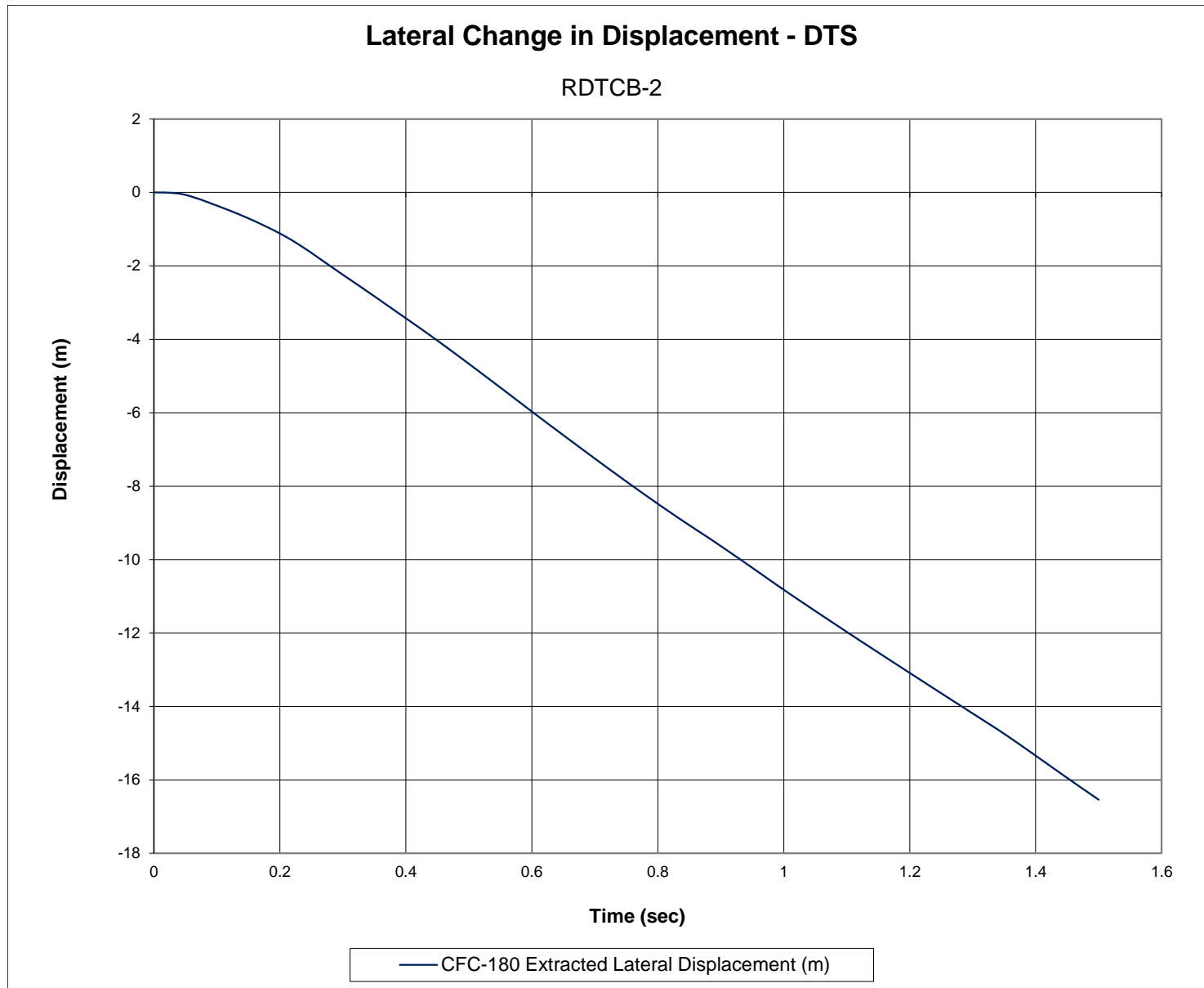


Figure G-6. Lateral Occupant Displacement (DTS), Test No. RDTCB-2

349

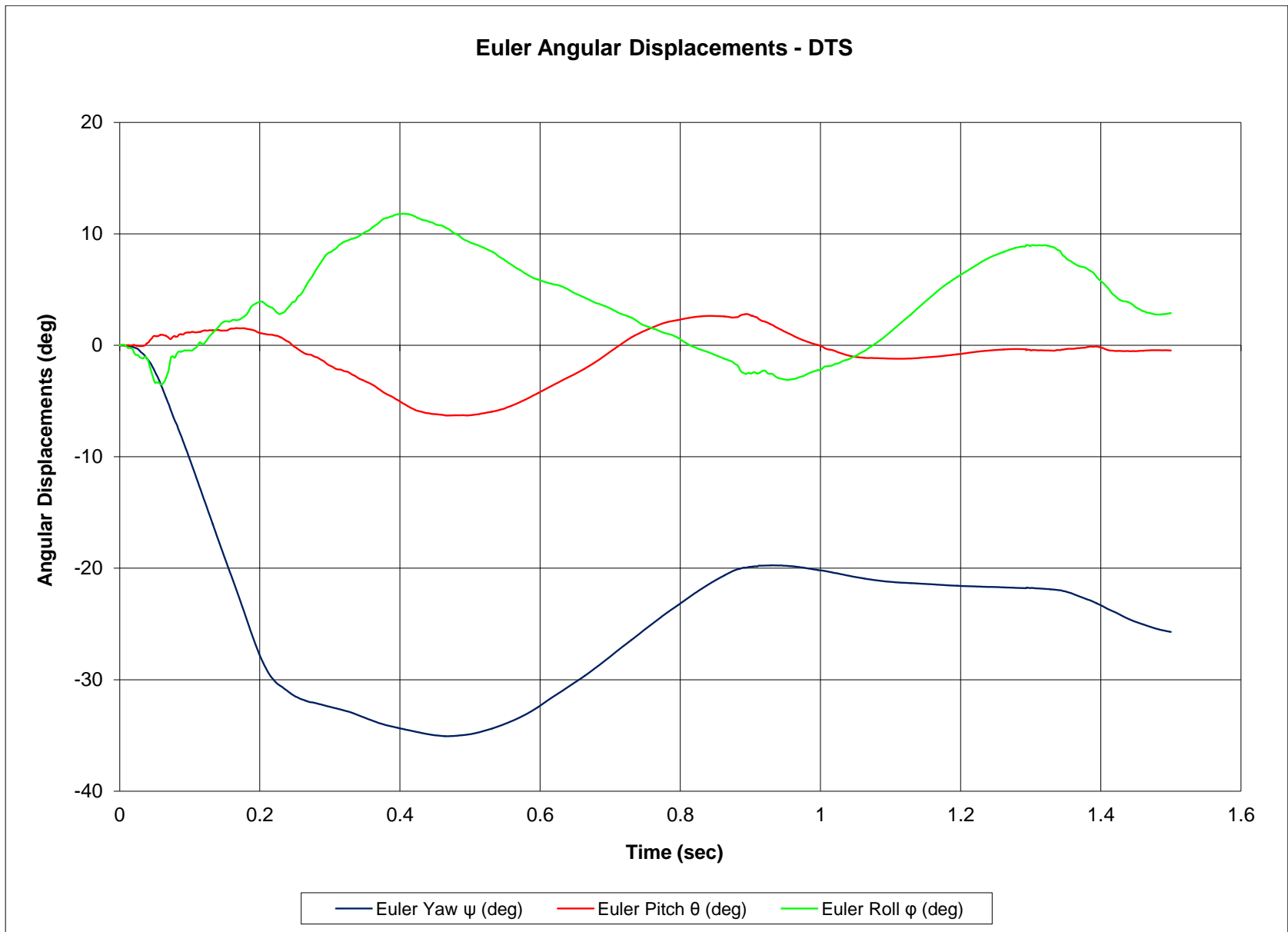


Figure G-7. Vehicle Angular Displacements (DTS), Test No. RDTCB-2

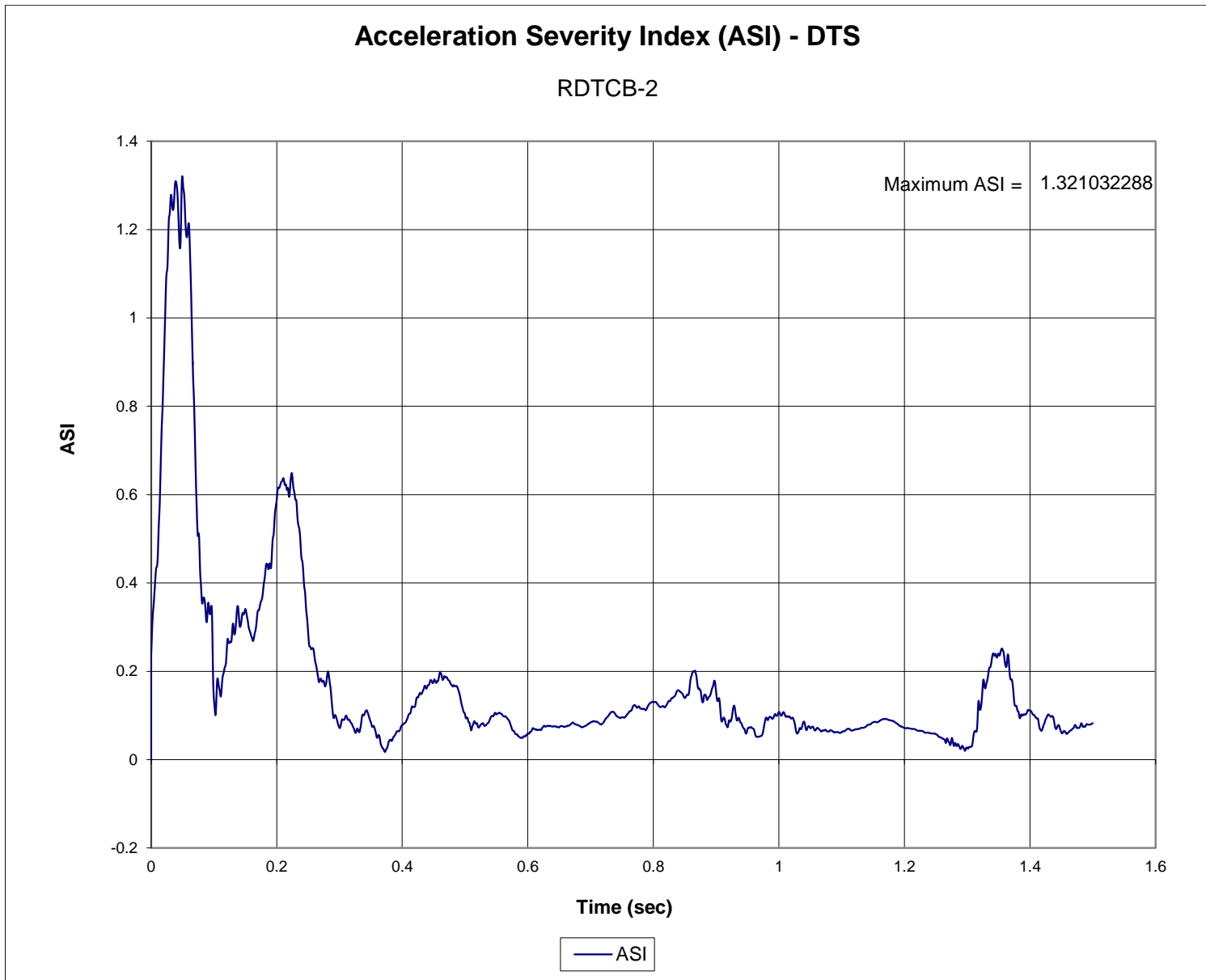


Figure G-8. Acceleration Severity Index (DTS), Test No. RDTCB-2

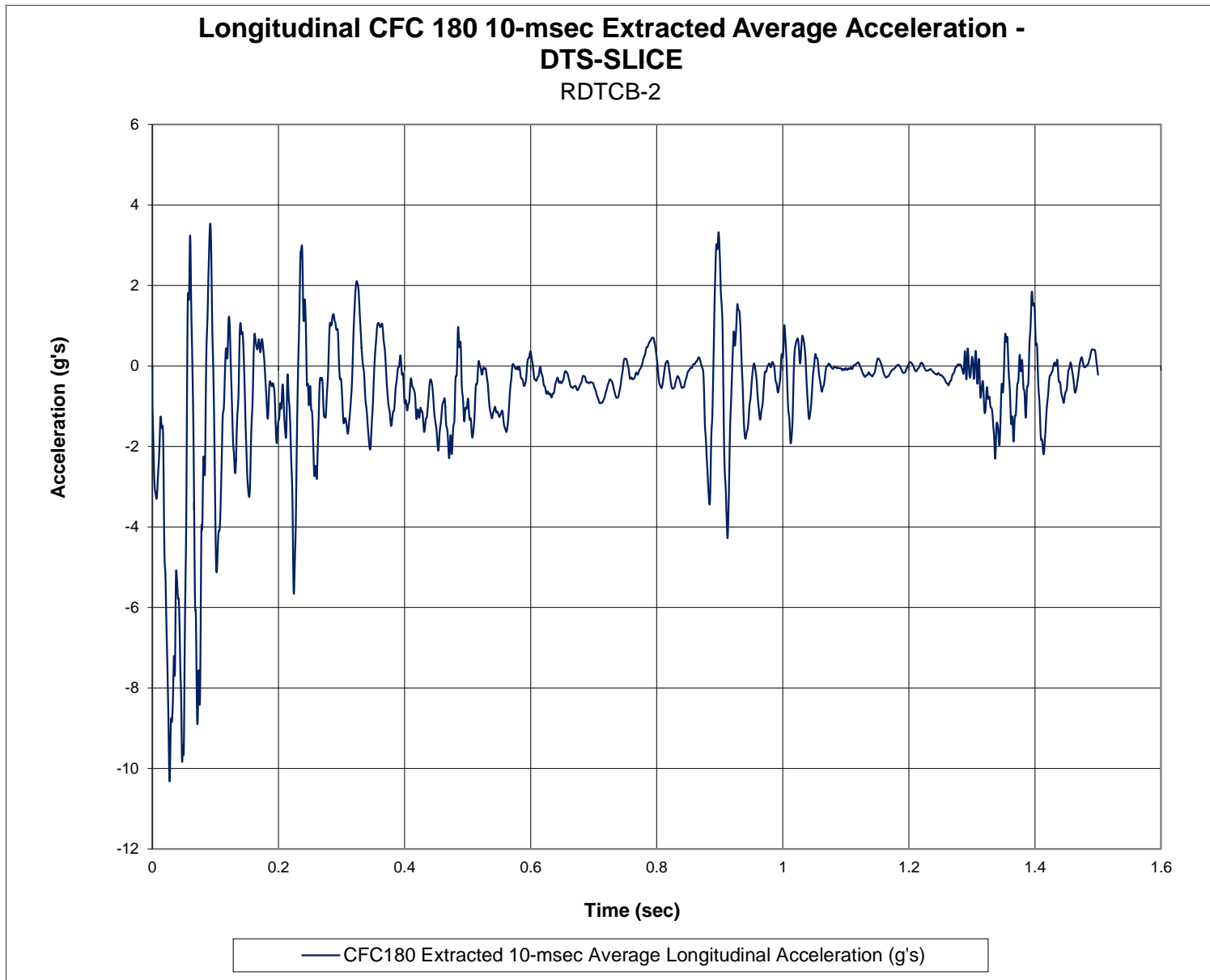


Figure G-9. 10-ms Average Longitudinal Deceleration (DTS-SLICE), Test No. RDTCB-2

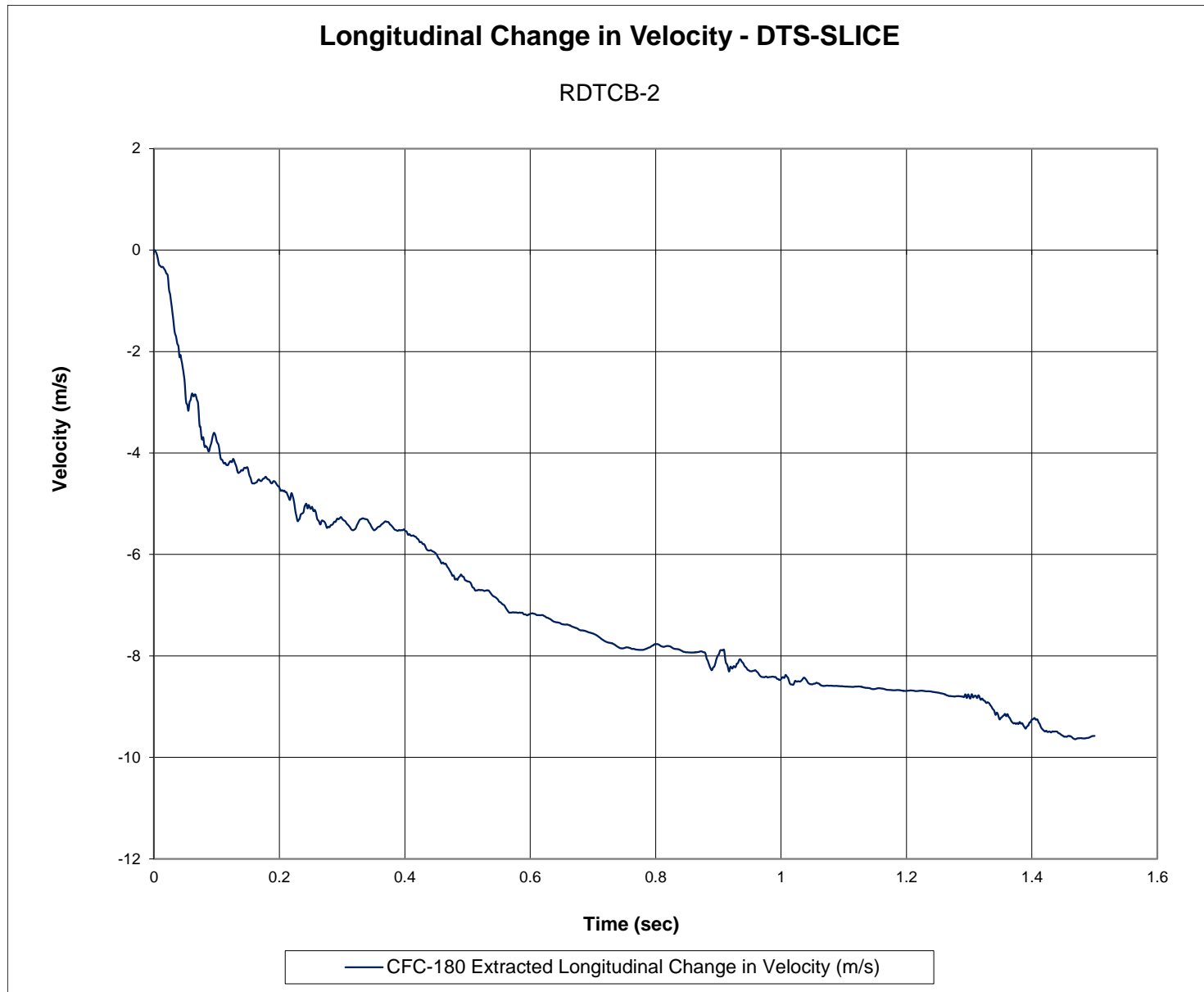


Figure G-10. Longitudinal Change in Velocity (DTS-SLICE), Test No. RDTCB-2

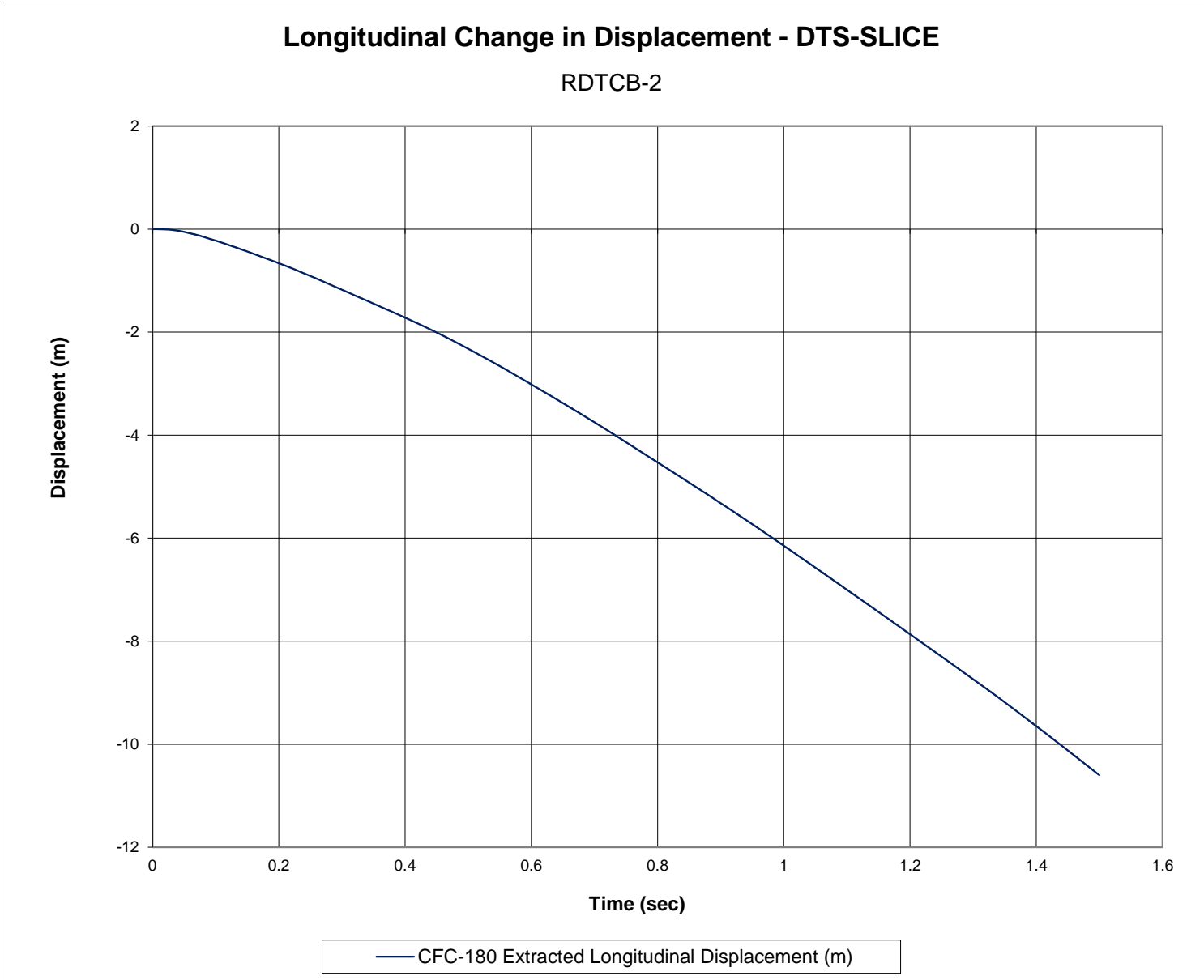


Figure G-11. Longitudinal Change in Displacement (DTS-SLICE), Test No. RDTCB-2

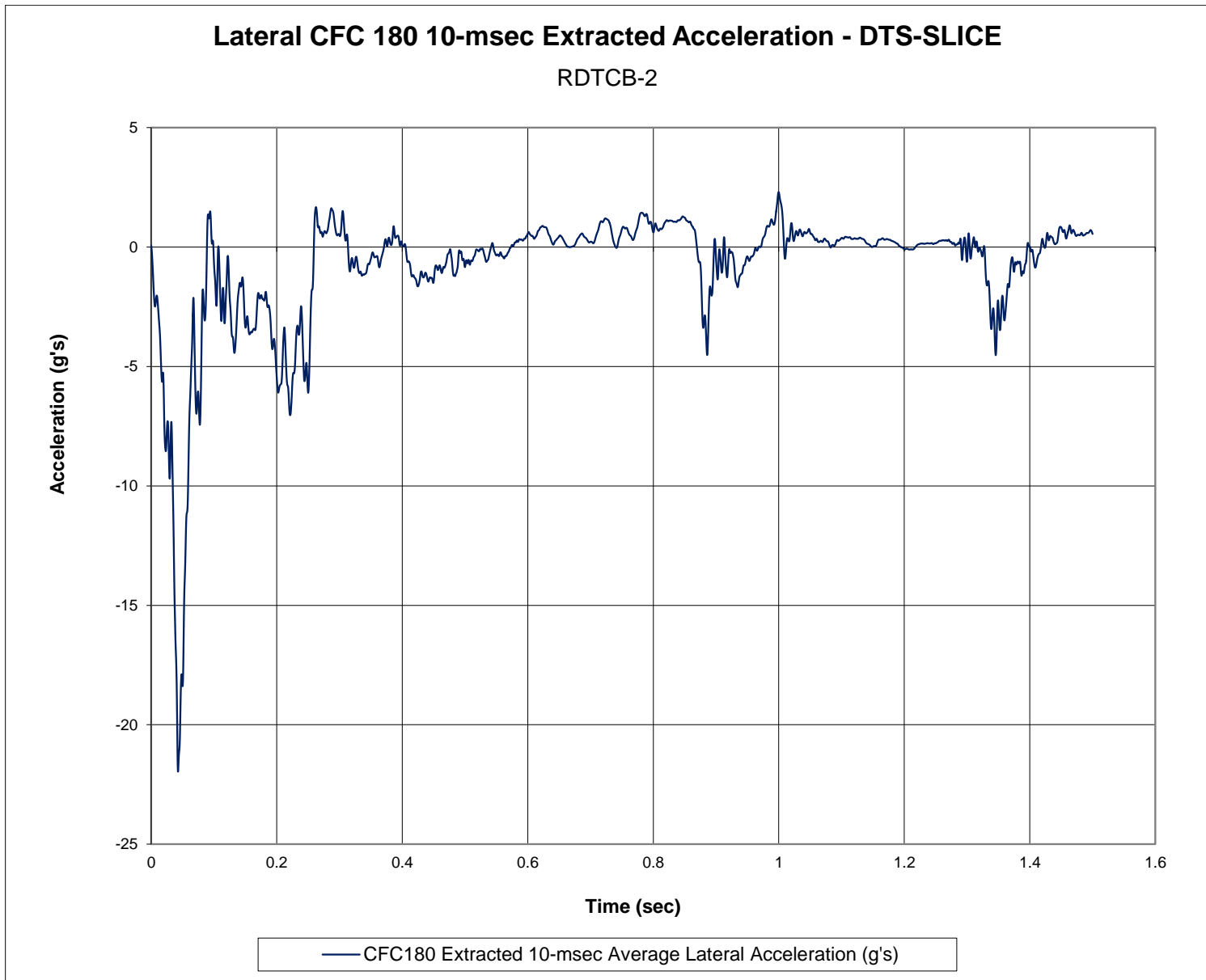


Figure G-12. 10-ms Average Lateral Deceleration (DTS-SLICE), Test No. RDTCB-2

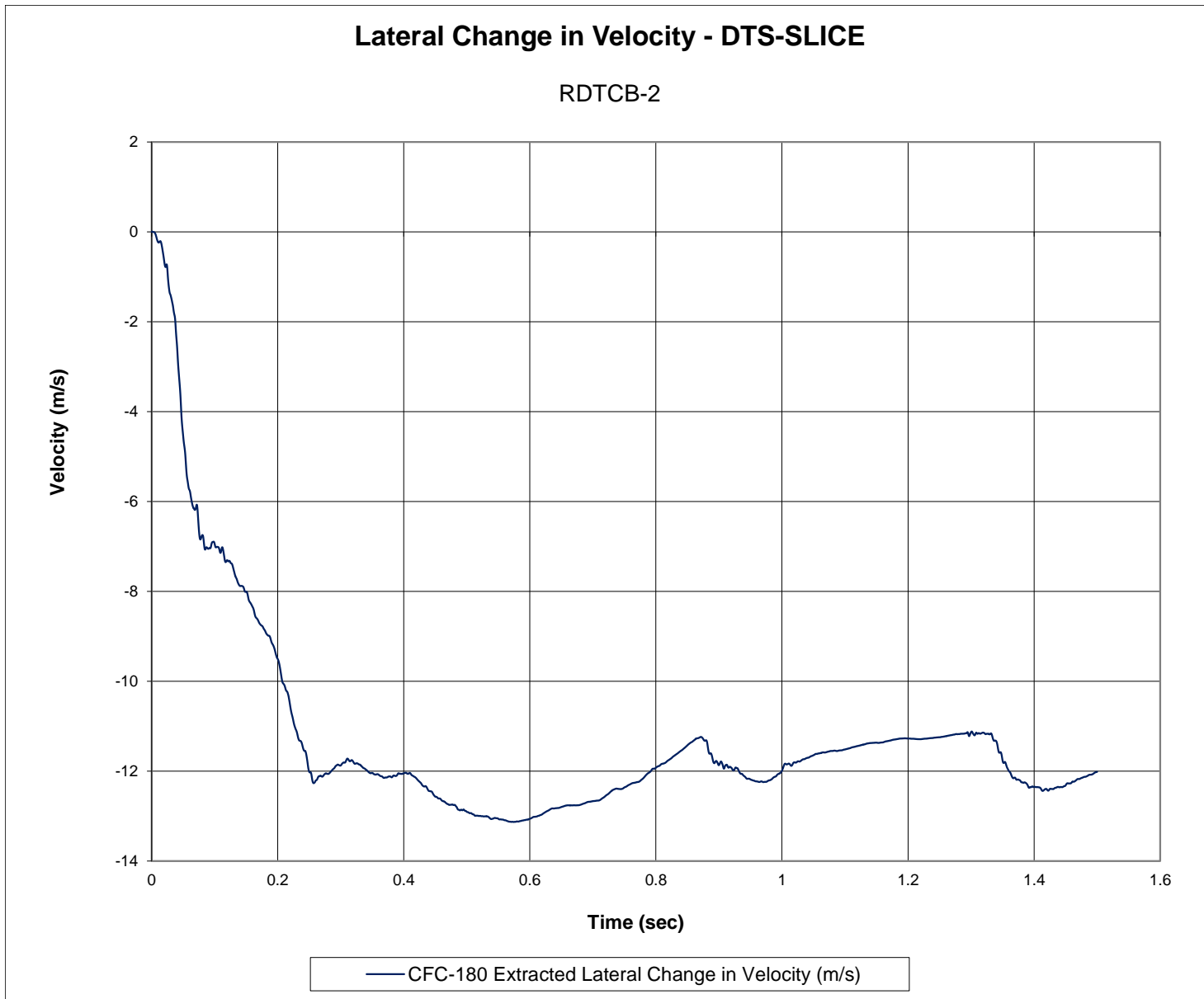


Figure G-13. Lateral Change in Velocity (DTS-SLICE), Test No. RDTCB-2

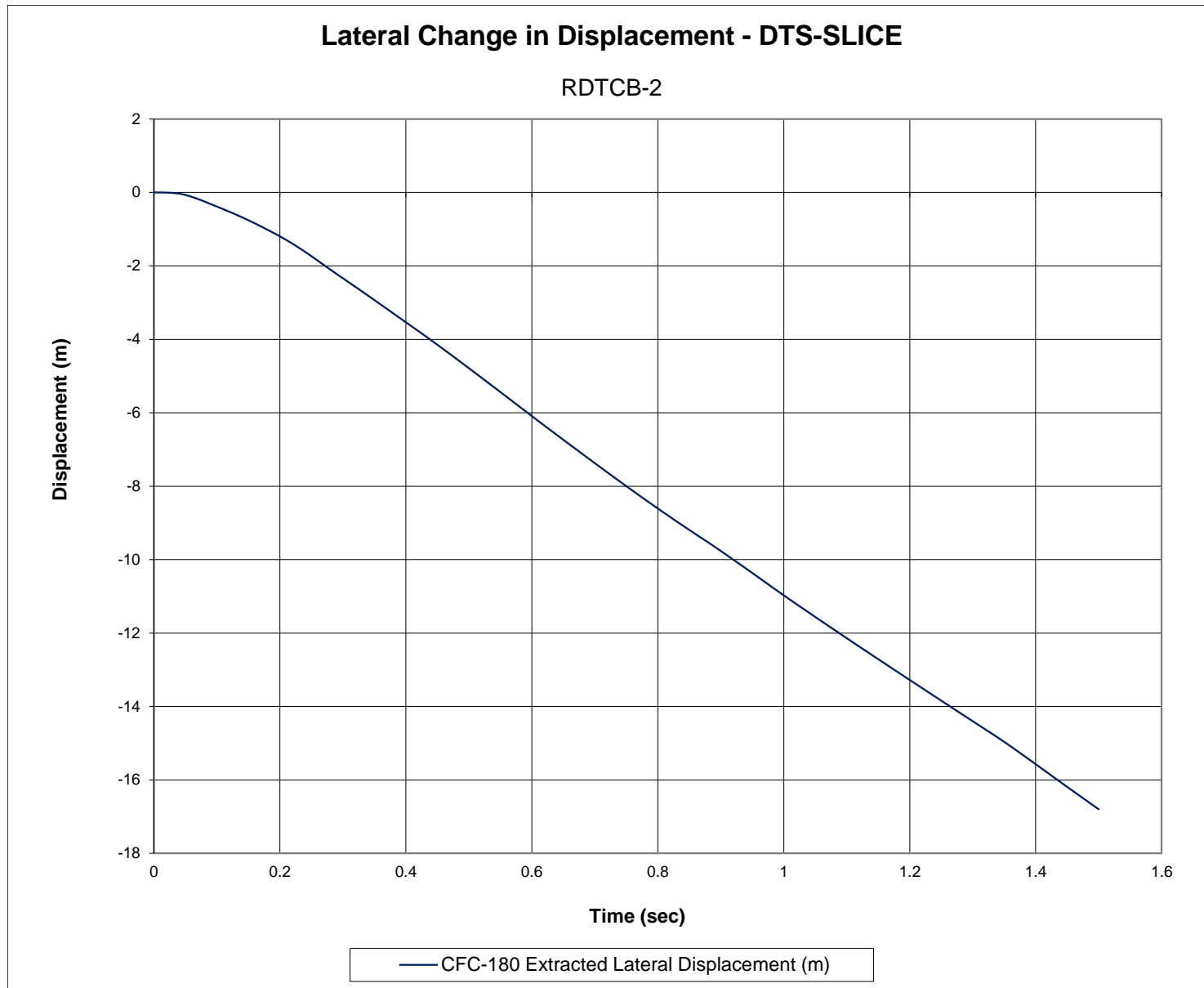


Figure G-14. Lateral Change in Displacement (DTS-SLICE), Test No. RDTCB-2

357

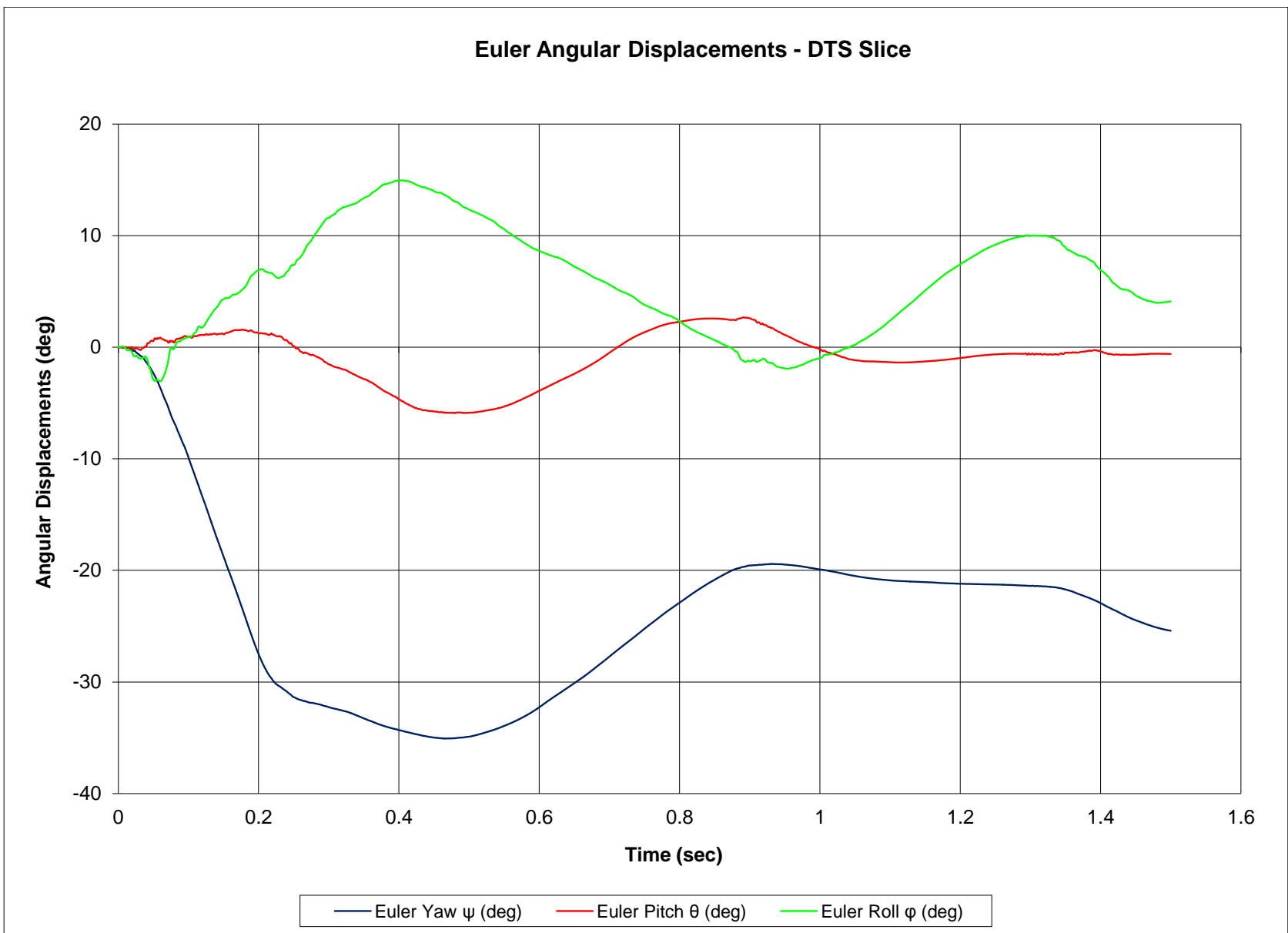


Figure G-15. Vehicle Angular Displacements (DTS-SLICE), Test No. RDTCB-2

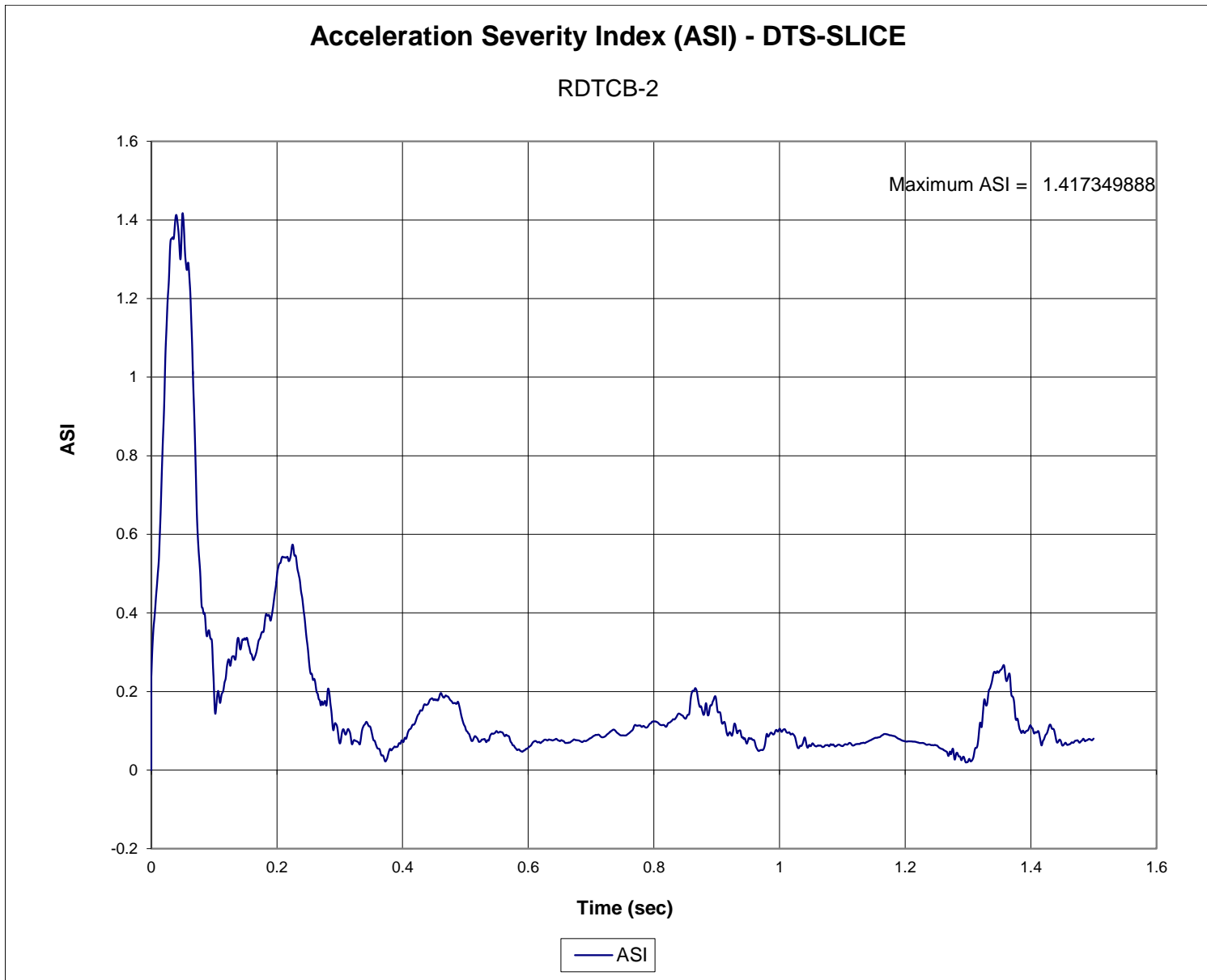


Figure G-16. Acceleration Severity Index (DTS-SLICE), Test No. RDTCB-2

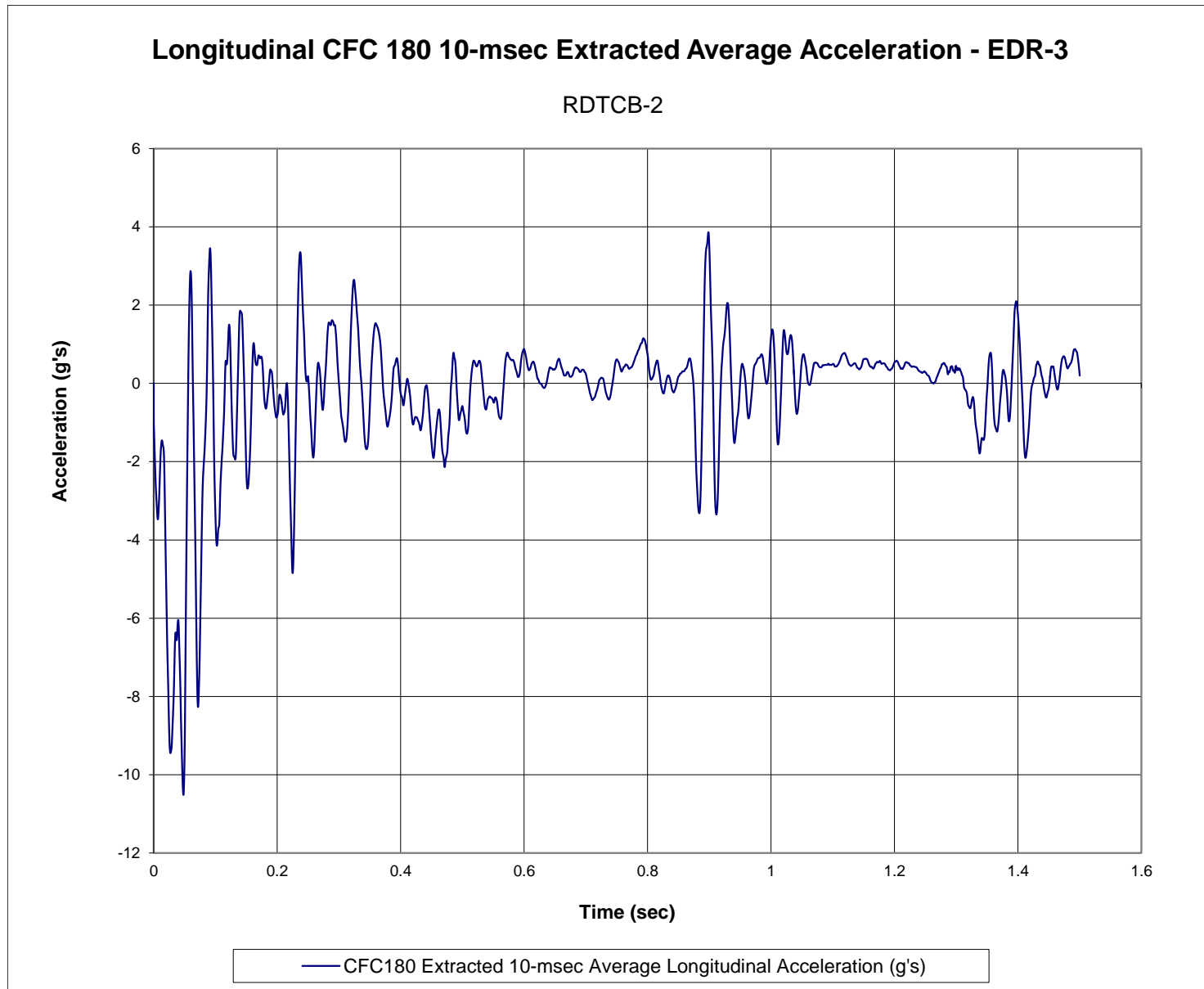


Figure G-17. 10-ms Average Longitudinal Deceleration (EDR-3), Test No. RDTCB-2

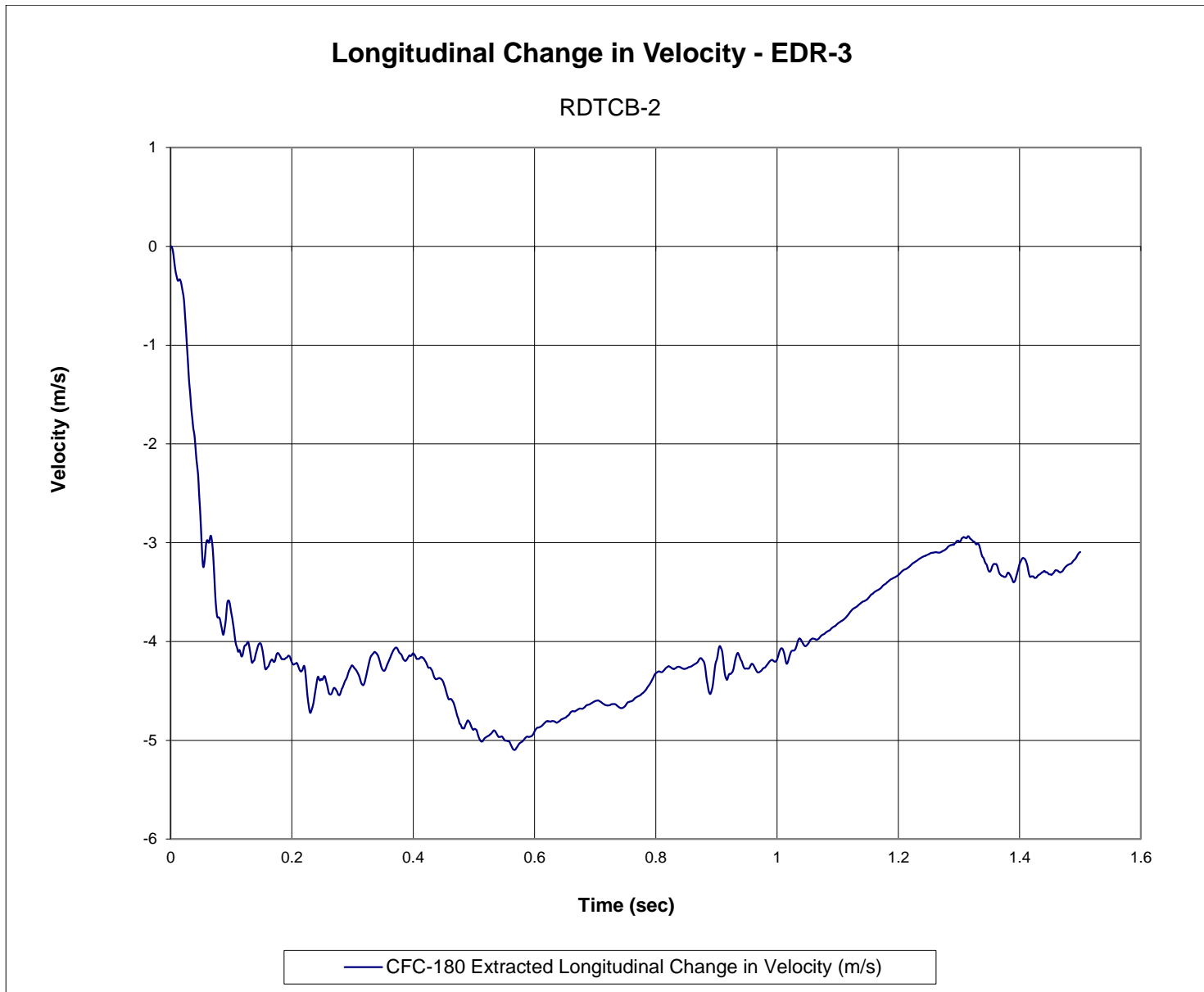


Figure G-18. Longitudinal Change in Velocity (EDR-3), Test No. RDTCB-2



Figure G-19. Longitudinal Change in Displacement (EDR-3), Test No. RDTCB-2

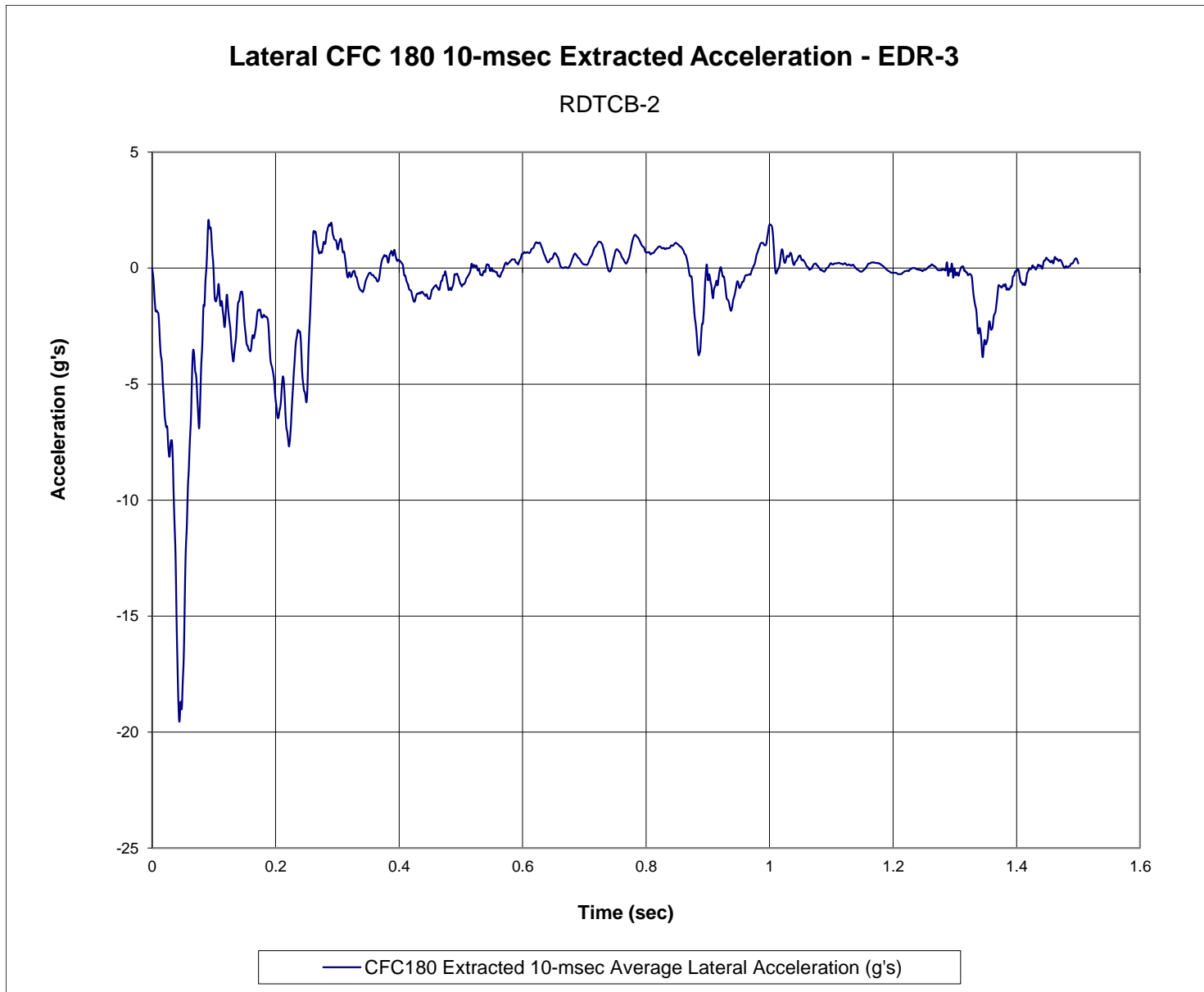


Figure G-20. 10-ms Average Lateral Deceleration (EDR-3), Test No. RDTCB-2

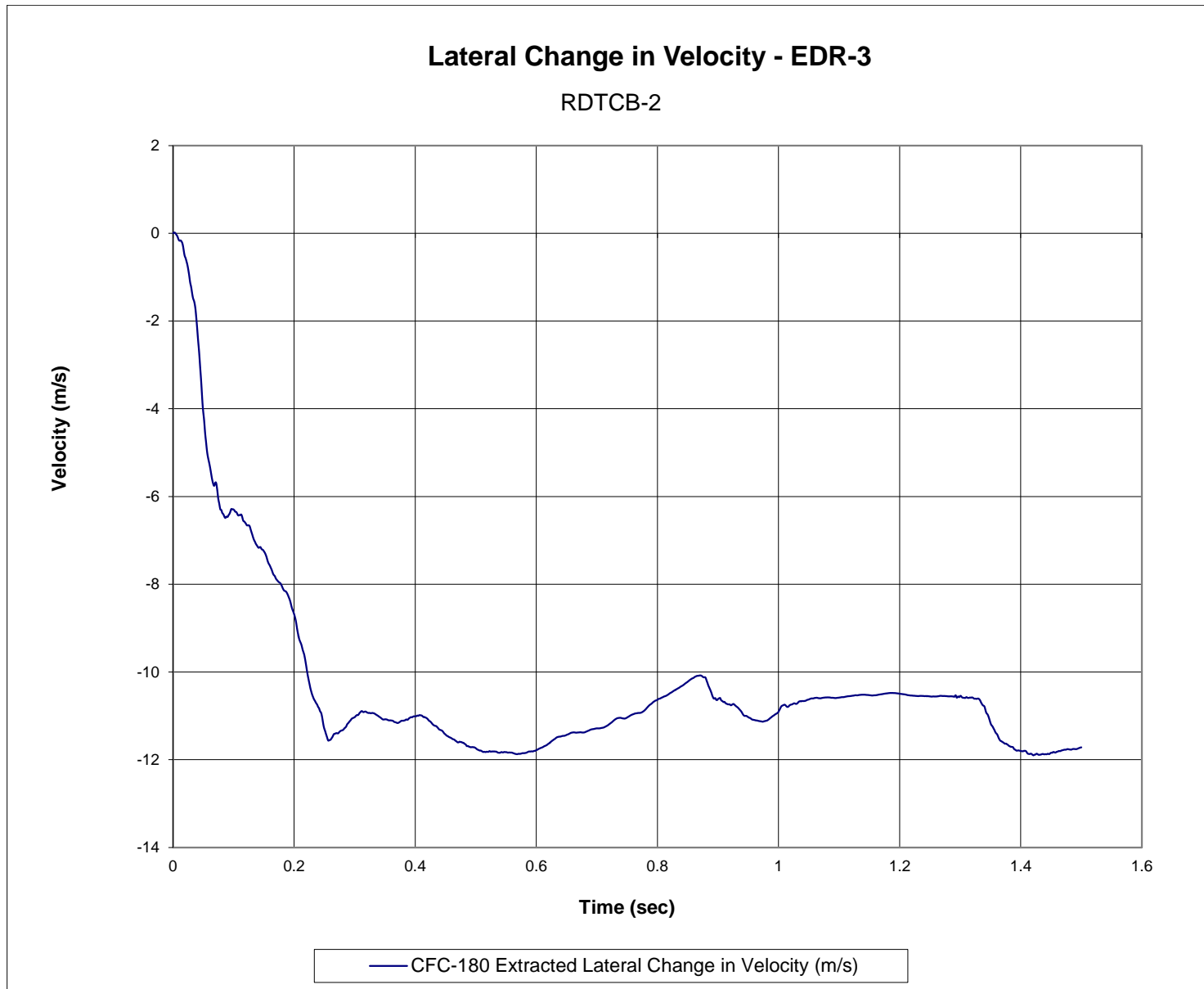


Figure G-21. Lateral Change in Velocity (EDR-3), Test No. RDTCB-2

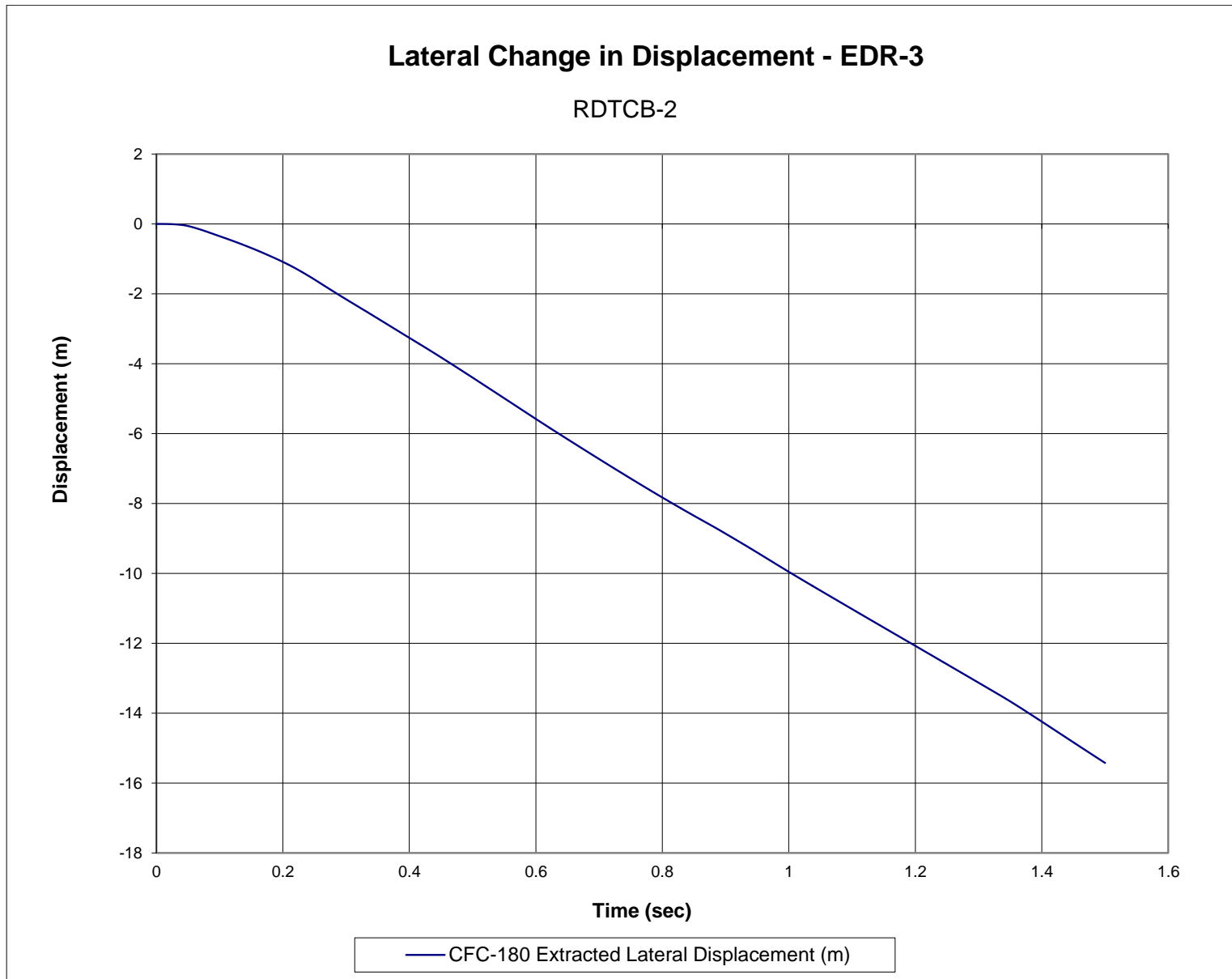


Figure G-22. Lateral Change in Displacement (EDR-3), Test No. RDTCB-2

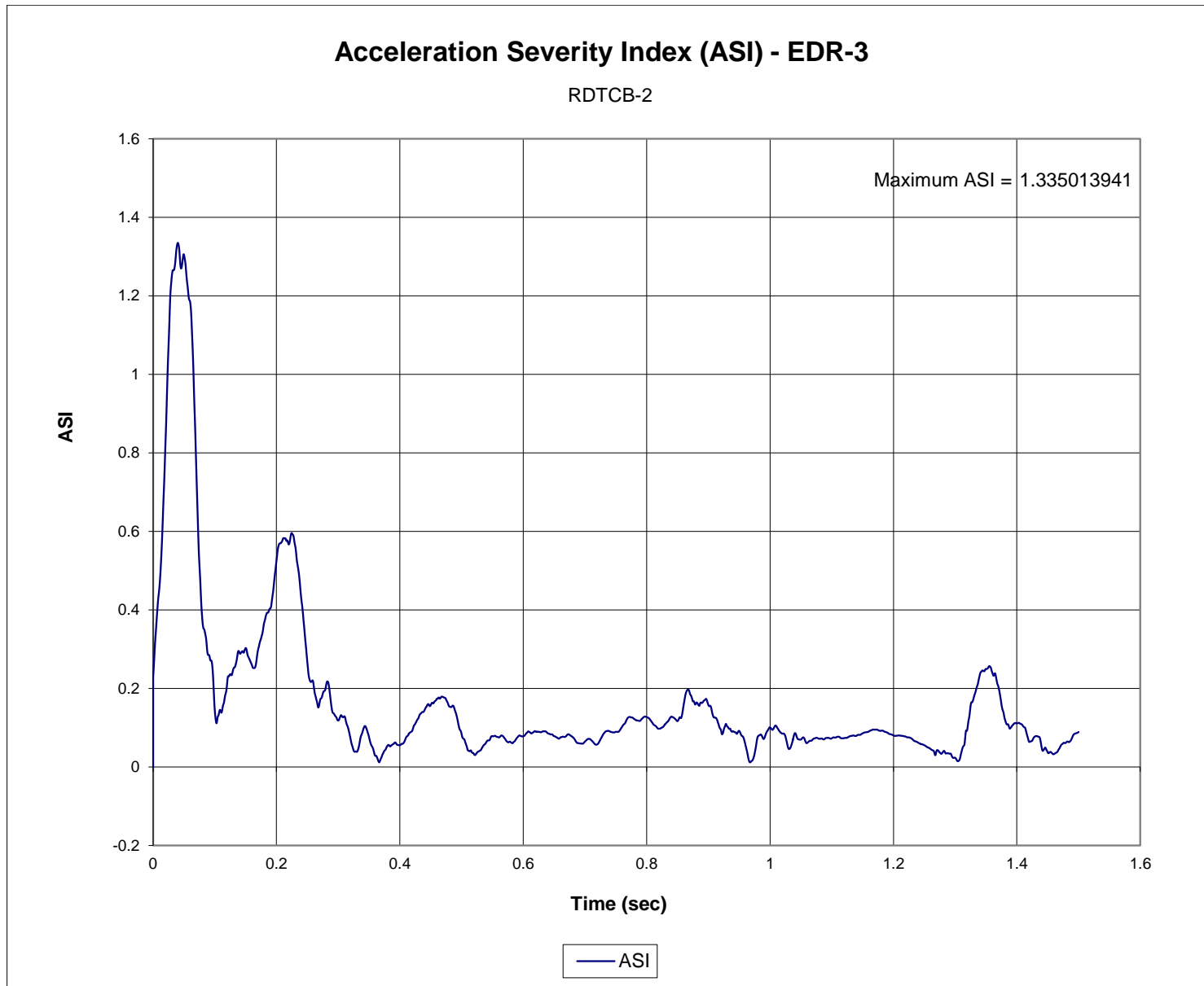


Figure G-23. Acceleration Severity Index (EDR-3), Test No. RDTCB-2

**END OF DOCUMENT**